



Grant Agreement No.: 226479

# SafeLand

Living with landslide risk in Europe: Assessment, effects of global change and risk management strategies

7<sup>th</sup> Framework Programme  
Cooperation Theme 6 Environment (including climate change)  
Sub-Activity 6.1.3 Natural Hazards

## Deliverable 4.5

Evaluation report on innovative monitoring and remote sensing methods and future technology

Work Package 4.2/4.3 - Remote sensing technologies for landslide detection, monitoring and rapid mapping/ Evaluation and development of reliable procedures and technologies for early warning

Deliverable/Work Package Leader: UNIFI

Revision: 1 – Final

July, 2011

Rev.	Deliverable Responsible	Controlled by	Date
0	UNIFI	Contributors	01-05-2011
1	UNIFI	UNIL	27-07-2011

## SUMMARY

In this deliverable the most innovative landslide monitoring and remote sensing technologies are reviewed and evaluated, with the aim to address their future scientific and technological developments.

Amongst all the ground based techniques employed in landslide studies, the ones which in recent years showed the most promising improvements have been selected and reviewed, emphasizing the recent trends in their development and application and stressing the latest scientific and technological advances.

The same approach has been pursued with remote sensing techniques, making a clear distinction between the use for detection and mapping and the use for monitoring purposes.

A relevant part of the deliverable has been focused on the application of these innovative techniques within SafeLand case studies, clearly stating which technical and scientific improvements have been achieved for each technique thanks to SafeLand project.

Additionally, the current use of both ground-based and remote sensing techniques in Europe has been evaluated by means of two questionnaires. These questionnaires have been used to make a picture of how ground based monitoring and remote sensing technologies are used in landslide study nowadays. They have been circulated within and outside Europe to Universities, Research Institutes, Public Institutions and Private Companies.

Based on the literature review, on the aforementioned questionnaires and on the results coming from the Safeland case studies, all the considered ground based, airborne and spaceborne techniques have been evaluated listing their main advantages and limitations and highlighting the needs for research and future developments.

It's worth noticing that most of the other deliverables of the Area 4 (D4.3, D4.4, D4.6) are deeply linked to D4.5. In particular in order to avoid a strong content overlapping we make reference for an in-depth examination to the other deliverables:

- D4.1 "Review of monitoring and remote sensing methodologies for landslide detection, fast characterisation, rapid mapping and long-term monitoring", concerning the technical description of the ground-based, airborne and spaceborne techniques examined in this deliverable.
- D4.3 "Creation and updating of landslide inventory maps, landslide deformation maps and hazard maps as input for QRA using remote sensing technology", concerning the methodology for setting up and updating landslide inventories and for feeding and maintaining adaptive hazard maps, providing a common tool for updating these products at regional/catchment scale.
- D4.4 "Guidelines for the selection of appropriate remote sensing technologies for monitoring different types of landslides", concerning the selection of suitable remote sensing techniques by the stakeholders.
- D4.6 "Report on geo-indicator evaluation", concerning a more specific description of the parameters monitored (geoindicators) and an advanced knowledge on the correlation between different indicators, their role as early warning parameters and quantification of thresholds.

## NOTE ABOUT CONTRIBUTORS

The following organisations contributed to the work described in this deliverable:

**Lead partner responsible for the deliverable:**

Università degli Studi di Firenze (UNIFI)

Deliverable prepared by:

*Veronica Tofani, Samuele Segoni, Filippo Catani, Nicola Casagli*

**Partner responsible for quality control:**

Université de Lausanne (UNIL)

**Other contributors:**

Analisi e Monitoraggio del Rischio Ambientale (AMRA Scarl)

*Fornaro G., Picarelli L., Minardo A., Guida A., Damiano E.*

Bureau de Recherches Géologiques et Minières (BRGM)

*Raucoules D., De Michele M.*

Centre National de la Recherche Scientifique (CNRS)

*Malet J.-P., Travelletti J., Delacourt C., Allemand P., Masson F., Ulrich P., Déprez A., Walter M., Joswig M.*

C.S.G. S.r.l. Centro di Servizi di Geoingegneria (CSG)

*Gozzi A., Garbarino E., Foglino L., Lovisolo M.*

Geological Survey of Austria (GSA)

*Supper R., Baron I., Jochum B., Winkler E., Ottowitz D., Römer A., Tilch N., Motschka K., Jaritz W.*

Geological Survey of Slovenia (GeoSZ)

*Carman M., Kumelj S.*

International Centre for Geohazards (ICG)

*Oppikofer T., Pfaffhuber A.*

International Institute for Geo-information Sciences and Earth Observation (ITC)

*Stumpf A., Kerle N.*

Università degli Studi di Firenze (UNIFI)

*Tofani V., Segoni S., Catani F., Casagli N., Intreiri E., Antolini F., Del Ventisette C., Moretti S., Luzi G.*

Università degli Studi di Salerno (UNISA)

*Peduto D., Cascini L.*

Universitat Politècnica de Catalunya (UPC)

*Gili J., Corominas J., Moya J.*

Université de Lausanne (UNIL)

*Michoud C., Derron M.-H., Jaboyedoff M.*

## CONTENTS

<b>1</b>	<b>Introduction.....</b>	<b>8</b>
<b>2</b>	<b>Recent trends in ground-based techniques.....</b>	<b>10</b>
2.1	Monitoring of movement and deformations.....	10
2.1.1	GPS .....	10
2.1.2	Wire extensometers.....	12
2.1.3	3D displacement monitoring gauges.....	17
2.1.4	Automatic inclinometers.....	19
2.1.5	GB-InSAR .....	21
2.1.6	Terrestrial Laser Scanner (TLS).....	23
2.1.7	High-resolution terrestrial optical images correlation .....	26
2.1.8	Seismic monitoring.....	27
2.2	Monitoring of hydrological conditions.....	28
2.2.1	Optical fibres.....	28
2.2.2	Time Domain Reflectometry (TDR).....	30
2.2.3	Geoelectric monitoring .....	32
<b>3</b>	<b>Recent trends in airborne and spaceborne techniques.....</b>	<b>34</b>
3.1	Landslide detection and mapping.....	34
3.1.1	Aerial sensors.....	34
3.1.2	Satellite optical .....	39
3.1.3	Satellite radar .....	42
3.1.4	Airborne geophysics .....	44
3.2	Landslide monitoring .....	50
3.2.1	Aerial sensors.....	50
3.2.2	Satellite optical .....	51
3.2.3	Satellite radar .....	53
3.2.4	Airborne geophysics .....	55
<b>4</b>	<b>Questionnaire on ground based techniques.....</b>	<b>56</b>
4.1	Methods .....	56
4.2	Review of collected sites.....	58
4.3	Results .....	59
4.3.1	Evaluation of the investigation methods.....	59
4.3.2	Evaluation of the monitoring methods.....	61
4.4	Discussion and conclusions.....	63
4.5	Acknowledgements .....	65
<b>5</b>	<b>Questionnaire on airborne and spaceborne techniques .....</b>	<b>66</b>
5.1	Methods.....	66
5.2	Review of the collected answers .....	68
5.3	Results - Landslide detection and mapping.....	70
5.4	Results - Landslide monitoring .....	73
5.5	Discussion and conclusions.....	77

<b>6</b>	<b>Outcomes from Safeland project test cases .....</b>	<b>81</b>
6.1	Ground based techniques.....	84
6.1.1	GPS: La Valette landslide and Villerville landslide (France).....	84
6.1.2	Borehole wire extensometers, Vallcebre (Spain) .....	96
6.1.3	Automatic inclinometers: Bagnaschino (Torre Mondovì – Italy) .....	101
6.1.4	GB-InSAR: Castagnola landslide (Italy) .....	107
6.1.5	TLS monitoring of the Åknes rockslide (Norway).....	114
6.1.6	High-resolution terrestrial optical images correlation: Super-Sauze (South French Alps) .....	118
6.1.7	Micro-seismic monitoring of soft-rock landslides: Super-Sauze (France) .....	128
6.1.8	Optical fibres and TDR: experimental flume .....	138
6.1.9	Geoelectric monitoring: Gschliefgraben.....	142
6.2	Mobile platforms .....	148
6.2.1	Offshore laser scanning for coastal rockfall hazard assessment, coupling terrestrial LiDAR and GNSS/IMU systems: example of Sunndalsøra, Møre og Romsdal, Norway (detection and mapping).....	148
6.2.2	Satellite optical (detection and mapping): object-oriented landslide inventory mapping with variable image data using machine learning techniques.....	153
6.2.3	Satellite radar (detection and mapping): Liri-Garigliano and Volturno basins.....	162
6.2.4	Airborne geophysical survey: Stože, Log pod Mangrtom (detection and mapping) .....	169
6.2.5	Airborne geophysics: Schnepfau, Austria (detection and mapping).....	175
6.2.6	Airborne frequency domain EM mapping, Gschliefgraben, Austria (detection and mapping).....	182
6.2.7	Airborne time domain EM mapping (monitoring): Aurland fjord rock slide (Norway) .....	201
6.2.8	Airborne geophysics (monitoring): Sibratsgfall .....	207
6.2.9	High resolution space-borne SAR images correlation (monitoring): La Valette (France).....	224
<b>7</b>	<b>Evaluation of the ground-based techniques .....</b>	<b>230</b>
7.1	Landslide types.....	231
7.1.1	Slides (rotational and translational) .....	231
7.1.2	Topples and falls.....	232
7.1.3	Flows .....	232
7.1.4	Lateral spreads .....	233
7.1.5	Complex and composite mechanisms.....	233
7.2	Advantages and limitations of ground-based monitoring systems.....	234
7.2.1	GPS: advantages and limitations .....	234
7.2.2	Borehole wire extensometers: advantages and limitations .....	234
7.2.3	3D displacement monitoring gauges: TM71 advantages and limitations .....	236
7.2.4	DMS systems: advantages and limitations .....	237

---

7.2.5 GB-InSAR: advantages and limitations.....	238
7.2.6 Terrestrial laser scanner: advantages and limitations .....	239
7.2.7 High-resolution terrestrial optical images correlation: advantages and limitations.....	240
7.2.8 Seismic monitoring: advantages and limitations .....	241
7.2.9 Optical fibres: advantages and limitations.....	242
7.2.10 TDR: advantages and limitations .....	242
7.2.11 Geoelectrical monitoring: advantages and limitations.....	242
7.3 Needs for research and future developments .....	244
<b>8 Evaluation of airborne and spaceborne techniques.....</b>	<b>247</b>
8.1 Landslide types.....	248
8.1.1 Slides (rotational and translational).....	248
8.1.2 Topples and falls.....	249
8.1.3 Flows	249
8.1.4 Lateral spreads .....	249
8.1.5 Complex mechanisms .....	249
8.2 Advantages and limitations of airborne and spaceborne techniques for landslide detection and mapping .....	251
8.2.1 Aerial Sensors: advantages and limitations for landslide detection and mapping.....	251
8.2.2 Satellite optical: advantages and limitations for landslide detection and mapping.....	252
8.2.3 Satellite radar: advantages and limitations for landslide detection and mapping.....	253
8.2.4 Airborne geophysics: advantages and limitations for landslide detection and mapping.....	254
8.3 Advantages and limitations of airborne and spaceborne techniques for landslide monitoring.....	256
8.3.1 Aerial sensors: advantages and limitations for landslide monitoring.....	256
8.3.2 Satellite optical: advantages and limitations for landslide monitoring.....	256
8.3.3 Satellite radar: advantages and limitations for landslide monitoring.....	256
8.3.4 Airborne geophysics: advantages and limitations for landslide monitoring.....	257
8.4 Needs for research and future developments .....	258
<b>9 Conclusion .....</b>	<b>260</b>
<b>10 References.....</b>	<b>261</b>

## 1 INTRODUCTION

Remote sensing imagery is a powerful tool for the rapid assessment of surface motions over large areas and for the fast characterization of slope instability factors. In particular in the framework of Safeland project several types of remote sensing data will be exploited such as spaceborne radars, airborne and VHR spaceborne optical sensors and airborne geophysics.

These techniques have been used in combination with geomorphological data and traditional surveying methods for providing an integrated tool for landslide detection, characterization, rapid mapping and monitoring. Special techniques for landslide characterization based on remote sensing have been developed and tested. Starting from the characteristics of landslides, such as the topography, limits, and movements, deduced from remote sensing, it is possible to deduce the failure mechanisms and to provide a rapid estimation of the volume involved.

The Safeland project has focused also on the development and evaluation of advanced and adaptive methodologies for real-time monitoring and early-warning systems for selected landslide sites. The monitoring methods have covered all kinds of technologies, ranging from the application of traditional monitoring methods to the improvement of new and advanced technologies, including geoelectrical, self potential monitoring, acoustic noise measurements, DMS, optical fibres, acoustic emissions etc.

Currently, a high level of expertise exists within the different member states related to monitoring methodologies and early-warning strategies, mostly based on the results of national research projects and initiatives.

One of the main objective of the Safeland project is to merge this highly selective expertise and therefore to create synergies on EC-level towards creation of high end European technologies and recommendation for European standards for site remote sensing and monitoring and early warning and to make these results available to end user and local stakeholders.

In this framework this deliverable has the aim to make an evaluation of the most innovative landslide monitoring and remote sensing technologies used at present, as well as suggesting needs for research and technical developments of the existing methodologies.

These objectives will be achieved through these main steps:

- Overview of recent and emerging ground based techniques for landslide analysis. This part will highlight the recent trends in the development and application of ground based methods in landslide studies.
- Overview of recent and emerging remote sensing technologies for landslide analysis. This part will highlight the recent trends in the development and application of remote sensing (airborne and spaceborne) techniques in landslide studies.
- Set up of a questionnaire on landslide monitoring methods. The Questionnaire on National State of Landslide Site Investigation and Monitoring was prepared and was disseminated among European institutes and representatives within the frame of the SafeLand project. The results of the questionnaire are reported and discussed.
- Set up of questionnaire on remote sensing technologies. The aim of the questionnaire is to collect information about the usefulness of remote sensing for landslide study and to evaluate its applicability for landslide detection, mapping, monitoring and early warning. This questionnaire has been circulated within and outside Safeland consortium. The results of the questionnaire are reported and discussed.

- Description of the results of monitoring and remote sensing techniques in Safeland case studies.
- Evaluation of ground based, airborne and space-borne techniques based on the literature review, on the aforementioned questionnaires and on the results coming from the Safeland case studies. The evaluation will be carried out for the different types of landslides according to the Cruden & Varnes (1996) classification. Limitations of each technique will be highlighted in order to define the needs for research and future developments.

It's worth noticing that most of the other deliverables of the Area 4 (D4.3, D4.4, D4.6) are deeply linked to D4.5. In particular in order to avoid a strong content overlapping we make reference for an in-depth examination to the other deliverables:

- D4.1 "Review of monitoring and remote sensing methodologies for landslide detection, fast characterisation, rapid mapping and long-term monitoring". It provides the technical description of the ground-based, airborne and spaceborne techniques examined in this deliverable.
- D4.3 "Creation and updating of landslide inventory maps, landslide deformation maps and hazard maps as input for QRA using remote sensing technology". It provides the methodology for setting up and updating landslide inventories and for feeding and maintaining adaptive hazard maps, providing a common tool for updating these products at regional/catchment scale.
- D4.4 "Guidelines for the selection of appropriate remote sensing technologies for monitoring different types of landslides". It provides the guidelines for the selection of suitable remote sensing techniques by the stakeholders.
- D4.6 "Report on geo-indicator evaluation". It provides a more specific description of the parameters monitored (geoindicators) and an advanced knowledge on the correlation between different indicators, their role as early warning parameters and quantification of thresholds.

## 2 RECENT TRENDS IN GROUND-BASED TECHNIQUES

This chapter contains a brief overview of the most recent developments in the application of the ground-based technologies in landslide studies. This chapter is further divided into two sections, section 2.1 "Monitoring of movement and deformations" and section 2.2 "Monitoring hydrological conditions". The techniques examined in this chapter are the ones considered as the most innovative and they have been selected among all the existing techniques by the project partners.

### 2.1 MONITORING OF MOVEMENT AND DEFORMATIONS

#### 2.1.1 GPS

*CNRS: Malet J.-P., Masson F., Ulrich P., Déprez A.*

A large variety of techniques is available for the monitoring of landslide displacements, ranging from classical geodetic methods providing a local (e.g. point) measurement of the deformation to advanced laser and radar methods providing a global image of the deformation. Among these techniques, distancemeters, total stations and *Global Positioning Systems* (GPS) receivers allow to precisely locate the position of targets installed within a landslide over time (Duranton, 2000). These conventional geodetic methods remain the most commonly used because it is possible to reach an accuracy of a few millimetres on short baselines of a few kilometres and to access to precise 3D coordinates. These techniques are also commonly used for the precise co-registration of the images acquired with high-resolution cameras, LiDAR and radar systems.

The GPS is a radio-navigation, timing and positioning system with a wide set of applications. By tracking the electromagnetic waves that the GPS satellites are sending continuously, the system can obtain the antenna position (Longitude, Latitude, and Height, or X, Y, Z coordinates). The use of the phase measurements allows determining the relative positions of points located as far as several hundred kilometres apart with an accuracy of 2-5 mm in the X-Y plan and 5-10 mm in altimetry. This accuracy allows the fast detection of weak displacements and, thus the survey of the temporal evolution of crustal deformation (Dixon, 1991) and natural hazards (volcanoes, tectonic faults, ice glaciers, landslides). A review of GPS monitoring applications is given in Malet et al. (2002). According to ClimChalp (2008), continuous monitoring with low-cost GPS receivers is currently object of research. Another way to adjust the installation budget is to implement a multi-antenna scheme, where one receiver is able to sequentially log or process the GPS signal acquired by several antennas spread in the area (Chen et al., 2005).

In France, several GPS receivers have been installed on active landslides (e.g. *La Clapière* rockslide, *Avignonet* and *Villerville* rotational slides, *Super-Sauze* and *La Valette* mudslides) since a few years. These landslides show very different displacement rates (ranging from a few centimetres to several meters per year) and different kinematic regimes (e.g. continuous displacement of nearly constant rate or succession of periods of acceleration/deceleration). All landslides are part of the French '*Observatory of Landslides*' (e.g. OMIV), a collaborative structure aiming at collecting the same type of kinematic, hydrologic and seismic

observations on landslides and at disseminating the data to the scientific community (e.g. <http://eost.u-strasbg.fr/omiv>).

The application of GPS techniques is mainly dedicated for the monitoring of slow-moving landslides, creeping slopes and the pre-failure stage of rockslides.

### 2.1.2 Wire extensometers

*UPC: Gili J., Corominas J., Moya J.*

In the last decade, the interest to improve our understanding of landslide behaviour and to use this knowledge to mitigate the risk and to warn population has promoted a great development of monitoring techniques; particularly those which allow an automatic and continuous recording of ground displacement. Wire extensometer is one of these techniques. Wire extensometers can be installed on the ground surface (Bonnard and Steinmann, 1990) or into a borehole (Angeli et al. 1988; 1989). In any case the extensometer integrates the displacement occurred between two points, one fixed in the stable zone outside the landslide area (in superficial extensometers) or below the landslide mass (in borehole extensometers), and the other one in the ground surface of the moving mass. Few new developments have been found on the superficial extensometers; hence, in this section the focus is centred on borehole ones. Displacements integrated along the vertical in a borehole wire extensometer can be easily compared with displacements measured by inclinometers and also with changes of the water table.

Borehole wire extensometry has been applied to a reduced number of landslides till now (Angeli et al. 1988, 1989; Corominas et al. 2000, 2005) and still is a little-known monitoring technique, but a growing use is expected due to its simplicity, low cost and excellent performance.

The wire extensometer consists of a steel wire anchored to the borehole bottom below the slip surface of the landslide. The other wire end is attached to pulley system located on the ground surface. The wire is placed around the pulley and is kept in tension by means of a counterweight (Figure 1 and Figure 2). The movement of the landslide displaces the wire either inside or outside the borehole with the consequent rotation of the pulley. Here, the displacement is transformed into an electrical voltage by means a potentiometer and is recorded in a data logger at the desired time interval (e.g., each 20 minutes) (for a more complete description see deliverable 4.1; Angeli et al. 1988, 1989; Corominas et al., 2000).

#### Recent developments

The first prototype of wire extensometer for borehole was designed by Angeli et al. (1988, 1989). Another prototype based on this first design was built at the Technical University of Catalonia (UPC), it was tested in the Vallcebre landslide (chapter 6.1.2) (Corominas et al., 2000). The new prototype incorporated some changes to improve the performance of the device:

- **Checking of the potentiometer readings**

To check the readings of displacement obtained by the potentiometer, a dial with tick marks every millimetre was added to the pulley. The precision of the direct readings in the dial is about half a mm (0.5 mm), only a little worse that those achieved with the automatic reading (potentiometer and data logger), that is a tenth of mm (0.1 mm). Dial readings can be made regularly during the field campaigns to check the performance of the instrumentation of a landslide, or to download data from data loggers, whether the data transmission is not telematic.

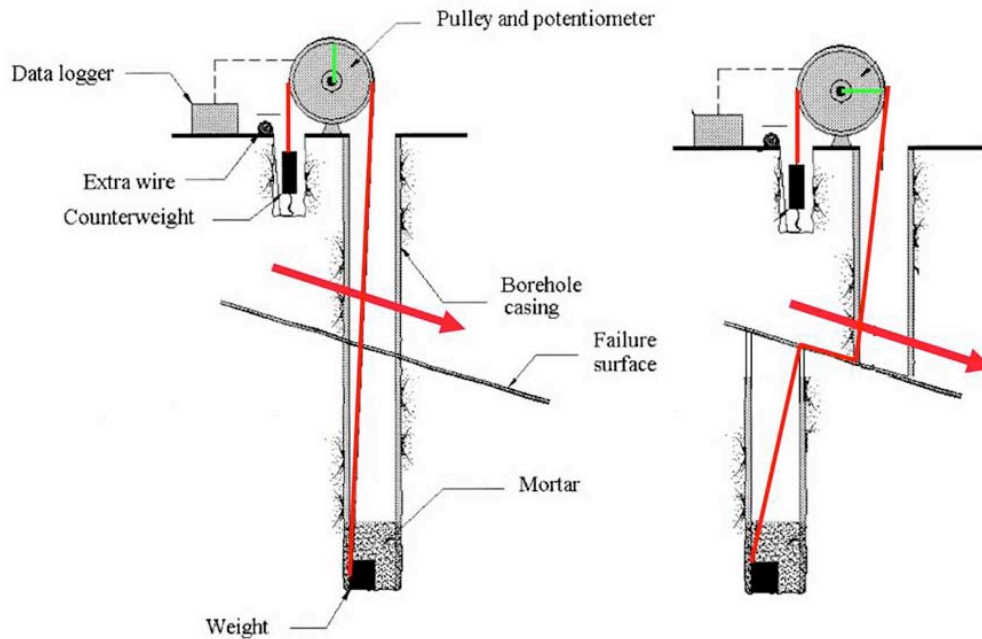


Figure 1: Scheme of the wire extensometer, modified from Corominas et al., 2000. Left: as installed. Right: after some sliding displacement of the upper mass downhill.



Figure 2: View of the upper part of the wire extensometer. In the centre, the pulley, the dial and the potentiometer.

#### • Improvement of the anchoring of the pulley system

Performance of the prototype was tested in the Alverà landslide (Eastern Dolomites, Italy; Angeli et al., 1988). The results revealed the occurrence of cyclic displacements up to 1.5 cm that were probably related to freezing and thawing of the upper layer of the soil. Swelling of

the ground surface is not an unusual phenomenon in mountain regions, where periglacial climate prevails during winter. In dry climates, soil or mudrocks can also swell periodically by changes of the ground moisture. To minimize displacements of the ground surface caused by swelling of the surficial layer, the pulley system should be anchored under this swelling layer. The pulley system was anchored to a depth of one meter in the Vallcebre landslide (Corominas et al., 2000).

- **Protection of the wire of the extensometer**

Some ground waters rich in carbonate, in sulphate, or in sulphides can be chemically aggressive and corrode the steel wire. In order to protect the wire against corrosion, it was inserted into a plastic sheath and sealed with silicone.

- **Assessment of superficial landslide displacement from the wire extensometer**

A main improvement of this monitoring technique was the calculation of the landslide displacement from the reading of the extensometer (Corominas et al., 2000). Wire extensometer readings cannot be properly interpreted unless the general pattern of the movement is known. There is no direct relationship between displacements of the landslide and the displacements of the wire extensometer. This is because the total displacement of the wire depends on several factors such as the diameter of the borehole, the type of landslide mechanism, the dip angle of the failure surface, and the existence and thickness of a basal shear zone instead of a slip surface. Displacements measured with the wire extensometer are global and the device cannot detect separately the vertical and the horizontal components of the movement neither identify the presence of several slip surfaces.

The relation between both wire displacement and superficial landslide displacement for translational slides was determined analytically by three equations for the case of a translational slide with a single basal shear zone (Corominas et al., 2000). Each equation corresponds to a stage characterised by the type of contact of the wire with the borehole casing. Initial negative displacements of small magnitude were foreseen for the wire extensometer (and afterwards observed) as a result of the shortening of the borehole length, which occurs approximately while the cumulative landslide displacement is less than the diameter of the borehole casing (Figure 3). During this stage, the displacements of the wire are smaller than those measured at the ground surface and show a non-linear relationship (Figure 3). For larger cumulative displacements of the landslide, the wire is pulled into the borehole which results in positive increments of the wire displacement. A theoretical analysis showed that, for landslide displacements much larger than the thickness of the shear zone, the rates of displacement of both ground surface and wire extensometer tend to coincide. The thicker the shear zone, the greater the differences between both measurements. Translational landslides with a single slip plane correspond to the particular case of a shear zone with null thickness.

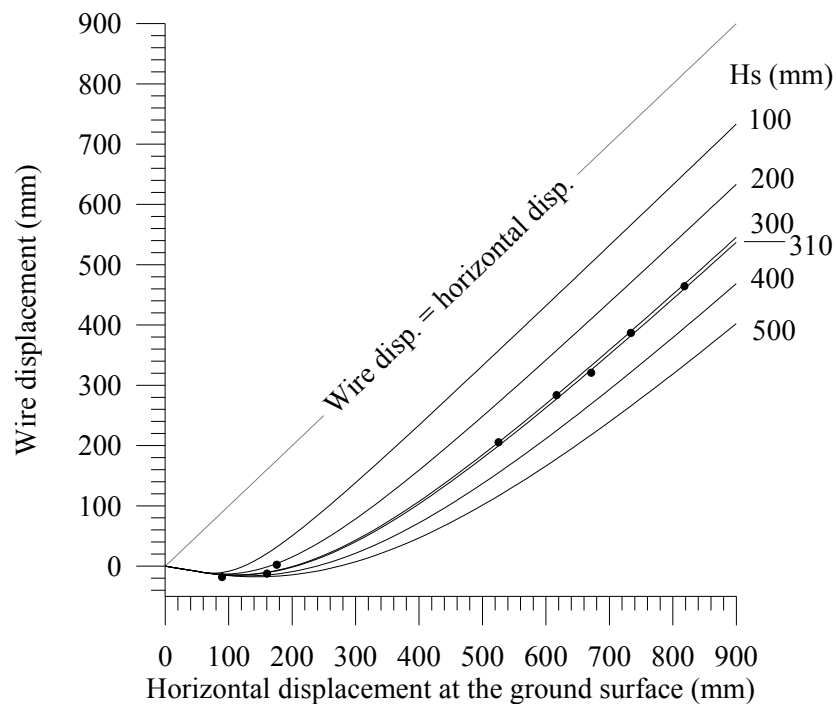


**Figure 3: Fitting of the measured displacements (dots) to a calculated curve relating both the horizontal and wire displacements for the borehole S-2 of the Vallcebre landslide. The set of curves (solid lines) has been prepared solving equations landslide displacement and wire displacement for several thicknesses of the basal shear zone. The thickness estimated for the shear zone by non-linear regression was 31 cm (Corominas et al., 2000).**

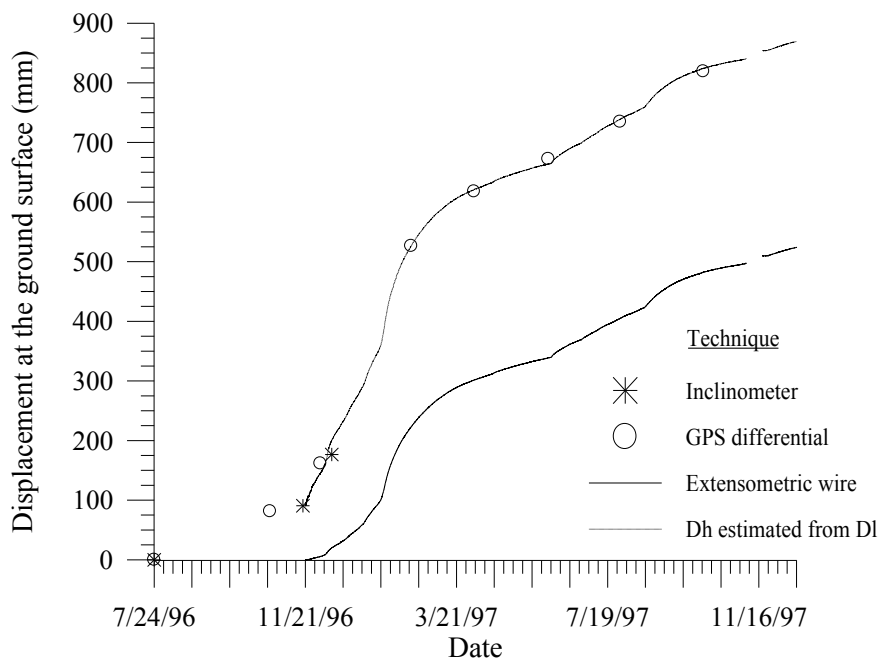


**Figure 4: Cumulative displacement of the Vallcebre landslide at the borehole S2 measured with the GPS and the probe inclinometer (open circles and stars), and the total wire extensometer displacement (solid line). Each minor tick on the time axis corresponds to 1 week. A continuous record of the horizontal component of displacements was calculated from the wire measurements using the displacement equations mentioned in the text (dashed line) (Corominas et al, 2000).**

The calculation of the landslide displacements from the wire displacements requires the values of some parameters that can be directly measured (as the diameter of the borehole casing). But, it also requires the determination of other parameters by indirect methods, as the dip of the slip surface (or the basal shear zone), that can be calculated from a landslide cross-section including several inclinometric boreholes. The thickness of the basal shear zone can be fitted by non-linear regression using the equations relating the landslide and wire displacement; this is possible if some values of the landslide displacement has been measured by an independent method, as inclinometry (for small displacements) or differential GPS (for large cumulative displacements) (Figure 3). This fit can be actually regarded as a calibration of the displacement of the wire extensometer. Once this calibration is made, the *continuous time series* (e.g. each 20 minutes) of real landslide displacements can be easily calculated from the extensometer readings (Figure 4). This latter is the key result of the technique, because a continuous displacement record allows for the assessment of the instantaneous velocity of the landslide, which is of great importance for comparing landslide movement with the changes of pore water pressure and for the implementation of early warning systems.

### 2.1.3 3D displacement monitoring gauges

*GSA: Baron I.*

*Institute of Rock Structure and Mechanics, Czech Academy of Sciences: Klimeš J.*

Monitoring of very slow and/or micro-displacement movements usually require very accurate devices recording the movement in 3D. These devices, moreover, have to sustain stable in common field conditions with high humidity, device soiling and temperature fluctuations.

All those requirements have successfully met in a special crack gauge, the TM71 (Košťák 1991). This device is based on the principal of mechanical interference between two optical grids. Glass grids used in the gauge represent stable elements. The gauge can be permanently installed across cracks and joints, allowing 3D monitoring of the blocks related to a joint (Figure 5). The displacement vectors in two perpendicular planes are supplemented with angular deviations and they are calculated from fringe patterns registered by the gauge indicators (Figure 6). The principle has been described by Košťák (1969) and the monitoring procedure by Košťák (1977, 1991). The accuracy of the gauge system can be effectively governed by the density of applied grids, which ranges from 5 to 100 lines\*mm<sup>-1</sup>. Sensitivity of the TM71 gauge system is 0.05–0.0125 mm in all three spatial coordinates of displacement, and 3.2\*10<sup>-4</sup> rad in angular deviations of the two planes. Based on field experience of its performance in harsh environmental conditions, one can confidently and systematically obtain results with an accuracy of at least of 0.03 mm.

The TM71 gauge is a very sturdy instrument that can be used even at remote locations with no electricity connection or signal coverage, such as in mountains or caves. In such locations it is accepted that monitoring can be hand-driven and readings taken at intervals of weeks or months. The frequency of readings is adjusted according to the characteristics of the observations.

The TM 71 device is industrially produced by GESTRA in Sedloňov, Czech Republic and it has been frequently applied by scientist of the Institute of Rock Structure and Mechanics in Prague since the 1960's with some observations of slope deformations extending over periods of more than 30 years. At the present days, more than 120 sites across Europe and Asia are being monitored with this instrument ([http://www.tecnet.cz/index\\_en.php](http://www.tecnet.cz/index_en.php)). Slope movements as low as 10<sup>1</sup> to 10<sup>-2</sup> mm/year have been registered. Block-type slope movements were studied first with this instrumentation and many seemingly stable structures were found to be moving as a result of creep at the base of huge rigid blocks in bedrock, where plastic movement in clayey deposits causes block instability (Košťák & Avramova-Tacheva 1984).



**Figure 5: The TM71 crack gauge installed underground to bridge a joint. It is equipped with two planar moiré indicators in two perpendicular planes, horizontal xy, and vertical xz, that define 3D displacement between the two joint faces in the wall. The TM71 crack gauge is a product of GESTRA, Sedloňov, Czech Republic.**



**Figure 6: A view of one of the TM71 indicators, in detail. The indicator shows several moiré patterns and a spiral thermometer. Displacement vectors in the vertical plane XZ are defined by the actual positions and densities of the moiré fringe patterns. The thermometer serves for calculations needed to compensate for temperature variation effects.**

#### 2.1.4 Automatic inclinometers

CSG: Gozzi A.

In-place inclinometers are typically used for monitoring subsurface deformations around excavations when rapid monitoring is required or when instrumented locations are difficult to access for continued manual readings and also is used to monitor landslide areas. The device consists of a series of gravity-sensor transducers (uniaxial or biaxial), joined by articulated rods, positioned at intervals along the borehole axis or concentrated in zones of expected movement. The main advantages include rapid automatic data logging and real-time monitoring, while a disadvantage is the great complexity and expense of the hardware. For further details, please read Dunnycliff and La Fonta (2001), La Fonta and Beth (2002), Machan and Bennett (2008).

In-place inclinometers can be used in combination with a conventional inclinometer in two possible modes:

- In-place version is installed before the conventional inclinometer to define the location of any transverse deformation, with minimal labour costs for reading. If deformation occurs, the in-place version is removed and the zone is monitored by a conventional inclinometer probe.
- Conventional inclinometer is first installed to indicate any deformation and the in-place system is installed later to minimize subsequent effort and to provide an alarm trigger.

Several innovations have been introduced since 2000 in the automatic inclinometers by the DMS 2D and 3D systems (patents CSG srl, Italy). This type of in place instrumentation is specifically designed for the real time stability control of landslides, cuttings, engineering works, allowing the differential monitoring of the major physical and mechanical parameters of the soil-bedrock and of the structures in 2D/3D, as well as of the piezometric level, variations of the movement acceleration, temperature (Figure 7).

DMS column is like a “spiral cord” composed of a sequence of hard tubular modules (hosting sensors and AD control), connected with each other by special joints, and endowed with the degree of freedom specific for the type of measurement performed. Depending on the instrumentation version, vertical, horizontal and inclined installations are possible.

Thanks to the modular structure DMS can operate in harsh environments with continuous adaptability to bend and twist of the casing (or borehole with the 3D version), also bearing very high deformation rate compared to standard instrumentation. It is possible to use a wide range of transducers on a modular basis that may be interfaced with the same digital control unit: mono/biaxial inclinometers, extensometers, accelerometers, piezometers, thermometers, digital compasses.

For column with considerable length (>30m) installation is made easier by means of a DMS reeler, which allows to install and retrieve the column inside the drilling hole/casing. The robust structure of the columns allows also transporting and installing the system directly by means of a helicopter (mountain areas and harsh environments).

Considerable continuous depths have been reached in installation. The deepest DMS column has been installed in 2009 inside the Åknes rockslide (Åknes Tafjord Beredskap, Norway)

---

where the real time continuous monitoring is active in the interval 8-128 m below ground level, a total of 245 transducers are connected at the same time.

For further details, please read Giuffredi et al. (2003) and Lovisolo and Della Giusta (2005).



**Figure 7: DMS 2D and DMS 3D columns on their reeler.**

### 2.1.5 GB-InSAR

#### *UNIFI: Intriери E.*

In the last years GB-InSAR technique has been demonstrated as a reliable tool to monitor slope instability. An extensive literature about the working principle of this instrument and some of its applications can be found in Luzi (2010) and also in the Deliverable 4.1 – Review of techniques for landslide detection, fast characterization, rapid mapping and long-term monitoring. Some further steps have been made in more recent times involving in particular innovative applications, improvements in the hardware and new software.

Concerning the first point it has been showed how GB-InSAR can be used in new geological contexts as well as with new approaches. For instance Luzi et al. (2010) from the Institute of Geomatics (IG) developed a specific procedure that allows one to use multitemporal discontinuous data sets lasting one day and repeated after more than one month, when maintaining coherence is often a problem. This permits to perform several short-term campaigns in different times and to merge them afterwards.

Very interesting is also the use of GB-InSAR as a tool for early warning systems; this has been proved in Casagli et al. (2009) where it is described how with a GB-InSAR it was possible to detect the bulging of the NW flank of the Stromboli volcano, anticipating the opening of a new vent during the 2007 crisis. The importance of this application is easily understood if we think how early warning systems have become more and more used all around the world.

Recently innovative applications to different types of landslides have been carried out. For example it has been demonstrated that this apparatus can be valuable for assessing the stability conditions of a deep seated gravitational slope deformations (Barla et al., 2010) in the Alps; with this type of landslides the problem could come from the wide areas to be monitored and therefore the long distance and the atmospheric effects connected to it.

Other works also highlight how GB-InSAR can be integrated with other novel techniques such as the Terrestrial Laser Scanner (TLS) and the Persistent Scatterer Interferometry (PSI) technique. Examples of this can be found in Casagli et al. (2010a) and in Tapete et al. (2011) where this integrated approach was used in order to assess the stability conditions of important structures with a high cultural heritage meaning, such as the Palatino Hill (Rome) and the Roman Forum. Here the monitoring was carried out at multiple scales, from “archaeological site scale” to “single monument scale”.

GB-InSAR has also proved to be efficient for assessing rockfall susceptibility (Mazzanti & Brunetti, 2010). In fact the study of movements of some portions of a rock mass, integrated with the use of TLS, permits to establish the state of activity of potentially unstable blocks. This approach can be used instead of (or together with) conventional instruments (such as extensometers) that, conversely, are installed only once the unstable blocks have already been detected.

Some innovations involve new software for the elaboration of interferometric data and atmospheric correction. Aresys, a spin-off the Polytechnic of Milan, developed GRAPeS, a program which integrates the Permanent Scatterers technique (Ferretti et al., 2001) also for ground-based systems. The procedure developed by the IG for discontinuous experimental campaigns has already been cited above (Luzi et al., 2010). Following the experience of the GALAHAD Project, IG also developed a cross-platform software, at the moment just for research purpose, able to operate on different commercial GB-InSAR apparatuses.

---

In the last years the hardware of GB-InSAR experienced some improvements as well. With respect to 10 years ago, now modern apparatuses are much smaller and mobile (although, in some cases, to the detriment of the number of electromagnetic bands that can be employed). Also, with some modern instruments, the time occurred to acquire a single radar image can be as short as 3-5 minutes (depending on several factors, especially the distance from the target). This enables the monitoring of moderately rapid landslides, such as some earth flows, which can exceed the velocity of 3 m/day. Applications like these were extremely difficult if not unthinkable with the first models.

All these innovations are also due to the fact that many research centres and societies are now able to produce a GB-InSAR, which has become, despite the cost, relatively popular. Some examples of developers and producers are, among others, the Department of Electronics and Telecommunications of the University of Florence (Pieraccini et al., 2003), the Joint Research Center of ISPRA (Leva et al., 2003), its spin-off Ellegi-Lisalab (Casagli et al., 2010b), Gamma Remote Sensing from Switzerland (Wiesmann et al., 2008), Ingegneria Dei Sistemi from Pisa (Barla et al., 2010), the Institute of Geomatics of Barcelona (Luzi et al., 2010), the Institute of Electronics Chinese Academy of Sciences from Beijing (Hong et al., 2010) and others.

### 2.1.6 Terrestrial Laser Scanner (TLS)

*ICG: Oppikofer T.*

The applications of TLS in landslide investigation and monitoring have greatly increased over the last 10 years (Derron and Jaboyedoff, 2010). Jaboyedoff et al. (2010) provide an overview of the most common applications of TLS (and ALS) in landslide studies. This chapter is based on this review article and on Oppikofer (2009).

#### **Landslide mapping and characterization**

The high-resolution topography data provided by TLS are useful for mapping and characterization of landslides: Rowlands et al. (2003) used a TLS-DEM to map the limits of a shallow landslide, Dunning et al. (2009) analysed a rockslide scar by TLS and estimated its volume, and based on the morphology of the head scarp Jaboyedoff et al. (2009a) demonstrated that shallow landslides in river banks possess a spherical failure surface. One of the major uses of TLS on rockfalls and rockslides is the characterisation of main structures (orientation, spacing, persistence, roughness of discontinuities). This is particularly useful for inaccessible, remote or hazardous rock walls.

Several tools exist to perform structural analyses of discontinuity sets on the basis of TLS point clouds. A basic approach to measure the orientation of a discontinuity is to fit planes on selections of the TLS point cloud (Abellán et al., 2006; Oppikofer et al., 2008b; Sturzenegger and Stead, 2009a; Sturzenegger and Stead, 2009b), which is a similar approach as field measurements with a compass. Methods for the automatic delimitation of discontinuities and measurements of their orientation are based on the meshing of the TLS point cloud followed by the computation of the spatial orientation of each facet and the automatic segmentation into contiguous areas with similar orientation (Slob et al., 2002; Kemeny and Post, 2003; Kemeny et al., 2006; Lato et al., 2009a). Another approach is the orientation-specific colouring of the TLS point cloud (or a DEM) in Coltop3D. This software computes the orientation for each point with respect to its neighbourhood and attributes a unique colour for each spatial orientation using a Hue-Saturation-Intensity (HSI) wheel in combination with a stereographic projection (Jaboyedoff et al., 2004; Jaboyedoff et al., 2007; Oppikofer et al., 2009).

TLS datasets have also been used for surface roughness analyses of rock fractures, using either fractal methods (Fardin et al., 2001; Fardin et al., 2004; Kulatilake et al., 2006) or by computing the residuals between the real fracture surface and a best-fitted plane (Sturzenegger and Stead, 2009a). Oppikofer et al. (in press) adapted Barton's (1982) asperity-amplitude method to obtain Joint Roughness Coefficients from TLS point clouds.

#### **Susceptibility and hazard assessment**

In landslide susceptibility and hazard assessment TLS is useful for the creation of high-resolution DEMs for site-specific slope stability modelling (e.g. Jaboyedoff et al., 2009b) and run-out modelling (Alba et al., 2005; Nguyen et al., 2011), especially when precise topographic information is not available from other sources (e.g. ALS-DEM).

Multi-temporal TLS point clouds provide crucial input for rockfall hazard assessment by enabling the localisation of rockfall activity and the quantification of rockfall volumes and mechanisms (Rosser et al., 2005; Abellán et al., 2006; Rosser et al., 2007; Rabatel et al., 2008; Abellán et al., 2010; Lim et al., 2010; Pedrazzini et al., 2010). Using a post-event TLS

point cloud, Abellan et al. (2006) performed a back-analysis of a large rockfall to obtain its volume and failure mechanism. Rosser et al. (2007) have shown increased activity of small rockfalls prior to a larger failure, while Pedrazzini et al. (2010) interpreted the decrease of such rockfall activity as temporary stabilization of a large unstable rock mass.

A promising application of mobile TLS, i.e. TLS acquisitions from a moving vehicle, to monitor rockfalls along a highway or a railroad track is presented by Lato et al. (2009b). Although mobile TLS provides less accuracy and resolution than static TLS, the obtained point clouds still allow for detection and quantification of rockfalls along the monitored corridor.

### **Monitoring**

Landslide displacements can be efficiently monitored by multi-temporal TLS acquisitions. In opposition to conventional, point-based surveying techniques (GPS, total station etc.), TLS is an area-based technique and provides information over the entire landslide area. This enables a more complete understanding of the landslide displacements.

Several studies computed the landslide displacements as differences between multi-temporal TLS-DEMs, but changes are only detected in the altitude (1D) (Bornaz et al., 2002; Bitelli et al., 2004; Avian et al., 2009; Prokop and Panholzer, 2009; Kasperski et al., 2010). More advanced methods enable the computation of 3D displacements, using for example the shortest distance between matching points in two TLS point clouds (Teza et al., 2007; Oppikofer et al., 2008b; Teza et al., 2008; Travelletti et al., 2008; Abellán et al., 2009; Jaboyedoff et al., 2009a; Oppikofer et al., 2009; Abellán et al., 2010; Pesci et al., 2011). On active landslides such shortest distance comparisons between two epochs of TLS acquisitions (days, months to years between acquisitions depending on landslide velocity and monitoring purpose) is a quick method to quantify displacements over the entire scanned area (Oppikofer et al., 2008b; Travelletti et al., 2008; Jaboyedoff et al., 2009a; Oppikofer et al., 2009), but it does not take advantage of the high point density of TLS data and has relatively high errors on single points (cm-scale). More advanced techniques compute the rigid body transformation between the initial and final state of a landslide, using the piece-wise alignment method on subsets of the TLS point cloud (Teza et al., 2007) or individual compartments in a rockslide (Oppikofer et al., 2009). These techniques are able to completely describe the landslide displacement in terms of translational and rotational components and have smaller errors than shortest distance comparisons.

For rock slope instabilities, the combined interpretation of the main discontinuity sets and the 3D displacement pattern increases the understanding of the failure mechanisms. Oppikofer et al. (2008b; 2009) propose geometric instability models for large rockslides by taking into account the measured displacements and the structures affecting the rock mass.

The spatial prediction of rock slope failures becomes possible by means of sequential TLS datasets, which enable the detection of areas with increased rockfall activity (Rosser et al., 2007; Oppikofer et al., 2008b; Pedrazzini et al., 2010) or precursory displacements in a rock mass (Oppikofer et al., 2008b; Abellán et al., 2009; Abellán et al., 2010). Oppikofer et al. (2008b) have shown large rockfall activity and up to 125 cm/day velocity in a rockslide prior to a large partial collapse of the rockslide. Abellán et al. (2009; 2010) have successfully measured precursory displacements prior to a large rockfall by reducing the instrumental noise and data treatment errors with a nearest neighbour averaging technique.

**Conclusions**

The above examples of recent developments in TLS for landslide investigations and monitoring reveal the huge potential of this technique. As stated by Jaboyedoff et al. (2010) and Derron and Jaboyedoff (2010), the exploration of TLS applications in landslides investigation and monitoring is still ongoing research and future improvements and new techniques can be expected in the next years. Further advances can be achieved by new TLS systems, such as full waveform and/or multi-spectral scanners (Jaboyedoff et al., 2009a), and by coupling TLS with other techniques, especially with InSAR (Teza et al., 2008).

### 2.1.7 High-resolution terrestrial optical images correlation

*CNRS: Malet J.-P., Travelletti J., Delacourt C., Allemand P.*

Correlation of high-resolution terrestrial optical images is a very cost-effective technique with implementation, operating and equipment costs much lower than GB-InSAR and Terrestrial Laser Scanner.

The technique consists in acquiring digital optical images represented using a matrix of intensity values (brightness) recorded at each pixel of the Charge Coupled Device (CCD) of the camera. While aerial images are acquired on overhead photographs from an aircraft, correlation of optical images uses RGB images acquired from a spot very close to the ground (Jiang et al., 2008). In the last decades, camera self-calibration and analytical processing techniques allowed the use of non-metric cameras and of simplified camera calibration algorithms to compute digital elevation models using the principle of stereoscopic views (Mikhail et al., 2001; Jiang et al., 2008). In the current state, the application of terrestrial images for landslide monitoring is mostly related to the production of DEMs for image orthorectification and sediment budget analysis (Bitelli et al., 2004, Pesci et al., 2004; Cardenal et al., 2008), and more recently to the characterization of the slope morpho-structure (Lim et al., 2005; Sturzenegger and Stead, 2009).

Using correlation techniques, two-dimensional displacement fields can be derived by tracking objects in two images acquired at different time. So far, image correlation techniques have been applied only on aerial and satellite images (e.g. SPOT, QuickBird, OrbView, EROS) for the creation of landslide displacement maps (Casson et al., 2003; Delacourt et al., 2004; LePrince et al., 2008); the use of image correlation on terrestrial images has not been as popular for permanent landslide monitoring as in other application field such as in solid and fluid mechanics for the characterization of the deformation pattern of soil/rock samples (White et al., 2003; Chambon et al., 2003) or for the monitoring of other natural processes such as ice glaciers (Fallourd et al., 2010; Maas et al., 2008) or volcanoes (Honda & Nagai, 2002). Only Delacourt et al. (2007) demonstrated an efficient application of correlation of optical images for landslide monitoring which consisted in the determination of the landslide boundaries and in the qualitative estimation of the spatial variability of displacement at the La Clapière landslide (French Alps) with an image acquisition system installed at 1 km-distance.

The application of this technique is mainly dedicated for the monitoring of slow-moving landslides, mudflows and rockfalls.

### 2.1.8 Seismic monitoring

*CNRS: Walter M., Joswig M., Malet J.-P.*

Recording “seismic noise” consists in using seismic sensors (e.g. seismometers, geophones, accelerometers, acoustic emission transducers, hydrophones) to monitor passively potential events, also called “Acoustic Emission (AE)” events. The extent of the investigated area varies from some centimetres to thousands of kilometres, depending on (1) the magnitude and depth of the events, (2) the possible attenuation of the waves by the material, and (3) the type of seismic devices and the design of the seismic array. AE is generated by an event source which converts localised stress accumulation of elastic energy into the release and the propagation of elastic waves that are transmitted within a material. AE sources may characterize several types of material behaviours such as failure, friction, shearing and sliding, crack propagation, impact, and cavitation processes. For the monitoring of geohazards, AE is also referred to as “micro-seismicity” or “rock noise”. In the case of natural events, seismic noise monitoring may provide information on the characteristics of regional earthquakes to small material instabilities observed within a local slope failure. Seismic monitoring acts as a seismic “microscope” to detect small impulsive signals generated within a landslide.

A few application of micro-seismic monitoring for slope stability are related either to open mines and quarries (Hardy et al., 1991). Concerning natural mass movements, some rare experiments have been carried out mainly in rocky cliffs (Kolesnikov et al., 2003, Amitrano et al., 2004; Willenberg et al., 2004, Eberhardt et al., 2004; Amitrano et al., 2005). Slide-quakes and fracture processes in hard rocks were monitored by e.g. Brückl and Mertl (2006) in the Austrian Alps, Spillmann et al. (2007) in the Swiss Alps and Roth et al. (2005) at the Åknes fjord in Norway. The detected fractures in these studies are probably caused by brittle deformation of the respective slope material. The micro-seismic monitoring technique has also been used for the monitoring and the warning of debris flows (Arratano, 1999; Itakura et al., 2005).

For mass movements developed in soft rocks and deforming continuously (such as mudslides), the high attenuation of the material generally avoids the use of micro-seismic monitoring. Some authors have overcome this difficulty by using passive or active waveguides (Dixon et al., 1996; Dixon et al., 2003). The passive waveguide is used to provide a shorter path for transmitting the elastic waves directly to the sensor, whereas the active waveguide generates AE signals by deforming itself within the moving mass (as the principle of vertical inclinometers). The system of waveguide allows using the micro-seismic monitoring technique even for very attenuating material such as clayey soils.

The application of this technique is mainly dedicated for the monitoring of landslide in hard rocks (rockslide, rockfall) and some very preliminary experiences are being developed on soft rocks (mudslides).

## 2.2 MONITORING OF HYDROLOGICAL CONDITIONS

### 2.2.1 Optical fibres

*AMRA: Minardo A.*

In the last few years there has been an increasing interest towards the use of distributed fiber-optic sensors for landslide monitoring (Dai et al., 2008; Iten et al., 2009; Liu et al., 2010; Iten et al., 2011). Fiber-optic sensors can be embedded inside the landslide body, enabling remote, real-time measurements of differential stresses such as shear and compression. Moreover, the distributed nature of the sensor provides lower costs per measurement point. This becomes an indispensable value for large projects. Furthermore, a continuous aligned sensor means that there are no gaps. Therefore, the detection of hazard zones and ground movements can be carried out much faster and with a higher precision in the localization.

The basic principle behind the use of optical fiber sensors for landslide monitoring is that any differential soil displacement along the embedded sensor will eventually translate into some stress in the sensor. The strain acting on the fiber can be continuously monitored by different mechanisms: the more relevant are Rayleigh scattering and Brillouin scattering. Rayleigh scattering in optical glass fibers arises from density variations of silica glass on a microscopic scale. As a consequence of these variations, a small fraction of propagating light is continuously backscattered. As Rayleigh backscatter is proportional to the intensity of the incident light, it provides a means to measure any localized loss occurring during propagation along the fiber due to, for example, external stresses. Spatial localization is typically obtained by using optical time-domain reflectometry (OTDR), which is based on a pulsed laser source and a direct detection system. The typical spatial resolution is 1m, dynamic range about 40dB, and sensitivity limited to about -50dBm (Gold, 1985). A remarkably higher spatial resolution (in the order of a few cm) and larger dynamic range (about 70dB) can be obtained by using optical frequency-domain reflectometry (OFDR), in which the backscattered light from a swept-wavelength laser source is coherently detected (Liu et al., 2011). While systems based on the detection of Rayleigh backscatter are simple and potentially low-cost, they suffer from the limitation that only perturbations inducing optical losses in the fiber can be detected. Therefore, if soil movement does not induce any optical loss, but, for example, only gives rise to longitudinal strain (elongation) on the fiber, this will not be detected by the monitoring system. On the contrary, systems based on Brillouin scattering are capable of measuring the longitudinal strain at each section along the fiber, offering a more quantitative approach to the problem of landslide monitoring (Iten et al., 2009; Olivares et al., 2009). In Brillouin scattering, a small amount of light propagating through the fiber is backscattered at every point by a nonlinear interaction between the light and the thermally excited acoustic waves. A higher signal-to-noise ratio can be realized by stimulating the process, i.e. by injecting two frequency-shifted light-waves at the two opposite ends of the fiber. The optical gain experienced by the Stokes beam (the one having the lowest frequency) is a Lorentzian function of the frequency offset with the pump wave, the maximum occurring for the so-called Brillouin frequency shift. As the latter is linearly dependent on longitudinal strain, any physical perturbation of the fiber condition can be measured by monitoring the changes in Brillouin frequency (Agrawal, 2008). Distributed fiber-optics sensors based on stimulated Brillouin scattering have evolved steadily in the last years, with ever improving performance especially in terms of spatial resolution and sensing range. Distributed strain measurements

with spatial resolution down to a few cm or sensing lengths up to several tens of km have been recently demonstrated [Li et al., 2008; Bernini et al., 2011; Soto et al., 2011). Therefore, they have an enormous potential in the field of geotechnical monitoring.

The practical application of these sensors as well as their widespread acceptance in the geotechnical field is strictly related to two important issues: fiber embedding and interpretation of strain data. As regards installation, the challenge is allowing transmission of strain from soil to fiber without inducing loss to the fiber core. Different solutions have been proposed, including a “micro anchor”-cable system (Liu et al., 2011), geotextiles and geogrids (Wang et al., 2009). Another relevant aspect is constituted by the optical fiber cable, as the latter must ensure mechanical robustness while performing an efficient strain transfer from the jacket to the fiber. Increasingly, specialty optical fiber cables for strain sensing are available from cable manufactures.

The second critical aspect is represented by strain data interpretation: distributed fiber-optics sensors produce large quantities of data, however this is not necessarily an advantage. Being able to extract useful information from the retrieved data requires the availability of specific geological models for accurate predictions. The problem is even more complex due to the fact that the soil is anisotropic and dishomogeneous: it includes randomly distributed rocks and roots, clays and compost. Therefore, an accurate modeling of the landslide phenomenon appears as important as an accurate sensory system, in order to be capable of predicting landslides with sufficient lead time (Picarelli et al., 2004).

As a final remark, we report the problem of strain/temperature discrimination, common to most optical fiber sensors: as Brillouin frequency shift is sensitive to both temperature and strain changes, sensor systems based on SBS cannot distinguish the two effects when they act simultaneously on the same fiber. Although various solutions have been proposed to overcome this problem, the most effective method is based on the use of two separate fibers, one sensitive to both temperature and strain, and the other one sensible only to temperature (via a loose cable). In this way, the readings of temperature from the second fiber can be used to subtract the temperature contribution from the measurements provided by the first fiber.

### 2.2.2 Time Domain Reflectometry (TDR)

*AMRA: Guida A.*

Time Domain Reflectometry (TDR) was founded in 1950 with the aim of testing the characteristics of lines transmission and determines the spatial location of failure along the cables. Subsequently the use of this technique has been extended to the geological sciences and, in particular it has been used for volumetric soil water content measurements.

Indeed, TDR provides easy and cheap water content estimations with relatively small disturbance to the investigated soil. TDR measurement of soil water content, based on the strong correlation observed between relative dielectric permittivity of wet soil and its volumetric water content  $\theta$  (Campbell, 1990), consists of measuring travel time  $T_p$  of an electromagnetic pulse along a metallic waveguide of known length  $L_p$  inserted into the soil. The volume averaged value of soil relative dielectric permittivity  $\epsilon_r$ , affecting the velocity of propagation of electromagnetic waves along the metallic waveguide, is given by (Topp et al., 1980)

$$\epsilon_r = \left( \frac{C_0 \cdot T_p}{2 \cdot L_p} \right)^2 \quad (1)$$

where  $c_0$  is the propagation velocity of electromagnetic waves in the vacuum space. Several expressions of the relationship between  $\epsilon_r$  and  $\theta$  have been proposed, empirically stated (Regalado et al., 2003; Roth et al., 1990) as well as based on semi-analytical approach to dielectric mixing models (Roth et al., 1990; Whalley, 1993). During its travel along the waveguide, electromagnetic pulse energy decays mainly because of the existence of a transverse electrical conductivity  $\sigma$  of the medium. Indeed, pulse attenuation has been used to estimate bulk soil electrical conductivity (Dalton et al., 1984):

$$\sigma = \frac{\sqrt{\epsilon_r}}{120\pi L_p} \ln \left[ \frac{V_T}{V_R} \right] \quad (2)$$

where  $V_T$  and  $V_R$  represent, respectively, the voltage of incident and reflected electromagnetic pulse, measured at the beginning of the probe. Measurements of soil electrical conductivity have been widely used for monitoring solutes movement through soil (Kachanoski et al., 1992; Nissen et al., 2000).

TDR applications suffered the limitation due to the capability of the technique of estimating only the mean water content in the volume investigated by the probe. Whereas the knowledge of non-homogeneous vertical water content profiles was needed, it was necessary to install either several vertical probes of different length or several horizontal probes placed in the soil at different depths, in both cases strongly increasing soil disturbance as well as the complexity of the measurements. Recently, several studies investigated either theoretically or experimentally the possibility of extracting information about in homogeneous soil moisture distribution along the probe from dielectric measurements in monodimensional transmission lines. In particular several efforts have been recently dedicated to the development of inversion methods aimed to extract more information from TDR waveforms, in some cases concerning soil dielectric properties (Weerts, 2001; Lin, 2003), in others dealing with

estimating non-homogeneous moisture profiles along the probe axis (Greco, 2006). A common feature of all these methods is that the electromagnetic transient through the wet soil along the metallic probe is mathematically modelled, assuming that the unknown soil properties correspond to the best agreement between simulated and measured waveforms. In some cases the soil is modelled as a series of small layers with different dielectric properties, and the waveform is obtained as the result of the superposition of multiple reflections arising from impedance discontinuities between the layers (Moret et al., 2006). Other methods consider the dielectric properties of the soil as smoothly variable along probe axis (Greco, 2006; Greco, 2009; Oswald et al., 2003). The retrieval of non-homogeneous water content profiles along TDR probes measured with this technique has been successfully applied both under controlled laboratory conditions (Bernini et al., 2011) with a monotonic moisture measurements that in experimental field where non-monotonic moisture profiles could be observed in the topsoil (Greco and Guida, 2008).

### 2.2.3 Geoelectric monitoring

*GSA: Supper R., Baron I., Jochum B.*

The direct current (DC) geoelectric method is at present the most routine geophysical method to investigate subsurface geometry and structural pattern of landslide bodies in Europe (Baron & Supper, 2010), thus gaining the status of a state-of-the-art-method in civil engineering (Supper et al. 2000, 2001, 2002, 2008; Perrone, 2001; Mauritsch & Seiberl, 2000; Meric et. al., 2005; Jongmans & Garambois, 2007).

Most of the European landslide events are closely connected with precipitation and the influence of underground water on slope stability (pore-water pressure, change of water flow regime, saturation). Thus registering temporal changes of geoelectric parameters seems to be a promising method for monitoring of landslides. Three main geoelectrical parameters promise success in landslide monitoring, i.e.: ground resistivity, self- (or spontaneous-) potential and induced polarisation.

With DC geoelectrical measurements it is possible to determine the distribution of the specific electrical resistivity within the subsurface. The electrical resistivity is a physical property of the substratum, which depends mainly on porosity, water saturation, conductivity of pore fluid and clay content (e.g. Archie, 1942; Atkins 1961; Jackson et al., 1978; Schlumberger, 1987; Winsauer et al., 1952).

Self potentials are related to natural electrical currents in the subsurface. They are of electrokinetic (interaction between moving pore fluid and electric double layer at the pore surface), thermoelectric or electrochemical (diffusion of ions due to a concentration gradient between two regions) origin or caused by "Electro-redox" potentials (Jouniaux et al., 2009; Zlotnicki & Nishida, 2003). The electrokinetic effect could provide additional information on fluid flow and its variations within a landslide body. Although a few results for applications on landslides exist (e.g. Lapenna et al., 2003, 2005; Meric et al., 2005, 2006), Garambois & Jongmans (2007) concluded in their review that there is a demand for further long term monitoring experiments and improvements in processing techniques.

The Induced Polarization (IP) method is based on measuring the decaying potential differences with time after disconnection of the injection current, which depends on pore scale properties. Recent studies have shown that it could be used to estimate, e.g., the hydraulic conductivity based on empirical equations in unconsolidated sediments (Hördt et al., 2006, 2007) or the specific surface area normalized to pore volume (e.g. Slater et al., 2006). A reconciled model of IP is still lacking (Slater et al., 2006). Although Auken et al. (2006) considered IP as a possibly emerging method, this technique has been applied on landslides quite rarely (Marescot et al, 2008; Jongmans & Garambois, 2007). This parameter could eventually provide information on changes in pore geometry due to deformations of the landslide body.

Permanent geoelectrical monitoring of temporal resistivity and self-potential changes was already successfully tested for different applications, e.g., for detecting the internal erosion and anomalous seepage in embankment dams (Sjödahl, 2006), leachate injection monitoring (Clément et al., 2010), wind-driven barotropic transports of marine water (Nilsson et al., 2007), exploration and monitoring in rock salt for the safety assessment of underground waste disposal sites (Yaramanci, 2000), monitoring of geological CO<sub>2</sub> storage sites (Kiessling et al., 2009), for permafrost monitoring (Aaltonen, 2001; Hauck, 2001; Kneisel, 2004, 2006; Lambiel & Baron, 2007; Marescot et al., 2003; Noetzli et al., 2008; Supper et al., 2007),

wetting and drying of masonry walls on historic stonework (Sass & Viles, 2010), in karst studies or for earthquake engineering (Kamshilin et al., 2008). However only some sporadic studies have been performed to investigate its usefulness as a monitoring method for landslides (e.g. Bell, 2008; Chambers, 2009; Jongmans and Garambois, 2007; Supper et al., 2000, 2002, 2008, 2009, Wilkinson et al., 2010). To our knowledge no case study was published before the time of the commencement of the SafeLand project applying permanent geoelectrical monitoring together with permanent, high resolution monitoring of displacement. Therefore there is an urgent demand for such combined applications to prove the practical applicability of geoelectrics for landslide monitoring and early warning.

Consequently several test sites with different characteristics are planned to be equipped with Geomon<sup>4D</sup> systems in frame of the SafeLand project to obtain relevant data on the temporal change of geoelectric parameters and to correlate them with the mass movement dynamics. The Geomon<sup>4D</sup> is a geoelectrical instrumentation that was specifically developed by the Geological Survey of Austria for remote controlled monitoring applications (Supper et al., 2003) and will be operated for at least 2 seasonal cycles on each of the sites. Hereby, to minimize costs, the strategy is followed to equip several SafeLand test sites, where permanent monitoring systems (especially of displacement) are already in operation. The following test sites have recently been / will soon be equipped: Gschliefgraben, Bagnaschino, Hausruck, Ancona, Recice, Rosano, Sonnblick/Mölltal and Super-Sauze.

### **3 RECENT TRENDS IN AIRBORNE AND SPACEBORNE TECHNIQUES**

This chapter contains a brief overview of the most recent developments in the application of airborne and spaceborne technologies in landslide studies. In particular we will deal with aerial sensors, satellite optical, satellite radar and airborne geophysics. This chapter is further divided into two sections related to two different applications of these techniques, chapter 3.1 "Landslide detection and mapping" and chapter 3.2 "Landslide monitoring".

#### **3.1 LANDSLIDE DETECTION AND MAPPING**

##### **3.1.1 Aerial sensors**

*UNIL: Michoud C., Derron M.-H., Jaboyedoff M.*

As described in the deliverable 4.3 of the SafeLand European project "Creation and updating of landslide inventory maps, landslide deformation maps and hazard maps as input for QRA using remote sensing technology", aerial technologies and sensors have been used in Geosciences in order to detect and map landslides for many years. For example, the French territory is covered by aerial imagery since 1937 with a time span of five years between two acquisitions (Delacourt et al., 2007). Up to now, the photogrammetry is still considered as the traditional way to extract the topography. Nevertheless, new research and development trends are steadily more used for geohazard purposes. They will be introduced in this section, first describing last technological improvements and then processing algorithm enhancements for aerial survey purposes.

##### **3.1.1.1 Hardware improvements:**

General trends in all micro-electronic domains have improved the overall acquisition device performances and have decreased the costs: better lenses and image capture chipsets, lighter electronic components and efficient stabilization processes (Delacourt et al., 2007). For example, in 2007, the camera Sony DSC-H5 had a sensor of 7 Megapixels, with a sensibility range between 80 and 1000 ISO, without optical stabilization and weighted 490 grams (Les numériques, 2006). Now, one of the last compact cameras of Sony, the Cyber-shot HX7V, has a sensor of 16 Megapixels, with a sensibility range between 125 and 3200 ISO, with an optical stabilization and it weights 208 grams (Les numériques, 2011). Moreover, in Aerial and Terrestrial Laser Scanning (resp. ALS and TLS), better technological manufactures have drastically improved the maximal range and frequency of acquisitions (Figure 8). For example (Optech Inc., 2011), in 2006 the Optech Inc.'s LiDAR Ilris-3D had a maximum range of acquisition of 1200 meters (for 80% reflectivity) with a Laser repetition rate of 2.5 kHz. Now in 2011, the Ilris-LR, the newest Optech Inc.'s LiDAR, has a maximum range of 3000 meters in the same conditions and a repetition rates four times faster, i.e. 10 kHz.

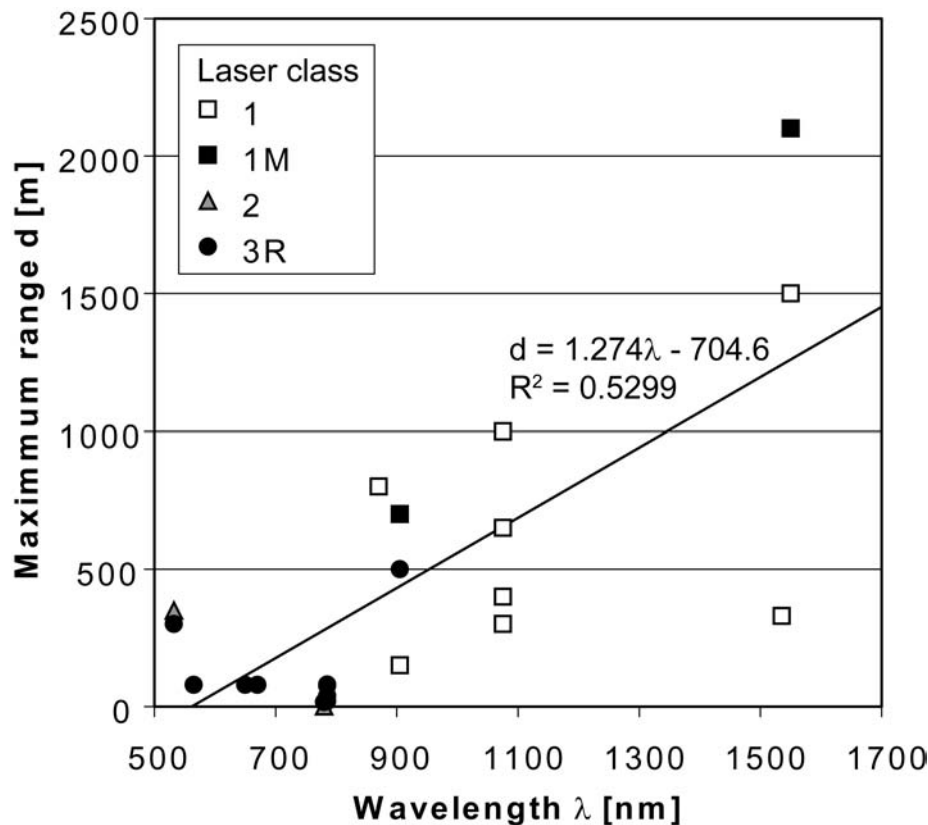


Figure 8. Maximum range of TLS from several manufacturers according to their wavelength (Jaboyedoff et al., 2009).

In the same line of sensor improvements, new platforms are under fast developments too. Indeed, now Unmanned Aerial Vehicles (UAV) benefit of the recent improvements of in board navigations systems, i.e. of better performances of lighter and cheaper Inertial Navigation Systems (INS), Inertial Measurements Units (IMU) and Global Navigation Satellites Systems (GNSS) antennas (Eisenbeiss, 2004; Nagai and Shibasaki, 2005; La Parra and Angel, 2005; Joyce et al., 2009; Nagai et al., 2009). Thus, cheap and light cameras with enhanced auto-focus, resolutions and stabilization systems can be mounted on stable UAV (Delacourt et al., 2007) to acquire images at low altitude (Figure 9, Figure 10). For natural hazard purposes, UAV are more and more used in order to investigate and map landslide areas (Delacourt et al., 2007; Eisenbeiss, 2004, 2007 and 2008; Zongjian, 2008; Joyce et al., 2009; Nagai et al., 2009; Niethammer et al., 2009, Walter et al., 2009).

Finally, more marginal researches are done by the German Aerospace Center (DLR) in the application of the Radar interferometry (InSAR) from aerial acquisitions. Their system, the F-SAR merges five frequency bands (X-, C-, S-, L- and P-band) in order to generate 2 m resolution Digital Elevation Models (DEM) thanks to interferometry principles (DLR, 2011a). New investigated ways concern the Airborne Repeat-pass SAR Interferometry which could allow differential radar interferometry processing with very low normal baselines (DLR, 2011b), decreasing geometrical decorrelations (Bamler and Harlt, 1998).



**Figure 9.** Small UAV developed by the Universität Stuttgart, used in the Super-Sauze landslide to acquire aerial images with small compact cameras (Walter et al., 2009).



**Figure 10.** Big UAV design by Fuji Heavy Industries Ltd., used in Nagai (2009).

### ***3.1.1.2 Algorithms and software improvements:***

Different research works introduce investigations performed from multisensors coupling. Nagai et al. (2009) coupled on an UAV passive (visible and Near Infra Red) and active (LiDAR) sensors. Supervised classifications from optical and NIR data can be more reliable and robust; furthermore, thanks to the additional information provided by NIR scenes, an improved automatic detection of vegetation on ALS point clouds can be achieved. The Swiss federal office of the topography (swisstopo) acquires now aerial scenes including NIR bands,

in order to enhance environmental applications with better land use classifications too (swisstopo, 2011). Roering et al. (2009) coupled ALS and air photos with spaceborne InSAR data in order to properly constrain landslides areas and activity states. Buckley et al. (2008) and Kurz et al. (2008) developed tools to identify and classify geological outcrops according to lithology and sedimentological features, merging data from aerial photos, Terrestrial Laser Scanning (TLS) and hyperspectral images.

Regarding classification algorithms, several researches are performed to improve and optimize existing ones, or to develop totally new approaches. As remember by Joyce et al. (2009), emerging algorithms try to improve the extraction steadily more automatically and robustly of unstable areas, using supervised (Nichol and Wong, 2005; Joyce et al., 2008a, 2008b) and unsupervised (Dymond et al., 2006) classifications from optical datasets. Plaza et al. (2009) introduced recent developments improving the reliability of hyperspectral images, integrating spatial and spectral information. As the spectral signatures of minerals are available within the USGS libraries, the authors identified and mapped cuprite outcrops from pictures acquired thanks to an Airborne Visible Infra-Red Imaging Spectrometer (AVIRIS, in Green, 1998).

New software and algorithms are under constant development in order to create and analyze High Resolution Digital Elevation Models (HRDEM). In photogrammetry, recent applications allow for everyone to build simple 3D models. For instance, with newly available softwares (such as the MS-Photosynth application), the topography can be built from pictures acquired with normal cameras, from the ground or from UAV. Up to now, these low cost processed models are not as accurate as the professional solutions, but the democratization of photogrammetric processing has begun. Concerning Aerial Laser Scanning data, recent applications deal with a huge number of point; furthermore, they are geologist-oriented, easily allowing the visualization and the extraction of structural information, such as the orientation and the persistence of discontinuities (Figure 11) (Jaboyedoff et al., 2007; Ferrero et al., 2009; Sturzenegger and Stead, 2009; Gigli and Casagli, 2011).

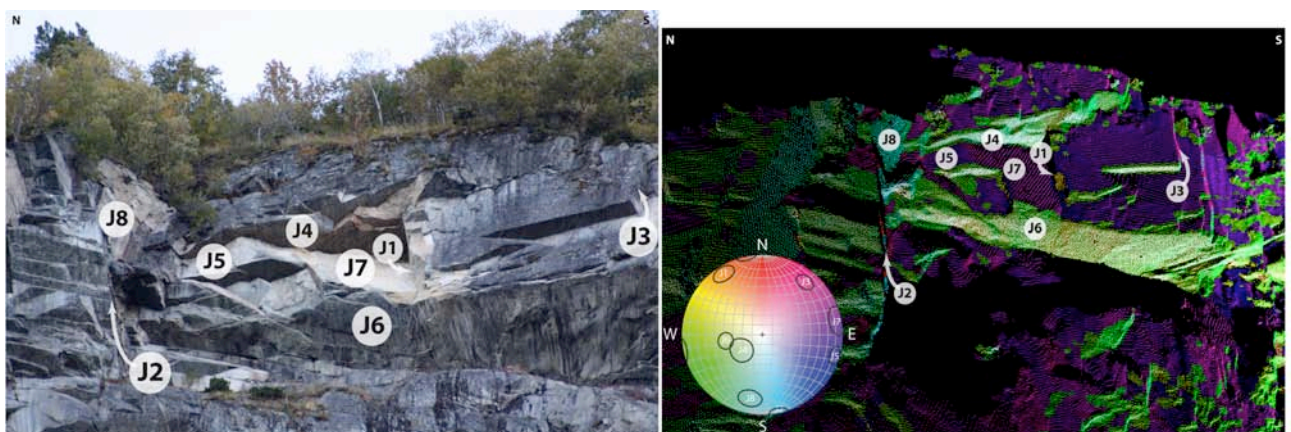


**Figure 11. Comparison between a real cliff and its structural settings analyzed thanks to the software Coltop3D from LiDAR acquisitions.**

Finally, GIS-based models progress rapidly in order to extract landslide source areas and to assess potential propagation zones from aerial dataset (Figure 12), both for rockfall events (Guzzetti et al., 2002; Crosta and Agliardi, 2003; Dorren et al., 2006; Lan et al., 2007; Frattini

et al., 2008; Loye et al., 2009; Jaboyedoff and Labiouse, 2011; Michoud et al., submitted) and debris flows (Huggel et al., 2003; Horton et al., 2008).

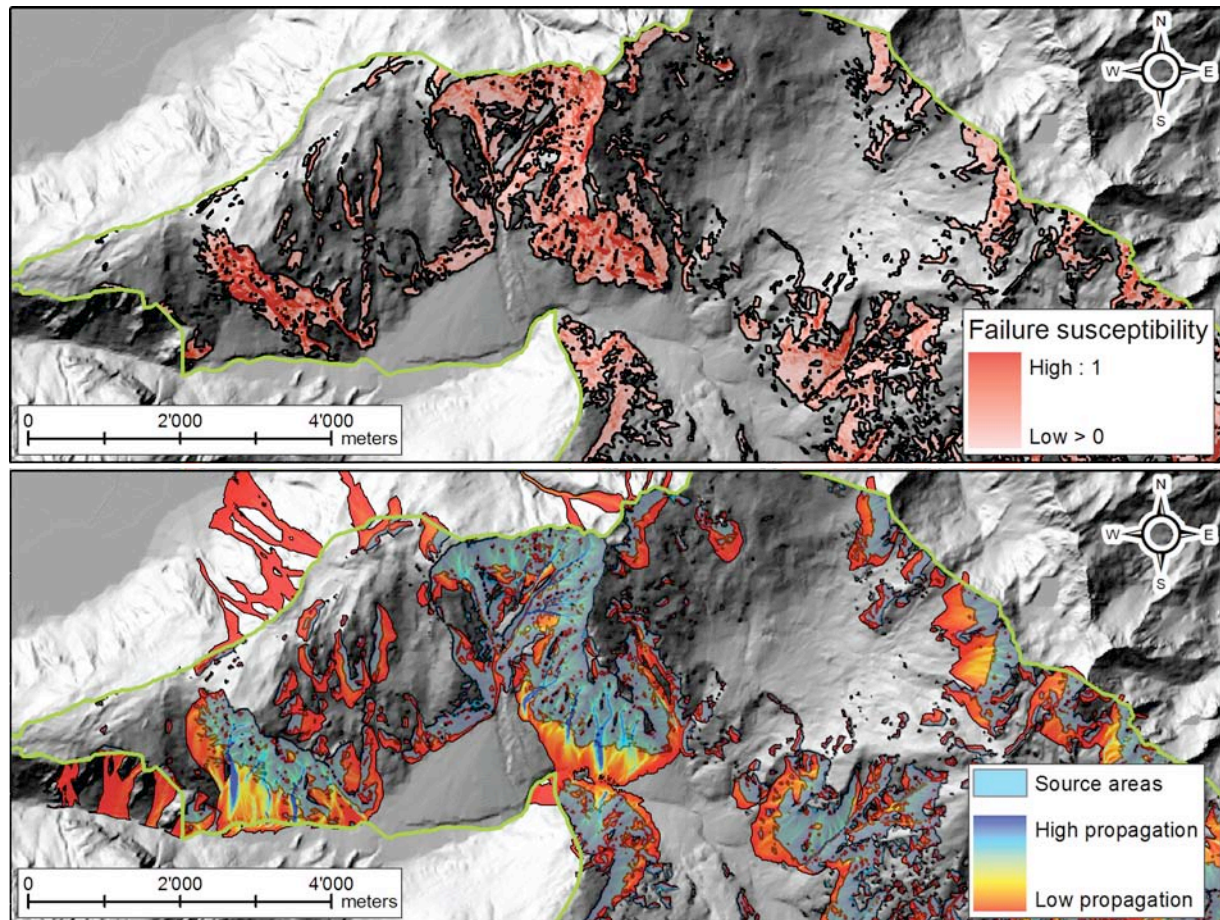


**Figure 12.** Creation of rockfall susceptibility map based on 10m-DEM. Top: identification of rock-mass-failure probabilities according to the slope, using a Slope Angle Distribution approach. Bottom: runout assessment, using the Flow-R model (modified after Michoud et al., submitted).

### 3.1.2 Satellite optical

*ITC: Stumpf A., Kerle N.*

The most notable innovations in optical satellite remote sensing are certainly, the enhanced spatial resolution which is now available to a broad public, and the greater diversity of available systems. This leads to better availability of imagery timely after major landslides events and improves the revisit times for areas where frequent monitoring is needed. A few most interesting sensors are highlighted here, whereas for a comprehensive overview of current and future satellite missions, the reader is referred to the SafeLand deliverable D4.1 or comprehensive online databases (<http://database.eohandbook.com/>, [http://gdsc.nlr.nl/gdsc/en/information/earth\\_observation/satellite\\_database](http://gdsc.nlr.nl/gdsc/en/information/earth_observation/satellite_database)).

Long-term work horses of optical satellite remote sensing such as LandsatETM+, TerraASTER, SPOT 5, Resourcesat-1 or ALOS are continuing their service and archived imagery from those sensor becomes an increasingly inexpensive source for past-events and change detection applications (e.g. Yang and Chen 2010). Several data continuity missions target the seamless continuation of such the observations with technological updated sensors providing comparable datasets. Such missions are the Landsat Data Continuity Mission (LDCM), SPOT 6/7 scheduled for 2012/2013, Resourcesat-2 or ESAs Sentinel-2, which is scheduled for launch as a part of GMES in 2013 and targets consistency with Landsat and SPOT observations. All those missions target spatial resolutions of at least 10 m and can hence be expected to be suitable for landslide mapping purposes (cf. Joyce et al. 2009). While most current studies focused on the exploitation visible and near-infrared bands of VHR images it might also be interesting to explore the potential thermal and hyperspectral bands as they become now available with resolutions of with 10-30 m (e.g. EO-1). Already Metternicht et al. (2005) noted a lack of studies in this direction.

There are still technological tradeoffs between the image footprint and the resolution which leads to generally smaller swath width and consequently lower revisit times if VHR images are desired. However, using constellations of identical sensors can solve such problems and an increasing number of microsatellites (mainly manufactured by SSLT) have entered this segment. The German company RapidEye operates five microsatellites capable of recording imagery daily at five multispectral bands and a GSD of 6.5 m. Similarly the Disaster Monitoring Constellation (DMC) includes currently five satellites (UK-DMC-1&2, Deimos-1, NigeriaSat-1, Beijing-1) with similar instruments. At present they still offer a relatively low spatial resolution between 22 m and 32 m (except Beijing-1 including a 4 m panchromatic channel), whereas finer resolutions are planned for future satellites of the constellations. The first constellation of sub-meter resolution satellites sensors is planned to be added to the current line-up of VHR satellites (Ikonos, Quickbird, Eros, WorldView, Geoeye) by the French CNES this year. The Pleiades constellation involves two identical satellites recording 4-band multispectral imagery at 2 m and panchromatic imagery at half a meter resolution. Both satellites can be rotated rapidly in three dimensions and will allow (tri-) stereoscopic imaging capabilities and image acquisition on request in down to only 8 hours. With the later integration of Spot 6/7 into the constellation it will be possible to record VHR imagery of the same place twice a day.

For landslide detection and mapping optical data is at present most commonly applied for the inventory mapping in the aftermath of major events. As long as limited areas are affected and

the amount of available images is limited manual image interpretation might still be a feasible option. However, considering the increasing availability of VHR data and large scale events with thousands of individual landslides such as recently in China (earthquake, 2008), Haiti (earthquake, 2010) and Brazil (rainfall, 2011) the restrictions of manual mappings become obvious. Proposed approaches for more automated mappings fall into image analysis techniques including pixel-oriented and object-oriented approaches, and the analysis of DEMs derived from stereo imagery.

The most recent studies using pixel-based techniques have been carried out in the context of the great Wenchuan earthquake and rely on change detection with moderate resolution satellite imagery (Di et al. 2010; Yang and Chen 2010). Although, there are differences in the detailed implementation of the workflows, the proposed processing chain typically include co-registration, radiometric cross-calibration, image transformation, differencing and the selection of a threshold to separate changes and non-change areas (Figure 13).

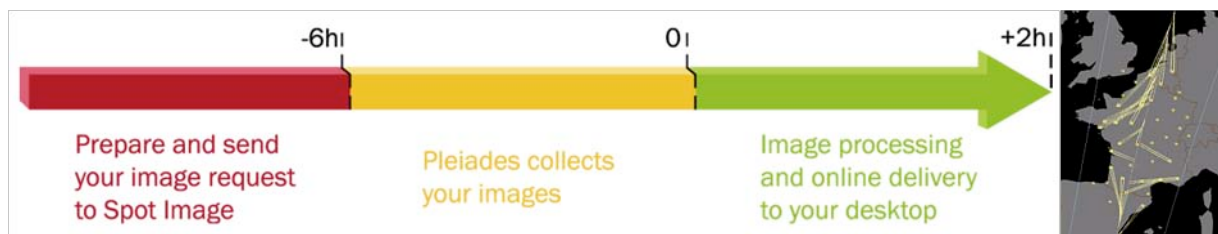


**Figure 13. Rapid steerable platforms such as Pleiades will allow rapid acquisition of VHR images on demand (Image source: CNES).**

Recently developed approaches for object-oriented image analysis (OOA) include mono-temporal and multi-temporal analyses workflows using mainly VHR imagery but also additional spatial datasets such as topographic models and river networks (Barlow et al. 2006; Lu et al. 2011; Martha et al. 2010a; Stumpf and Kerle forthcoming). Image segmentation enables the exploitation of additional features such as texture, shape and generally the spatial context of object primitives. An exemplary workflow of OOA inventory mapping is displayed in Figure 14 and shows the possibility for an enhanced integration of imagery and topographic data, both from VHR optical satellite sensors.

Lu et al. (2011) presented a workflow for rapid mapping via a joint-analysis of multi-temporal Quickbird images and a post-disaster LiDAR DSM (see also SafeLand deliverable 4.3) using image segmentation and multi-temporal image transformation to simplify the integration of multiple data layer. The SafeLand case study “Object-oriented landslide inventory mapping with VHR imagery using machine learning techniques” presented in 6.2.2 addresses several current issues such as the adaptability of mapping workflows to a wide range of different ground conditions and imaging sensors. The study demonstrates that advanced machine learning algorithms can be trained efficiently with samples provided by an expert and enable robust and accurate semi-automatic mapping with a wide variety of state-of-the-art datasets.

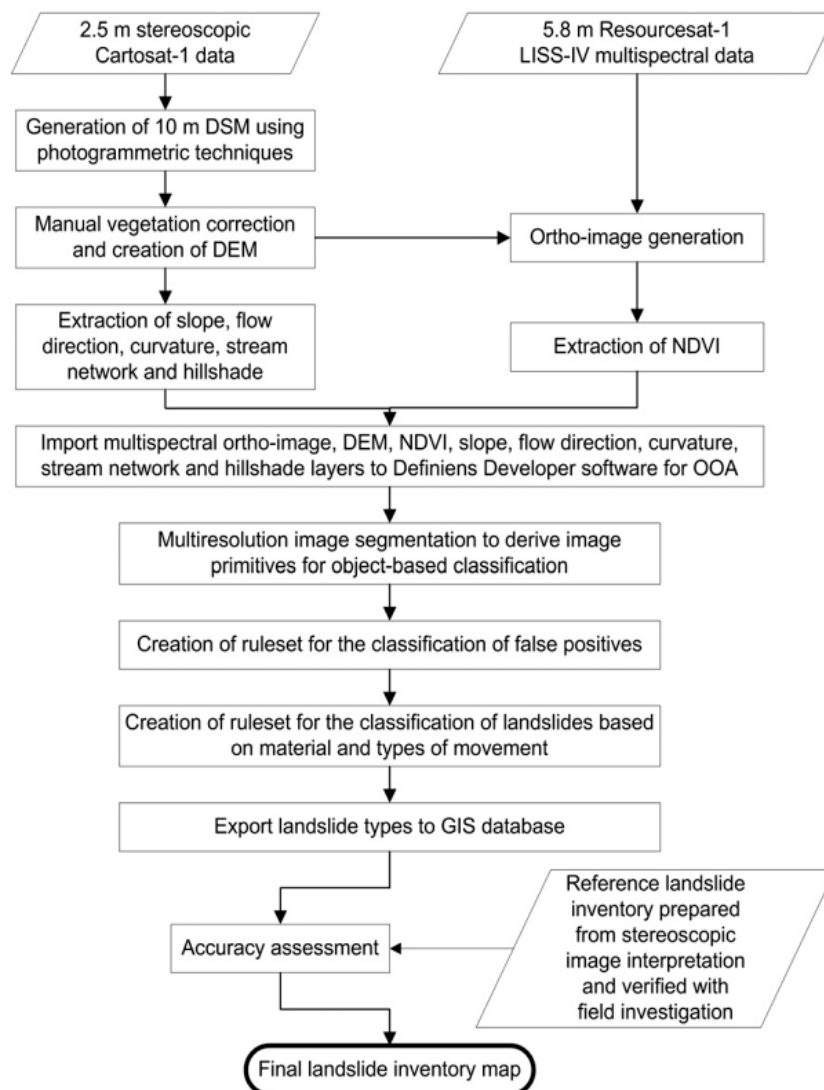


**Figure 14. Typical workflow for an object-oriented approach to landslide mapping including multi-source data (Martha et al. 2010a).**

The increasing availability of VHR stereo imagery and enhanced algorithm for DSM generation (e.g. Zhang and Gruen 2006) make use of multi-temporal DSMs more attractive. Especially for slope failures that involve large volumes it has already been demonstrated that DSM differencing can be used to map landslides over wide areas and estimate involved volumes simultaneously (Tsutsui et al. 2007). There are still very few reference studies using such technique for regional mappings, whereas in the light of above mentioned innovations in stereo image acquisition their application might become more common in the future.

### 3.1.3 Satellite radar

*UNISA: Peduto D., Cascini L.*

*AMRA: Fornaro G.*

The application of multipass DInSAR techniques to the study of slow-moving landslides is a relatively new and still challenging topic. The scientific literature reports some successful case studies dealing with the detection and the mapping of landslide phenomena, as discussed in Fruneau et al.(1996), Squarzone et al.(2003), Berardino et al.(2003), Colesanti et al.(2003), Colesanti and Wasowski (2004), Farina et al.(2006), Hilley et al.(2004), Strozzi et al.(2005), Cotecchia (2006), Canuti et al. (2007), Catani et al. (2005a-b), Casagli et al. (2009); Cascini et al. (2009, 2010), etc.

These works apply DInSAR data derived from different algorithms and sensors to the analysis of either single phenomena (Fruneau et al., 1996; Berardino et al., 2003; Hilley et al., 2004; Cascini et al. 2010) or wide areas (Farina et al., 2006; Casagli et al., 2009; Cascini et al., 2009, 2010). DInSAR measurements are usually interpreted by using the data on the LOS direction and they are rarely projected along the steepest slope direction as in Hilley et al. (2004), Colesanti and Wasowski (2006), Cascini et al. (2010).

The interest of the scientific community in these techniques is testified by an increasing number of workshops and demonstration projects supported by space agencies, e.g. European Space Agency's (ESA) projects MASMOV, ALPS, SLAM, and TERRAFIRMA. Key issues (e.g. Carnec et al., 1996; Singhroy et al., 1998; Wasowski and Gostelow, 1999) are the reduction of the most significant constraints such as the coherence loss, a typical problem affecting vegetated areas, and the atmospheric effects that significantly limit the utility of many currently available radar satellite datasets. These difficulties were partly overcome by using the multipass DInSAR techniques (e.g. Ferretti et al., 2001; Lanari et al., 2004, Fornaro et al., 2009) which exploit long series of SAR images.

Moreover, the insufficient appreciation of inherent limitations of EO systems and relevant processing techniques, coupled with natural complexities of landslide movements and related ground deformation phenomena, may result in misinterpretations of satellite SAR data.

The recent trends in this kind of applications pursue the development of procedures for the use of DInSAR data at different scales of analyses, in particular:

- when dealing with studies over large areas an integrated approach can be followed with the help of geomorphological analyses (Farina et al., 2006; Cascini et al., 2010; etc.), information derived from sensors operating at different wavelengths (Strozzi et al., 2005), the mixture with optical images and ortophotos (Casagli et al., 2005; etc.), the cross-comparison with damage survey dataset (Cascini et al., 2008).
- as for studies at the scale of the single phenomenon the integration with ground-based monitoring techniques and advanced landslide displacement monitoring as well as the use of corner reflectors (Novali et al., 2005; Gili et al., 2009) must be pursued.

Thanks to the development of applications of the DInSAR techniques in several areas of natural hazard, many international space agencies have invested in the launch of new platforms equipped with SAR sensors. This is the case of Italian constellation COSMO-SKYMED, composed of four satellites orbiting around the earth in a configuration that allows a sensible reduction of the area access time to four hours and an average revisiting time of

---

four days. Another example is the German TerraSAR-X/TANDEM-X system which is composed of two twin satellites orbiting in a formation scheme allowing the simultaneous acquisition of interferometric data for precise topographic mapping. Both systems operate at X-band and are characterized by high and very high spatial resolution reaching one meter. Further population of the space from the point of view of SAR sensing systems is foreseen in the near future. This is the case of the C-band RADARSAT constellation whose launch is planned for 2014-2015 which should add two satellites to the system planned for launch as a continuity of RADARSAT-2. Similarly the twin satellite Sentinel system whose first satellite is envisaged to be launched in 2013.

The reduction of the revisiting time in conjunction with the improved spatial resolutions of the above sensors provides an enhancement in terms of the coherence properties of the interferometric data from the point of view of both temporal correlation and the reduction of clutter thus improving the quality of the response of natural scatterers. These advanced peculiarities appear promising and hold the premise for increasing practical use of radar satellite data in landslide investigations.

### 3.1.4 Airborne geophysics

*GSA: Supper R., Baron I.*

*ICG: Pfaffhuber A.*

Airborne geophysics has been intensively applied for exploration of raw materials within the last decades. Recently it developed into a promising approach for landslide investigation and rapid mapping (Nakazato et al. 2006, Pfaffhuber et al. 2010, Sasaki & Nakazato 2004, Supper et al. 2008). Reasons for that are significant technological improvements in the area of hardware and software within the last 5 – 10 years. Thus accurate and well calibrated data can be provided for further processing and reliable inversion algorithms are available.

However, due to the rough topography usually encountered in landslide susceptible areas, performing a high quality multi-parameter airborne survey in such areas within the limits of usual research budgets still poses a big challenge to geophysicists. Consequently hardly any successful case studies were reported before commencement of the SafeLand project in 2009.

The airborne geophysical technology uses sensors that are either mounted on an aircraft or dragged on a cable several tens of meters below the aircraft (Figure 15). Commonly used platforms are fixed wing airplanes or helicopters. Due to the fact that mass movements are usually located in rugged terrains and that a maximum distance between sensor and topography has to be kept because of the rapid signal decay, helicopters are in most cases the only choice for the acquisition platform for such surveys.



**Figure 15.** Left: helicopter borne electromagnetic (HEM) system; right: helicopter borne skytem system (photos: R. Supper, 2009).

Airborne geophysical data acquisition systems usually apply a combination of different sensors to investigate the target area from different perspectives (e.g. Motschka, 2001). Out of

the available measurement technologies, the electromagnetic method seems to be the most appropriate one for investigating landslide areas. AEM ultimately provides resistivity depth sections of the subsurface down to a depth of 40 – 300 m (depending on the general resistivity structure), which are mainly related to porosity, fluid and clay content and thus may act as an indicator for weakness zones and destabilized and partly saturated landslide bodies. Supplementary methods e.g. gamma ray measurements can be used to characterize the surface soil/rock layers in combination with passive microwave sensors, which map the soil humidity of the surface layer. Interpretation of data for landslide investigation coming from airborne methods is a matter of ongoing research.

Additionally to the core sensors, auxiliary instrumentation has to be employed for precise location of the actual position of each of the sensors (precise differential GPS with base station, laser altimeter, dip-meters) and for applying necessary corrections to the data (infrared sensor, air temperature, sensor temperature, flight path digital camera...).

Traditionally a research area is covered by parallel lines (Figure 16 shows a typical flight line map at the research area of Sibratsgfall in 2001) at a separation between 50 and 250 m. However for landslide mapping, smaller line spacing has to be favoured (25 - 100 m). Since in rugged terrains these parallel lines are not easily maintained by the pilots at a maximum clearance of 90 m, alternative schemes (e.g. flight lines parallel to topography, Figure 17) have to be tested.

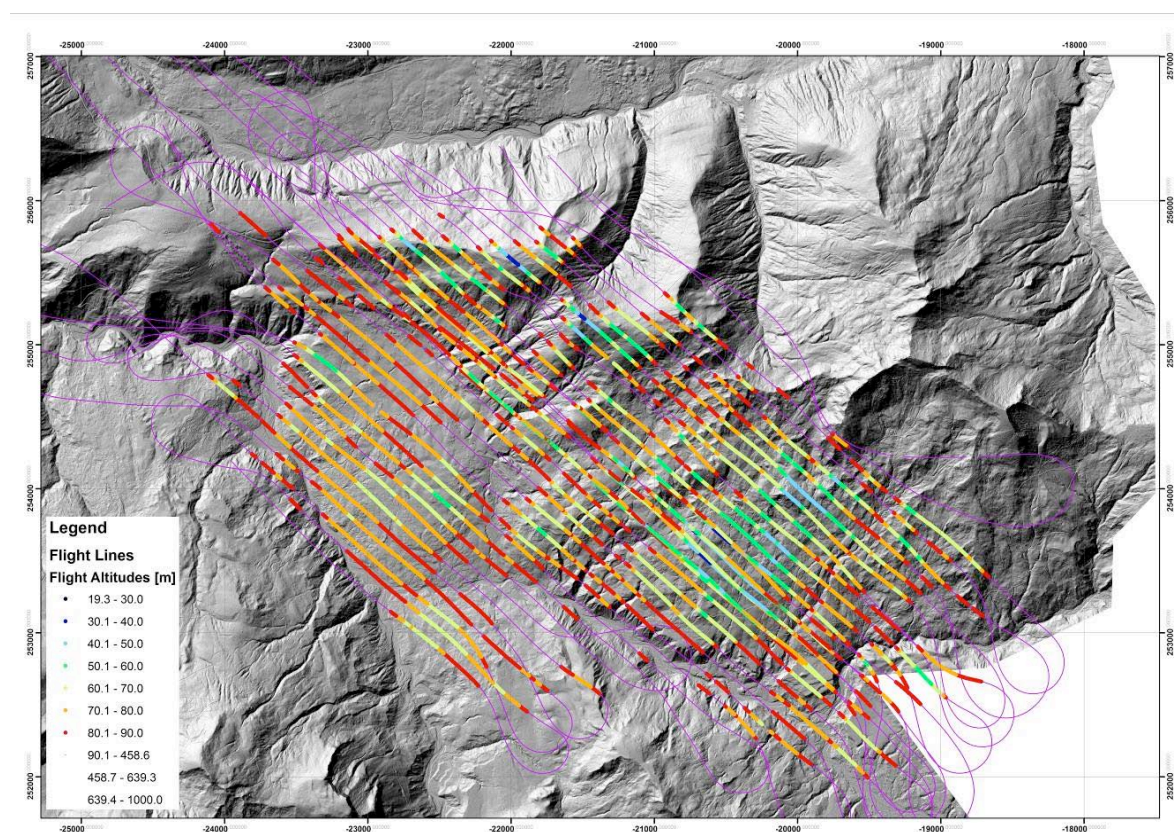


**Figure 16. Typical flight path map covering the landslide of Rindberg and Sibratsgfall 2009 (Vorarlberg, Austria), colours are indicating the actual sensor altitudes above topography.**

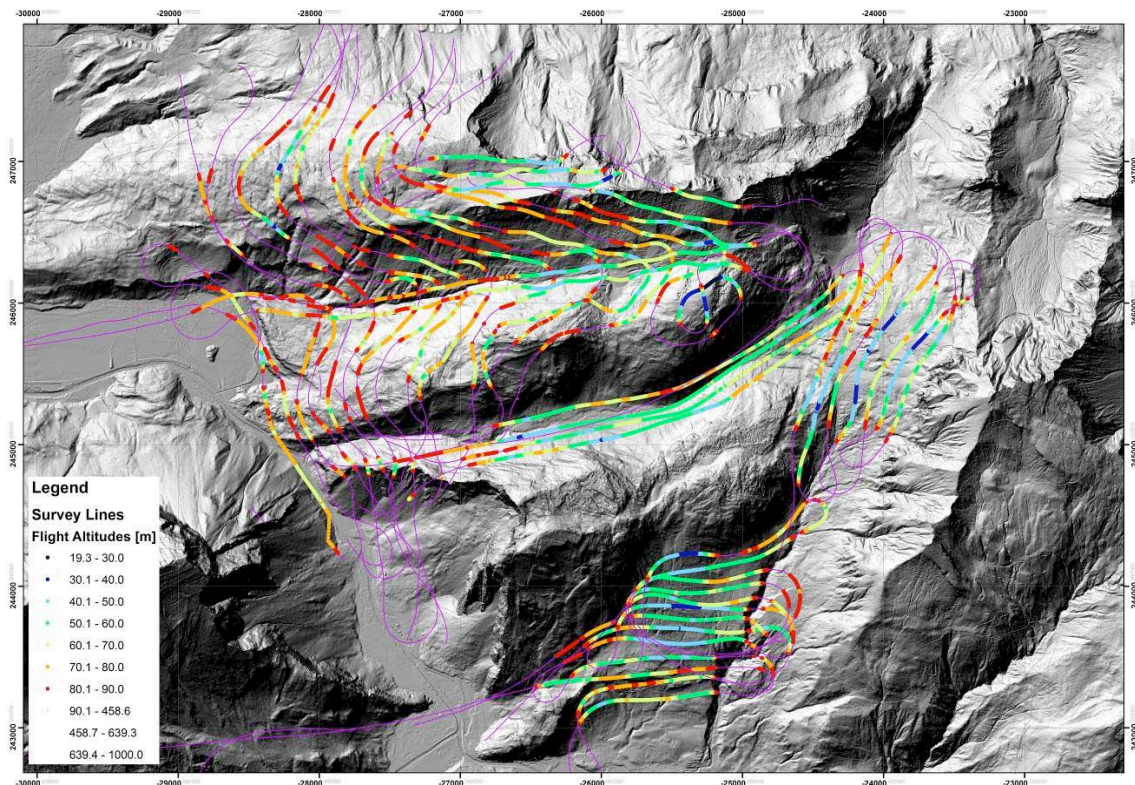


**Figure 17. Unconventional flight paths covering the area of Schnepfau (Vorarlberg, Austria), an area with rough topography; colours are indicating the actual sensor altitudes above topography**

### *3.1.4.1 Available parameters for landslide investigation*

#### **Subsurface Resistivity**

The electromagnetic method it is intended to determine the distribution of the specific electrical resistivity within the subsurface. This parameter is a physical property of the subsurface. Under the assumption of a non-conductive rock matrix it mainly depends on porosity, water saturation, conductivity of the pore fluid and clay content and to a minor extent on particle shape and pore geometry. By the use of airborne electromagnetics a rough overview of the resistivity distribution within the subsurface over large areas at different depths can be derived within relatively short survey times. Since areas affected by recent movements are in many cases correlated with higher water contents than the surroundings, the special mapping of subsurface resistivity could be applied to detect landslide susceptible areas.

#### **Measurement technology**

##### **FDEM – Frequency domain airborne electromagnetics**

The main part of a frequency domain electromagnetic system consists of a probe (also called “bird”) of several meters of lengths which is towed on a cable 30 m below a helicopter. Inside the probe there are several transmitting coils as well as receiving coils in different geometric arrangements (co-axial, co-planar loops). The transmitting coils generate an electromagnetic alternating field with certain frequencies e.g. of 340 Hz, 3200 Hz, 7190 Hz and 28850 Hz. This primary field induces eddy currents inside conductive subsurface layers. In turn the

corresponding (secondary) magnetic field generated by these currents induces a current in the receiver coils. Based on the amplitude and the phase shift of the secondary field relatively to the primary field, conclusions can be drawn on the electrical resistivity of the subsurface (Avdeev, 2005; Seiberl et al, 1998; Sengpiel et al, 1988; Winkler et al, 2003). Variable frequencies and different geometric arrangements of the coils are used in order to allow depth-specific sounding of the subsurface. The lowest frequency determines the total penetration depth of the method (approx. 120 m below ground surface).

### **HTEM – Helicopter time domain airborne electromagnetics**

Airborne EM systems used to be separated in two classes being fixed wing time domain systems and rotary wing frequency domain systems. Traditionally fixed wing systems provided large transmitter moments and thus large penetration depth with limited lateral and depth resolution. Helicopter towed systems fly lower, are able to follow rough topography providing better resolution and logistical advantages. With the new millennium these two concepts were merged into helicopter borne time domain systems combining the advantages of both platforms, namely high resolution, versatile and deep penetrating AEM systems (Allard, 2007).

The majority of these new HTEM systems tow a big horizontal transmitter loop more or less rigidly connected with receiver coils at 30 to 40 m above ground. A strong current in the transmitter loop is rapidly switched off, providing a step impulse inducing currents in the ground that diffuse downward with time. The secondary field induced by this ground current is picked up by the receiver(s) over a time range from some  $\mu\text{s}$  to ms after turn off. Early time responses are governed by the shallow subsurface while the late time signals provide information down to several hundred meters depth (depending on resistivity). Early time and late time in HTEM correspond to high frequency and low frequency in FDEM, respectively.

### **Natural radiation - Gamma-ray spectroscopy**

This methodology determines the natural and artificial radioactivity, which depends on the content of radioactive minerals within the first decimetres of the subsurface. Potassium, uranium and thorium are the only naturally occurring elements with sufficient gamma-ray energy and intensity to be measured at airborne survey heights (Minty 1997). Natural gamma radiation is essentially caused by the decay of three unstable isotopes, which occur as fixed proportions of the total Potassium, Uranium and Thorium content of subsurface rocks/soils:  $^{232}\text{Th}$  (energy peak: 2.62 MeV),  $^{238}\text{U}$  (energy peak: 1.76 MeV) and  $^{40}\text{K}$  (energy peak: 1.46 MeV).

With 2.33 weight % Potassium is one of the major elements of the Earth's upper crust. Potassium occurs mainly in alkali-feldspars and micas in felsic rocks. It has only a low content in mafic rocks (basalt) and a very low content in ultramafic rocks (dunite, peridotite). The maximum values were found at around 5 % in granites and mudstones. Since potassium is soluble under most conditions, there is a general tendency for the potassium concentration in rocks or soils to decrease during weathering. After being released by its host, potassium can be taken up in the formation of K-bearing minerals or absorbed into clays (Dickson & Scott, 1997). In soil, Potassium is usually enriched compared to the concentration in the parent rock. It also intensively takes part in the biological cycle.

Thorium is present in the rocks huttonite, thorite and uranorite, in accessory minerals and as trace elements in the major rock forming minerals. The average abundance of Thorium in the

Earth's crust is about 12 ppm. In the magmatic cycle it is enriched in course of the differentiation and it is mainly integrated into minerals of the late crystallisation phase. It is not easily soluble in natural occurring fluids. However it is transported in suspensions. Thorium shows a high adsorption power to clay minerals, oxides and hydroxides. Therefore high contents of Thorium can be found e.g. in bauxite, bentonite and manganese nodules (Siehl A., 1996).

Uranium appears in rocks like uranite and uranorite, in accessory minerals and as trace elements in the major rock forming minerals. Mafic minerals (pyroxene, mica, hornblende) generally show a higher uranium content than felsic minerals (feldspar, quartz). It is enriched in course of the differentiation of magma in the fluid phase and it is therefore mainly integrated into minerals of the late magmatic and pegmatitic crystallisation phase. Consequently the primary sources of Uranium are granites and pegmatites.

Uranium is soluble under oxidising conditions and insoluble under reducing conditions. Enrichments of uranium are therefore mainly caused by chemical precipitation from aqueous solutions (e.g. due to change from oxidising to reducing conditions). In sedimentary rocks quartz rich sandstones and limestones contain low concentrations of Uranium, whereas due to the adsorption of Uranium in clay minerals, clayey sediments exhibit rather high value (Siehl A., 1996). The average concentration in the Earth's upper crust is 3 ppm.

So far hardly any case studies are available for gamma ray surveys on landslides. However since, as described above, these elements can be found in different rocks and soils at various concentration levels, the spatial distribution of these elements and/or their ratio can provide information about soil parent material and soil and rock properties, such as composition, weathering, leaching clay types and others. This information could be used to determine areas with a higher susceptibility to sliding. Thus this methodology could provide relevant additional data for landslide susceptibility mapping.

### **Measurement technology**

The measuring sensor consists of several sodium-iodide crystals, which convert gamma radiation into flashes of light. Appropriate survey instruments determine their energies. With conventional measuring systems the energy spectrum between 0.2 to 6.0 MeV is resolved in 256 channels.

Since the air layer between helicopter and ground is absorbing gamma radiation (depending on the physical condition of the air), the exact flight altitude, air pressure, air temperature as well as air moisture have to be taken into consideration when correcting survey data.

The recorded data has to be corrected for background radiation, Compton scattering and variation of sensor altitude (for details of gamma-ray processing see Minty et al. 1997) and vegetation thickness (Ahl et al., 2010).

### **Magnetic field anomalies - Airborne Magnetics**

With this methodology the total intensity of the earth's magnetic field is measured. Deviations from a reference earth magnetic field (IGRF) are considered as anomalies and assist e.g. in the discovery of differently magnetized bodies (i.e. ore bodies, young volcanic rocks, metallic contents of waste repositories) or fracture zones.

Magnetic measurements are mostly used for exploration of raw materials and geological and volcanological mapping.

For investigation of landslides this methodology seems to be of less importance. However it can be useful to derive information on the general geological settings of the area if contrasts in the magnetic susceptibility of the involved geological units or magnetized fault zones exist.

#### **Surface soil moisture - Passive microwave surveys**

The content of soil water is of great importance for many hydrological, agro-meteorological, ecological, as well as biological processes since the water content close to the surface controls the energy exchange between soil and atmosphere. The link between soil moisture, evaporation and transpiration is of utmost importance for predicting reciprocal influence of ground surface on climate and weather. Conventionally such survey systems are mainly used for determining water movements near ground surface and estimating the spread of precipitation over large areas.

For estimating soil moisture (in water content percentage) within the first centimetres of the subsurface a passive L-band antenna can be used, which is attached to the bottom a helicopter. The antenna measures the radiation from the ground, reflected in the L-Band (1400 to 1427 MHz). The intensity of this radiation correlates to the water content in the soil and is influenced by the surface temperature, surface roughness as well as vegetation. The “penetration” depth of this method is 5-10 cm.

#### ***3.1.4.2 Conclusions***

High resolution airborne geophysics is an emerging method, which so far has only very rarely been applied to landslide investigations. By evaluating the results available from before 2008 we conclude that the application for landslide mapping seems very promising. However due to the significant improvements in data acquisition as well as in data processing and interpretation during the last years more delicate results could be expected by incorporating latest improvements in airborne technology. Therefore several test studies are planned within the SafeLand project in cooperation with other projects to advance interpretation for landslide mapping and to explore the prospects of this methodology and evaluate the usability of the results for fast detection and mapping of landslides.

In 2009 the landslide of Gschliefgraben and Rindberg / Sibratsgfäll and the area of Schnepfau and Rankweil were mapped in frame of the SafeLand project. In May 2010 a survey at the Stovze landslide in Slovenia was performed.

Data processing and interpretation of all case studies is currently performed.

## **3.2 LANDSLIDE MONITORING**

### **3.2.1 Aerial sensors**

*UNIL: Michoud C., Derron M.-H., Jaboyedoff M.*

To date, aerial sensors are usually not used directly to monitor landslides. Actually, the monitoring that can be achieved with aerial sensors is more related to back-analysis of continuous phenomena or single events, comparing non-continuous datasets, such as aerial photos. However, as for the satellite optical monitoring, recent trends in aerial techniques concerning acquisitions and processings (see chapter 3.1.1) have a positive impact on monitoring too. Indeed, thanks to images with steadily better resolutions and steadily shorter temporal baselines, smaller displacements can be detected between two acquisitions, allowing a finer detection and monitoring of earth's surface changes.

### 3.2.2 Satellite optical

*ITC: Stumpf A., Kerle N.*

The recent innovation in the sensor systems, already explained in chapter 3.1.2, have a positive impact also on the landslide monitoring.

A frequently repeated application of one of the techniques (especially change detection) mentioned in chapter 3.1.2 must be considered as a form monitoring. The high temporal and spatial resolution of the imagery delivered by modern optical satellites is suitable to monitor a large spectra of landscape changes including those induced by landslide (Rau et al. 2007). Object-oriented methods are featuring many advantageous for image classification and change detection applications with VHR imagery, whereas only recently frameworks for the spatially and temporally consistent integration of time-series through backdating and updating are being proposed (Linke and McDermid 2010; McDermid et al. 2008) (Figure 18). Typically, even if no changes occur between two time steps, image differences lead to small mismatches between the same objects among different time steps. Linke and McDermid (2010) proposed the use of a minimal mapping width (MMW) to suppress such effects when combining multiple time steps. The MMW could be estimated statistically on the corresponding datasets and, if co-registration errors are kept at a minimum, 2-4 pixels might be acceptable threshold.

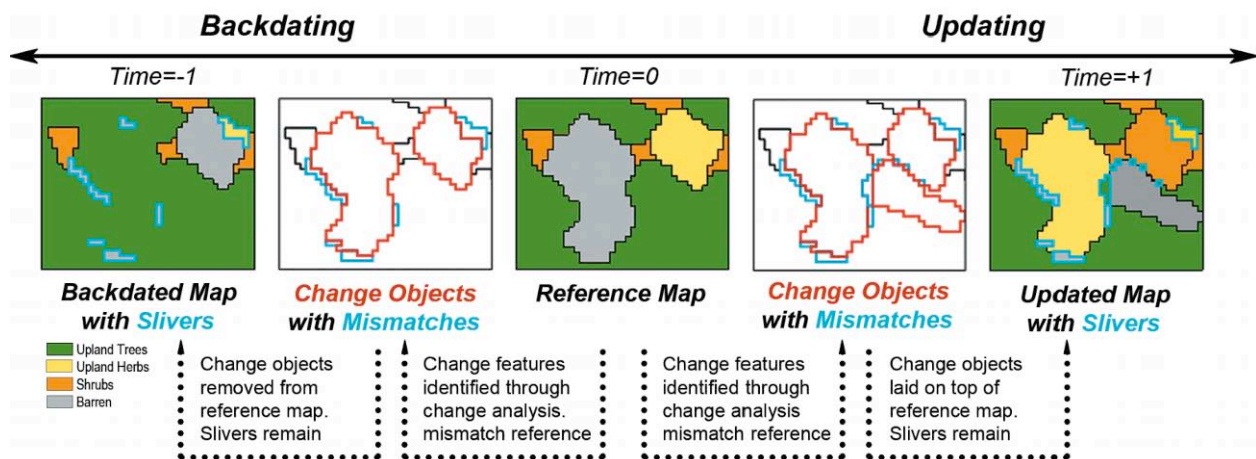


**Figure 18.** Object-oriented backdating and updating for the construction of time series maps representing temporal and spatial changes. Spurious effects of mismatches (slivers) between reference objects can be addresses by defining a minimum mapping width (figure from McDermid et al. 2008).

Among monitoring techniques that target to measure displacement and deformation from optical satellite images two distinct techniques are available. Differencing of multi-temporal DSMs generated from satellite stereo images can be used to estimate involved volumes and/or vertical surface deformation. Dewitte et al. (2008) demonstrated that aerial optical data can be used to track surface displacement over decades but still relatively few studies addressed a similar use of spaceborne imagery (Martha et al. 2010b; Tsutsui et al. 2007). Martha et al. (2010b) showed recently that Cartosat-1 can be used to automatically derive accurate volume estimates for relatively small landslides and without the necessity of GCPs. This may encourage further tests of such techniques on imagery from upcoming satellites with enhanced stereo imaging capabilities.

An important innovation for the measurement of horizontal displacement fields from optical satellite data has been the development algorithms for digital image correlation. Recently user friendly software implementations of this technique have become available (Leprince et al. 2007), whereas generally different algorithms are kept being used to measure for instance co-seismic slip (e.g. Konca et al.) or glacier flow (Debella-Gilo and Kääb 2011). The capability of DIC to monitor landslide surfaces over multiple time steps has been demonstrated with aerial photographs (Casson et al. 2005). Only few studies demonstrated the usefulness of satellite images in this context (Delacourt et al. 2007; Delacourt et al. 2009; Leprince et al. 2008) and research that addresses the analysis of longer available VHR satellite time series is still lacking.

### 3.2.3 Satellite radar

*BRGM: Raucoules D., De Michele M.*

*CNRS: Malet J.-P.*

A SAR (Synthetic Aperture Radar) system sends radar pulses to the ground and measures both the amplitude and the phase of the backscattered signal. Here we propose the use of the radar amplitude data to construct ascending and descending correlograms following the sub-pixel correlation described in Michel et al. (1999) or Leprince et al. (2007), which is today a widely used technique for retrieving ground surface deformation such as co-seismic surface displacements (e.g. Fialko et al., 2005). Figure 19 shows an example of generation of deformation maps based on space-borne SAR images correlation.

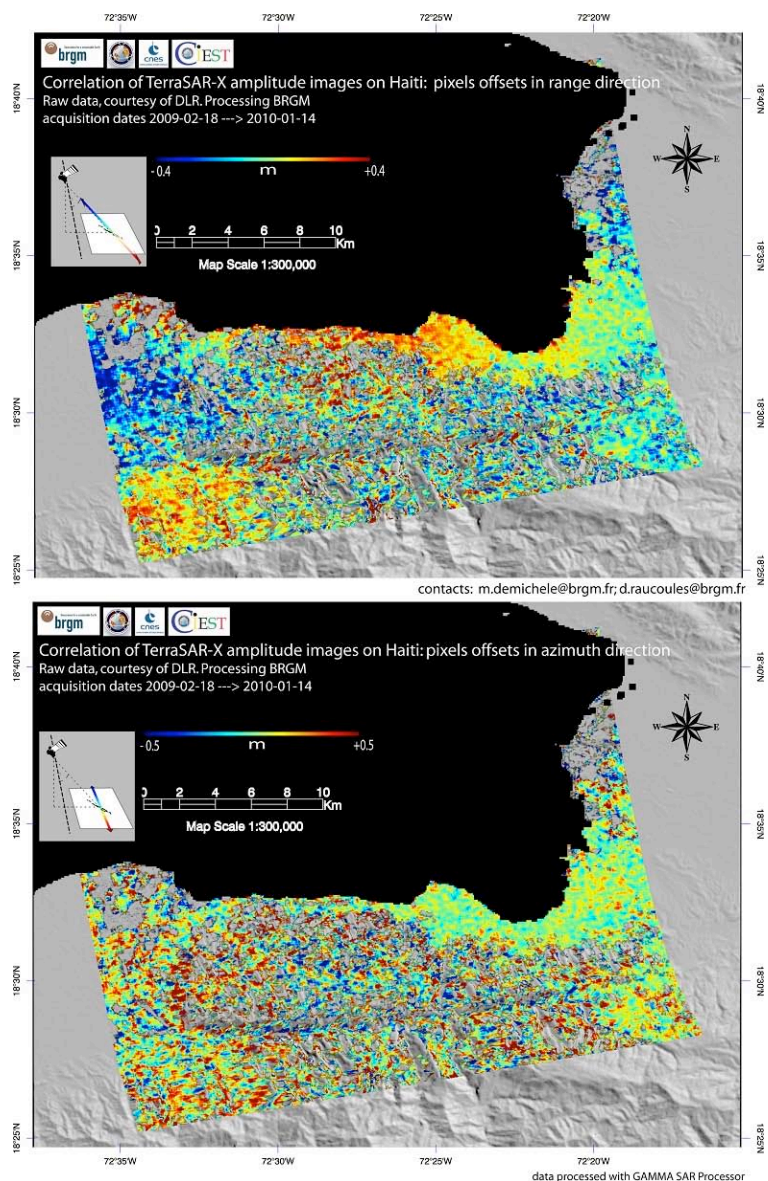


**Figure 19. Example of surface deformation obtained using radar images (TerraSAR-X) correlation on the Haiti earthquake (12/01/2010) (BRGM/CIEST).**

Typically, the sub-pixel algorithms can reach 1/10 to 1/20 pixel precision (in the most favourable cases – Le Prince et al., 2007).

For landslides, the use of the correlation techniques based on SAR data was therefore limited by the resolution of the previous generation of space-borne SAR sensors (e.g. EnviSAT/ASAR or RadarSAT 1) that limited the precision of the result and the possibility of covering small (in size) landslides. Therefore, the technique could be applied only to specific cases of landslide with metric displacements over large areas. In this context, interferometric techniques were generally more adapted for using such SAR data on landslides. Therefore, image correlation techniques were more suitable to be applied to space-borne optical data (e.g. Delacourt et al., 2009) than radar data.

Now, with the recent launches of TerraSAR-X and Cosmo-SkyMed missions offering sub-metric resolutions, the situation has changed and the characteristics of the radar images in terms of resolution are equivalent to those provided by optical sensors widely used for image correlation (such as Spot 5, Quickbird, etc.).

In this context, the SAR data is becoming an interesting alternative to optical data for image correlation techniques applied to ground surface deformation.

### **3.2.4 Airborne geophysics**

*GSA: Supper R., Baron I.*

Airborne geophysical survey is not enough reliable for landslide monitoring due to many technological, processing and financial restrictions. Currently the main applications regard landslide detection and mapping survey. However, in the framework of the SafeLand project, some applications confirmed the actual feasibility and effectiveness of airborne geophysics monitoring of landslides (see chapters 6.2.7 and 6.2.8) and it cannot be excluded, that if the technological progress would continue in the future, the method could be applied also for monitoring.

## 4 QUESTIONNAIRE ON GROUND BASED TECHNIQUES

*GSA: Supper R., Baron I.*

Mass movements are one of the worst natural threats worldwide. Consistent information about individual unstable slopes, especially in very vulnerable areas, on their internal structure, dynamics of deformation, triggers, history and possible magnitude is an essential base for any proper evaluation the actual hazard and for eventual warning of people before a catastrophic event in advance. Such knowledge is obtainable only through a complex interdisciplinary approach consisting of investigations by many different methods and techniques, long-time monitoring of deformation and triggering factors and by establishing early warning centres.

The approaches differ, of course, regarding the affected mass parameters, behaviour, activity state, local infrastructure, and national tradition as well.

Studies, which evaluated and compared those approaches and individual techniques complexly throughout the world, are really scarce. Therefore a Questionnaire on National State of Landslide Site Investigation and Monitoring was prepared and was disseminated among European institutes and representatives within the frame of the SafeLand project. Some answers out of Europe were obtained as well. The principal goals and expected output of the questionnaire study were:

- Assessing general state of the slope-instability investigation and monitoring in different countries,
- Assessing effectiveness / reliability of each method for slope-instability investigation and monitoring,
- Applicability of the monitoring techniques for early warning.

### 4.1 METHODS

The questionnaire study was concerned on landslides which have been investigated with at least two independent methods and monitored for a longer time than 1 year. A Word-Doc Application was prepared in the way to be as comprehensive and user friendly for collecting the answers as possible (Figure 20). Most of the parameters were pre-defined; however some free fields were left for specific answers. The answering was done through ticking and was an input for further statistical assessment.

The **general information on monitored mass movement** consisted of information such as on slope failure typology, activity state and recent movement rates. The classification was adopted and modified from CRUDEN & VARNES (1996). Abundance of different types of the phenomena was then expressed relative to the total number of the described monitored sites - *relative occurrence* (%).

The next section was focused on methods of **investigation** of the structure and character of the landslide to be monitored. The investigation **methods** consisted of **mapping, testing, ground-based geophysical surveys** and **remote-sensing data**. Such methods, where the sensors are placed on aeroplanes, helicopters or satellites, are here considered to be the “remote-sensing” ones, whilst the ground-based (GB) methods have the sensors placed at or under the ground surface. The methods were evaluated by *relative occurrence* (%), i.e.: abundance of the method / technique per total number of the collected case-study sites and the *relative reliability* (%) of the method, evaluated subjectively by authors of the answers.

---



Methods of **landslide monitoring** (monitoring of **displacement and deformation, hydrometeorological factors, and geophysical factors**) were assessed by their *relative occurrence* (%) per total number of case-study sites as well. The next parameter, the applicability of the monitoring method for an early warning – shortly called the *early warning potential* (%), was given by number of positive answers on the possibility to use the method for EW, divided by the total number of the collected sites, and multiplied by 100.

## 4.2 REVIEW OF COLLECTED SITES

An information on totally 86 investigated and simultaneously monitored landslides has been obtained from 14 European and Asian countries (Table 1). Most answers came from Italy (totally 22 monitored landslides), the Slovak Republic (16), the Czech Republic (11) and Kyrgyzstan (8). The most abundant slope failures that have been monitored were active rotational (29 %) and translational (22 %) slides and complex failures (19 %) with recent movement rates less than 10 mm/month (Figure 21 and Figure 22).

**Table 1. Review of the number of sites and countries included in the study. Explanations: AD – Andorra, AT – Austria, CH – Switzerland, CZ – Czech Republic, ES – Spain, FR – France, GB – Great Britain, IT – Italy, JP – Japan, KG – Kyrgyzstan, NO – Norway, RU – Russian Federation, SI – Slovenia, SK – Slovak Republic.**

Country	No.	Monitored landslides	Author
AD	1	Canillo	J. Corominas
AT	7	Kerschbaumsiedlung, Blaubach, Murenbach, Sibratsgöl / Rindberg, Gschlifgraben, Maesstobel, Wagrain Ache	V. Kaufmann, Ch. Ihrenberger, M. Wöhrer-Alge, W. Gasperl
CH	3	Gruben, Ruedlingen, Tössegg	S. Springman
CZ	11	Pustevny, Halenkovice, Holstejn, Přihrazy, Třebeňovice, Čeřeniště, Ondřejník, Karolinka, Ujala, Obří Hrad, Pravčická brána	J. Klimes, M. Bil, V. Hanzl, J. Rybar, P. Blaha, F. Hartvich, Z. Varilova
ES	1	Vallcebre	J. Corominas
FR	5	Mas d'Avignonet, Super Sauze, Villerville, La Valette, Séchillienne	D. Jongmans, J.-P. Malet, S. Garambois, A. Helmstetter
GB	1	Hollin Hill	C. Foster
IT	22	Cervinara site, Castagnola, Masseria Marino mudslide, Santo Stefano d'Aveto, Monteforte Irpino area, Ponti, Ruinon, Idro, Bagnaschino, Ancona, Chervaz, Comba Citrin, Cherz, Passo della Morte, Tessina, Magliatica, Bosmato-Stadelte, Vollein, Letze-Bosmato, Becca di Nona, Pitigliano, SanMiniato	L. Picarelli, N. Casagli, G. Urciuoli, M. Lovisolo, S. Cardellini, M. Broccolato, J. Blanc, A. Passuto, G. Truffelli
JP	4	Kuchisakamoto, Aratosawa, Yui, Takisaka	G. Furuya, S. Tosa, H. Marui
KG	8	Gulcha-Basar, Kambar-Ata, Kok-Jangak (Kapitalnaja), Min-Kush, M-Suu Izolit, M-Suu Tektonik, M-Suu, Koy-Tash, Taran-Basar	I. Torgoev
NO	3	Aaknes, Jettan Nordnes, Mannen Romsdalens	L.H. Blikra
RU	1	Zagorsk	M.M. Ilyin
SI	3	Macesnik, SlanoBlato, Stože	M. Carman, S. Kumelj
SK	16	Banska Stiavnica, Bojnice, Demjata, Dolna Micina, Fintice, Handlova 1960, Handlova - Kunesov road, Hlohovec, Klecenov, Liptovska Mara, Morovno Estate, Okolicne, Slanec, Velka Izra, Velka Causa, Vistuk	P. Wagner

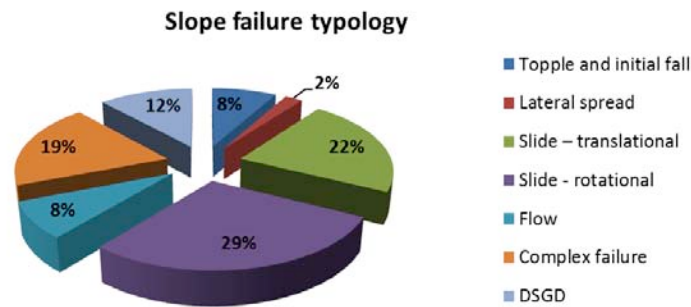


**Figure 21. Review of monitored slope failures included in the study (modified classification of CRUDEN & VARNES, 1996).**

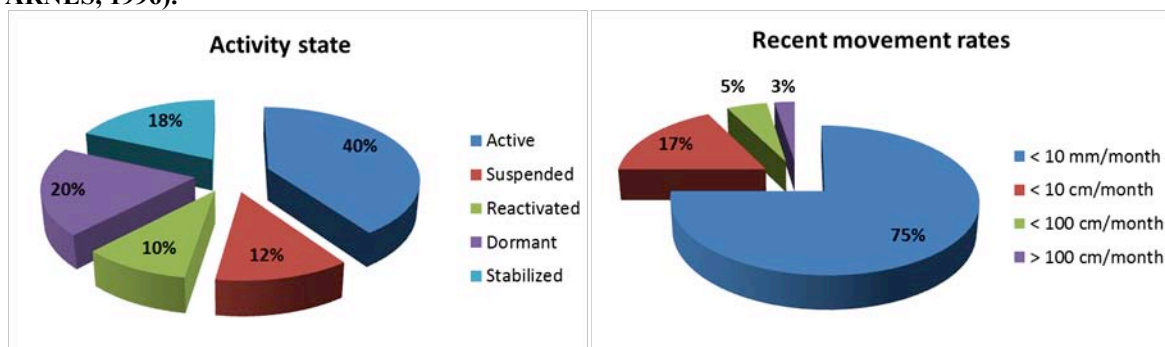


**Figure 22. Review of slope failures included in the study by their activity state (after WP / WLI, 1993) and actual movement rates.**

## 4.3 RESULTS

### 4.3.1 Evaluation of the investigation methods

The geological (applied at 87 % of the sites), engineering-geological (86%) and geomorphic (72%) **mapping surveys** were the most abundant ones (Figure 23). Strength properties/deformability (at 72% of the sites), clay mineralogy testing (43%) and borehole testing (26%) represented the most abundant **testing surveys** of the monitored sites (for the graphical presentation and for the methods review see Figure 24).

DC resistivity (applied at 62 % of the sites) and refraction seismic (41 %) were the most abundant **ground-based geophysical methods** of investigation at the reported landslides. Other frequently used methods were the reflection seismic (17% occurrence), self-potential survey (15 %) and ground-penetrating radar (15 %). Geophysical logging (85% reliability), the resistivity (82 %) and the refraction seismic (80 %) were considered as the most reliable ground-based geophysical methods (for the graphical presentation and for the methods review see Figure 25).

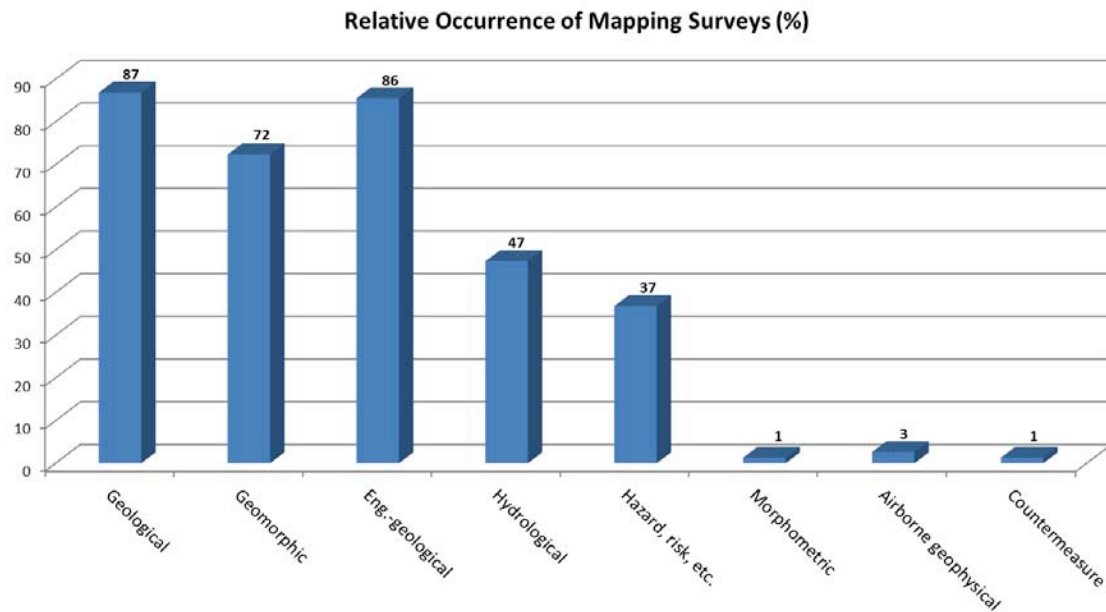


**Figure 23.** Review of relative occurrence of different mapping approaches (per number of sites) applied in the case sites.

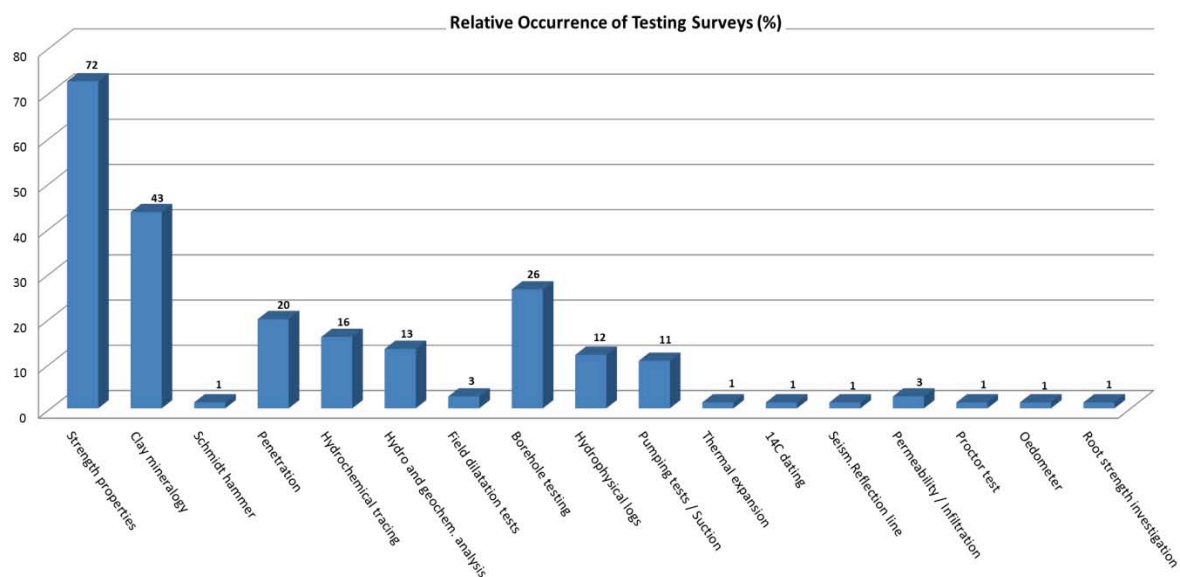


**Figure 24.** Review of relative occurrence of different testing approaches applied in the case sites.

The most frequently applied **remote sensing data and techniques for landslide investigation** were aerial photographs (applied at 36 % of the sites), radar interferometry (17 %) and LiDAR ALS (17 %) (see Fig. 7). Reliability of remote sensing methods was jointly evaluated for structural investigation and for monitoring of movement. As the most reliable **remote sensing methods** were unequivocally evaluated LiDAR ALS (91% reliability), then aerial photographs (83 %) and satellite optical very-high resolution images (76% reliability). For the graphical presentation and for the methods review see Figure 26.

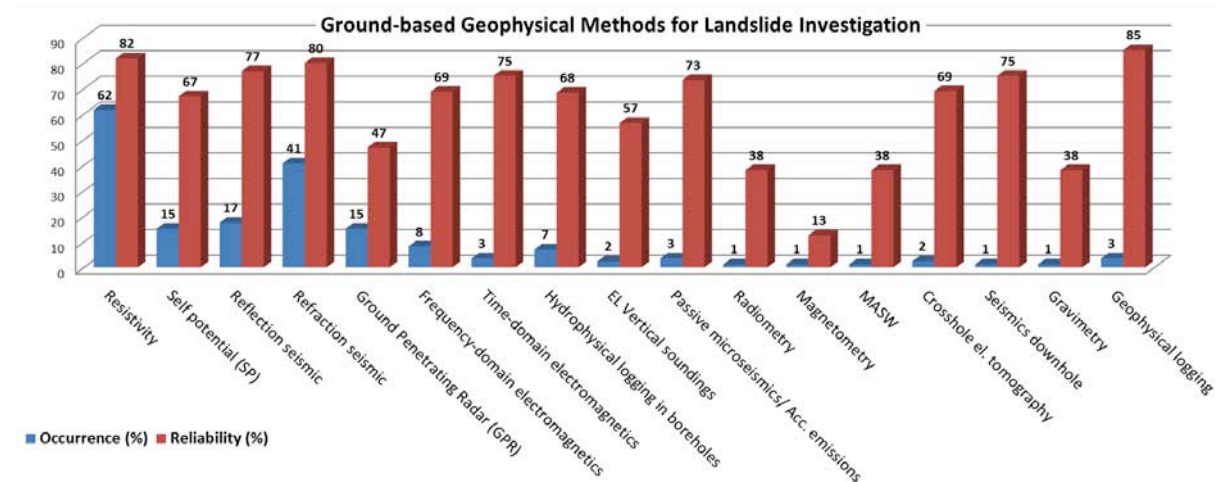


Figure 25. Review of relative occurrence and reliability of different geophysical methods applied for investigation of the case sites.

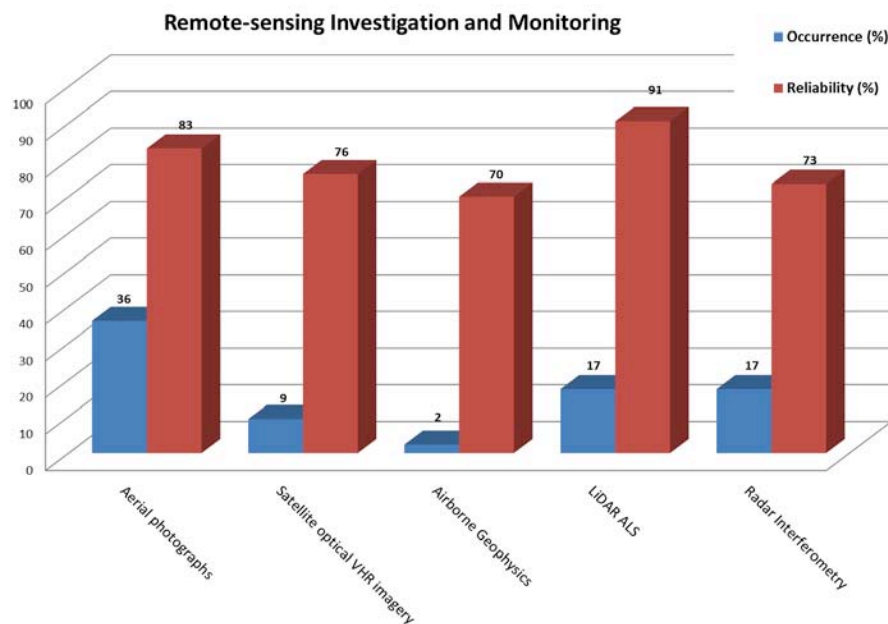


Figure 26. Review of relative occurrence (blue) and relative reliability (red) of different remote-sensing data applied for investigating or monitoring of the case sites.

#### 4.3.2 Evaluation of the monitoring methods

Classical inclinometers (47 %), dGPS (38 %) and wire extensometers (33 %) were the most frequently applied **ground-based methods of displacement and deformation monitoring**. Those methods have also the highest early-warning potential (for the graphical presentation and for the methods review see Figure 27).

As the most abundant methods of **hydro-meteorological factors monitoring** of landslides, precipitation amount (at 74 % of collected case-study sites), pore-water pressure (57 %) and, especially in the case of topples and initial rockfalls, air temperature (52 %) were evaluated.

Those methods were also the most promising ones for an early warning (for the graphical presentation and for the methods review see Figure 28).

Passive seismic/acoustic emissions (at 17 % of collected case-study sites), electromagnetic emissions (13 %) and direct current resistivity (15 %) were the most frequently monitored **geophysical parameters** and the most promising ones for early warning as well (for the graphical presentation and for the methods review see Figure 29).

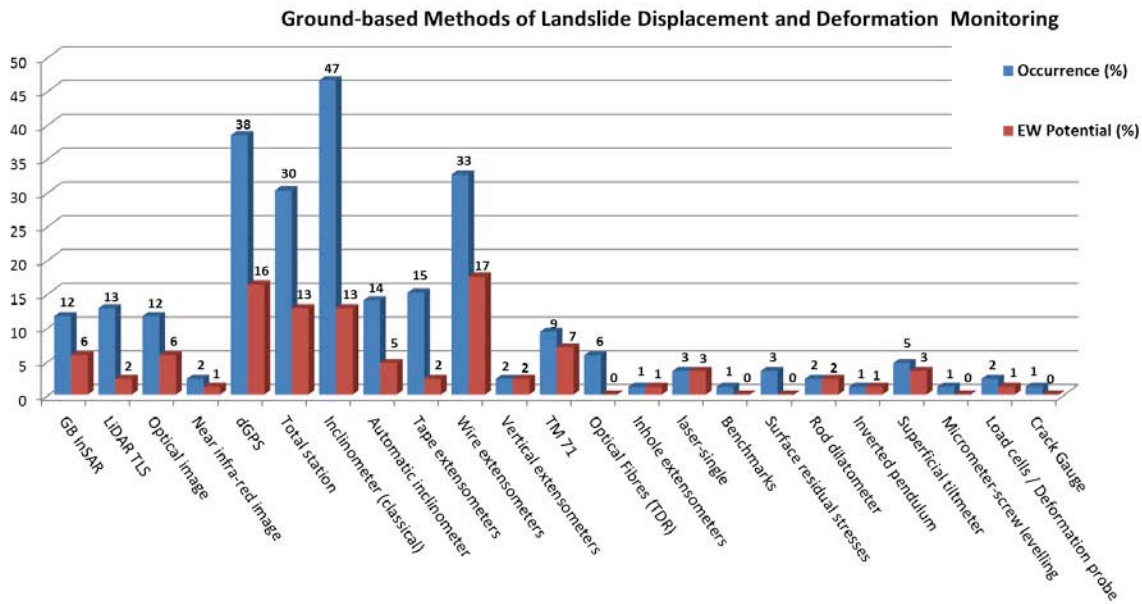


Figure 27. Review of relative occurrence and early-warning potential of ground-based techniques applied for displacement and deformation monitoring of the case sites.

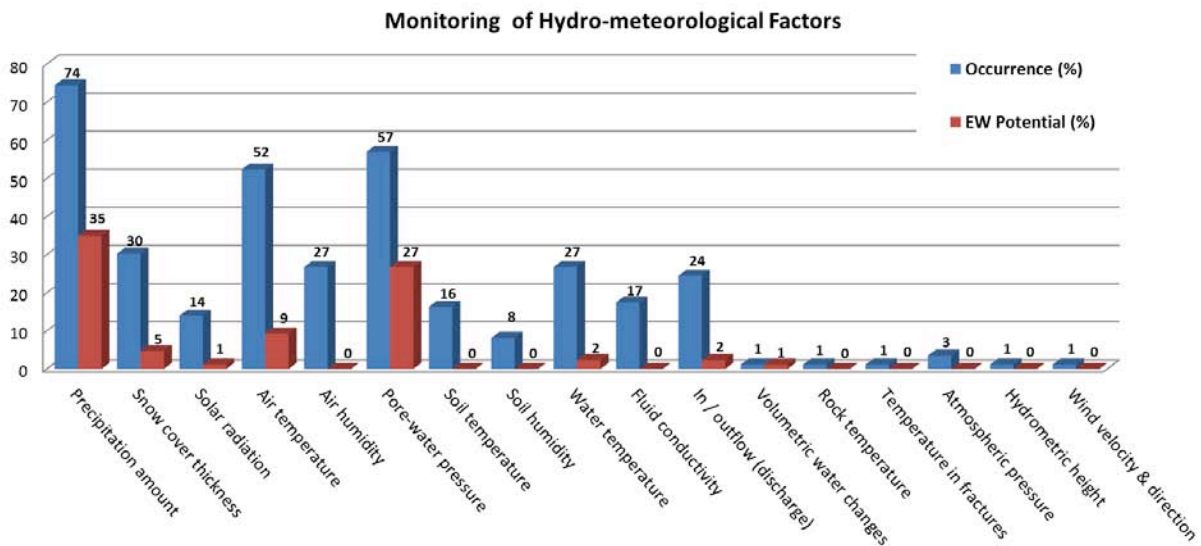
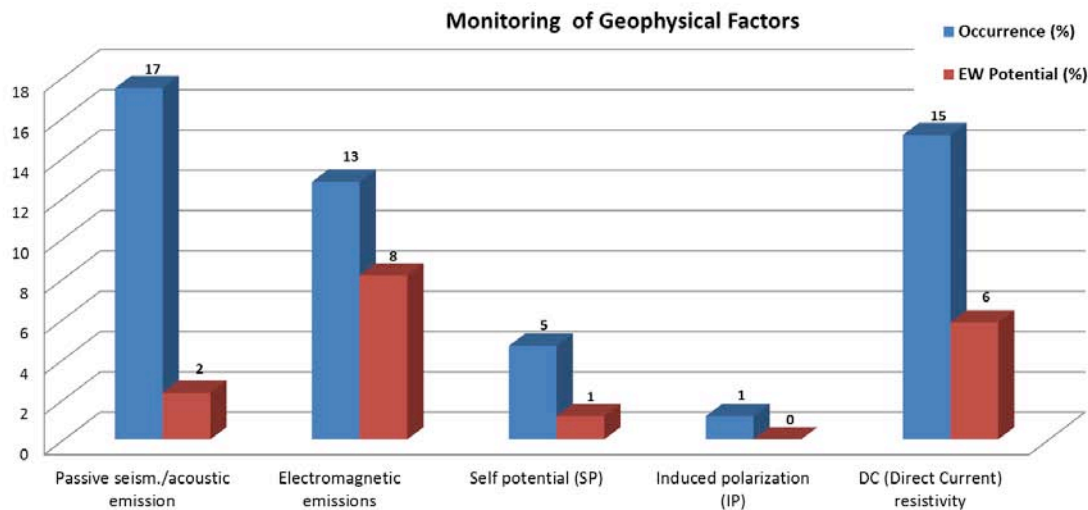


Figure 28. Review of monitoring of hydrometeorological factors at the case sites, and their early-warning potential.



**Figure 29. Review of monitoring of geophysical factors at the case sites, and their early-warning potential.**

#### 4.4 DISCUSSION AND CONCLUSIONS

The presented study has evaluated the recent general state of the slope-instability investigation and monitoring, the reliability of applied remote sensing and ground based methods, and the applicability of monitoring techniques for early warning. The study was based on information collected from 86 prominent landslides in 14 European and Asian countries, which have been investigated with at least two independent methods and monitored for a longer time than 1 year.

Slope instabilities comprising rotational and translational slides, topples, falls, ground flows and their complexes are being investigated and monitored by completely different methods. E.g., some specific methods, applicable only for less abundant rockfalls, could appear in the evaluation (relative occurrence) less than methods applicable for large spectra of mass-movements or more abundant landslide types. Therefore any comparison of the relative occurrence of those methods is very difficult and contains many approximations and much omitting. The same restriction must be regarded to monitoring methods and parameters, and their early warning potential.

Certain degree of subjectivity of the answers could be considered as rather weak aspect of the study, because the reliability and early warning potential of applied methods, parameters and factors were assessed by the experts with different experience and profession. The authors of the study respect this fact. However, the study brought as complex and comprehensive information as possible.

Based on the answered forms, LiDAR ALS, geophysical logging, aerial photographs, resistivity surveying, GB InSAR and the refraction seismic were considered unequivocally as the most reliable methods of the investigation of structure and character of landslides. See Figure 30 and Figure 31 for the graphical presentation and for the review of all of the methods. Especially LiDAR ALS and geophysical logging seem to be very challenging methods because they have been evaluated so high, despite their application at relatively few landslides worldwide.

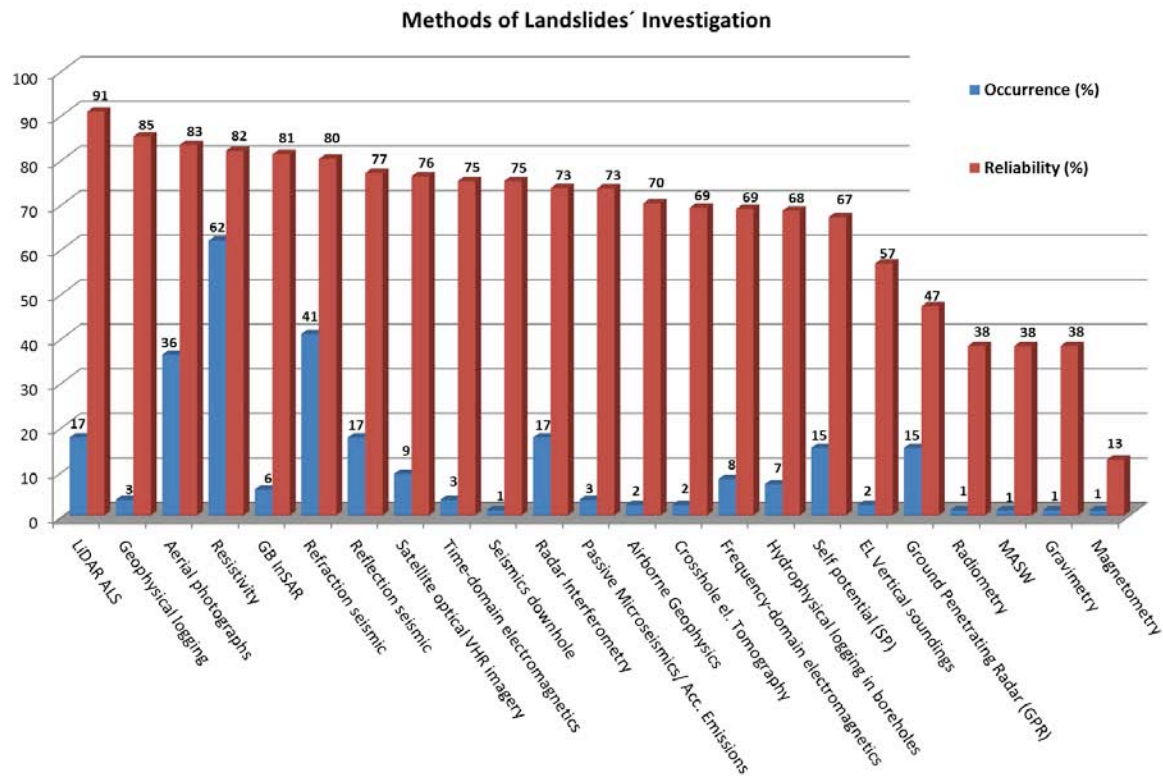


Figure 30. Comparison of all of the evaluated methods of landslide investigation ordered by their reliability.

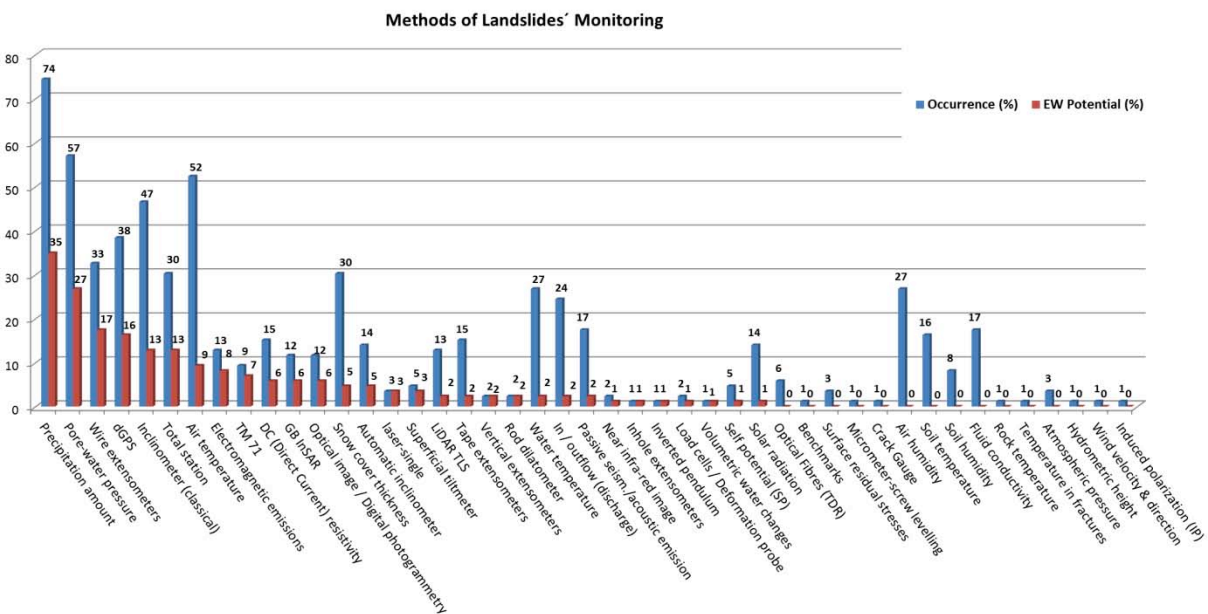


Figure 31. Comparison of all of landslide monitoring methods included in the study ordered by their early-warning potential.

Precipitation amount, pore-water pressure and displacement monitored by wire extensometers, dGPS and total stations, followed by air temperature and EM-emissions

monitoring and displacement monitored by the TM 71 crack gauge were considered the most promising parameters for early warning.

#### **4.5 ACKNOWLEDGEMENTS**

The authors would like to acknowledge everyone who helped through discussions to improve the form to be as comprehensive and "user-friendly" as possible. Special thanks go to all the local national coordinators who helped to disseminate the questionnaire effectively and to obtain as many answers as possible; and, of course all specialist and responsible persons, who filled in the form, must be thanked, i.e.: M. Bil, P. Blaha, J. Blanc, L.H. Blikra, M. Broccolato, S. Cardellini, M. Carman N. Casagli, J. Corominas, C. Foster, G. Furuya, S. Garambois, W. Gasperl, V. Hanzl, F. Hartvich, A. Helmstetter, Ch. Ihrenberger, M.M. Ilyin, D. Jongmans, V. Kaufmann, J. Klimes, S. Kumelj, M. Lovisolo, J.-F. Malet, H. Marui, S. Novosad, A. Passuto, L. Picarelli, J. Rybar, K. Sassa, S. Springman, I. Torgoev, S. Tosa, G. Truffelli, G. Urciuoli, Z. Varilova, P. Wagner, and M. Wöhler-Alge.

## **5 QUESTIONNAIRE ON AIRBORNE AND SPACEBORNE TECHNIQUES**

*UNIFI: Tofani V., Segoni S., Catani F., Casagli N.*

In the framework of the SafeLand project the Department of Earth Sciences of the University of Firenze has prepared a questionnaire on remote sensing in order to investigate the role of remote sensing for landslide study.

The SafeLand project, among many other the issues, addresses the development of monitoring technology, especially early warning systems and remote sensing techniques. The research develops remote sensing technologies for the detection, monitoring and efficient mapping of landslides. The work within SafeLand involves an evaluation of existing technology and development of new technology, including procedures and techniques, hardware and software, for early warning of sliding movements. The technologies will be applicable to both the local scale for individual slopes, and the regional scale.

In order to make an evaluation of the existing remote sensing techniques, the aim of the questionnaire is to collect information about the usefulness of remote sensing for landslide study and to evaluate its applicability for landslide detection, mapping, monitoring and early warning.

The questionnaire wants to make a picture of how remote sensing is used in landslide study nowadays. To this end, whoever fills the questionnaire has been requested to compile it according to his/her actual use rather than to the one he/she would have theoretically used.

The questionnaire has been circulated among Safeland partners, Safeland end-users and Researchers involved in landslide study within and outside Europe. All over the world 52 answers have been collected.

In section 5.1 the description of the structure of the questionnaire is reported, while in section 5.2 it can be found an overview of the type of answers. In sections 5.3 and 5.4 the description of the results of the questionnaire is provided by means of simple statistical analysis.

Since the number of charts is high, in sections 5.3 and 5.4 only the most important ones are provided. For an in-depth examination all the charts can be found in Appendix 1.

### **5.1 METHODS**

The questionnaire was set up as a Google form. In this way the answers were automatically collected in a Google spreadsheet (Figure 32). The questionnaire was prepared in a way to be comprehensible and user friendly as much as possible. The majority of the questions are checkbox; this means that more than one answer could be picked. Some of them are open questions and at the end of each section some space is left for comments related to the answers. At the beginning of the questionnaire a sort of help text was provided in order to guide the compiler throughout the questionnaire.

The questionnaire is structured into three different sections.

The first section is related to the general information on the questionnaire compiler (Institution, Location, Country, Contact person, e-mail) (Figure 32).

The second section is devoted to landslide Detection and Mapping. Eleven questions have been prepared concerning the use of remote sensing for landslide detection and mapping, an overview of the questions is reported in Figure 32.

---

The third section is devoted to Landslide Monitoring. 13 questions have been prepared concerning the use of remote sensing for landslide monitoring; the overview is reported in Figure 33.

### Questionnaire on remote sensing

Dear all,

In the framework of the SafeLand project the Department of Earth Sciences of the University of Firenze has prepared a questionnaire on remote sensing in order to investigate the role of remote sensing for landslide study.

SafeLand is a Large-scale integrating Collaborative research project funded by the The Seventh Framework Programme for research and technological development (FP7) of the European Commission.

The SafeLand project among all the issue addresses the development of monitoring technology, especially early warning systems and remote sensing techniques. The research will develop remote sensing technologies for the detection, monitoring and efficient mapping of landslides. The work will involve an evaluation of existing technology and development of new technology, including procedures and techniques, hardware and software, for early warning of sliding movements. The technologies will be applicable to both the local scale for individual slopes, and the regional scale.

In order to make an evaluation of the existing remote sensing techniques, the aim of this questionnaire is to collect information about the usefulness of remote sensing for landslide study and to evaluate its applicability for landslide detection, mapping, monitoring and early warning. The Questionnaire wants to make a picture of how remote sensing is used in landslide study nowadays. To this end, whoever fills the Questionnaire is requested to compile it according to his/her actual use rather than to the one he/she would theoretically use.

The Questionnaire is structured into three different sections. The first section is related to the general information on the Questionnaire compiler, the second one to Landslide Detection and Mapping and the third one to Landslide Monitoring and Early warning. At the end of each section some space is left for comments related to the answers. The questions marked by a red asterisk are compulsory. All the questions are multiple choices, this means that more than one answer can be picked.

We would be really grateful if you could provide your contributi. It should take only 10 minutes of your time.

Thanks for your cooperation.  
Kind regards

Veronica Tofani, Samuele Segoni, Nicola Casagli & Filippo Catani

\* Required

---

#### Landslide detection and mapping

Remotely sensed data used for landslide detection and mapping

Satellite optical

Satellite radar

Airborne geophysics

Aerial photos

Other:

Landslide parameters identified trough remote sensing

geometry

typology

state of activity

volume

velocity

Other:

Optical spectral ranges

VIS

NIR

SWIR

TIR

multispectral

hyperspectral

data fusion

Other:

#### General information

Institution \*

Location \*

Country \*

Contact person \*

Email \*

---

#### Landslide monitoring and early warning

Remotely sensed data for landslide monitoring

satellite radar

satellite optical

airborne geophysics

aerial photos

meteorological sensors

Other:

Parameters monitored through remote sensing

velocity

displacement

deformation

triggering factors

rain/fall

soil wetness

Other:

Optical spectral ranges

VIS

NIR

SWIR

TIR

multispectral

hyperspectral

data fusion

Other:

**Figure 32. Print screens of the questionnaire distributed as an online document. At top left the help text provided at the beginning of the questionnaire, at top right the first section of the questionnaire, at bottom left the beginning of the second section on landslide detection and mapping and at bottom right the beginning of the third section on landslide monitoring and early warning.**

Concerning the landslide type and velocity classification, the one adopted is the classification of Cruden and Varnes (1996) while concerning the scale of analysis it has been adopted the classification proposed by Fell et al. (2008).

Landslide detection and mapping	<ol style="list-style-type: none"> <li>1. Remotely sensed data used for landslide detection and mapping</li> <li>2. Landslide parameters identified through remote sensing</li> <li>3. Optical spectral ranges</li> <li>4. Optical techniques for landslide detection and mapping</li> <li>5. Radar spectral bands</li> <li>6. Radar techniques for landslide detection and mapping</li> <li>7. Type of landslide detectable through remote sensing</li> <li>8. Scale of analysis for landslide detection and mapping through remote sensing</li> <li>9. Integration with other thematic data</li> <li>10. Landslide predisposing factors detectable through remote sensing</li> <li>11. Effectiveness/reliability of remotely sensed data for landslide detection and mapping</li> </ol>
Landslide monitoring and early warning	<ol style="list-style-type: none"> <li>1. Remotely sensed data for landslide monitoring</li> <li>2. Parameters monitored through remote sensing</li> <li>3. Optical spectral ranges</li> <li>4. Optical techniques for landslide monitoring</li> <li>5. Radar spectral bands</li> <li>6. Radar techniques for landslide monitoring</li> <li>7. Type of landslide monitored through remote sensing</li> <li>8. Scale of analysis for landslide monitoring through remote sensing</li> <li>9. Landslide velocities monitored through remote sensing</li> <li>10. Integration of remotely sensed data with ground-based techniques</li> <li>11. Integration with other thematic data</li> <li>12. Duration of landslide monitoring by means of remote sensing data and main reason for the interruption of monitoring, if any</li> <li>13. Effectiveness/reliability of remotely sensed data for landslide monitoring</li> </ol>

Figure 33. Overview of the questions.

## 5.2 REVIEW OF THE COLLECTED ANSWERS

All over the world 52 answers were collected. In particular 45 answers came from Europe while 7 answers came from outside Europe (Canada, USA, China, Malaysia, and Korea) (Figure 34). Inside Europe, 16 countries provided at least one answer with a peak of 16 answers from Italy, which corresponds to a percentage of 36% of total European answers (Figure 35).

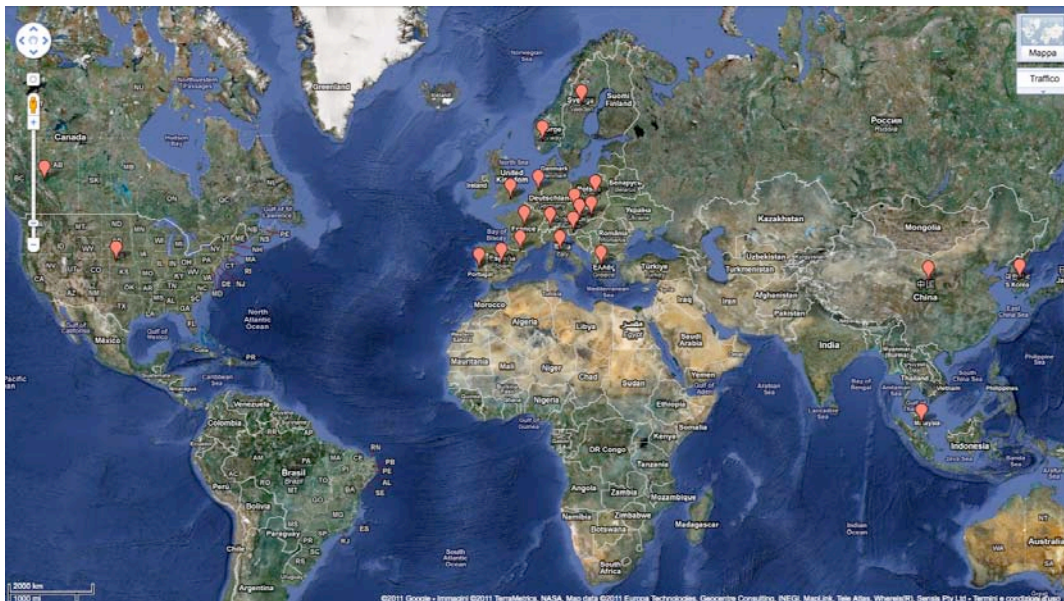


**Figure 34. Geographical distribution of the answers to the questionnaire.**

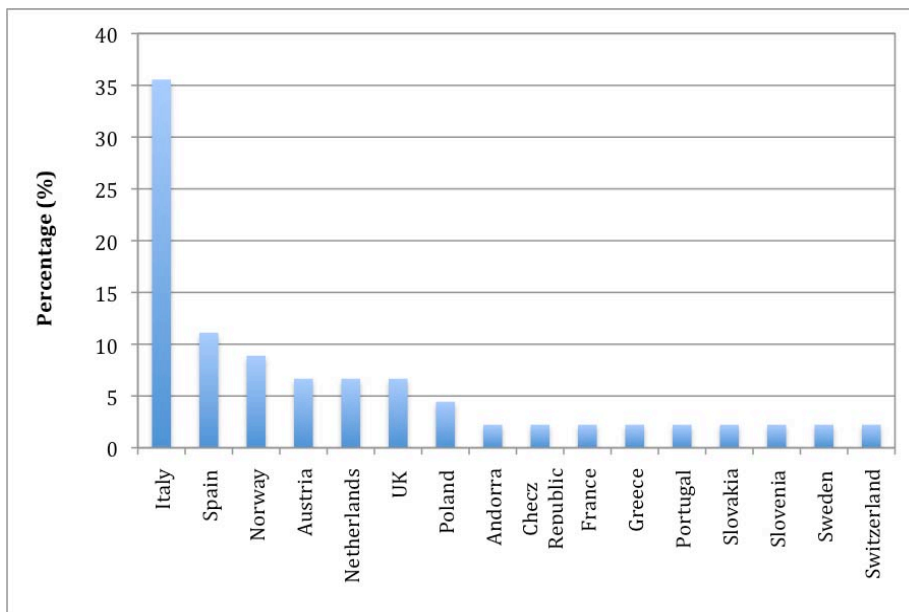


**Figure 35. Distribution of answers in Europe.**

Concerning the affiliation the 43% of the compilers worked at Universities, 21% at Research Institutes, 34% at Public Institutes (Geological Survey, River Basin Authorities etc) and 2% at private companies (Figure 36).

25% of the answers come from partners or end-users of the Safeland project.

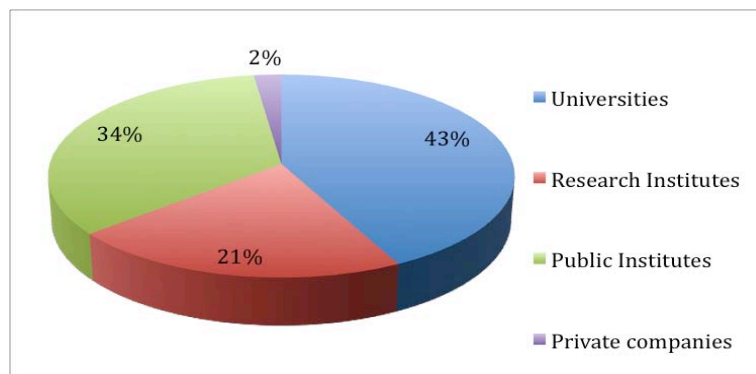


Figure 36. Affiliation of the compilers of the questionnaire.

### 5.3 RESULTS - LANDSLIDE DETECTION AND MAPPING

This section provides with the analysis of the results of the section on “Landslide detection and mapping” of the questionnaire.

Concerning the remotely sensed data for landslide detection and mapping the most frequently used are aerial photos (71 % of the answers), followed by satellite radar (56% of the answers) and satellite optical (52% of the answers). The 15% of the answers indicated also the LIDAR while the 8% the airborne geophysics (Figure 37).

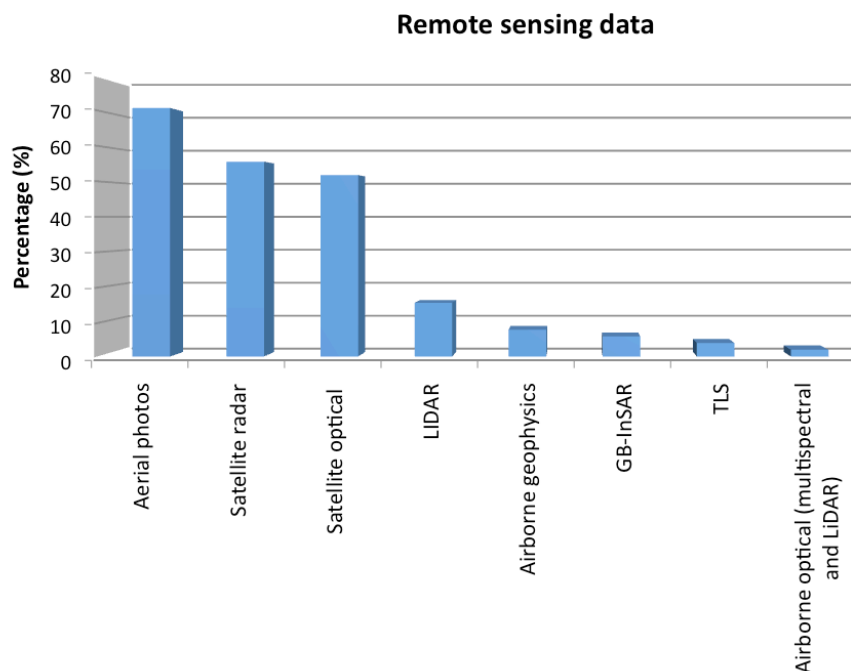
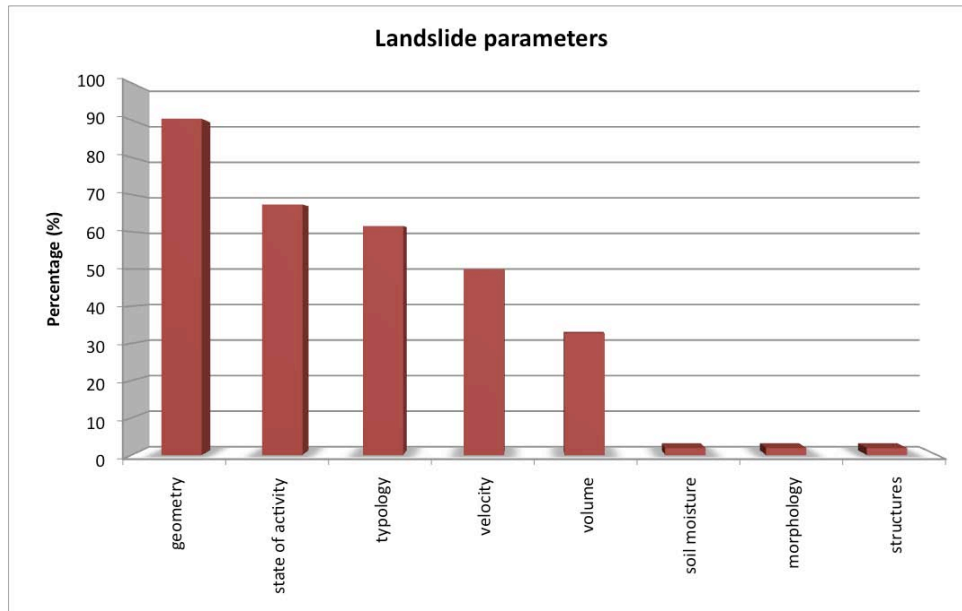


Figure 37. Remotely sensed data for landslide detection and mapping.

Around the 75% of the compilers use more than one remote sensing type of data. In general the use of satellite optical and satellite radar goes with the use of aerial photos (Appendix 1). The most frequent combinations of different type of data are reported in Appendix 1.

Concerning the landslide parameters, the most frequently detected with remote sensing is the geometry (90% of the answers), followed by the state of activity (68%) and the typology (62%).



**Figure 38. Landslide parameters detectable by remote sensing.**

In the field of optical data imagery, the spectral range most frequently used is the visible (67% of answers) followed by multispectral (64%) and NIR (36%), while the optical techniques most reported are visual interpretation (86%), photogrammetry and change detection (Figure 39).

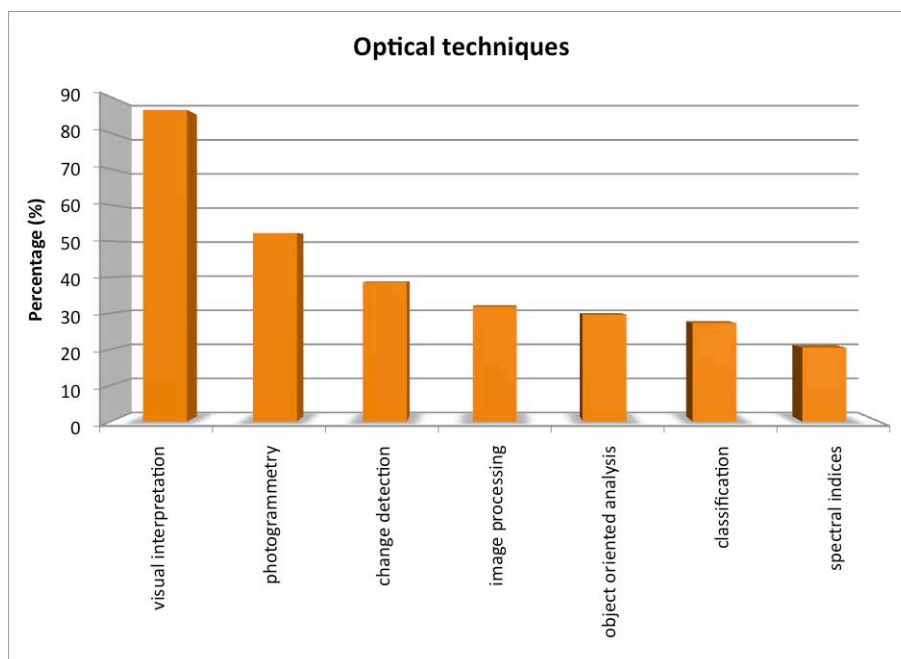


**Figure 39. Optical techniques to detect and map landslides.**

In the field of radar data imagery, the radar band most used is the C band, while the most used technique is A-DInSAR (PS-InSAR, IPTA, SBAS, etc) with a percentage of the 67% of users (Figure 40).

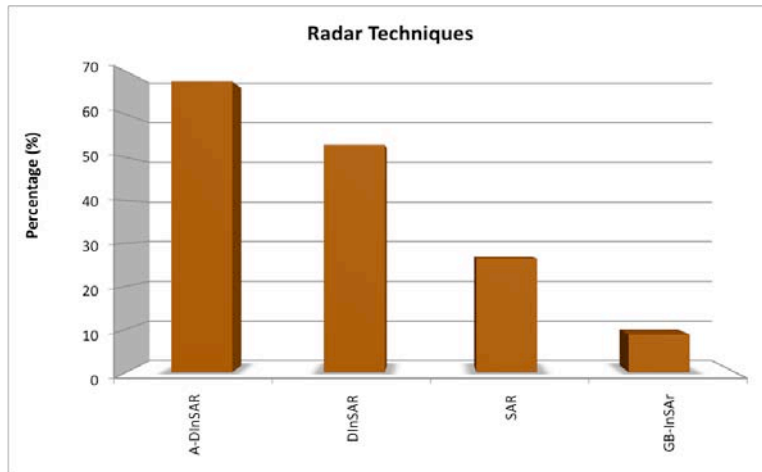


**Figure 40. Radar techniques to detect and map landslides.**

All the compilers agree that with remote sensing is possible to map slides (both rotational and translational), the 78% of them report to map flows, while few of the users can detect lateral spreads, falls and topples (Figure 41).

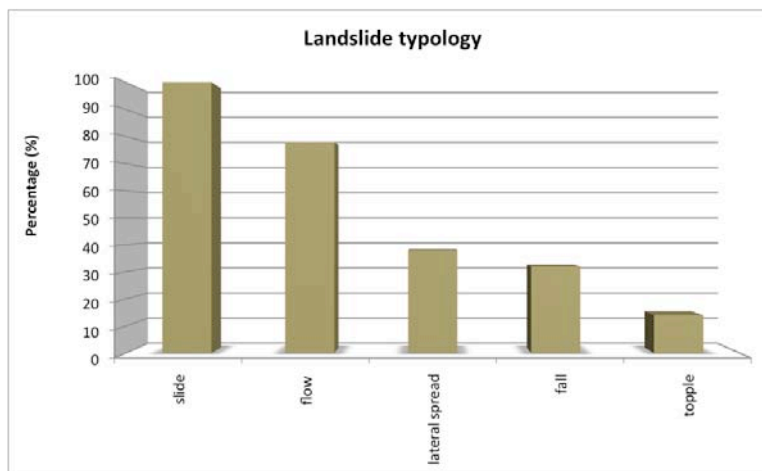


**Figure 41. Type of landslide detectable through remote sensing.**

By means of remote sensing the detection and mapping of landslides is carried out mostly (84% of the answers) at large scale (1:25000 – 1:5000). More than half of the compliers report to map landslide at more detailed scale (> 1:5000) (Appendix 1).

When detecting and mapping landslides through remote sensing, all the users agree on the necessity to make use of other thematic data such as DTM and derived maps (88%), geological maps (86%), pre-existing landslide inventory maps (84%). All the thematic data are reported in Figure 42.

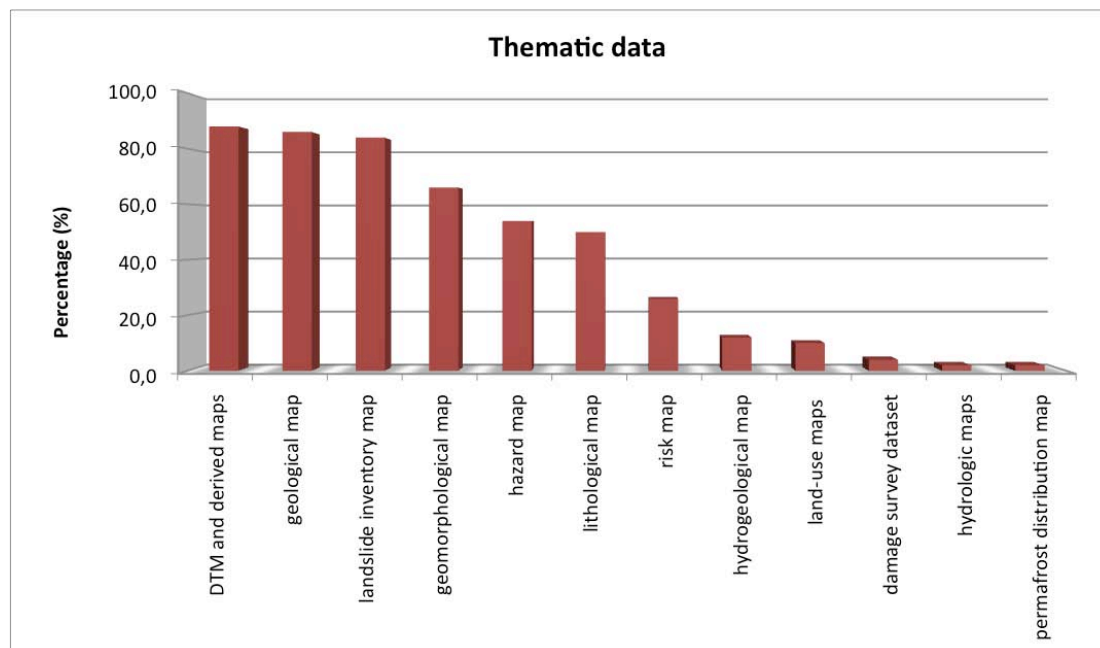


**Figure 42. Integration of remote sensing data with other thematic data for landslide detection and mapping.**

Remote sensing is a useful tool to detect landslide predisposing factors over large areas. The 78% of the compilers use remote sensing to detect predisposing factors. Among them the 90% have indicated DTM and derived parameters, the 63% lands use, the 42% hydrology and 32% lithology.

#### 5.4 RESULTS - LANDSLIDE MONITORING

This chapter provides the results of the section “Landslide monitoring and early warning” of the questionnaire.

Concerning the remotely sensed data for landslide monitoring, the most frequently used type of data is satellite radar (69%) followed by aerial photos (49%), meteorological sensors (38%) and satellite optical (26%). Just 8% of the users have indicated GB-InSAR and LIDAR. (Figure 43)

The 31% of the compilers use only 1 type of remote sensing data. The same percentage is related to 2 types of data while the 26% use 3 types of data and the 13% use 4 types of data.

In landslide monitoring by means of remote sensing the parameters measured are displacement (100% of the answers), deformation (73%), velocity (55%), rainfall (40%) and triggering factors (20%). (Figure 44).

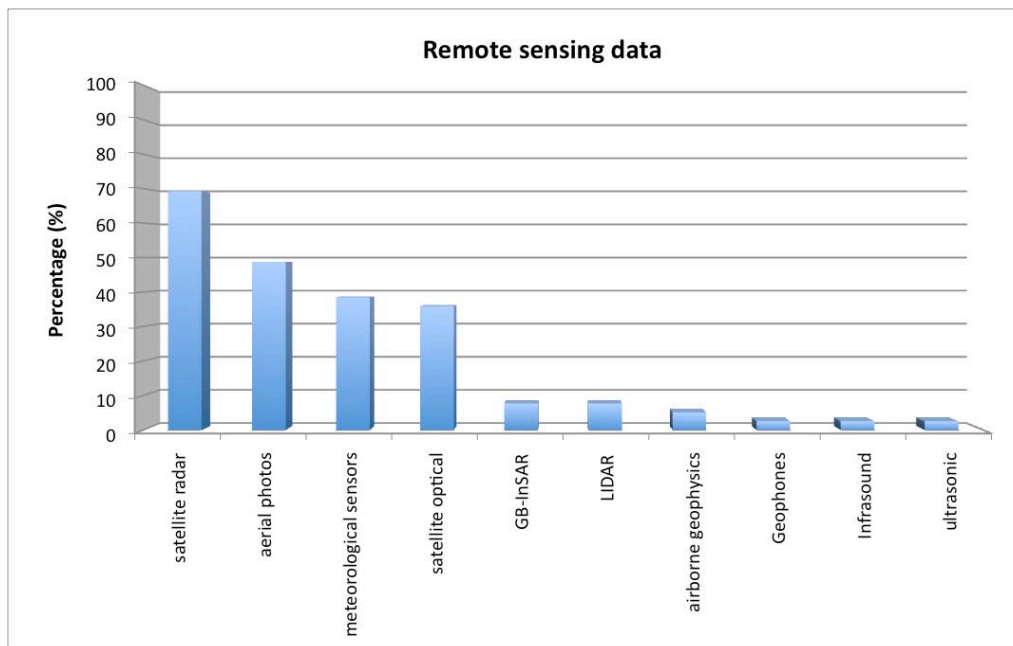


Figure 43. Remotely sensed data for landslide monitoring.

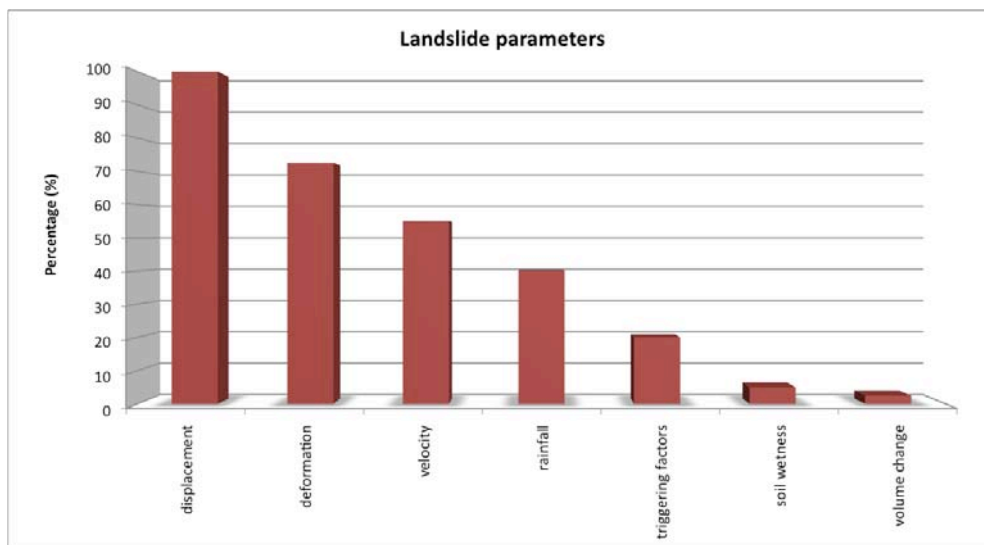
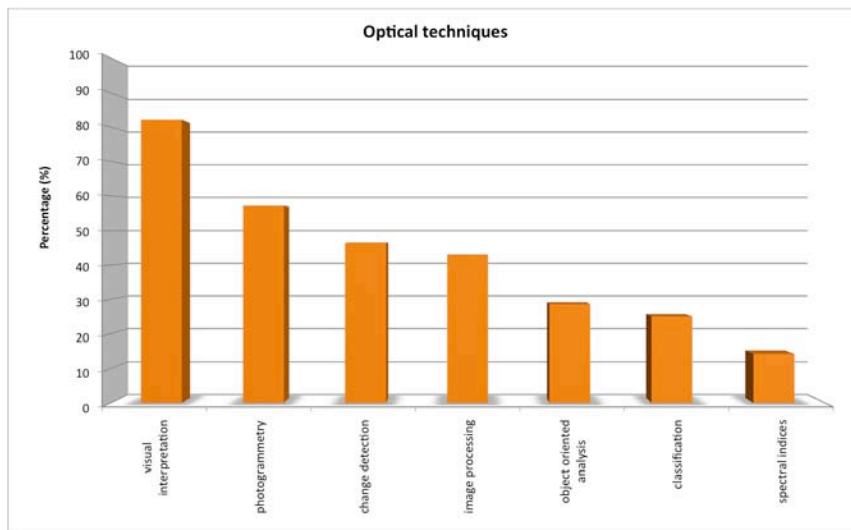


Figure 44. Landslide monitoring factors detectable with remote sensing.

Concerning the optical imagery the visible and multispectral ranges are the most reported, both of them with a percentage of 62%. As for landslide detection and mapping, the more frequent optical techniques are visual interpretation, photogrammetry and change detection (Figure 45).



**Figure 45. Optical techniques for landslide monitoring.**

In the field of radar imagery the A-DInSAR technique is the most used (67% of the answers) followed by D-InSAR (40%) (Figure 46). Concerning radar bands the 85% of the compilers use C band.

Monitoring with remote sensing is common for slides (rotational and translational) with 100% of the answers. The 60% of the users have indicated also the flows while the monitoring of lateral spreads, falls and topples is less common (Figure 47). The most recurrent velocities of the monitored landslides range from extremely slow to very slow (respectively 68% and 70% of the users). Slow movements are monitored by the 46% of the users.

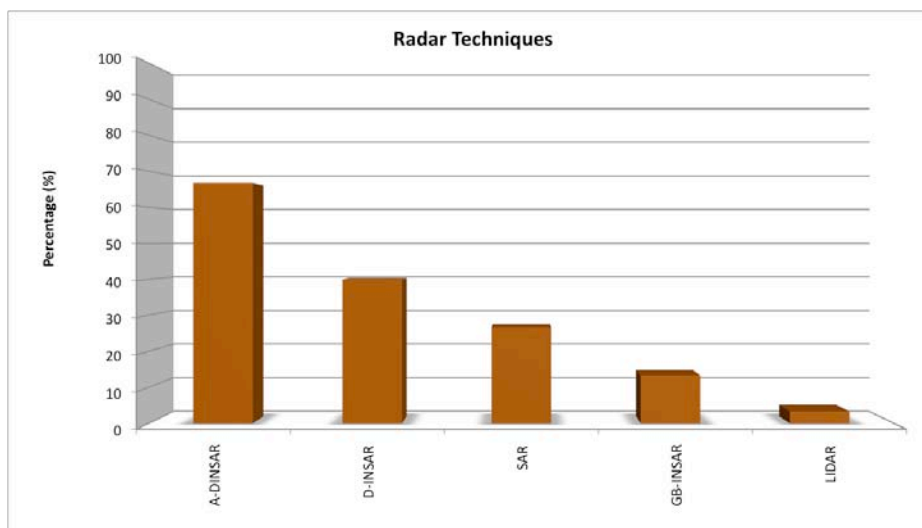


**Figure 46. Radar techniques for landslide monitoring.**

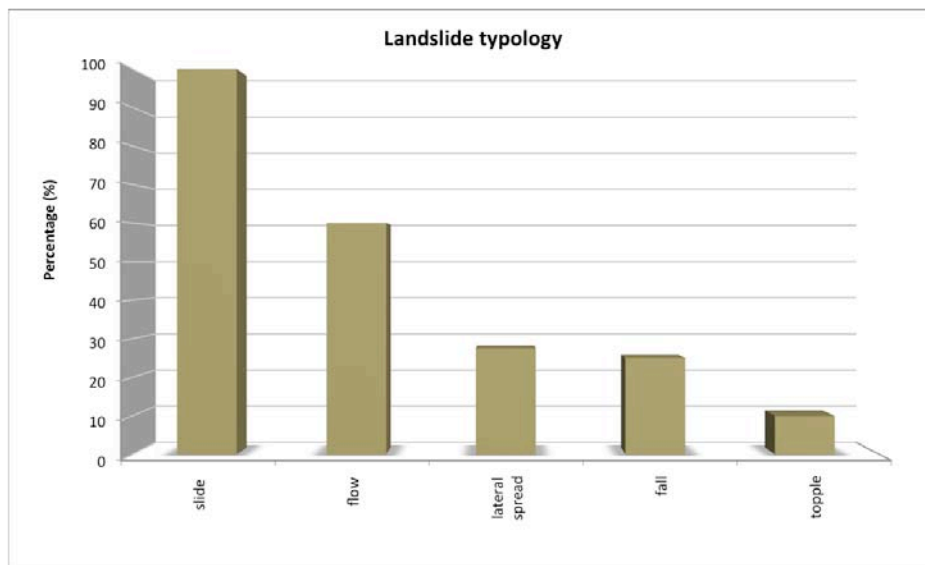


**Figure 47. Type of landslides detectable through remote sensing.**

In landslide monitoring the most common scale of analysis is the same adopted also for landslide detection and mapping (large: 1:25000- 1:5000), followed by the detailed scale.

The integration of remote sensing data with ground-based monitoring data is common. Among the ground-based techniques the most used are GPS (81%), LIDAR TLS (67%), Inclinometer (67%), GB-InSAR (64%), Total Station (50%) and Wire extensometer (50%) (Figure 48).

The integration with other thematic data is common as well, especially with geological maps, landslide inventory maps and DTMs and derived maps (Figure 49).

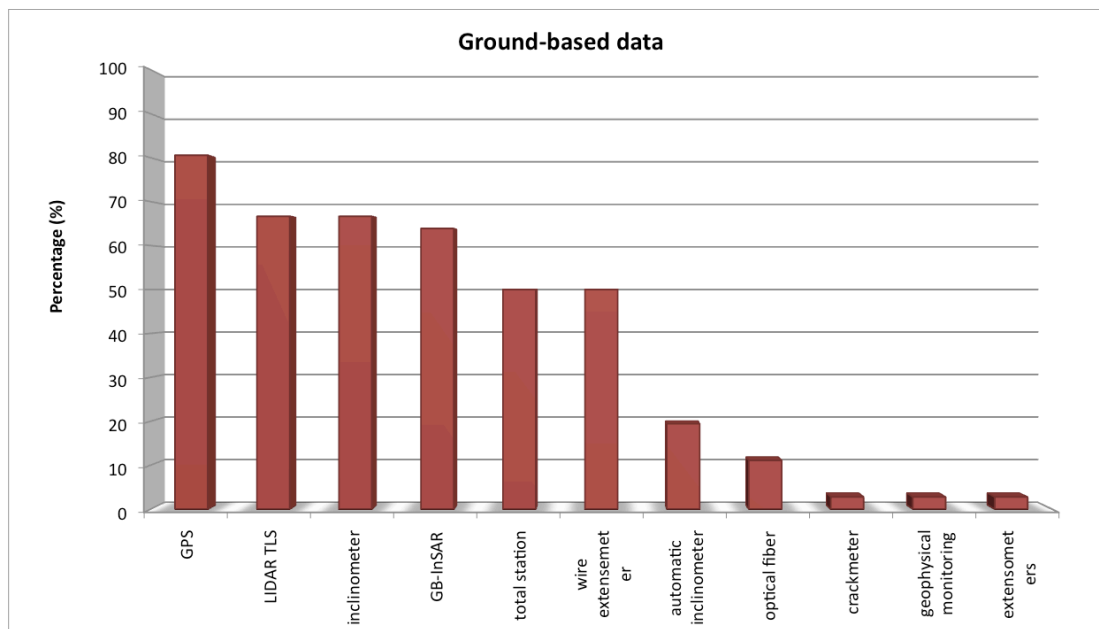


**Figure 48. Integration of remote sensing data with ground-based monitoring data.**

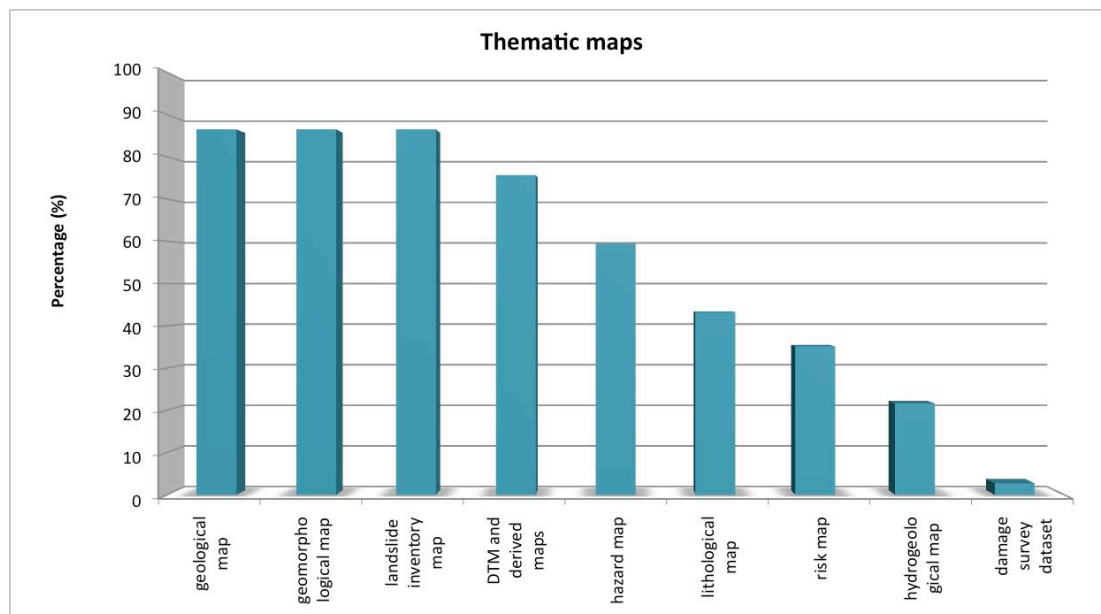


**Figure 49. Integration of remote sensing data with other thematic data.**

The monitoring duration is variable from a few weeks to some decades. This wide range is closely related to the used technique (i.e. few days-weeks for GB-InSAR, 1-2 years with TLS, decades for optical photos and satellite images surveys, depending, in this latter case, on the archives), of type of landslide and obviously on the landslide mechanism and velocity. Main reasons for the interrupting of monitoring are due to budget and fund problems. Temporary interruptions are caused by meteorological conditions (i.e. snow cover for both ground based and airborne techniques) and hardware malfunctions. Moreover, monitoring may be stopped after several years of inactivity of the landslide.

## 5.5 DISCUSSION AND CONCLUSIONS

The presented study evaluated the applicability of remote sensing for landslide detection and mapping and for landslide monitoring. This study was based on the evaluation of the answers to a questionnaire prepared as a Google form with multiple choices questions. The answers came from 21 countries all over the world.

In section 5.3 and 5.4 the results of the questionnaire are reported. In general it was observed that landslide detection and mapping is mainly made with aerial photos, often associated to optical and radar imagery. Concerning landslide monitoring the satellite radar prevails on the other types of data.

Both the detection/mapping and the monitoring of landslides concern slides, flows and lateral spreads. Rarely other types of movements (falls, topples) are mentioned. The scale of analysis is usually the large scale (1:25000- 1:5000).

All the compilers reported that detection/mapping and monitoring are performed integrating the remote sensing data with other thematic data, mainly geological maps, DTMs and derived maps and landslide inventory maps.

The users' evaluation of the effectiveness/reliability of remote sensing for landslide detection and mapping and landslide monitoring is reported in Figure 50 and Figure 51.

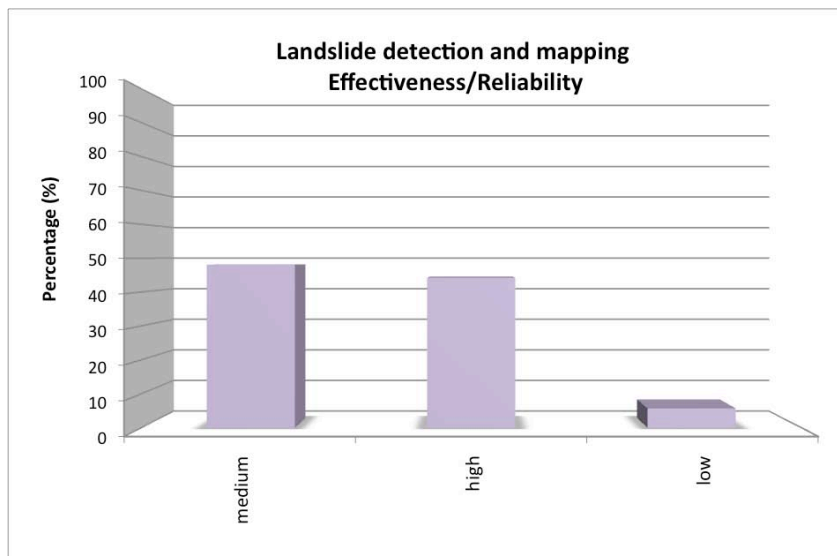


**Figure 50: Remote sensing effectiveness/reliability in landslide detection and mapping.**

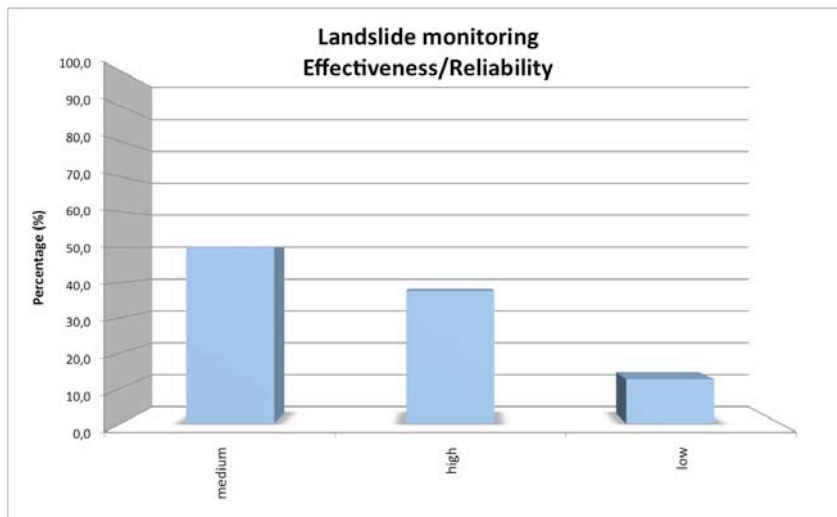


**Figure 51: Remote sensing effectiveness/reliability in landslide monitoring.**

Concerning landslide detection and mapping the degree of effectiveness/reliability was considered medium by 48% of the users, high by 46% of the users and low by 6% of the users (Figure 52), while for landslide monitoring the degree of effectiveness/reliability was considered medium by the 50% of the users, high by 38% of the users and low by 12% of the users (Figure 53). A certain degree of subjectivity in these answers can be considered as a weak point in the analysis since the answers were provided by people with different expertise and backgrounds.

Concerning the effectiveness, it has been observed that increasing the number of remote sensing type of data (aerial photos, satellite optical, satellite radar etc) used by the compilers, there is an increase in the effectiveness/reliability of the remote sensing for landslide study. In particular, concerning the landslide detection and mapping (Figure 52), it can be noted that the degree "low" disappears when more than two different type of data are considered. Consequently the degrees "medium" and "high" increase. Concerning landslide monitoring

(Figure 53), the high degree of effectiveness/reliability increases if the number of data increases

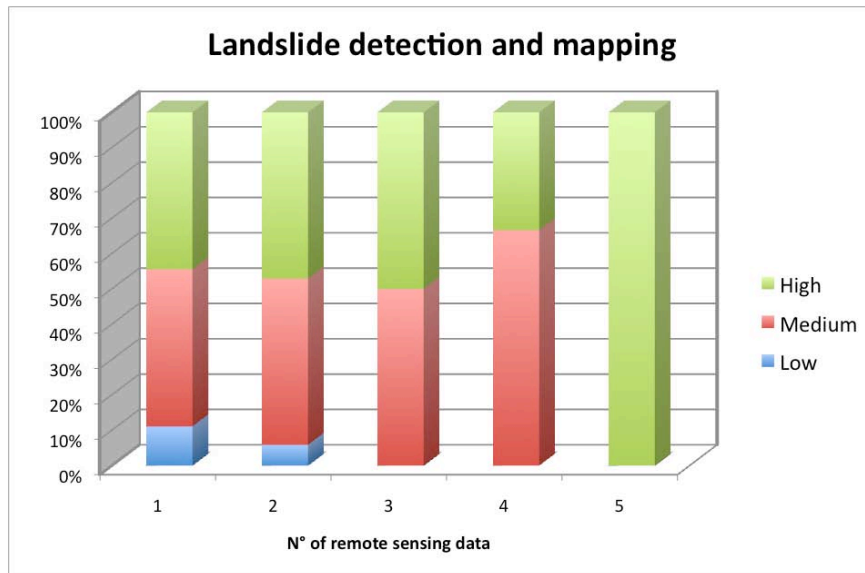


**Figure 52: Effectiveness/reliability of remote sensing in landslide detection and mapping versus the number of remote sensing type of data.**

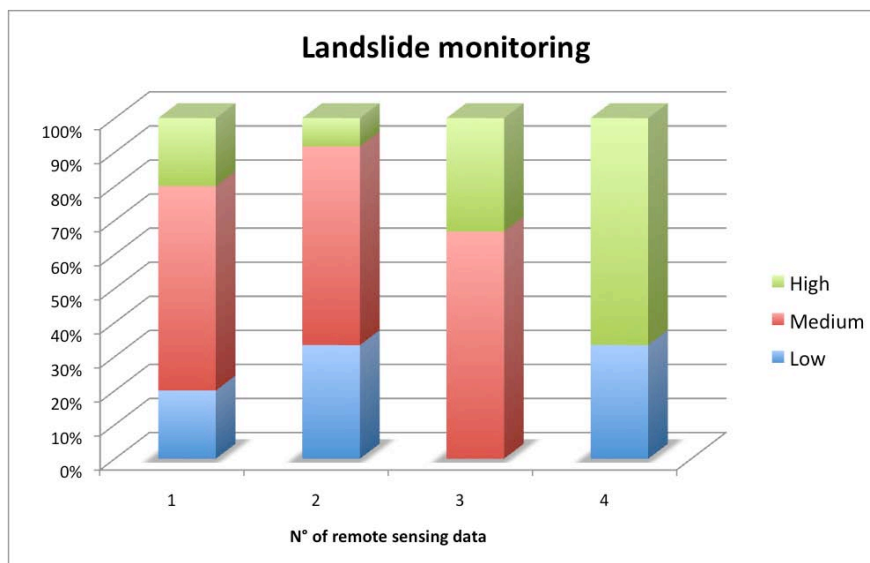


**Figure 53: Effectiveness/reliability of remote sensing in landslide monitoring versus the number of remote sensing type of data.**

In general the number of remote sensing techniques (both optical and radar), is proportional to the number of parameters detectable through remote sensing. In Figure 54, concerning landslide detection and mapping, it can be observed that the increase in the number of techniques used is related to an increase in the number of parameters measured. This behaviour can be recognized also for landslide monitoring (Figure 55). Obviously this behaviour would be clearer if the numbers of answers was higher.

The results of the questionnaire represent an interesting picture on the use of remote sensing in landslide study nowadays. However, in order to have more sound results and to give a general overview of the procedures and methodology currently in use at the world level, it's necessary to enlarge the number of answers, especially outside Europe.

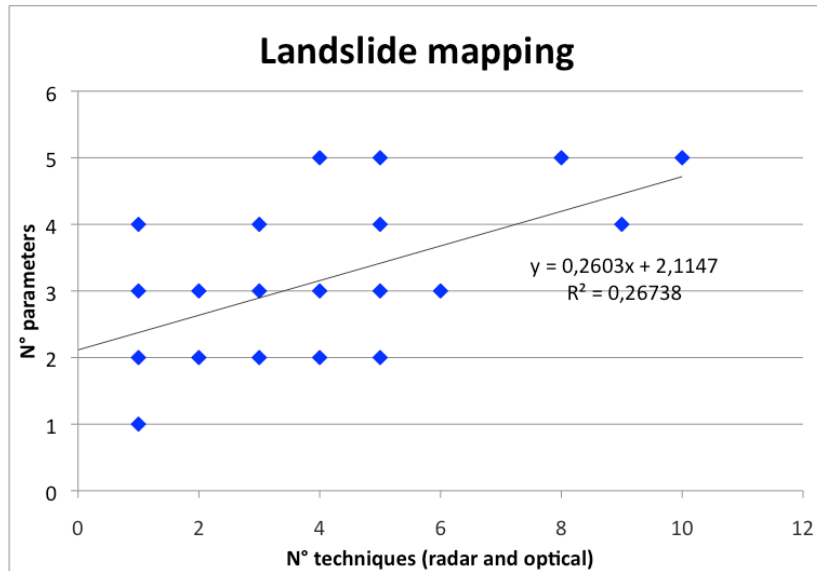


Figure 54: Number of techniques (radar and optical) versus the number of parameters.

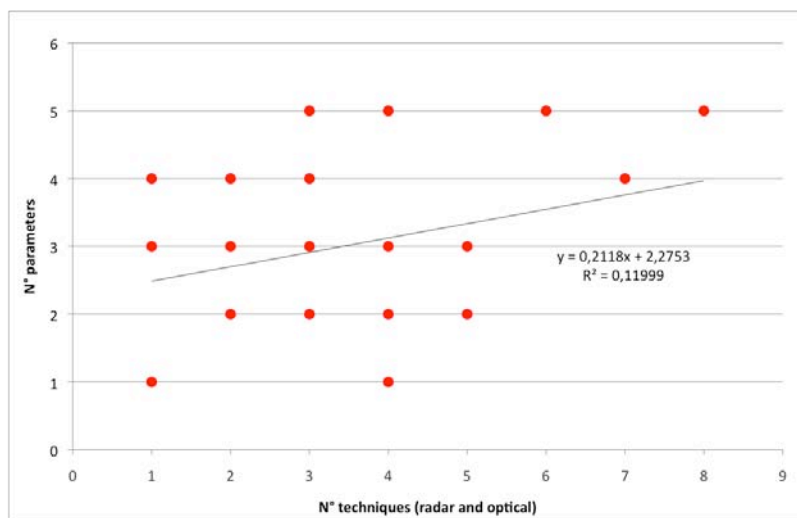


Figure 55: Number of techniques (radar and optical) versus the number of parameters.

## 6 OUTCOMES FROM SAFELAND PROJECT TEST CASES

This chapter highlights the new technical developments achieved in the framework of the Safeland project, including technical or scientific improvements and making reference to Safeland case studies.

The chapters 6.1 and 6.2 will include the contributions related to ground-based and airborne/spaceborne techniques, respectively.

Table 2 summarizes the content of each sub-chapter, highlighting the main improvements achieved by each technique in the selected SafeLand case study.

**Table 2: Main improvements achieved within SafeLand case studies.**

Chapter	Technique	Case study	Main improvements with respect to previous applications
6.1.1	GPS	La Valette landslide Villerville landslide (France)	Development of a specific landslide-focused script for the automatic collection, storage, processing and visualization of GPS observations. Displacement rates with an accuracy of 0.5-1.0 mm (horizontal component) and 1.0-2.0 mm (vertical component). It allows a day+1 data processing.
6.1.2	Borehole wire extensometers	Vallcebre landslide (Spain)	Towards an early warning system: - Telematic transmission of the wire and water level data (GSM modem) - Water pressure and velocity reactivation thresholds Cross checking of the results obtained with emerging techniques (calibration of spaceborne DInSAR; validation of GBSAR results)
6.1.3	Automatic inclinometer (DMS column)	Bagnaschino (Italy)	Early warning system (thresholds) + real time monitoring during the events + at different depths Perspective of long term monitoring (fully operational during/after displacements)
6.1.4	GB-InSAR	Castagnola (Italy)	Demonstration of the applicability as an effective real time monitoring and early warning tool. Use of GB-InSAR for -evaluating the possible landslide evolution -defining deformation thresholds
6.1.5	TLS	Aknes rockslide (Norway)	Application of the roto-translation matrix technique: -Complete 3D movement of each compartment (displacement + type of movement) -Interpretation of the movement in terms of landslide mechanism (rotation, translation...) -Complex rockslide mechanism model

6.1.6	Terrestrial optical images correlation	Super-Sauze (France)	First time application of this newly developed methodology
6.1.7	Micro-seismic monitoring	Super-Sauze (France)	First application in soft-rock landslides: quantitative characterization of the type of seismic signals within a mudslide; location and characterization of their sources
6.1.8	Optical fibres and TDR	Experimental flume	Demonstration of the potential effectiveness in geotechnical monitoring
6.1.9	Geoelectric monitoring	Gschliefgraben	One of the first known cases where geoelectric and high resolution differential displacement monitoring were coupled for several years. It was demonstrated: -reliability of the method for long term monitoring. -long term stability of geoelectrical parameters and their response to changes in the hydrological system of the landslide.
6.2.1	OLS (Offshore Laser Scanning)	Sundalsøra (Norway)	New technique Compared to Aerial Laser Scanning (ALS), OLS provides more points with a better resolutions for sub-vertical planes
6.2.2	Satellite optical (detection and mapping)	Various (Haiti – China – Italy – France)	Workflow combining object-oriented image analysis with a modern machine learning algorithm (Random Forest)
6.2.3	Satellite radar (detection and mapping)	Liri-Garigliano and Voltorno basins (Italy)	Implementation of original procedures based on the merging of DInSAR data with simple geomorphological models and geometric considerations: -A priori visibility map (information on the applicability of DInSAR data to slow-moving landslide detection and mapping in certain regions) -Advanced landslide velocity map (further step towards the quantitative interpretation of remote sensing data)
6.2.4	Airborne geophysics (detection and mapping)	Stoze	Application of the multi-parameter airborne geophysics in a site specific study. Demonstration of the feasibility with good results (even if at high costs).
6.2.5	Airborne geophysics (detection and mapping)	Schnepfau (Austria)	-Innovative layout of survey lines to get high quality data in rough topographic conditions in a wide area -First time application of gamma ray to

			generate conceptual soil maps for landslide susceptibility mapping
6.2.6	Airborne frequency domain EM mapping	Gschlifgraben (Austria)	Quick determination of low resistivity areas. Use of passive microwaves as indicator of active mass movements. Content of radioactive elements was related to the original geological structure (and contributed to assess weathering degree and displacement). Information about the internal structure of the subsurface down to 30-70 m.
6.2.7	Airborne time domain EM monitoring	Aurland (Norway)	Use of the latest generation of helicopter borne time domain EM systems, combining the high penetration depth of time domain systems with the high resolution and versatility of a helicopter system.
6.2.8	Airborne geophysics (monitoring)	Sibratsgfall (Austria)	In 2001 the first airborne survey in Austria for natural hazard mitigation was carried out. In 2009 the survey was repeated in frame of the SafeLand project in order to make use of the technological innovations of the last 8 years. The flight direction was changed from the original 2001 plan to make minimum sensor clearances possible.
6.2.9	Satellite radar (monitoring)	La Vallette (France)	Use of high resolution SAR imagery produced by recently launched platforms. <ul style="list-style-type: none"> <li>- Same precision of satellite optical (sub-metric resolutions)</li> <li>- Not affected by weather conditions</li> <li>- Short revisiting time (week to month)</li> </ul>

## 6.1 GROUND BASED TECHNIQUES

### 6.1.1 GPS: La Valette landslide and Villerville landslide (France)

CNRS : Malet J.-P., Masson F., Ulrich P., Déprez A.

#### 6.1.1.1 Study areas

The SafeLand case studies for the evaluation of the capability of permanent GPS to monitor landslide displacements in near-real time are the La Valette landslide (South French Alps) and the Villerville landslide (Normandy coast, North-West France).

#### La Valette landslide

The La Valette landslide, triggered in 1982, is one of the most important large and complex slope movements in the South French Alps. The landslide associates two styles of activity: a mudslide type of behaviour with the development of a flow tongue in the medium and lower part, and a slump type of behaviour with the development of several rotational slides in the upper part at the main scarp. The landslide extends over a length of 2 km for a variable width of 0.2 km in the lower and medium parts, to 0.45 m in the upper part (Figure 56). The maximum depth, estimated by seismic and electrical resistivity tomography and geotechnical boreholes, varies from 25 m in the lower and middle parts (Evin, 1992; Travelletti et al., submitted) to 35 m in the upper part (Le Mignon, 2004). The volume of the mudslide body is estimated at  $3.5 \cdot 10^6 \text{ m}^3$ .

From a geological viewpoint, the La Valette landslide is located at the tectonic contact between two major geological formations (Figure 56a):

- an autochthonous formation represented by the closely stratified Callovo-Oxfordian black marls (e.g. “Terres Noires”);
- an allochthonous formation represented by two sheets thrusts and in which the upper part of the landslide has developed.

From a hydro-geological viewpoint, the tectonic discordance has an important role on the landslide mechanism creating a contrast of permeability between the black marls and the flysch conditions, and the spatial occurrence of several springs and marshy areas at the direct vicinity of the tectonic discordance between the elevation 1870 m and 1950 m (Figure 56 a, b). According to Le Mignon (2004), a spring (the “Rocher Blanc” spring at 1900 m) is currently partially buried by the landslide. Consequently a deep water circulation affects the hydrological regime of the upper part of the landslide but the characteristics of the water flows (fluxes, quality) are unknown.

The landslide exhibits a complex style of activity in space and time. It has developed first as a rotational slide affecting the Autapie sheet thrust. The failed mass has progressively loaded the underlying black marls formation, and the landslide has developed by a series of rapid mudflows triggered in the marls such as in March 1982, April 1988, March 1989 and March 1992. The most important crisis occurred in 1988 when a mudflow of  $50.000 \text{ m}^3$  triggered at the elevation of 1400 m flows over a distance of ca. 500 m (Colas et Locat 1993). Up to now, these mudflows did not mobilize the complete failed mass.

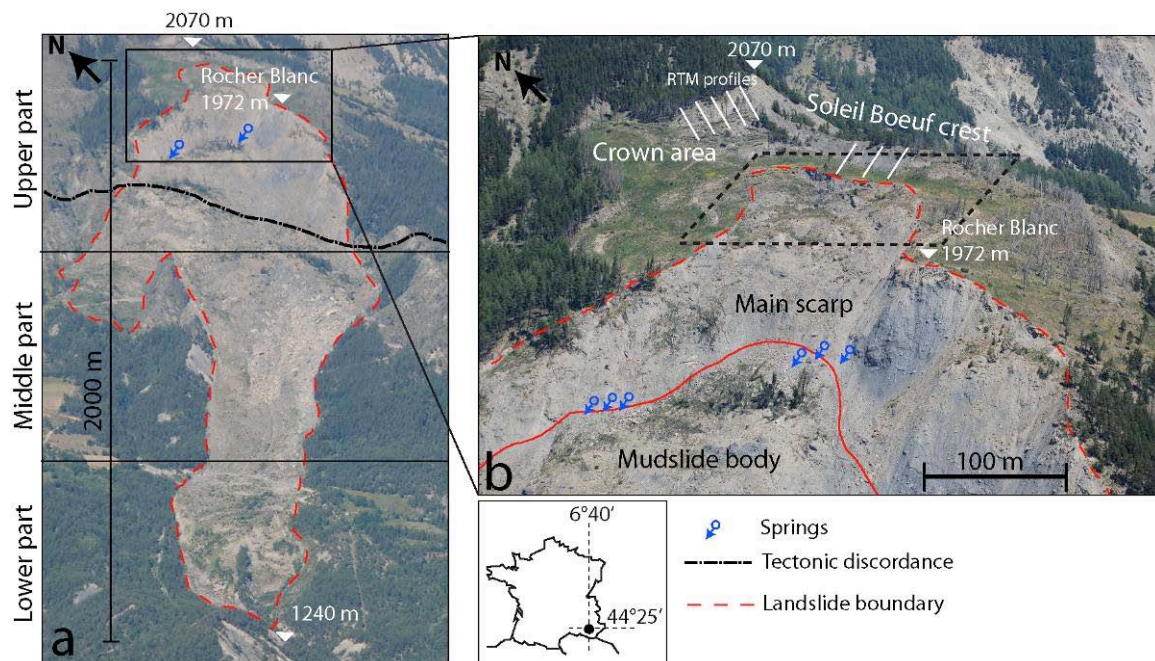


**Figure 56: Geomorphological setting of the La Valette landslide on the South-facing slope of the Barcelonnette basin. a) General view of the landslide to the North East. b) View of the main scarp and the crown areas; the dashed line delimitates the area investigated by TLS and seismic tomographies. The displacement profiles measured by the “Restauration des Terrains de Montagne” (RTM) office to monitor the retrogression of the crown are also indicated.**

The displacements are monitored in continuous with topometric benchmarks since 1991 (Squarzoni et al. 2005), differential dual-frequency GPS (Déprez et al. submitted) and an extensometer since 2008, and at regular periods by digital correlation of satellite images (Le Prince et al., 2007) and satellite radar interferometry (Squarzoni et al., 2003).

### Villerville landslide

The ‘Cirque des Graves’ and the ‘Fosses du Macre’ landslides, located nearby the municipality of Villerville (Normandy, France) are slow-moving rotational and translational coastal landslides characterized by surface displacement of a few cm per year. The landslides are located on the high cliffs of the Pays d’Auge plateau (up to 140 m, Figure 57 and Figure 58). Both landslides cover approximately 8 ha surrounding the village of Villerville. Both can be defined as active, slow-moving, rotational landslides.

The morphology is typical of rotational landslides with successive sliding blocks, often with counter slopes, separated by scarps of several decimetres to meters high. The oldest scarps are completely hidden by vegetation and/or modified by human intervention (Flageollet and Helluin, 1987) and correspond to the Cenomanian chalk panels (Figure 59) sliding on the Albian sands which overlay Kimmeridgian marls. The toe of the landslide is characterized by a chaotic morphology with shallow clayey flows overtopping sandy limestones.

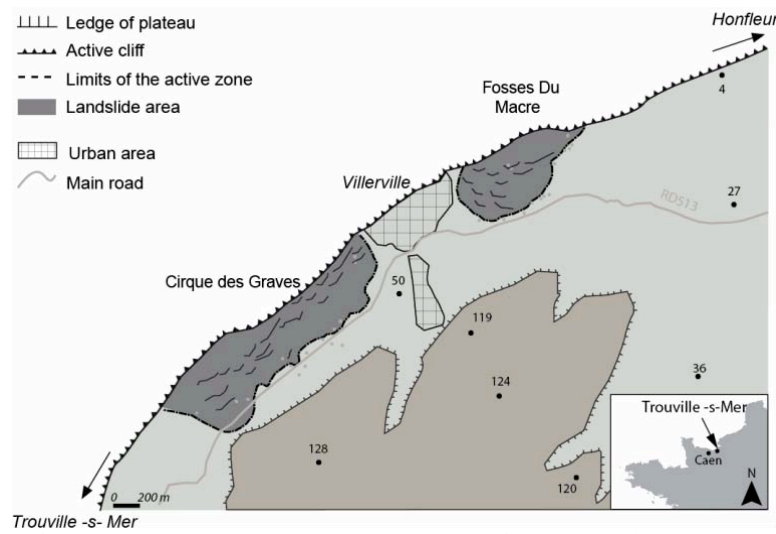


Figure 57: Location of the study area on the North-East part of the Pays d'Auge coast.

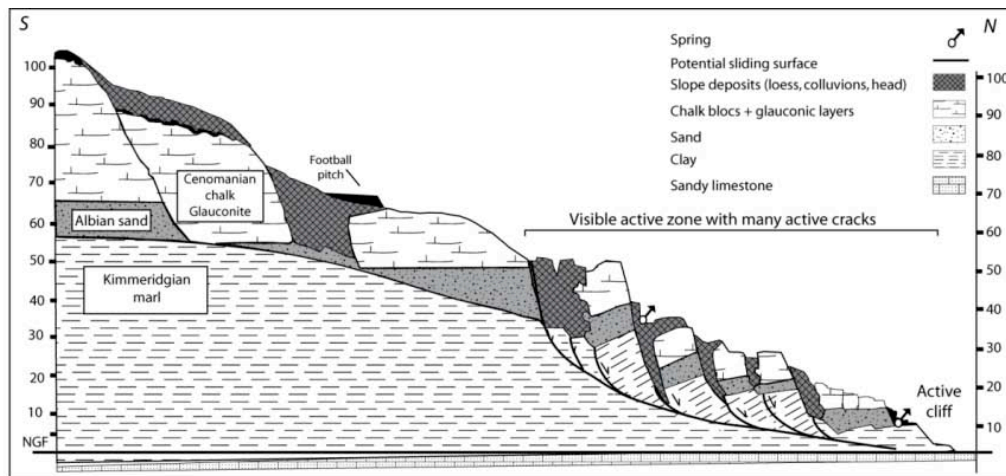


Figure 58. Aerial view of the landslides surrounding the municipality of Villerville, North-East part of the Pays d'Auge coast.

The landslides are officially considered as active since an important reactivation that occurred in January 1982; however the slopes were not stable since the last two centuries though not major crisis has been identified (Ballais et al., 1984). Since the first major reactivation of 1982, the slopes are permanently affected by seasonal slow movement ( $0.05-0.10 \text{ m.yr}^{-1}$ ). Three other main acceleration occurred (February 1988, January 1995 and March 2001) in close relation with the hydro-climatic conditions.

These multiple phenomena have generated many new scarps of several meters high and tensile cracks which are still evolving. The principal part of the 'Cirque des Graves' landslide is affected by horizontal displacement rate between  $0.005$  to  $0.1 \text{ m/yr}$ . The toe of the landslides is affected by superficial failure and the development of muddy flows characterized by a high velocity (around  $1 \text{ m/yr}$ ). The whole mass is affected by a combination of superficial

and deep movements, including possible retrogression, enlargement or advancement of the limits of the landslide during major acceleration.



**Figure 59: Geological cross-section of the “Cirque des Graves” landslide detailing the slip surface and the slumping blocks.**

The permanent landslide activity generates important economical and physical damages (building perturbations and destruction) in this area where the land pressure associated to coastal tourism is increasing. For these reasons, the landslides have been progressively monitored since 1984 (Lissak et al., 2010).

Further information on the La Valette landslide and on the Villerville landslide can be found at: <http://eost.u-strasbg.fr/omiv/>

### **6.1.1.2 Description of the analysis**

In the framework of the Safeland case studies, the objectives of this work are (1) to present the permanent GPS monitoring system and data transfer system installed on several landslides in France, (2) to present the automatic processing of the data, and (3) to define quantitatively the contribution of permanent GPS observations for the fast detection of small displacements.

#### **Description of the GPS permanent monitoring system at the two landslides**

At the two landslides, three GPS receivers have been installed. The GPS data were acquired using TRIMBLE NetRS dual-frequency receivers equipped with TRM41249.00 antenna with a TZGD radome. Every day, a 30-second daily file (i.e. 2880 sessions) and 24 1-second hourly files (i.e. 3600 sessions) are produced. The data are stored locally and, within 1 day, a wireless access point allows the data transmission to a database and the processing. A communication problem does not cause data loss. The Figure 60 presents the installation on concrete pillars for the ‘stable’ base GPS (LVAL at La Valette, VLRV at Villerville) outside the landslides, and on rigid but still flexible iron-tripods for the ‘moving’ GPS (lva1, lva2 for La Valette; vlrh, vlrb for Villerville) within the landslides.

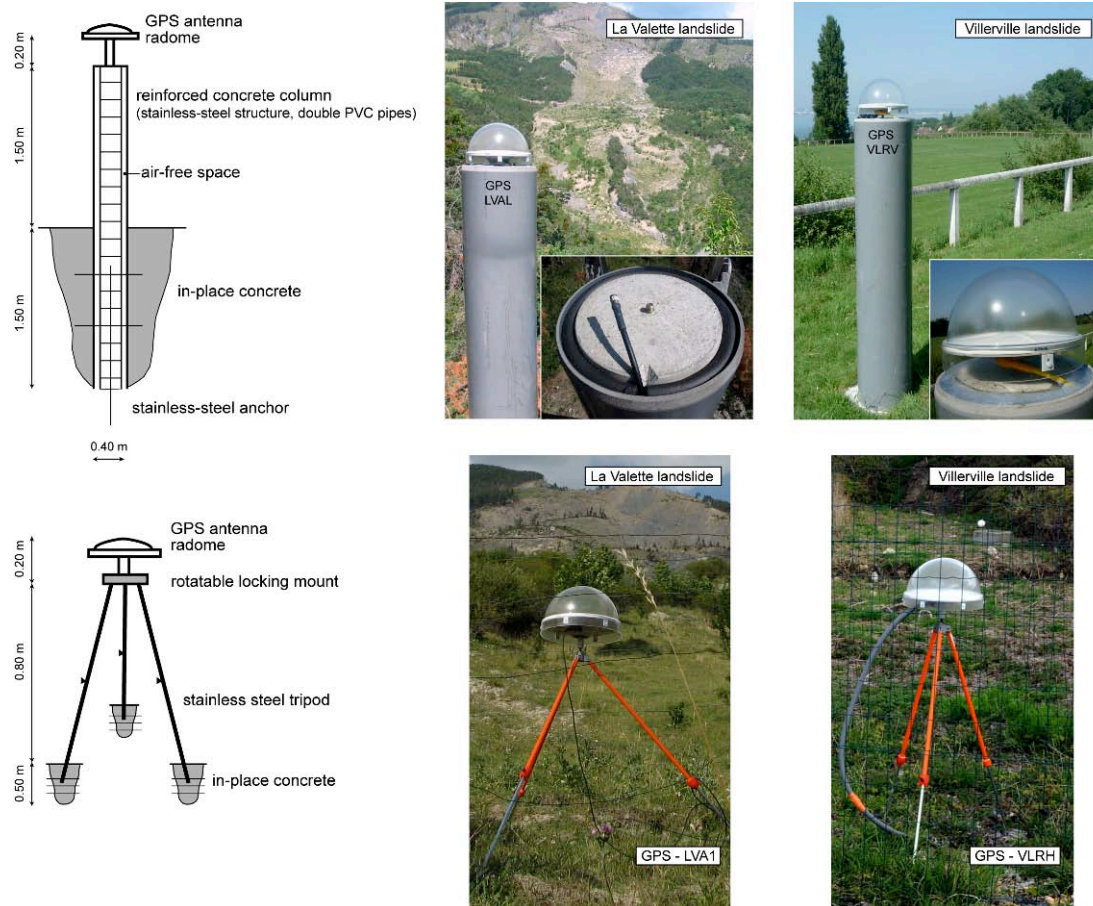


**Figure 60: GPS monitoring equipment installed on the Villerville and La Valette landslides.**

At Villerville, the three GPS are installed in the Eastern part of the landslide along a cross-section of ca. 450 m; the two moving GPS vlrh and vlrb are located nearby the sea on two different very active scarps (Figure 61 and Figure 62).

At La Valette, the base GPS is installed on a stable crest in front of the landslide, and the two moving GPS are located at respectively the toe (lva1) and the crown (lva2) of the landslide.

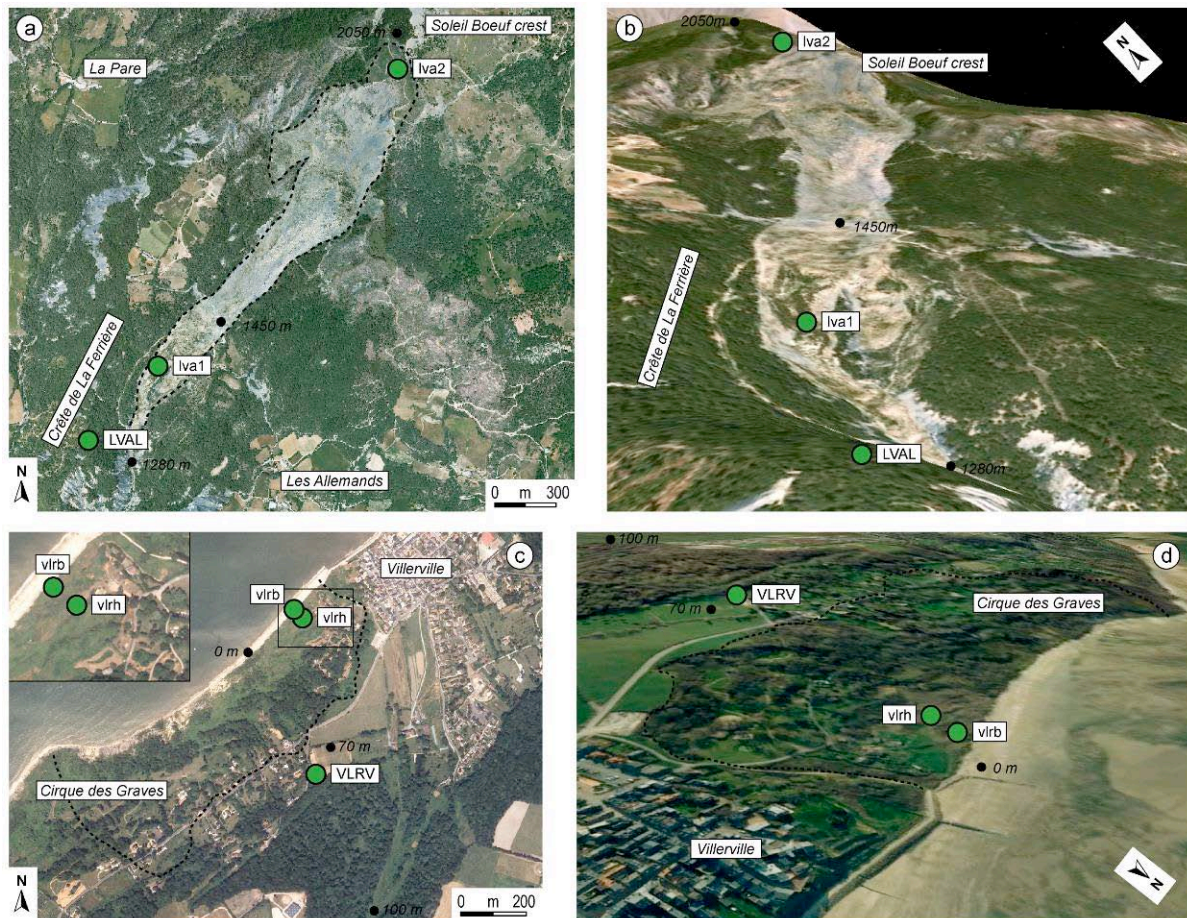


Figure 61. Location of the GPS monitoring equipment on the Villerville and La Valette landslides.

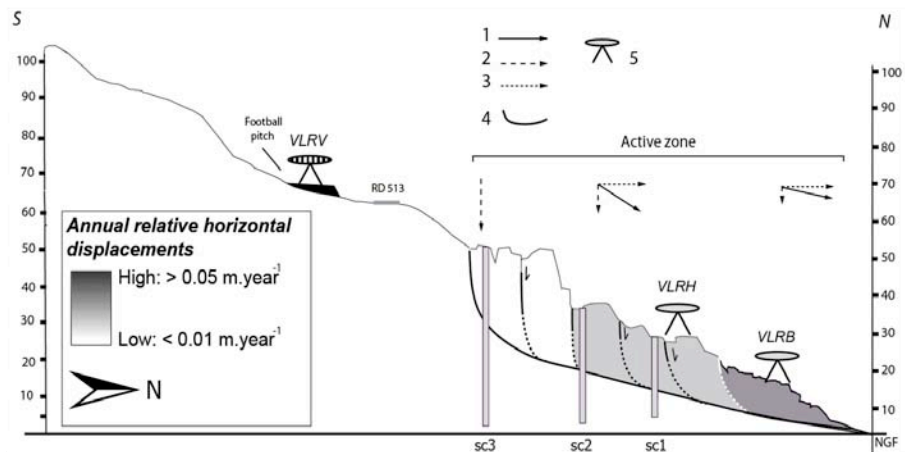


Figure 62. Displacement pattern and direction of movement observed at the Villerville landslide. The profile indicates the principal slip surface and the schematic displacement vectors at the surface: 1) Displacement vector measured by punctual GPS acquisitions, 2) Vertical component of the velocity vector, 3) Horizontal component of the velocity vector, 4) Slip surface, 5) Permanent GPS receiver.

### **GPS data processing**

The processing of the data has been performed following two main ideas: 1- the processing has to be as simple as possible in order to avoid heavy computations and 2- the precision of the results (i.e. the precision of the baseline from the GPS stations on the landslide to the GPS station on the bedrock) has to be better than the useful precision for modelling and/or for a warning procedure.

Data processing has been performed with GAMIT/GLOBK, an analysis package developed at MIT (Herring et al., 2003, 2003b). It is dedicated for the estimation of three-dimensional relative positions of ground stations and satellite orbits. A loosely constrained daily solution (H-) file of parameter estimates and covariances is the output of GAMIT. The GLOBK package combines the daily solutions to estimate station positions and velocities. Orbital and Earth-rotation parameters can also be estimated.

An automatic processing script (Figure 63) has been developed to obtain position of each station and monitor the landslide activity. Daily, the script runs thanks to a “crontab” program and integrates in the processing the more recent available GPS data to complete position and baseline time series. The geodetic coordinates (latitude, longitude and ellipsoid height) and baseline values are extracted from the output file of GLOBK (globk\_rep.prt). The geodetic coordinates are then converted to Lambert zone projection (North, East and altitude) using Circé, software developed by IGN (Institut Géographique National).

Two processing cycles of calculations are carried out: within two day by using the rapid orbits of International GNSS Service (IGS) and delayed of 30 days with the final ones. A test on a 100 days data sample showed that differences on baselines triggered by a processing with rapid orbits in comparison to the final ones were negligible, in the order of hundredth millimetres. The second step is nevertheless useful because it allowed updating the database with all RINEX files recorded. This two-step methodology overcame possible occasional broadcasting problems.

### **Identification of the best GPS data processing protocol**

Our objective is to evaluate baselines of hundreds meters with a very high precision, up to a few millimetres. The geometry of the GPS network processed and processing parameters were carefully chosen by performing numerous tests and bearing in mind that processing should be as simple as possible. A dataset of 175 days (slightly less than 6 months) acquired at the Villerville landslide has been used for the tests.

To check the stability of the results as a function of the GPS network, several network configurations have been designed (Figure 64):

- a European scale network of 6 international IGS stations, 8 French RGP stations and the 3 stations on the landslide;
- two regional networks, without the IGS stations;
- a local network, composed of only the 3 stations on the landslide and 4 RGP stations within a circle of about hundred kilometres.

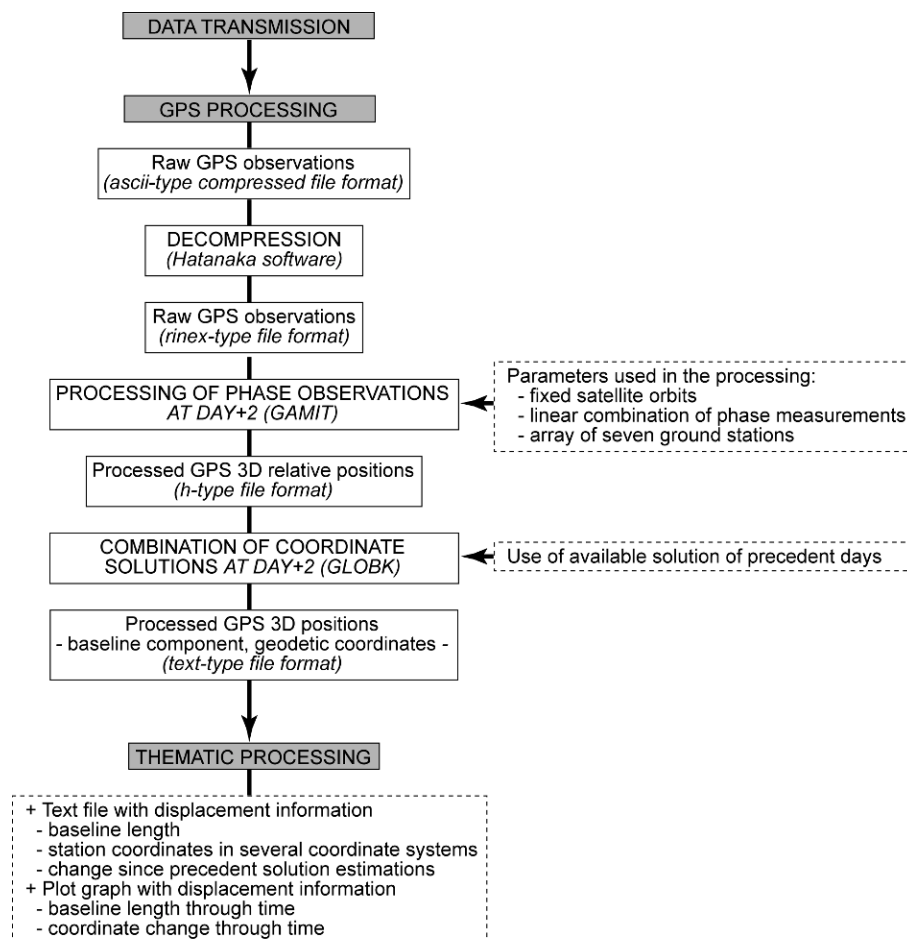


**Figure 63: Flowchart of GPS data automatic processing.**

The GPS observations have been processed with the GAMIT software (Herring et al., 2003a, b) which allows estimating position and orbiting parameters. The estimation of orbiting parameters needs the introduction into the processing of data from GPS stations far from the studied area (a European scale network is needed; e.g. Figure 64). This makes the processing more cumbersome without providing better accuracy on baselines (Figure 65). Therefore we preferred to use a strategy without reassessment of the orbits (Baseline option in GAMIT). The only position calculation requires only the introduction of some additional regional GPS stations. Because of the distance between the regional stations, using a linear combination of the two frequencies L1 and L2 is necessary to relieve ionospheric delay (LC-AUTCLN option in GAMIT).

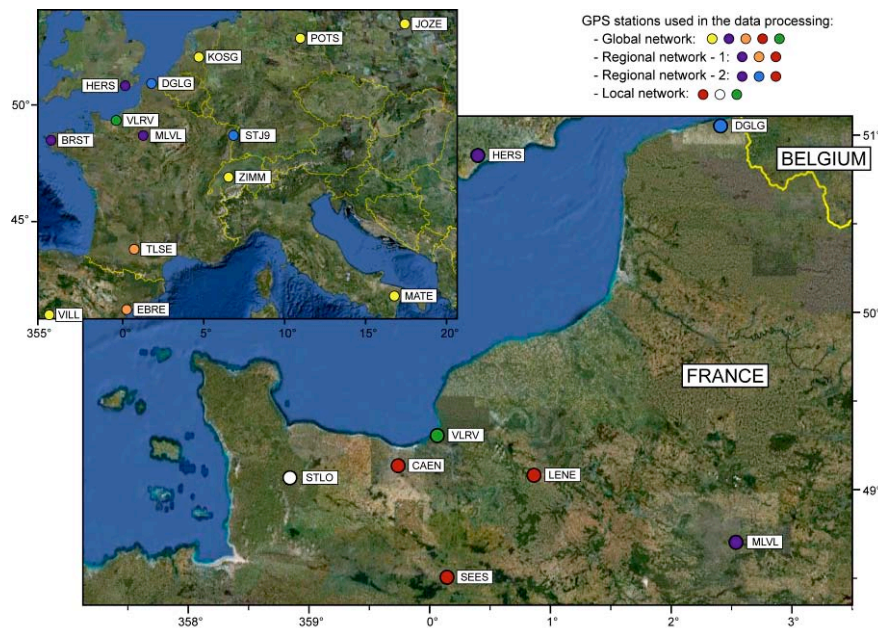


**Figure 64. Map of different networks used for the Villerville landslide data processing. Global network consisted in IGS stations (yellow stars: JOZE, MATE, POTS, KOSG, ZIMM, VILL), RGP stations (violet stars: MLVL, BRST, HERS, orange stars: TLSE, EBRE, rose stars: CAEN, LENE, SEES) and Villerville stations (VLRV). The first regional network is composed of violet, orange and red RGP stations without STLO and Villerville stations. The second regional network is composed of violet, blue and red RGP stations without STLO and Villerville stations. The local network chosen for the automatic processing consisted in rose stations.**

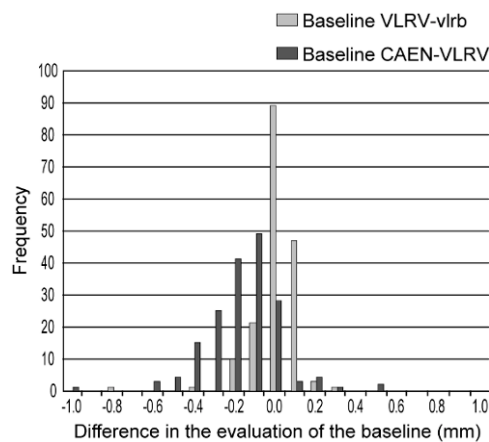


**Figure 65. Comparison of the baseline evaluations within a global network and with using fixed or not orbital parameters. The processing using an orbital parameter evaluation requires downloading additional data. The CAEN-VLRV baseline is about 50 km long and the VLRV-vlrb baseline (the longest baseline on the landslide) is about 450 m long. Standard deviation of 0.18 mm for CAEN-VLRV baseline and of 0.11 mm for VLRV-vlrb baseline.**

Figure 66-Top shows the differences for the global and regional networks. They are close to 0 and without bias for the baseline on the landslide (VLRV-vlrb), slightly larger and with a small bias for a longer baseline (CAEN-VLRV). Even if the differences are slightly higher, the same result is globally observed for the global and local networks (Figure 66-middle). The evaluations of local baselines within two different regional networks were almost the same whatever the network configuration around the landslide (Figure 66-bottom). With the local

network, evaluations are made with each station successively omitted. The differences observed on local baseline values are of a few tenth millimetres.

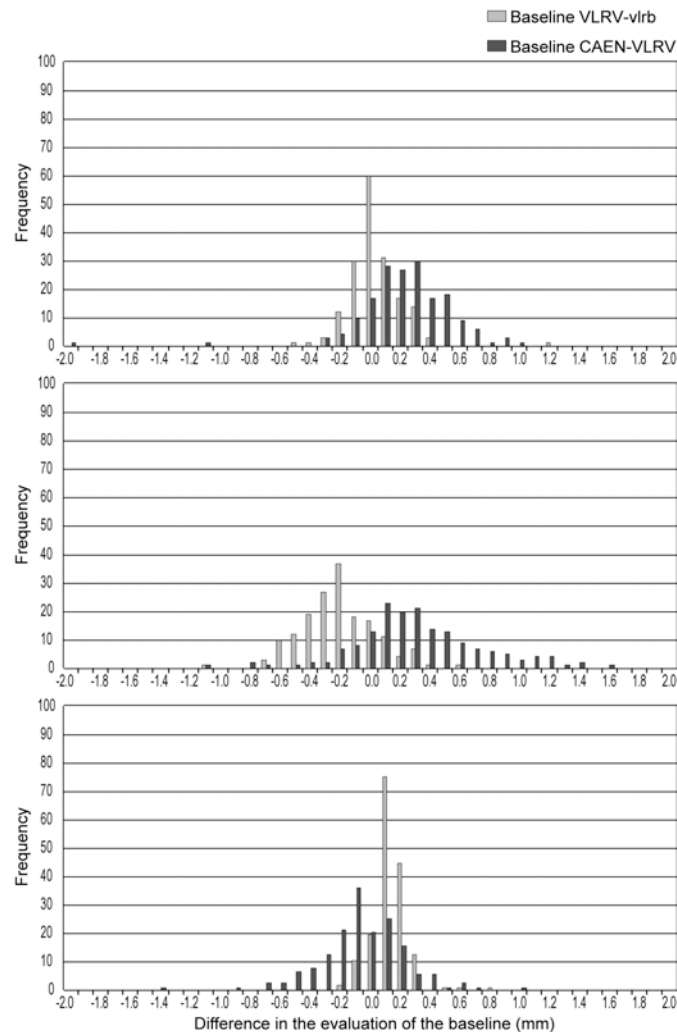


**Figure 66. Top - Comparison of the baseline evaluation with a global network and a regional one. Standard deviation of 0.26 mm for CAEN-VLRV baseline and of 0.18 mm for VLRV-vlrb baseline. Middle - Comparison of the baseline evaluations with a global network and a local one. Standard deviation of 0.47 mm for CAEN-VLRV baseline and of 0.25 mm for VLRV-vlrb baseline. Bottom - Comparison of the baseline evaluations with two different regional networks. Standard deviation of 0.30 mm for CAEN-VLRV baseline, of 0.19 mm for VLRV-vlrb baseline, of 0.23 mm for VLRV-vlrb baseline, of 0.12 mm for vlrb-vlrb baseline.**

These results are confirmed by the time series. The value of the VLRV-Vlrb time series computed using a global, a regional and a local network are indicated on Figure 67. Differences are always smaller than 1 mm, and generally smaller than 0.5 mm.

From these results, a processing protocol with a local network and 24h sessions has been defined. It is composed of 7 stations to avoid a lack of result in case of technical problem on one or two stations (antenna breakdown, broadcast problem...). The quality of this processing is in agreement with the requested accuracy. The script allows the data collection and storage, the data processing and the visualization of the results in graphs and text files which are updated daily. Daily, the figures and the text-files generated by the automatic processing are

sent by e-mail. The latter contains also a synthetic file of the latest data: baseline values, station coordinates, the observed differences between the position of the previous day and the first evaluation.

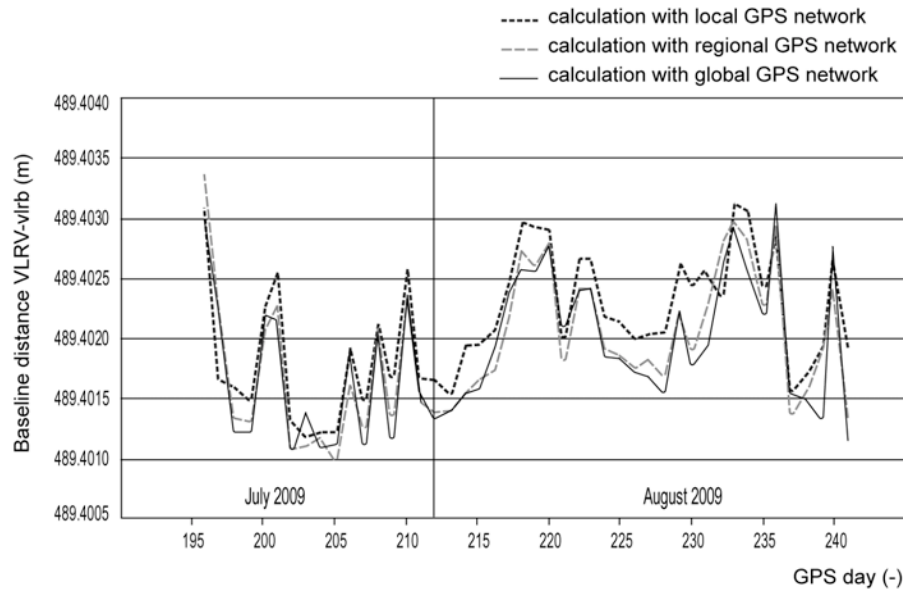


**Figure 67. Temporal variations of the VLRV-vlrh baseline within different networks.**

### Interpretation of the results

The observed displacement rates and the spatial variations of the velocity within the landslides are in accordance with previous knowledge on the sites. For instance, at Villerville, several acceleration periods are observed for the two ‘moving’ GPS stations in 2010. For the February acceleration, vlrh began to record a displacement about two days after the vlrh station recording. A displacement lag time of about 2 or 3 days between the stations (Figure 68) can be explained by a required lag time between the two nested chalk panels to move downstream one after another.

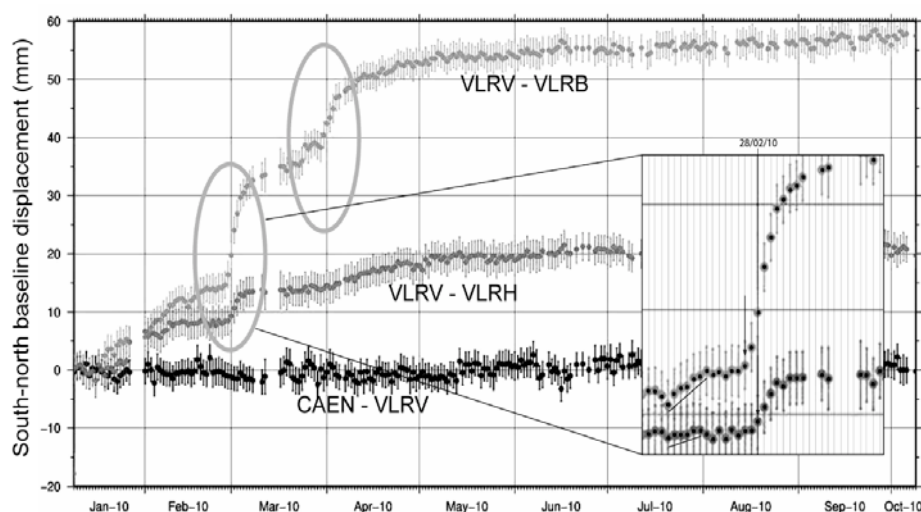


**Figure 68: GPS baselines between VLRV (local reference station) – Caen (regional reference station, and VLRV-vlrh; VLRV-vlrh since January 2010. The baseline VLRV – CAEN allows to determine the accuracy on the GPS solutions, which is estimated at ca. 0.05 cm in all directions.**

At the end of March, an acceleration of about 0.01m of displacement was observed only for the vlrb station. The station is located on the landslide toe which is directly in contact with the sea during high tides. A few days before the vlrb acceleration, the tidal coefficients were high. During the same periods South-North winds were recorded with a speed of 30-35 km.h<sup>-1</sup> (Figure 69).

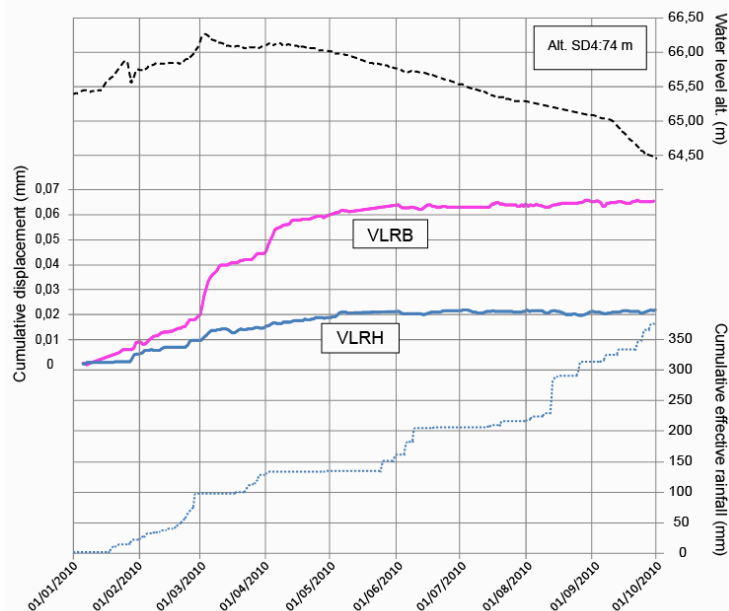


**Figure 69: Cumulated horizontal displacements of vlrb and vlrh stations and observed rainfall between July 2009 and August 2010.**

After one year of a continuous GPS survey, an approximate critical water level threshold about 65.90 alt. at piezometer SD4 correlated can be estimated.

### ***6.1.1.3 Improvements with respect to previous applications***

The expected improvement comes from the development of a specific landslide-focused script for the automatic collection, storage, processing and visualization of GPS observations and baseline distances and coordinates from permanent GPS receivers installed on landslide. The processing protocol is kinematic and is designed to characterize the displacement rates with an accuracy of 0.5 to 1.0 mm for the horizontal component and 1.0 to 2.0 mm for the vertical component. It allows a day+1 data processing.

## 6.1.2 Borehole wire extensometers, Vallcebre (Spain)

UPC: Gili J., Corominas J., Moya J.

### 6.1.2.1 Study area

According to Corominas et al. (2005) the Vallcebre landslide is a large, active slope failure located in the upper Llobregat river basin, in the Eastern Pyrenees, 140 km north of Barcelona, Spain (Figure 70).



Figure 70. General view of the Vallcebre landslide (Eastern Pyrenees, Spain).

The mobilised material consists of a set of shale, gypsum and claystone layers of continental origin gliding over a thick limestone bed, all of which are of Upper Cretaceous – Lower Palaeocene age. The slide mass is 1200 m long and 600m wide. The entire landslide involves an area of 0.8 km<sup>2</sup> that shows superficial cracking and distinct ground displacements (Figure 71).

The age of the landslide has not been determined but it is known to have been active for several centuries at least. From a geomorphological point of view, the Vallcebre landslide is of a translational type. A longitudinal profile shows a stair shape with three main slide units of decreasing thickness towards the landslide toe (Figure 72).

Each unit is formed by a gentle slope surface bounded in its downhill edge by a scarp of a few tens of meters high. At the base of each scarp an extension area develops in the form of a graben. This fact is interpreted as the lower units moving more rapidly than upper ones, which has been confirmed by the monitoring network installed. The average slope of the landslide is about 10°. Most of the evidence of surface deformation is situated at the boundaries of the slide units in the form of distinct shear surfaces and tension cracks. At the base of each transverse scarp, both the ground surface and the trees are tilted backwards due to the development of a graben along with a slight rotation of the head. In contrast, within the units, the ground surface is only disturbed by minor fissures, scarps less than 50 m long, and by some cracking of the walls of farm-houses standing on the landslide.

The most active area is the lower unit, which is bounded, at the south-western side, by the torrents of Vallcebre and Llarg and, at its north-eastern side, by a well developed lateral shear surface.

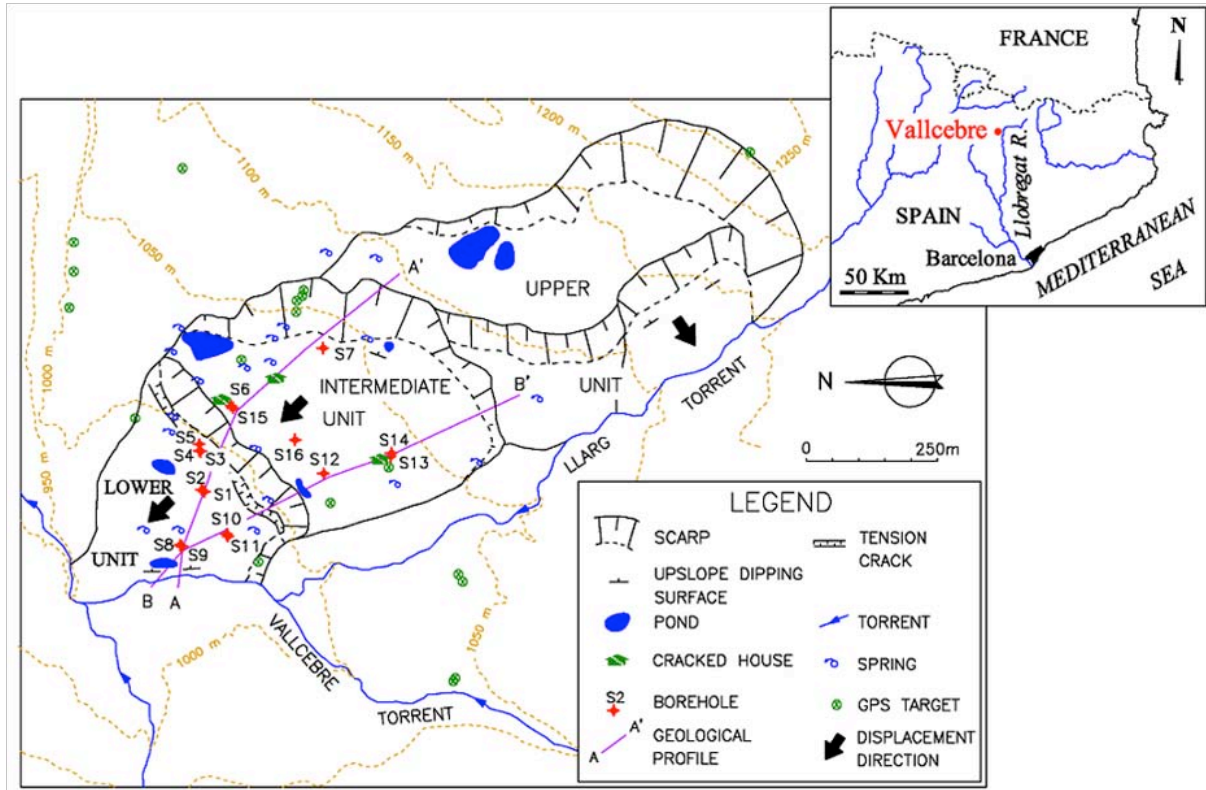


Figure 71. A geomorphological sketch of the Vallcebre landslide (Corominas et al, 2005).

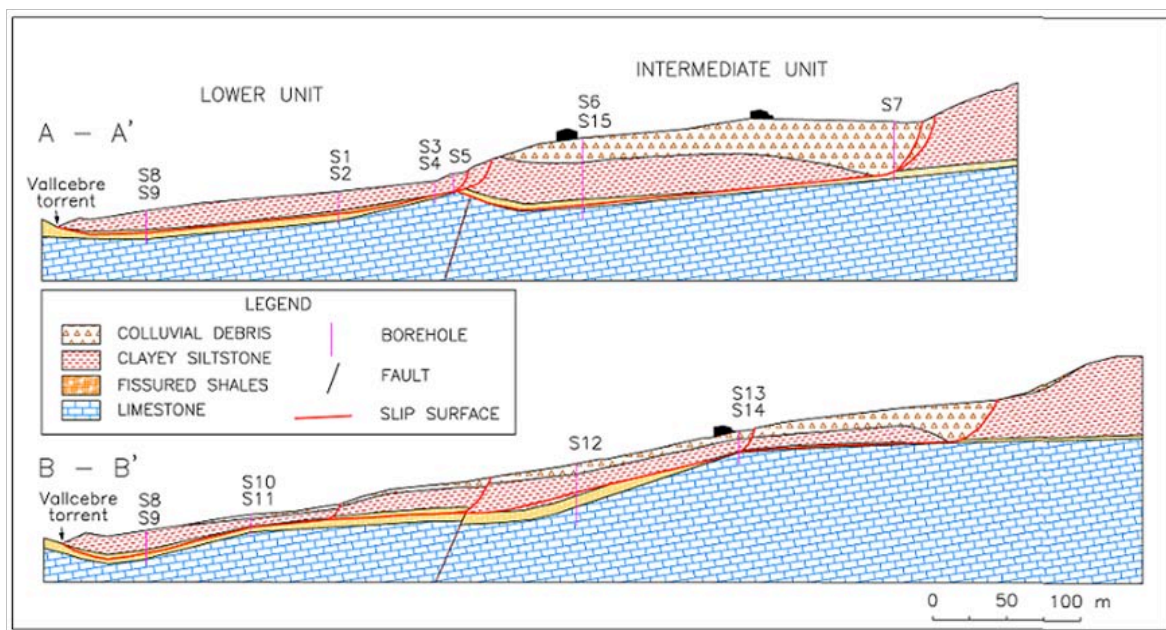


Figure 72. Geological cross-sections of the Vallcebre landslide (Corominas et al., 2005).

### 6.1.2.2 Description of the analysis

During July 1996, March 1997 and April 1998, sixteen boreholes were drilled in the landslide in order to: log the geologic materials of the landslide; provide undisturbed samples for laboratory tests; allow in-situ hydrological testing; and set up a monitoring network. Boreholes were equipped with inclinometers, wire extensometers and piezometers.

Since 1996, systematic logging of rainfall, groundwater level changes, and landslide displacements has been carried out every 20 min. Piezometric readings have indicated that changes in groundwater levels occur quickly. The extensometer has recorded sudden changes in displacement rates that can be directly related to the fluctuations of the water table governed by rainfall. The wire extensometer measurements show that the landslide has never completely stopped moving since we started the continuous monitoring in November 1996, although velocities reduced significantly during dry periods.

As an example of recent results, in Figure 73 the wire displacements measured in the borehole S11 during the 2010 are shown against the depth of the ground water. In Figure 74 the landslide velocity is plotted for the same period. As can be seen, the correspondence between the groundwater and the mobility is clearly shown.

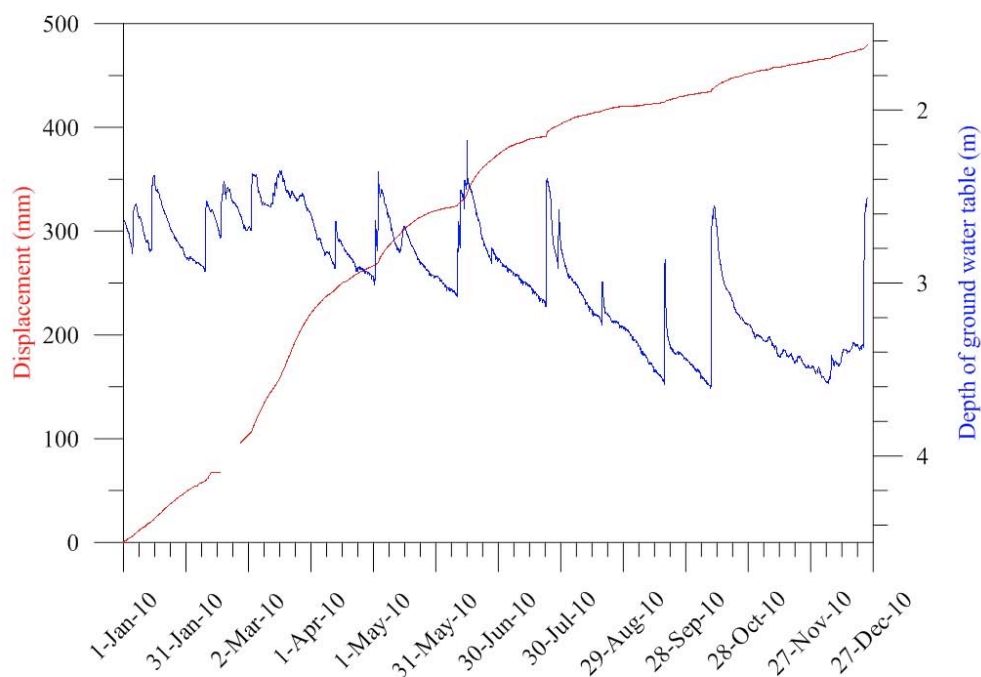


**Figure 73. Accumulated wire displacements and water table depth at borehole S11 during 2010.**

The wire extensometers have been used to calibrate some new techniques under development. In Gili et al. (2009) and Crosetto et al. (2009) the calibration of satellite based DInSAR versus the wire extensometer is reported. In November 2006 seven corner reflectors were installed to enhance the performance of the DInSAR techniques. The cross-checking of the DInSAR results versus the displacements derived from the wire extensometers has been carried out in 2007 and 2008, and some preliminary results have been obtained (Figure 75).

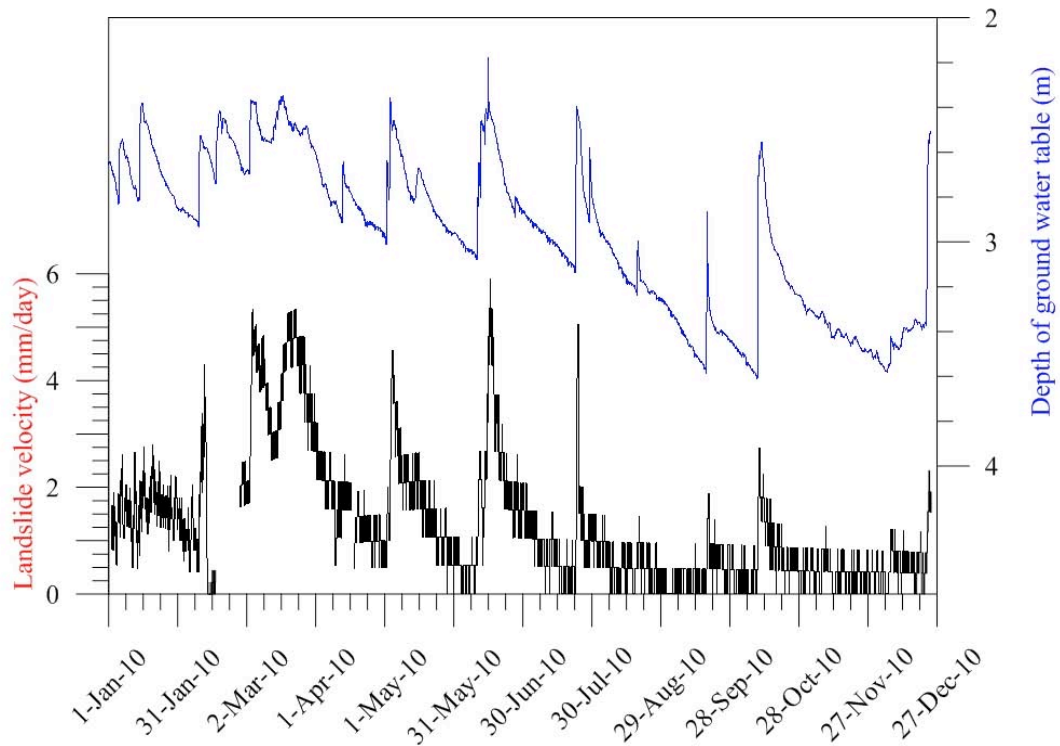


Figure 74. Landslide velocity vs. water table depth at borehole S11 during 2010.

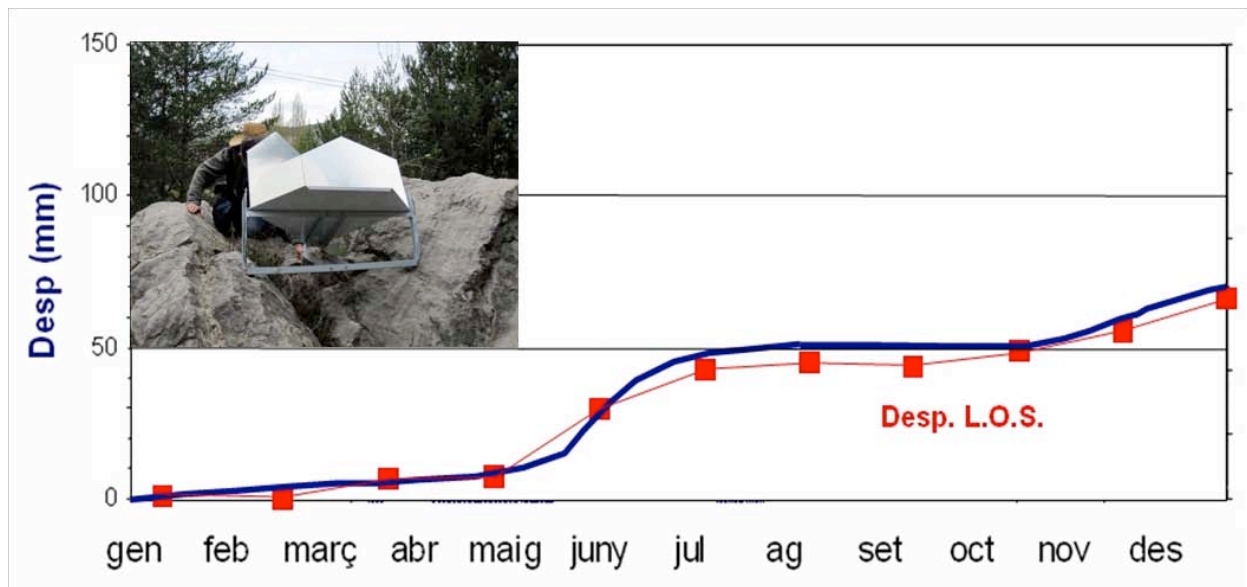


Figure 75. Wire extensometer readings at borehole S5 (blue line) vs “Line Of Sight” displacements obtained with DInSAR (red dots, corner CR4) during 2008.

### 6.1.2.3 Improvements with respect to previous applications

A summary of the last achievements in the Vallcebre monitoring follows:

In relation to the wire extensometer, a GSM modem has been installed in most of the data loggers. Therefore, the telematic transmission of the wire and water level data allows implementing an early warning system.

On the other hand, the analysis of the monitoring data in the recent years (wire readings, water pressure and rainfall) has permitted to establish certain water pressure and velocity thresholds for the Vallcebre landslide: if the water inside the slide reaches a given pressure threshold, the movement is reactivated, the velocity will start growing and several weeks will pass until the original situation is recovered.

Finally, the wire measurements enable the cross checking of the results obtained with emerging techniques. In the previous page the calibration of the spaceborne DInSAR has been presented. Additionally, the extensometer has been used to validate the first results of the ground based Radar (GBSAR) works carried out in Vallcebre by the Institute of Geomatics (Figure 76).

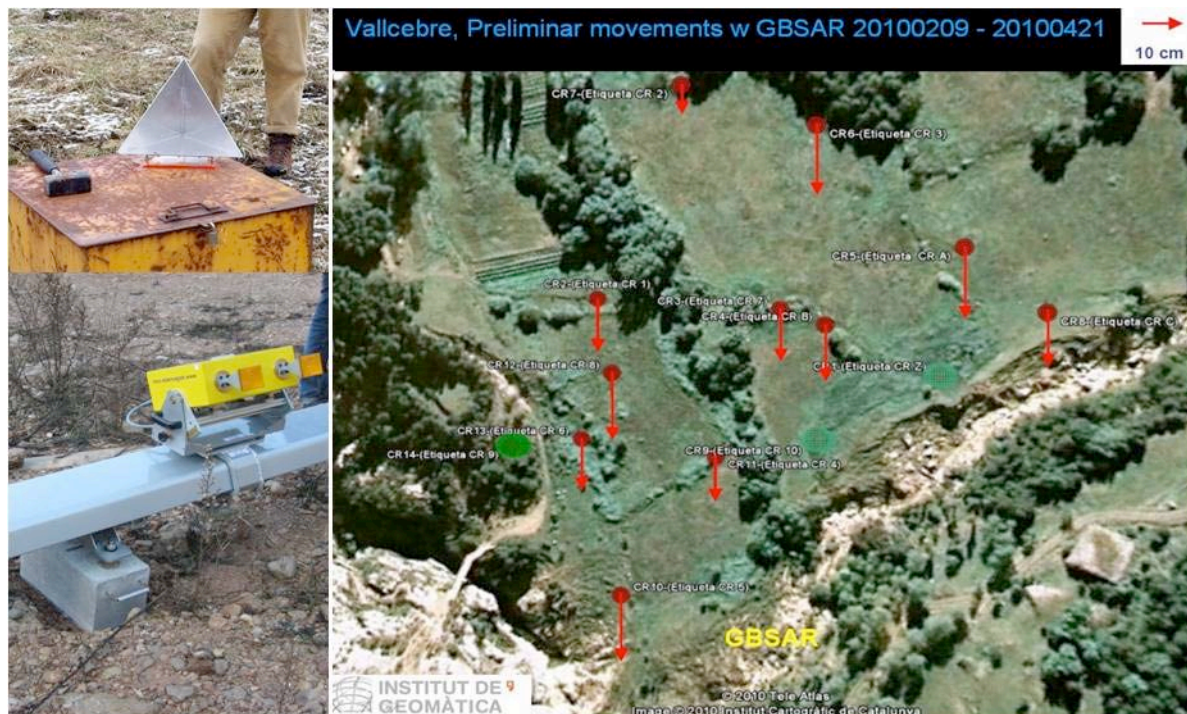


Figure 76. The IBIS-L-IDS GBSAR system (left) installed in front of the Vallcebre landslide by the Institute of Geomatics for the first preliminary results (right). A number of mini-corners (upper left) were deployed in the red points (right) where the movements are computed.

### **6.1.3 Automatic inclinometers: Bagnaschino (Torre Mondovì – Italy)**

*CSG: Garbarino E., Foglino L., Lovisolo M.*

#### **6.1.3.1 Study area**

The study area is in the Municipality of Torre Mondovì, Cuneo County, Piedmont Region. During the flood event occurred in 1994 the highway n. 194 was seriously damaged by a composite landslide activated in Bagnaschino site.

In proximity of km 1+400 the landslide invaded the carriage way.

Type: composite, flow 5-8m bgl (below ground level), deep creep 30-44m bgl.

Estimated area: 150.000m<sup>2</sup>

Estimated volume: 1.2M m<sup>3</sup>

Element at risk: Regional highway S.P. 164, potential lake formation

Early warning systems: DMS + surface systems

#### **Geological setting**

Basic geological data are summarized in the sheets “Cuneo” (80) and Boves (91) of Italian Geological Map (1:100000 scale) and in the sheet “Gap” of French’s Geological Map (1:250000 scale). On the basis of the mentioned cartography, the instable area implicates materials belonging to the Axial Perm Carboniferous (in particular gneissic, sericitic and filladic schists), sericitic quartz, and generally paragenetic rocks. We observed, during the inspection, wide outcrops of prasinite and ofiolites. Being geomechanically rigid rocks, these heaps suffered a tectonics of disjunctive type, resulting very fractured and predisposed to an aggressive action of weathering and to a raising distension.

#### **Geomorphologic setting**

The Geomorphologic structure of the whole valley bottom of T.Casotto and of the underlying slopes, results very conditioned by the litology of the bedrock and from his tectonic grade. So in the sector which structure is made by high tectonized rocks and/or high schistose (which appear covered by an abundant debris and soil), the valley bottom is quite large and the form of the reliefs are little hard, whereas, in the zones where the substrate of gneissic rocks or amphibolites rocks is present we have very steep scarps, and the valley bottom is narrow and the riverbed is embedded. In many areas of these side’ sectors we notice evident indications of deep gravitative morphogenesis (crowns and scarps, zone of accumulation of large paleoslides) which lead to suggest that the current slopes are in a condition of limit-equilibrium and are predisposed to slow movements or to rough landslides (total or partial), facilitated or caused by the temporary arise of triggering factors (large water’s infiltrations, pronounced river erosion at the foot...).

#### **Lito-stratigraphics characteristics**

On the basis of the geotechnical surveys, the stratigraphy of the landslide area (the upper part) is made by a considerable power (20 -30 m) of heterometric and heterogeneous debris in an abundant sandy silt and clayey matrix, with a low permeability primary porosity and endowed a high water retention and imbibition. These materials lay on a bedrock highly weathered, intensely fractured and clayed, given by laminated micaschists, overlapping to metabasites and prasinites, highly weathered and fractured, no mapped in the geological maps. During the

drillings several levels of perched water table were found, generally included in the most superficial levels, and the crossing of the bedrock generated a lot of problems because of the lost of the drilling fluids caused by the highly fractured system. The movement affects the recently reactivated portion, due to an alluvial event, of a biggest deformation of the slope of D.S.S.G.D type. The trigger of these movements is generally attributable to several factors; for the big paleoslides of Bagnaschino the glacier decompression, after the withdrawal of the quaternary ices, and the presence of tectonically dislocations and fragile deformation, due to the presence of faults, had a crucial role.

### ***6.1.3.2 Description of the analysis***

In order to monitor in continuous the stability conditions, the Cuneo County established in 2008 a slope monitoring plan with DMS system.

The monitoring system is composed by n.1 multiparametric DMS column, 60 meter long, installed in a borehole conditioned with an inclinometric pipe. It's linked respectively to a local control unit, with its solar power supply, and a GSM transmission system for the collected data.

The column is composed by a series of 60 modules stainless steel aisi 304 containing transducers and digital electronic, linked by special joints, having the necessary freedom degrees for the type of measurement required, allowing the single unit to adapt to the characteristics of the borehole and to the movements of the landslide, preserving the azimuthal direction compared to an external presetting reference system.

The instrumentation was installed in 28.10.2008 and in the same day linked in wireless to the monitoring centre by the GSM network (Figure 77).



**Figure 77: DMS installation.**

The modules contain 60 biaxial digital inclinometric sensors (range  $\pm 20^\circ$ , resolution  $0.005^\circ$ ), 1 piezometric sensor (range: 0-100 psi, resolution 1cm), 60 temperature sensors (resolution  $0.1^\circ\text{C}$ ).

Data acquisition is continuous (24/24 h) checking for the warning every minute, and information is recorded in a data base every hour. The remote control station checks the system automatically through G.S.M. remote data transmission.

Correlation between DMS column and precipitation data allowed to identify critical events that have reactivated the landslide on the sliding surface at 7 m bgl, with direction  $30^\circ$  NE. During the observation period it was possible to monitor in continuous different kinematics and different weather conditions.

DMS system allowed investigating 5 triggering events and their relative period of stasis, with a clear delay time after rain events or snow melting.

### ***6.1.3.3 Improvements with respect to previous applications***

The Cuneo County was able to control the landslide displacement in real time during the events by remote control, enabling the Civil Protection to intervene quickly in order to prevent potentially dangerous situation along the road, as soon the warning threshold was passed.

Data for the first time were relating to the overall landslide body (both superficial landslide zone and deep creep zone) and water table at the same time in order to model the complex phenomenon. Thanks to a multiparametric approach it was possible in this way to deepen the knowledge of the geotechnical and kinematic model in a short time.

Moreover, for each event it was calculated a particular value, the critical intensity, that corresponds to the ratio between precipitation (calculated in mm) that caused triggering movement and its duration (calculated in hours).

The interpolated line in the bi-logarithmic plot can be considered a site specific deterministic approach to the limit equilibrium threshold that separates the stability and instability field (Figure 78).

The site specific equation describing the rainfall thresholds for the initiation of the Bagnaschino landslide (rainfall, duration) can be written in the following way:

$$I = c + \alpha D^{-\beta}$$

Where in the specific site:

$$c = 0$$

$$\alpha = 9.1376$$

$$\beta = 0.3901$$

The following diagram shows the site specific experimental equation elaborated by the DMS data, compared with the regional analysis available in literature basic on national and international cases (Figure 79).

The DMS column allowed to obtain with continuity the kinematics of the landslide in action, not only limited to the initial stages of trigger, but also during the evolution up to achievement of stasis conditions.

The integrity of DMS column is preserved in spite of the displacement recorded of 600 mm; this is a significant improvement, probably the largest deformation recorded at only one module (length = 1m) considering also that the instrumentation was still active and operating correctly.

---

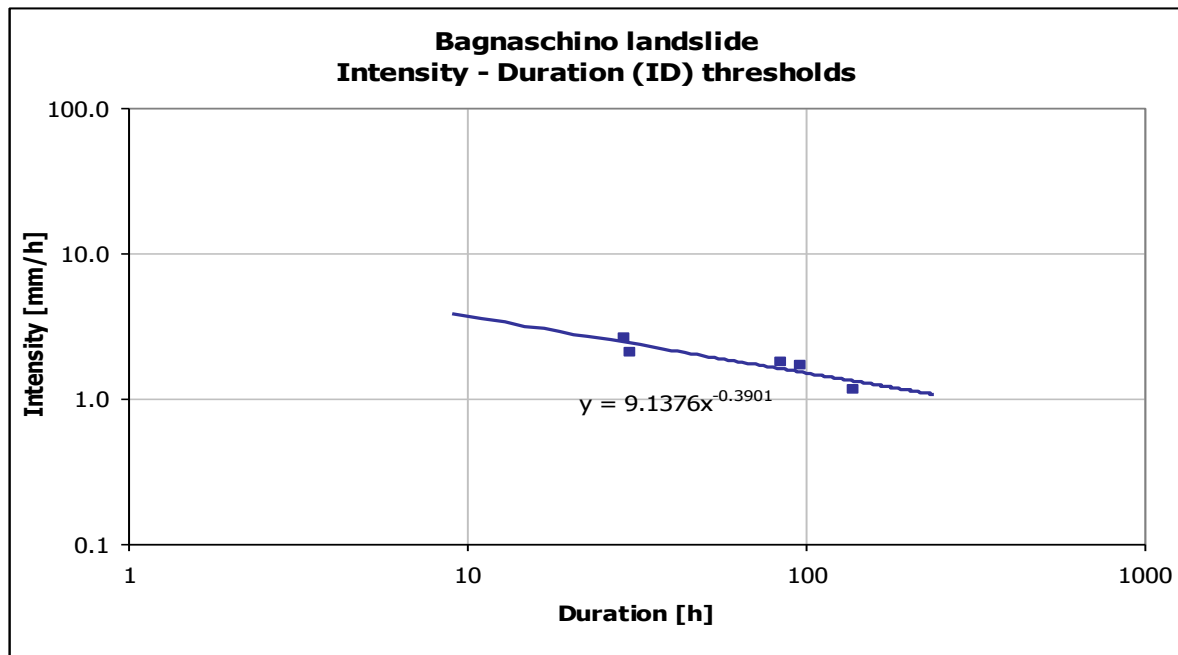


Figure 78: Bagnaschino site specific rainfall thresholds

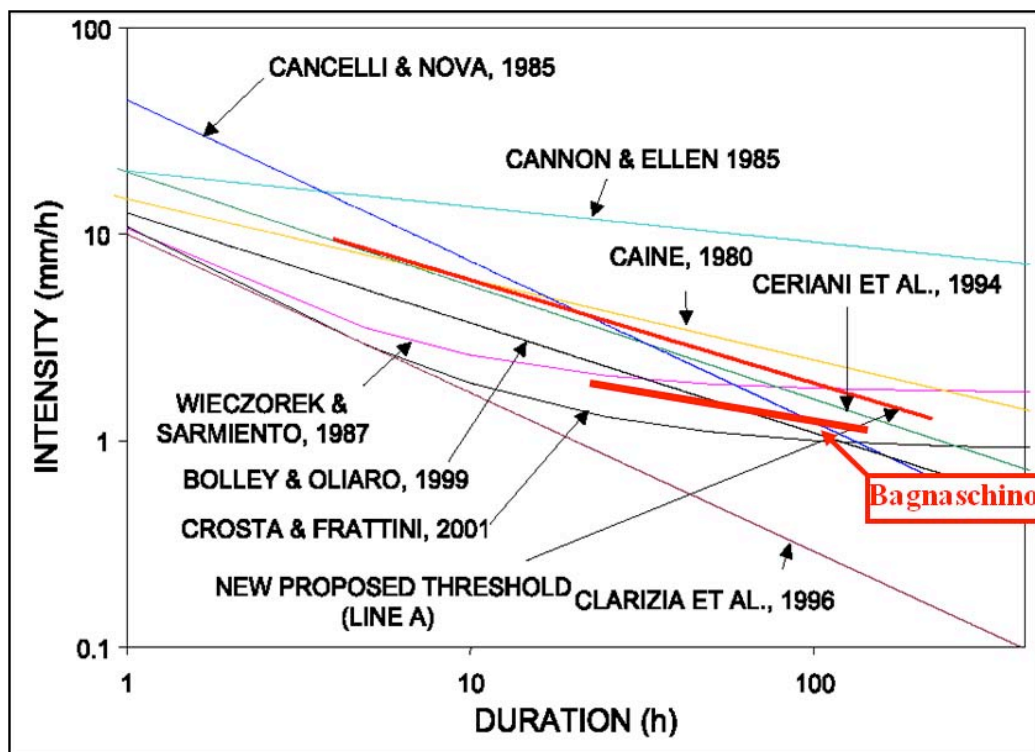


Figure 79: Bagnaschino site specific rainfall thresholds compared to literature thresholds.

The excavation realized subsequently to release the column confirmed depth, direction and extent of the displacement, allowing the complete recovery of the instrumentation (Figure 80). The activity in Bagnaschino with the cooperation of the Cuneo County allowed also repairing the inclinometer Al pipe that was replaced and protected by another pipe with a larger diameter in the interval of interest reaching the surface. This solution tested specifically in

Bagnaschino will allow maintaining a long term monitoring both in the shallow zone and in the lower part of the landslide.



**Figure 80: DMS column removal (13th July 2009), and displacement check after excavation**

Continuous monitoring of the landslide allowed noticing weak deep creep in the interval 30-44 m bgl in addition to considerable shallow movements. The activation of deep movements is delayed in respect to shallow movements, with a well defined behaviour.

DMS systems have been installed permanently in June 2010 for Early Warning function by means of 2 columns (DMS 1-60 and DMS 2-10 active in the intervals depths 20-60m and 0-10m).

During this week (March 2011) another event is starting after the heavy precipitation in these days in the Piedmont region (Figure 81).

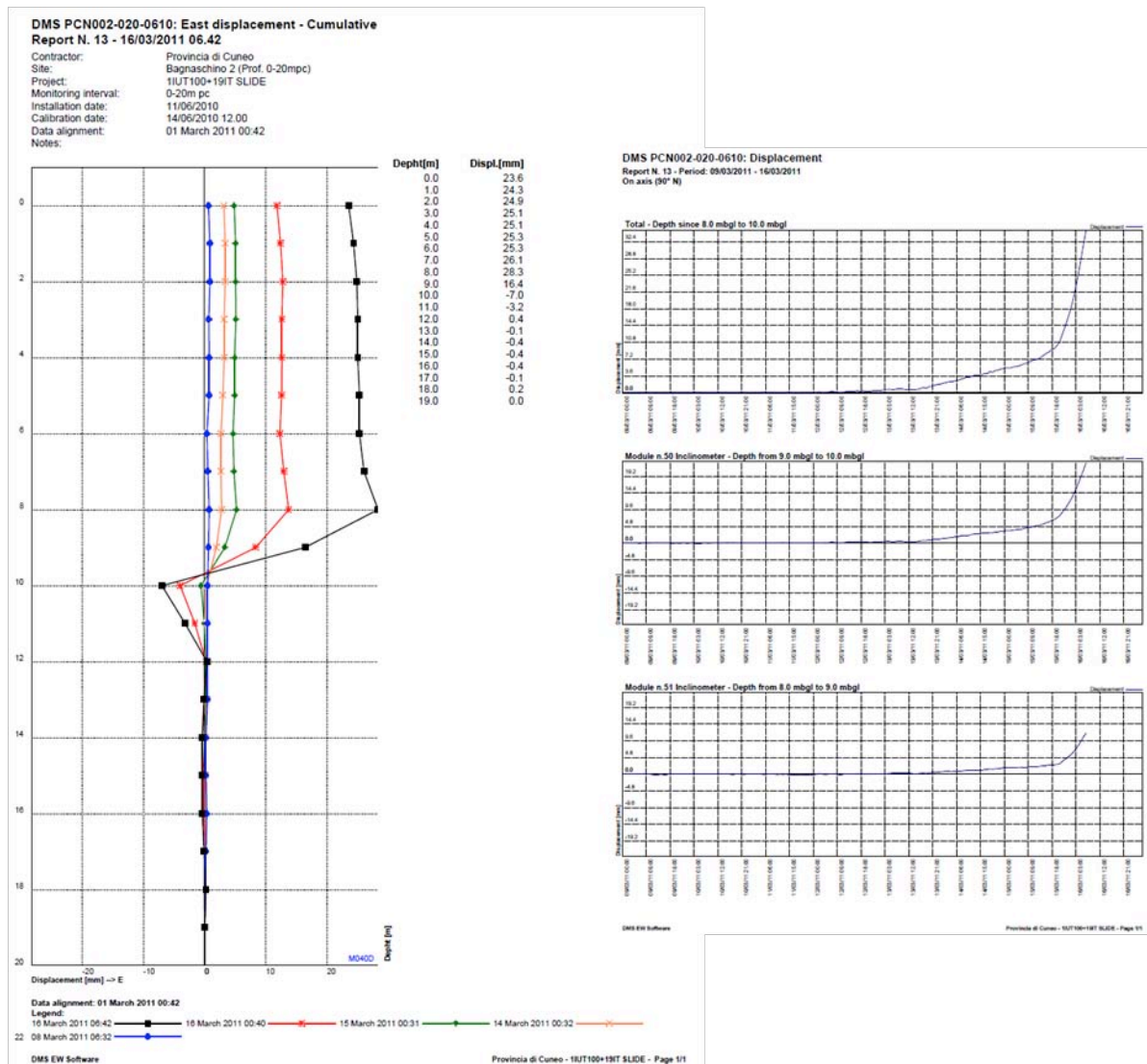


Figure 81: DMS data monitoring, new activation event (March 2011)

## 6.1.4 GB-InSAR: Castagnola landslide (Italy)

UNIFI: Antolini F., Tofani V., Del Ventisette C., Casagli N., Moretti S., Luzi G.

### 6.1.4.1 Study area

The Castagnola landslide is a large composite landslide with an estimated volume of about 3 Mm<sup>3</sup> (Cruden & Varnes, 1996) located in the Northern Apennines, about 25 km to the N of La Spezia city and 2.5 km to the N-NE from the Eastern Ligurian coast (Figure 82). The Ligurian Apennines and their coastal area are characterized by extensive outcrops of rocks belonging to the Internal Ligurian Domain. These successions consist of a Jurassic-Paleocene oceanic sequence (“Supergruppo della Val di Vara”, Abbate et al., 1980), with ophiolites. The latter include a gabbro and serpentinite basement and a portion of a volcano-sedimentary complex (ophiolitic breccias and basaltic lavas) followed upward by a marine sedimentary cover (Monte Alpe Cherts, Calpionelle Limestone and Palombini Shales) of Callovian - Santonian age (middle Jurassic – late Cretaceous, Principi et al., 2004).

The tectonic framework of the Castagnola area is characterized by the transport toward the foreland (E-NE) and the subsequent overlap of the Internal Ligurian Units over both External Ligurids, Canetolo (Sub-Ligurids) and Tuscan Units (Figure 82). The ophiolitic basement is disjointed in small tectonic sub-units (Velva, S.Nicola and Pavereto sub-units, Menna, 2008) and it is affected by two series of normal faults trending respectively parallel (NW-SE) and orthogonal to the mountain chain (NE-SW).

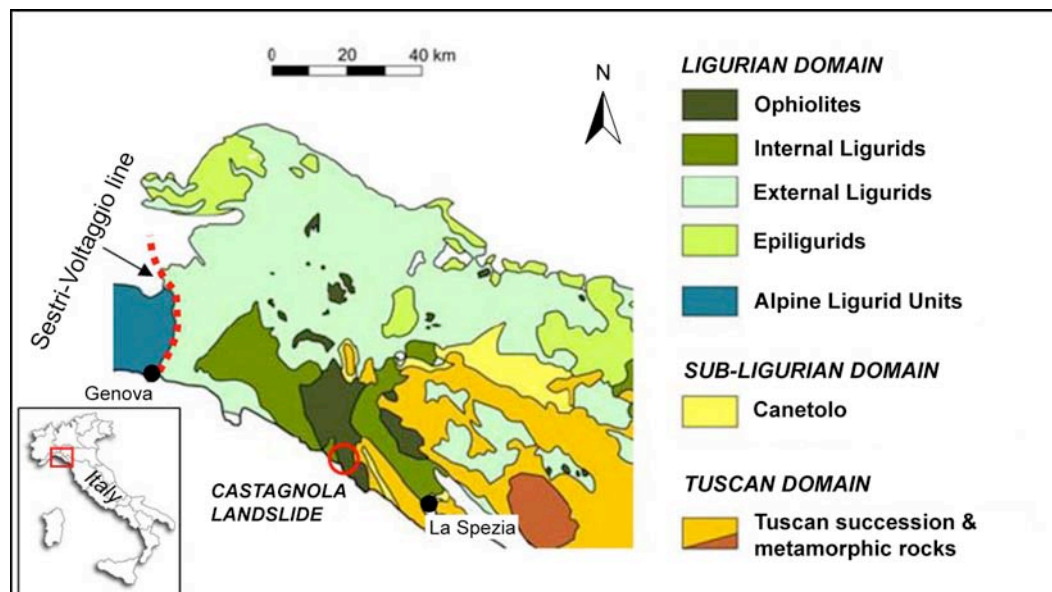


Figure 82. Geological sketch of E Liguria. In the red circle is shown the study area.

The geological model of the landslide was developed by integrating a new detailed geomorphological investigation with sub-surface data acquired from 10 boreholes drilled between February and March 2001 (Vannini et al., 2004). The boreholes were subsequently equipped with inclinometric tubes on which also piezometric levels were monitored. The inclinometric and piezometric survey lasted one year (from April 2001 to April 2002), being the instrumentation monitored monthly.

The aerial photo interpretation, the morphological characteristics and the geological arrangement of the area highlight the presence of several rotational slips on which are superimposed minor shallow planar and, in a less extent, flow-like instability phenomena (Figure 83). The different landslide portions are characterized by a different state of activity and have undergone distinct reactivation phases. On surface the landslide structure is therefore partially masked by the presence of discontinuous terraced alluvial deposits, colluvial and talus debris. The landslide mass lithology is heterogeneous and predominantly consists of altered argillite with limestone and ophiolitic blocks interbedded with clays and silty-clays layers with cobbles and gravels. The bedrock along the slope is constituted predominantly by Palombini Shales and on a lesser extent by Ophiolitic rocks (Serpentinites and Gabbro). The thickness of the altered and loose materials vary across the different slope sectors and progressively increases from the N area close to the head scarp (7-10 m) toward the toe of the landslide (Figure 83), reaching a thickness of 25 m on the borehole S7.

The landslide activity has disrupted the vegetation cover which, in the slide area, now consists of sparse olive trees, rows of vines and bushes, delineating a noticeably different pattern with respect to the surrounding stable area. The landslide interaction with the civil infrastructures is extensively documented: many buildings in Castagnola village and the surroundings show structural damages due to the landslide activity.

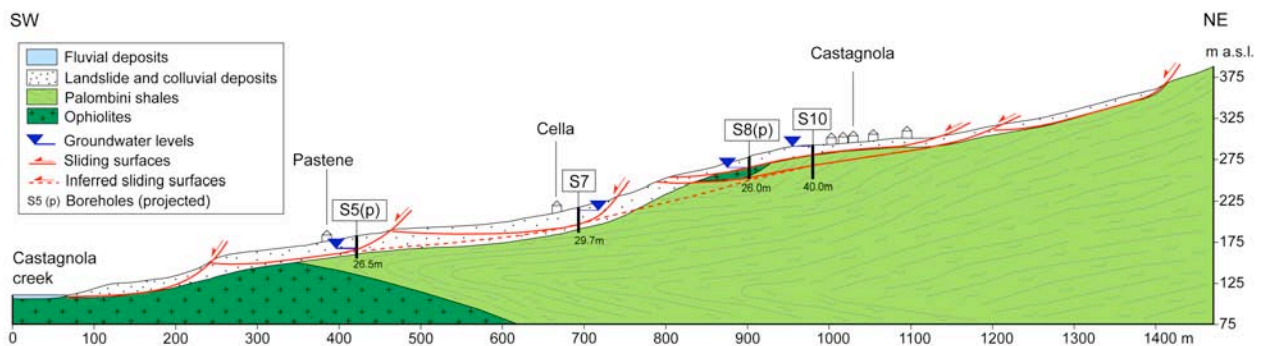


Figure 83. Geologic section across the landslide.

#### 6.1.4.2 Description of the analysis

The GB-InSAR system installed in Castagnola belongs to the interferometer series called LISA (Linear Synthetic Aperture high-resolution radar) designed by JRC - Joint Research Centre of the European Commission (Rudolf *et al.*, 1999) and manufactured by Ellegi-LISALab Company. In the last few years the LISA radar system has been already applied to monitoring different typologies of unstable slopes, volcano deformations and civil infrastructures (Antonello *et al.*, 2008; Atzeni *et al.*, 2002; Barbieri *et al.*, 2004; Casagli *et al.*, 2009; Luzi *et al.*, 2006; Tarchi *et al.*, 1997; 1998; 1999; 2000a; 2000b; 2002; 2003a; 2003b; Pieraccini *et al.*, 2000a; 2000b; 2003).

GB-InSAR system consists of a coherent microwave transceiver unit based on a precision network analyzer (PNA) working at Ku band which generate a sweep of electromagnetic waves of proper duration at different frequencies. The signal is then amplified and transmitted to the antennas. The synthetic aperture is realized by moving, via a linear positioner, a motorized sled hosting the radar head along a 2.7 m long straight rail (Figure 84). The main operational parameters adopted during the monitoring surveys are summarized in Table 3.

**Table 3. Summary of the main operational parameters of the radar measurement campaigns.**

Central frequency	17.05 GHz
Bandwidth	100 MHz
Synthetic aperture	2.7 m
Minimum target distance	100 m
Maximum target distance	1500 m
Range resolution	1.5 m
Cross-range resolution (at 100 m)	0.33 m
Cross-range resolution (at 800 m)	2.60 m
Cross-range resolution (at 1500 m)	4.95 m
Polarisation	VV
Antenna gain	-20 dB

Using these acquisition parameters the ground resolution in the range direction, which is a function of the employed bandwidth, was about 1.5 m. The cross-range resolution (perpendicular to the range direction) was variable from 0.3 to 2.6 m, with a higher resolution for the landslide sector located close to the radar station. GB-InSAR system was installed on the roof of a municipal warehouse, at a mean distance of about 700 m from the landslide area (Figure 84). The first survey campaign was carried out over 7 days, between the 23<sup>rd</sup> and the 29<sup>th</sup> of October 2008. Image acquisitions were repeated at time intervals of about 10 minutes, acquiring a total of 907 radar images. During the second periodical check survey (from the 10<sup>th</sup> to the 18<sup>th</sup> of February 2009) the GB-InSAR system was installed again in the same position (zero baseline) acquiring a total of 1231 images.

**Figure 84. Close-up view of the GB-InSAR system installed in front of the monitored area.**

The daily analysis of the interferograms has revealed conspicuous slope deformations with respect to the displacements observed during the first campaign. To follow the evolution of the landslide and to avoid possible phase wrapping effects in the long-term interferograms, it has been decided to rapidly resume the radar survey in order to provide the local authorities with a near real-time monitoring service (*Short- Term Monitoring*). The last survey campaign

was performed from 23<sup>rd</sup> of February to 13<sup>th</sup> of March 2009, spanning 17 days and 22 hours and acquiring 2727 images. During each campaign, radar data were daily transferred via FTP to the processing unit for the generations of both the interferograms and the cumulative displacement maps.

The analysis of the interferograms sequence related to the October 2008 campaign did not show any significant slope movements. The total displacements recorded during the second (February 2009) and third (February – March 2009) campaigns are represented by the cumulated displacements map of Figure 85. At the same time a total of 9 significant points (P\_01 to P\_09 in Figure 85) distributed over the slope were analyzed in order to determine velocity trends in key sectors of the landslide.

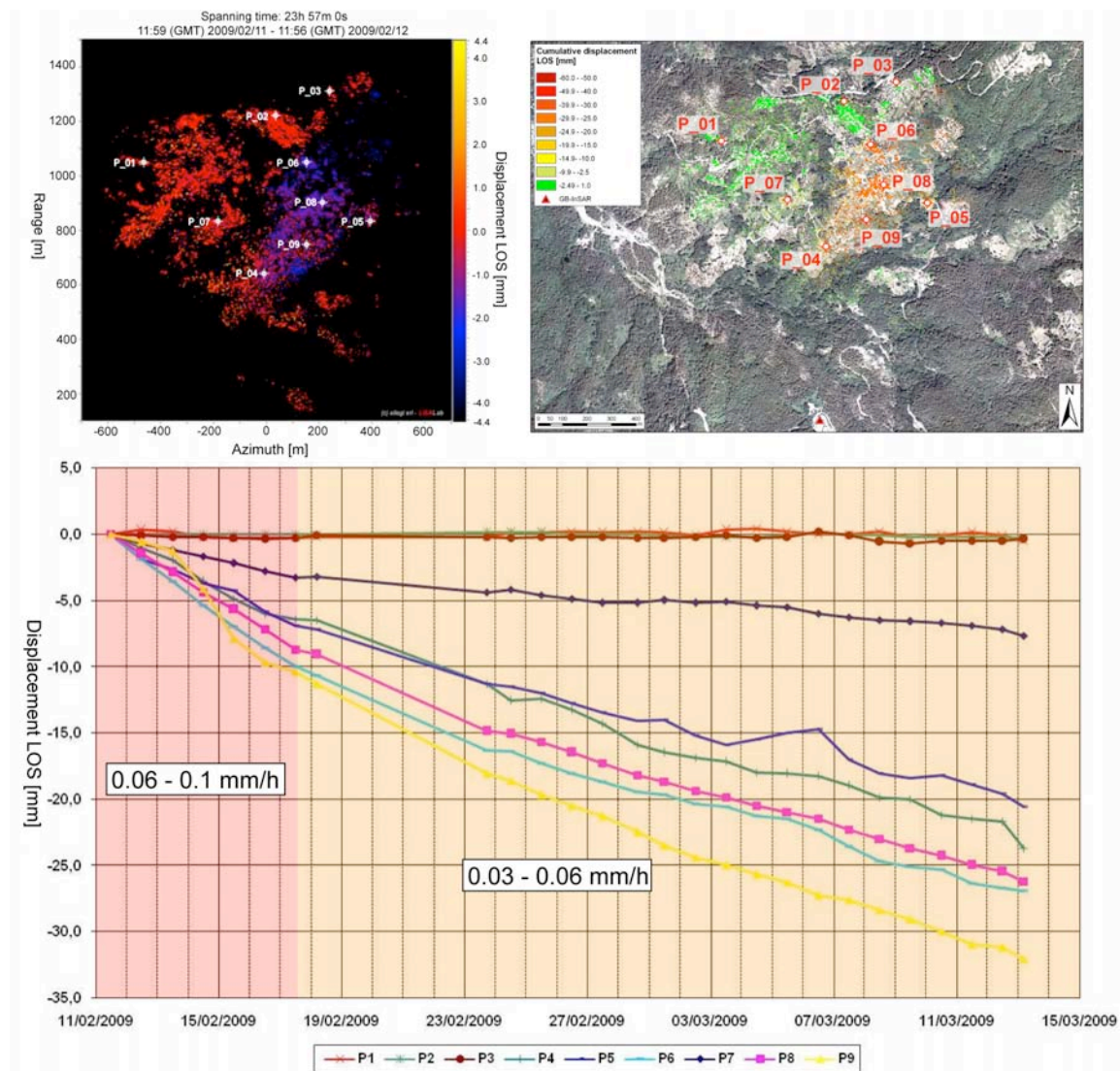


**Figure 85. Time series analysis of 9 points in the monitored area. The location of the points is shown both on the interferogram (upper left corner) and on the landslide map (upper right corner).**

The displacement map analysis highlights a huge sector affected by movements, which extends approximately between 500 and 1300 m away from the radar sensor and corresponds to the SE sector of the landslide. The cumulative displacement map shows a maximum

displacement rate of about  $60 \text{ mm month}^{-1}$  in the head scarp area, near the Rovereto abandoned village and on the left side of the Rovereto creek valley (Tari area). The area where the Castagnola village is located is instead characterized by a lower deformation rate, equal to  $20 - 25 \text{ mm month}^{-1}$ . Moving towards the NW landslide sectors, ground deformation decreases dramatically, reaching a value of  $4 - 5 \text{ mm/ month}^{-1}$  in the vicinity of Passano, Posata, Lazzino, Narà and Voltorara villages. Regarding the state of activity of the landslide toe (SW landslide sector close to Castagnola creek), the area was not covered by the radar signal and therefore the displacement information are missing. The time series analysis concerning some points of interest extracted from the interferograms (Figure 85) denotes that the displacement rate has decreased during the radar survey: maximum velocity was between  $0.06 - 0.1 \text{ mm hours}^{-1}$  during the first week changing to  $0.03 - 0.06 \text{ mm hours}^{-1}$  since the end of the second campaign (17<sup>th</sup> - 18<sup>th</sup> of February 2009). In the second and third monitoring week (third campaign) the deformation rate remained nearly constant although it has been possible to recognize slightly velocity increases. The overall decrease of the velocity also corresponds to a decrease in the surface area affected by deformations. In the N monitored area (see point P\_01, P\_02 and P\_03 in Figure 4), the overall velocity is close to zero and the area can be considered stable.

The long-term interferogram spanning 122 days (from October 2008 to February 2009) reveals a paucity of coherent pixels in the radar image due to the application of a coherence mask with an high threshold value which has discarded the low coherence areas from the images (Figure 86). On the basis of the long-term analysis results, the Castagnola landslide can be subdivided into three distinct sectors (Figure 86): the “A” sector has been characterized by a substantial stability while the “C” sector has been instead characterized by displacements close to instrument precision. Finally, in the “B” region, a marked loss of coherence of the signal backscattered from the scene, has prevented a long-term satisfactory analysis. This fact can be related both to the geometric changes of the monitored scene due to the displacements occurred since the end of October 2008 and partially to the growth of the vegetation cover.

Based on the results of the GB-InSAR campaign, the boundaries of the Castagnola landslide (Casagli et al., 2008) have been updated and extended (Figure 87) towards NE (main scarp area) and towards S (Rovereto - Pallareto area). Moreover it has been possible to differentiate an E sector (red in Figure 16) characterized by an average rate of deformation of about  $0.055 \text{ mm h}^{-1}$  and a W sector (yellow in Figure 6) characterized by a lower average deformation rate ( $0.025 \text{ mm h}^{-1}$ ). With regard to the landslide toe (light blue area in Figure 87) any consideration about the state of activity cannot be drawn since the area was not covered by the radar signal.

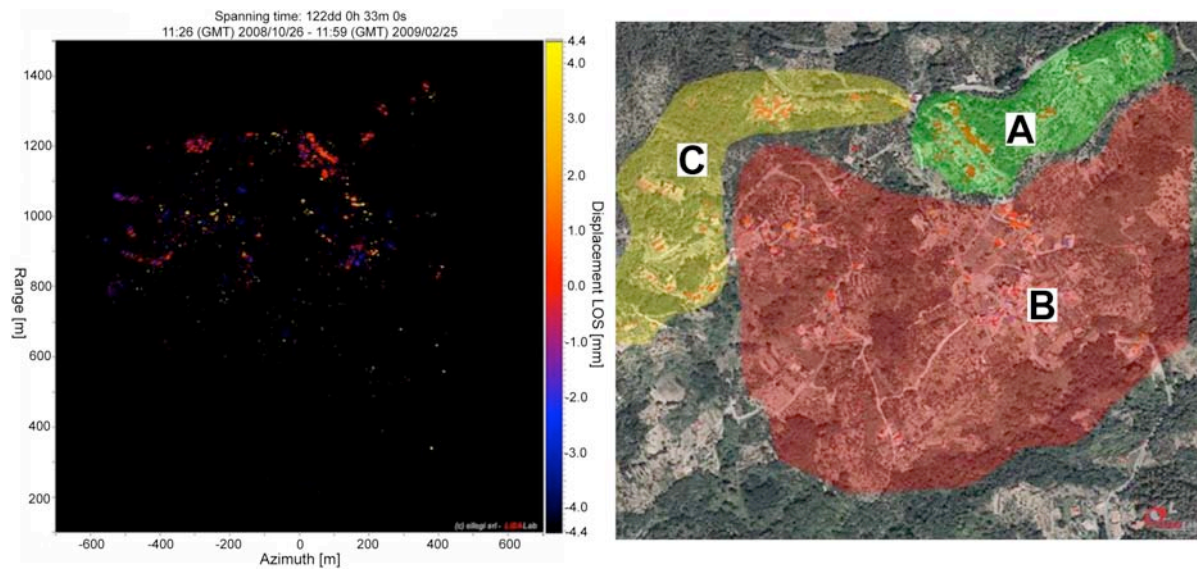


Figure 86: Interferogram spanning 122 days (left) obtained through radar images acquired during the first (October 2008) and the second (February 2009) periodical check campaigns and subdivision of the monitored area (right) on the basis of the results of the long-term analysis of displacements (see text for explanations).

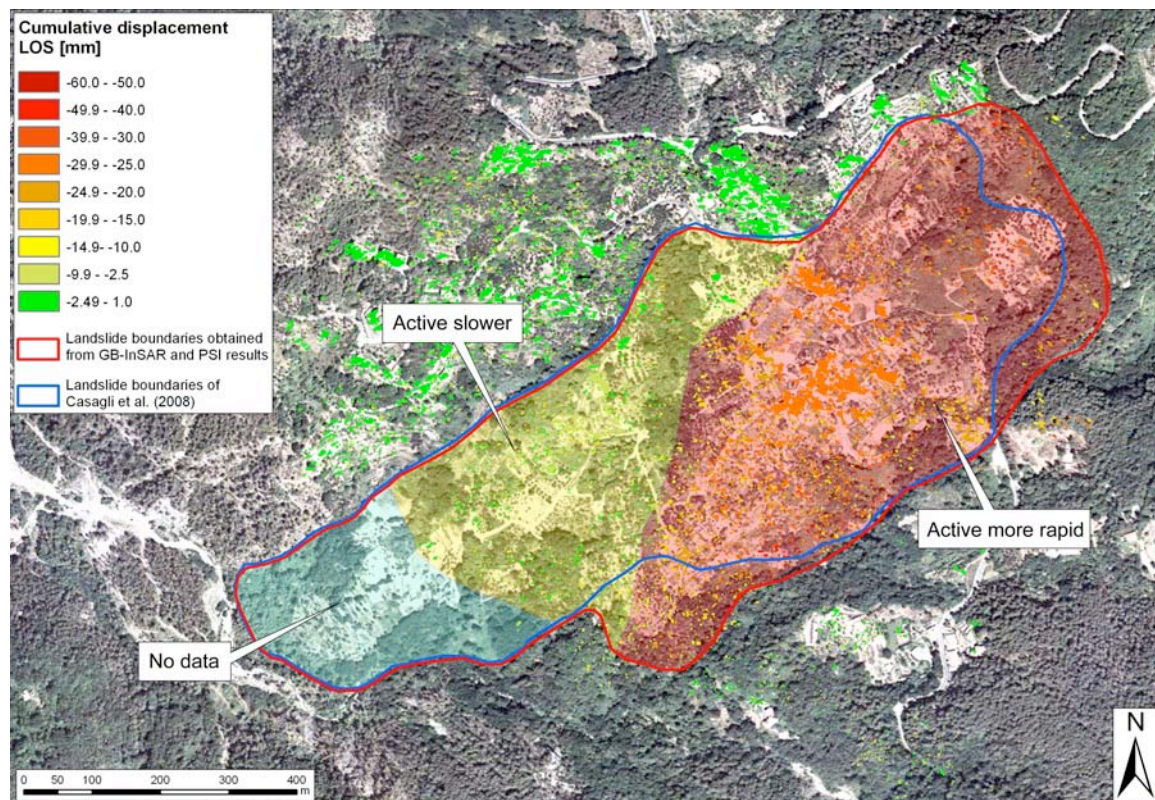


Figure 87: New landslide boundaries obtained from the GB-InSAR and PSI monitoring results and distinction of two landslide main sectors characterised by different deformation rates.

#### ***6.1.4.3 Improvements with respect to previous applications***

The application of GB-InSAR to the Castagnola has demonstrated its applicability as an effective early warning tool for risk management, able to provide near real time information which can be employed in civil protection actions and plans.

Furthermore this type of analysis gives information on spatial and temporal deformation pattern and is fundamental for evaluating the possible landslide evolution, defining deformation thresholds, and setting real time monitoring systems for early warning purpose.

## 6.1.5 TLS monitoring of the Åknes rockslide (Norway)

*ICG: Oppikofer T.*

The present chapter is based on the paper of Oppikofer et al., 2009.

### 6.1.5.1 Study area

The Åknes rockslide is situated on the western flank of Sunnlyvsfjord, a branch of the Storfjord in western Norway (Figure 88). The volume of the Åknes rockslide was first estimated to be 5 to 6 million m<sup>3</sup>. Detailed investigations however revealed that the whole rockslide covers a much larger area (approximately 550000 m<sup>2</sup>) and stretches from 900 m down to 100 m above sea level with a total estimated volume of 30-40 million m<sup>3</sup> (Derron et al., 2005; Blikra, 2008). Its failure might cause a catastrophic tsunami in the fjord that would reach the nearby villages of Hellesylt and Geiranger (Figure 88) within 4 and 10 minutes respectively, creating run-up waves of up to 40 m in these localities (Eidsvig and Harbitz, 2005).

Since 2005, the Åknes rockslide has been investigated as part of the Åknes/Tafjord Project and is now continuously monitored by the Åknes/Tafjord Early Warning Center ([www.aknes.no](http://www.aknes.no)). It is one of the biggest landslide monitoring projects in the world employing a multitude of geological, structural, geophysical and borehole investigations (Blikra et al., 2006a; Blikra, 2008; Ganerød et al., 2008). The monitoring focuses not only on the measurement of slope movements using a large variety of techniques, but also includes measurements of meteorological, seismic and groundwater conditions (Blikra et al., 2006a; Blikra, 2008). The measured slope movements reach about 1–3 cm/year (Braathen et al., 2004; Derron et al., 2005; Ganerød et al., 2008), but higher annual displacements are recorded in the most unstable parts (7–20 cm/year) (Blikra et al., 2006b) (Figure 88c).

A detailed investigation of the Åknes rockslide was undertaken in 2006, 2007 and 2008 by TLS. The primary goal of this survey was the detection of movements in the uppermost part of the rockslide by comparison of sequential TLS points clouds and the structural analysis of the scarp area. This case study summarizes the main findings of the complete TLS survey, which is described in Oppikofer et al. (2009).

### 6.1.5.1 Description of the analysis

On the fast-moving ridge in the uppermost part of the Åknes rockslide, the shortest distance comparison between the scans taken on 3 August 2006 and 7 August 2007 shows a horizontal displacement of 6 to 8 cm towards the South and a vertical displacement of 4 to 6 cm (Oppikofer et al., 2008a). The shortest distance comparison of the 3 August 2006 and 24 August 2008 datasets is shown in Figure 89. This comparison gives evidence of a southward movement of the whole ridge by 12 to 18 cm (orange colours at the front of the fast-moving ridge in Figure 89) along with a downward movement by approximately 6 cm (light blue colours on the top of the ridge). This comparison also reveals the subsidence of the debris (up to –24 cm) in the graben which opened between the main scarp and the fast-moving ridge (Figure 89). In this subsidence area, two small freestanding columns with high displacements (up to +24 cm) are detected. The debris at the foot of the fast-moving ridge are also moving towards the South with displacements varying between 6 cm and 24 cm for individual blocks (yellow to red colours in the foreground of Figure 89).

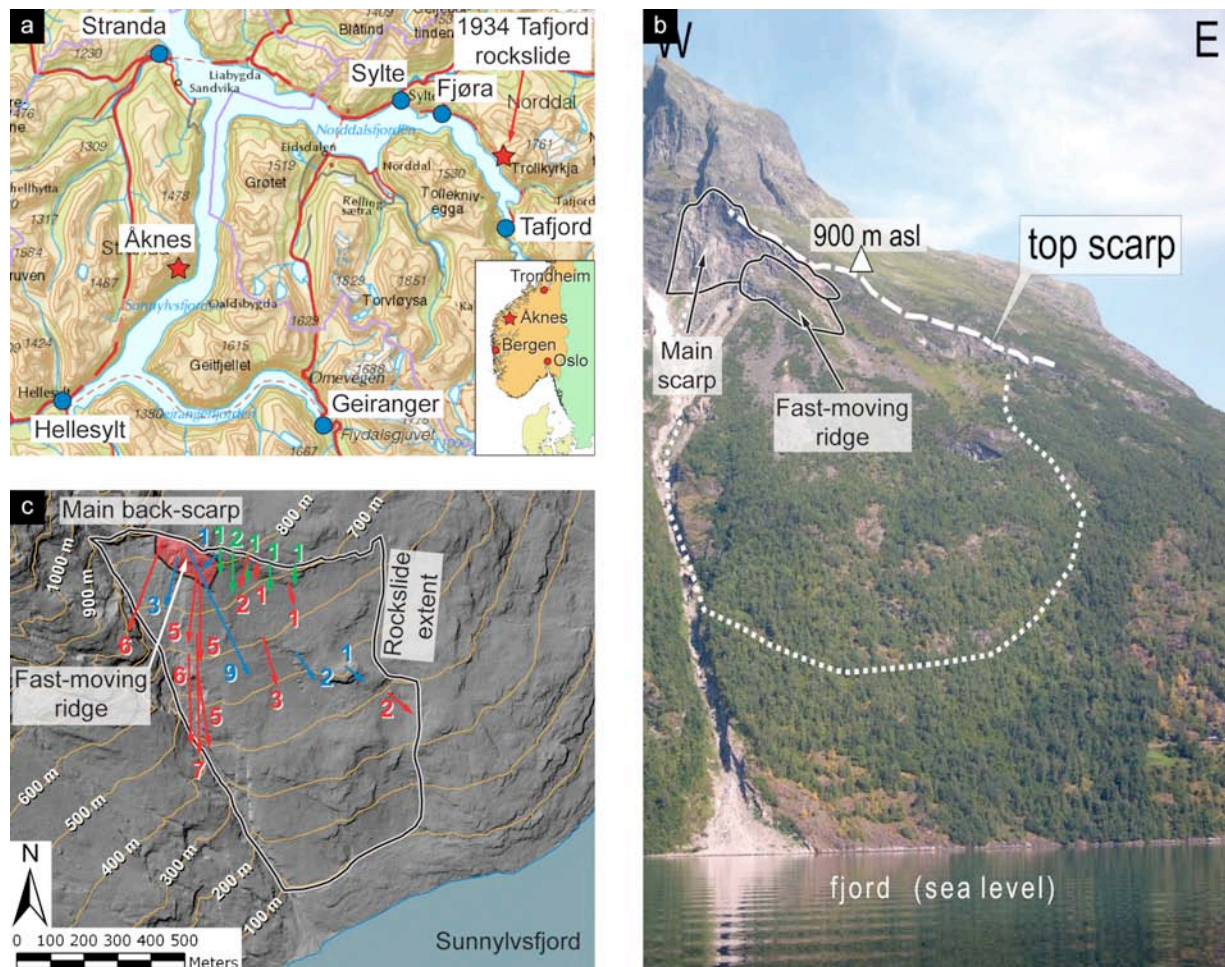


**Figure 88:** a) Location map of the Åknes rockslide in Western Norway (© Statens Kartverk, Norwegian Mapping Authority); b) picture of the Åknes rockslide seen from the Sunnylvsfjord showing the areas of interest (modified from Derron et al., 2005); c) shaded relief map of the rockslide showing its extent, the location of the main scarp and the fast-moving ridge, as well as the annual displacement vectors in cm/year obtained by GPS (blue), extensometers (green) and total station (red) (displacement data from Ganerød et al. (2008); ALS digital elevation model © Åknes/Tafjord Project, 2005).

For the detailed analysis of the displacements, the fast-moving ridge was divided into 11 compartments – labelled R1 to R10 – on the basis of the shortest distance comparison and the morphology (Figure 89). For each compartment, a mesh of the 2006 TLS scans was created and aligned first onto the 2007 point cloud and afterwards on the 2008 dataset. Using the roto-translation matrix technique (see Oppikofer et al., 2009 for a detailed methodological description), the complete 3D movement of each compartment was calculated for each possible comparison (2006 vs. 2007, 2007 vs. 2008 and 2006 vs. 2008). Figure 90 shows the translation vectors and toppling directions and angles for the 2-year period between August 2006 and August 2008. All of the measured translation vector lengths and most toppling angles are significant since they are greater than the accuracy of the roto-translation matrix technique.

The compartment R1 is a detached column sliding and toppling towards the graben in the North (translation length of 36.4 cm and toppling angle of  $0.818^\circ$  in two years) and shows a clearly different displacement pattern than the other compartments of the ridge. R1 was therefore excluded from the displacement analysis of the fast-moving ridge.

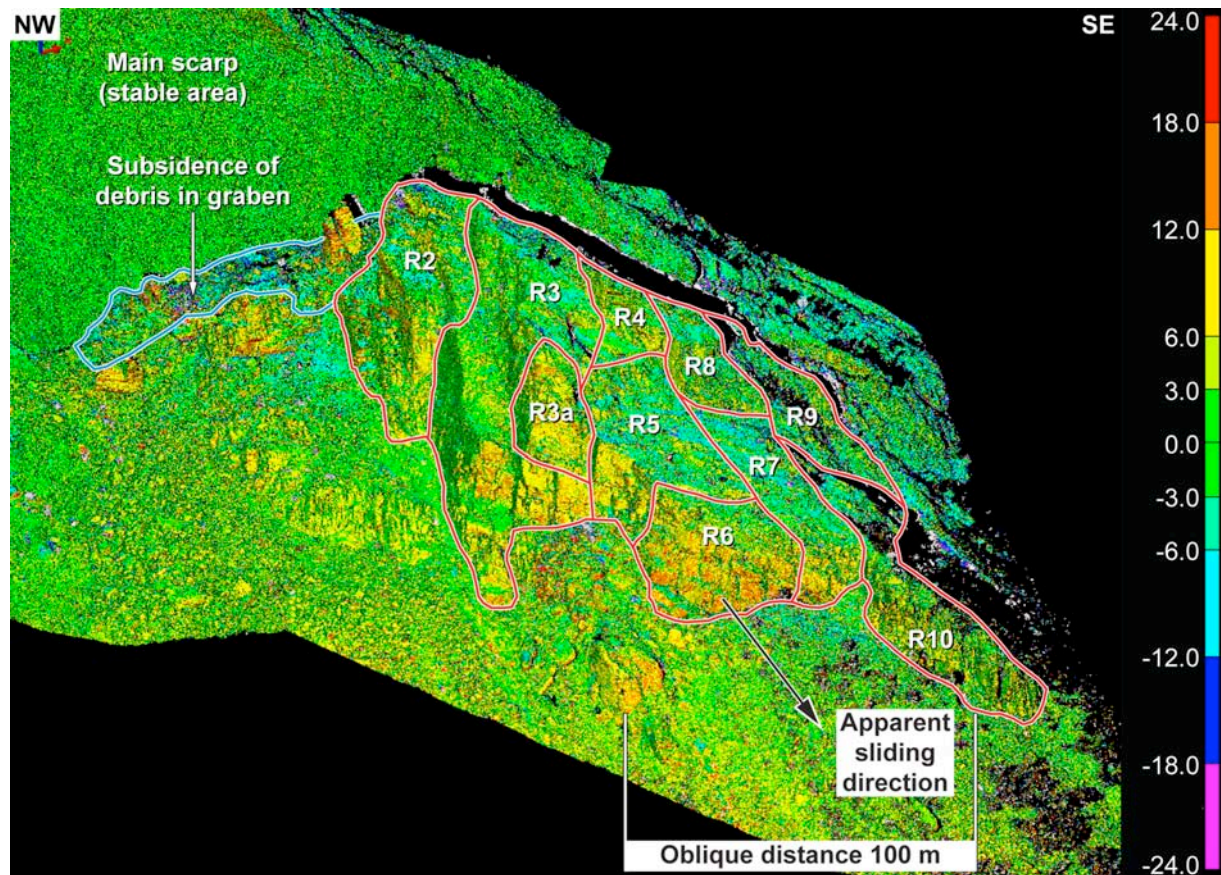


Figure 89: Comparison of the TLS point clouds from 3 August 2006 and 24 August 2008. Positive differences up to +24 cm are shown in yellow to red colours and negative differences up to -24 cm in light to dark blue colours. The 10 compartments on the fast-moving ridge (R1 is hidden by R2) used for the detailed displacement analysis using the roto-translation matrix technique are outlined.

The translation vectors of the compartments R2 to R10 are quite homogenous in length and direction. The different compartments move towards the SSW to SW (between  $N196^\circ$  and  $N227^\circ$ ) and the length of the translation vectors varied between 13.1 to 19.3 cm between 2006 and 2008. The translation direction of the northern compartments is more to the SW and steeper plunging (between  $57^\circ$  and  $64^\circ$  for R2, R4, R8 and R9) than the southern compartments (between  $41^\circ$  and  $50^\circ$  for R3, R3a, R5, R6, R7 and R10). This higher subsidence can be explained by the opening of the graben structure between the back scarp and the ridge.

The global displacement of the fast-moving ridge can be described by the average of the displacement vectors ( $208^\circ/53^\circ$ , 14.9 cm in two years) or the mean value weighted by horizontal surface of each compartment ( $206^\circ/52^\circ$ , 14.5 cm between 2006 and 2008). These calculated displacements are similar to the shortest differences visible in the comparison image (Figure 89).

Except for R3a that is toppling towards the SW, the compartments topple towards the North (ranging from  $N331^\circ$  to  $N037^\circ$ ; weighted mean toppling direction:  $N001^\circ$ ). Toppling angles are low ( $< 0.1^\circ$ ) with a weighted mean angle of  $0.048^\circ$ . Nonetheless, a toppling by  $0.048^\circ$  of a 50 m high compartment, as found on the ridge in Åknes rockslide, leads to a displacement of 4.2 cm at its top. This toppling component is in good agreement with the different

displacement patterns detected by the SDC (Figure 89). The northward toppling combined to southward sliding leads to higher SD at the foot of the fast-moving ridge (> 12 cm, orange to red colours at the foot of R3, R5 and R6 in Figure 89), smaller SD at the top of the cliff (< 12 cm, green to yellow colours in the upper part of the compartments in Figure 89) and higher negative SD on the top of the ridge (< -6 cm, light blue colours on the top of the ridge compartments in Figure 89).

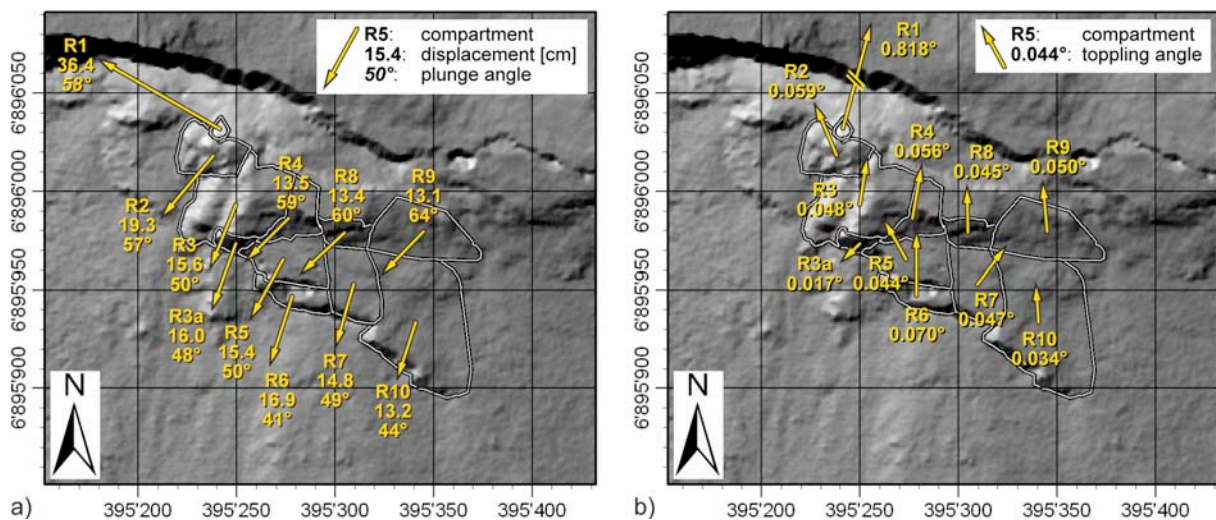


Figure 90: Map of the 11 compartments on the ridge: a) the arrows indicate the direction and amplitude of the displacement vector between August 2006 and August 2008; b) shows the toppling direction (indicated by the azimuth of the arrow) and the toppling angle (indicated by the length of the arrow and the number) from August 2006 to August 2008.

### 6.1.5.2 Improvements with respect to previous applications

The terrestrial laser scanner survey of the upper part of the Åknes rockslide shows the potential of this new method. TLS is able to detect global slope movements over the whole landslide area and not just at single monitoring points. In contrast to many other monitoring techniques, TLS provides information not only on the total amount of displacement in the line-of-sight, but also on the type of movement, i.e. translation and/or rotation. Comparisons of TLS point clouds of the upper part of the Åknes rockslide reveal displacements as low as a few centimetres and up to several decimetres. In contrast to other area-based monitoring techniques, the range of measurable displacements by TLS is very large leading to a wide range of potential landslide monitoring applications.

The roto-translation technique is well suited for displacement measurement and the interpretation of the movement in terms of landslide mechanism. The measured displacements are consistent with the overall movement of the Åknes rockslide. On the basis of the TLS data, a possible rockslide mechanism model for the uppermost part of the Åknes rockslide was established including planar sliding as well as toppling and vertical settlement (see Oppikofer et al., 2009 for details).

## 6.1.6 High-resolution terrestrial optical images correlation: Super-Sauze (South French Alps)

CNRS: Malet J.-P., Travelletti J., Delacourt C., Allemand P.

This chapter is based on the work described in Travelletti et al., submitted to International Journal of Photogrammetry & Remote-Sensing, 2010.

### 6.1.6.1 Study area

The Super-Sauze landslide (Alpes-de-Haute-Provence, France) is the SafeLand case study for the evaluation of the capability of correlation of terrestrial optical images to monitor the displacement of landslides; (Figure 91). The test site is located in the Barcelonnette Basin (South East France).

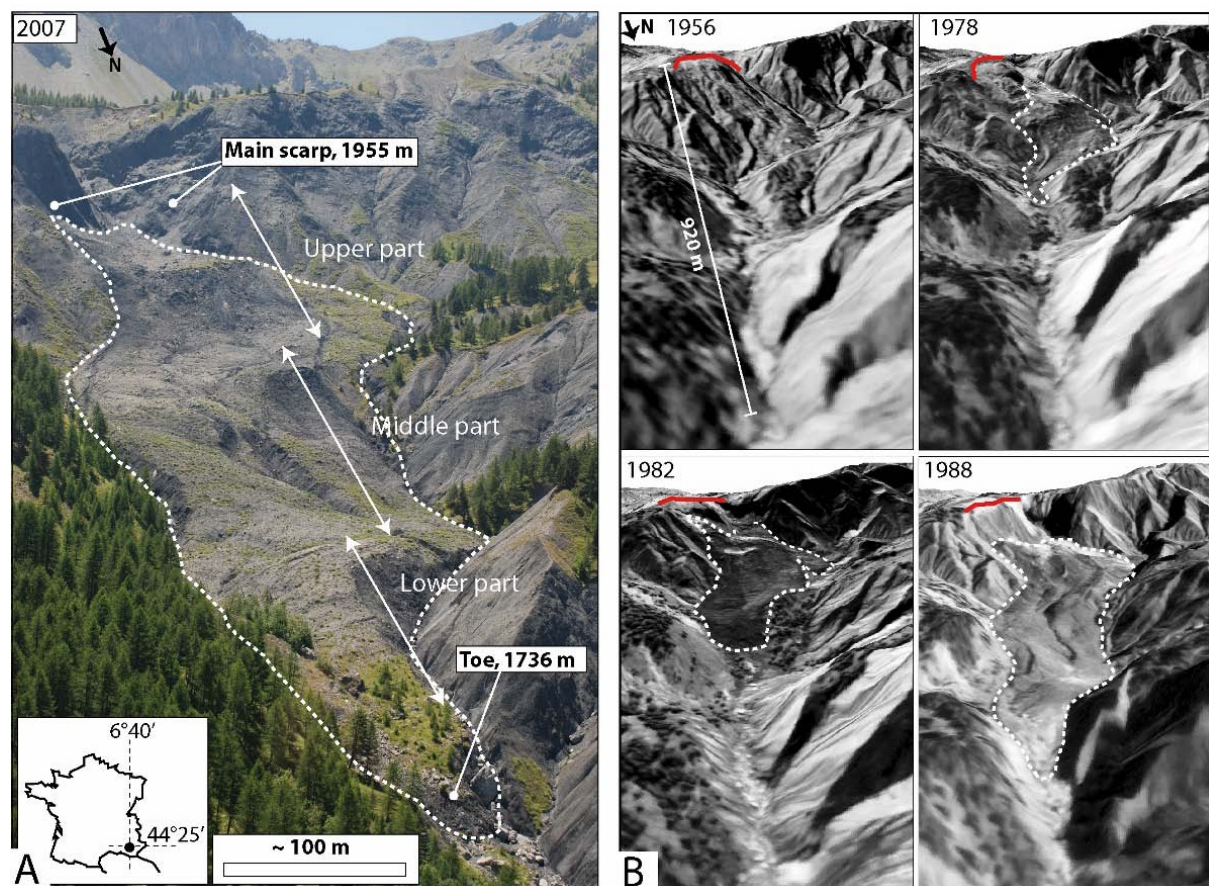


Figure 91. A) View of the Super Sauze mudslide from the North. B) Main evolution steps of the mudslide from the main failure in 1960's to the development of the mudslide in 1988. The original torrential channel is progressively covered by the material.

The landslide is located in the upper part of the Sauze torrential catchment. In the 1960s, the area was affected by rock failures in the scarp area. The failed material composed of rocky panels progressively transformed into a silty-sandy matrix integrating marly fragments of heterogeneous sizes through successive weathering cycles (Malet, 2003). Figure 91 presents the main development periods of the Super-Sauze mudslide. Before the destabilization event

in the 1960's, the scarp area was probably affected by a deep seated slope deformation controlled by regional faults which initiated the slope collapse. In the 1960's, additional shallow failures occurred in the scarp area. They mainly consisted in successive plane and wedge failures affecting the crests. The collapsed material of rocky panels progressively transformed into a silty sandy matrix integrating marly fragments of heterogeneous size through successive drying/wetting and freeze/thaw cycles. In the late 1970s, the mobilized material started to accumulate in the gullies. Since the 1970s until today, the mudslide is gradually covering the torrential stream located downstream with typical range of velocity between 1 to 3 cm/d and acceleration peak until 40 cm/d in the spring season. In 2007, the mudslide was extending over a distance of 920 m between an elevation of 2105 m at the crown and 1736 m at the toe with an average width of 135 m and an average slope of 25°. The total volume is estimated at 560,000 m<sup>3</sup> (Travelletti et Malet, in press).

Geomorphologic, geologic, geophysical, geotechnical and displacement monitoring studies have been conducted over 15 years in order to monitor the landslide dynamics. The kinematics of the landslide is currently monitored by Differential Global Positioning System (DGPS) and Terrestrial Laser Scanning (TLS), and by a remote camera monitoring system. The latter consists in a low-cost D70 Nikon non-metric reflex digital camera installed on a concrete pillar located on a stable crest in front of the landslide at a distance of 300 m from the lower part and 900 m from the main scarp (Figure 92 A, B, C). The acquisition system is controlled by a data logger (Campbell CR10) and the power is provided by a 40 W solar panel. The characteristics of the acquisition are presented in Table 2. Each four days, four images are acquired at 11:00, 12:00, 13:00 and 14:00 GMT in order to increase the probability of having at least one image with good meteorological conditions. Each photograph (6 Mb) is stored in a native file format to avoid any loss of information.

Further information on the Super-Sauze landslide can be found at: <http://eost.u-strasbg.fr/omiv/>

#### ***6.1.6.1 Description of the analysis***

The steps in the data processing workflow consist in (1) correlating the images by pairs in their original acquisition geometry to prevent any loss of information, and (2) orthorectifying the calculated displacement fields using a high-resolution digital elevation model interpolated from airborne LiDAR data. The daily images (an example is provided in Figure 93 together with a projection of the images on the real topography in the local coordinate system) presenting the best ground texture contrast and the most homogeneous lightening are selected based on expert judgment.

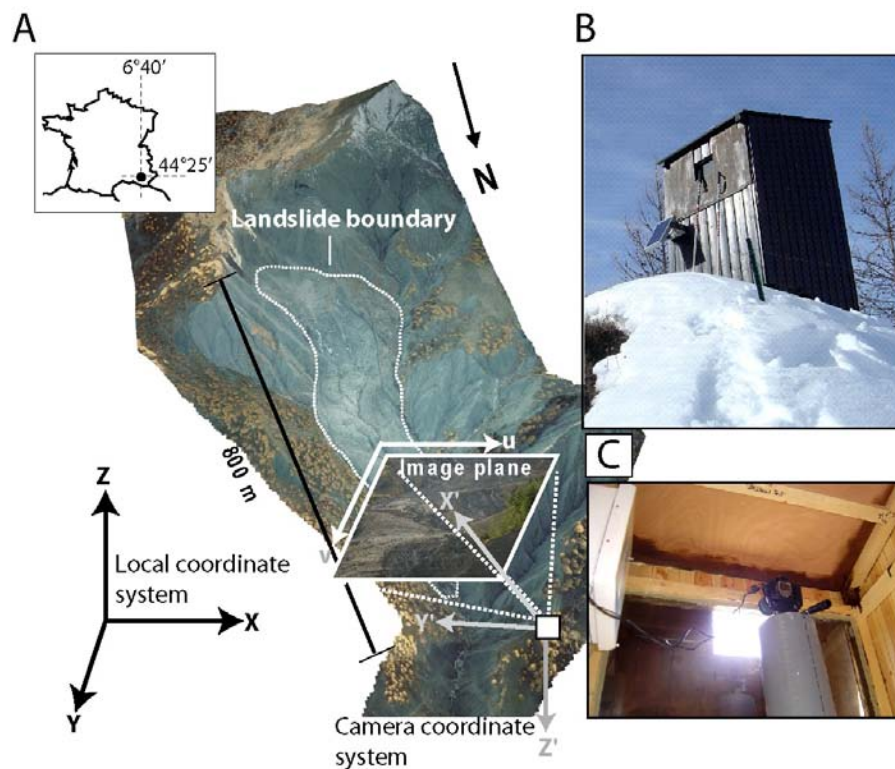


Figure 92. (A) View of the Super-Sauze landslide towards the south with the different coordinate systems used in the georeferencing procedure. (B) Location of the camera monitoring system (C) View of the concrete pillar on which the camera is installed.

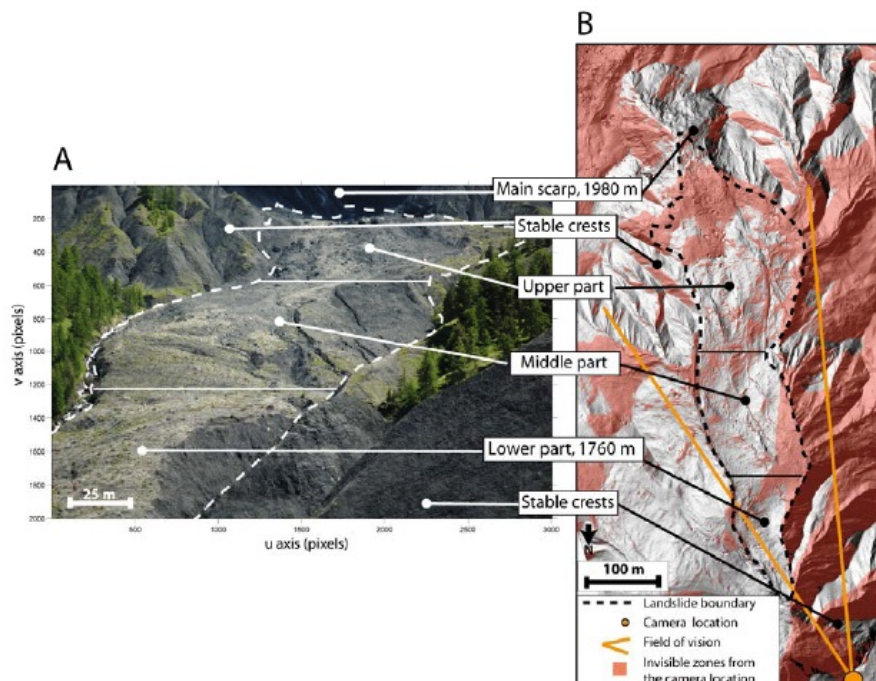


Figure 93. Views of the landslide in the image geometry and in the local coordinate system (A) Image acquired by the monitoring system showing the different parts of the landslide from the camera location. (B) View of the landslide morphology in the local coordinate system on a shaded relief computed with a 0.25 m mesh DEM interpolated from airborne-LiDAR data sets acquired in July 2009. The invisible areas from the camera location are also shown.

The detailed methodology is summarized in Figure 94 and described below.

### **Image correlation technique**

The 2D displacement field is obtained by correlating two optical images acquired at different time. The image correlation technique is based on the automatic identification of identical texture patterns within an image by maximizing a correlation function (Debella-Gilo & Käab, 2010). Its principle adapted for landslide kinematics analysis is described in Delacourt et al. (2007). Visible ground features have to be superimposed on two successive images on stable parts located outside the landslide. On the areas affected by landslide movements, the visible and recognizable features are shifted by the displacements. In order to quantify the ground displacements, a correlation window is defined on a reference (often the oldest) image. The corresponding window is searched in a pre-defined explored area belonging to the second image. In this work, a sub-pixel hierarchical correlation technique is used (Chambon, 2003). The RGB images are first converted in gray-scale images on which a 3x3 pixel Sobel convolution matrix is applied to highlight the ground surface texture. The gradient values are then correlated. Four successive degradations of the image resolution are applied following a pyramidal approach for changing the physical size of the correlation window and of the explored area.

The correlation results consist in matrices of displacements  $\Delta u$  and  $\Delta v$  along the  $u$ - and  $v$ -axes in the image plane with their associated correlation index (Figure 94). Because the pixel size is not constant in the image due to the oblique acquisition, the displacements field correlated in the image plane cannot be directly interpreted in terms of metric displacements. Therefore an orthorectification procedure is necessary for a quantitative analysis of the displacement fields.

### **Ortho-rectification of the displacement field using high-resolution digital elevation models (DEMs)**

The orthorectification procedure consists in transforming the central projection of the image into an orthogonal view of the ground by correcting the effects of various distortion sources such as camera orientation, topographic effects and lens characteristics (Kraus & Waldhäusel, 1998). In terrestrial photogrammetry, distortions induced by topography effects are the most important due to the oblique acquisition of the images. The orthorectification is used to convert the initial  $(u, v)$  and the final  $(u + \Delta u, v + \Delta v)$  positions of the displacement vectors in a local coordinate system. The conversion is possible if a Digital Elevation Model (DEM) of the object is available. In our approach, the rotation angles defining the external orientation of the camera are first determined using the relationship between the image coordinates  $(u, v)$  and the local coordinates system  $(X, Y, Z)$  given by the collinearity equations. Knowing the exact location of the camera and assuming that the principal point coordinates is at the centre of the image, the external angle defining the absolute orientation of the camera in the local reference system can be determined with Ground Control Points (GCPs; Corripio, 2004). In our case, the GCPs located on the landslide by DGPS measurements consisted in red-yellow squared metal targets with a dimension of 0.5x0.5 m identified both in the image plane and in the local coordinate system. A series of 95 pairs of GCPs distributed on the image plane and in the local reference system were measured. The centres of the GCPs are positioned in the local coordinate system with an average 3D accuracy of 0.02 m and a standard deviation of 0.01 m. The coordinates  $(u, v)$  of the GCPs in the image plane are determined by manual picking with

an estimated accuracy of about 2 pixels. Among the 95 GCPs, 45 are used to compute the external parameters and 40 are kept to calculate the accuracy of the transformation. A least mean square minimization technique based on Singular Value Decomposition (SVD) between observed and calculated GCPs in the image plane is used to determine the external parameters that satisfy the collinearity equations (Heikkilä & Silven, 1997). Then, a backward projection method is applied to allocate a 3D coordinate to each pixel coordinate in the image plane (Mikhail et al., 2001). In the backward projection, instead of interpolating in the local reference system, the interpolation is carried out in the image geometry.

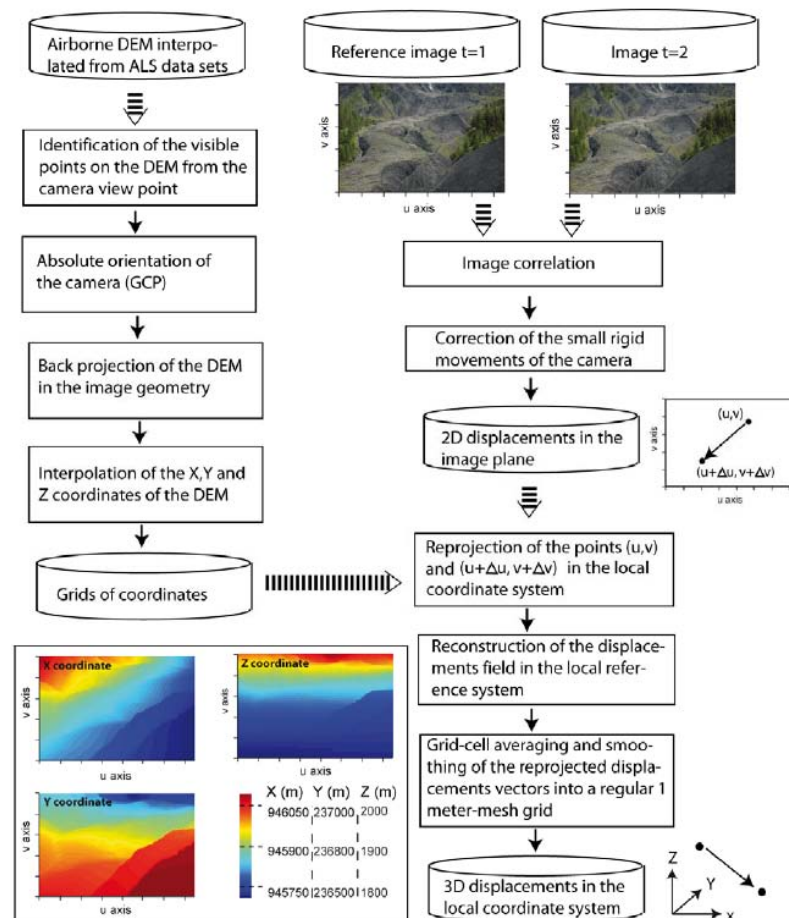


Figure 94. Flowchart of the methodology

### Image resolution at the terrain surface

The effective (e.g. ground) pixel size is calculated using the 2009 DEM projected in the image geometry. The effective pixel size is one limiting parameter for the accuracy of the correlation. The pixel size depends on (1) the distance between the object and the camera (Figure 95A) and (2) the angle of incidence which is defined as the complementary angle between the line of sight of the camera and the normal of the terrain surface (Figure 95B).

The pixel size determines the minimum theoretical displacement that can be detected by the Image Correlation technique for a pixel-level correlation. Below this displacement threshold, the accuracy solely depends on the accuracy of the sub-pixel correlation. Globally, the incidence angle on the landslide ranges from  $0^\circ$  to  $40^\circ$  and the pixel size varies from  $1.10^{-2} \text{ m}^2$  in the lower part (at an average distance of 300m) to  $3.10^{-2} \text{ m}^2$  in the upper part of the

landslide (at an average distance of 900 m; Figure 95A,B). The upper part is characterized by a pixel size often larger than  $0.04 \text{ m}^2$ , especially in areas where the angle of incidence is less than  $5^\circ$ . Therefore the lowest accuracy is expected in this region because a small  $\Delta v$  and  $\Delta u$  displacement can lead to an important  $\Delta X$ ,  $\Delta Y$ ,  $\Delta Z$  metric displacement.

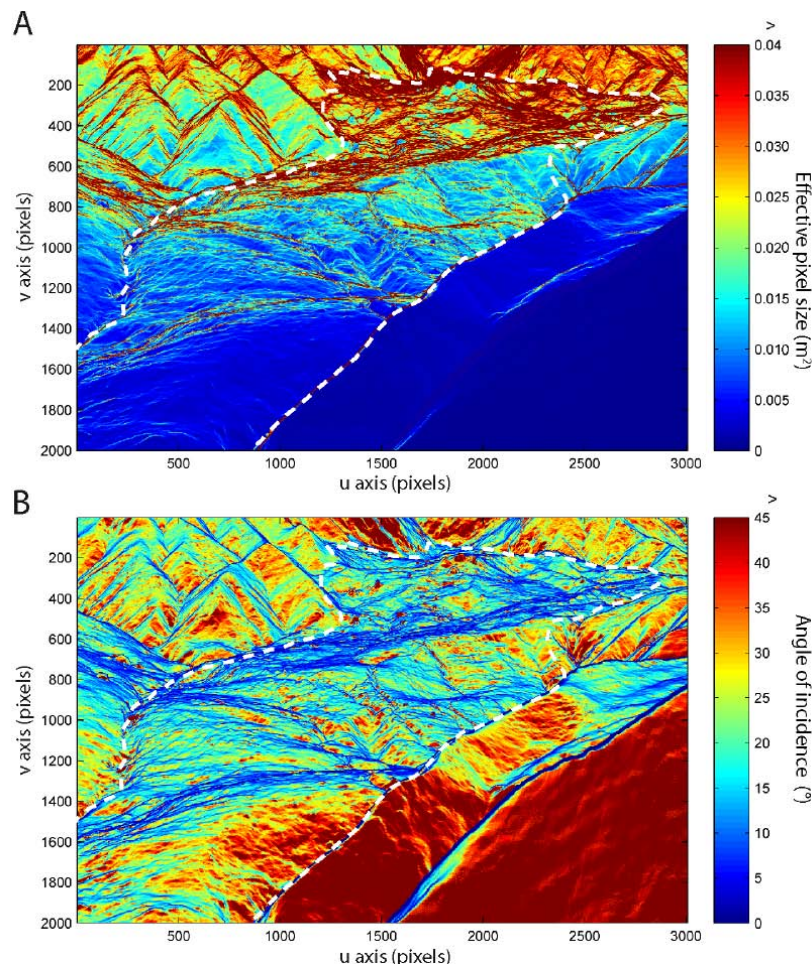


**Figure 95. Image resolution characteristics: (A) Effective pixel size in square meters (B) Angle of incidence in degrees. A low angle means that the line of sight is nearly tangential to the topography.**

### Post-processing: displacements filtering

Filtering criteria are necessary to remove the badly correlated points and improve the signal to noise ratio (Casson et al., 2003; Debella & Käab, 2010). Three criteria are used in this study to filter aberrant displacements in the image plane coordinate system and in the local coordinate system, and are based on: (1) the value of the correlation peak coefficient, (2) the value of displacement amplitudes and directions and (3) the displacements assigned to invisible areas from the camera viewpoint because of small orthorectification errors in the conversion to the local coordinate system.

### 6.1.6.2 Results

#### Displacement maps of the landslide

A set of images over the period May–July 2008 is used to illustrate the potential of the technique for the characterization of the kinematics during an acceleration period triggered by high rainfall amounts and a fast melting of the snow cover (Figure 96).

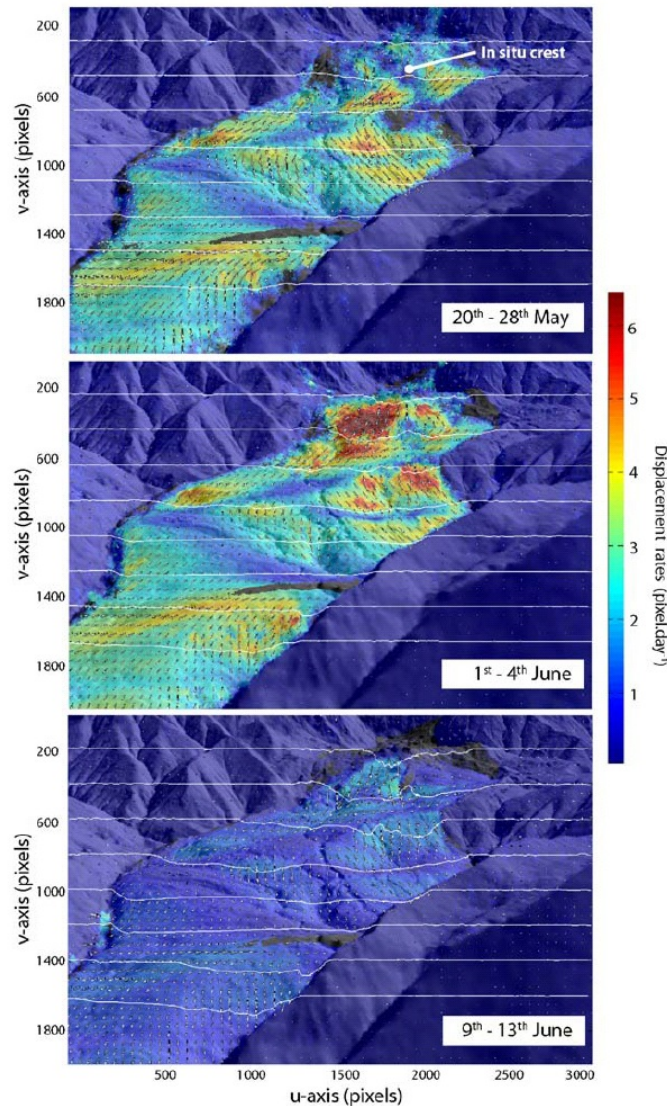


**Figure 96. Displacement rates amplitude (colour) and displacement direction (arrows) in the image plane and cumulated displacements along 8 profiles crossing the landslide over the period 20th May to 25th June 2008. In order to highlight the displacement direction, the arrow length is normalized in each image.**

Figure 96 shows an example of displacement rate (in  $\text{pixel}\cdot\text{day}^{-1}$ ) of the ground surface in the image plane derived from image pairs of 20–28 May, 1–4 June and 9 June–13 June. The reference is the image of 20 May. The contrast in displacement rates between the landslide area and the stable area gives confidence on the calculated velocity field. The pattern of displacement rate is spatially and temporarily heterogeneous. The upper part of the landslide displays the highest velocities ranging from 1 to 7  $\text{pixels}\cdot\text{day}^{-1}$  while the lower part displays velocities of less than 4  $\text{pixels}\cdot\text{day}^{-1}$ . No quantitative comparisons can be carried out at this

stage because the pixel sizes vary strongly in the image. From the 20 May to the 13 June, cumulated displacements up to 110 pixels are observed in the upper part. The maximum of displacement rate is observed around the 1<sup>st</sup> June. Then the landslide decelerates to displacement rate of about 1 pixel.day<sup>-1</sup>. Some local specific displacement patterns are also clearly highlighted; for instance, the presence of a stable *in-situ* crest located in the landslide body is perfectly identified in the correlated images.

Figure 97 presents the amplitude of the 3D orthorectified displacement rates for the period 1<sup>st</sup> June– 4<sup>th</sup> June in the local coordinate system. The difference of kinematics among the upper (until 3 m.day<sup>-1</sup>) and the lower (until 1 m.day<sup>-1</sup>) parts becomes more evident than in the image plane. The geometrical effect induced by the presence of the stable *in-situ* crest on the landslide kinematics is also clearly pointed out. The difference of displacement rates between the upper and the lower part of the landslide is particularly pointed out.

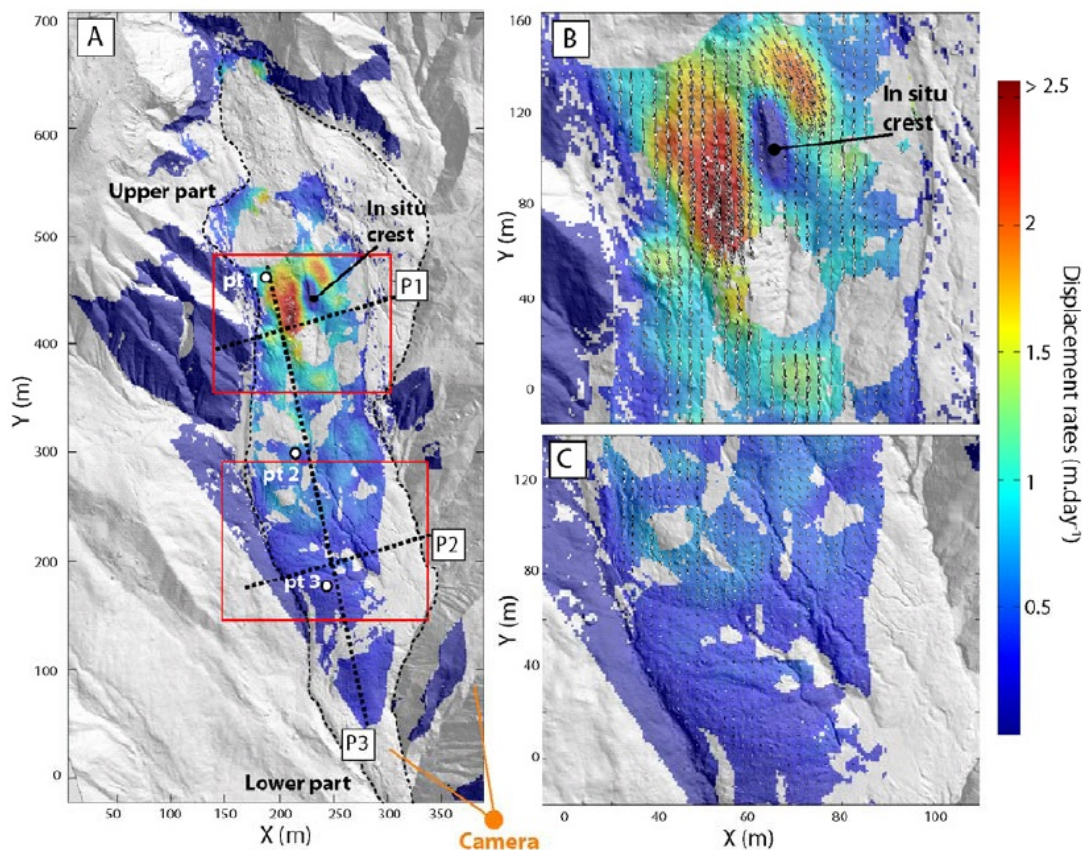


**Figure 97. Displacement rates map for the period 1st – 4th June 2008. (A) Displacement rates observed on the whole landslide. (B) Details on the displacement rates and displacement direction of the velocity amplitude and direction in the upper part. (C) Details on the displacement rates and displacement direction in the lower part.**

The precision of the computed displacements is assessed by performing a null hypothesis on the stable areas (Berthier et al., 2005; Casson et al., 2003). Only the points with a correlation coefficient  $r > 0.8$  are taken into account. In the image plane coordinate system, the average errors  $\mu$  range from 0.5 to 0.9 pixels with standard deviations  $\sigma$  of 0.3 to 1.2 pixels for the image pairs between the 20 May and the 25 June. In the local coordinate system, the average

errors  $\mu$  range from 0.03 m to 0.11 m with standard deviations  $\sigma$  of 0.10 to 0.31 m for the image pairs between the 20 May and the 25 June.

### Comparison with DGPS displacements

In order to estimate the accuracy and validate the calculated displacements, comparisons with independent and more accurate geodetic technique is necessary. Sixty benchmarks distributed in the stable parts and on the landslide body were monitored by DGPS with a horizontal and a vertical average accuracy of  $\pm 0.02$  m and  $\pm 0.05$  m. In total, 219 DGPS measurements are available for the period 2008–2009. In order to validate the displacements computed in the image plane, the DGPS benchmarks are projected in the image plane using the collinearity equations. The pixel displacements derived from the image correlation are then averaged in a perimeter of 16 pixels around each benchmark. The results are presented in Figure Figure 98A. A correlation coefficient of  $r=0.98$  is found between DGPS measurements and Image Correlation, and an average relative accuracy of 11% is determined (Figure 98C). In order to validate the metric displacements in the local coordinate system, the orthorectified displacements are averaged in an area of  $4 \text{ m}^2$  around each benchmark and compared with the DGPS displacements. A correlation coefficient of  $r=0.95$  is found (Figure 98B), and an average relative accuracy of 20% is determined (Figure 98D).

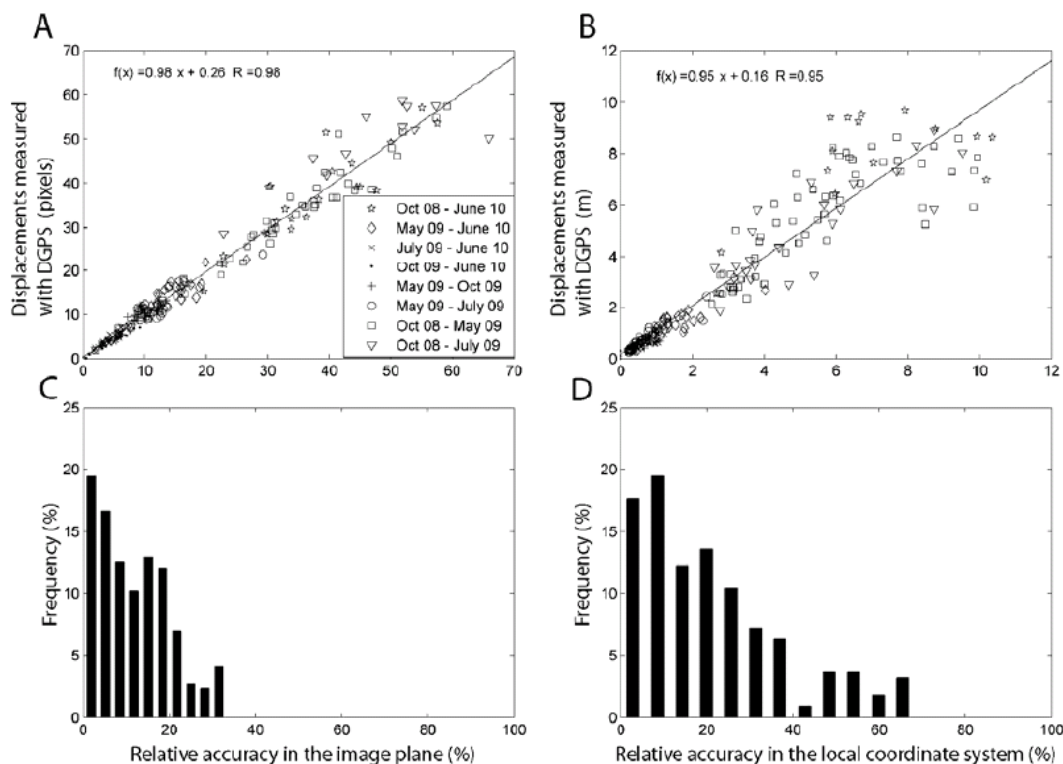


**Figure 98.** Assessment of the accuracy of the Image Correlation technique. Relationships between the displacements observed by Image Correlation and the displacements observed by DGPS on sixty benchmarks in the image plane (A) and in the local coordinate system (B). Relative accuracy of the Image Correlation technique in the images plane (C) and in the local coordinate system (D).

### ***6.1.6.3 Improvements with respect to previous applications***

There are no specific improvements with respect to previous works as this analysis is a first application of correlation of terrestrial optical images to (1) quantitatively characterize the displacement field (pixel and metric displacements) of landslides, (2) propose a methodology and (3) discuss the main sources of errors. The present application could therefore be considered a benchmark for further developments of the technique.

### **6.1.7 Micro-seismic monitoring of soft-rock landslides: Super-Sauze (France)**

*CNRS: Walter M., Joswig M., Malet J.-P.*

This chapter is based on the paper Walter, M., Arnhardt, C., Joswig, M. 2011 (accepted, in press).

#### **6.1.7.1 Study area**

The SafeLand case study for the evaluation of the capability of micro-seismic monitoring to analyse the slide quakes and associated fractures processes observed on landslides is the Super-Sauze landslide located in the Barcelonnette Basin (Alpes-de-Haute-Provence, South East France).

A complete description of the study area is contained in 6.1.6.1.

#### **6.1.7.2 Description of the analysis**

Since 2008, a pilot study on the characterization of seismic signals caused by the dynamics of soft rock landslides (e.g. developed in clay-shales lithology) is carried out at the Super-Sauze mudslide as collaboration among the Institute of Geophysics of the University of Stuttgart and the Institute of Earth Science of the University of Strasbourg. The results of the seismic observations in the year 2008 are presented.

#### **Data acquisition**

Micro-, nanoseismic monitoring (Joswig, 2008) must be seen in a line of several approaches to extend the capabilities of seismic event location down to the level of ambient noise. Seismicity is recorded by individual stations, reliable phase picking demands clear onsets and location utilizes the iterative Geiger approach. The quality control of location results is based on residual analysis of onset times. The complete opposite of microseismic networks properties is an approach recently adapted from exploration seismics, named Passive Seismic (e.g. Kochnev et al., 2007). The region of interest is covered by a large number of sensors, seismograms are stacked automatically in a grid-search method and potential events are identified by accumulation of radiated energy. Depending on the number of stacked channels, signal-to-noise ratios of more than -15 dB can be handled. Between these two methods, nanoseismic monitoring offers a kind of third approach to improve the sensitivity of seismic monitoring down to background noise but to maintain the aspect of single event identification. The improvement is based on the increase in instrumental efforts by upgrading selected microseismic network sites to small arrays. Any small array (Seismic Navigating System – SNS) is comprised of a centre, 3-c sensor, and a minimum of three outer instruments, 1-c seismometers in about 25-30 m distance. An even greater rate of success is due to an innovative concept for seismogram processing and event location, realized by the software HypoLine (Joswig, 2008), for which detailed information is available at: <http://www.geophys.uni-stuttgart.de/lehre/summerschool/tutorial.pdf>

For this study in Super-Sauze, seismic data was acquired during a 10-day campaign (July 14-24, 2008) by deploying four SNS on the mudslide (Figure 99). Data was recorded in continuous mode with a sampling rate of 400 Hz. The layout of the four SNS at the Super-Sauze mudslide during the field campaign was chosen in order to cover seismically most of the mudslide and to concentrate on the mid-part of the slope which shows the highest

dynamics at the surface (Figure 99). The raw-data was high-pass filtered above 5 Hz to eliminate anthropogenic noise sources and to increase the SNR.

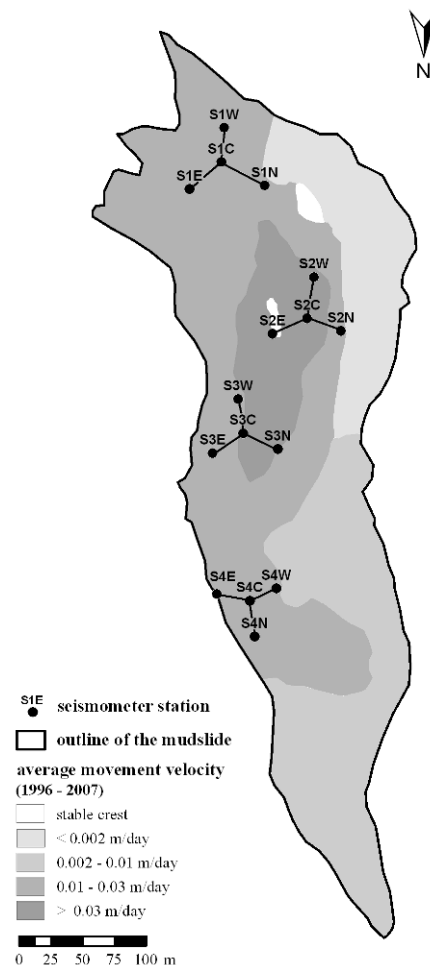


**Figure 99. Location of the installed seismometer stations (black dots) and average movement velocity of the mudslide between 1997 and 2007 determined by Amitrano et al. (2007).**

### Signal analysis and classification

During the campaign in July 2008 we detected and located different types of events caused by material failure within the source area and the mudslide itself. The event types differed in signal duration, number of seismometer stations which recorded the signal, amplitude, frequency content and consequently in sonogram patterns. These characteristics as well as the analysis of further site-effects, like amplitude decrease, absorption and attenuation effects caused by the heterogeneity of the slope material, allowed a classification of the recorded signals (Table 4).

During a pilot study of monitoring slope dynamics of soft rock landslides in the Austrian Alps, we observed only one type of event caused by fracture processes during its movement (Walter and Joswig, 2008). Therefore, we expected at the beginning of the field campaign to record similar seismic events, with a higher amount of them due to the stronger deformation processes at Super-Sauze. Surprisingly, we identified three different types of events on the basis of the aforementioned attributes, which are caused by varying slope dynamics: rockfalls, 155 subsurface fracture processes and superficial fissure development (Table 4).

**Table 4. Classification criteria of seismic signals caused by different slope dynamics.**

Classification criteria	Rockfalls	Fracture events	Fissure development
Signal duration [s]	20-1200	2-5	2-20
Frequency content [Hz]	10-130	10-80	5-150
# of Seismometer stations [-]	8-16	4-12	4
Signal Amplitude [nm/s]	50-1500	40-2000	20-7500

### Seismic signals of rockfalls

During the field campaign, we recorded hundreds of signals with durations between a few seconds (single event) and up to 20 minutes (multiple events) caused by rockfalls which occurred frequently in the source area of the mudslide. The signals show a “noise band” between  $\sim 5$  Hz up to  $\sim 50$  Hz with broadband spikes (Figure 100).

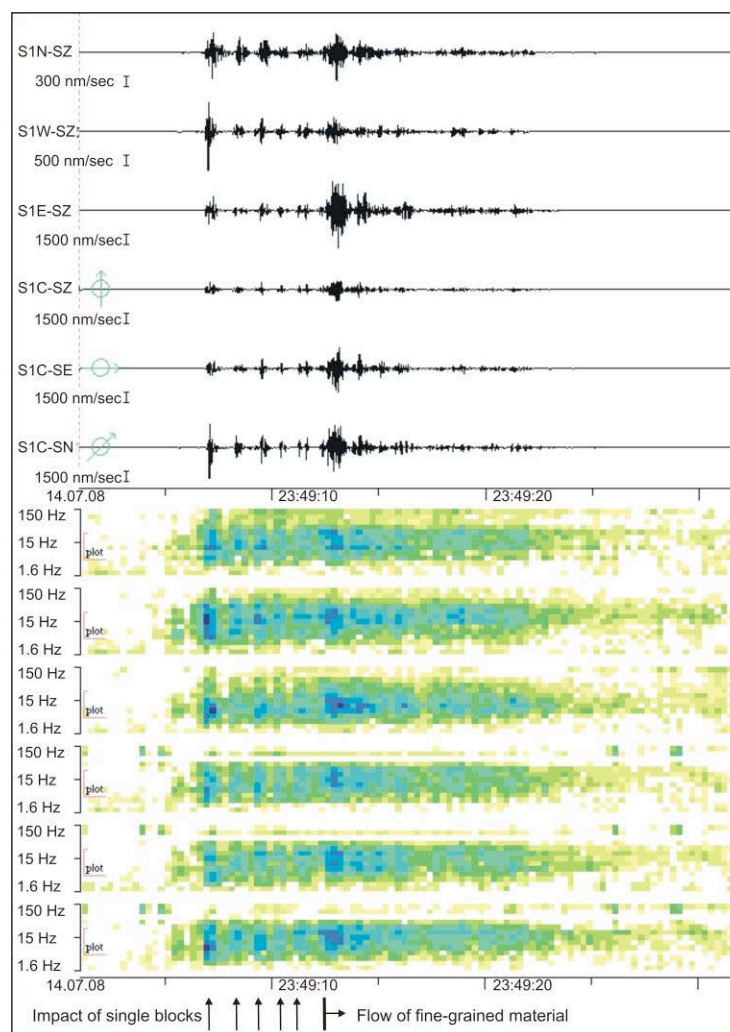


**Figure 100. Typical waveforms and sonograms of a rockfall event, recorded on July 14, 2008, with SNS; the upper three traces belong to the three outer 1c-stations while the lower three traces represent the 3c-central station.**

The “noise band” is caused by the flow of fine-grained material resulting in signals comparable to those of avalanches (Suriñach et al., 2005). The spikes are caused by the

impact of falling blocks, a fact that has been proven by experiments and visual observations in the field. The stronger events show maximum amplitudes (peak to peak) of 500 nm/s - 1500 nm/s and were recorded on all seismometer stations; the weaker ones were recorded at the seismometer stations of only two SNS with amplitudes varying between 50 nm/s and 500 nm/s. The source area of the rockfall events was estimated by determination of the back-azimuth for each SNS which recorded the signal. All these events occurred in the steep, north facing hillsides, on the main scarp of the mudslide.

### Seismic signals of subsurface “slide-quakes”

During the field campaign, we detected 34 signals which show clear phase onsets (Figure 101), allowing their localization by standard seismological procedures. The duration of these events lies between 2–5 seconds, the maximum amplitude varies between 40 and 2000 nm/s (peak to peak) and the frequency content of the P-phase is concentrated between 10–80 Hz while the later arriving phases prevail in lower frequencies between 10-30 Hz. The observed events at the mudslide in Super-Sauze show remarkable similarities to the fractures we recorded at the creeping Heumoes slope in Austria (Walter and Joswig, 2009). For this reason we interpret these signals as results of subsurface stress relief such as “slide-quakes” (shearing, friction, fracturing).

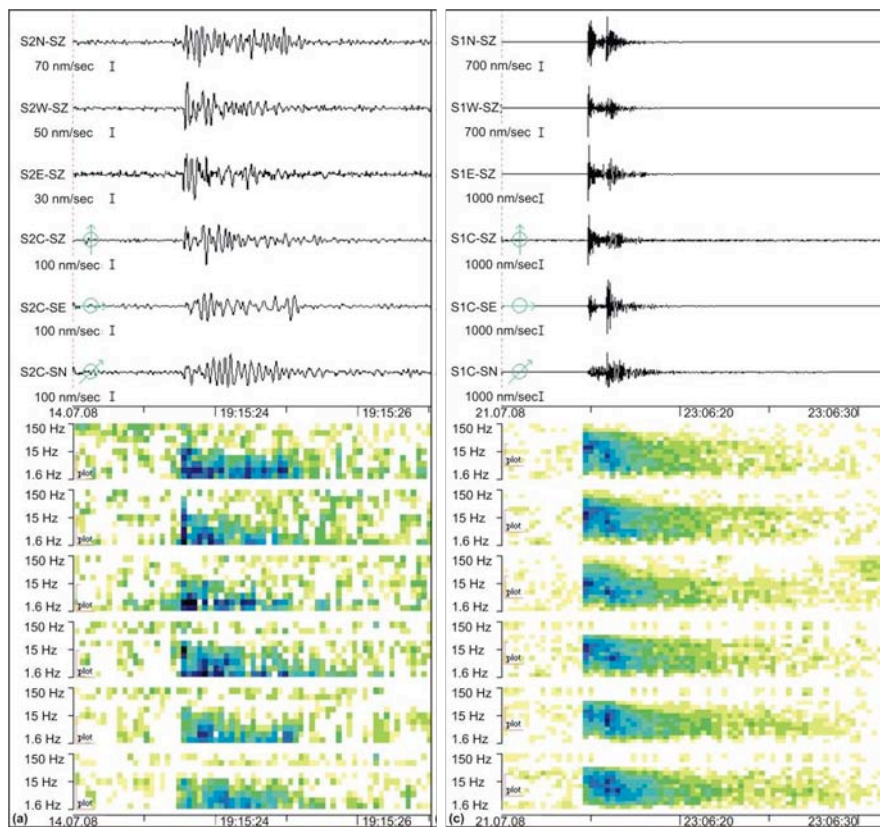


**Figure 101. Typical waveforms and sonograms of fracture processes and local earthquakes recorded with one single SNS: the upper three traces belong to the three outer 1c-stations while the lower three traces represent the 3c-central station. Left: fracture process  $ML = -2.2$  in  $\sim 120$  m distance in Super-Sauze, recorded with SNS 2; Right: local earthquake  $ML = 2.0$  in  $\sim 15$  km distance in Super-Sauze, recorded with SNS 2. Note the different time and amplitude scales.**

The signals had to be recorded on at least 2 SNS to be localizable, where the distance range for reliable detection was within some 200 m. The accuracy of localization was determined to be ~10% of the epicentre distance by the localization of the calibration shots. The emergent onset, the lack of higher frequencies above 80 Hz, and the signal incoherency indicate intense scattering caused by the high heterogeneity of slope material (Figure 101). However, the frequency content of these signals is rather similar to those of weak local earthquakes (Figure 101). Only the amplitudes and the signal lengths of these signals differ distinctly from each other. The amplitude scale of the fracture event of figure 4a, which was recorded in Super-Sauze, varies between 30 – 100 nm/s, and the one of the local earthquake between 700 – 2000 nm/s. These observations can be explained by the varying energy release in dependence of the epicentre distance of the different sources.

The magnitudes of the fracture processes observed at Super-Sauze vary between  $-3.2 \leq ML \leq -1.3$ . They are ~one magnitude order lower than the recorded fracture processes at the Heumoes slope in Austria where the magnitudes range between  $-2.4 \leq ML \leq -0.7$  (Walter and Joswig, 2008). The magnitudes were determined by the maximum amplitude of the S-phase. The ML distance correction curve is based on the analysis of seismic events with short slant distances, done by Wust-Bloch and Joswig (2006). The magnitude variation between the events observed in Super-Sauze compared to the ones at the Heumoes slope in Austria has two reasons: First, the noise-level in Super-Sauze is about 10dB lower, which equates to ~one order of magnitude. Second, the lack of magnitudes  $ML > -1$  in Super-Sauze indicates a lower stress relief for single events, but they occur with a much higher frequency caused by the higher movement velocities compared to the Heumoes slope.

The located fractures are mainly clustered in the middle part of the mudslide (Figure 102). The cluster corresponds to the part of the slope showing the highest velocities at the surface. A cluster of fracture events is located directly at the boundary between the mudslide material and one of the emerging in-situ crests in the central part of the slope (Figure 102) indicating higher deformation processes close to the crest. Not displayed in Figure 102 are three events which were localized in the south, outside of the slope catchments. They were probably generated by material failure in the hard rock mass in the source area of the mudslide. As the event depth could not be evaluated due to the sparse station distribution, it is impossible to estimate at which depth and along which material interface the source processes took place exactly.

Figure 103 displays the localized fracture processes mapped on an aerial picture from 1957, before the mudslide occurred (by courtesy of *Institut Geographique National*, Campaign F3139-3639). Most of the epicentres are located on top of the in-situ crests or in the vicinity of them, today hidden by the mudslide material. This observation supports prior investigations of a direct interaction between the mudslide behaviour and the topography of the bedrock below (Malet, 2003).

Statistics related to the Gutenberg-Richter power law should be drawn from a sufficient number of events. Schorlemmer and Wiemer (2004) propose 50-100 events for reliable  $b$ -value estimation. On the other hand, Neunhöfer and Hemmann (2005) expect only a small  $b$ -value error for a calculation with  $\geq 10$  events. The  $b$ -value of the recorded fracture processes in Super-Sauze was calculated with 22 events with magnitudes  $ML \geq MC$ , where MC is the magnitude of completeness or the detection threshold during the measurement period. The error of magnitude determination was estimated to be  $\pm 0.1$ . Hence the magnitude of completeness is  $MC = -2.6 \pm 0.1$  (Figure 104). The cumulative and the incremental number of fracture events as well as the  $b$ -value are illustrated in the frequency magnitude distribution in

---

Figure 104. The  $b$ -value was calculated to be  $0.84 \pm 0.18$ ; the standard error was estimated after Utsu (1965) with  $berr \approx b/\sqrt{N}$ , where  $N$  is the number of events with  $ML \geq MC$ .

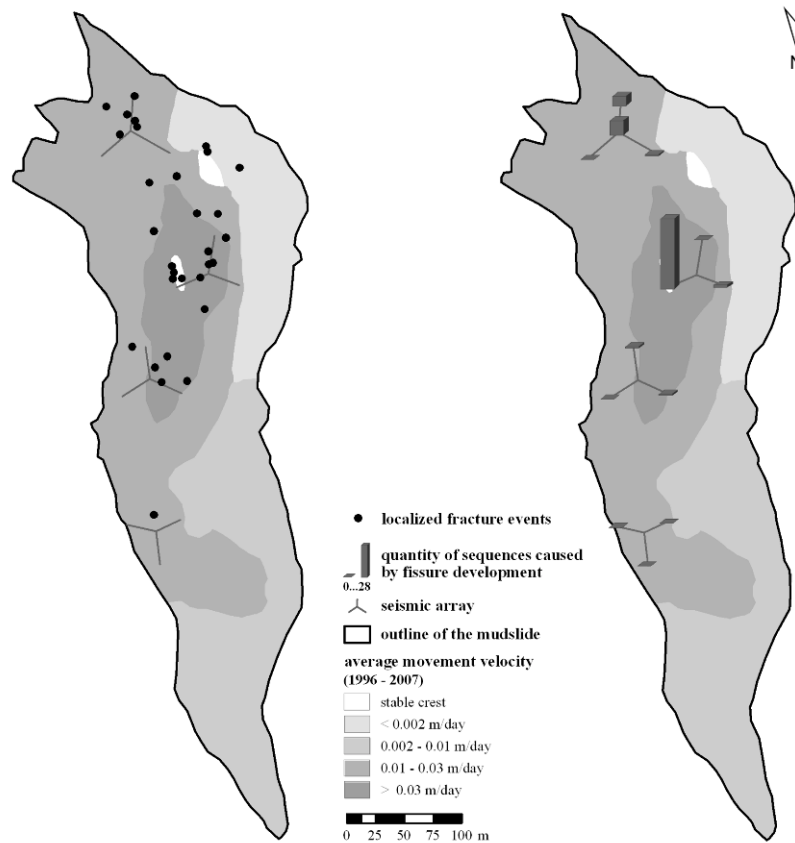


Figure 102. Epicentres of the fracture processes (left) and quantity of sequences caused by superficial fissure development (right) mapped on the average movement velocity of the mudslide (1997-2007) determined by Amitrano et al. (2007).

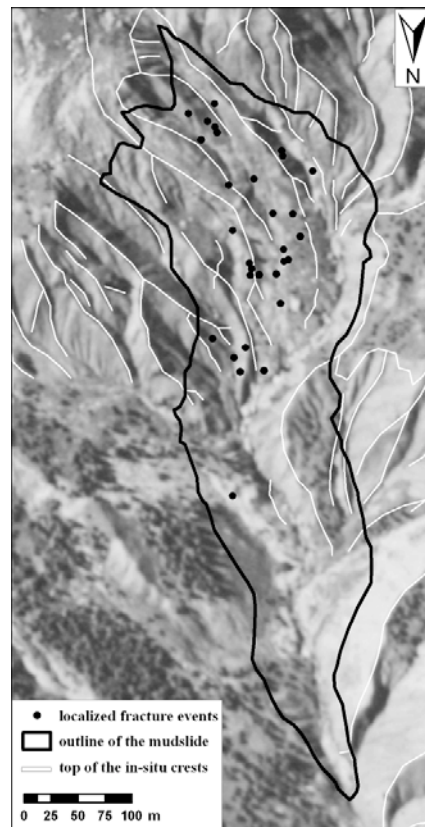


Figure 103. Epicentres of the located fracture processes mapped on an airborne picture from 1956, courtesy of IGN (Institut Geographique National, Campaign F3139-3639). Highlighted are the tops of the in-situ crests of the bedrock's topography.

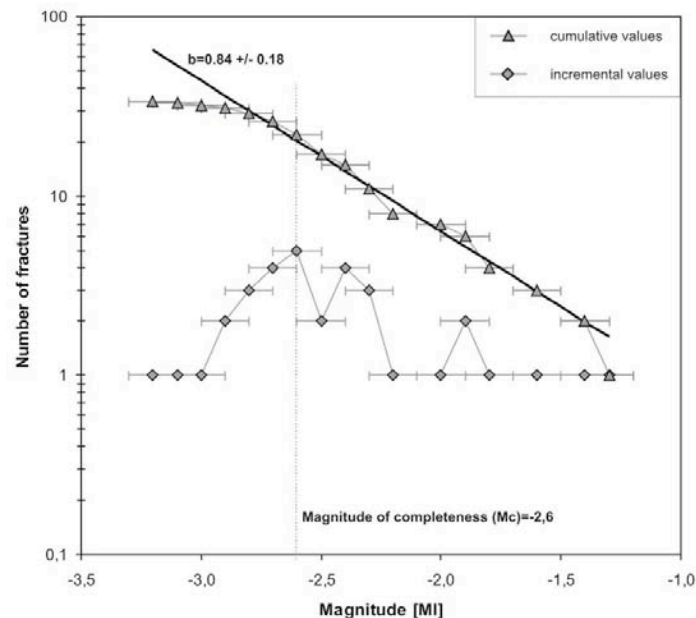


Figure 104. Frequency-magnitude distribution and b-value of the recorded fracture events in July 2008 at the mudslide in Super-Sauze. The determined magnitude of completeness (MC) is shown with the black dashed line. The horizontal error bars mark the uncertainty of magnitude determination of  $\pm 0.1$ .

### **Seismic signals of superficial fissure development**

Besides seismic signals caused by rockfalls and subsurface fracture processes, we recorded and identified 44 signals showing significant differences (Table 4). The increased sensitivity at the mudslide in Super-Sauze compared to our seismic measurements at the Heumoes slope in Austria resulted in the detection of signals caused by the movement of the slope, which lay barely above the low, ambient noise level. For this reason, these events were not observed at the Heumoes slope and were not expected at the mudslide in Super-Sauze. The duration of these events, which were only recorded at one single SNS, varied between 2-20 seconds. Compared to the other event types, the signal energy prevailed at higher frequencies: up to 150 Hz at the closest station in the array (Figure 105). Due to the heterogeneity of the slope material, we saw enormous attenuation effects within one single SNS; the signal amplitude decreased about 30 times within one single 308 SNS at the same time (Figure 105).

Similar to the rockfall events, no wave phases could be identified in the signals, which prevented their localization by standard seismological procedures. Therefore we could only estimate the source area, which is for obvious reasons, in the vicinity of the closest station with the highest recorded amplitude.

A first model of the generation of these seismic signals interprets these events as a result of “scratching” and “grinding” sequences of the mudslide material against the (emerging) in-situ crests (Walter and Joswig, 2009). The joint analysis by nanoseismic monitoring and UAV (Unmanned Aerial Vehicle) based remote sensing (Niethammer et al., 2009; Walter et al., 2009; Niethammer et al., 2011) reveals the generation of these signals by fissure development on the mudslide’s surface. The high-resolution pictures of the mudslide in Super-Sauze by UAV-based remote sensing show specific deformations of the mudslide material at (emerging) in-situ crests and lateral boundaries resulting in particular fissure patterns at the surface (Niethammer et al., 2009; Niethammer et al., 2011).

#### ***6.1.7.1 Synthesis of the results***

By applying the nanoseismic monitoring, we were able to detect and partially locate distinct types of events caused by the activity of the Super-Sauze mudslide. Waveform and sonogram analysis were applied to discriminate the event types. We identified signals caused by rockfalls, subsurface fracture processes and fissure development at the mudslide surface. The rockfall signals show remarkable similarities to those of avalanches. The “noise band” with a frequency range between ~5 Hz and ~50 Hz is caused by fine-grained material, while the broadband spikes represent the impact of blocks, which has been proved by experiments and visual observations in the field.

The source area of the rockfalls is estimated to be at the uppermost part of the slope, where rockfalls with particles of varying size occur frequently. Beside rockfalls, we recorded 34 fracture events with magnitudes between  $-3.2 \leq ML \leq -1.3$  which show significant similarities to the ones we observed at the creeping Heumoes slope in the Austrian Alps. The spatial distribution of the localized fracture events correlates quite well with parts of the slope showing the highest movement velocities. The highest magnitudes of these events were observed a few hours after a rainfall event on July 21, 2008. Besides that, the temporal occurrence of these fracture processes was more or less uniformly distributed over the whole measurement period. The analysis of the magnitude-frequency distribution shows that the fracture events follow the empirical Gutenberg-Richter relationship, with a  $b$ -value of  $b = 0.84 \pm 0.18$  for events with magnitudes higher than the magnitude of completeness  $MC = -$

2.6 +/-0.1. The calculated  $b$ -value is in accordance with  $b$ -values ( $\sim b < 1$ ) which were observed during brittle rock deformations by Scholz (1968). The magnitude of completeness has to be considered regarding the spatio-temporal occurrence of the fracture processes, but does not influence the observations and interpretation in general.

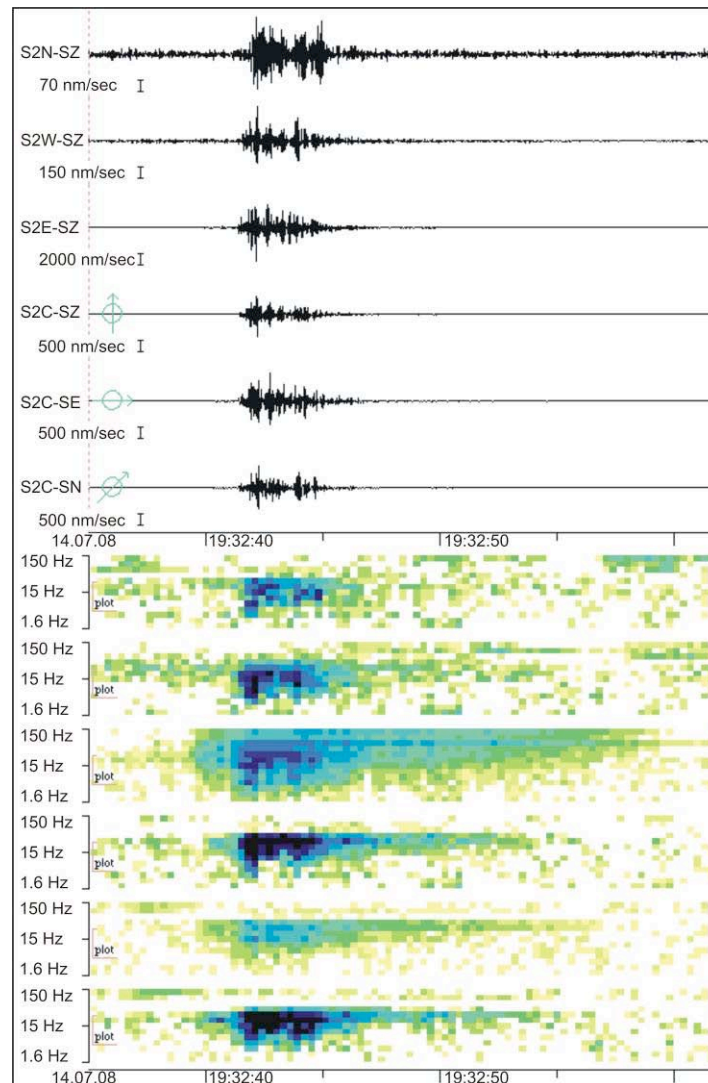


**Figure 105.** Typical waveforms and sonograms of an event caused by fissure development at the mudslide's surface (see text), recorded with SNS 2: the upper three traces belong to the three outer 1c-stations while the lower three traces represent the 3c-central station. Note the different amplitude scales, signal duration and frequency content.

Additionally, we identified seismic signals caused by fissure development at the surface of the mudslide. The signals, which were only recorded with one single SNS, show an enormous amplitude decrease and attenuation of high frequencies within a few meters. The majority of these events are generated, again, close to the emerging in-situ crest of the slope.

Simultaneous measurements of fissure development by nanoseismic monitoring and extensometer devices in July 2009 proved that these signals were generated by fissure development. The temporal occurrence of the seismic events correlates well with the measured opening of an existing fissure. Further signal analyses were carried out in order to

determine the source processes. The sonograms of rockfall events show remarkable similarities to those events generated by fissure development indicating comparable slope processes. We assume that the fall of small particles in existing fissures generated the observed seismic events.

Stress relief within weak sediment material can be generated depending on its water saturation. Shear strength analysis of the material of the mudslide at Super-Sauze, depending on its water saturation, shows the highest values between 12-15 % water content, up to 27-28 % water content the material generally deforms in a brittle manner (Malet, 2003). These values are consistent with those of the first few meters beneath the surface of the slope. Below, the material is almost water saturated. As a brittle material deformation is needed for both impulsive stress relief and fissures generation, we presume that the fracture processes as well as the signals caused by fissure development are generated close to or directly at the surface, respectively. The fact that we located most of the fracture events as well as the majority of events caused by fissure development directly at the boundary between the sliding material and one of the emerging in-situ crests suggests the possibility of higher stress relief in general at that boundary. To prove this assumption, we overlaid the location of all these events with an airborne picture taken in 1956, before the mudslide occurred. Most of the epicentres are located on top of the in-situ crests, today hidden by the mudslide material. Specific fissure patterns at the mudslide surface in that area observed by UAV-based remote sensing prove the observation of differing dynamics in that area (Niethammer et al., 2011; Walter et al., 2009).

In close collaboration with colleagues from the OMIV-project (Observatoire des Instabilités de Versants), a hydrological model will be developed in the future in order to verify the spatio-temporal occurrence of seismic signals and the hydrological properties of the mudslide's material. The joint investigations of the mudslide in Super-Sauze by nanoseismic monitoring and UAV-based remote sensing will be extended, focusing on spatially limited areas of the slope, e.g. focusing on the emerging in-situ crest where specific deformations take place. A permanent seismic network was installed in summer 2009 on the mudslide by colleagues from the University of Strasbourg in order to prove our first observations and to investigate the spatio-temporal occurrence of the seismic events by long-term observations.

#### ***6.1.7.2 Improvements with respect to previous applications***

There are no specific improvements with respect to previous works as this analysis on soft-rock landslides is a first application of micro-seismic monitoring to (1) quantitatively characterize the type of seismic signals within a mudslide, (2) locate and characterize the sources.

## 6.1.8 Optical fibres and TDR: experimental flume

AMRA: Guida A., Minardo A., Damiano E., Picarelli L.

### 6.1.8.1 Description of the analysis

An instrumented small-scale flume was set-up at the Second University of Naples to investigate the mechanics of rainfall-induced landslides. The experiments have been conducted on air-fall unsaturated cohesionless pyroclastic soils, taken at the experimental fields of Cervinara and Monteforte Irpino, north-east of Naples, Southern Italy. The soil is a silty sand with a high sandy component and a significant amount of non-plastic silt. In the flume, controlled evaporation and infiltration processes taking place in model slopes of various geometries can be reproduced. The flume is equipped with a series of sensors allowing accurate monitoring of a number of hydrological and mechanical variables during the experiments. The infiltration experiments can be continued until slope failure is reached. A sketch of the flume is given in Figure 106. Artificial rainfall is applied by several spray nozzles installed above the lateral sides of the flume, allowing producing vertical rainfall intensity between 10 mm/h and 110 mm/h. In order to prevent erosion of the soil surface, the adopted nozzles produce atomized water particles 0.1 mm in diameter. Applied rainfall intensity is measured by a horizontal tipping bucket rain gauge located at the foot of the slope. Two experiments were conducted: (test 1) on homogeneous slope made up of ashes, (test 2) on layered slope (alternation of ashes and pumices). The deposits were reconstituted at porosities similar to the in situ ones (about 70% for ashes and 55% for coarse pumices), varying the geometry, the initial conditions and the rainfall intensity.

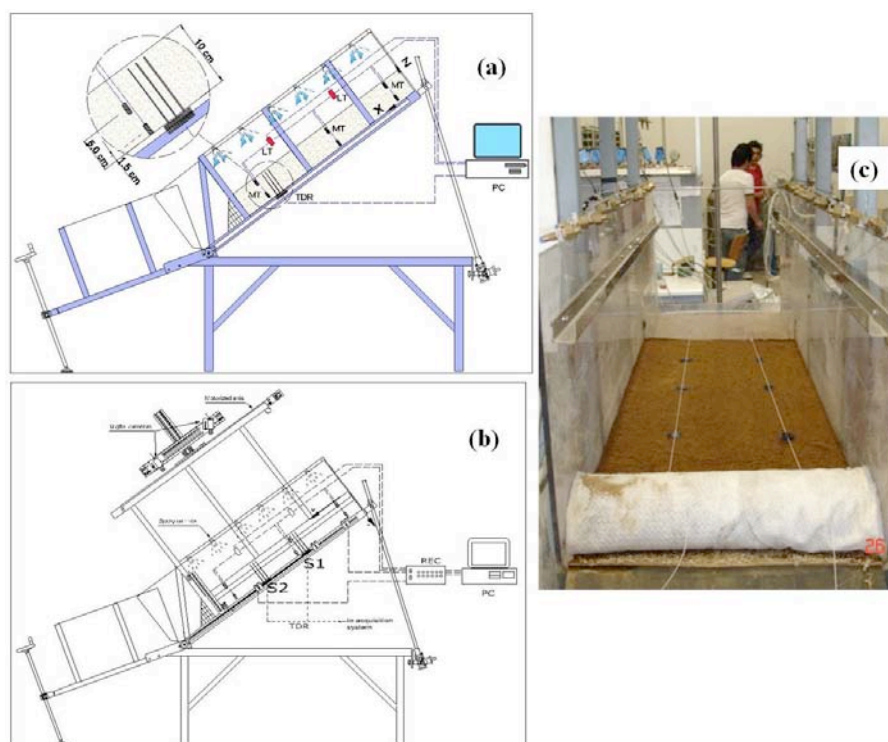
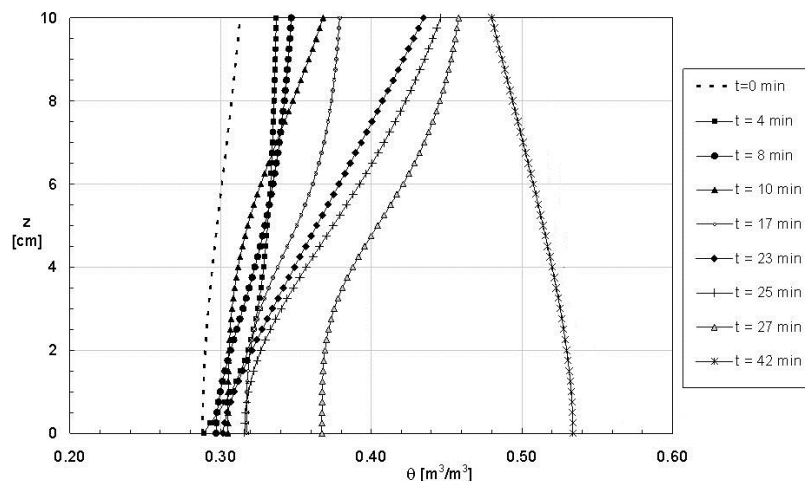


Figure 106: Sketch of the instrumented flume employed for test 1 (a) and test 2 (b), and disposition of the embedded fibre strands in both tests (c).

In both tests soil water content profiles were measured by Time Domain Reflectometry (TDR) metallic probes. Soil water content measurements were carried out with a recently proposed method allowing retrieving moisture distribution along a TDR metallic probe buried into the soil (Greco, 1999; Oswald et al., 2003; Greco and Guida, 2008). TDR experimental apparatus consists of a cable tester connected to a three rods metallic probe (one for Test 1 – two for Test 2) buried in the slope orthogonal to soil surface, as shown in Figure 106(a-b).

In conjunction with the TDR equipment, a distributed optical fibre sensor based on Brillouin scattering was also employed during the experiments in order to detect soil movements. The fibre-optics equipment had a strain resolution of  $\pm 20 \mu\epsilon$ , and a spatial resolution of 1 m. The fibre employed for the experiments was a single-mode standard optical fibre, protected by an outer PVC tight jacket with a diameter of 900  $\mu\text{m}$ . Two 1-m-long strands of fibre were placed within the soil layer, along two parallel longitudinal directions of the flume, as shown in Figure 106c.

We show in Figure 107 and Figure 108 the results of Test 1. In particular, Figure 107 reports the volumetric water content profiles retrieved by TDR during the infiltration experiment. During the initial phase of the infiltration process, the water content profiles were characterized by the presence of steep water content vertical gradients. This behaviour is typical of very coarse soils, for which hydraulic conductivity dramatically reduces at low water contents. Afterwards, also the deepest part of the soil profile started wetting and the acquired profiles tend to smoothen up.



**Figure 107: Volumetric water content profiles acquired by TDR probe at various stages of infiltration experiments.**

Figure 108 shows the strains measured along one of the two buried fibre strands, by use of the optical fibre sensor. The readings were performed with a time-lag of about five minutes, starting from the onset of the artificial rainfall. Note that the reported strain values were obtained by converting the measured Brillouin shifts with a calibration factor of  $20 \mu\epsilon/\text{MHz}$ .

The two vertical red dashed lines indicate the time in which rainfall began ( $t=0$  min) and the time when slope failure was observed ( $t=65$  min). It can be seen that the fibre strain increased gradually during the experiment, with a higher gradient in the last twenty minutes. It can be noted that the initial strain was not zero, due to a pre-tensioning given to the fibre during the embedding procedure.

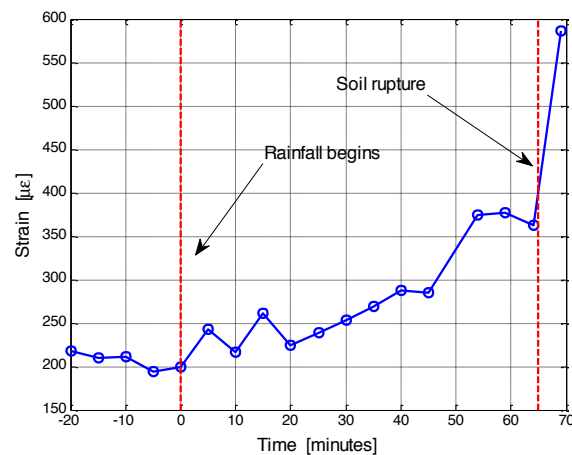


**Figure 108: Longitudinal strain acquired along a fibre strand immersed into soil.**

It is interesting to search for a correlation between data provided by TDR equipment and those provided by fibre-optics sensor. Comparing Figure 107 and Figure 108, it can be seen that larger soil movements occurred after wetting of the deepest part of the soil layer i.e., after about 40 minutes the beginning of the infiltration, as a result of volumetric collapse due to progressive suction decrease in a deposit of such high porosity.

Figure 109 and Figure 110 report the results of test 2 on a layered slope. This test was carried out with a slope gradient of  $38^\circ$ , with a rainfall intensity of 50 mm/h, and had duration of 180 min. The test can be considered as representative of a very persistent and intensive meteoric event.

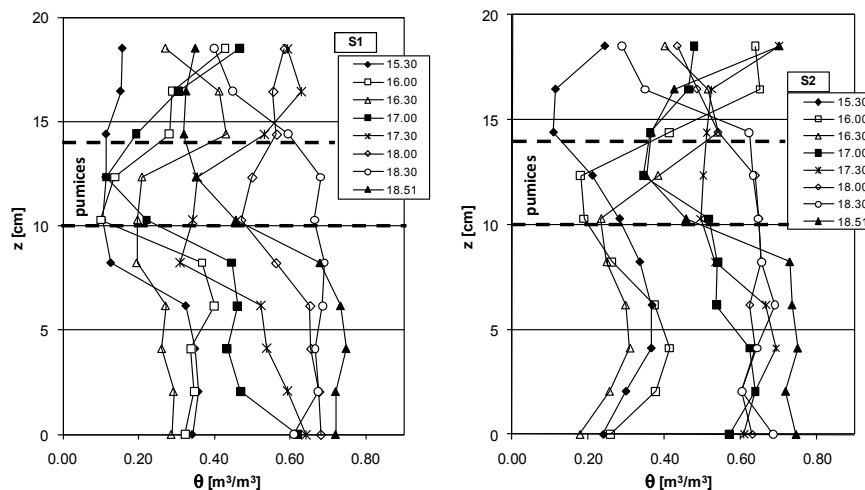


**Figure 109: Moisture profiles measured during Test 2 by use of probe S1 (left) and probe S2 (right).**

Figure 109 shows some moisture profiles measured by the two probes S1 and S2 located respectively upstream and downstream. It can be noted that the TDR inverse method is able to capture the presence of a layered deposit: looking at each profile it may be noted that the location of the pumice layer was clearly identified since the presence of coarsest grains determined lower values of volumetric water content.

The water content profiles were very similar during the initial and final stages. Instead, during the intermediate phase of the test the profiles measured by the two probes were very different;

the downstream part of the slope, where the probe S2 is installed, remained always more humid than the upstream part, especially in the more superficial ashy layer. Probably this event is due to the three dimensionality of the infiltration process, caused by the presence of the pumice layer and the slope inclination. In unsaturated conditions the flow in the slope direction through the superficial layer (ash) is due to the lower hydraulic conductivity of the pumice layer which acts as a barrier. Close to saturation the release of stored water from the upper ashy layer towards the bottom of the flume is due to the strong increase of the hydraulic conductivity of the pumices. This mechanism can justify why, at the bottom of the slope, the deepest ashy layer reached a condition close to saturation more rapidly.

As regards fibre-optic measurements (Figure 110) it can be seen that the embedded fibre recorded a rapid increase of tensile strain after about 90 minutes the beginning of the infiltration. This result is coherent with the acquired moisture profiles shown in Figure 109. Actually, after about 90 minutes the water content in the deepest soil layer increased abruptly, indicating an infiltration of the water through the middle layer of the soil. At this point, the water reached the deepest layer where the fibbers were embedded, producing soil deformation and then inducing stress acting on the fibbers.

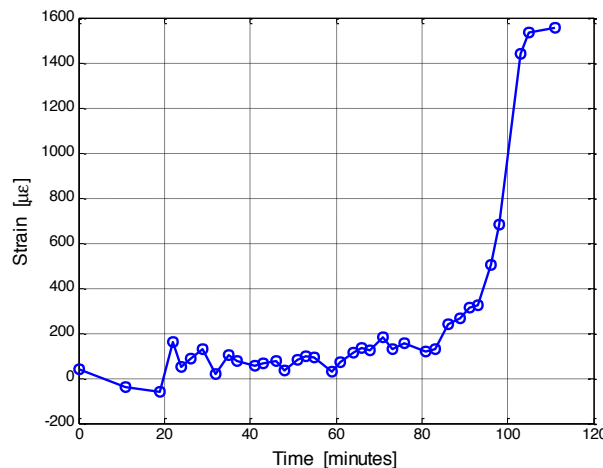


Figure 110: Longitudinal strain acquired along an immersed fibre strand.

### 6.1.8.2 Improvements with respect to previous applications

We have shown that both TDR and fibre-optics sensing technologies offer great potentialities in the field of geotechnical monitoring. Two test-cases were reported, for which data provided by TDR and fibre-optics sensor were shown to be somewhat correlated. Indeed, the fibre-optic-detected soil movements occurred after wetting of the deeper soil, as detected by TDR. In conclusions the simultaneous measurement of different physical quantities (e.g., moisture profiles and soil movements) may be also of usefulness in order to provide an accurate modelling of soil behaviour in real test-cases.

## **6.1.9 Geoelectric monitoring: Gschlifgraben.**

*GSA: Supper R., Baron I., Jochum B.*

### **6.1.9.1 Study area**

The Gschlifgraben site is one of the most prominent and extensively studied slope failures in Central Europe. In December 2007 the large landslide system inside the Gschlifgraben valley (located at the east edge of the Traun lake, Upper Austria), known over centuries for its repeated activity, was reactivated. Although a hazard zone map was already set up in 1974, giving rise to a complete prohibition on building, some hundreds of people are still living on the alluvial fan close to the lake. Consequently, in frame of the first emergency measures, 55 buildings had to be evacuated. At the beginning the displacement velocity was up to 4.7 m/day. A more detailed geological description appears in another chapter of this report, dealing with the airborne geophysical survey of this site (6.2.6.1).

Within the first phase of mitigation in 2008, major measures were focused on property and infrastructure protection. About 220 wells and one deep channel were implemented to drain the sliding mass. Additionally a big quantity of sliding material was removed close to the inhabited areas. Differential GPS and water level measurements were performed to evaluate the effectiveness of the measures, which led to a significant slowdown of the movement. During the second phase (soon after the suspension of the evacuation), multi-disciplinary investigations including drilling, borehole logging and complex geophysical measurements (e.g., geoelectric, seismic and GPR surveys), were performed to investigate the structure of the landslide area in order to evaluate maximum hazard scenarios as a basis for planning further measures. Based on these results, monitoring techniques for an early warning system are currently being tested within the third phase. This early-warning system should enable local stakeholders to provide an appropriate response in any case of further landslide reactivation. Several innovative approaches were applied, such as the airborne multiparametric geophysical survey, differential ALS, automated D.M.S. inclinometers, discharge monitoring and DGPS surveys.

### **6.1.9.2 Description of the analysis**

The electrical resistivity of the subsurface mainly depends on porosity, saturation, pore fluid conductivity and clay content. Therefore the geoelectric method is a reliable method to investigate the structure of a landslide and its surroundings. Since mass wasting is often triggered by rising water pore pressure and other hydrogeological changes, monitoring of geoelectrical parameters, like subsurface resistivity or self-potential could be an emerging tool for observing those triggering factors.

Before the installation of the monitoring equipment at the Gschlifgraben site, a multi-electrode geoelectrical survey was performed in a broader area of the active earthflow to verify the subsurface structure and to optimise the location for a geoelectric and displacement monitoring system. Figure 111 clearly highlights the correlation of the geoelectric pattern with areas of different displacement characteristics. The low resistivity structure at the top correlates with the most active top layer, whereas the region with higher resistivity below exhibits only a slowly creeping behaviour. The sliding surfaces detected by the DMS inclinometer are clearly marked by high gradients of resistivity.

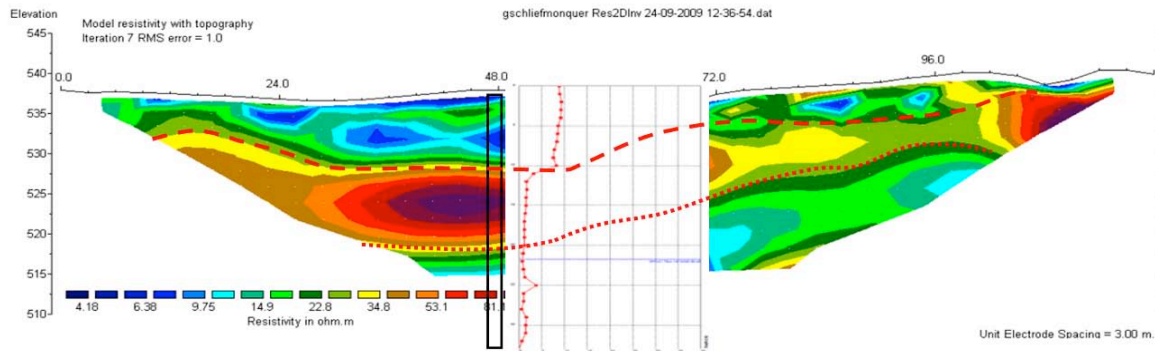


**Figure 111. Correlation of resistivity layers with sliding surfaces determined by a permanent inclinometer (red curve) in the area of Gschliefraben.**

Based on these promising results, a geoelectric monitoring system of the type Geomon<sup>4D</sup> was installed in the upper central part of the active earthflow of Gschliefraben in September 2009 (Figure 112, Figure 113) as a part of the early warning approach at the Gschliefraben test site.

The Geomon<sup>4D</sup> was specifically developed for monitoring applications by the Geological Survey of Austria (Supper et al. 2003, 2009, and 2010). The completely open architecture of the instrument allows installation of any number of current or potential electrodes by adding parallel or serial cards. Furthermore, data acquisition at a speed of about 3000 measurements/hour in single channel mode and usually 1000 samples per single configuration including recording of the full signal enable an effective noise analysis and filtering. The GPRS (General Packet Radio Service) data transfer allows the maintenance to be performed fully remote-controlled. Data (such as measurement results, test sequences and log files, containing information about system and GPRS connection status) are sent automatically via email to the data processing centre at GSA. Consequently, immediate availability of information for local stakeholders could be guaranteed. For power supply a 500 m long cable was installed to connect to the local power grid. The length of the two perpendicular profiles (for location see Figure 112) is 120 m (electrode separation 3 m, 41 electrodes) and 192 m (electrode separation 4 m, 49 electrodes).

To define correlation between geoelectric anomalies and the triggering of movements, a multiparametric monitoring system of stability D.M.S. (Differential Monitoring of Stability; Centro Servizi di Geingegneria, Italy) was installed at the crossing point of the GEOMON<sup>4D</sup> profiles. The D.M.S. tool measures differential displacements with an extremely high accuracy (fractions of a millimetre) in 2 or 3 directions (both horizontal and vertical at all the prefixed depths), piezometric ground-water level and soil temperature up to the depth of 32 m below the ground-surface. Thus it allows a complex analysis of the dynamics of the mass movement, e.g.: deformation analysis, displacement, velocity, acceleration, and depth of failure or piezometric variations (Fogolino et. al., 2006).

Along each of the geoelectric profiles a complete tomographic data set, each consisting of around 1000 single values of Gradient configurations, was measured every four hours. The self-potential sequence was repeated every hour. The interval of the displacement measurements was set to half an hour.



Figure 112. Location map showing the position of the geoelectric monitoring profiles (red lines) on the landslide of Gschlifgraben.

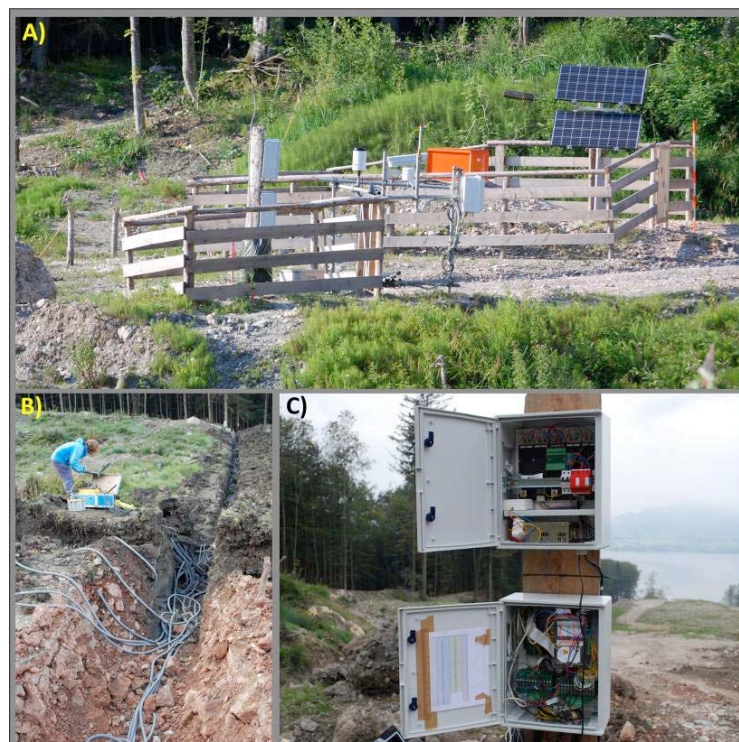
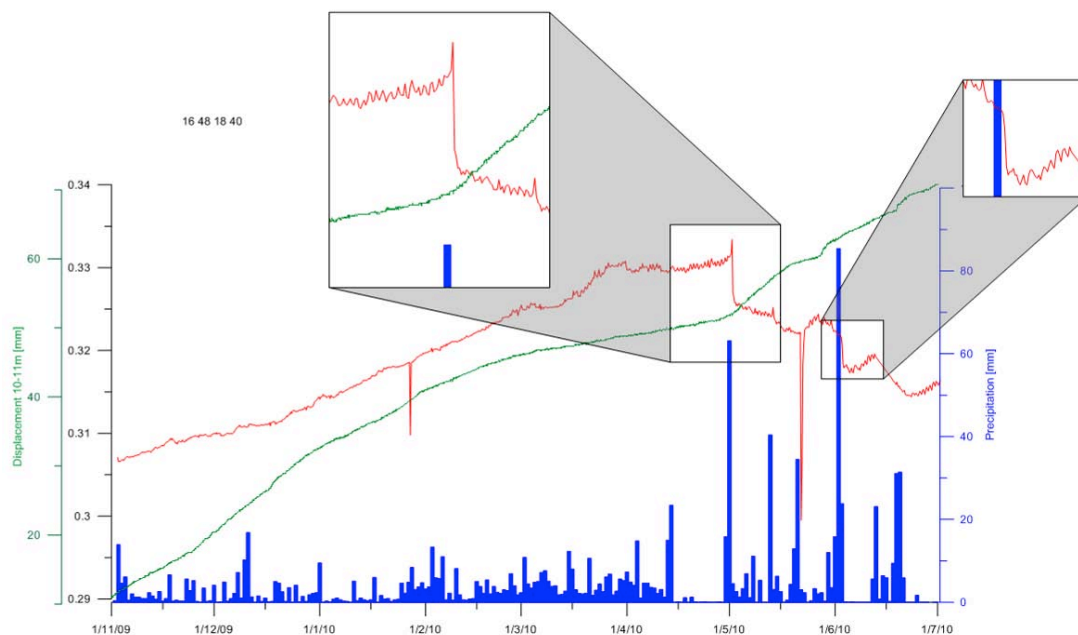


Figure 113. GEOMON<sup>4D</sup> instrument at the Gschlifgraben site: A) the control panel and the central unit were placed close to crossing of both monitoring profiles and close to the D.M.S. automatic inclinometer; B) the electrodes and cables were buried up to 1 m below the ground surface to protect them against major meteorological and mechanical circumstances; C) general appearance of the control unit (Photo by: Ivo Baron 2009 and 2010).

Figure 114 and Figure 115 show the monitoring results in the time interval from November 2009 till July 2010. In the period from August 2010 till February 2011 hardly any changes in the displacement velocity were detected. Therefore these results are not displayed.

The most significant change took place on the 1<sup>st</sup> of May 2010, when a thunderstorm passed by Gschliefraben and triggered a small mudflow. The retention basin in the upper part of the landslide was flooded and started a torrent which filled up the deep drainage trench at the base of the geoelectric monitoring line. This event immediately caused an increase of the displacement velocity and a small but significant decrease of the electrical resistivity after the rainfall event. Later, but even heavier rainfalls did not cause changes of the same quantity of displacement as the event on May, 1<sup>st</sup>. Therefore we conclude that the flooding of the deep drainage trench was mainly responsible for the increase of the displacement velocity. The long periodic trend in the curve of the electrical resistance is due to seasonal temperature variations. An algorithm to properly correct for this influence is still under development.



**Figure 114. Results of monitoring at the landslide of Gschliefraben in the period of November 2009 till July 2010: precipitation (blue), cumulative displacement (green) and normalised electrical resistance (red; configuration 16-48-18-40).**

Since the rainfall events had an almost immediate impact on the displacement and subsurface resistivity at this test site, no statement can be passed on the ability of geoelectrics to predict displacements based on the available data. The same is also true for the self-potential anomalies (Figure 116), which are directly related to rainfall events. However the recorded changes in the displacement velocity can be characterized as very small events which did not change the general behaviour of the earthflow or endanger any settlements or infrastructure. Rainfalls had only impact on the near surface layers, but did not change the hydraulic conditions in the deeper subsurface. Consequently to evaluate the prediction ability of geoelectrics, we have to wait for larger events, which hopefully will not happen in the near future. Therefore other test sites have also to be equipped.

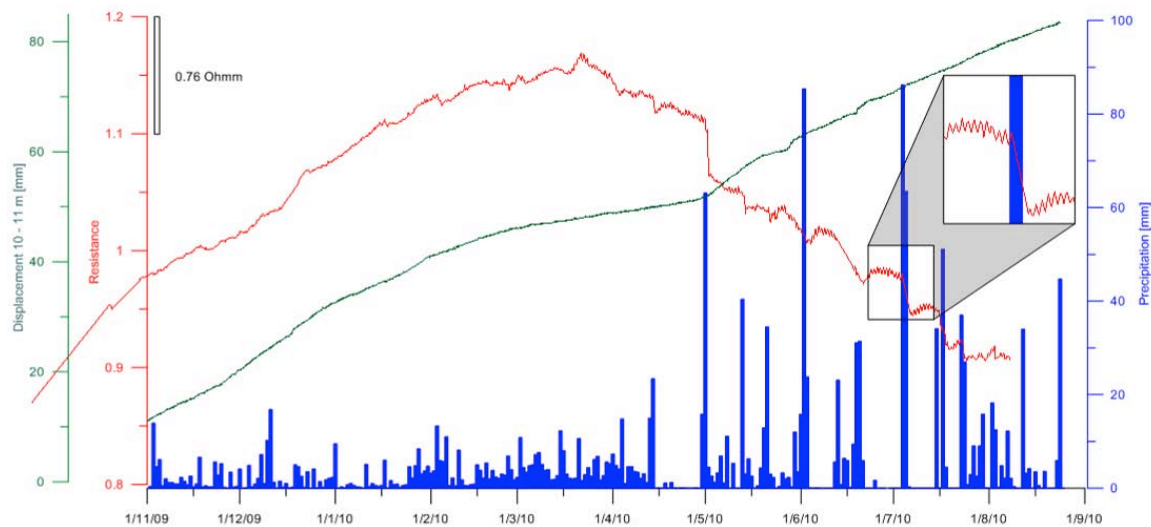


**Figure 115. Results of monitoring at the landslide of Gschlieflgraben in the period of November 2009 till July 2010: precipitation (blue), cumulative displacement (green) and normalised electrical resistance (red; configuration 108-120-111-114).**

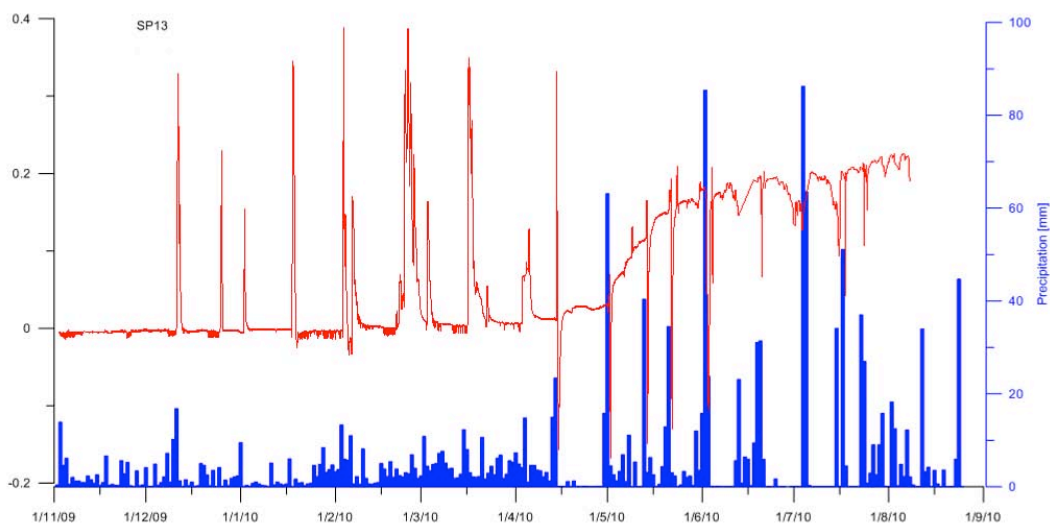


**Figure 116. Results of monitoring at the landslide of Gschlieflgraben in the period of November 2009 till July 2010: precipitation (blue) and normalised self-potential (red).**

### ***6.1.9.3 Improvements with respect to previous applications***

The monitoring system in Gschlieflgraben is one of the first known cases where geoelectric and high resolution differential displacement monitoring were coupled for several years. The monitoring was started in September 2009 and the system is operating since that time with only one short interrupt due to a torrential rain event, which flooded the retention channels and damaged the geoelectrical cables.

Consequently from the aspects of measurement technique (concerning transmitter, receiver as well as automatic data transfer, remote controlled maintenance, power supply and lightning protection) we can conclude that geoelectric monitoring is, after several years of specific development, a mature technology.

The monitoring initiative at Gschlifgraben is furthermore integrated into a complex airborne and ground- based investigation program to allow proper interpretation of the data.

The case study so far proved the reliability of the method for long term monitoring. It clearly shows the long term stability of geoelectrical parameters and their response to changes in the hydrological system of the subsurface. The results showed that intense rainfalls had a direct and immediate impact without any delay on the displacement and resistivity pattern causing very small, but clearly identifiable changes in both parameters.

However, since during the observation period no significant changes in the displacement pattern took place in that area, a direct evaluation of the ability of geoelectrics as an early warning parameter could not be performed. For this purpose, longer observation periods as well as additional case studies at several landslides showing different displacement characteristics are necessary. Therefore several other sites were equipped with the Geomon4D monitoring equipment. However for these installations the observation period is still too short to evaluate the results. This will be included in deliverable D.4.6 of the SafeLand project.

## 6.2 MOBILE PLATFORMS

### 6.2.1 Offshore laser scanning for coastal rockfall hazard assessment, coupling terrestrial LiDAR and GNSS/IMU systems: example of Sunndalsøra, Møre og Romsdal, Norway (detection and mapping).

*UNIL: Michoud C., Derron M.-H., Jaboyedoff M.*

This chapter is mainly based on the papers Michoud et al., 2010 and Derron et al., 2011.

#### 6.2.1.1 Study area

The Institute of Geomatics and Risk Analysis (IGAR) of the Faculty of Geosciences and Environment of the University of Lausanne was sub-contracted by Dr. Lars Harald Blikra of the Åknes/Tafjord Beredskap (IKS) to acquire LiDAR datasets of unstable cliffs above the Oppdølstrand road (from Sunndalsøra to Oppdøl, Møre og Romsdal county, Norway) shown in Figure 117.

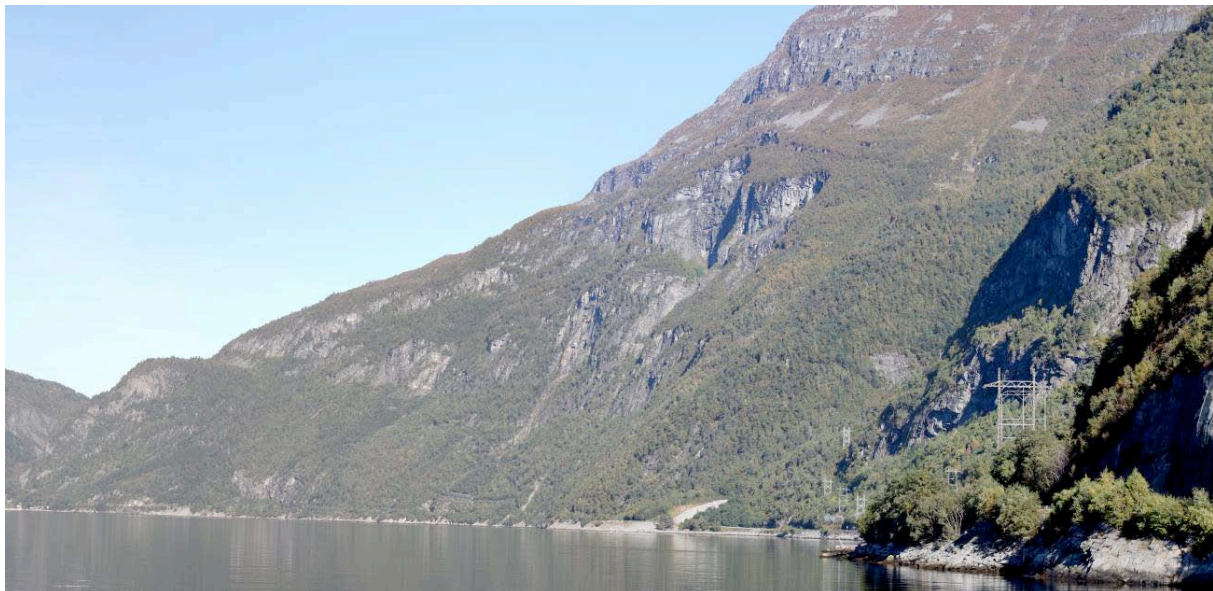


**Figure 117: picture of the unstable cliffs, which threaten the coastal road between Sunndalsøra and Oppdøl.**

Mainly composed by diorites and gneiss (NGU's geological atlas, 2011), local GSI (Geological Strength Index introduced in Hoek et al., 1998) evaluations show fair rock mass quality ( $45 < \text{GSI} < 55$ ), due to very blocky structures (Figure 118) and moderately weathered surfaces. After many inventories of fragmental rockfall events, investigations and ground-based monitoring are performed, focusing on four main sites along the road.

The acquisition of LiDAR point clouds allowed a better understanding of the structures of the sites which are presently monitored by a Ground-Based Interferometric Radar (GB-InSAR) system. It allowed the identification of the most hazardous cliff areas and then, to highlight the most exposed road sectors, from regional scale to outcrop analysis.

---



**Figure 118: example of an outcrop affected by an important fracturing; some anchors have been installed to stabilize the unstable blocks.**

As some unstable cliffs are high and wide, it appeared that several sites had to be scanned from a long range distance. But the fjord is too wide (~2.5 km) to allow an acquisition by laser scanning from the other side. Thus laser scanning was performed from a boat, with an Offshore Laser Scanning (OLS) system using an Inertial Measurement Unit (IMU) coupled with two Global Navigation Satellite System (GNSS) antennas. Furthermore, all the accessible sites were scanned from land with a classic Terrestrial Laser Scanning (TLS) system at a high-resolution.

#### ***6.2.1.2 Description of the analysis***

The off-shore laser scanning (OLS) is a new development of laser scanning used for coastal cliff stability assessment. An Applanix POS MV system was coupled with a LiDAR Optech ILRIS-3D-ER to combine an accurate dynamic positioning and orientation system with a long range LiDAR (Figure 119 and Figure 120). The main particularity of this system is to be mounted directly on a marine vessel and to be able to acquire in motion georeferenced LiDAR point clouds. The high resolution digital elevations models (HRDEM) derived of these point clouds are an important data for rockfall assessment along the shores of lakes and fjords.

The Terrestrial Laser Scanning (TLS) is an active optical sensor which allows providing (xyz) points clouds of the topography with a high resolution. The LiDAR (the device used for laser scanning) emits laser pulses in directions perfectly known, thanks to 2 internal mirrors. Pulses get back-scattered by the terrain, vegetation, etc. The TLS records the Times Of Flight (TOF)

that the pulses take to go forth and back. Then a TOF is converted in a distance, the range, and a 3D image of the topography is created.

When performing scans from moving platforms such as boats, the directions of emitted pulses cannot be known with only the orientations of the 2 internal mirrors of the LiDAR. However, coupling the LiDAR with an Inertial Measurement Unit (IMU) and 2 GNSS antennas, it is possible to do surveys from a vessel. This technique is called Offshore Laser Scanning (OLS). Indeed, the IMU records the angles of roll, pitch and heading of the platform on the boat, according to three fixed orthogonal axes; furthermore, the GNSS antennas localize the instrument. Then, as the LiDAR knows its position, the direction of sight and the TOF for each pulse, it is possible to post-process all the points in order to reconstruct the 3D topography.



**Figure 119: Onshore calibration of the coupled TLS Optech ILRIS-3D-ER with the IMU/GNSS Applanix POS MV.**



**Figure 120: Offshore acquisition with the OLS system setup on a boat, in the Norwegian fjord.**

### ***6.2.1.3 Improvements with respect to previous applications***

The laser spot size increases with the range, following the equation  $D=0.17 \times R+12$ , where  $D$  is the laser spot size (in mm) and  $R$  the Range (in m). As the spot diameter get wider (around 10 cm at 500 m), it covers a larger area of rock. Then the return pulse is a kind of average of the signal back-scattered from the surface covered by the spot and details within this surface cannot be distinguished. As the ranges from the vessel and the land were respectively 400-600 m and 50-300 m, the TLS scans can provide more details of the rock surface than the OLS scans. Nevertheless, comparing to Aerial Laser Scanning (ALS) dataset, OLS provides more points with a better resolutions for sub-vertical planes, often not well detected by ALS (Figure 121).

Furthermore, with new terrestrial LiDAR generations acquiring five times quicker (such as the new Optech Iris 3D LR), OLS techniques will provide more and more accurate and dense point clouds.

To sum up, thanks to its ability to provide a continuous record from an extended and wide area along coastal cliffs, this new OLS technique knows a promising start, being useful for large and small coastal rockfall hazard assessment.

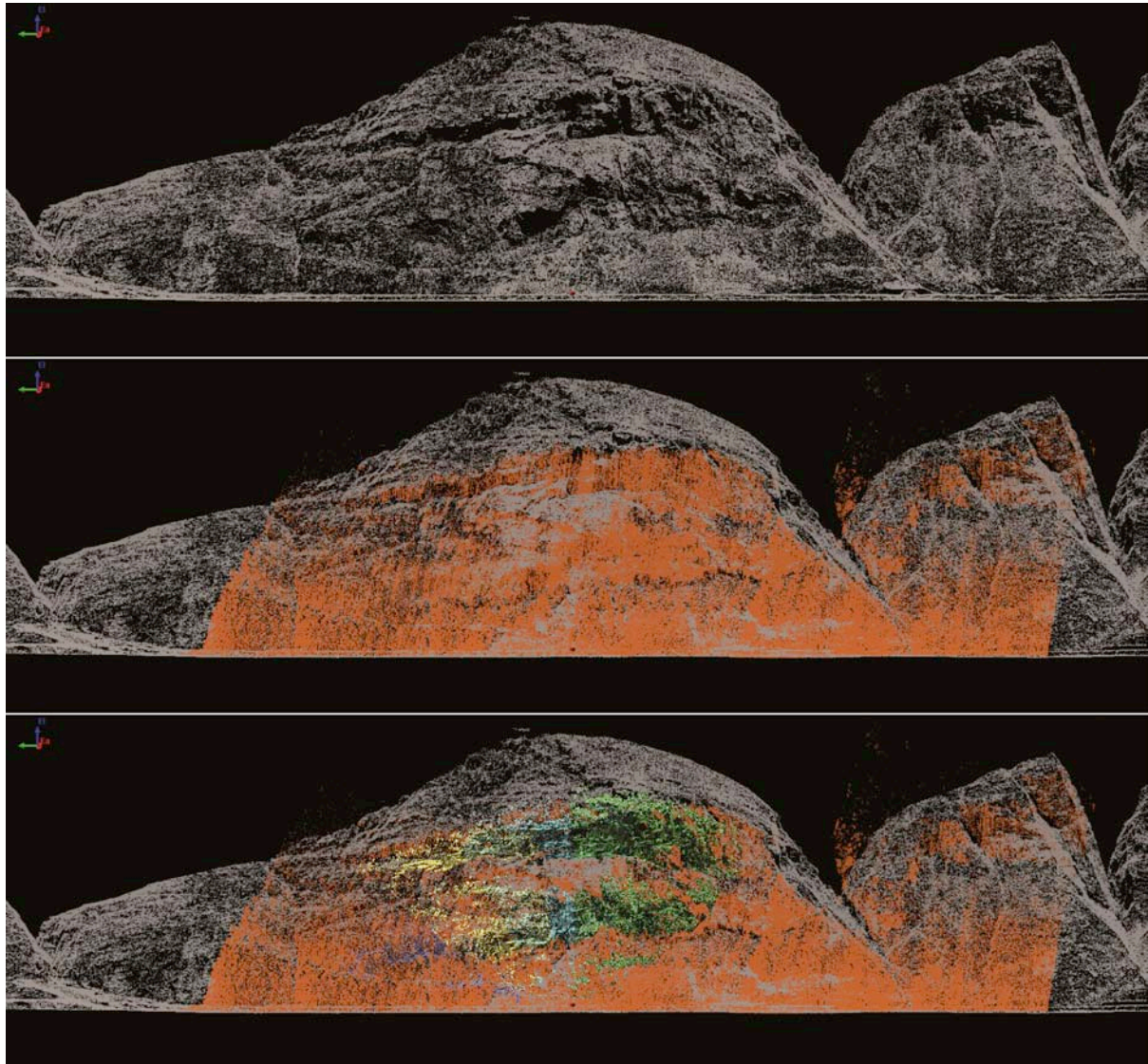


**Figure 121: Top: view of the HR-DEM provided by IKS. Middle: view of the ALS's and OLS's points clouds overlapped. The unstable cliffs, which were not detected by the ALS, are covered by OLS. Bottom: view of the ALS's, OLS's and TLS's points clouds overlapped. The unstable cliffs are covered with a high point density (Michoud et al., 2010).**

## 6.2.2 Satellite optical (detection and mapping): object-oriented landslide inventory mapping with variable image data using machine learning techniques.

ITC: Stumpf A., Kerle N.

### 6.2.2.1 Study area

VHR images collected in the immediate aftermath of two recent major earthquakes, as well as from two sites affected by a large number of non-seismic landslides, were used in this study (Table 5). The areas (Figure 122) are characterized by a great diversity of environmental settings, landslide processes and image acquisition conditions, and in this manner simulate realistic test cases with imagery that is typically available shortly after major events.

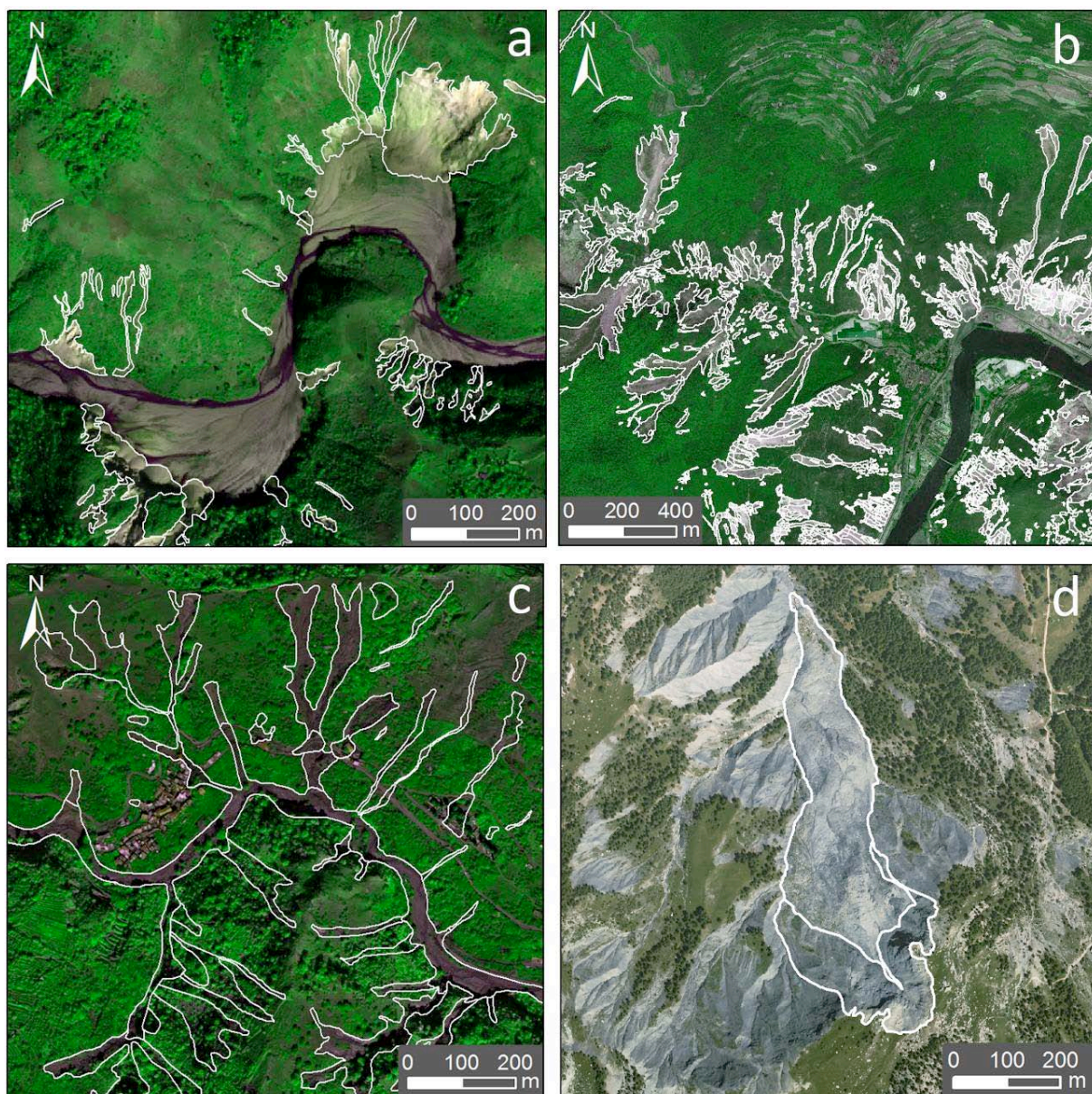


Figure 122. Analyzed subsets at the different test sites. a) Haiti, b) Wenchuan, c) Messina, d) Barcelonnette area. White outlines indicate the landslide areas.

**Test site 1: Momance River - Haiti**

On January 12, 2010 an MW 7.0 earthquake struck Haiti and recent studies reveal that ground shaking resulted from the rupture of a previously unknown system of a blind thrust fault, whereas strain accumulated at the Enriquillo–Plantain Garden fault zone remains to be released in future surface ruptures (Hayes et al. 2010). Mainly due to unsound construction an estimated 230,000 people were killed, and the total value of the damage and losses approximates US\$ 7.8 billion (PDNA 2010). The direct impact of landslide was rather small, whereas an increased frequency of slope failures and debris flows can be expected during future rainfall events. The study site is located at the Enriquillo fault line, which in the particular section finds a strong morphological expression in the tectogenetic valley of the Momanche River. The fault separates basaltic rocks in the south from marine sedimentary rocks (chalk, sandstone, and limestone) in the north (Eberhard et al. 2010). The slopes are between 20° to 50°<sup>steep</sup> and show a large number of shallow debris and rock slides. Most of the gentler terrain sections are under agricultural use by hundreds of scattered family farms. Due to erosion bare soils are exposed at several locations and the valley bottom is filled with non-vegetated fluvial deposits. Geoeye-1 imagery was recorded one day after the event.

**Test site 2: Wenchuan town - China**

The rupture of the Longmenshan fault system on May 12, 2008 ( $M_L=8.0$ ) triggered more than 60.000 individual slope failures (personal communication T. Gorum, 2010) and approximately 30.000 of the 80.000 casualties can be attributed to the impact of landslides (Tang et al. 2010). The county capital Wenchuan town is located on both sides of the Minjiang River and surrounded by steep terrain with average slopes of approximately 30° up to 3600 m.a.s.l. The town and its surroundings were seriously affected by a large number of mainly shallow translational landslides, which are concentrated on the steepest slopes in proximity to the drainage lines. Already before the event those terrain units were rather sparsely vegetated and showed bedrock outcrops at several locations. The predominant rock-types are flysch-type sediments and smaller outcrops of an older crystalline formation in the northeast of the study area. The main land cover types are degraded mountain forest and terraced field crops, which extend to slopes of up to 35°.

**Test site 3: Messina - Italy**

On 1<sup>st</sup> of October 2009 a series of debris flows struck several catchments a few kilometres south of the city of Messina/ Sicily. The debris flows were triggered by extraordinarily intense rainfalls on the afternoon of the 1<sup>st</sup> of October that was preceded by prolonged intense rainfall at the end of September. Thirty-one people were killed during the event and the direct economic loss was estimated as almost € 600 million (Civil-Protection-Sicily 2010). The study area comprises ten small and medium size catchments that rise from sea level to about 700 m in the Peloritani Mountains, which are composed of a metamorphic basement overlaid by sequences of younger pelitic and conglomeratic sediments. The present land cover types comprise bare ground, crop-, shrub- and grassland, deciduous forest and rural built-up areas. Most of the landslides were initiated as shallow debris flows or slides at the upper slopes and evolved into rapid hyper-concentrated flows along their way through the drainage network. The Quickbird imagery was recorded 7 days after the event.

#### Test site 4: Barcelonnette Basin - France

The Barcelonnette Basin is located in the South French Alps and characterized by a mountain climate with Mediterranean influence. The area is known for the large number of active landslides, whereas for in the present study a small subset comprising the Super Sauze active mudslide (Malet 2003) was examined. The task here was mainly to distinguish the landslide body from the surrounding badlands and as the affected area is one compact object this corresponds rather to an image segmentation task. The available imagery is a natural colour aerial photograph recorded in summer 2004.

**Table 5. Overview of analyzed images and topographic data.**

Test site	Haiti	Wenchuan	Messina	Barcelonnette
Sensor	Geoeye-1	IKONOS	Quickbird	Aerial photograph
Spectral band	4-band multispectral	4-band multispectral	4-band multispectral	3-band natural colour
Pixel size (multispectral / panchromatic) [m]	2 / 0.50	4 / 1	2 / 0.61	0.5 / -
Sensor Tilt [°]	2.7	15.7	3.1	n.a.
Nominal Collection Azimuth [°]	343.8	62.7	343.3	n.a.
Solar Zenith Angle [°]	45.6	19.2	45.6	-
Sun Angle Azimuth [°]	150.2	119.3	161.7	-
Date (days after the event)	13/01/2010 (1)	23/05/2008 (11)	10/8/2009 (8)	07/2004 (n.a.)
Test area [km <sup>2</sup> ]	1	2	1	1
DEM Resolution (Source resolution)	10 m (1 m LiDAR DSM)	10 m (20 m contour lines)	10 m (1 m LiDAR DSM)	10 m (1 m IFSAR DSM)

#### 6.2.2.2 Description of the analysis

The purpose of this study was the development and testing of a workflow combining object-oriented image analysis with the advantages of a modern machine learning algorithm termed Random Forest (RF, Breiman 2001). The underlying assumption was that landslide inventory mapping from VHR optical imagery could be organized more efficient if a human operator labels only a fraction of the image, whereas the rest of the image would be classified with the algorithm that has been trained on the provided examples. The training of the algorithms comprises a number of challenges such as the selection of suitable image features and the compensation of the general encountered imbalance between landslides and non-landslide areas.

For our experiments we selected at each test site subsets that include landslides and spectrally similar objects, such as river plains, urban areas, roads, badlands and barren fields (Figure 122). A scalable image segmentation algorithm was applied on the images from each area, and a comprehensive set of metrics characterizing the image objects was calculated. Subsequent to segmentation and metric calculation (Figure 123A) landslide inventories compiled from field work and manual image analysis were used to create a sample database with all objects assigned either as landslide object ( $O_{LS}$ ) or non-landslide objects ( $O_{NLS}$ , Figure 123B). Each image object containing at least 50% of landslide-affected area was labelled as

$O_{LS}$  and all others as  $O_{NLS}$ . To evaluate a comprehensive set of object-metrics (including colour, texture, shape and topographic variables) for the discrimination of landslides and unaffected areas, all  $O_{LS}$  and an equal number of  $O_{NLS}$ , drawn randomly without replacement, were used at all test sites and scales, respectively. They were introduced in the RF-based approach for feature evaluation and reduction (Figure 123C) proposed by *Diaz-Uriarte and Alvarez de Andres (2006)*.

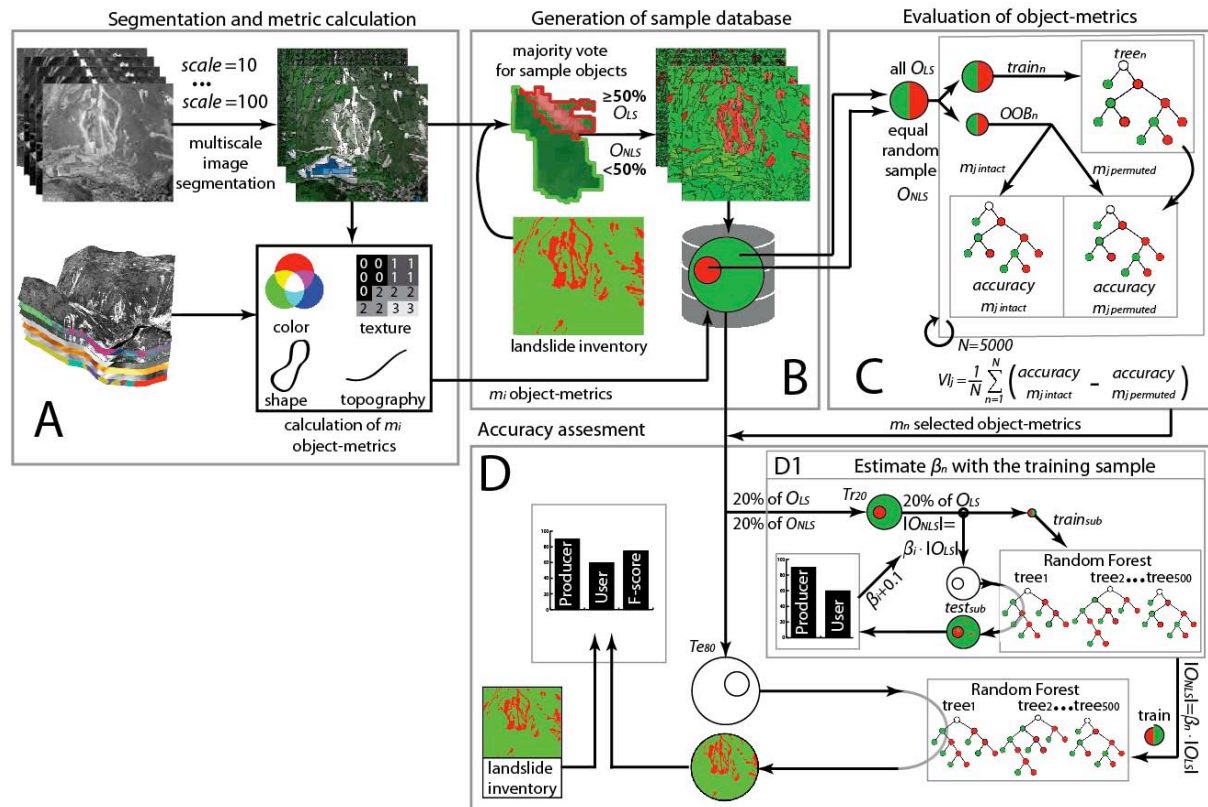


**Figure 123: Overview of the processing steps followed in this study.** A: The images were segmented with 15 different scale factors, and at each scale a number of object-metrics ( $m_i$ ) was calculated. B: Based on the landslide inventory all segments were either assigned as landslides ( $O_{LS}$ ) or non-landslide objects ( $O_{NLS}$ ). C: Training samples including approximately two third of the cases ( $train_n$ ) were repeatedly ( $N=5000$ ) sampled from a balanced subset ( $|O_{LS}|=|O_{NLS}|$ ). The remaining out-of-bag test sample ( $O_{OB_n}$ ) was classified with the decision tree ( $tree_n$ ) built from  $train_n$ . Sequentially, and one at a time, each object-metric  $m_j$  used in  $tree_n$  was randomly permuted within the  $O_{OB_n}$  sample. The respective decrease of the classification accuracy was measured, and the variable importance ( $VI$ ) of each  $m_j$  calculated as the average decrease from 5000 trees. D: 20% of the image objects ( $Tr_{20}$ ) and all selected object-metrics  $m_n$  were employed for the training of the Random Forests (RF). D1: An iterative procedure was adopted to estimate the class ratio of  $O_{LS}$  and  $O_{NLS}$  for the training sample ( $\beta_n$ ), which yields balanced error rates on the test set. In the first iteration 20% of  $O_{LS}$  and an equal number of  $O_{NLS}$  ( $\beta_i=1$ ) were randomly sampled from  $Tr_{20}$  ( $train_{sub}$ ) to train a RF. The remainder ( $test_{sub}$ ) was sent through the RF to assess user's and producer's accuracies. The next iteration started with  $\beta_i+0.1$  and the complete procedure was repeated until the balance between user's and producer's accuracies clearly reversed.  $\beta_n$  was determined as the ratio where the difference between user's and producer's accuracies reached a minimum. D: The estimated  $\beta_n$  was applied to the complete  $train$  set, which was subsequently used to train the final RF. Accuracies in terms of correctly classified areas and objects were finally assessed with the remaining 80% test set ( $Te_{80}$ ).

To account for spurious effects of class-imbalance and class-overlap, an iterative scheme for the adjustment of the training sets was developed (Figure 123D1) and tested at three different sites. In this last step the accuracy was assessed on a test set comprising 80% of all image objects, and hence in a scenario where 20% of the data would be available for training (Figure 123D).

### 6.2.2.3 Results

Among the tested sites and segmentation scales in average one third of the tested image features (96) was useful to increase the separability of landslide and non-landslide areas. Unsurprisingly, metrics related to spectral information resulted as the most important ones for all test cases and scales. Band ratios and principal component transformations that depict the contrast between vegetated and non-vegetated areas ranked with a particularly high variable importance (*VI*). Object means of the slope and hillshade layers significantly reduced the error rates, whereas in most cases their relative importance decreased with larger segmentation scales. Shape metrics displayed a rather contrary behaviour, and generally contributed little to the reduction of the error rates. Only for larger segmentation scales at Wenchuan and Messina, where the segments more closely approached the elongated shape of the landslides, shape metrics were selected by the selection procedure. They have been reported as useful after initial spectral classification steps (Martha et al., 2010a; van der Werff and van der Meer, 2008) but provide little additional information within the tested sample-based framework.

Topographically guided versions of the grey-level co-occurrence matrix (GLCM, Haralick 1973) were calculated on all bands along the hydrological flow direction and across the slope, respectively, and corresponding derivatives included GLCM Contrast, Correlation, Entropy, Standard Deviation and Mean. As Figure 124 illustrates such features capture well the contrast between the downslope oriented structures of landslides and other spectrally similar object oriented differently. The topographically guided *GLCM Con.*, *Cor.* and *Ent.* helped to reduce the classification error significantly at all tested sites and largely outperformed all other omnidirectional *GLCMs*. The modified *GLCM Con.* was apparently more efficient when derived from the higher resolution panchromatic channels.

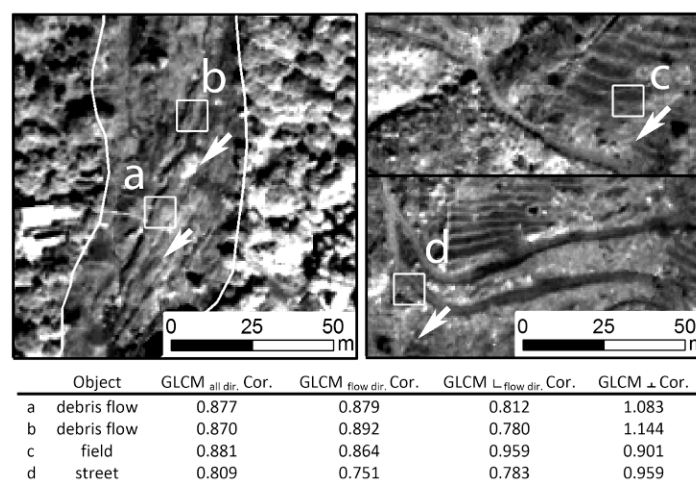


Figure 124. Exemplary comparison between omnidirectional (GLCM<sub>all dir.</sub> Cor.) and topographically guided texture measures calculated on the panchromatic channel. White arrows indicate the hydrological flow direction within the measured cells. For linear structures along the flow direction (debris flows)

texture measure calculated along the slope ( $GLCM_{\text{flow dir. Cor.}}$ ) tend to be lower and across the slope ( $GLCM_{\perp \text{flow dir. Cor.}}$ ) they tend to be higher. Hence, their ratio ( $GLCM_{\perp \text{Cor.}}$ ) is typically lower for linear structures perpendicular to the flow direction (field, street).

At all four test sites landslides covered only minor fractions of the scene, which is a typical situation leading to an imbalance between  $O_{LS}$  and  $O_{NLS}$  potentially introduces a bias of the classification towards the over-represented non-affected area. Preliminary test runs adopting naturally imbalanced training sets for the training of the Random Forest algorithm indeed demonstrated seriously lower classification accuracies for the landslide class. On the other hand a strong over-prediction of  $O_{LS}$  was observed if a class-balanced training sample was employed. In order to estimate a suitable ratio of  $O_{NLS}$  and  $O_{LS}$  ( $\beta$ ) that would yield equal accuracies for both classes the training samples (20% of the data) were repetitively resampled as illustrate in Figure 123D1. While altering the class ratio user's and producer's accuracy on subsets of the training sample balance and  $\beta$  can be determined as the point where they reach equilibrium (Figure 125). The estimate was adopted to resample the entire training sets and the accuracy of the RF classification was assessed on the remainder test set comprising 80% of the data. The accuracies in terms of correctly predicted area generally decreased for larger segmentation scales. At the test sites Haiti and Wenchuan this must be attributed to an increasing misfit between segmented object boundaries and the reference inventory leading to greater impurities within mixed objects, whereas the predictive accuracy of the RF (expressed by  $F_{obj}$ , Table 6) remained nearly constant among the different scales. Conversely, for Messina and Barcelonnette  $F_{obj}$  was consistently lower than Farea (Table 6), and the classifier performance decreased significantly with larger scale factors. Spectral confusion and hence the importance of additional textural and topographic features was unlikely higher for the classification of the datasets from Barcelonnette and Messina. In summary, the RF classifier provided relatively high accuracies of up to 87% for the test sites Haiti and Wenchuan, while in the case of Messina the best model reached an accuracy of 73%. This encourages the use of the technique in further applied studies.

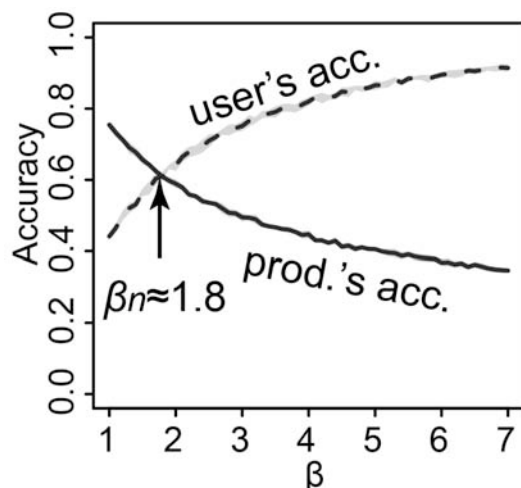


Figure 125. Graph showing exemplarily the result of the iterative resampling procedure.  $\beta$  is determined where user's and producer's accuracy reach equilibrium

Table 6. Final accuracy assessment for all test sites at three exemplary segmentation scales. Accuracies show the average performance of RFs (ntrees = 500), trained with 20% of the OLS and  $\beta n$ -fold amount of

ONLS, applied to the test set Te80.  $\beta_0$  is the original class-ratio of the entire population. The mean accuracies and their standard deviations were calculated over 50 randomly resampled (without replacement) replicates of Tr20. The best results for each test site are indicated with bold numbers

	Scale	$\beta_n(\beta_0)$	user's accuracy [%]	producer's accuracy [%]	$F_{area}$ [%]	$F_{obj}$ [%]	$\beta_n$ -adjusted $Tr_{20}$		
							$O_{LS}$	$O_{NLS}$	% of all objects
Haiti	10	3.0 (5.8)	<b>88.8</b> $\pm 0.1$	<b>85.7</b> $\pm 0.2$	<b>87.1</b> $\pm 0.1$	<b>89.7</b> $\pm 0.1$	4512	13536	11.7
	30	2.3 (4.2)	82.8 $\pm 1.2$	87.1 $\pm 0.9$	84.9 $\pm 0.7$	88.3 $\pm 0.3$	564	1297	12.8
	70	2.6 (4.0)	88.5 $\pm 1.1$	72.4 $\pm 1.3$	79.6 $\pm 0.7$	88.5 $\pm 0.5$	149	387	14.3
Wenchuan	10	2.7 (3.4)	<b>81.3</b> $\pm 0.1$	<b>81.1</b> $\pm 0.1$	<b>81.2</b> $\pm 0.1$	<b>80.5</b> $\pm 0.1$	6535	17645	17.0
	30	2.5 (3.0)	81.2 $\pm 0.4$	77.1 $\pm 0.5$	0.791 $\pm 0.2$	80.3 $\pm 0.2$	570	1425	17.4
	70	2.0 (2.6)	77.7 $\pm 0.9$	75.3 $\pm 1.1$	76.5 $\pm 0.6$	79.9 $\pm 0.6$	125	250	16.5
Messina	10	1.8 (4.2)	<b>72.9</b> $\pm 0.3$	<b>74.6</b> $\pm 0.2$	<b>73.7</b> $\pm 0.1$	<b>73.0</b> $\pm 0.1$	6135	11043	10.8
	30	1.9 (4.1)	69.0 $\pm 1.2$	60.9 $\pm 0.9$	64.7 $\pm 0.4$	59.2 $\pm 0.4$	663	1260	11.3
	70	1.9 (3.7)	64.3 $\pm 2.0$	59.8 $\pm 1.3$	62.0 $\pm 0.8$	60.5 $\pm 1.1$	125	238	11.9
Barcelonnette	10	4.7 (9.5)	<b>77.8</b> $\pm 1.0$	<b>78.0</b> $\pm 0.5$	<b>77.9</b> $\pm 0.4$	<b>76.5</b> $\pm 0.2$	1810	8507	10.8
	30	5.5(11.5)	74.7 $\pm 2.1$	75.9 $\pm 1.8$	75.2 $\pm 1.0$	67.4 $\pm 0.8$	237	1304	10.1
	70	4.9 (12.1)	63.3 $\pm 5.6$	88.6 $\pm 2.3$	73.3 $\pm 3.5$	65.3 $\pm 2.7$	46	226	8.9

#### 6.2.2.4 Improvements with respect to previous applications

Previously proposed methods for object-oriented mapping of landslides from VHR images are highly reliant on manual thresholding and a subjective selection of suitable features, making it difficult to adapt them to new locations and datasets. To overcome such issues this study investigated the use of image segmentation and the Random Forest framework for feature selection and image classification. A variety of VHR remote sensing images and different landslide processes was analyzed with the RF data-mining technique to evaluate useful image object-metrics, the influence of the segmentation scale, and the consequences of class-imbalance.

Class-imbalance and class-overlap initially caused severely imbalanced error rates at all test sites, but an iterative scheme to estimate a compensating class balance for the training data was found to enhance substantially the balance of user's and producer's accuracies. In the presented setup, accuracies between 73% and 87% were achieved when 20% of the total area was provided for training.

Those figures are in a similar range as the results of other recent studies on landslide mapping from optical imagery (Barlow et al. 2006; Lu et al. 2011; Martha et al. 2010a). Though the quantities of employed samples are not always explicitly mentioned (Barlow et al. 2006; Nichol and Wong 2005), all proposed solutions depend on the availability of some sort of training data. The main advantage of workflow proposed here is its great adaptability

including an automated classification of unknown image objects and the selection of relevant features.

Although the optimal set of object-metrics varies considerably from case to case, a number of spectral, topographic, and textural features are generally useful. Omnidirectional and directional GLCMs provide complementary information to distinguish affected from non-affected areas. Though GLCMs have been previously adopted for landslide mapping (e.g. Martha et al. 2010a) the proposed topographic control on their calculation provides significant enhancement, and makes such object-metrics potentially useful for the automated mapping of various geomorphological processes. Although the optimal choice of the texture measures depends to a certain degree on the application, it is interesting to note that Clausi (2002) highlighted Con., Cor. and Ent. as particularly useful GLCM derivatives for the recognition of sea ice, and Laliberte and Rango (2009) concluded that Con., Ent. and Stdv. are the most suitable texture measures for rangeland mapping. The range of potentially useful object metrics for landslide mapping and other applications seems still not fully exploited, and data mining techniques such as RF are valuable tools to ease feature selection for machine learning, or to guide experts during the elaboration of knowledge-driven rule sets. Further results that are not detailed here indicate that feature reduction leads to an improved image classification, but also that not all significant features can be fully exploited with one particular segmentation scale.

At each of the four test sites a medium resolution DEM, one VHR resolution image, and the reported numbers of training objects were sufficient for an efficient performance of the RF classifiers. In most practical situations such kind of data will be available and the described algorithms may provide a generic approach to map the overall affected area more efficiently before site and data specific tasks, such as the classification of landslide types (Barlow et al. 2006; Martha et al. 2010a), are targeted. In situations where more data (e.g. pre-event imagery) are available the proposed framework is suitable to accommodate a large variety of additional datasets and object-metrics, which may be used to further increase the mapping accuracies.

In the short term further enhancements are certainly possible through the integration of ancillary datasets such as pre-event imagery, or the exploration of additional object-metrics such as Gabor filters or higher level contextual information. More research is needed to optimize the segmentation process, which at present is based on spectral information solely. An initial sample-based estimate of the variable importance might thereby be an interesting tool to decide which further layers should be included in the segmentation. The processing time for a small test area can be streamlined to a few hours on a standard desktop PC, while for larger areas the RFs can easily be implemented for parallel processing, and the scale factor may provide an interesting parameter to trade between accuracy and processing time.

In order to differentiate individual landslides and provide map products with less dispersed class distributions (Figure 126) the current architecture still needs enhancements. This is closely related to the observed fact that high-level features such as shape are better exploited on larger scales. The design of a hierarchical algorithm that robustly and efficiently incorporates sample data and relevant features in the classification and constitution of image objects among a number of different scales remains a major challenge, and with potential benefits for many remote sensing applications.

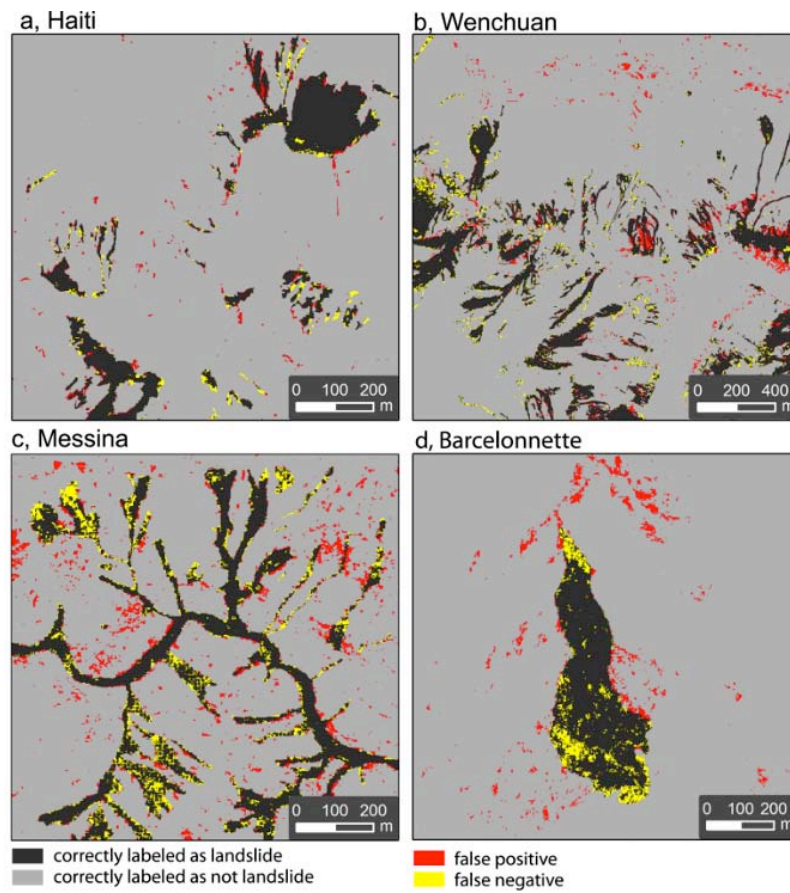


**Figure 126.** Results with a segmentation scale of 10, after feature selection and balancing of the error rates as indicated in 1 at a, Haiti b, Wenchuan c, Messina and d, Barcelonnette. Correctly classified areas include the samples used for training.

### 6.2.3 Satellite radar (detection and mapping): Liri-Garigliano and Volturno basins.

UNISA: *Peduto D., Cascini L.*

AMRA: *Fornaro G.*

#### 6.2.3.1 Study area

The procedures developed by UNISA for DInSAR data analysis (see section 3.1.3) were tested within a sample area belonging to the northern portion of the territory of the National Basin Authority of Liri-Garigliano and Volturno rivers (NBA LGV) in Central-Southern Italy (Figure 127). This territory was selected due to the availability of both base and thematic maps furnished by the NBA LGV at 1:25,000 scale. These maps were produced in 2001 as results of the activities of the PSAI (Piano Stralcio per l'Assetto Idrogeologico) project, carried out by a group of experts and technicians working for NBA LGV in accordance with the Act of Italian Parliament (L. 365/2000), aimed to develop emergency plans at national scale (Cascini, 2008).

The test area has an extension of around 489 km<sup>2</sup> and includes eleven municipalities, belonging to two Regions (Lazio and Abruzzo) (Figure 127). The geological map highlights that the bedrock mainly consists of Upper Miocene arenaceous units mantled by Quaternary Age superficial deposits, characterized by talus and alluvial fans. Landslide phenomena are widespread all over the area (covering around 5% of the whole territory) as it can be noticed in the available landslide inventory map at 1:25,000 scale, derived from aerial photographs and surface surveys. This map furnishes detailed information for each mapped phenomena with reference to location, typology, state of activity and areal extension (Cascini et al., 2005).

Owing to the phase ambiguity limitation of DInSAR data processing (see section 1.2), the analysis was focused on the typology of phenomena ranging from extremely to very slow velocity classes (i.e. lower than 1.6 m/year according to Cruden and Varnes, 1996).

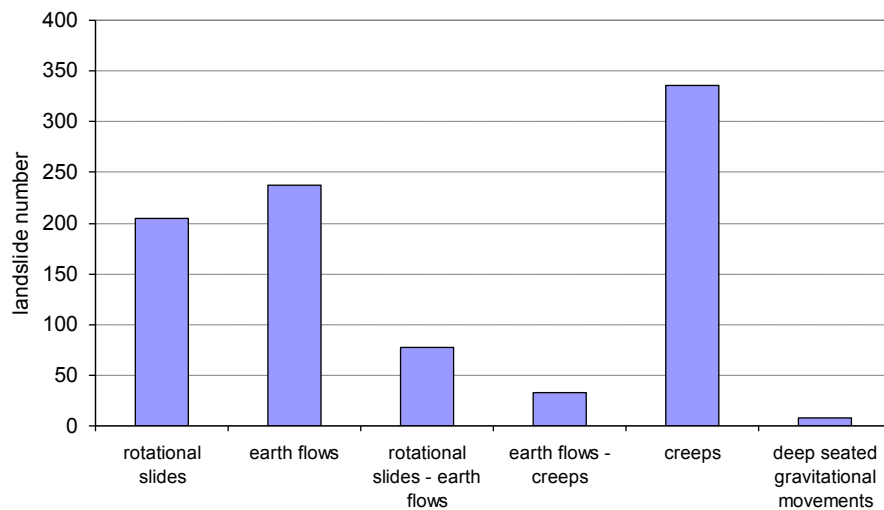


Figure 127. The study area

In the study area a total number of 897 slow-moving landslides (Figure 128) were mapped (Peduto, 2008; Cascini et al., 2009); according to Varnes (1978) they are classified as: 204

rotational slides, 238 earth flows, 78 rotational slides–earthflows, 336 creeps, 33 earthflows—creeps, and 8 deep-seated gravitational movements. On the basis of geomorphological criteria, three different states of activity were distinguished for these landslides, defined as follows: “active” (including active, reactivated and suspended), “dormant” and “inactive” (relict) phenomena (Cruden and Varnes, 1996). The selected landslide typologies (Figure 129) exhibit a significant predominance of dormant phenomena (428) on active ones (92).

As for the typical extension of landslide phenomena, the landslide inventory highlights that around 14% exceed 50,000 m<sup>2</sup> and around 15% of landslides have an area smaller than 10,000 m<sup>2</sup>. Moreover, the total length (minimum distance from tip of landslide to crown, according to IAEG commission on Landslides, 1990) ranges between less than 50 m up to more than 1350 m; the width of landslide body (maximum width between flanks of landslide perpendicular to length, according to IAEG Commission on Landslides, 1990) ranges between 50 m and 1000 m.



**Figure 128.** Number of mapped phenomena for each typology within the study area (Cascini et al., 2009).

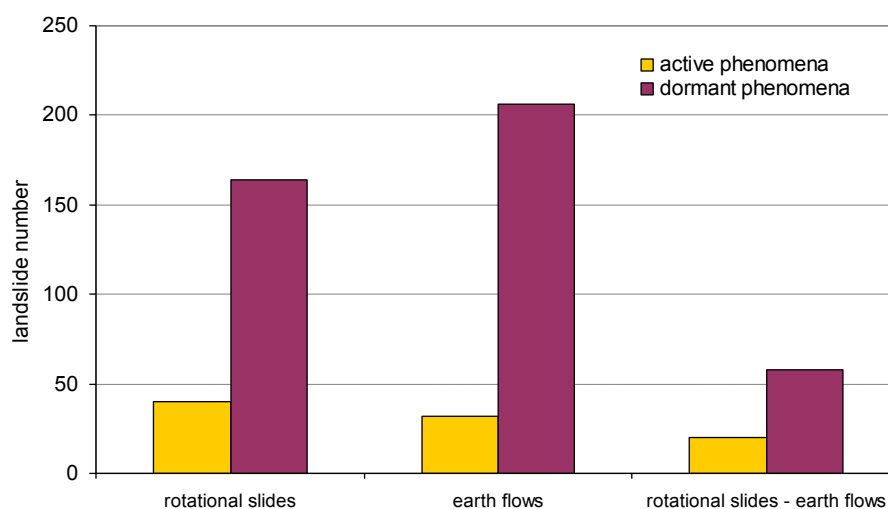


**Figure 129.** Number of mapped phenomena for each typology distinguished on the basis of the state of activity (Cascini et al., 2009).

### 6.2.3.2 Description of the analysis

The radar images were processed on a two step approach. In particular, the low-resolution analysis was performed via the Enhanced Spatial Differences (ESD) approach (Fornaro et al., 2009a), which represents an upgrading of the original SBAS algorithm (Berardino et al., 2002); the full-resolution analysis was carried out via the tomographic analysis (Fornaro et al., 2009b).

UNISA developed an original procedure for DInSAR data analysis at different scales as sketched in the framework in Figure 130. The first step consisted of the generation of the a priori DInSAR landslide visibility map (Peduto, 2008; Cascini et al., 2009), which can be used to distinguish in advance whether an area is expected to be visible from space-borne SAR sensors thus driving data-users through the image dataset selection. Once SAR images were processed, a procedure for 1D-LOS DInSAR data projection (Cascini et al., 2010) was implemented to generate the advanced DInSAR landslide velocity map. As for the scale of the study, low-resolution DInSAR data were used for landslide analyses at 1:25,000 scale, according to the dimension of both the landslide phenomena and the coherent DInSAR pixels on the ground; whereas full-resolution DInSAR data allowed studies at more detailed scale (i.e.1:5,000) according to the almost point-wise information and the dimension of single portions of landslides and structures/infrastructures.

The above procedure was tested within the territory of the National Basin Authority of Liri-Garigliano and Volturno rivers.

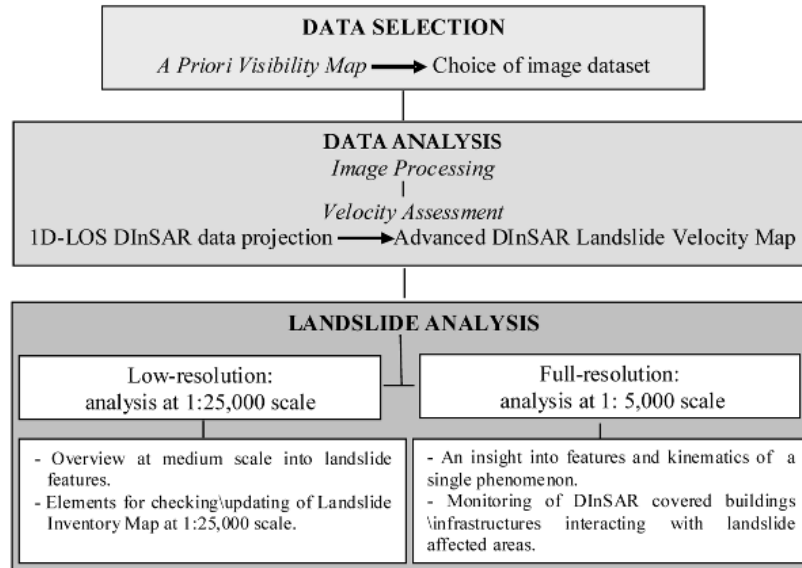
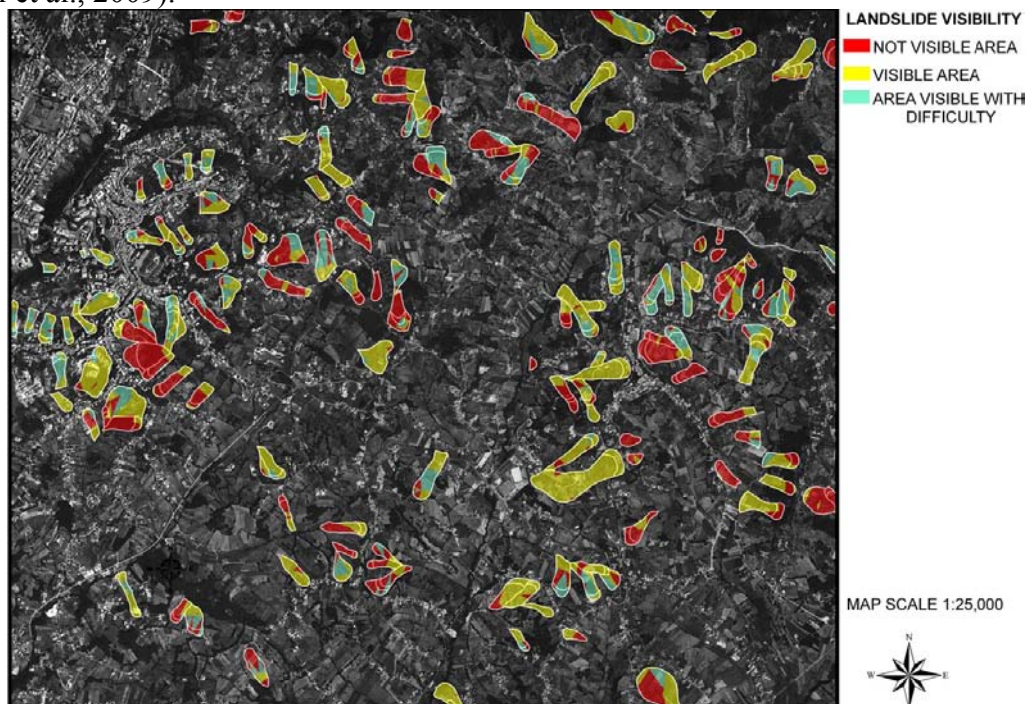


Figure 130. The framework of DInSAR data analyses for landslide studies (Cascini et al., 2010).

An example of the a priori DInSAR landslide visibility map over a portion of the study area, obtained via low-resolution ESD DInSAR data deriving from an ERS1-ERS2 descending orbit image dataset, is presented at 1:25,000 scale (Figure 131). The input data consisted of the following available maps: landslide inventory map; aspect map; slope angle map; land-use map; urbanized area map. The map in Figure 131 distinguishes the visible areas from the not visible areas as well as from the areas where a quantitative interpretation of the measured

velocity value can turn out to be misleading (for slopes facing north and south directions, see Cascini et al., 2009).



**Figure 131.** An example of a priori DInSAR landslide visibility map on descending orbits for a portion of the test area (Cascini et al., 2010).

Within the same test area, low-resolution DInSAR data were then used to generate the advanced low-resolution DInSAR landslide velocity map at 1:25,000 scale (see Figure 132). The map was generated starting from along LOS low-resolution DInSAR velocity values, a DEM at 1:25,000 scale and introducing simplified geomorphological schemes (see Cascini et al., 2010), which take into account the landslide geometrical features suggested by Cruden and Varnes (1996). According to these criteria the advanced low-resolution DInSAR landslide velocity map was generated in order to firstly check the potential of DInSAR data to detect already mapped landslide; the results showed that more than 30% of slow-moving landslide were covered. Moreover, a check of the state of activity of the mapped phenomena over the whole study area was carried out thus highlighting that almost 84% of the DInSAR covered dormant landslides (144) exhibit evidence of no movement. On the other hand, the percentage of active landslides (25) with moving coherent DInSAR pixels is about 24%, on the average (Cascini et al., 2008).

The advanced low-resolution map was then used to detect new landslide phenomena by extending the analysis of moving/not moving coherent pixels on those portions of the territory mapped as hollows in the geomorphological map at 1:25,000 scale (Cascini et al., 2009). These zones (1263 within the study area) are characterized by geomorphological settings quite similar to landslide-affected areas, also exhibiting the same landslide predisposing factors. The proposed procedure allowed the detection of 63 hollows where a clear evidence of movement was recorded; this can provide elements for a check/update of the landslide inventory map.

A further step dealt with analyses of landslide phenomena at more detailed scale (i.e. 1:5000) via full-resolution DInSAR data. Since these analyses call for significant computational

efforts they were concentrated on limited areas. Accordingly, full-resolution DInSAR data were processed via tomographic analysis (Fornaro et al., 2009b) with reference to an area of 64 km<sup>2</sup> corresponding to the municipalities of Frosinone and Torrice. Full-resolution DInSAR data analysis pursued two main goals: the preliminary analysis of landslide features (i.e. check of mapped boundaries; detection of ground displacements out of mapped areas); an insight into different kinematic behaviour characterizing different portions of the same phenomenon.

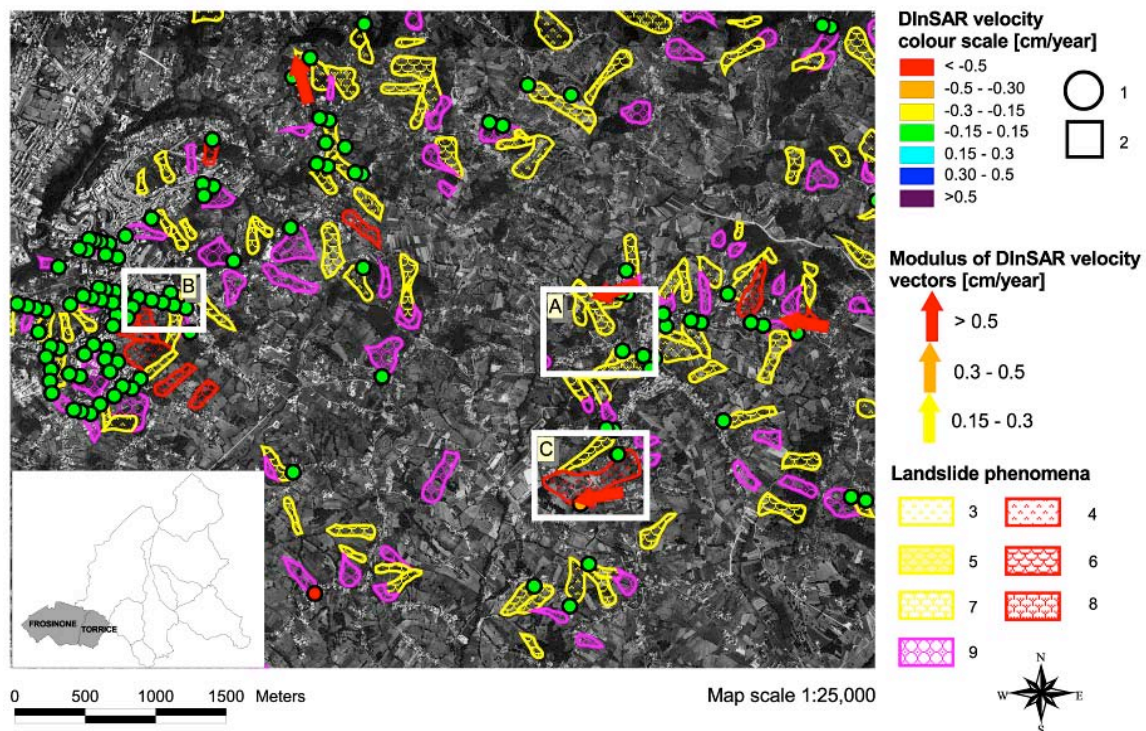


**Figure 132.** An example of advanced low-resolution DInSAR landslide velocity map for the municipality of Frosinone and Torrice (Lazio Region, Italy) with boxes selecting areas where full-resolution DInSAR landslide velocity map are shown, respectively in: A, B and C, see Cascini et al. (2010). Not moving DInSAR coherent pixel or on flat areas; 2) DInSAR coherent pixel moving on vertical direction; 3) dormant rotational slide; 4) active rotational slide; 5) dormant earth flow; 6) active earth flow; 7) dormant rotational slide–earth flow; 8) active rotational slide–earth flow; 9) creep phenomenon (Cascini et al., 2010).

In order to test the potential of the proposed procedures for the check of possible changes in landslide boundaries, the entire full-resolution coherent pixel dataset was considered including pixels out of the mapped landslides and assuming translational movements along the steepest slope direction. For instance, referring to the dormant rotational slide–earth flow, labelled as A in Figure 9, the proposed procedure highlights evidence of movements exceeding 0.3 cm/year both in the head (orange squares) and in the nearby built-up area located just up the head. This means that geomorphological in situ investigations, a more detailed map of the landslide as well as a building damage survey are necessary to check the landslide boundary and the current state of activity. As it concerns the dormant earthflow labelled as B, in Figure 133 full-resolution DInSAR data exhibit evidence of movement in a built-up area located along a road above the head of the phenomenon. To further investigate this case, the analysis of the geomorphological map at 1:25,000 scale revealed the presence of

a hollow (labelled with stripes in Figure 133) located between the road and the head of the earth flow. Actually, this latter is bordered by moving full-resolution DInSAR velocity vectors, thus suggesting that the head of the earthflow is likely to be retrograding, involving the hollow and, in turn, the buildings along the road.

The description of other examples can be found in details in Cascini et al., 2010.

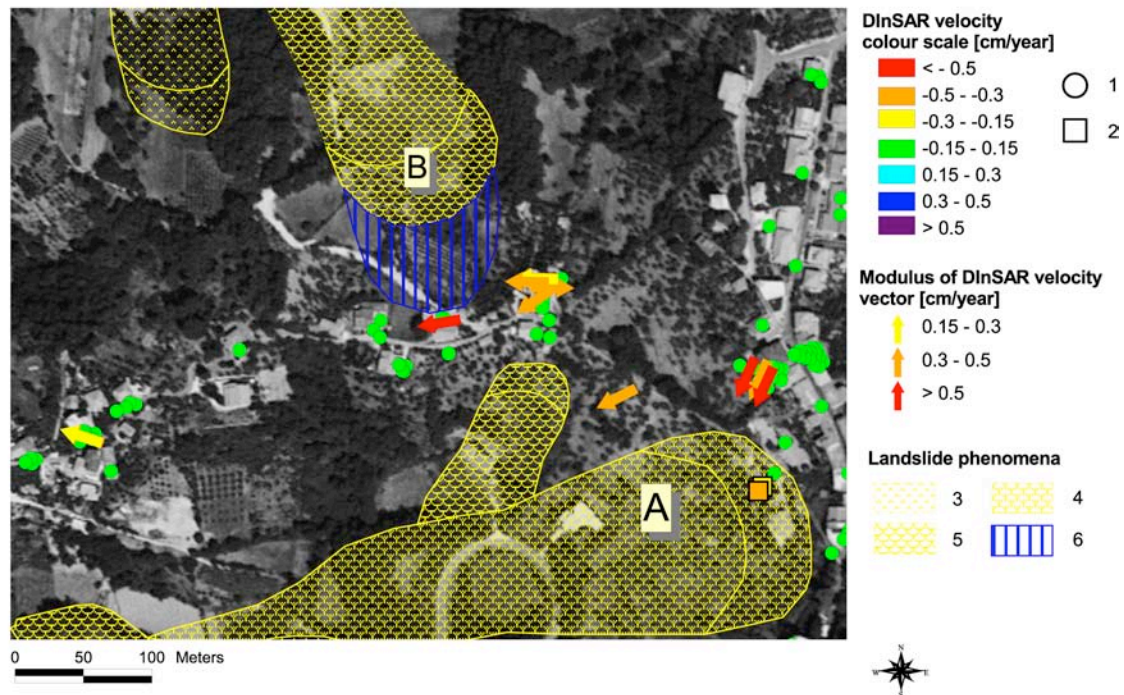


Figure 133. Advanced full-resolution DInSAR landslide velocity map of a portion of Torrice urban area (Lazio Region, Italy). 1) Not moving DInSAR coherent pixel or on flat areas; 2) DInSAR coherent pixel moving on vertical direction; 3) dormant rotational slide; 4) dormant rotational slide–earth flow; 5) dormant earth flow; 6) hollow (Cascini et al., 2010).

### 6.2.3.3 Improvements with respect to previous applications

The improvements achieved in the presented activities derive from the implementation of original procedures based on the integrated approach which merges DInSAR data (at both full- and low-resolution) with simple geomorphological models and geometric considerations. Key results are the generation of the a priori visibility map and the advanced landslide velocity maps. These two maps has turned out to be innovative and helpful in landslide detection and mapping processes.

The a priori visibility map is a valuable tool which can furnish useful information on the applicability of DInSAR data to slow-moving landslide detection and mapping in certain regions. In fact, the use of this map allows the zoning of the areas where it is possible to achieve a good DInSAR data coverage in order to develop analyses pursuing the detection/mapping of landslides, thus enabling to save both money and time for image processing.

Then, the generation of the advanced landslide DInSAR velocity map represents a further step towards a quantitative interpretation of remote sensing data since the projection of the

velocity/displacement vector along a precise direction may prevent the end-users from misleading interpretation of the typically adopted along-LOS measurements.

Accordingly, once the visible areas have been individuated low-resolution DInSAR data can provide useful elements for activities concerning checking/updating of landslide inventory maps either within or outside areas mapped as landslide phenomena. Further interesting aspects can be deepened via the analysis of full-resolution DInSAR data. Indeed, isolated structures located on landslides can act as ground benchmarks providing the researchers with useful information on the local kinematics of the phenomenon to study. In this regard the characterization of a given landslide with the help of DInSAR data mainly depends on the scale of the analysis, the extension and the complexity of the phenomenon.

In conclusion, notwithstanding the sometimes limited visibility the proper use of these techniques within areas sufficiently covered by DInSAR data has proved to hold the premise for furnishing valuable contributions to landslide detection/mapping at different scales.

## 6.2.4 Airborne geophysical survey: Stože, Log pod Mangrtom (detection and mapping)

GSA: Supper R., Baron I.,

GeoZS: Carman M., Kumelj S.

### 6.2.4.1 Study area

On the 17th of November 2000, a debris flow occurred in the Stože area (1,340-1,580 m a.s.l.), close to Mangart mountain (2,679 m a.s.l.), within the Julian Alps in NW Slovenia, demolishing about 20 ha of forest and the Predel pass road, and destroying part of the village of Log pod Mangartom, which is 4 km downstream in the Koritnica valley. There the landslide killed seven people. In the first stage of the event, a huge rotational landslide occurred (300 m wide, 1.5 km long and up to 10 m, locally even 50 m thick) at an altitude of 1,525 m, which later turned into a debris flow (Figure 134). The source of triggering of the landslide and debris flow can most properly be found in a combination of unfavourable geological and relief structure combined with intense rainfalls in October and November 2000 (1,800 mm). During this event approximately 1 million m<sup>3</sup> of material was displaced. However, in the tension zone of the landslide a huge amount of moraine deposits is still loosened and ready-to-slide (Figure 135). It was estimated that more than 1.5 million m<sup>3</sup> of unstable material could be mobilized within the landslide area (Komac 2001, Majes 2001, Petkovšek 2001).

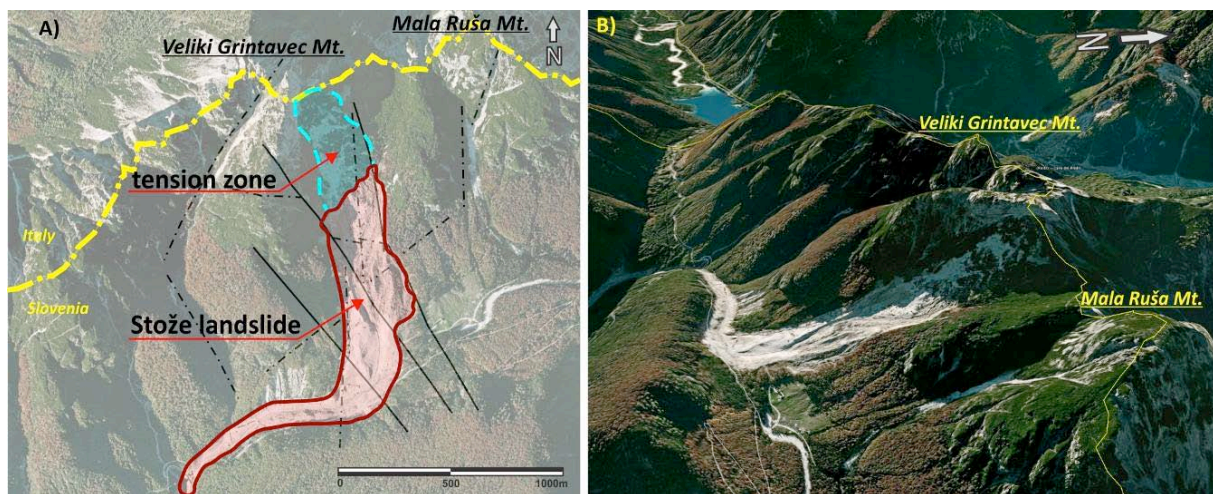


Figure 134: Stože landslide: (A) General settings with mapped faults (full black lines) and with faults interpreted from topography (dot-and-dashed black lines), and (B) oblique 3D view of the landslide from E (Source of data: Google Earth).

The whole region of NE Slovenia is a seismically very active area. On the 12<sup>th</sup> of April 1998, the strongest earthquake of the last 100 years occurred in the Upper Soča valley, with the epicentre 10 km away from the Stože area. Its magnitude was 5.8 and its maximum intensity was between the VII and VIII degrees according to EMS. The epicentre was located at a depth of 9 km. Another strong earthquake shook this area on July 12<sup>th</sup>, 2004. The earthquake with magnitude 4.9 caused the highest effects of VI to VII intensity according to EMS-98. The focal depth was located at a depth of about 8 km (Vidrih & Ribičič, 1999, 2004). Although the landslide of the year 2000 was most likely triggered by heavy rainfalls within November,

those strong seismic tremors probably had loosened the substrate of the subsequent landslide some time before the event and had been one of its most important controlling factors.

The Koritnica is an alpine valley lying in the direction SW-NE, which was reshaped by glaciers. The annual precipitation in this area is about 2500 mm. In contrast to other parts of the Julian Alps, the superficial river network prevails over the karst outflow and it is controlled by the dolomite outcrops in the Koritnica river valley.

The Mangart Mountain and its west ridge are mainly composed of Upper Triassic rocks, which consist of three different lithostrathigraphic units: (i) Cordevol dolomite in the lower part; (ii) Julian-Tuvalian calcareous marlstone, claystone and limestone; and (iii) the main dolomite in the upper part. Geological mapping of the site proved the existence of very unfavourable geological conditions which controlled the landslide. The landslide occurred in glacial moraine sediments and slope debris, deposited on tectonically highly fractured dolomite lying on impermeable layers of Triassic marly limestone. Dolomite is an excellent aquifer and during heavy precipitation, the water level in the rock rises substantially, saturating the overlying soils, which are rich in clay, with water. Also three major fault systems with general strike NW-SE, N-S and NE-SW were determined.

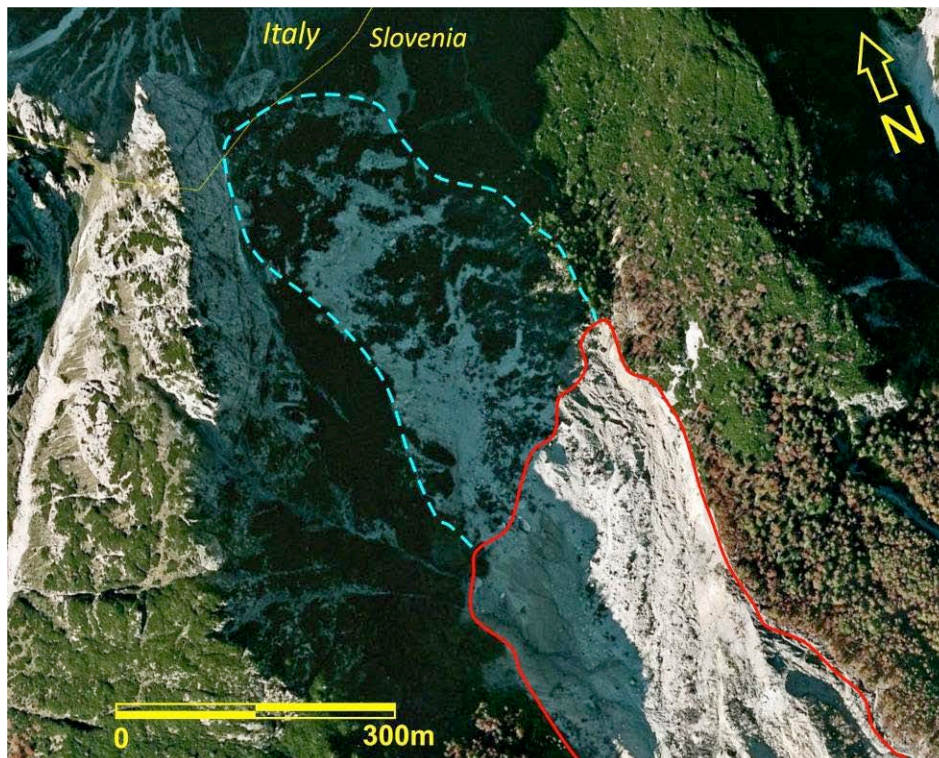
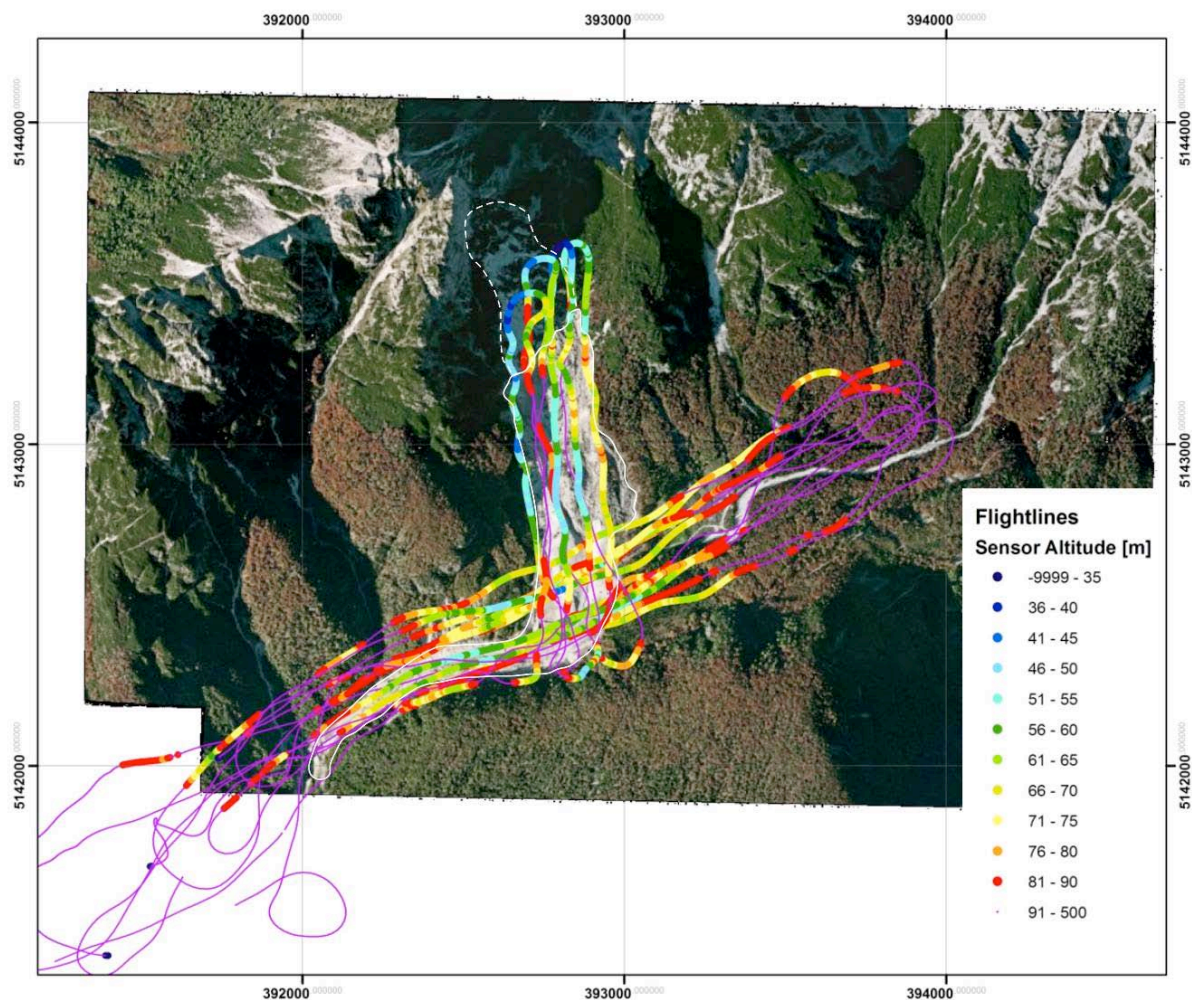


Figure 135. Orthophoto of the upper part of the landslide with bare surface of the marly rock (appearing in the shadow), and of the tension zone comprising loosened moraine deposit (Source of data: Google Earth).

#### 6.2.4.2 Description of the analysis

The airborne geophysical survey at the Stože landslide was performed on May, 21<sup>st</sup> 2010. This area was selected as a worst case test site for airborne geophysics since it shows a very rough topography with altitude differences of 700 m along a distance of just 1.7 km. At the beginning it was not possible to decide if a proper survey in this area would be possible at all.

The survey was performed with a rental helicopter of the type Ecureuil AS 350, which is a widely available type of aircraft, but with limited engine power for such surveys. However, due to the limitation of the budget, not much time could be given to the pilot for training flights. Last but not least, weather condition during the survey period was quite bad with strong winds at the top of the mountain ridge. Because of these strong winds the electromagnetic system could not be calibrated in between the lines at high altitudes, thus resulting in a much lower data quality than usual. Consequently the basic conditions for the survey were far from being ideal.



**Figure 136. Stožice landslide: Map of the helicopter flightlines (Source of data: Geological Survey of Austria and Google Earth).**

According to the steep mountain ridges all around the survey area, flight lines had to be squeezed inside the valley. Additionally some lines were flown up and down the landslide body itself to cover as much area as possible with data. Figure 136 shows the final flight line map. It is obvious that only a small quantity of the total area could be covered with data. Consequently interpretation of the airborne results is quite difficult since the integration of the results measured on the landslide body into the geophysical signature of the background of the area around is hardly possible. Moreover the average sensor altitude within the survey

area was at 89 m, thus significantly limiting the survey resolution, especially of the electromagnetic results.

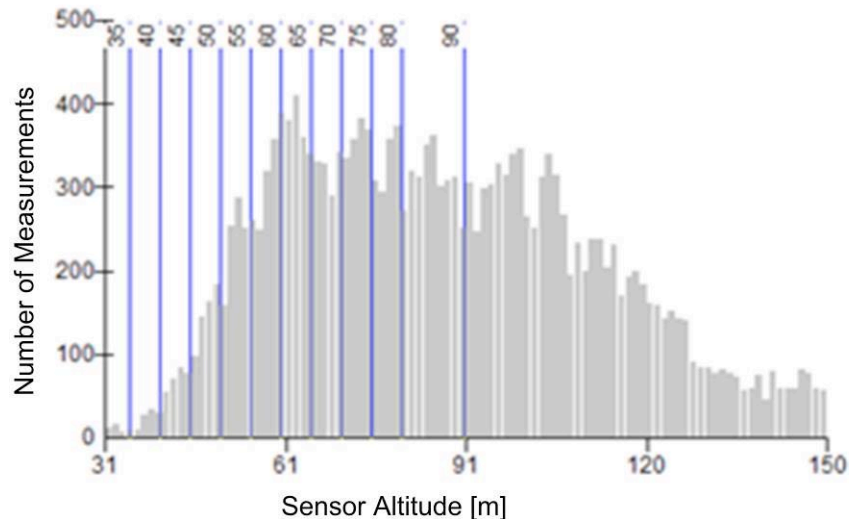


**Figure 137. Distribution of sensor altitudes within the survey area; blue lines indicate the bin classifications used in the flight line plan.**

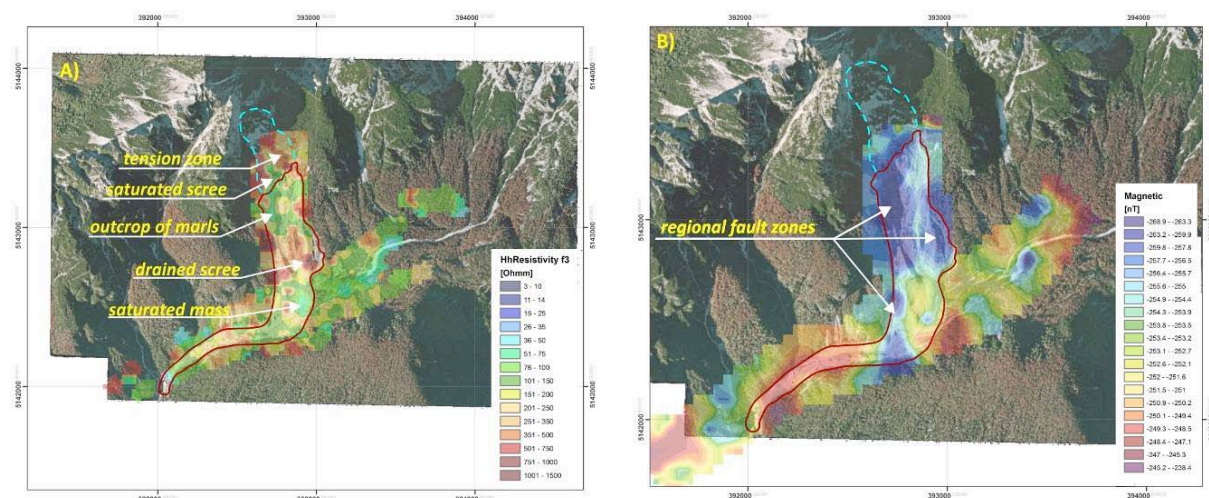


**Figure 138. Geological interpretation of the airborne geophysical survey: (A) subsurface resistivity and (B) Magnetics (Source of data: Geological Survey of Austria and Google Earth).**

However, in spite of the unfavourable boundary conditions, the multi-parametric airborne geophysical survey brought interesting results concerning information on the subsurface structure and about actual slope-related processes. The resistivity (HEM) survey confirmed the lithological pattern and water saturation. The high resistivity regions mostly indicated the dolomite and limestone rock, drained slope scree, drained landslide mass, moraine deposit and loosened material of the tension zone of the landslide with present cracks and cavities (Figure 135). The low resistivity indicated outcrops of marls, which are rich in clay, or water-saturated scree. The magnetic survey discovered an elongated minimum, located at the centre of the landslide and running in parallel to the main sliding direction, indicating most probably a major regional tectonic fault (Figure 138B). The gamma-ray survey consisted of Cesium,

Uranium, Potassium and Thorium. The Cesium content in European soils is mostly related to the contamination due to the Chernobyl Nuclear Accident. Although the Cs has already decayed in most areas of Europe to the background value, significant amounts can still be found in regions mostly exposed to rainfalls after the accident, like in northern Slovenia. Figure 139A clearly show that the Cs minima well correlate with bare surface of landslides, since the contaminated material was removed there by the landslide. Thus this parameter could be used to study the slope-related material removal and erosion after the 1986 event. The Uranium (Figure 139B), and especially the Thorium and Potassium pattern (Figure 140A) well identified the regions of tension inside the landslide zone, outcrops of marls and dolomite, clay-rich colluvia, weathered zones along a regional tectonic fault (perpendicular to the landslide) and deposits of moraines and debris flows.

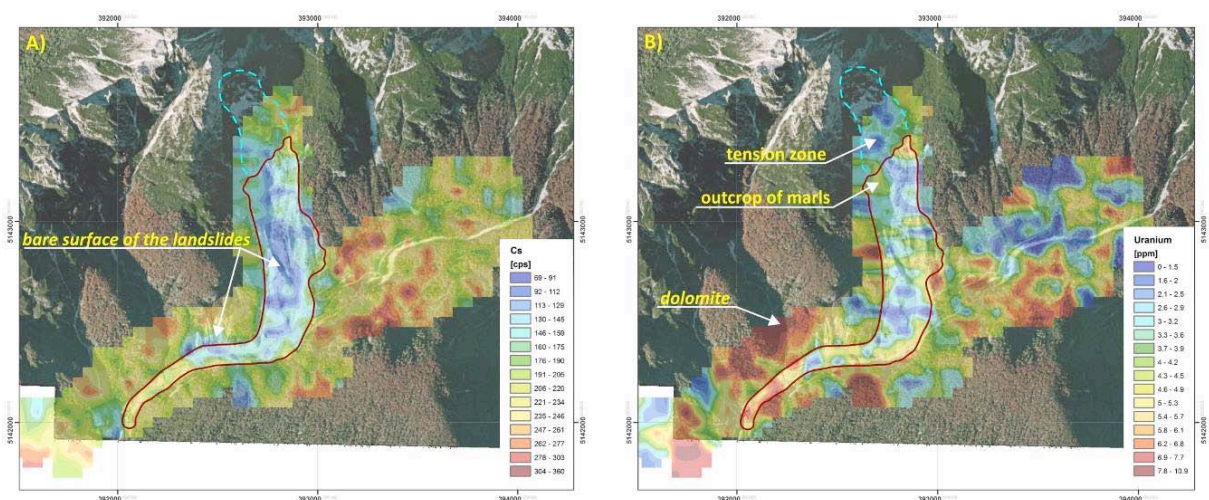


**Figure 139. Geological interpretation of the airborne geophysical survey – gamma ray: (A) Cesium and (B) Uranium (Source of data: Geological Survey of Austria and Google Earth).**

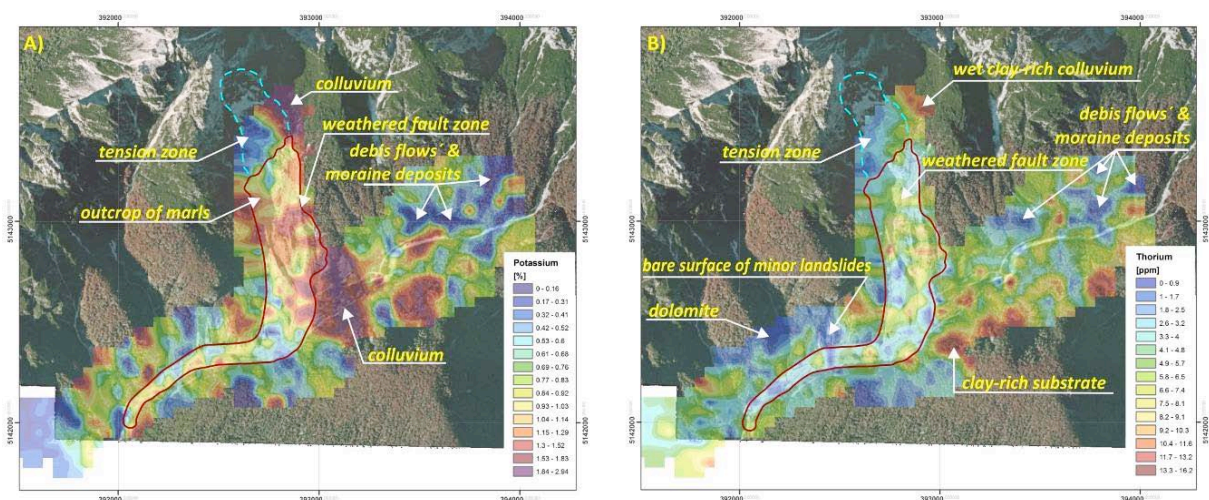


**Figure 140. Geological interpretation of the airborne geophysical survey – gamma ray: (A) Potassium and (B) Thorium (Source of data: Geological Survey of Austria and Google Earth).**

#### ***6.2.4.3 Improvements with respect to previous applications***

Although the airborne geophysical survey at the Stože landslide had to deal with many difficulties, it provided new data on the application of the multi-parameter airborne geophysics at such a local scale and brought new experience on surveying in such an exposed topography. The methodology proved its performance for landslide detection, geological structure investigation, mapping of actual slope-related processes and mapping of landslide susceptibility even under worse survey conditions.

However if the budget allows several hours of training flights for the pilot and permits to wait for optimum flying conditions, the average value of the sensor altitudes could be decreased, which would significantly improve the quality of the electromagnetic results. On the other hand this study also showed that even with a stronger helicopter not a much larger area could have been covered with data due to the steep cliffs. Consequently the question arises, if the limited coverage of the area justifies the high costs (mobilization of helicopter and data acquisition crew, flight costs, personal costs for the survey) of an optimized airborne survey for such a relatively small investigation area in such rough terrain conditions. Using the same budget, the area might be covered with ground geoelectrical profiles, which even provide a much higher resolution.

Therefore we conclude that for site specific, small scale studies under rough terrain conditions, like the one investigated at Stože, airborne geophysics might not be the method of choice taking into account the high costs and the limited resolution of the data. However if larger areas or several sites which are close together have to be surveyed, airborne geophysics would definitely be the method to be applied due to its multi sensor surveying ability.

## 6.2.5 Airborne geophysics: Schnepfau, Austria (detection and mapping)

*GSA: Tilch N., Supper R., Motschka K., Winkler E.*

### 6.2.5.1 Study area

In August 2005 a countless number of gravitational mass movements were triggered in the course of heavy rainfalls lasting for several days, which included intense episodic rainfall, in the Austrian Federal States of Vorarlberg, Tyrol and Styria. Due to the high number of triggered and quickly developing processes with large runout distances within unconsolidated rocks (such as earth flows and soil flows), several buildings and traffic infrastructures were damaged or destroyed (Figure 141). In the Federal State of Styria even two fatalities were recorded.

Such scenarios clearly show that there is an urgent need for planning criteria, which allow in an objective way the identification (based on the natural and anthropogenic conditions, e.g. geology, pedology, land use, morphology) of areas with variable susceptibilities to the genesis of such dangerous types of gravitational mass movements.

So far in Austria, only such hazard maps were used in frame of land use planning, which solely contain semi-quantitative information on hydrological hazards. However the events of the year 2005 clearly show that there is an increasing need to upgrade the content of hazard maps with information on hazard potentials due to gravitational mass movements (more holistic and process-orientated hazard maps, Tilch & Schwarz 2010, Tilch et al. 2009).



**Figure 141. Earth flows in Berbigen-Rehmen-Au (Bregenzer Wald, Vorarlberg, Austria).**

For the compilation/modelling of process-oriented susceptibility maps of the disaster region of “Schnepfau-Au August 2005”, area-wide maps containing information on the process relevant geosphere are needed. However no commonly available maps exist in Austria, which contain such information in a detailed, spatially inclusive and comprehensive way. The available geological maps for example only comprise partial information on granular soils (unconsolidated rocks) and are only partly adaptable for such a purpose due to their scale (1:200,000, 1:50,000). Solely for some areas, like for Vorarlberg, maps with a more suitable scale (1:10,000) exist, which are based on results from detailed mapping campaigns. The conceptual soil maps (= geological basic disposition/susceptibility map, see Tilch & Schwarz 2010), which are adapted from an interpretation of available geological maps by methods

---

developed at the Geological Survey of Austria, are of course subject to the scale of these underlying base maps (Figure 142). The delineation of areas with comparable dominant soil types is based on the spatial extension of geologic-lithological units, which is definitely not always the case in nature. Consequently there are several limitations for the derived conceptual soil maps as regards the spatial delineation of homogenous areas as soil types (units).

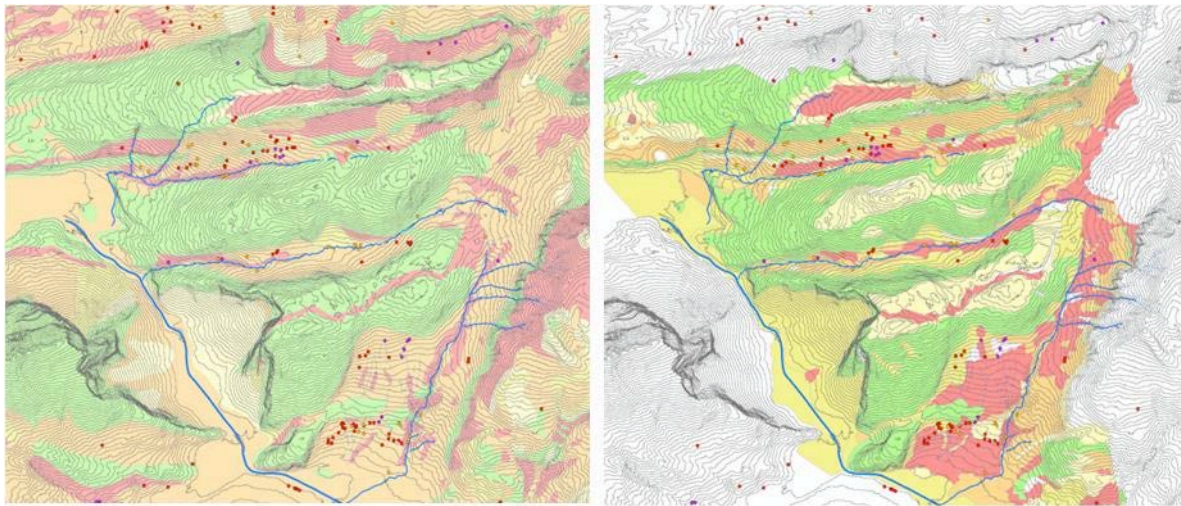


**Figure 142. Available geological maps, interpreted to conceptual soil maps with information to potential autochthone soils (conceptual soil maps): left: a section of the available digital geological map), right: a section of the digitalized geotechnical map after Seijmonsbergen et al. 1988); Legend: green to red (green: supported by rough-grained, gravel-rich soil/sediment, very high portion of stones, small or very small portion of fine-grained soil/sediment (silty) and partly loamy (sandy slope cover); red: supported by fine-grained silty-claylike soil/sediment, small portion of stones and very strongly loamy (from silty clay to clay).**

#### **6.2.5.2 Description of the analysis**

Until now area wide maps of unconsolidated rocks, which represent the basis for the identification of areas of different geological basic disposition for spontaneous gravitational mass movements, are lacking for the area of “Schnepfau-Au”. Keeping in mind that area wide mapping is very time consuming and always also subjective in some degree, alternative sources of data, like those derived from geophysical airborne and ground measurements, could be used to support the compilation of such maps. These methods provide comprehensive and objective data, covering a large area within a relatively short time of investigation. Hence this study is an attempt to investigate, in which way airborne and terrestrial geophysical results, in combination with other methodologies, can support the delineation of areas with comparable integrated geo-disposition.

The airborne survey in Schnepfau was performed on the 27<sup>th</sup> of August 2009 using the Austrian airborne system (Motschka 2001). Since topographical preconditions made it impossible to fly straight lines over the steep flanks of the mountains maintaining sensor altitudes of less than 90m, the lines were flown at constant altitude above sea level following the topography at a maximum distance of 120 m (Figure 143). Even with this alternative layout of survey lines, only a part of the whole area could be mapped.

One of the major outcomes supplied by airborne geophysics is the spatial mapping of the subsurface resistivity. This parameter reflects the spatial heterogeneity as well as the spatially and temporally variable hydrological characteristics of the subsurface as an integral response. Additionally airborne gamma ray mapping was applied to delineate areas of variable granular soils. For calibration of the airborne results 8 geoelectric ground profiles were performed. On one hand these lines were positioned according to the results of the geological and process-related field mapping campaign, selected in a way to cover as much as possible areas showing different characteristics related to geology, lithology and stability. On the other hand they were aligned to cross regions of maximum resistivity contrast based on the results from the airborne survey.

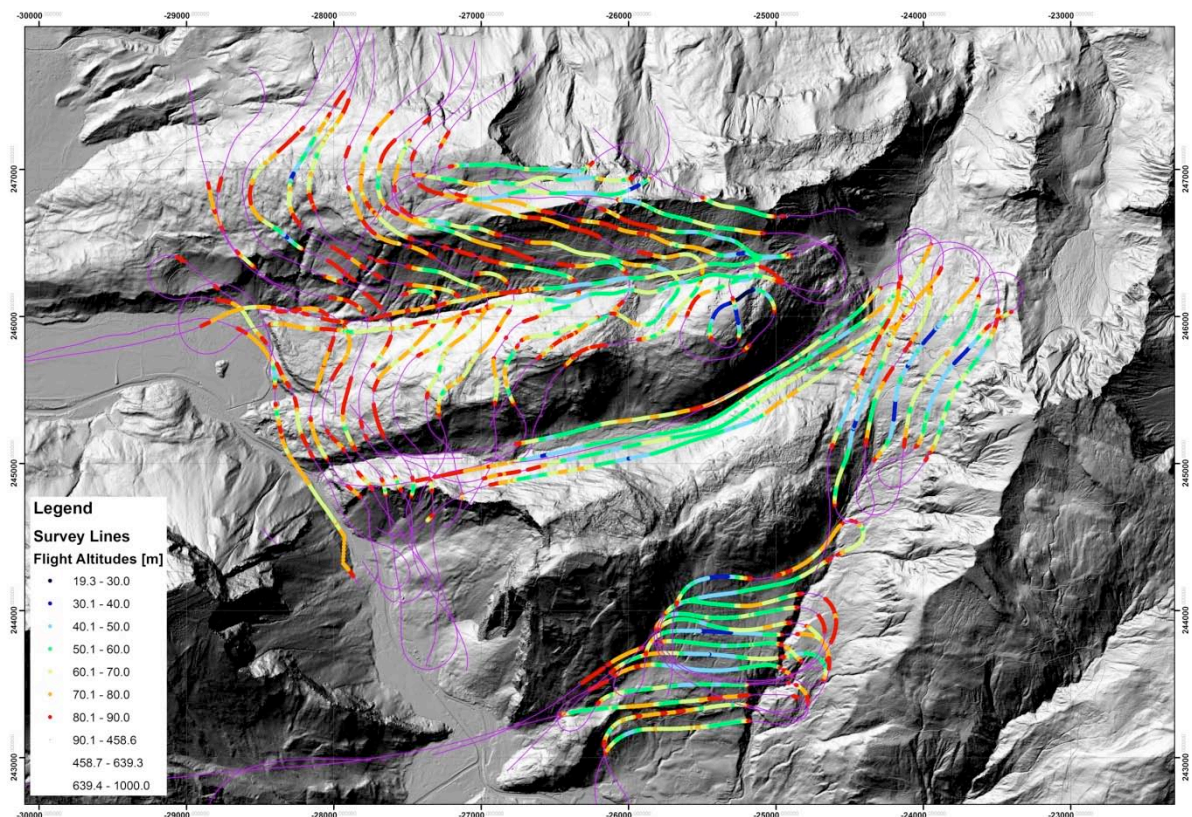


**Figure 143. Flight line map of the SafeLand test area SCHNEPFAU, colours indicate sensor altitudes above topography according to the legend; purple colours indicate sensor altitudes above 90 m (=data not used for interpretation).**

### 6.2.5.3 Results

Based on the outcome of airborne electromagnetics, the results of area by area field mapping of the lithological condition of the process-relevant geosphere could not only be verified but even improved. For instance it is nearly impossible to map gradual changes of soil and rock conditions in the field; in contrast airborne geophysics makes it possible. Additionally the results of airborne electromagnetics allowed mapping the basement and the overlaying unconsolidated rocks (soil cover), which could be delineated well by interpreting the two-layer inversion results (Figure 144). For instance it was possible to properly define the spatial

boundaries between fine grained granular rocks, which are very susceptible to sliding (moraines and running-grounds), and rather coarse grained granular soils (e.g. coarse scree material), which usually show a higher resistance against sliding.

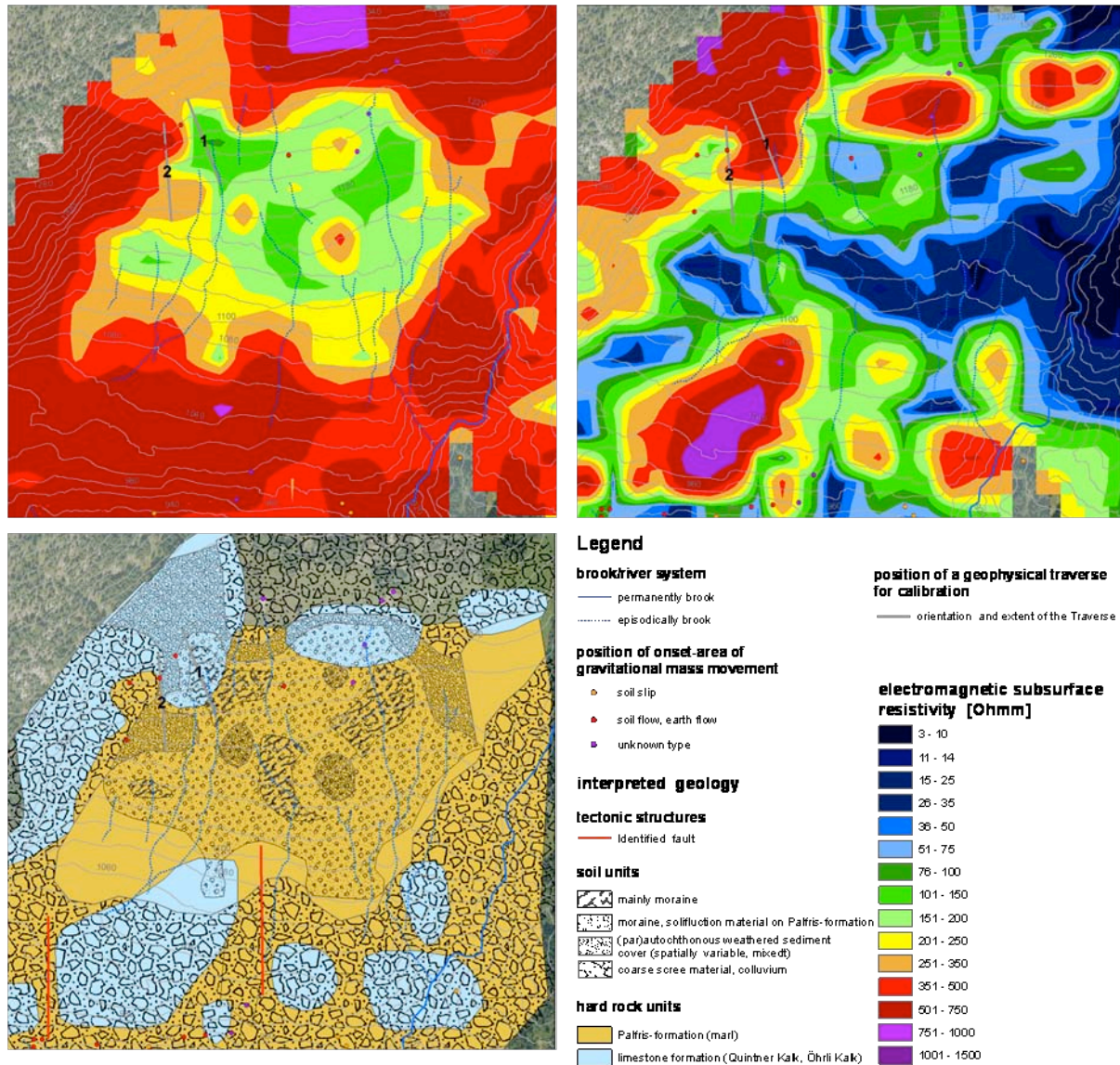


**Figure 144. Model results of 2-layer-inversion of airborne electromagnetic measurements in a subarea of the test region Schnepfau/ Vorarlberg (Austria): Upper left: Electrical resistivity of the first layer [Ohmm], upper right: Electrical resistivity of the second layer [Ohmm], lower left: Geological interpretation; gray lines: location of ground geoelectric calibration profiles.**

Additionally gamma ray mapping results could be interpreted well for the test area. Based on values of high Thorium content it was possible to confine the allochthonous sediments of glacial and periglacial displacement processes (moraines, sediments of solifluction) as well as relatively fine-grained parautochthonic colluvial deposits, originating from marlstone, which are very susceptible to weathering (see Figure, right and Figure 145, left). In case of the glacial sediments the high thorium content can be attributed to the fraction of sandstones

contained, whereas for the pure colluvia high thorium values are due to weathering scree of silicate rich marly and clayey rocks.

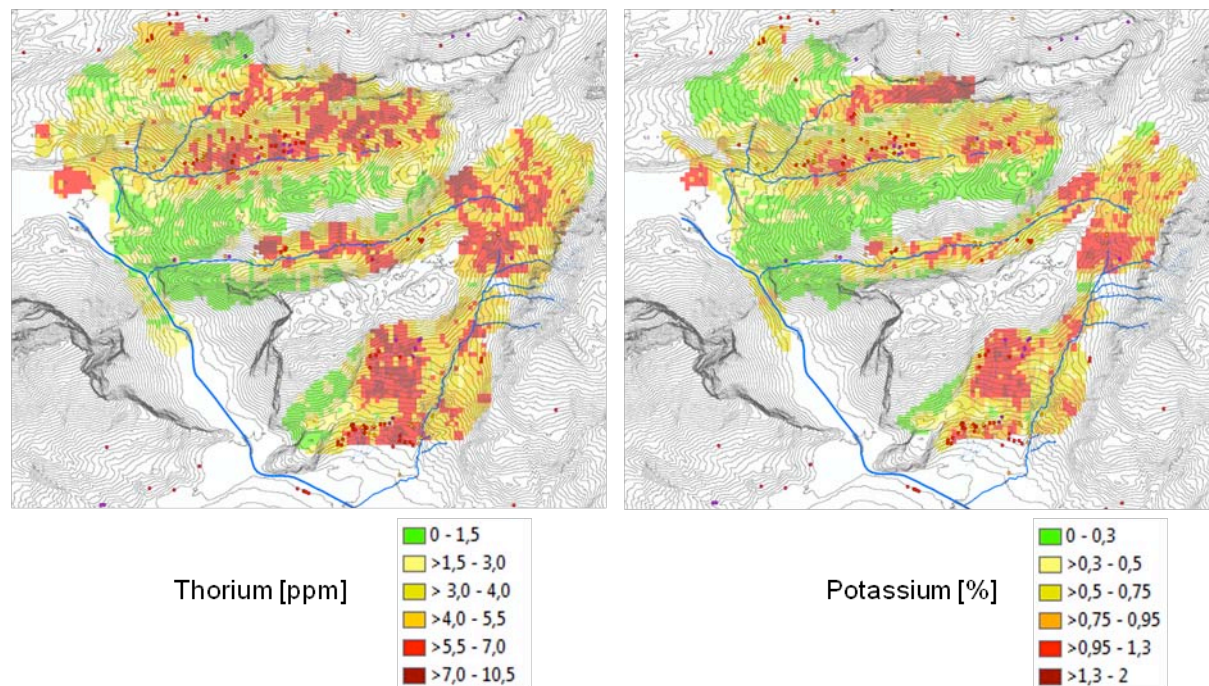


**Figure 145.** The derived “radiometric conceptual soil map”. The definition of value intervals is based on field knowledge and the available site-specific conceptual soil map (see Fig. 2, right): based on Thorium (left) and on Potassium (right).

#### 6.2.5.4 Conclusions

The results from this study support the assumption that glacial sediments as well as fine grained (par)autochthonic colluvia of the marlstone formation are exceptionally prone to spontaneous mass movements within unconsolidated rocks. So far an area wide, detailed and objective mapping and assessment of these units regarding their geological and lithological basic disposition was very difficult if not impossible. However the results of this study show that based on the outcome from the airborne geophysical mapping this seems to be possible for the examined region since the pattern of potassium and thorium correlates very well with the conceptual soil maps, which were derived from the available geological maps of the area. Moreover gradual lithological transitions inside of the colluvia and glacial sediments can be identified. Such information cannot (or only with large efforts) be derived from the available geological maps and field investigations. Due to successive adjustment and determination of the radiometric bin intervals to site knowledge and to available detailed geological maps it was possible to generate “radiometric conceptual soil maps” adapted from the potassium and thorium pattern (Figure 145). Both approaches lead to similarly good validation results (Figure 146) compared to the site-specific conceptual soil map (= geological basic disposition/susceptibility map, scale 1:10,000), but to a better outcome as the one derived from the commonly available Geological Map of Austria (= geological base disposition/susceptibility map, scale 1:50,000).

We can further conclude that results obtained for this specific test area concerning the definition of adapted geophysical bin classes and their correlation with process-relevant

properties and relations of unconsolidated and consolidated rocks (e.g. wetness, conceptual soil unit, landscape-specific geologic-lithological conditions) should be applied to other areas where airborne geophysical data is already available. When necessary, landscape specific value intervals have to be defined to improve the interaction of methods towards a general, large scale applicability.

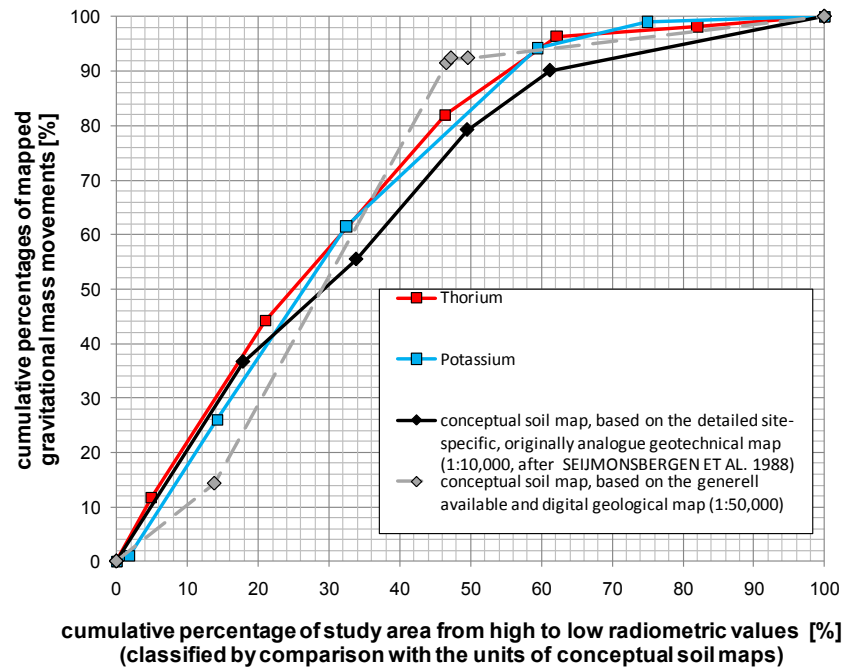


Figure 146. Validation according to Chung & Fabbri (2003) of the obtained conceptual soil maps (= geological basic disposition/susceptibility maps), based on different geological maps and radiometric measurements.

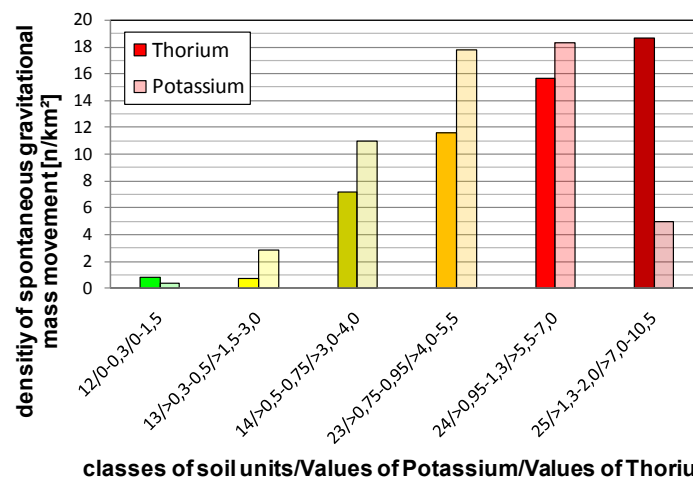


Figure 147. The density of spontaneous gravitational mass movement in soil in different value-intervals of radiometric measurements for Thorium [ppm] (full colour bars) and Potassium [%] (transparent bars), and interpreted soil units (12(coarse grained), ..., 25 (fine grained)).

#### ***6.2.5.5 Improvements with respect to previous applications***

To summarize, despite of the rough topographic conditions, airborne geophysics was successfully applied within the SafeLand test site Schnepfau. To cope with the steep mountain ridges an unconventional layout of survey lines was used to cover as much area as possible with high quality data. Additionally, for the first time, the applicability of gamma ray measurement to support the generation of conceptual soil maps as a base for landslide susceptibility mapping was proven for a test area and a strategy to adopt this method to larger scales was suggested.

## **6.2.6 Airborne frequency domain EM mapping, Gschlifgraben, Austria (detection and mapping)**

*GSA: Supper R., Baron I., Winkler E., Jochum B., Ottowitz D., Römer A.*

### **6.2.6.1 Study area**

The Gschlifgraben site (Figure 148) is one of the most prominent and extensively studied slope failures in Central Europe. It comprises a large complex of geologically controlled landslides, earth flows, topples, rockfalls and deep-seated gravitational deformations in the Gschlifgraben valley and along the slopes of the Northern Calcareous Alps. In late November 2007, an earth flow of about 3.8 million m<sup>3</sup> of colluvial mass was reactivated in the central and western parts of the valley. The displacement velocity was up to 4.7 m/day at the beginning. Consequently, in frame of the first emergency measures, 55 buildings had to be evacuated. Recently, the Gschlifgraben landslide has been a test site of the European FP7 project SafeLand where new techniques have been tested for rapid mapping monitoring and effective early warning, consisting of, e.g., airborne and ground-based geophysical surveys and the GEOMON4D (continuous geoelectrics) and DMS (automatic inclinometer) monitoring systems.

### **Geological and Geomorphic settings**

The area of Gschlifgraben is a 2.85 km long and 0.85 km wide valley along the foot of the Northern Calcareous Alps (Figure 148) south of the town of Gmunden. The front of the Northern Calcareous Alps there forms a steep cuesta with the summit at Mt. Traunstein (1691 m a.s.l.). The valley is divided into small sub-parallel catchments; its topography is strongly controlled by complicated tectonics and a very complex lithology, as well as by mass wasting that has been active here since the end of the last glacial period.

The surveyed area of Gschlifgraben covered three main geological units with completely different lithology and geological structure (Figure 149), i.e.: (i) Northern Calcareous Alps and the "Marginal Nappe" (NCA), (ii) Ultrahelveticum (UHV) and (iii) the Rhenodanubian Flysch Zone (RFZ).

The NCA unit (Triass-Cretaceous age) is generally composed of densely fractured, diversely stratified, steeply dipping and frequently faulted competent brittle rock. Dolomite and Limestone are the most abundant rock types. The substrate is highly permeable and the joints often have a character of opened cracks. Generally this unit shows the highest electrical resistivity and the lowest content of radioactive elements.

The UHV unit (Cretaceous-Paleogene age) comprises tectonically strongly deformed variegated marl, claystone, nummulitic limestone, sandstone, arcose etc. This unit is the most incompetent one in the study area. The material contains a relatively high fraction of swelling clay minerals. Moreover the soft rocks are intensively tectonically fragmented. The rocks of the UHV are locally quite permeable (fractured sandstone, limestone etc.), however impermeable zones prevail. Tectonic joints used to be filled with secondary or tectonic clay. Due to these facts, this zone shows a relatively low resistivity, and a high U, K and Th content.



**Figure 148. General setting of the Gschliefgraben site: A) Position within Austria, B) Airborne photo of the Gschliefgraben valley and Mt. Traunstein from the west (Photo by: R. Supper, 2009).**

The RFZ (Cretaceous age) is built up mostly with slate, shale, cemented marl and sandstone of different thickness. The alteration of competent vs. incompetent and permeable vs. impermeable rocks exhibit high local contrast resulting in a distinct local contrast of resistivity and U, K, and Th content.

The main mass wasting processes are represented by sliding and flowing in the central part, which is built up mostly of the UHV unit. The UHV emerge here in a form of the tectonic window between the RFZ and the NCA. On the other hand, falling, toppling, and spreading are the most characteristic types of mass movement in the eastern and southern marginal areas of the Gschliefgraben valley along NCA, where hard rock dominates (dolomite, limestone, cemented Pleistocene breccia). At some places, great portions of the NCA and the below situated RFZ and UHV units are subject to Deep-seated Gravitational Deformations in a rather initial evolution stage.

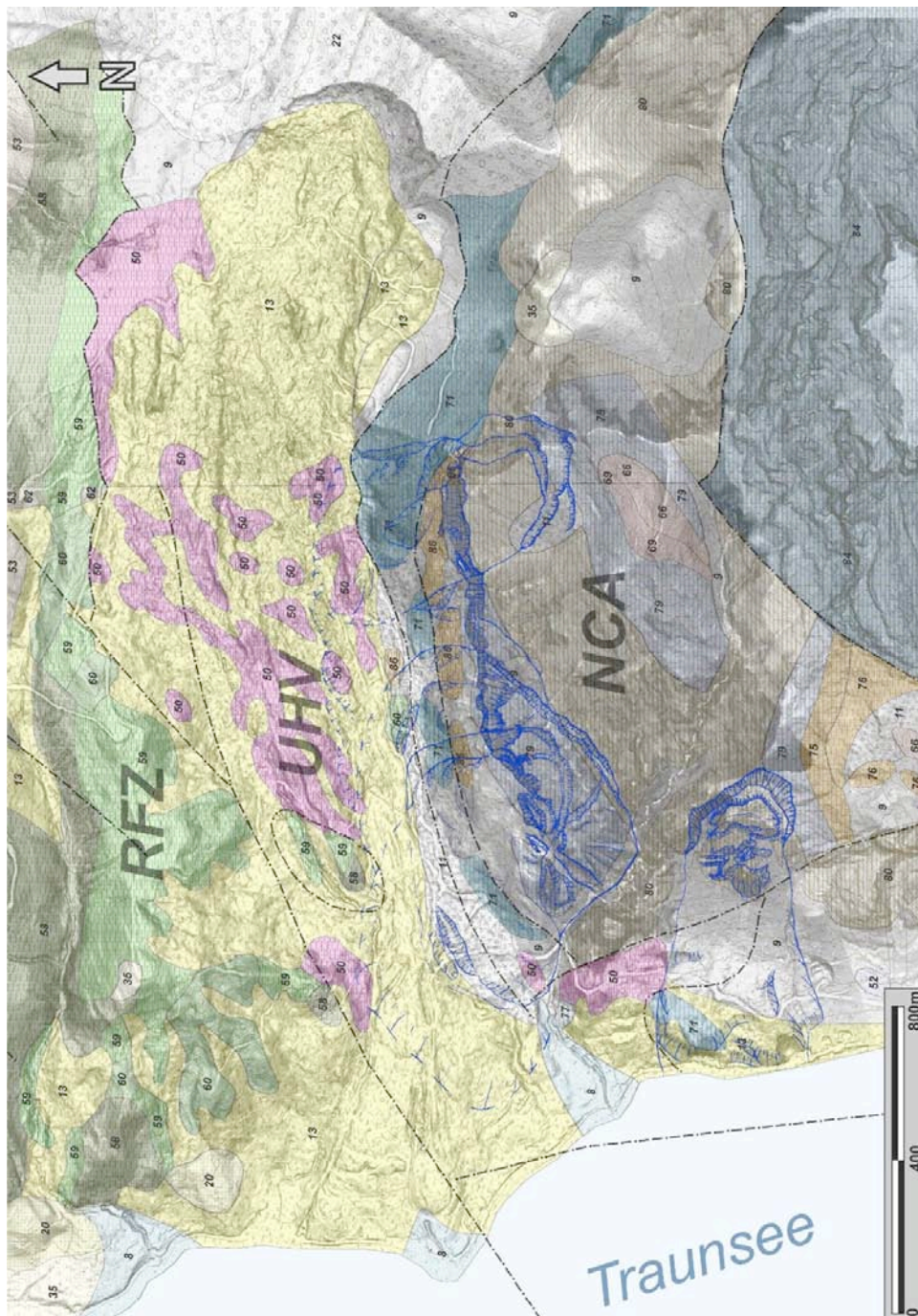


**Figure 149. Geological map of the area of Gschlifgraben. The blue contours indicate the Deep-Seated Gravitational Deformations. Legend: Quaternary deposits: 8 - Alluvial Fan, 9 - Slope Scree, 11 - Block Fields, 13 - Landslide Deposits, 20 - Glacilacustrine deposits, 22 - Slope Breccia, 35 - Moraine deposit; UHV: 50 - Buntmergel Fm., 52 - Greisten Fm.; RFZ: 53 - Altliengbach Fm., 57 - Perneck Fm., 58 - Zementmergel Fm., 59 - Seiesenburg Fm., 60 - Rieselsberg Fm., 62 - Gaultflysch Fm.; NCA: 66 - Schrambach Fm., 69 - Ruhpolding Fm., 71 - Calcarenite Fm., 75 - Koessen Fm., 76 - Koessen Fm., 77 - Koessen Fm., 79 - Plattenkalk Fm., 80 - Hauptdolomit Fm., 84 - Wetterstein Fm., 85 - Guttenstein Fm., 86 - Haselgebirge Fm.; the major tectonic faults are as dot-and-dashed lines (modified after Schoenlaub et al. 1996, Krenmayer 2007 and Moser et al. 2009).**

### 6.2.6.2 Description of the analysis

The remote sensing part of the investigations carried out at the Gschlifgraben test site consisted of a detailed morphostructural and morphodynamical analysis of the mass movement (landslide inventory), and of a complex airborne geophysical survey. The interpretation was supported by geological maps compiled by Schoenlaub (1996), Krenmayr (2007) and Moser et al. (2009), structural palaeostress analysis (not published yet), and by a detailed ground geoelectrical survey (12 profiles).

#### Landslide inventory and activity assessment

A set of 5 high-resolution Airborne Laser Scan (ALS) scenes, which were taken at different times in April 2007, January, February, March and September 2008 (Table 7), represented the ground surface topography of Gschlifgraben just before, during, and after the major recent landslide event of winter 2007/08.

Slope gradient maps in inverted greyscale (“pseudohillshade”), derived from the ALS Digital Terrain Model (DTM) were applied for visual inspection of the area. Such slope-gradient maps have a much better and more continuous performance of the ground topography than the classical hillshade maps representing only one illumination azimuth (Figure 150). Although the vertical orientation of individual slopes on such a map could be difficult to be determined, the advantages of its expressivity prevailed. This small disadvantage was eliminated by applying contour lines. The recent activity state of individual slope failures (since 2000) was assessed by analyzing bare surfaces on ortophotos from 2000 (application Google Earth) and 2008, by analyzing differential ALS DTM in ArcGIS software, and by comparing individual “pseudohillshades” (Figure 151). The ALS analysis was complemented with field inspections and field morphostructural mapping.

**Table 7. Parameters of the ALS campaigns in the site of Gschlifgraben.**

Date	Ordering party	Company	Plane	Sensor	Resolution [mm]	Flight Height [m]	Processing by
2007-04-05	GeoL	Topscan	x	ALTM 2050, ALTM 3100	~20	1000	Topscan
2008-01-03	WLV	Diamond Airborne sensing GmbH	Diamond HK36 MPP	Riegl LMS – Q 560	20	650	Area-Vermessung ZT-GmbH
2008-02-11	WLV	Diamond Airborne sensing GmbH	Diamond HK36 MPP	Riegl LMS – Q 561	20	650	Area-Vermessung ZT-GmbH
2008-04-28	GeoL	Topscan	x	ALTM 3100	~20	1000	Topscan
2008-09-05	WLV	Diamond Airborne sensing GmbH	Diamond HK36 MPP	Riegl LMS – Q 561	20	650	Area-Vermessung ZT-GmbH

*Note: WLV – Austrian Service for Torrent and Avalanche Control, GeoL – Abteilung Geoinformation und Liegenschaften, Upper Austria*

The detailed morphostructural and morpho-dynamical analysis of the ALS DTMs and ortophotos enabled us (i) to recognize individual slope failures and their deposits and (ii) to distinguish the active landslides and earthflows from the dormant (inactive) and old ones (Figure 152, Figure 153). In total, the study area was affected by morphologically expressive mass movements at more than 50 % (Table 13). The mass-movement phenomena in the area include different types of landslides at different volumes, evolutionary stages and activity level, forming a complicated complex. Due to the limited time available, the inventory could only deal with a rough classification. Shallow and deep-seated slides (slumps), their transitions to earthflows, earthflows alone, fallen boulders or sagged slopes and toppled rock

towers were the most abundant landslide types. The active landslides and earthflows (active between 2000 and 2008) had affected about 5 % of the study area.

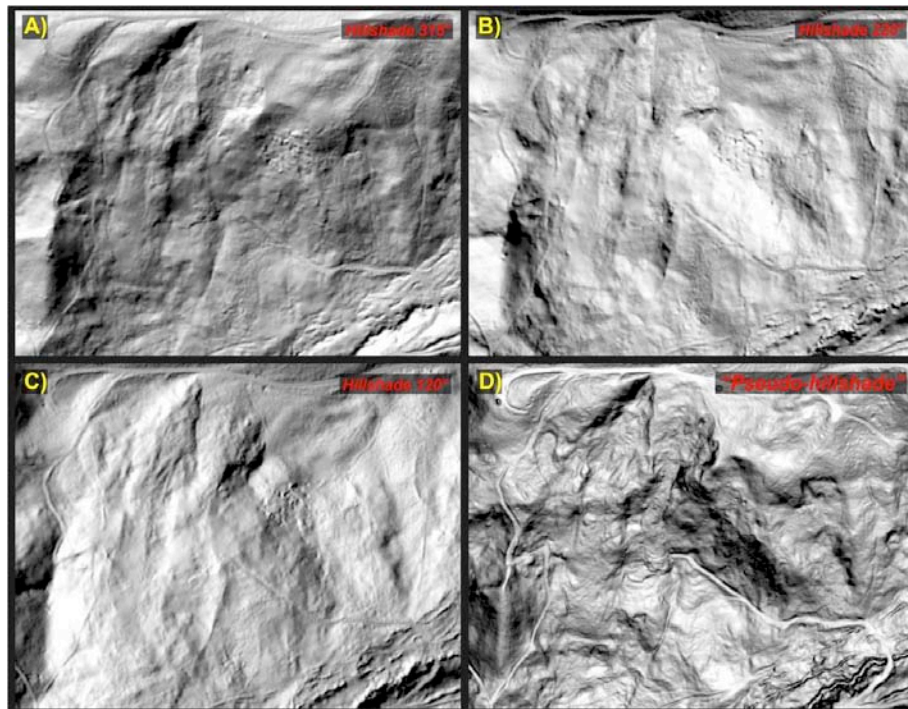


Figure 150. Comparison of hillshade DTM with different azimuths of illumination (A-C), and the slope-gradient map in inverted greyscale, the “pseudo-hillshade” (D). Each of the frames covers the same 512 m wide area.

Table 8. Review of the spatial extent of different landslide types vs. stable area.

Index	Type	Area [km <sup>2</sup> ]	Area [%]
0	Stable area	2,17	48,69
1	Active landslides	0,01	0,30
2	Active earthflows	0,21	4,77
3, 4, 5	Inactive landslides and earthflows	1,20	27,05
6	Old landslide	0,85	19,18
<b>Total:</b>		<b>4,45</b>	<b>100,00</b>

The major recent landslide event in winter 2007/08 and subsequent remedial works were well documented by the differential ALS. The main recent earthflow mobilized older mass-movement deposit in the central and lower western part of the Gschlifgraben valley. Distinct subsidence in the upper earthflow portion, as well as the uplift of about 14 m in the accumulation zone was registered by the differential ALS (Figure 153A). The remedial works comprised of distinct material removal from the active earthflow, managed by the Austrian Service for Torrent and Avalanche Control Survey (WLV Austria) in spring and summer 2008 (Figure 153B).

Three distinct Deep-seated Gravitational Deformations (DSGDs) were identified at the ALS DTM in the area built-up by NCA and adjacent UHV rocks (Figure 154). They were approved

by field geomorphic and structural mapping. Toppled rock towers, crushed limestone and dolomite, pseudo-karst caves of open joints, cracks with intensive cold wind out blow and active rockfall zones were documented there. The entire DSGDs are most probably in the initial evolutionary stage and they comprise of typical topography including smooth trenches or smooth pressure ridges in the lower portion and along the flanks. The easternmost DSGD is about 683 m long, 320 m wide with an estimated thickness of 300 m and volume of about 34.3 million m<sup>3</sup>. The western one is about 800 m long, 712 m wide with an estimated thickness of 250 m and estimated volume of 74.5 million m<sup>3</sup>, while the third DSGD facing to Traunsee (out of the area of interest) is about 1 km long, 220 m wide with an estimated thickness of 250 m and volume of 31.1 million m<sup>3</sup>.

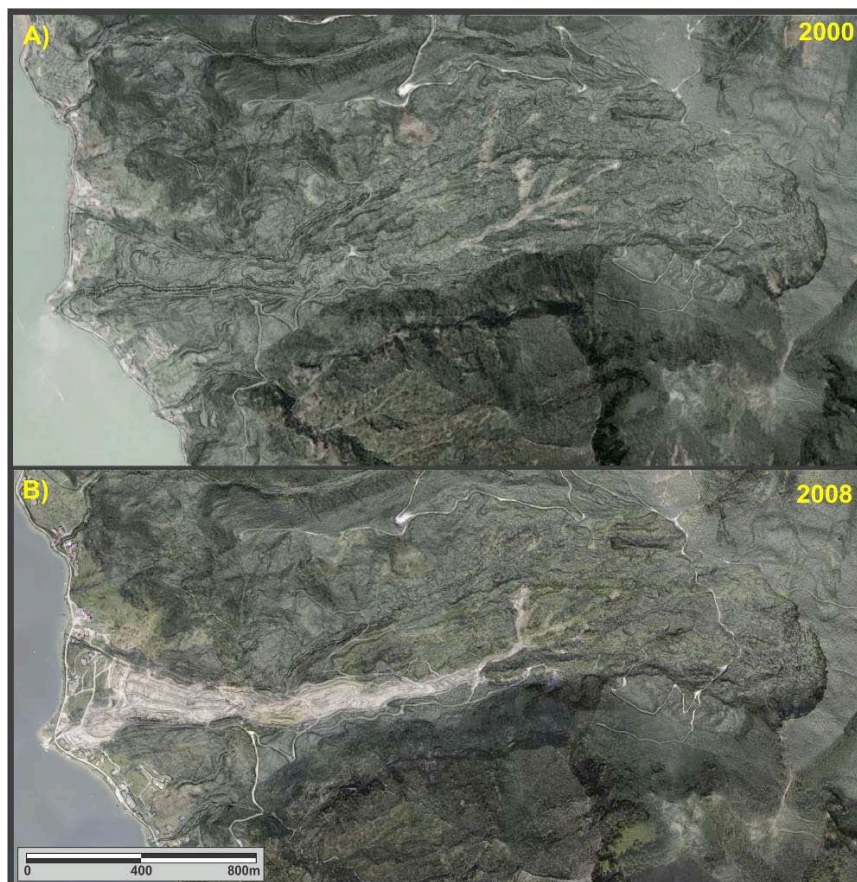


**Figure 151.** The identification of bare surfaces on set of two orthophotos from 2000 and 2008 was a base for assessing the activity of the earthflow complex. The orthophotos are superimposed on the ALS pseudo-hillshade.

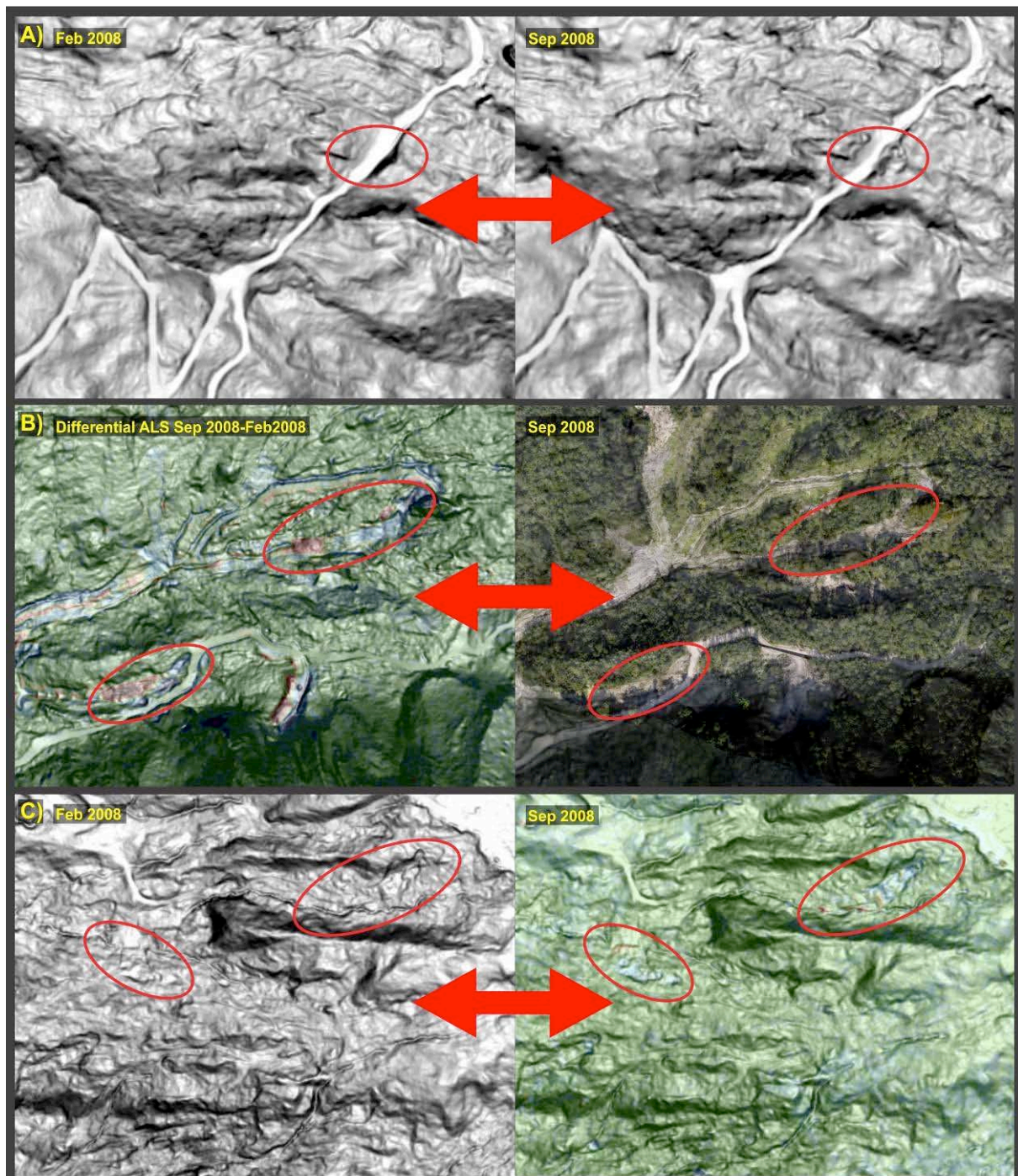
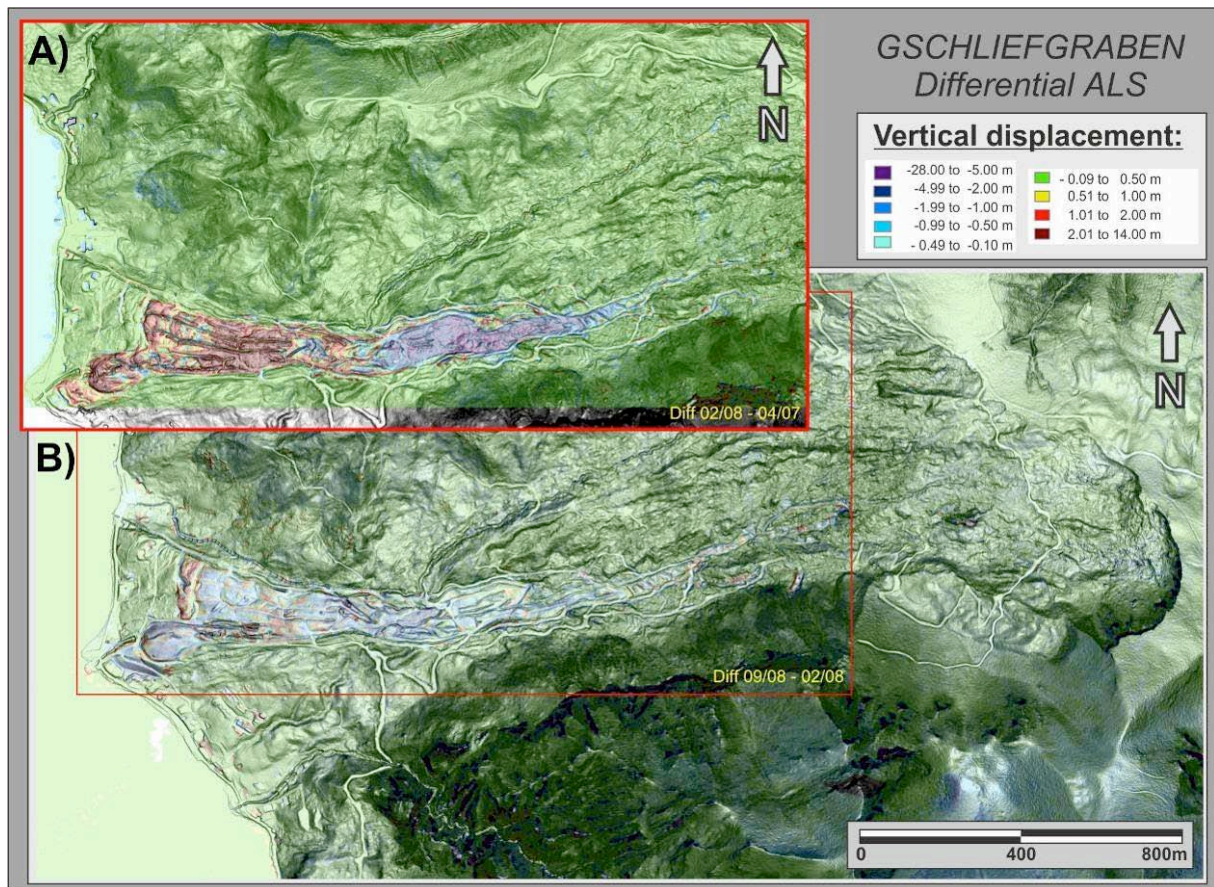


Figure 152. A more-detailed activity assessment of landslides was based on differential ALS, which had the best expressivity, as evidenced by comparison of A) two separate ALS pseudohillshades taken in different time, B) differential ALS model and the orthophoto, and C) pseudohillshade and superimposed differential ALS model.



**Figure 153.** Two differential ALS scenes highlight mass transport due to (i) the major recent landslide event in winter 2007/08 (above) and (ii) latter remedial works comprising of distinct material removal from the active earthflow (below). The presented individual ALS surveys took place in April 2007, February 2008 and September 2008.

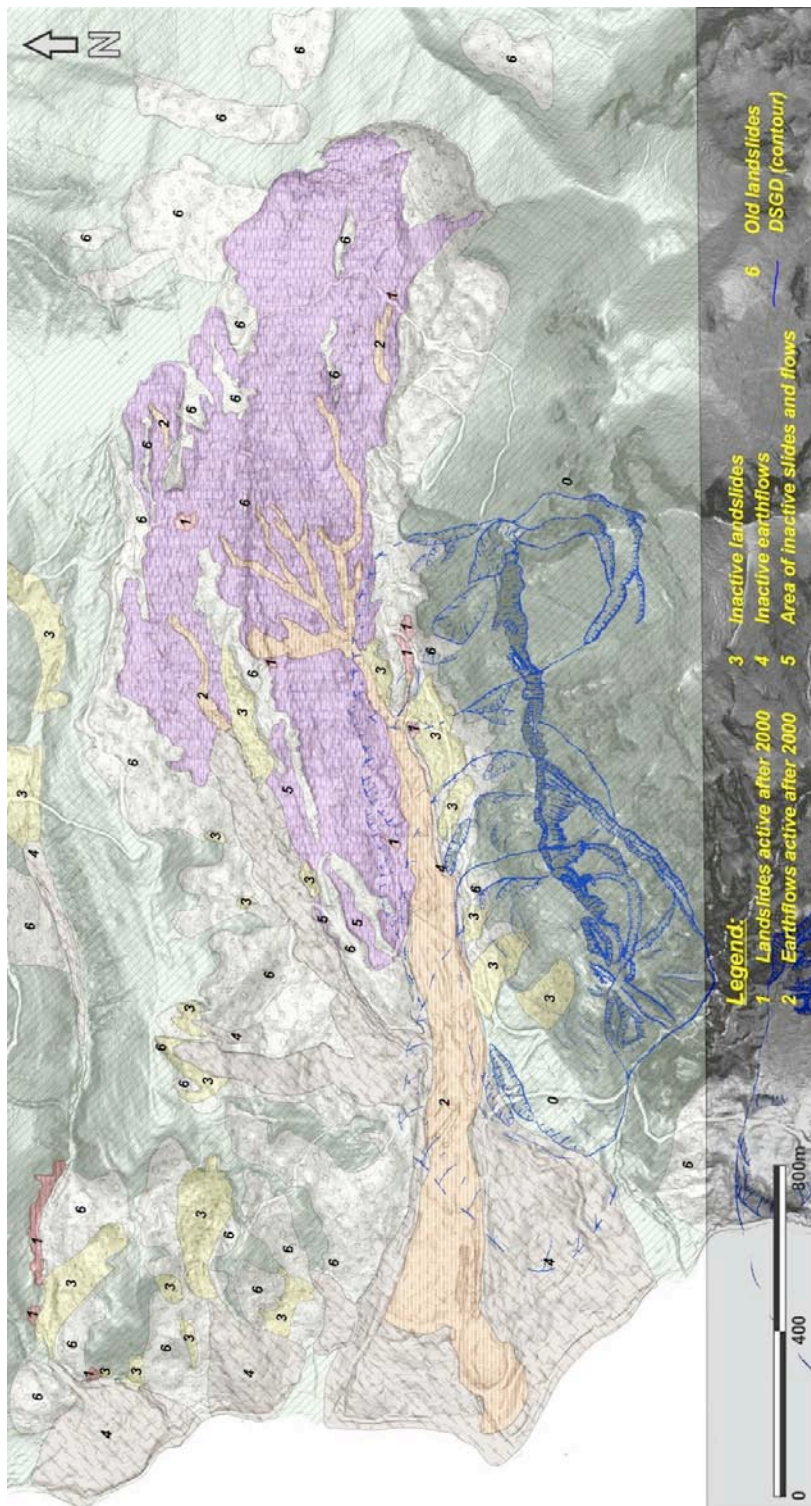


Figure 154. Landslide inventory map of the area of Gschlifgraben. Slope failures comprise more than 50% of the area, even the Deep-seated Gravitational Deformations (DSGD) were not included in the summary.

## Airborne geophysics

The big advantage of the application of airborne geophysics compared to other remote sensing or ground methods is, that multi-sensor, area wide information on subsurface parameters down to several tens of meters depth can be derived within a comparably short time. For a general description of the different applicable sensors please refer to the state-of-the-art description of airborne geophysics given before within this deliverable.

The multi-parameter helicopter borne geophysical campaign was performed in September 2009 by the Geological Survey of Austria (GSA) in close cooperation with the Austrian Army, the Austrian Service for Torrent and Avalanche Control and the civil engineering company Moser/Jaritz (Gmunden, Austria). The complete instrumentation of the Austrian airborne system (Motschka, 2001) was applied for the survey, consisting of a multi-frequency electromagnetic bird, a gamma spectroscopic unit consisting of two crystal packages of a total volume of 32 l, a passive microwave antenna and a magnetic sensor. The radiometer used by GSA has a sensitivity of  $0.3^\circ\text{C}$  and is equipped with an aperture angle of  $19^\circ$ . At a flight altitude of 80 m this results in a survey diameter of 26.8 m. In order to avoid any influences of temperature, the antenna is equipped with a heater, as well as a cooler and can be constantly operated at  $49.9^\circ\text{C}$ .

Due to the rough topography the survey area was separated into two parts, one part covering the area of the recent activity and the other one the probable catchment area in the east, with different line orientations (Figure 155) to ensure a maximum sensor altitude of 90 m. Due to the high cliffs in the surrounding area, lines could only be flown in one direction. Thus twice as much flight time had to be used than for usual survey flights.

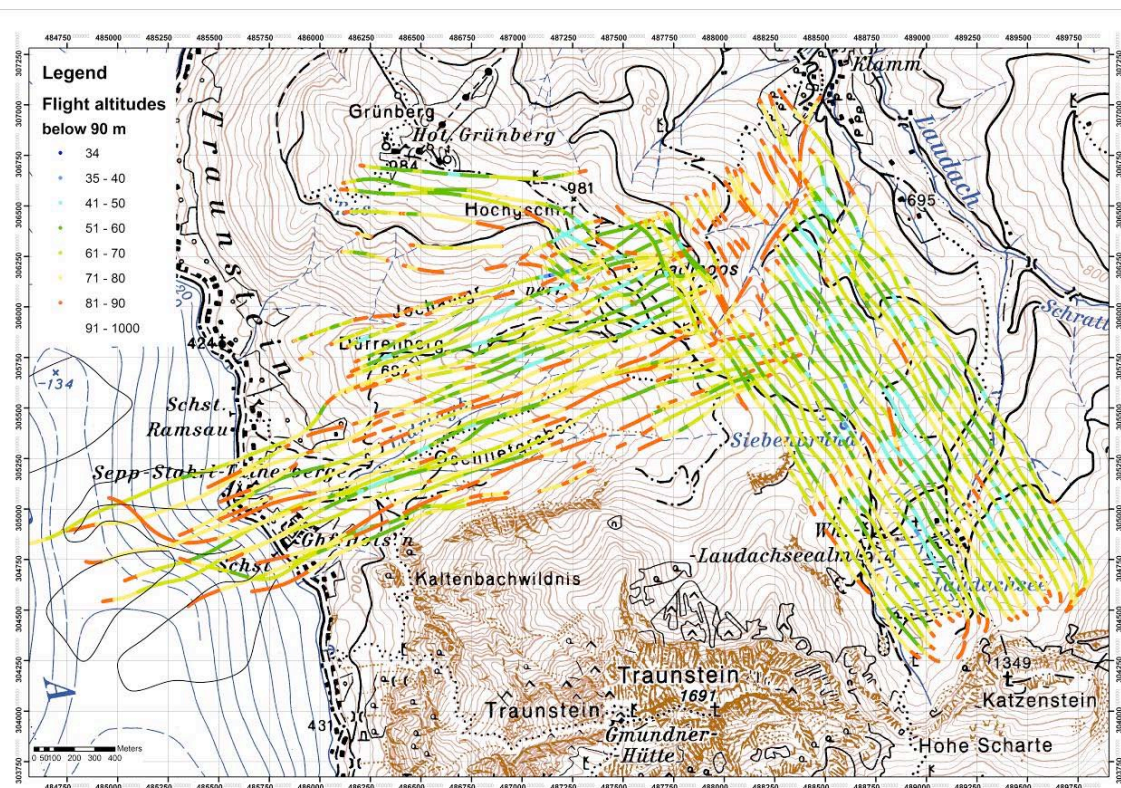


Figure 155. Flight lines of the Gschlifgraben airborne survey; colours indicate the actual sensor height above topography.

After applying the usual processing steps, the data (or the derived model outputs in case of electromagnetics) were analyzed and compared to the landslide inventory map and the geological map. The geological map was compiled after Schoenlaub et al. 1996, Krenmayr 2007 and Moser et al. 2009.

### **Subsurface resistivity**

The subsurface resistivity results show a very distinct pattern differing as well with location and with depth. The central and upper northern parts of the Gschlifgraben valley comprised the areas of the lowest resistivity (Figure 167Figure 156 to Figure 159). Relatively intermediate values of resistivity prevailed in the western part of the study area and the highest values occurred in the southern, northern and eastern parts. The ground resistivity generally decreased with the depth; only isolated high-resistivity areas occurred in mapped deep-seated gravitational deformations, and in the NW, NE and SE parts of the study area at the depths below 30 m. However one has to take into account that the very low surface resistivity limits the penetration depth of the electromagnetic system significantly. Consequently no information about structures below can be derived.

The highest resistivity can be contributed to limestone and dolomite rocks, slope scree (and cemented slope breccia) crushed zones and opened cracks in NCA, weathered sandstone and limestone and their colluvium in RFZ. Rather intermediate resistivity occurred in sandstone and nummulitic calcarenite rocks, clayey and stony colluvium in NCA and the main earthflow accumulation. In contrary, the lowest resistivity is typical for major portion of the UHV, which is rich in clay, and for tectonically jointed areas of the RFZ (Figure 156, Figure 158).

By the 1D multilayer inversion, well confined high resistivity blocks of crushed limestone and dolomite were detected in deep parts on the south. Those blocks well correlate with the mapped deep-seated gravitational deformations of N slopes of Kaltenbachwildniss / Traunstein (Figure 160). A rough correlation between the airborne resistivity and the spatial pattern of shallow and intermediate landslides was observed (Figure 157, Figure 159). The results clearly show that those landslides most frequently occurred in the low resistivity zones within the UHV and RFZ. Thus the method could be applicable for defining broader zones which might be susceptible to mass wasting. However, due to the limited special resolution of the method and the absent resistivity contrast, further results on the detailed structure of single landslide bodies could not be derived. Some correlation was observed between the surface resistivity pattern derived from multi-layer inversion results and gamma-ray data. High resistivity often occurred in the zones of low thorium content, and reversely low resistivity well correlated to high Th content. This is due to fact that both parameters are related to high clay content.

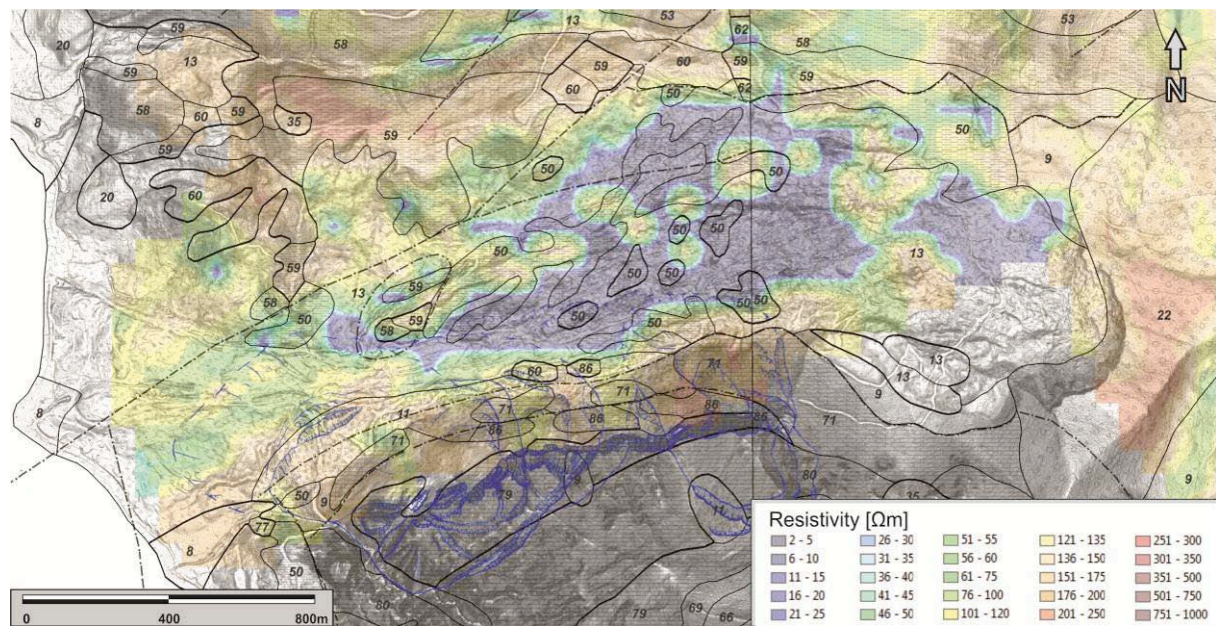


Figure 156. Map of the ground resistivity (depth slice) at depth 5 to 7.5 m below the ground surface compared to geological map. The blue contours define expected extent of the DSGDs at northern slopes of Mt. Traunstein. Explanations of the geological map: Quaternary deposits: 8 - Silt, Sand, Gravel, 9 - Angular fragments of rocks, 11 - Blocks of Rocks, 13 - Diverse Diamictic Colluvium, 20 - Sand, Gravel, 22 - Cemented angular fragments of rocks, 35 - Sand, Gravel; Ultrahelveticum: 50 - Variegated Shale; Rhenodanubian flysch zone: 53 - Quartz- to calcitic sandstone, 57 - Variegated Shale, siltstone, claystone, 58 - Calcarenite, Siltstone, Shale, Marlite, 59 - Variegated Shale, siltstone, claystone, 60 - Sandstone-dominant flysch, 62 - Dark quartzitic sandstone, variegated shale; Northern Calcareous Apls: 71 - Calcarenite, 77 - Grey limestone, 79 - Thick-bedded limestone, 80 - Dolomite, 86 - Sandstone, Anhydrite, Claystone; major tectonic faults in dot-and-dashed line.

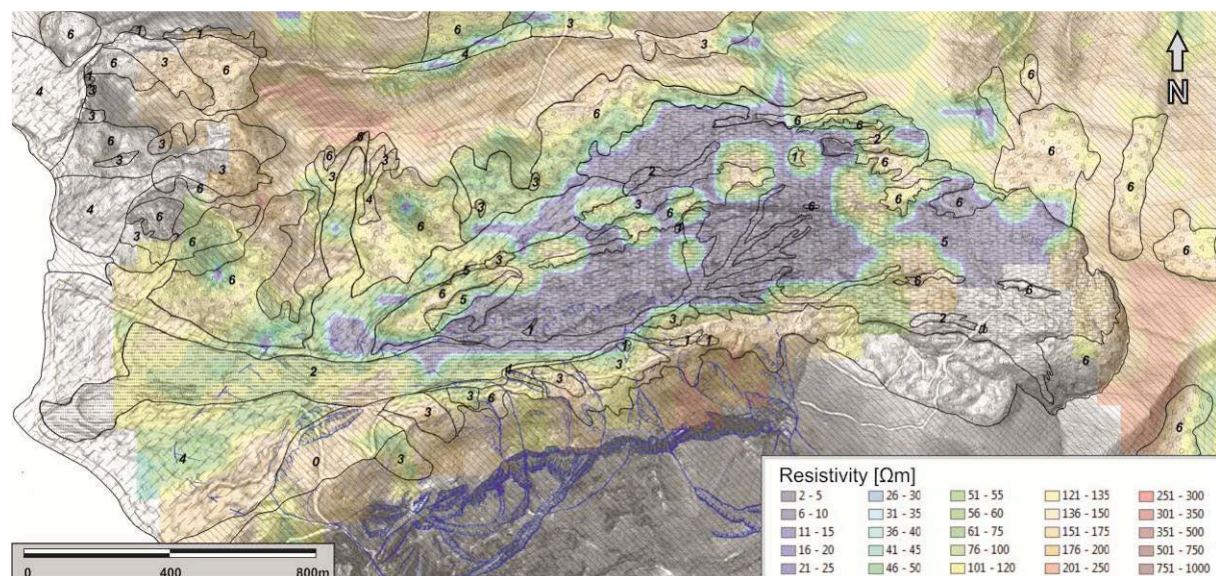
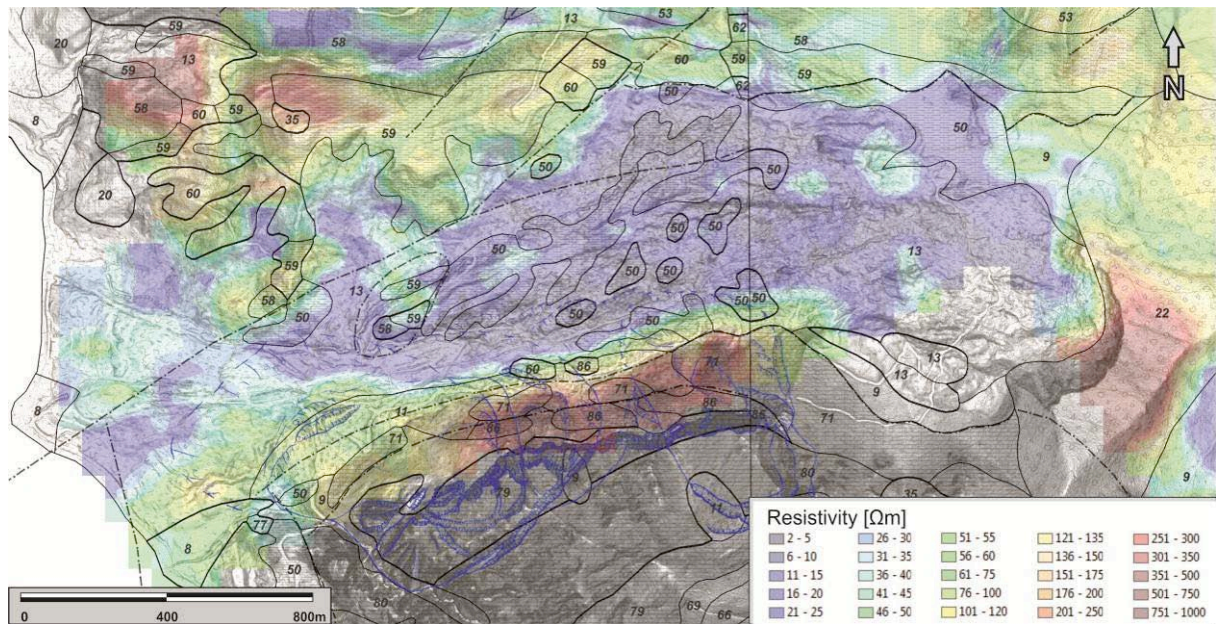
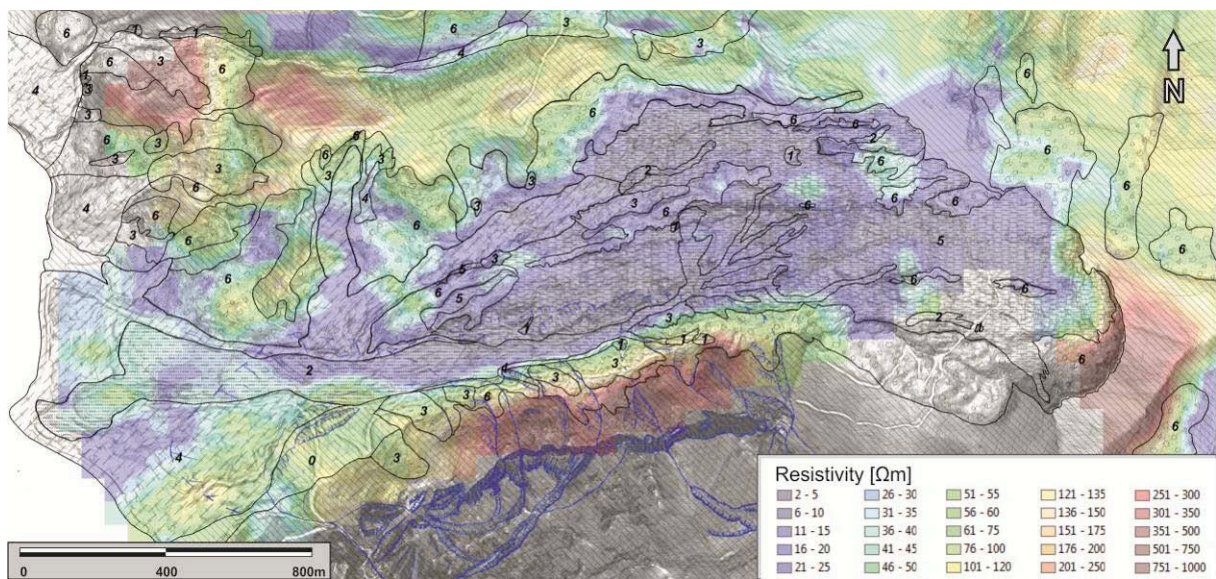


Figure 157. Map of the ground resistivity (depth slice) at depth 5 to 7.5 m below the ground surface compared to the landslide inventory map. The red contours define expected extent of the DSGDs at northern slopes of Mt. Traunstein.



**Figure 158.** Map of the ground resistivity (homogenous halfspace 1+2) at shallow depths compared to geological map. The blue contours define expected extent of the DSGDs at northern slopes of Mt. Traunstein.



**Figure 159.** Map of the ground resistivity (homogenous halfspace 1+2) at shallow depths compared to the landslide inventory map. The red contours define expected extent of the DSGDs at northern slopes of Mt. Traunstein.

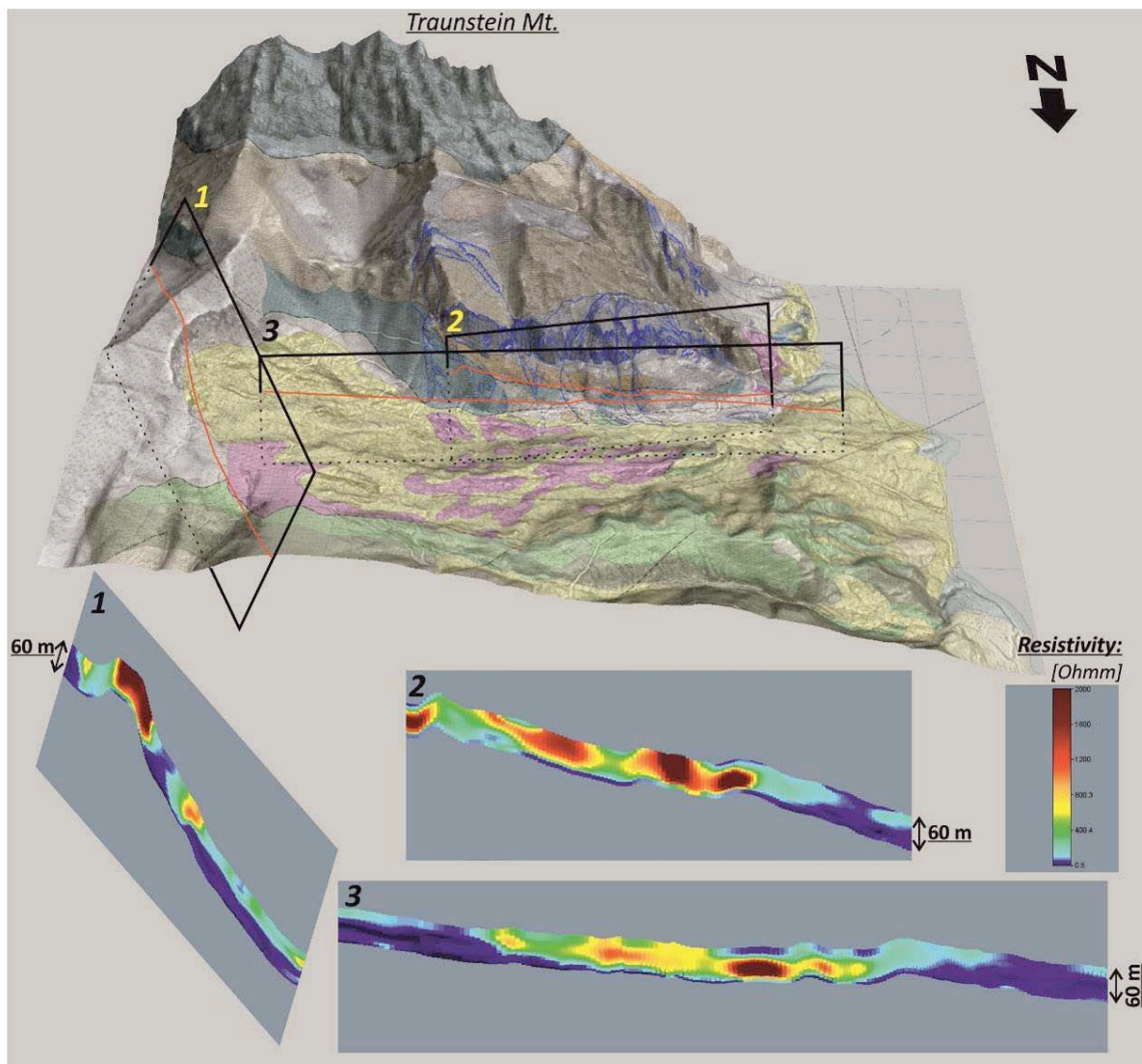


Figure 160. HEM cross-sections obtained from the 1D multilayer inversions; their position is marked on the 3D view of the geological map seen from the N.

### Radiometry

In general the results of the gamma-ray survey clearly show that the content of the radioactive elements Potassium and Thorium is expressively related to the original geological structure. Both elements show very similar pattern. The highest concentration is found in the area of shale, claystone and sandstone of the UHV and RFZ, whereas the lowest contents occur at the limestone, breccia and slope scree along the NCA (Figure 161, Figure 162) in the south of the investigation area.

The occurrence of Potassium showed the most regular spatial pattern (Figure 163, Figure 164). A low content of Potassium was observed in the southern and eastern portion of the study area. Generally rocks and slope scree of the entire NCA and in the zone of a cemented breccia in SE on the surveyed area, as well as large alluvial fans and the lowermost portion of the Gschlifgraben earthflow exhibit low concentrations, whilst the lowest ones were observed along loosened and crushed limestone, opened cracks as well as along the zones of detachment of the DSGD. The intermediate or relatively higher Potassium concentrations

were observed in the major regions in the centre and in the N of the study area. The highest ones were related to colluvial deposits of inactive dormant or old landslides in the RFZ, as well as in the active and dormant landslides/earthflows' deposits in the UHV. The highest Potassium occurrence most probably correlates with high clay content. High Potassium values can be also found in the upper and middle part of the earthflow indicating that most of its material (at least at the surface) originates from that area. As mentioned above, the lower section of the earthflow shows medium to low Potassium values. From this fact we can conclude that limestone material plays a significant role in the composition of the lower part of the earthflow.

In the area north of the recent slide, high contents of **thorium** can be related to slope deposits in the UHV and RFZ, frequently at old landslide deposits. Here only at few locations low values appear, which can be correlated with the claystones and mudstones of the Seisenburg formation and the Rieselsberg Fm. (both of RFZ). In the southern part of the survey area, distinct low concentration of Thorium are observed along detached and crushed limestone and in the zones with opened cracks in the NCA. This pattern of low concentration coincides with the limits of the deep-seated gravitational deformations (Figure 162).

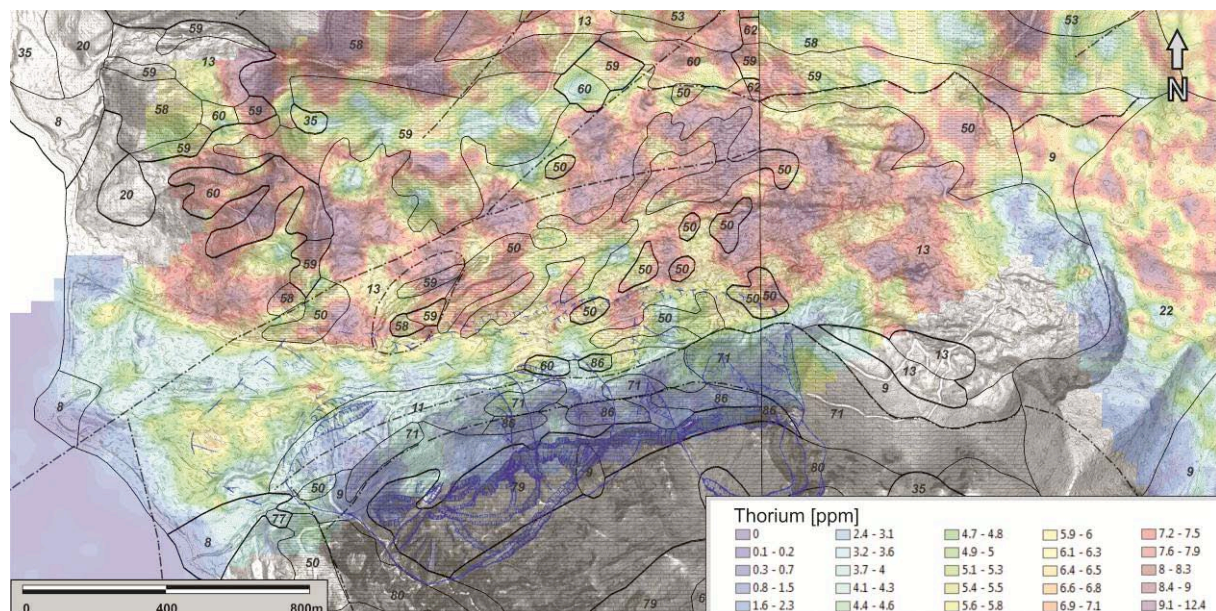


**Figure 161. Map of the Thorium content at the ground surface compared to geological map. The blue contours define expected extent of the DSGDs at northern slopes of Mt. Traunstein.**

The relation between the content of radioactive elements and individual landslide bodies is, however, quite a difficult task due to the relatively low spatial resolution of the survey and very complex mass wasting processes at the Gschlifgraben site. However some interesting general conclusion can be derived on landslide dynamics. Focusing on the area mostly involved by the recent events, a clear separation into areas with different characteristics or radioactivity can be recognised. Just west of the main scarp of the landslide complex, which is clearly detectable from the laser scan, quite low values show, that probably due to mass wasting processes, the underlying limestones or limestone and dolomite scree are uncovered, which is indicated by a very low natural radiation. Further to the west, in the most eastern (highest) part of the recent landslide, the results show high contents of Potassium as well as

Thorium, indicating that the surface material is dominated by clay and marl components of the UHK unit. In the middle part of the recent sliding area, an alteration of high and low values (mostly expressed in the Th pattern) can be determined from east to west. This pattern is most probable due to different, alternating inputs of material from the UHV unit (high values) and rockfall material (limestones, low values) from the NCA.

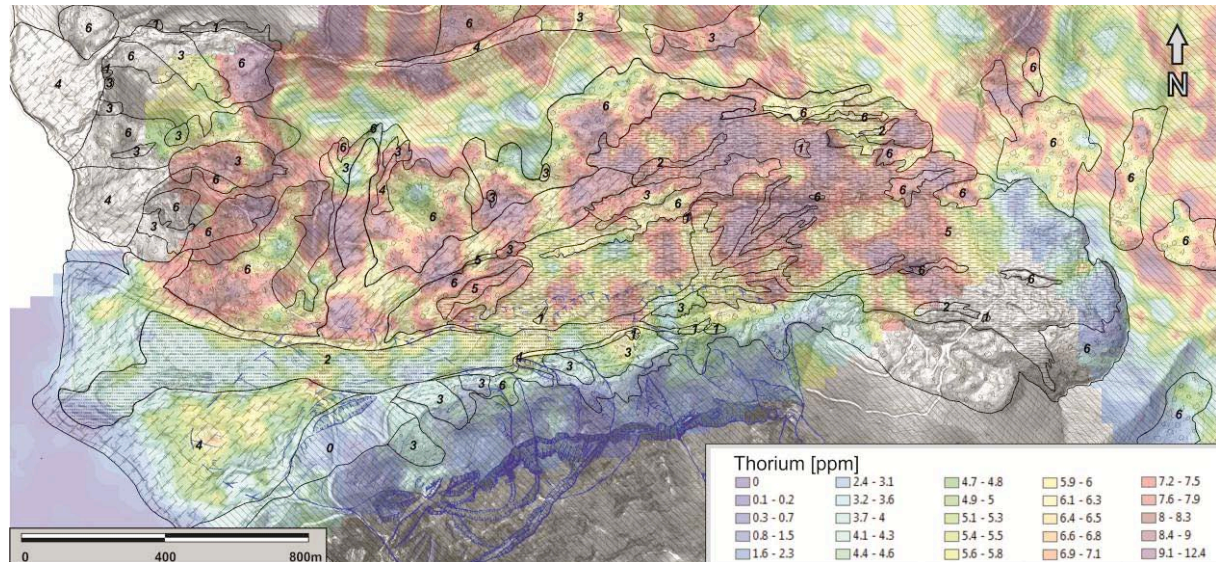


**Figure 162. Map of the Thorium content at the ground surface compared to landslide inventory map. The blue contours define expected extent of the DSGDs at northern slopes of Mt. Traunstein.**

In the most western part, the area influenced by recent sliding is sharply delineated to adjacent historical landslide material in the north by a sharp contrast from low to high values. Field inspection proved the occurrence of coarser sediments with higher limestone content thus causing lower count rates. However in this region the top layer of the original landslide material was removed during the phase of remediation. An isolated anomaly with higher values in the south-western area can be correlated with historic landslide bodies.

The distribution of **uranium** does not display a distinct pattern and seems rather randomly distributed. This is most probably due to the fact that distinct Uranium sources are missing in the investigation area. Therefore a further interpretation cannot be provided.

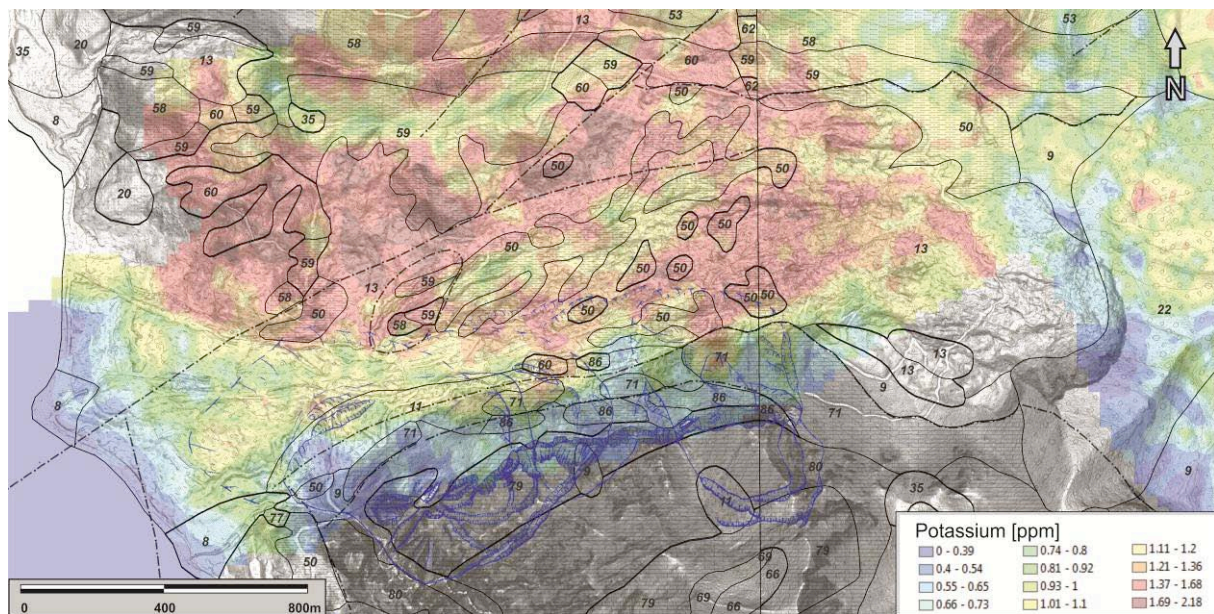


Figure 163. Map of the Potassium content at the ground surface compared to geological map. The blue contours define expected extent of the DSGDs at northern slopes of Mt. Traunstein.

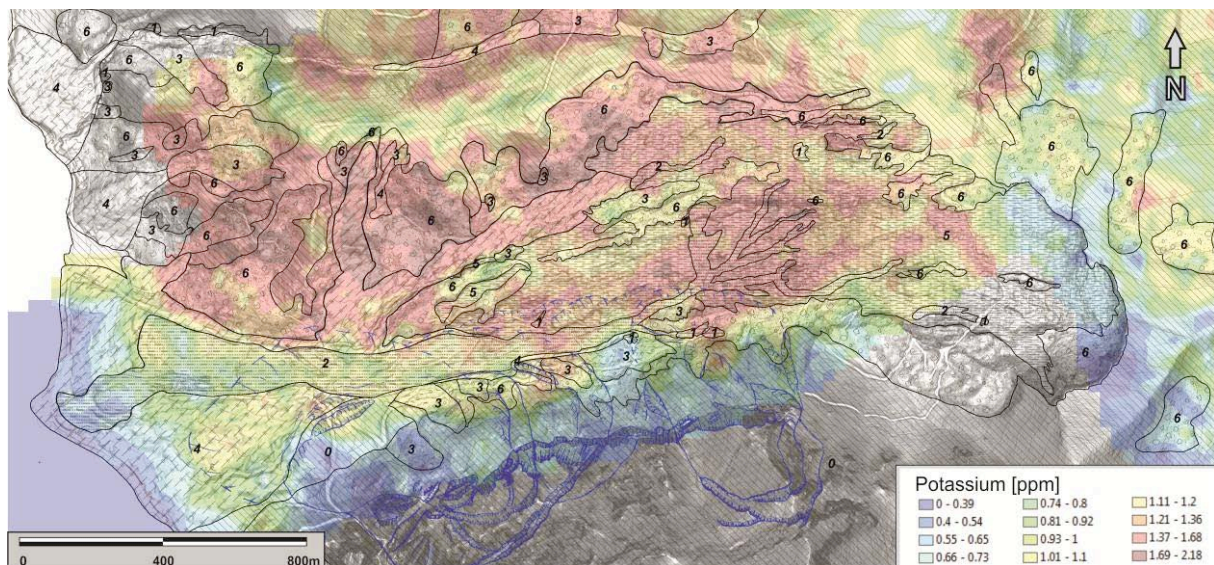


Figure 164. Map of the Potassium content at the ground surface compared to the landslide inventory map. The blue contours define expected extent of the DSGDs at northern slopes of Mt. Traunstein.

### Passive microwave

The passive microwave survey (Figure 165, Figure 166) provides information on the superficial soil moisture. The highest soil water content was mapped within the zone of the recent earthflow, especially along the foot of the NCA in the central part of the valley. It could indicate intensive infiltration of karst-water from the NCA. The soil moisture surveying seems to be a promising indicator of active mass movements.

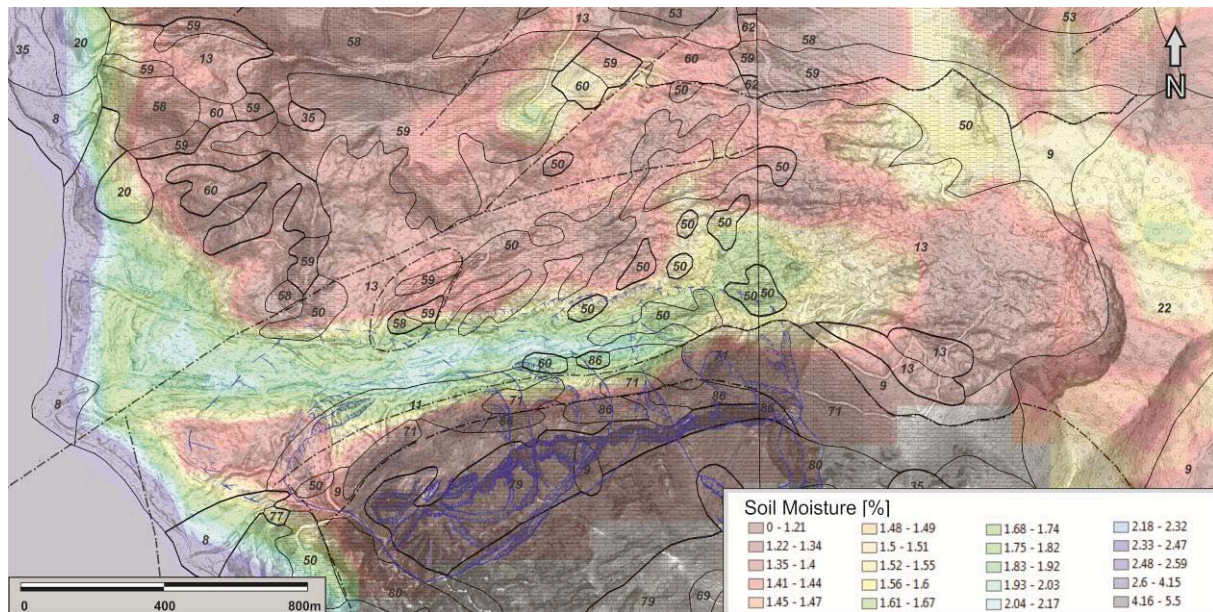


Figure 165. Map of the soil moisture near the ground surface, which was obtained from the passive-microwave survey, compared to the geological map.

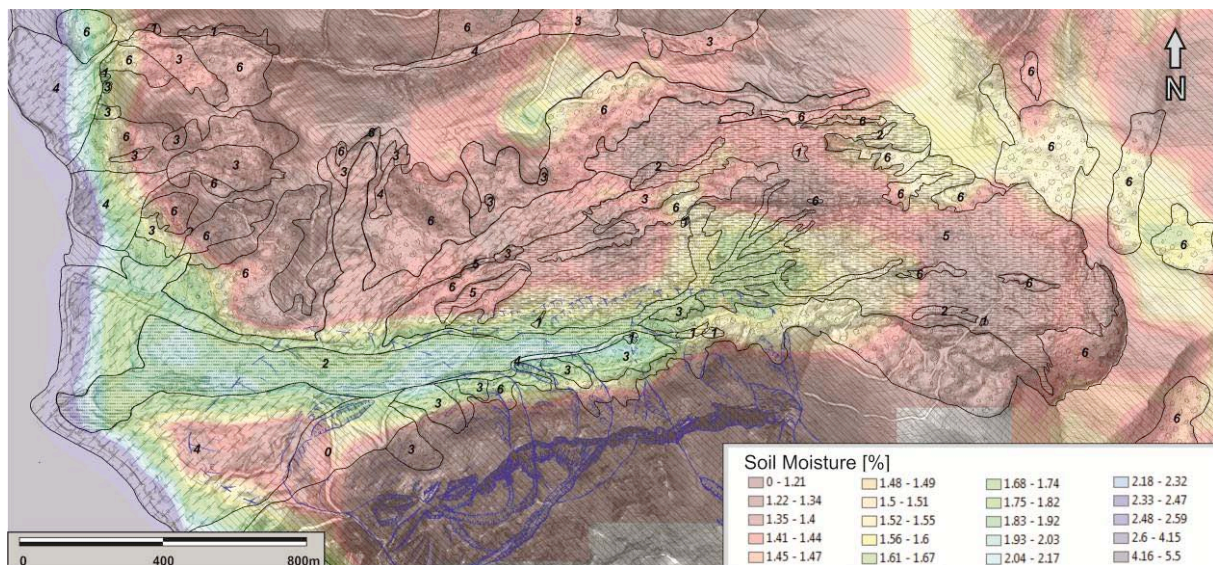


Figure 166. Map of the soil moisture near the ground surface, which was obtained from the passive-microwave survey, compared to the landslide-inventory map.

### 6.2.6.3 Improvements with respect to previous applications

The comprehensive case study at the Gschliefgraben site proved that a complex airborne geophysical survey is a reliable innovative method for landslide investigation. This methodology could quickly determine low resistivity areas, which actually mark areas most susceptible to mass wasting. High soil moisture content surveyed by passive microwave seems to be a promising indicator of active mass movements. Additionally the content of radioactive elements was expressively related to the original geological structure and this information could, e.g., contribute to studying displacement, source areas of earthflows or

studying the weathering degree at the local scale. One of the big advantages of this approach is the ability to survey large areas within relatively short time to derive a model of the subsurface structure. Furthermore it is the only remote sensing methodology which can provide information about the internal structure of the subsurface down to 30-70 m (electromagnetic mapping).

#### ***6.2.6.4 Acknowledgements***

The authors would like to acknowledge the excellent close cooperation with the Austrian Service for Torrent and Avalanche Control (WLV), Section Upper Austria – especially to Wolfgang Gasperl and Harald Gruber – and to Centro Servizi di Geingegneria, Ricaldone (Italy), and ZT Büro Moser/Jaritz, Gmunden (Austria).

## 6.2.7 Airborne time domain EM mapping (monitoring): Aurland fjord rock slide (Norway)

ICG: Pfaffhuber A.

### 6.2.7.1 Study area

The inner Aurland fjord with the adjacent Flåm valley (Western Norway) is one of Norway's most famous tourist destinations with up to 450,000 visitors and more than 100 cruise ships a year visiting the area.

The main road between Oslo and Bergen (E16) passes through Flåm, bypasses the fjord and enters the 24.5 km long Lærdalstunnelen in Aurlandsvangen. Evidence of large rockslides in the geological past has been documented in the area with ground movements evident to the present day. The area is subject to potential rockslides composed of creeping rock and debris masses extending over roughly 5 km<sup>2</sup> and 20 km<sup>2</sup>, respectively (Figure 167). A rock slide would likely trigger a tsunami in the fjord devastating for the area. The intent of our study was to provide geophysical input to the ongoing natural hazard assessment program in Aurland municipality covering an overall area of about 100 km<sup>2</sup>.

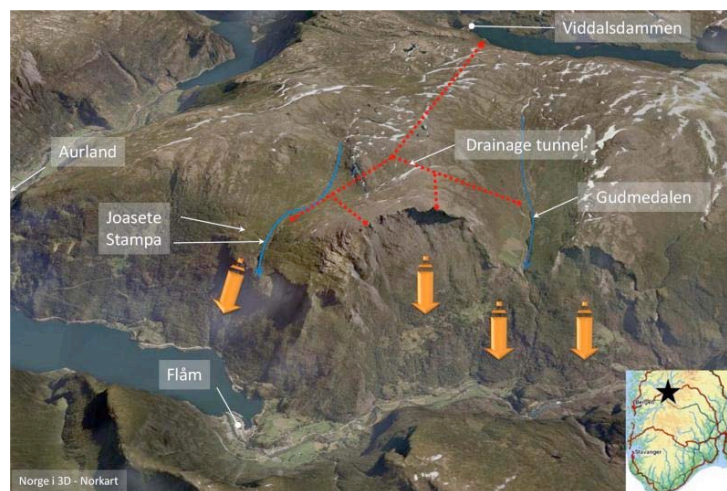


**Figure 167. Study area (aerial photography draped over topographic model courtesy of [www.norgei3d.no](http://www.norgei3d.no)) indicating areas with known previous rockslides and creeping movements (orange arrows) of both massive rock (fjord) and loose debris (valley) partly driven by pore water delivered by the Stampa and Gudmedalen catchments. Red lines indicate the potential water drainage tunnel system.**

Based on repeated GPS measurements and anecdotal observations in the area, rock and debris movements are likely influenced by precipitation and snow melt. Based on this empirical evidence the local municipality and regional hydroelectric company E-CO Vannkraft are evaluating the potential of draining the unstable area to a nearby hydropower reservoir (Viddalsmagasinet) with the aid of a 10 km long drainage tunnel. Here preliminary interpretations of an airborne electromagnetic (AEM) mapping survey conducted in June 2009 reveal indications of the sliding planes and assess the tunnel corridor for potential tunneling hazard areas.

From a geological standpoint, the investigated area consists of a basement of high grade Precambrian metamorphic gneisses overlain by a nappe (sheet) of phyllite with another layer of high grade metamorphic gneisses with minor layers of quartzite and other rock types

resting on the phyllite layer. During the formation of the nappe the weaker phyllite acted as lubrication in the thrust zone between the basement of Precambrian gneisses and the overlying gneisses. The thrust zone recrystallized to a schistose layer during post-movement low grade metamorphism.

Unstable rock in the study area (about 1,000 meters above sea level) has been mapped as massive phyllite broken by numerous tension cracks with openings up to several meters. Field observations also document significant amounts of surface water in streams on the mountain plateau around Joasete (Figure 167) that disappears into some of these cracks and reappear on the surface several hundred meters down the slope.

Potentially sliding planes provide pathways for the water with changes in water pressure potentially causing instability. Since the phyllite can be crushed to fine grained clay under certain conditions the water saturated sliding planes should be an ideal target for AEM since they are very conductive (1-10  $\Omega\text{m}$ ) compared to the more resistive, undisturbed phyllite or nearby gneiss ( $> 1.000 \Omega\text{m}$ ). Earlier ground resistivity measurements in the area, strengthened this hypothesis. Note that these geological conditions are in strong contrast to other Norwegian rock slides, like Åknes, which is within gneiss where resistivities of several 1,000 to 10,000  $\Omega\text{m}$  are possible even in the water saturated zones (Heincke et al. 2010).

#### ***6.2.7.2 Description of the analysis***

The AEM survey was carried out with SkyTEM, a helicopter borne, time domain EM system (Sørensen and Auken, 2004). A total of ~250 line km were flown at 125 m line spacing with some infill lines spaced 60 m in the central part of the survey area. To improve lateral resolution in this area of large topographic relief, flight speed was a nominal 7 m/s at 30 m above ground (sensor height). The system was operating with dual transmitter moments 63  $\text{kAm}^2$  and 2.5  $\text{kAm}^2$  at 100 Hz and 200 Hz base frequency, leading to off-time windows from 8.4  $\mu\text{s}$  to 2.5 ms. Standard processing and spatially constrained inversion, SCI (Viezzoli et al. 2008) were applied to the data resulting in resistivity maps and profiles. Only the vertical magnetic field component (Hz) was considered for inversion. Since SkyTEM also acquires the horizontal field component (Hx), future analysis and interpretations could include 3D data components.

#### **Results**

From our preliminary AEM data interpretation we find widespread areas with high conductivity, which are most likely caused by either water saturated, fine grained sliding planes or fault zones at the phyllite / gneiss interface (Figure 168).

Based on our initial survey concept, we expected limited signals from phyllite that had been reworked to clay but no significant response from the undisturbed phyllite and gneiss environments. Much to our surprise, we found strong and consistent signals covering nearly the entire survey area (Figure 168). In the following we highlight some examples; however, we are only beginning to understand the sub-tiles of the processed data:

- **Lines over the fjord**

Some flight lines were extended over the fjord water to test the bathymetry sounding capability of the TEM system. Since the fjord is filled with old debris, the water column was expected to be shallow enough ( $< 50 \text{ m}$ ) for complete signal penetration. The high sea water

conductivity is evident in the shallow (40-50m) resistivity map (Figure 168, left), while the deep (100-110m) depth slice probes the seafloor (Figure 168, right). The conductivity depth section from multilayer, smooth inversion (Figure 169) shows the limited thickness of the conductor (sea water). Further, 4-layer inversion (not shown) indicates water at depths between 40 m and 60 m, in remarkably good agreement with bathymetric charts indicating depth ranges from 43 to 59 m in the area.

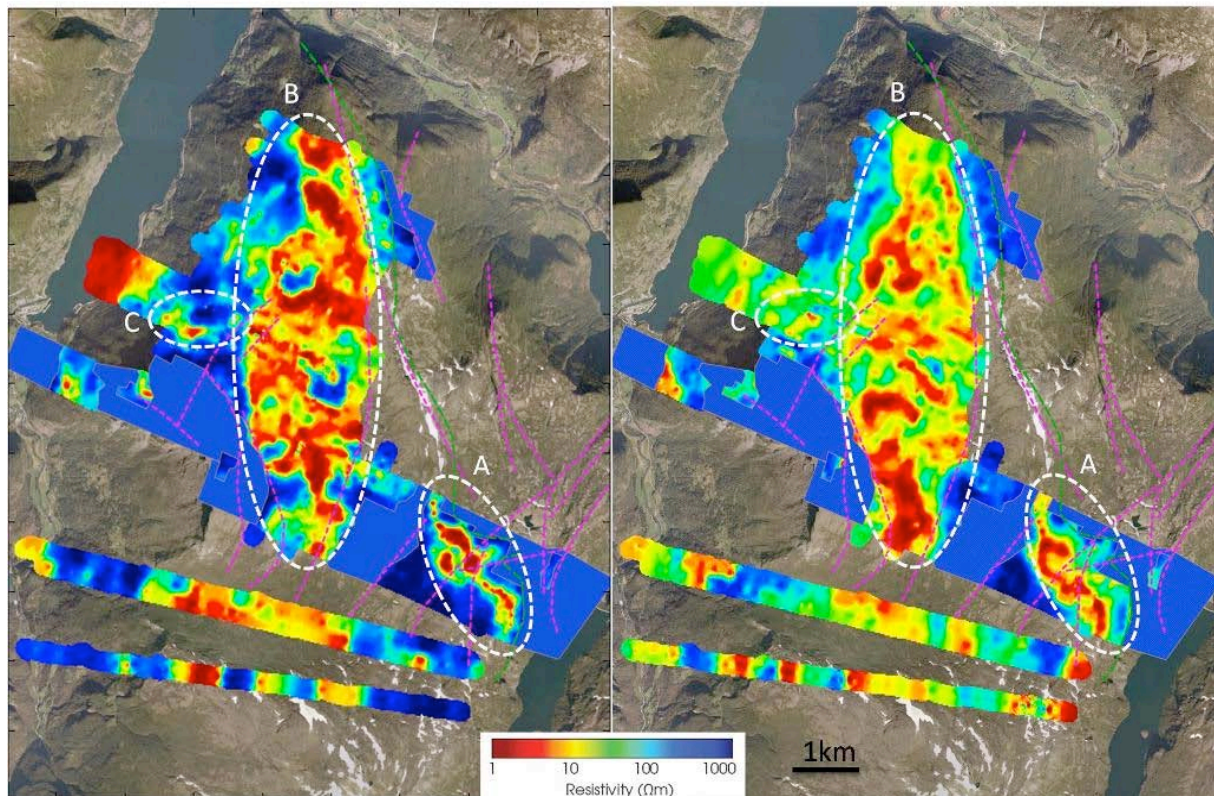


**Figure 168:** Spatially constrained inversion (SCI) result: interval resistivity averaged from 40 m to 50 m (left panel) and 100 m to 110 m (right panel) below ground (depth slice) mapped over survey area. Purple and green lines roughly outline mapped weakness zones and phyllite/gneiss interface, respectively. Bright blue areas are areas where minimal AEM signal was recorded due to highly resistive ground.

- Lineament in the SE

A meandering distinct conductor close to Viddalsdammen roughly coincides with the phyllite / gneiss boundary known from surface mapping (Figure 168, Area A). Following the feature through different depth slices indicates a fairly flat dip towards SW (Figure 170).

- Central dominant conductor

Consistent from line to line, covering a large area (some 10 x 2 km) 10 to 80 m below the surface is a massive conductor that expands to a thickness of up to 100 m (Figure 168, Area B and Figure 169). Given the inductive nature of the AEM measurements, the depth to the base of the conductor can only be roughly estimated. The data indicate clearly, however, that a resistor underlays that structure. Generally this conductor dips conform to the topography. The lateral extent of this feature frequently co-aligns with topographic or geological features (Figure 168).

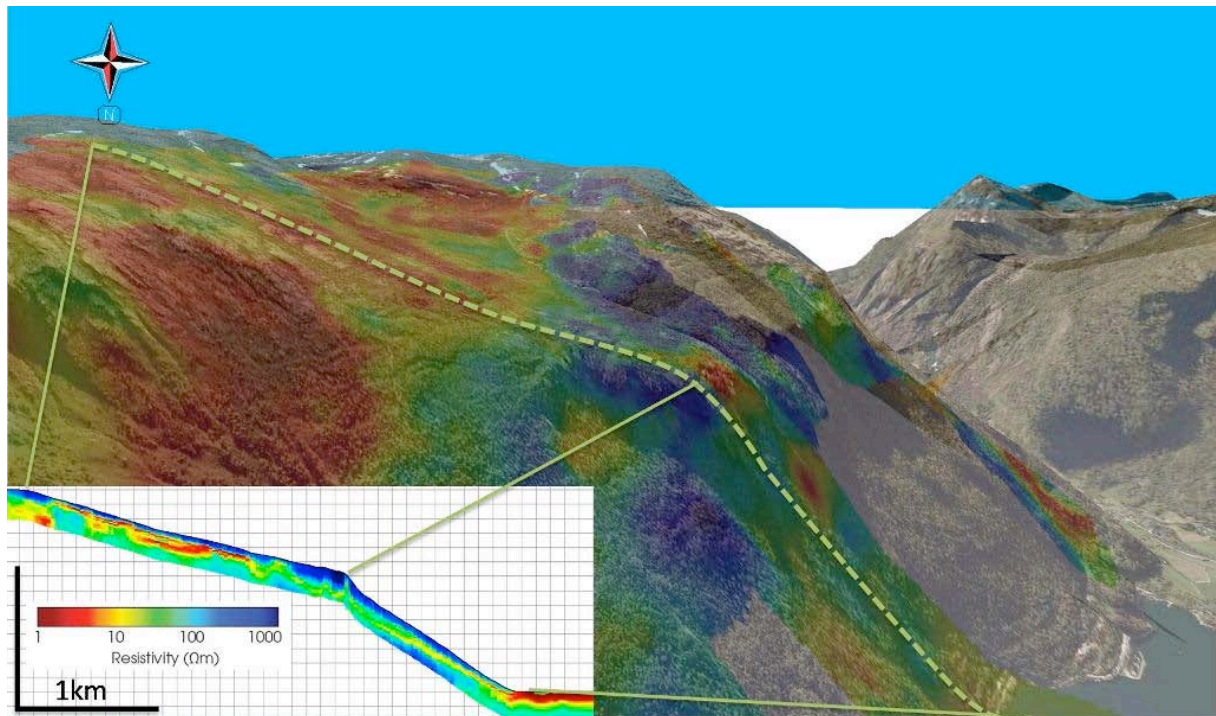


**Figure 169: 3D visualization of area C around Joasete (Figure 2) looking south. A slightly transparent aerial photo is draped over topography with no vertical exaggeration. The 70-80 m resistivity depth slice draped 75 m below the topography shines through the aerial photo. An exemplary conductivity depth section derived from SCI results represents a cross section at the profile indicated with a green, stippled line.**

- **Anomalies along the slopes**

The subsurface around Joasete but also along the slopes down to Aurlandsfjorden and Flåmsdalen features widespread conductive anomalies (Figure 169). The debris covered slopes usually feature consistent, thin conductors while the anomalies at Joaste and Stampa (Figure 168, Area C) are more complex, most likely caused by sub vertical 3D structures.

#### **6.2.7.1 Conclusions**

Even though we have gained significantly more information about the area's geology from the AEM survey, care has to be taken when interpreting the measurements. Even though SkyTEM is a versatile system for rough topography (slow flight speed, acquisition of system altitude and attitude with lasers and inclinometers), the SCI algorithm has been designed for efficient mapping of layered structures with limited topography both on the surface and the geology. Here we are faced with a high relief (up to 80%) and evidence for strong 2D and 3D contrasts that exceed the assumptions and approximations, which apply to SCI processing. Hence, detailed follow up of 3D artefacts in the results involving the acquired Hx component is crucial before final decisions are made.

Based on the geophysical data and knowledge from geological pre-investigations we can draw the following preliminary conclusions:

The known, outcropping phyllite / gneiss interface close to Viddalsdammen (Area A, Figure 168 and Figure 170) appears as a strong conductor dipping SW, consistent with outcrop data. This is an indication of the presence of crushed phyllite potentially with graphite infill thereby

representing a formerly unknown potential tunneling hazard. This anomaly has been followed up by ground ERT measurements and been confirmed by detailed geological mapping.

A similar feature appears over large areas on the west flank of the mountain plateau (Figure 168 Area B and Figure 169), which may indicate a thin, 50 to 150 m thick layer of phyllite overlaying gneiss.

More complicated anomalies appear around Joasete (Figure 168, Area C) potentially indicative of the anticipated sliding plane response. Further down the slope a consistent, conductive layer most likely indicative of the base of a debris field filed with fines and thus the sliding plane for the creeping debris along the fjord and valley. A follow up ERT survey in area C found a dipping conductor outcropping in a river bed, supporting the assumption of water fed clay rich sliding planes.

No final conclusions can be drawn from geophysical data alone, however. At this point, only limited drilling is necessary to transform the geophysical maps to a firm geological model.

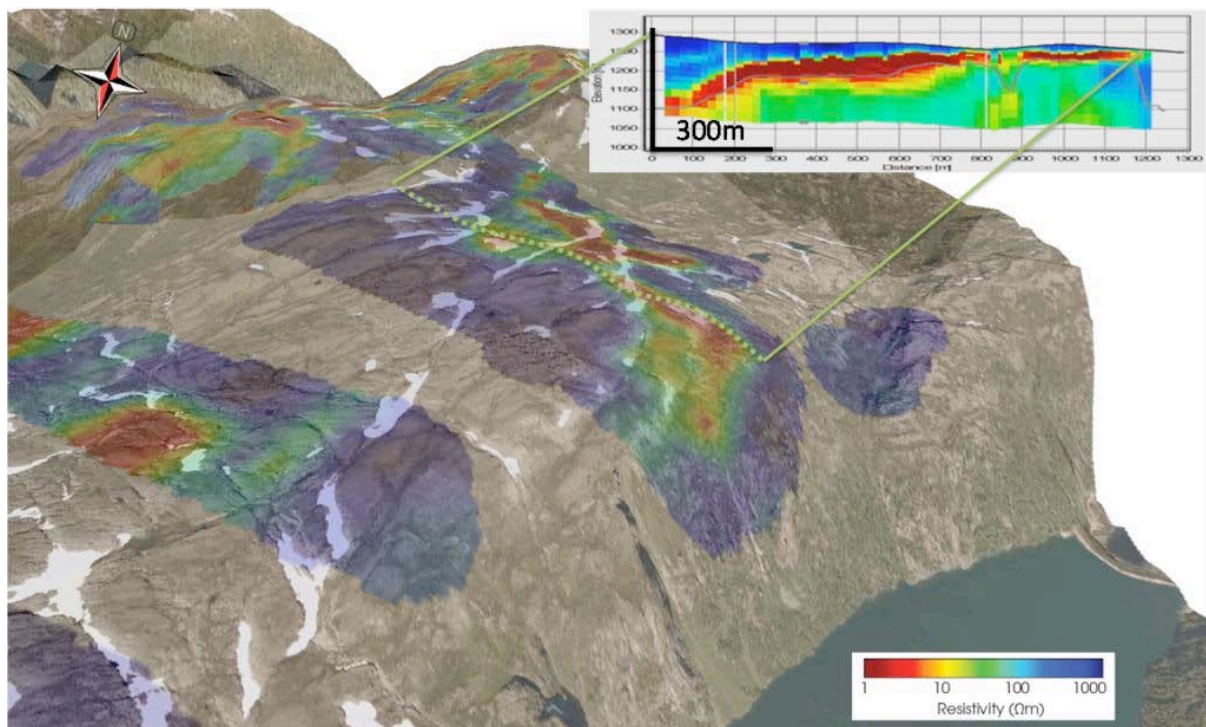


**Figure 170: Area A adjacent to Viddalsdammen (Figure 3) looking NNW. The 30-40 m resistivity depth slice is draped 35 m below the topography. For a more detailed description refer to Figure 169.**

#### ***6.2.7.2 Improvements with respect to previous applications***

The latest generation of helicopter borne time domain airborne EM systems combines the high penetration depth of strong, time domain systems with the high resolution and versatility of a helicopter system. Thus this conductivity mapping technology opens new opportunities for geohazard assessment as large areas can be investigated at comparably low cost. In the past airborne EM has largely been used for mineral exploration and also in a rather qualitative fashion. New accurate and well calibrated systems, developed for high resolution groundwater mapping have brought significant improvements also to the possible use of this technology. An alternative tool to investigate water saturated weakness zones, Electrical

Resistivity Tomography, can provide somewhat better resolution but demands very elaborate ground field work. ERT is however an excellent tool to follow up AEM anomalies in higher detail and also full 3D resolution.

## 6.2.8 Airborne geophysics (monitoring): Sibratsgfäll

*GSA: Supper R., Jaritz W., Winkler E.*

### 6.2.8.1 Study area

The settlement area of the community Sibratsgfäll is characterised by two large-scale mass movements: the Sibratsgfäll Dorf landslide and the Rindberg landslide.

**The Sibratsgfäll Dorf landslide** affects the main settlement area of the community Sibratsgfäll with approximately 70 residential houses over an area of around 2.5 km<sup>2</sup>.

The areas affected by the landslides are built up from thick, complex compositions of unconsolidated rocks, mostly from the late glacial period. In terms of their process, the slope movements can be classified as continuous slides in accordance with AGNA (2004), with rates of about 1 – 2 cm/year and 5 – 7 cm /year. In terms of the proposed criteria by the Federal Office for the Environment (Leutwiler, 2009), this is a mildly active, slow slope movement.

The movement is predominately related to the fine-grained waterlain till along a few of the shear planes, some of which lie at considerable depths. The moving horizons were discovered at depths of 10 – 12 m, around 15 m and at 35 m. According to Leutwiler (2009), these slides represent medium-depth (0 – 10 m) up to very deep (> 30 m) slope movements.

Besides the recorded movements along discrete shear planes which proceed at varying rates in different parts of the village, secondary slope movement processes are present in the affected area. These contribute to the slope abrasion in the form of creep and flow. The results are faster movements of the flow type. This type of slope movement is superimposed on the existing morphology which is characterized by terraces and steps.

Within the survey area, two development stages can be distinguished within the six mapped flows close to the Subersach River, at the bottom of the slope:

1. Already fast moving systems (flowing, rates of about 0.5 – 1 m/a) with clear boundaries at the sides (shear tracks) but mostly unclear or even anthropogenically superimposed scarps.
2. Slope sections which can be seen as pre-stages of fast movements, where shell-shaped scarps superimpose the stepped terrain morphology. Examples can be found to the south-east of Mähmoos as well as in the forest region below the district of Wieseln.

**The Rindberg landslide** lies to the east of the main settlement area of Sibratsgfäll in the district Rindberg. The Feuerstätte nappe in this area is particularly susceptible to soil movements due to their high percentages of changeable hard rock (Junghansen layers and Schelpen series).

Such geological settings provided the initial susceptibility for the frequent large-scale events within this section of the valley. Using radiocarbon dating (<sup>14</sup>C-Method) on tree trunks exposed in the course of the mass movements, it was possible to distinguish four geological events.

The Rindberg landslide was reactivated in May 1999 and affected an area of approx. 1.4 km<sup>2</sup> with movement rates of 1 m/day and in some places up to 5 m/day.

In the course of the accelerated movements during the first half of the year 1999, a rapid decrease in mass in the upper slope area arose (failure), while the middle and lower slope

initially reacted with a gradual mass increase. The additional mass and the subsequent bulging of the bottom of the slope were confirmed by land surveys. The bulging and thus over-steep slope base balanced out the uneven mass distribution through secondary slope movements such as debris flows. These compensation movements set in at a delay of several weeks after the main movement.

In terms of its process, AGNA (2004) describes the slope movement of Rindberg as a reactivated and currently blocked movement of highly complex composition. Some parts of the complex composition are active. The mechanics of the movement can be described as deep creep on the upper slopes and flows on the lower slopes.

Along the upper slope, the rate of movement is around 1 – 2 cm/a, hence it is classified as a sub-stable, very slow movement according to the Federal Office for the Environment (FOEN). The movement rate for the biggest active debris flow “Bader” on the lower slope is currently (latest measurements 2010) 2 – 3 cm /a. These movements are classified as mildly active, slow slope movement.

The movements in 1999 took place in the unconsolidated sediments (mostly old slide masses and slope sediment redistributions) as well as in variable hard rock of the Junghansen layers and the Schelpen series. Accordingly, the shear planes were sometimes found in the unconsolidated rock and sometimes along the boundary unconsolidated/hard rock. The movement horizons in the debris flow deposits were found at depths of 5 – 10 m and at around 47 m depth (boundary between hard/unconsolidated rocks). According to Leutwiler (2010), these slides represent medium-depth (0 – 10 m) up to very deep (> 30 m) slope movements.

Like in the district of Sibratsgfall Dorf, secondary processes are also found in the area of the Rindberg slope movement. These contribute to the slope abrasion in the form of creep and flow processes. The results were and currently are faster flow movements.

Within the survey area, three different debris flow systems on the lower slopes can be distinguished in two different stages of development:

1. A fast proceeding, active system (flowing; rates of around 2 – 3 cm/a = *Bader flow*) with clear boundaries at the sides (shear tracks) but mostly unclear or even anthropogenically superimposed scarps.
2. Two dormant systems in the middle (*Heidegger flow*) and western section of the slope movement area (*Ferienhäuser flow*).

### **6.2.8.2 Geological overview**

The survey area lies in the outer northern region of the Eastern Alps, which extends as a narrow strip of land on the northern edge of the Limestone Alps and is composed of four tectonic units in the wider survey region. Going from the underlying stratum to the top, the rock series are Helvetic Zone, Liebenstein Nappe, Feuerstätte Zone and the Rhenodanubian Flysch. An overview of the geological setting can be seen in Figure 171 and Figure 172.

The general strike direction of these series and the overall tectonic elements (nappe boundaries, thrust faults, etc.) is approximately SW-NE, the general dip, except for the small tectonic structures, is of medium steepness and oriented SE.

---

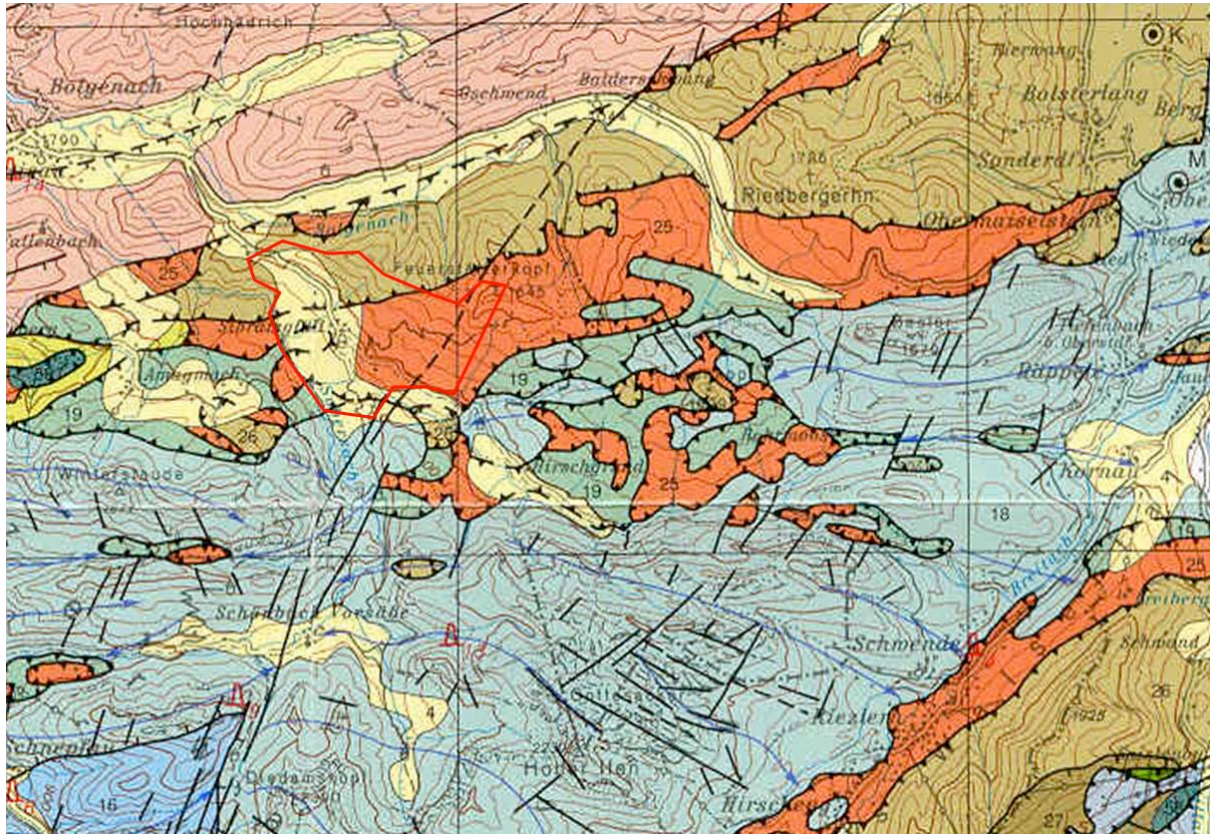


Figure 171: Section of the geologic-tectonic map of Vorarlberg 1:200.000 (OBERHAUSER & RATAY 1998: blue: Helvetic; orange: Feuerstätte nappe; olive: Rhenodanubian Flysch; green: Liebenstein nappe; pink: Molasse; yellow: Quaternary); red line: survey area.

### Liebenstein Nappe (Aptian – Mid Eocene)

The rocks of the Liebenstein nappe are coast-distant sedimentary formations. Following the Liebenstein chalk, the Leimern layers form the bulk of the Liebenstein nappe. The Leimern layers are generally described as light colored, slightly yellow weathered marl and calcareous marl.

### RHENODANUBIAN FLYSCH

Like the Flysch sediments of the Feuerstätte nappe, this sedimentary region is characterised by pelagic sedimentation of suspension currents with the following lithological contents:

**Reiselberger Sandstone**  $f_R$  (Cenoman – Turon): These sediments consist of mica sandstones and fine conglomerates with high feldspar concentrations. Pelitic layers recede.

**Piesenkopf layers**  $f_P$  (Turon - Santon): In the Piesenkopf layers, the sedimentation is again characterised by pelitic material. The layer thickness varies in the range of 100 m. The sequence is characterised by thin-layered alterations between chalks, argillaceous limestone and silty clay with marl and argillaceous marl.

**Zementmergelseries**  $f_Z$  (Santon – Campan): There is a gradual transition from the Piesenkopf layers to the Zementmergel. The boundary between the two layers is defined at a marl layer thickness of  $> 0.3$  m (REICHELDT; 1960).

**Hällritzer series**  $f_H$  (Campan – lower Maastricht): Beginning with the Hällritzer Series, the sequences show an increase in grain-size, the argillaceous limestones recede.

### **Feuerstätter nappe**

The facies of the Feuerstätte Zone were originally situated south of the sedimentary region of the Liebenstein Zone (FESSLER et. al; 1992, OBERHAUSER; 1980, 1984, 1998). It is an extremely heterogeneous rock series, which is tectonically disrupted, imbricated and sheeted, and occurs at the basis of the Rhenodanubian Flysch.

**Junghansen layers:** This comprises a strongly tectonic, imbricated and sheared alternating sequence of black pelites and slate with changing sand content, dark marl, different psammites, as well as conglomerates and breccia.

**Schelpen series:** The Schelpen series is composed of gray/brown argillaceous marl and light brown/ochre weathered sandstones and sandy chalk. The series shows lithological similarities to the rocks of the Junghansen layers.

**Feuerstätter sandstone:** These are dense, glauconite-containing sandstones with sharp fractures. Occasionally, coarse insets with grain sizes up to 4 cm can be found.

**Aptychen layers:** These are mostly light gray, thin-layered Mikrites, whose colour spectra vary gradually from green to red. They occur in alternating sediment layers with dark to light gray marl, sometimes reddish to greenish clays and argillaceous marl. In the reddish chalk banks, Hornstein concretions are frequently embedded which can form up to 15 cm thick, red, green or black horizons.

### **Quaternary**

Glacigenic sediments form the biggest part of the quaternary sediments. Due to the glaciation of the northern edge of the Alps, the Flysch nappes were eroded and thick glacigenic sediment covers were formed in the valleys and on the mountain sides.

Furthermore, the considerable scree nappes take on an important role due to the loosening of the easily weathered Flysch. The post-glacial, fluvial sediments of streams and rivers in the valley basin only play a minor part. Post-glacial redistribution of unconsolidated sediments through former mass movements needs to be treated separately. During this process, considerable mud deposits in slope synclines can occur. Due to fractionation of grain sizes, these deposits have unique characteristics compared to mixed grain scree formations.

**Waterlain till sediments:** In general, waterlain-till sediments (i.e. deposits which are directly related to glacial lakes) comprise the bulk of the valley in-fill of the Sibratsgfall Basin. A characteristic feature of waterlain-till is their large matrix (clay-silt-fine sand-fraction). The matrix percentage varies between 60 vol. % and 100 vol. %.

**Glacier margin sediments:** Glacier margin sediments arose whenever the ice in the main valley dammed up the tributary valleys, retaining the melt water and streams (→terraces), or forced them to flow besides the glacier (→kames). The material is composed of horizontally and vertically rapidly changing layers, made up of different sand-gravel mixtures. The composition of the sediment body (mostly coarse clastic sediments), as well as the alternating layers and the orientation of the bedding planes, confirm a fluvial sedimentation setting.

**Ground moraine:** Evidence for sediments of the glacier floor – ground moraine deposits – could only be found in the upper and middle slope areas above approx. 950 m above sea level and up to a maximum of 1070 m a.s.l.

**Scree/slope sediment redistribution/recent valley in-fill:** Late- to post-glacial unconsolidated sediments are found in the survey area in the form of scree nappes, as well as redistributed sediments on slopes and at the foot of the slopes. The scree nappes of the Flysch zones are predominately mixed grained – in accordance with their parent material – and easily break into fine-grained loose rock masses, in which weathering-resistant rock fragments

(sandstones, calcium silicate, calcareous marl) are embedded. On the whole, these fragments are very sharp-edged due to the short transportation distances. Since the beginning of the late glacial, these scree nappes have formed in the ice-free regions and can reach thicknesses of several metres in the middle and lower slopes.

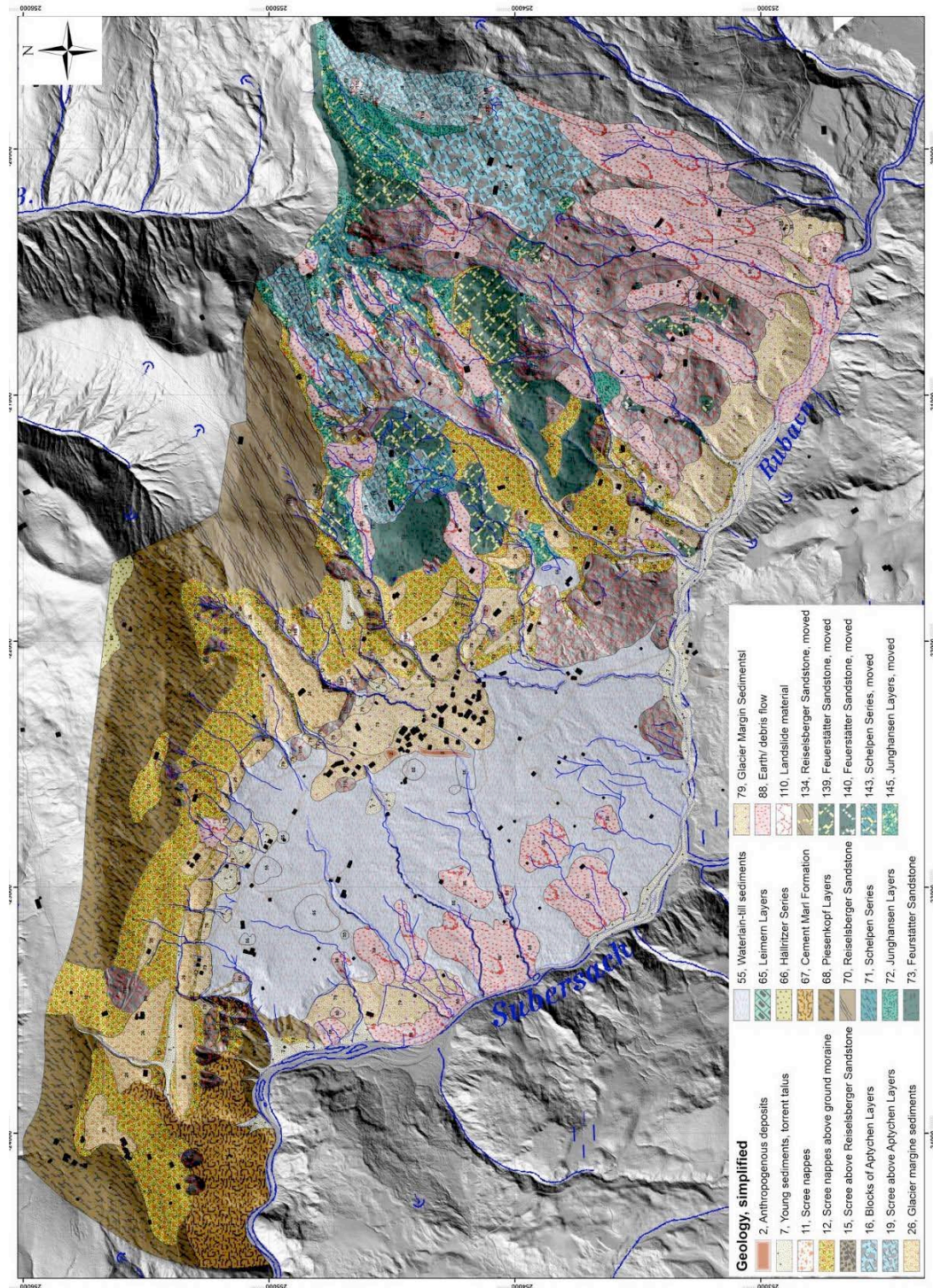


Figure 172: Simplified geological map of the research area Sibratsgfall.

### **6.2.8.3 Description of the analysis**

#### **Problems and Aims**

After the landslide event of the year 1999 the whole area of Sibratsgfäll was covered by airborne geophysical measurements to provide the basis for the upcoming detailed mapping of the area in frame of the design of a new land-use plan. The survey of 2001 was the first airborne survey in Austria devoted to the topic of natural hazard mitigation. However, data quality for the town area of Sibratsgfäll was not satisfying. Therefore in 2009 the survey was repeated in frame of the SafeLand project in order to make use of the technological innovations of the last 8 years. Figure 173 and Figure 174 show the flight line maps of the 2001 and 2009 survey respectively. The flight direction was changed from the original 2001 plan to make minimum sensor clearances possible in the area of Rindberg.

Geophysical surveys were conducted in the area of the slope failure of Sibratsgfäll in order to acquire further information concerning the lateral extent of unconsolidated sediments and hard rock, their depth profiles and their structure. The airborne measurements were complemented by more than 20 ground geoelectrical profiles, surface geological and structural mapping, several deep drillings, borehole geophysics and a detailed monitoring project in the area of Rindberg.

The survey results are going to be interpreted herein from a geological perspective. For this purpose, the data from 2001 will be compared to that from 2009. An evaluation of the applied methods will follow in terms of their usage and significance regarding the recognition of geological structures, the spread of lithological units, and potential regions of mass movement.

The survey results will be discussed in relation to the geological subdivisions in the area. These are:

- Quaternary valley in-fill of the Sibratsgfäll basin in which the main residential areas of Sibratsgfäll are to be found, including the places Nest, Wieseln, Mähmoos, Krähenberg and Sausteig. – SUBREGION SIBRATSGFÄLL BASIN.
- The slope region north of the Sibratsgfäll basin which is composed of Rhenodanubian Flysch. – SUBREGION RHENODANUBIAN FLYSCH.
- Places to the east of the main residential areas, such as Scheibladegg and Rindberg, which are located in rocks of the Feuerstätte nappe. The slope failure of Rindberg is also to be found here. – SUBREGION FEUERSTÄTTER NAPPE.

#### **Measurement setup and interpretation**

Within the survey area, the following parameters were logged along with the flight path documentation, allowing the following interpretation options regarding lithology of the ground, geological structures, water paths and moisture penetration, depth extents of geological bodies and possible areas of slope movement.

- Relative soil moisture: this parameter gives the soil moisture of the surface soil layers. It is strongly dependent on the meteorological condition during the survey.
  - Natural radioactivity / Thorium: The natural radioactivity of Uranium and Thorium provides information concerning the lithological build-up of shallow layers and is indicative for clay layers.
  - Natural radioactivity / Potassium: The natural radioactivity of Potassium is an indicator for high clay contents and potassium-rich minerals in the near-surface layers.
-

- Technogenic radioactivity / Caesium: The technogenic radioactivity of Caesium provides information about the local remaining contamination after the nuclear accident of Chernobyl. This parameter is indicative for landslides, which took place after the Chernobyl accident since deeply moved material exhibit very low values or in many cases do not contain Cs-137 at all. Consequently it could be used to map such areas. However, if the initial concentration was low, Cs-137 has already been removed by hydrological processes and decayed to the background value.
- Apparent resistivity / homogeneous half-space: The apparent resistivities of shallow layers deliver information about lithology and crop-out of potential slope movement. Grounds dominated by fine-grained materials, high clay content with high water saturation generally yield low resistance values, while dry, large-grained rock produces mostly large resistance values.

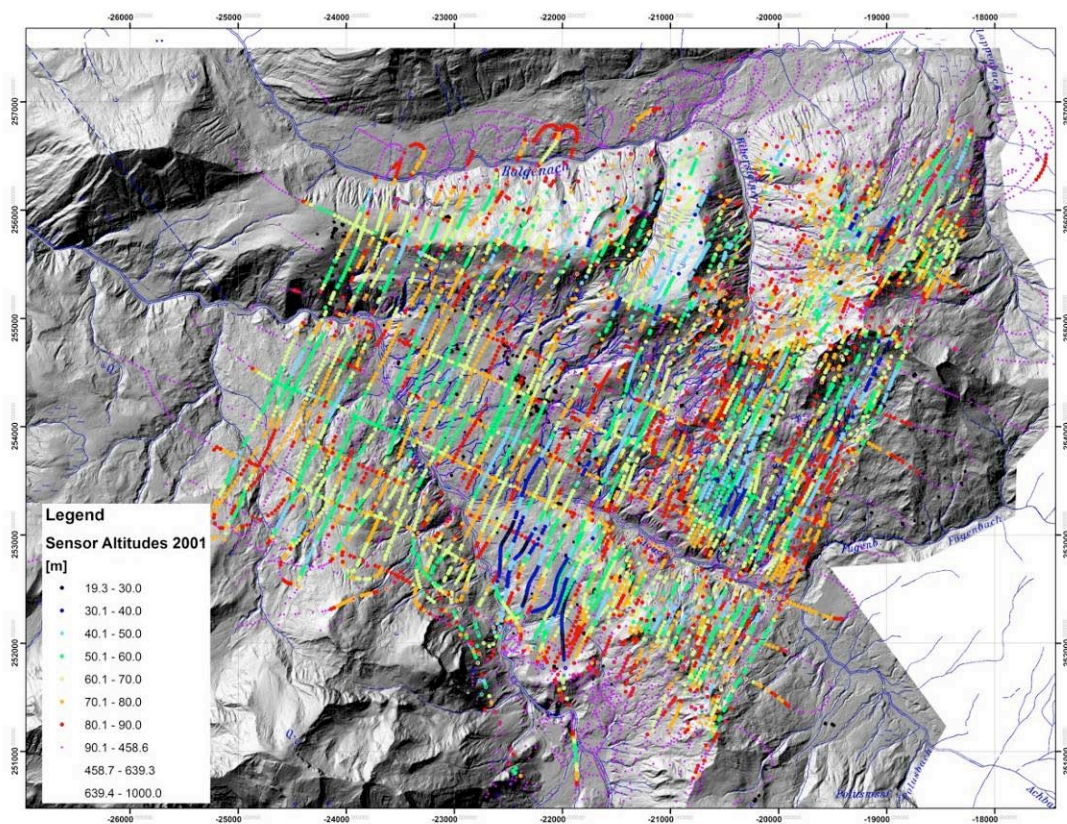


Figure 173: Flight lines of the survey at the Sibratsgfäll area in 2001; colors indicate sensor altitudes.

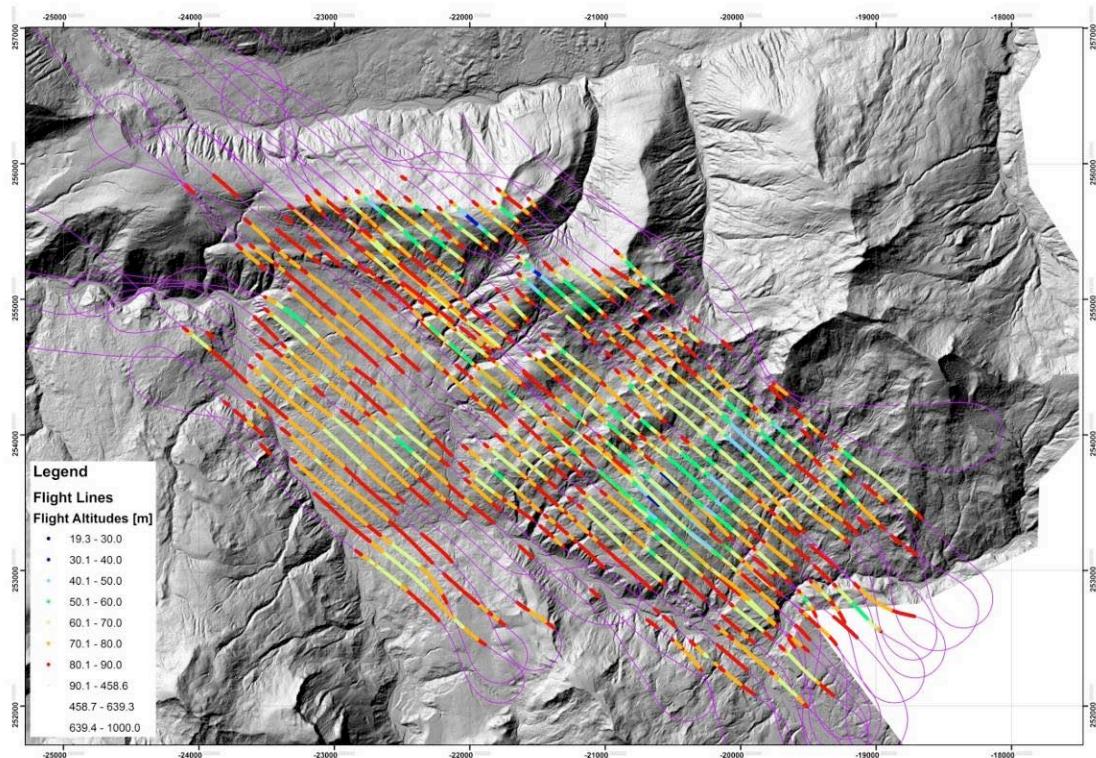


Figure 174: Flight lines of the survey at the Sibratsgfäll area in 2009; colors indicate sensor altitudes.

#### 6.2.8.4 Results and Interpretation

##### Measurement parameter: soil moisture (Figure 175)

Soil moisture is highly dependent on the time of flight for the airborne geophysical survey. Nevertheless, the parameter permits the differentiation between highly permeable, dry soils and soils where seepage is limited due to the fine particle content and thus shallow layers are (constantly) water permeated.

- Subregion Sibratsgfäll Basin. The Sibratsgfäll basin is filled with thick glacial and post-glacial sediments. The biggest part of the valley in-fill is comprised of waterlain-till. Lithologically speaking, these are thick, fine-grained sediments dominated by silt and fine sand deposits with low permeabilities and high clay contents. Accordingly, these soils are characterised by stagnant moisture, which manifests itself in the aerogeophysical surveys as high soil moisture. There is a sharp boundary with the highly permeable and thus dry sand-gravel mixtures of the glacier margin sediments.
- Subregion Rhenodanubian Flysch. The slope areas built up from Rhendanubian Flysch are found to the north of the quaternary valley in-fill of the Sibratsgfäll basin. The soil moisture values there are clearly lower than for the basin sediments, which can be explained through the shallow, dry hard rock and the dominant surface run-off. Areas with strong water emersion and springs are numerous. They are easily recognisable in the form of light blue patches within the survey area.
- Subregion Feuerstätte Nappe. Within the Feuerstätte nappe, there is a frequent alternation between fine-grained, low-permeability rocks (Junghansen layers and Schelpen series) and rocks which show a good permeability of surface water due to

their brittle behaviour (Feuerstätte sandstone and Aptychen layers). These alternating series with a general strike direction from south-west to north-east are visible in the soil moisture data: more permeated areas (Junghansen layers and Schelpen series) alternate with dry areas (Feuerstätte sandstone and Aptychen layers).

- The soil mass from the Rindberg slope failure in 1999 represents a further major anomaly in terms of soil moisture. This slope movement particularly affected the sequences of the Junghansen layers. Due to their fine particle content, stagnant moisture is very dominant, which in turn can be seen in the form of shallow permeation of the soil.
- Given the lithological settings, the glacier margin terraces composed of coarse-grained sedimentation, are clearly demarked at the foot of the slopes. The dry sand-gravel mixtures are well mappable using the soil moisture measurements.

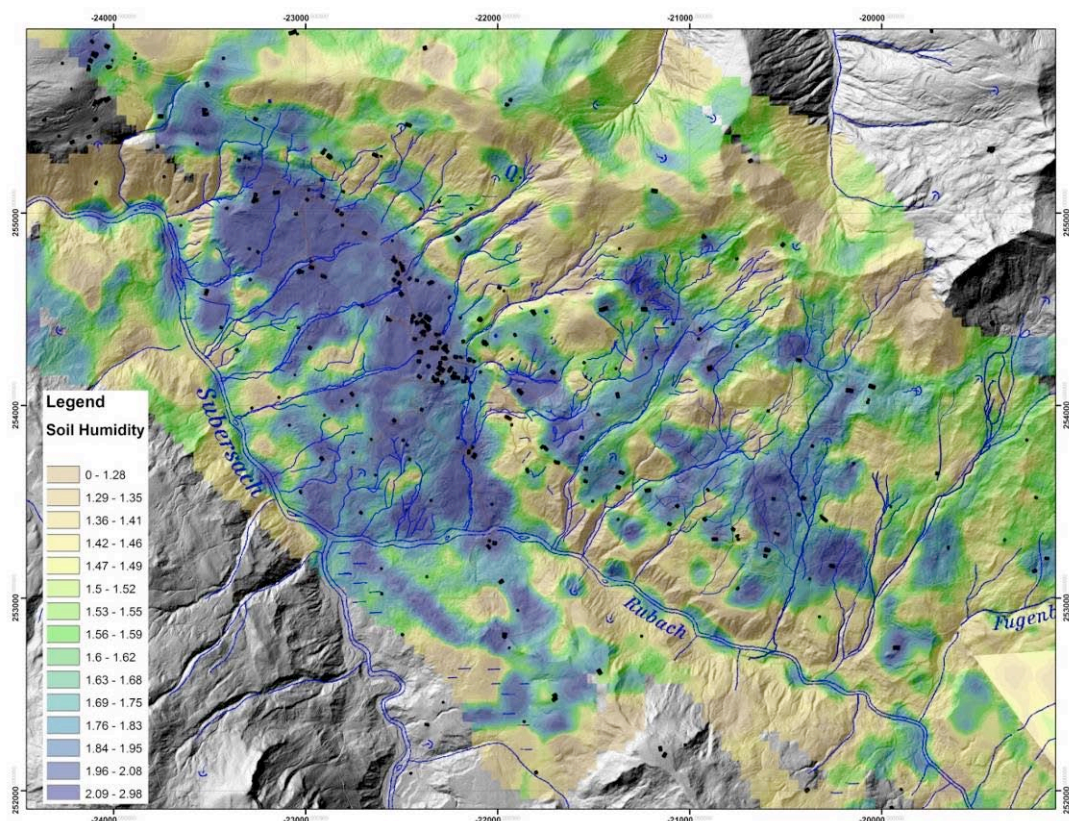


Figure 175: Results of the passive microwave soil humidity measurements of 2009.

## GAMMA RAY MEASUREMENTS

**Measurement parameter: potassium** (Figure 176 and Figure 177)

In order to interpret the potassium distribution, the underlying theory is that radioactive potassium is primarily found in clay minerals in the soil. In this respect, the following interpretations for the three survey regions are proposed:

- Subregion Sibratsgfäll Basin. In agreement with the fine-grained valley in-fill of the Sibratsgfäll basin, which is predominately composed of silt and clay sediments, the measurements reveal high potassium counts. Small anomalies concerning low potassium counts are noticeable within the valley in-fill, as they do not correlate with

the geological records. The source of these low potassium values in these areas remains unknown.

- Subregion Rhenodanubian Flysch. In the region of the Rhenodanubian Flysch north of Sibratsgfäll, the slopes in the western part are covered by a thin ground moraine. This thin-banked overlay of unconsolidated sediments is reflected in the potassium counts of the aerogeophysical survey. There is a noticeable anomaly in the boundary region between Feuerstätte nappe/Rhenodanubian Flysch. Seeing as the anomaly correlates well with the lateral extent of the Reiselsberg sandstone found in that area, the background contamination of potassium is associated with those rocks.
- Subregion Feuerstätte Nappe. In the area of the Feuerstätte nappe in the eastern part of the survey region, high potassium counts were found along the central depth contour of the slope failure Rindberg, between the break-off edge „Feuerstätter Kopf“ and Ruhbach. The distribution of the potassium radiation corresponds very well to the fine-grained slide mass of the upper, intermediate and lower slope sections delimited in the geological records. The high potassium count is thus a result of the high clay content of the Junghansen layers along the depth contour and their overhaul products. Also the Aptychen layers, dominated by carbonates, are clearly delineable and are expressed through low potassium values in the aerogeophysical data.
- Another low potassium contamination can be found in regions of Feuerstätte sandstone.

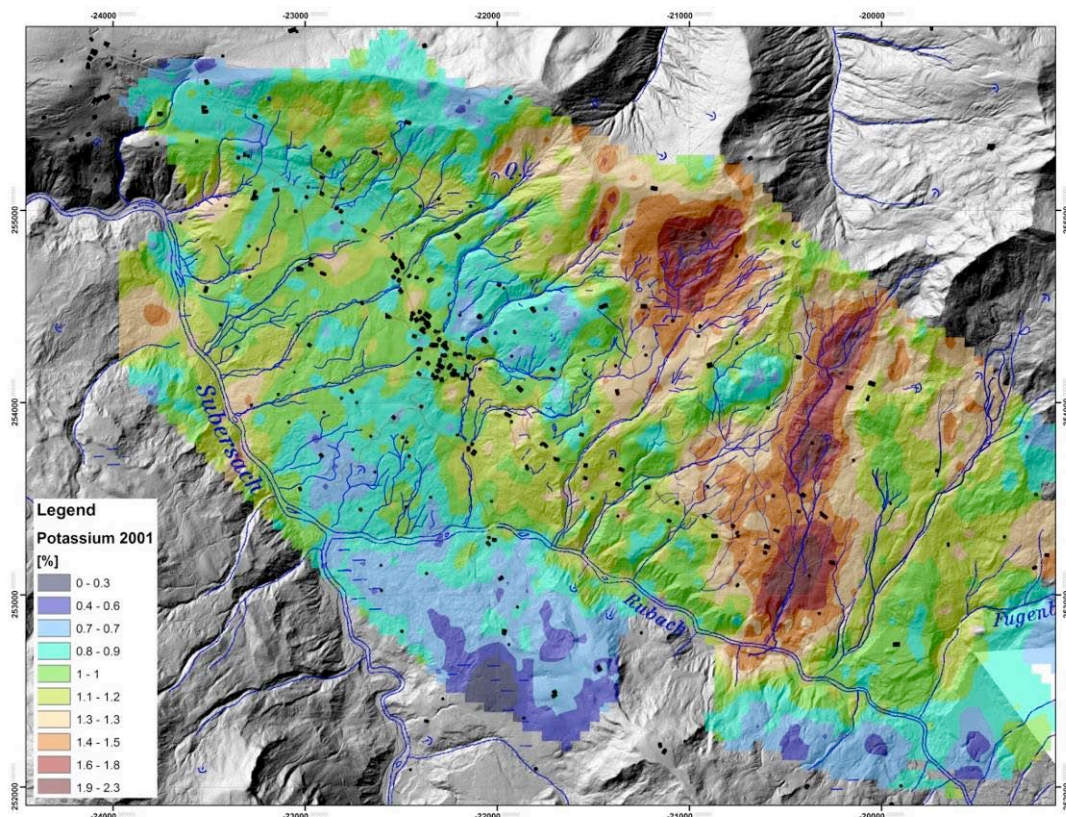
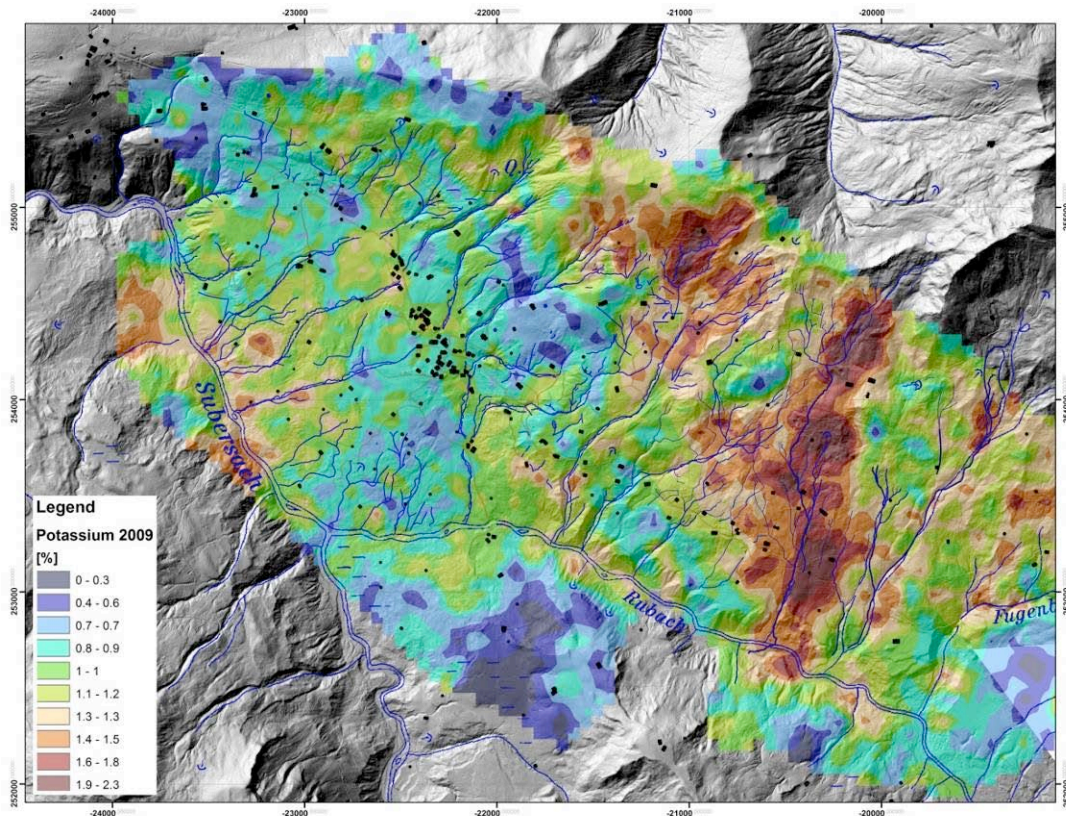


Figure 176: Results of Potassium mapping: survey 2001.



**Figure 177: Results of Potassium mapping: survey 2009.**

**Measurement parameter: Thorium** (Figure 178 and Figure 179)

Essentially, the Thorium values in the SIBRATSGFÄLLER BASIN, RHENODANUBIAN FLYSCH and FEUERSTÄTTE NAPPE show a similar distribution to those of the Potassium radiation. Variations occur in the differential intensity.

For instance, in the eastern part of the subregion Feuerstätte nappe, the differences in Thorium between rocks of the Aptychen layers and Feuerstätte sandstone are far greater than in areas with Junghansen layers and Schelpen Series. This is explicable through the respective content of heavy minerals in the series.

Due to this circumstance, the source and composition of gravels and sands in the quaternary i.e. glacial und post-glacial sediments can be interpreted. Because of the low Thorium radiation measured there, the source areas of the sediments in the Helvetic region with high carbonate contents (bordering in the south) can be held responsible for the low Thorium radiation.

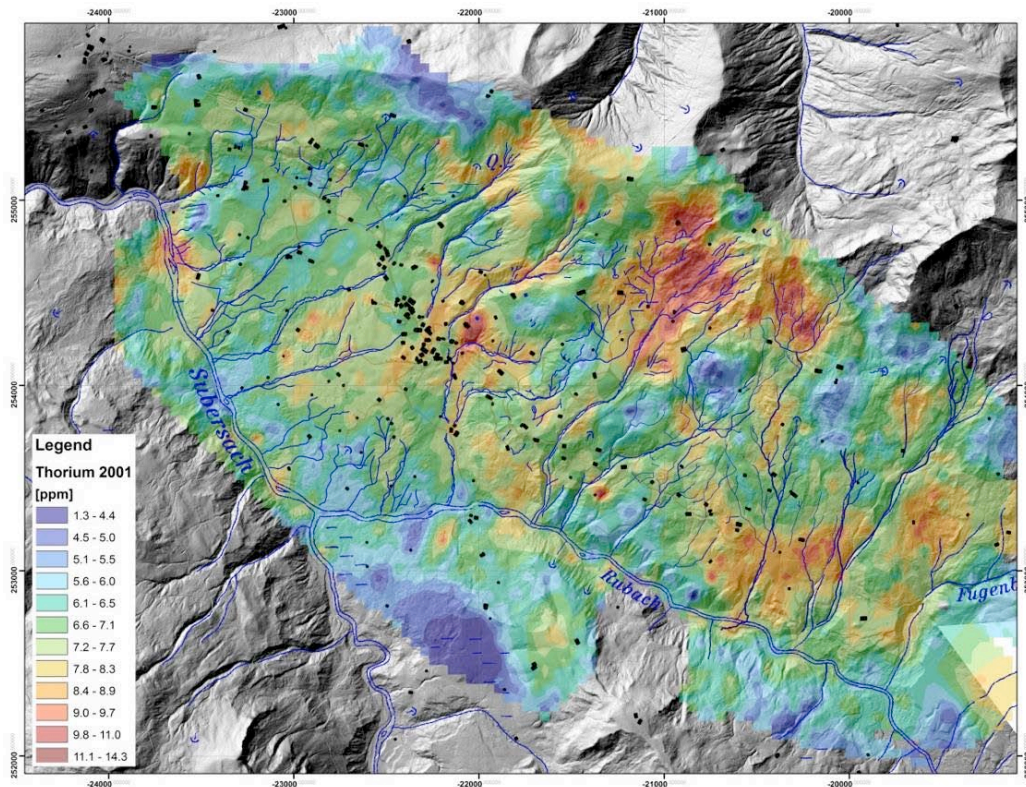


Figure 178: Results of Thorium mapping in 2001.

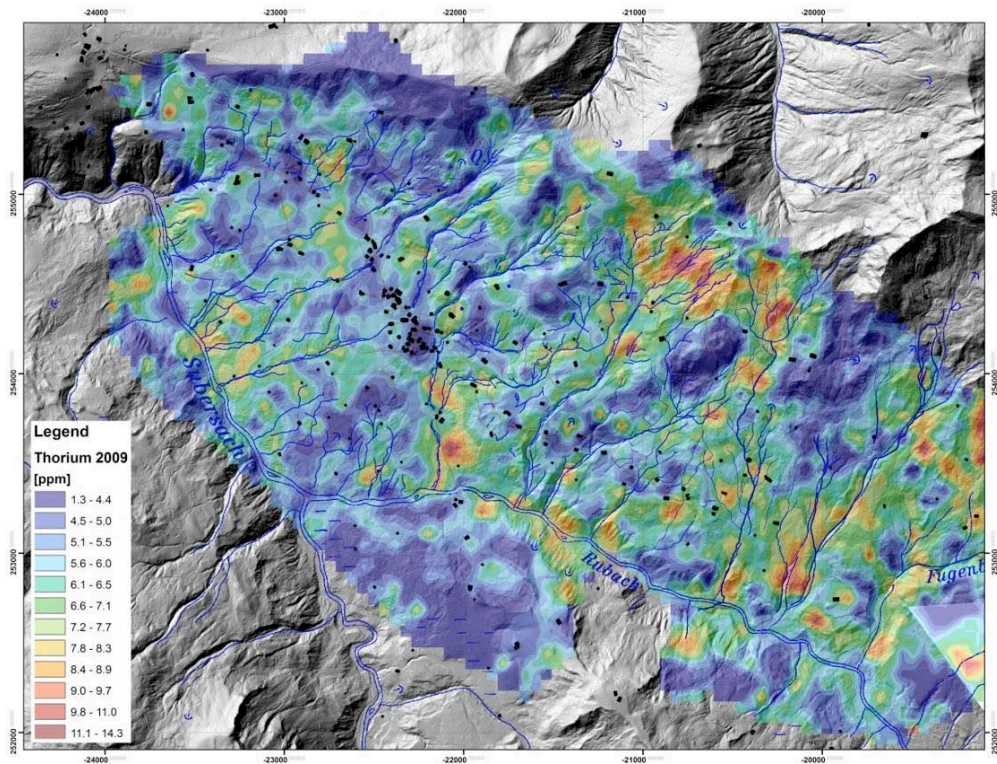
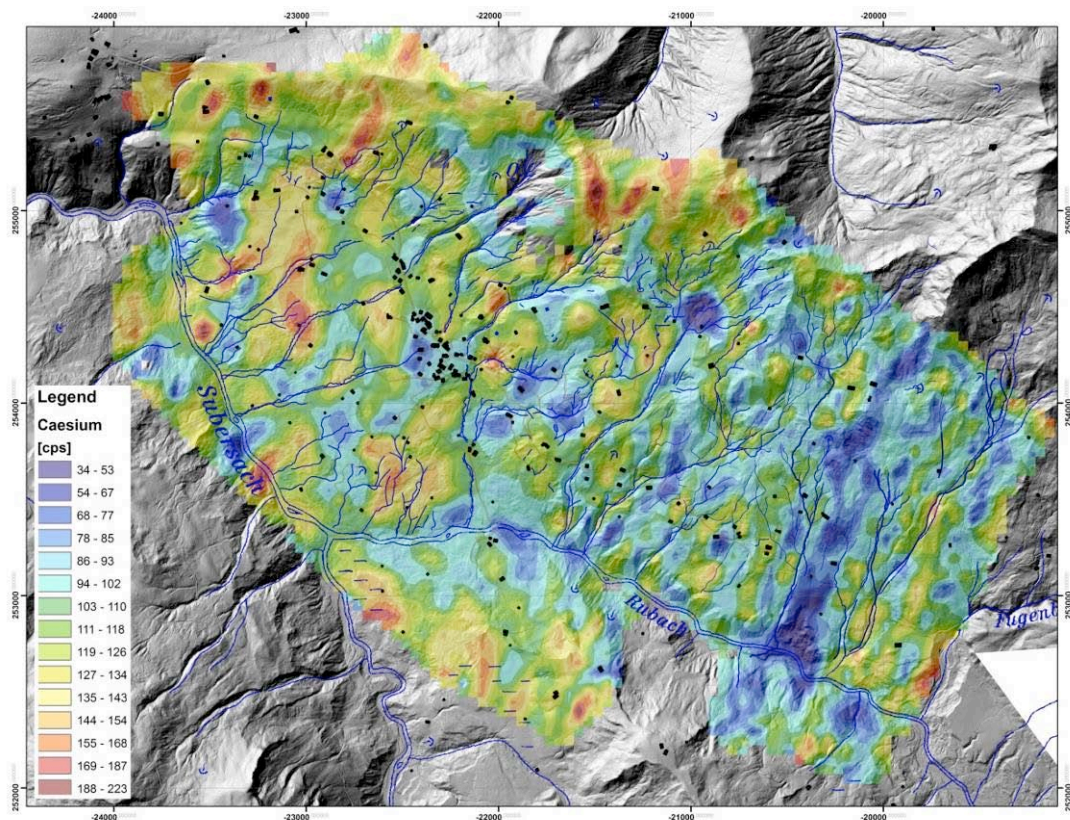


Figure 179: Results of Thorium mapping in 2009.

**Measurement Parameter: Cesium (Figure 180 and Figure 181)**

The parameter Caesium is termed “technogenically radioactive” and yields information concerning the remaining contamination after the nuclear accident in Chernobyl. Correspondingly, the initial Caesium values reflect the spread of particles transported by wind and precipitation. After the initial deposition, Cs was transported by hydrological and mass movement processes and decayed. Thus the measurement data of 2001 reveal structures which correlate well with the geological settings. This can be said in particular for the Eastern survey region around Rindberg. Especially the central depth structure of the mass movement with creep / flow of the unconsolidated sediments in the formerly activated Rindberg movement in 1999 is clearly visible in the Caesium distribution. This can be explained through a strong rearrangement or overhaul of the unconsolidated sediments and their displacement down to greater depths. The results from 2009 clearly show that hardly any Cs was left in 2009 within the area due to decay and transport. Consequently no clear pattern can be recognised.



**Figure 180: Results of Cesium mapping in 2001.**

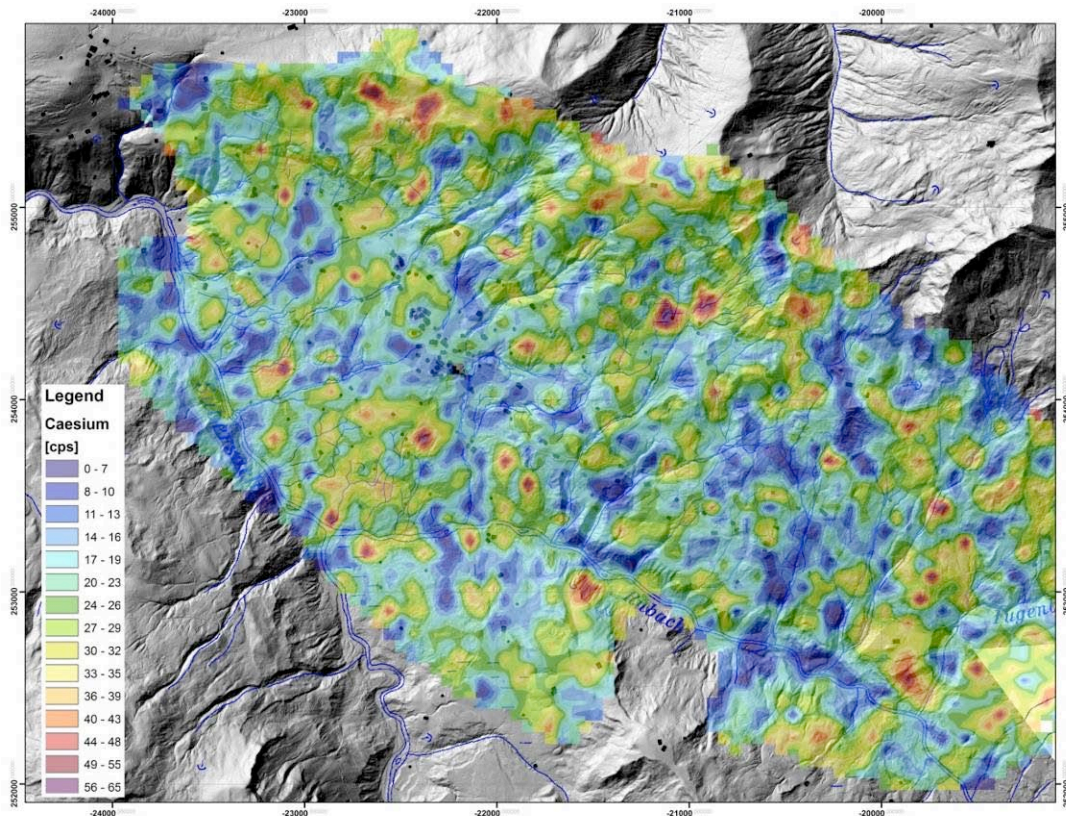


**Figure 181: Results of Cesium mapping 2009 (pay attention to the color scale different to the one of 2001)**

**Measurement parameter: Apparent Resistivity (Figure 182 and Figure 183)**

Like the terrestrial geophysical data, the apparent resistivity parameter delivers the clearest and easiest interpretable data in the survey region. Due to the dependence on fine-grain content, moisture penetration and water saturation, these differences in the data are clearly recognisable in the given geological settings with series being occasionally dominated by fine grain sizes and competent, compact hard rock regions.

- Subregion Sibratsgfäll Basin. In accordance with the ground structure, the lowest resistivities are expected in the thick, fine-grained valley in-fill. This was confirmed in the measurement data, where values were in the range of 3 – 25 Ohmmetre. The greater resistances in regions of the glacier margin, dominated by coarse grains (sand-gravel mixtures) at the northern boundary are also clearly marked in the data.
- Subregion Rhenodanubian Flysch. On the one hand, thin ground moraine overlaps are recognisable in the western part of the Rhenodanubian Flysch (low apparent resistivities) and, on the other hand, the coarse-grained sediments (high apparent resistivities, in particular Rieselberg sandstone) show up in the data.
- Subregion Feuerstätter Nappe. Within the subregion „Feuerstätter nappe“, the areas composed of Feuerstätter sandstone and Aptychen layers are marked by high resistivities. This circumstance is ascribed to the significant break-up of the structure and the associated dry character of the series. On the valley floor and the central depth contour of the moving mass – dominantly fine-grained moving masses and fine-grained parent rock – are characterised by low apparent resistivities. These large-scale

structures with the two main break-off edges (Feuerstätte Kopf and Vogt) are recognisable in the aerogeophysical data, even 20 years after the event in 1999.

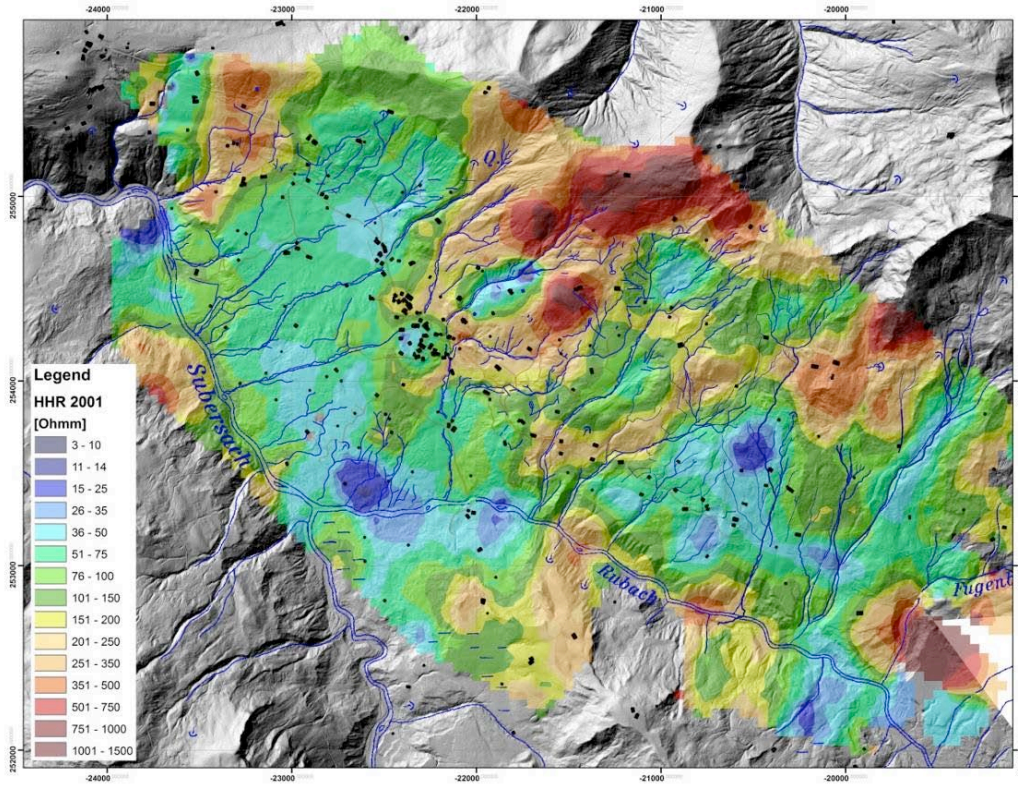


**Figure 182: Results of homogeneous halfspace inversion: survey 2001.**

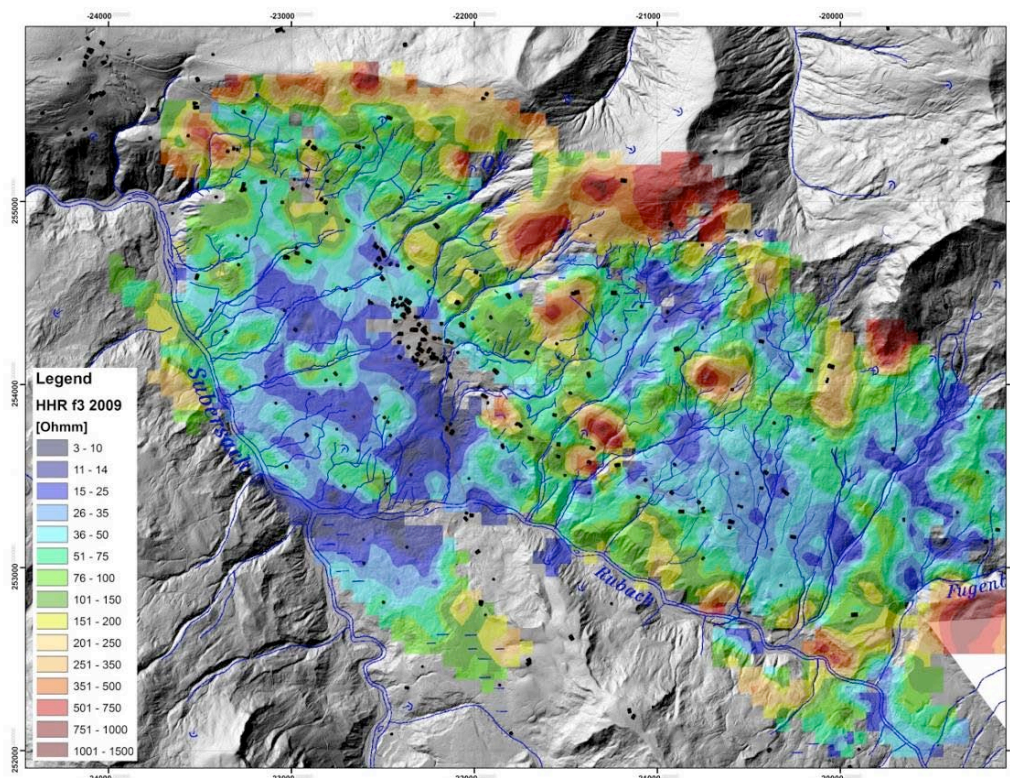


**Figure 183: Results of homogenous halfspace inversion: survey 2009.**

#### **6.2.8.5 Discussion and conclusions**

On the whole, the results from the 2001 and 2009 surveys correlate very well. There are no considerable differences in the parameters and data, and the macro-scale structures are recognisable in both the 2001 and the 2009 aerogeophysical mapping. Discrepancies are possible in the resolution of the data and in the small-scale differentiation, where it can be seen that the 2009 data permit a finer resolution.

With the survey at Sibratsgfäll in the year 2009 the first known repeated airborne survey at a landslide area was performed to investigate the “monitoring” capabilities of airborne geophysics. The results show, that in both campaigns the general geological framework could be mapped with high resolution. The 2009 survey further improved the resolution in the region around the town of Sibratsgfäll. However, due to the different technological settings of the measurement systems used in the 2001 and 2009 survey (especially the electromagnetic system was significantly improved), different calibration procedures and processing algorithms, the resolution of the results is not accurate enough to compare small differences related to changes within the hydrological system of the subsurface as regards the electromagnetic parameters. The same is true for the gamma mapping, where the general pattern of potassium and thorium content could be verified, whereas it was not possible to interpret very local changes in parameters. For a detailed interpretation further research is needed, especially since gamma ray measurements also depend on the prevailing meteorological conditions during the survey. There is still a lack of algorithms to correct for this effect. Furthermore the relatively high survey costs as well as the restricted availability of airborne surveys and the significant amount of time needed for data processing at the current state-of-the-art limit the applicability of airborne geophysics as a quasi permanent monitoring methodology to pure scientific applications.

#### ***6.2.8.6 Improvements with respect to previous applications***

The survey of 2001 was the first airborne survey in Austria devoted to the topic of natural hazard mitigation. However, data quality for the town area of Sibratsgfäll was not satisfying. Therefore in 2009 the survey was repeated in frame of the SafeLand project in order to make use of the technological innovations of the last 8 years.

The flight direction was changed from the original 2001 plan to make minimum sensor clearances possible in the area of Rindberg.

## 6.2.9 High resolution space-borne SAR images correlation (monitoring): La Valette (France)

CNSR : Malet J.-P.

BRGM : Raucoules D., De Michele M.

### 6.2.9.1 Study area

The SafeLand case study for the evaluation of the capability of TerraSAR-X data to monitor the displacement of landslides is the La Valette landslide located in the Barcelonnette Basin (South East France) (Figure 184).

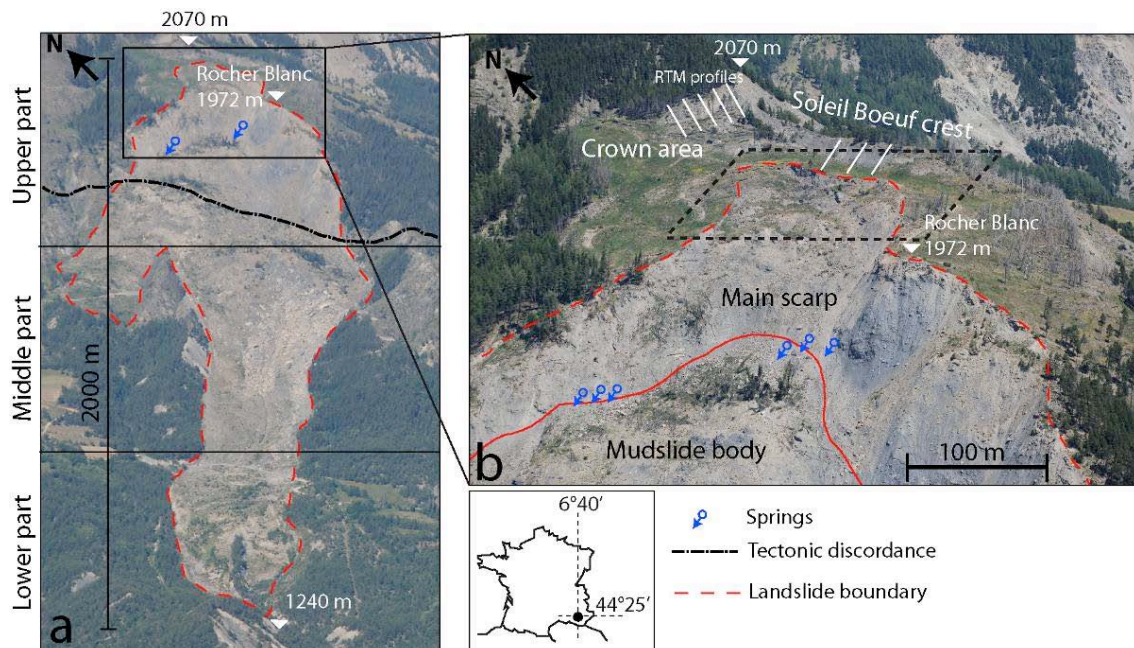


**Figure 184. Geomorphological setting of the La Valette landslide on the South-facing slope of the Barcelonnette basin. a) General view of the landslide to the North East. b) View of the main scarp and the crown areas; the dashed line delimitates the area investigated by TLS and seismic tomographies. The displacement profiles measured by the “Restauration des Terrains de Montagne” (RTM) office to monitor the retrogression of the crown are also indicated.**

The La Valette landslide, triggered in 1982, is one of the most important large and complex slope movements in the South French Alps. The landslide associates two styles of activity: a mudslide type of behaviour with the development of a flow tongue in the medium and lower part, and a slump type of behaviour with the development of several rotational slides in the upper part at the main scarp. The landslide extends over a length of 2 km for a variable width of 0.2 km in the lower and medium parts, to 0.45 m in the upper part (Figure 184). The maximum depth, estimated by seismic and electrical resistivity tomography and geotechnical boreholes, varies from 25 m in the lower and middle parts (Evin 1992; Travelletti et al. 2009) to 35 m in the upper part (Le Mignon, 2004). The mean slope gradient is ca. 30° in the scarp area and ca. 20° in the mudslide area (Figure 184b). The volume of the mudslide body is estimated at  $3.5 \cdot 10^6 \text{ m}^3$ .

The landslide affects a hillslope located uphill of the municipality of St-Pons (Department of Alpes-de-Haute-Provence), and is a important threat for the 170 community housings located downstream (Le Mignon and Cojean, 2002). The occurrence of rapid mudflows triggered from the mudslide body and in the scarp area in the 1980s and 1990s has motivated the development of an early-warning system since 1991 composed of benchmark topographical monitoring, optical and infra-red camera monitoring and the installation debris height detection sensors in the torrent, and the drainage of the lower part of the landslide.

### **Geological, geomorphological and hydro-geological setting**

From a geological viewpoint, the La Valette landslide is located at the tectonic contact between two major geological formations (Figure 185a):

- An autochthonous formation represented by the closely stratified Callovo-Oxfordian black marls (e.g. “Terres Noires”) characterized by a typical landscape of badlands. This formation is located in the middle and the lower parts of the slope;
- An allochthonous formation represented by two sheets thrusts and in which the upper part of the landslide has developed. The basal sheet thrust is a tectonic wedge belonging to the Pelat sheet thrust and is composed of highly fractured flysch and planctonic carbonates of the Turonian and Paleocene Superior age (BRGM 1974). This formation has a few dozen of meters of thickness at the location of the main scarp with an average dip direction and dip of 135°/30°. The Pelat sheet thrust is overlaid by the upper Autapie sheet thrust composed of highly fractured Helminthoid flysch, grauwakes, marls and schist.

From a hydro-geological viewpoint, the tectonic discordance has an important role on the landslide mechanism. Due to the high heterogeneity of the landslide material and of the highly dislocated texture of the flysch, both materials are considered as aquifers at the scale of the landslide. At the opposite, the black marls formation is considered as an aquitard (Dupont and Taluy 2000; Le Mignon 2004). Consequently, the contrast of permeability between the black marls and the flysch conditions the spatial occurrence of several springs and marshy areas at the direct vicinity of the tectonic discordance between the elevation 1870 m and 1950 m (Figure 185a, b). According to Le Mignon (2004), a spring (the “Rocher Blanc” spring at 1900 m) is currently partially buried by the landslide. Consequently a deep water circulation affects the hydrological regime of the upper part of the landslide but the characteristics of the water flows (fluxes, quality) are unknown.

### **Landslide historical and recent development**

The landslide exhibits a complex style of activity in space and time. It has developed first as a rotational slide affecting the Autapie sheet thrust in relation to a major thrust fault (Colas et Locat 1993; Le Mignon 2004). The failed mass has progressively loaded the underlying black marls formation, and the landslide has developed by a series of rapid mudflows triggered in the marls such as in March 1982, April 1988, March 1989 and March 1992. The most important crisis occurred in 1988 when a mudflow of 50.000 m<sup>3</sup> triggered at the elevation of 1400 m flows over a distance of ca. 500 m (Colas et Locat 1993). Up to now, these mudflows did not mobilize the complete failed mass.

The displacements are monitored in continuous with topometric benchmarks since 1991 (Squarzoni et al. 2005), differential dual-frequency GPS (Déprez et al. submitted) and an

extensometer since 2008, and at regular periods by digital correlation of satellite images (Le Prince 2008) and satellite radar interferometry (Squarzoni et al. 2003).

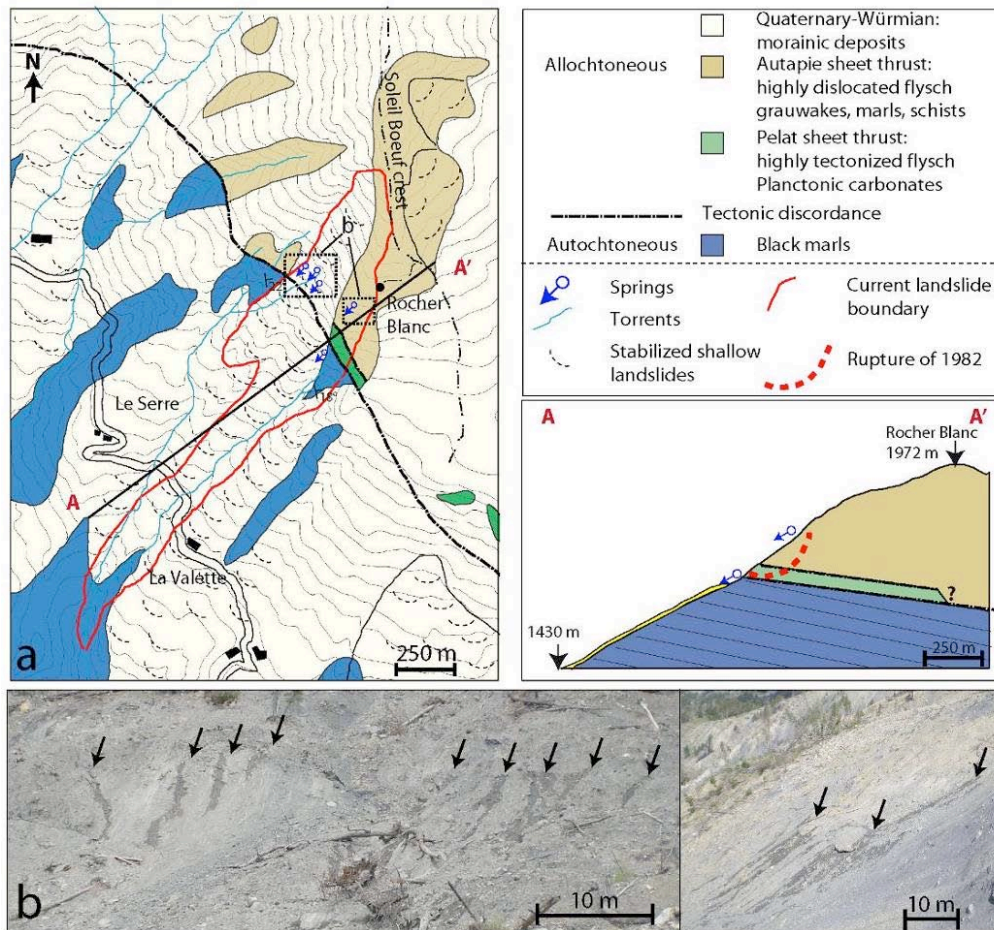


**Figure 185. Geological setting of the La Valette landslide. a) Extract of the regional geological map at 1:50.000 with the topography before the landslide event (adapted from BRGM, 1974) and schematic cross-section detailing the hydro-geological setting of the slope before the failure of 1982 (adapted from Colat and Locat, 2003). The interval between elevation contour lines is 20 m b) Photographs of the spring line at an elevation of ca. 1880 m along a possible weak zone above the tectonic discordance near the North West boundary and the Rocher Blanc location.**

Two main aspects can be pointed out from these studies and from the observations by the local stakeholders. The first one is the decrease of velocity (from  $0.4 \text{ m.day}^{-1}$  to about  $0.01 \text{ m.day}^{-1}$ ) in the middle and lower part of the landslide caused by the local groundwater drawdown since the installation of a drainage system in the 1990s. The second is the important activity since the year 2000 of the upper part at the Soleil Boeuf crest, which is characterized by a rapid retrogression of the main scarp towards the North-East and an enlargement of the landslide towards the North-West (Figure 186). In response to this worrying situation, the RTM Service has installed several additional benchmarks along profiles both in the unstable and stable parts of the Soleil-Boeuf crest to monitor the displacements in the crown area. Actually, an accumulation of material and a steepening of the slope are observed in the upper part of the mudslide because of the retrogression of the

scarp. Consequently, the possible hazard scenario consists in the undrained loading of underlying black marls formation and the triggering of new rapid and mobile mudflows.

Further information on the La Valette landslide can be found at: <http://eost.u-strasbg.fr/omiv/>

### **6.2.9.2 Description of the analysis**

In the framework of the Safeland case study, we propose to process a data set obtained from the TERRASAR-X sensor using correlation techniques. The data set was acquired at reduced scientific prices by BRGM (proposal LAN0666 accepted by the TerraSAR X Science Service). Twenty four Spotlight mode (1m resolution) images from our quota were planned on the test site (12 in ascending mode and 12 in descending mode) between October 2010 and mid-2011. The presented methodology will therefore be applied when the dataset is completed.

#### **Issues to be addressed**

The main objective of the study is to evaluate if such a technique is appropriate for monitoring landslide displacements and could be complement or replace other Remote Sensing or Ground based data. So the study should respond to the following questions:

- 1 Is the resulting precision is equivalent to the precision obtained with optical data with similar resolution?
- 2 How to retrieve a time series of 3D displacements using temporal correlation products?
- 3 How to extract time series with sampling appropriate for the monitoring of given typologies of landslides (velocity, size)?

#### **Methodology**

We propose to compute all the possible correlation products (offsets in range and azimuth estimated for two images acquired at different dates) to estimate the deformation between the acquisition dates of pairs of images included in the data set using semi-automated procedures. The tools we will use are mainly based on the GAMMA interferometric software (from Gamma RS) and additional scripts we developed. GAMMA provides both tools for processing the SAR images, sub-pixel correlation tools and tools for multi-baseline interferometric processing (that is designed for producing deformation maps at the dates of the SAR acquisitions from a set of interferograms larger than the initial image set) we adapted for processing offset maps.

We will therefore derive the displacement respect to the first acquisition date in range and azimuth for both ascending and descending modes. Using a least squares procedure such the one proposed in de Michele et al. (2010) for deriving  $\sigma$ , we will derive the 3 components of the deformation for each period (ascending and descending acquisitions does not correspond exactly to the same dates – incidence of this issue on the precision have to be assessed during the study).

The final product will therefore be bimonthly/monthly 3 D deformation maps.

#### **Validation/comparison with ancillary data**

The proposed methodology needs to be validated. We therefore propose to compare when possible the obtained results with those issued by the comprehensive monitoring ground based tool set of the la Vallette Landslide for the studied period. This analysis will be carried out in

collaboration with the CNRS (EOST-Strasbourg) that has a deep knowledge on the studied phenomenon and access to ground based data.

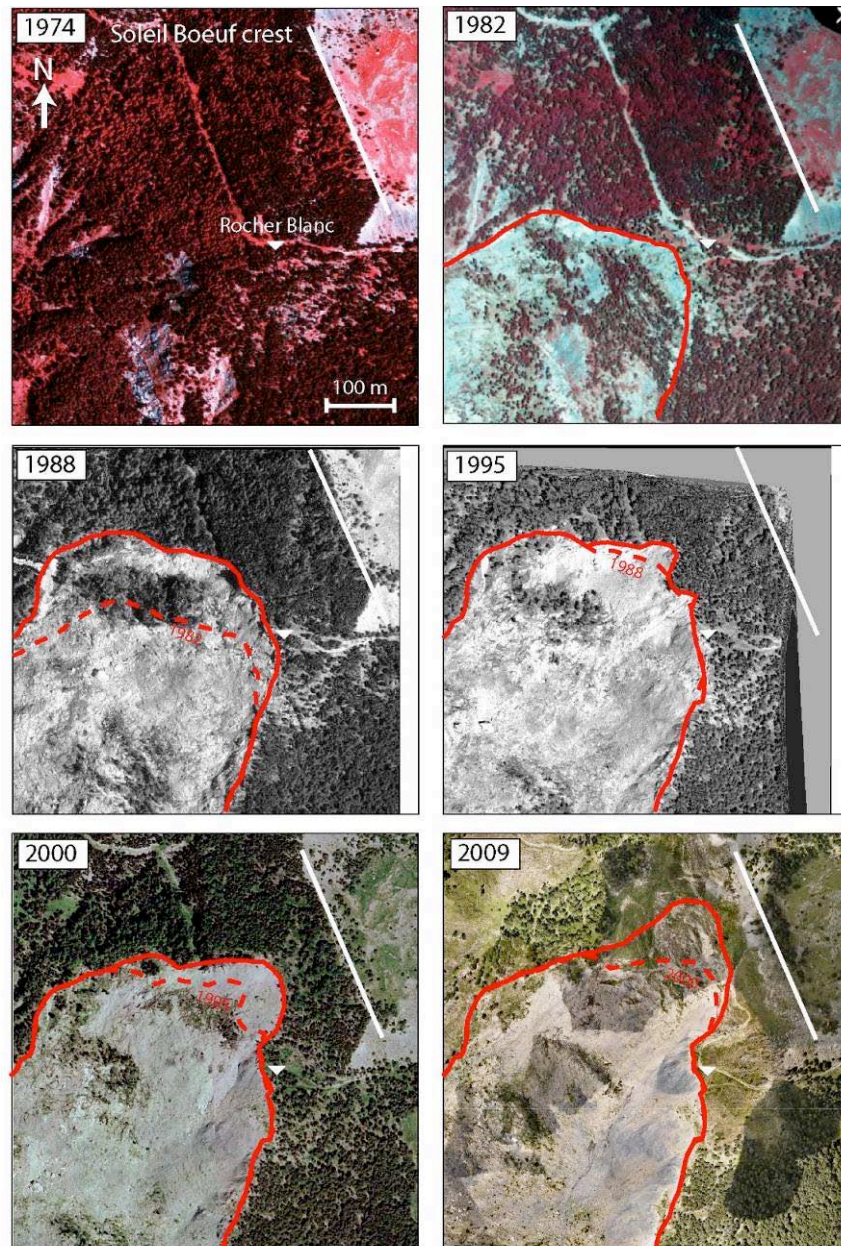


**Figure 186.** Development of the La Valette scarp since 1974 (before the failure) to 2009 from the analysis of aerial orthophotographs. From 1982 to 2009 a scarp regression of 200 m towards the North East is observed.

### **Additional analysis**

In addition to the work previously described, we plan to take advantage of a similar test presently carried out by BRGM on landslides located in the la Reunion Island (Figure 187) but based on a set of 25 COSMO-SKYMED images (with about 30 cm resolution). Comparison between results on both test sites will be valuable for a better understanding of the performances of the method. In particular, we will focus on the issues related to the

required precision in the perspective of an operational monitoring of the studied landslides (the studied landslides on La Valette and la Reunion have different characteristics in terms of displacement and extent of the slide).

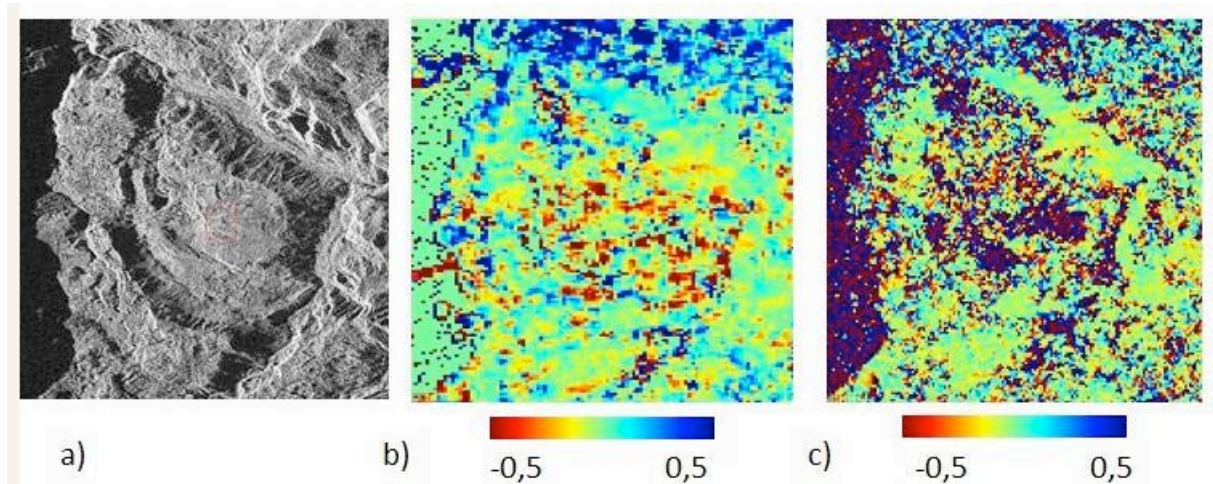


**Figure 187.** Example of computation of azimuth offsets on the Hellbourg landslide (La Reunion Island) using 2 Cosmo-SkyMed images acquired 10/13/2010 and 1/1/2011. a) averaged radar amplitude image b) azimuth offset (in pixels) derived using GAMMA software c) offsets obtained using Cosicorr (Caltech) software.

### ***6.2.9.3 Improvements with respect to previous applications***

The expected improvement comes from the use of high resolution SAR imagery produced by recently launched platforms. Previous radar based study used lower resolution images.

It is potentially equivalent to optical space-borne image correlations in terms of precision (due to similar sub-metric resolutions) but due to characteristics of the radar systems respect to the weather conditions (not affected) and the effective repetitiveness (week to month) of the proposed platforms an improvement can be achieved in the perspective of landslide monitoring.

This issues will be discussed and in a further document (to be annexed to the present document) when the data set is fully acquired, the processing done and the results evaluated.

## 7 EVALUATION OF THE GROUND-BASED TECHNIQUES

*UNIFI: Segoni S., Tofani V.*

*with the contribution of all the partners*

In recent years ground based techniques have been interested by several technical and scientific improvements. That has not led to clearly identify a technology which can be undoubtedly and universally considered better than others. Conversely, the reliability and effectiveness of every ground-based technique have been enhanced, providing for each geological problem a wide range of equally good solutions. As a consequence, at present end-users can select the most proper methodology with respect to their specific needs, which can be related to technical issues, economic budget, environmental factors and specific features of the landslide(s) to be monitored.

This chapter provides a list of the most effective methodologies with respect to the various landslide types and an overview of the main advantages and limitations of each technique, providing scientists and end users with a support for the selection of appropriate ground based techniques for their specific needs.

It should be also stressed that ground based techniques provide measurements of very different kind (e.g. punctual or widespread, related to the superficial or the deep displacements), therefore the proposed methodologies should not be considered alternative one to each other; on the contrary they could be conveniently used in close cooperation to obtain very effective monitoring systems.

## 7.1 LANDSLIDE TYPES

This chapter contains the evaluation of the performance of each ground-based technique with respect to the various landslide types (as defined by Cruden and Varnes, 1996). This evaluation can be considered a first crucial step towards the choice of the methodology to adopt, as it allows narrowing down the number of possible solutions to a smallest cluster of techniques which grant high-quality results (Table 9).

**Table 9: evaluation of the effectiveness and reliability of the emerging ground based techniques for the monitoring of different landslide types.**

Technique	Effectiveness / reliability				
	slides	topples and falls	flows	lateral spreads	complex mechanisms
GPS	High	Not applicable	Low	High	Medium
Terrestrial optical images Correlation	High	High	High	Low	Medium
TLS	High	High	High	High	High
Geoelectrics (monitoring)	High	Not applicable	Medium	Low	High
Geoelectrics (detection and mapping)	High	Low	High	Medium	High
Automatic inclinometers	High	Medium	High	High	High
Wire extensometer	High	Not applicable	Not applicable	Not applicable	Low
Micro-seismic monitoring	Medium	High	Low	Medium	Medium
GB-InSAR	High	Medium	Medium	High	High
Optical fibre	Low	Low	Medium	Not applicable	Medium
TDR	High	Not applicable	High	Not applicable	High

### 7.1.1 Slides (rotational and translational)

Generally speaking, slides can be effectively monitored by means of almost every ground based technique described in chapter 2. This could be due to the fact that rotational and translational slides are typically associated to a wide range of velocities ranging from medium to very slow and they could be found in very different lithological and geological settings. Chapter 6.1 shows how some of these techniques have been used to study such typology of landslide or complex\composite landslides that encompass a relevant sliding component (Table 10).

GPS, terrestrial laser scanner, automatic inclinometers, GB-InSAR, wire extensometers, TDR and geoelectrical methods have already been adopted in the monitoring of slides obtaining high quality results. In the framework of the SafeLand project, terrestrial optical images

correlation was applied for the first time obtaining successfully outcomes and seismic monitoring was applied to soft rocks slides for the first time with promising results.

**Table 10: Application of ground based technologies to slides in SafeLand case studies.**

Technique	Chapter	Test site	Landslide typology
GPS	6.1.1	La Valette	Complex (rotational slide + translational slide + flow)
GPS	6.1.1	Villerville	Rotational and translational
Borehole wire extensometers	6.1.2	Vallcebre	Translational slide
Automatic inclinometers	6.1.3	Bagnaschino	Complex (slide + flow)
GB-InSAR	6.1.4	Castagnola	Composite (rotational slide + translational slide + flow)
TLS	6.1.5	Åknes	Rockslide
Terrestrial optical images correlation	6.1.6	Super Sauze	Complex (fall + slide + flow)
Seismic monitoring	6.1.7	Super Sauze	Complex (fall + slide + flow)
Geoelectric monitoring	6.1.8	Gschlifgraben	Various (including slides)

### 7.1.2 Topples and falls

This type of movements is mainly characterised by brittle deformations in hard rocks. This is the optimal physic context for the application of 3D displacement monitoring gauges as the TM71 device described in chapter 2.1.3. Also micro seismic monitoring techniques can provide high quality results when applied to this landslide typology (as explained in the SafeLand case study reported in chapter 6.1.7). In particular these two techniques can provide useful information about the internal structure of the landslide and its behaviour at depth.

The superficial displacement, in turn, could be effectively assessed by means of terrestrial optical image correlation and terrestrial laser scanning. GB-InSAR should be taken into account as an option as well: when applied to topples and falls can provide high to low quality results, depending on the velocity of the landslide.

To sum up, the most complete insight in the behaviour of topple or fall landslides can be obtained when one of the latter methodologies (terrestrial optical image correlation, terrestrial laser scanning or GB-InSAR) is applied in conjunction with one of the former (micro seismic monitoring or 3D displacement monitoring gauges).

### 7.1.3 Flows

In this chapter flows are intended as slow movements, mainly because very fast movements such as debris flows cannot be effectively monitored with ground based technologies.

Terrestrial laser scanning, GB-InSAR and terrestrial optical images correlation can provide high quality results when applied to the monitoring of superficial deformations of large sections of flows (see e.g. the SafeLand test case applications in 6.1.4 and 6.1.6). Automatic inclinometers can provide highly reliable punctual information which can extend also to considerable depths (see also the SafeLand test case application in 6.1.3).

#### **7.1.4 Lateral spreads**

Unfortunately, no SafeLand test case reported in the present deliverable concerns this landslide typology. Anyway, amongst all the emerging techniques presented in chapter 2, automatic inclinometers and GPS systems are credited to be the most effective. The first methodology allows the monitoring of various parameters at varying depths in correspondence of specific points, the latter allows a constant monitoring of the vertical and horizontal displacements of the topographic surface at specific predetermined points (but a monitoring network could be implemented at relatively lower costs).

The application of Terrestrial laser scanners (TLS) and GB-InSAR techniques may lead to satisfactory results but it is conditioned by various environmental factors such as the landslide velocity and the line of sight from the instrumentation to the instable hillslope. Since lateral spreads often occur in very gentle slopes, and in areas characterized by a modest energy of relief, it may be difficult to find a proper location to install the instrumentation in order to avoid the presence of wide and disturbing shadow areas.

#### **7.1.5 Complex and composite mechanisms**

Complex landslides can be monitored at best using terrestrial laser scanning or GB-InSAR to track the superficial displacement of the moving material and geoelectrics or automatic inclinometers for gaining a more detailed understanding of the landslide behaviour at depth. Chapter 6.1 provides a selection of applications of emerging technologies to the monitoring of complex and composite landslides (see also Table 10).

Anyhow, since in complex and composite mechanisms different types of movement contribute to the landslide, a correct assessment of the best monitoring technique requires to analyse every single mechanisms separately. Therefore, the previous chapters (7.1.1 to 7.1.4) could be again considered as a reference.

## 7.2 ADVANTAGES AND LIMITATIONS OF GROUND-BASED MONITORING SYSTEMS

In the light of the recent developments discussed in chapter 2, this chapter synthesises the main advantages of each technique and the open issues and the general drawbacks which still affect them. Each following subchapter is devoted to a specific ground based technique and it was composed by the same authors in charge for the recent trends description reported in chapter 2.

### 7.2.1 GPS: advantages and limitations

#### Advantages

The GPS equipment has become progressively less expensive, lighter and easier to use. New field operating modes and softwares have been developed for data recording and post-processing (Gili et al., 2000; Malet et al., 2002, Brunner et al., 2003). GPS is thus increasingly used in a large variety of long-term and permanent monitoring applications. To acquire very precise and absolute 3D coordinates that can be used as a reference for other monitoring techniques and to develop early-warning systems based on real-time displacement analysis, permanent GPS with automatic transmission of the data is certainly the only solution that can be used on very constraining sites with either difficult accessibility, absence of long-term stability of the slopes around the landslide, or absence of direct visibility. GPS monitoring can be performed whatever the weather conditions and during the night.

The few permanent applications of GPS applications on landslides are by Malet et al. (2002) at the *Super-Sauze* landslide (France) using single-frequency (L1) GPS receivers, Chen et al. (2005) at the *Xiaowan* landslide (China) using multi-antenna systems, and Reid et al. (2008) at the *Fremont* landslide (California, USA).

#### Limitations

For the monitoring of landslides where the required degree of accuracy is millimetric, GPS has been mainly used for repeated measurements (Gili et al., 2000; Coe et al., 2003; Squarzoni et al., 2005; Brückl et al., 2007), as a complement to conventional geodetic methods. Permanent monitoring is still not usually performed operationally, mostly because of the cost of the GPS system compared to conventional deformation monitoring techniques. In addition, if GPS measurements can reach a millimetre-level of accuracy for long observation sessions (typically 12h), their accuracy decreases with the duration of the observation sessions, because of errors introduced by variations of the satellite constellation and multi-path effects at the sites (Genrich and Bock, 1992). Moreover, one millimetre-level accuracy requires sophisticated *a posteriori* data processing techniques.

### 7.2.2 Borehole wire extensometers: advantages and limitations

There is a long experience on the performance of the borehole wire extensometer mainly in the Vallcebre landslide (since the year 1996), in the Alverà landslide and from other landslides elsewhere.

### Advantages

- Borehole wire extensometer equipment is cheap, simple and robust. All the wire extensometers installed in Vallcebre landslide were still functioning almost 15 year later. The readings made with the potentiometer allow 0.1 mm accuracy in the measurements.
- The technique is applicable to landslides in which displacement occurs on a sliding surface or on a basal shear surface (translational and rotational slides, earthflows and mudslides) with moderate or slow velocity.
- Continuous record enables very frequent readings that may be stored in a data logger. The frequency of readings depends obviously on the maximum landslide velocity expected.
- Telematic transmission of data via modem allows implementing an early warning system.
- Long time record: long life batteries allow data storage for more than three months due the low power consumption of the device; which can be considerably enlarged if are recharged in situ by means of a solar panel. The device may last working for several meters of displacement, provided that enough wire has been left outside the borehole. Anyway, placing additional wire is always possible and can be carried out easily. While the inclinometer casings were out of order after movements of less than 15-20 cm, total displacements around 8 m have been recorded with the wire extensometer at the Vallcebre landslide.
- Low maintenance. Maintenance include a regular: a) control of the potentiometer voltage to avoid potentiometer pointer reaching the open zone of the resistor; b) lowering of the counterweight located on the external end of the wire when is close to the pulley, due to the pulling of the wire into the borehole; c) visual reading of the dial of the extensometer; and d) replacement of batteries, which can be delayed considerably if they are recharged by a solar panel.
- Complement of inclinometric readings. The use of probe inclinometers and wire extensometers complement each other very well. Inclinometers have a short life when the landslide is very active, but they produce high quality information on landslide displacement profiles, velocities and the position of the shear surface, immediately after its installation. Instead, at the early stages of deformation, the wire extensometer may only record negative displacements that are not directly related to the superficial ones. Once the inclinometer is lost, it allows a continuous recording and it is operational for very large displacements. The relationship found between the wire and superficial displacements makes possible the achievement of a continuous record of displacement of the landslide.
- Easy joint installation with piezometers. It is possible to install a wire extensometer and a piezometer in the same borehole (that was currently made in the Alverà and Vallcebre landslides). The wire extensometer has proved to be very useful in recording sudden changes in the rate of displacement that can be directly related to the change of groundwater table and indirectly, to the rainfall records. When combined with a

piezometer, the wire extensometer has a great capability to reproduce with high accuracy the response to the rainfall and groundwater fluctuations. Sudden changes in the rate of displacement due to short lasting rainy events were wholly recorded (Figure 188). This latter allows the observation of the temporal trend of the displacement during critical rainy events.

- **Calibration of other techniques.** The wire measurements enable the cross checking of the results obtained with emerging techniques of displacement measurement. For instance, in the Vallcebre landslide the extensometer data has been used to calibrate the results of the SAR spaceborne and ground based interferometry.

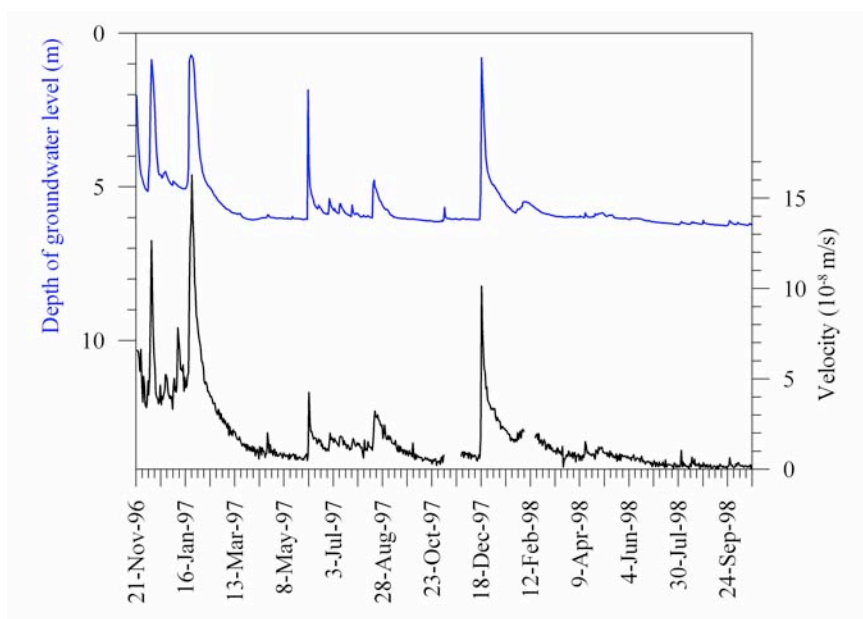


**Figure 188:** Piezometric record (blue line) and landslide velocity (black line) at borehole S2 of the Vallcebre landslide (from Corominas et al., 2005). Note the remarkable correspondence between the water level and the landslide velocity.

### Limitations

- The technique is not useful to locate the depth of the sliding surface, or to detect the existence of several sliding surfaces. The location (and number) of the sliding surface(s) should be determined by using other technique. Also on this matter, the wire extensometer complements very well the inclinometer.
- Anomalous wire measurements can be expected in case of freeze-thaw episodes of the upper soil layer whether the anchoring of the pulley system is not deep enough.

### 7.2.3 3D displacement monitoring gauges: TM71 advantages and limitations

#### Advantages

- Fully mechanical tool water/soiling proof.

- Very precise results in 3D. The accuracy of the device reaches up to about 0.05 to 0.0125 mm in all three axes x, y, z. A new version of the TM 71 device provides very accurate rotations up to  $3.2 \cdot 10^{-4}$  radians as well.
- Excellent tool for monitoring of initial and/or slow landslides, topples, initial rockfalls and active tectonic movements.
- Could be extended to provide remotely controlled operation and data transfer.

### **Limitations**

- Not applicable for rapid landslides with displacement higher than few cm/year.
- Results could be influenced by the diurnal and seasonal changes of temperature at the ground surface, and thus must be properly corrected or emplaced in a thermally stable environment like deep caves or artificial galleries.
- Applicable only for a single joint or crack.

## **7.2.4 DMS systems: advantages and limitations**

### **Advantages**

Advantages of the DMS systems compared to traditional in place instrumentation are several, in particular:

- There is no need for inclinometric pipe with 4 grooves.
- Simultaneous multiparametric monitoring in the same casing/borehole, extended to the overall landslide/rockslide body domain. Through the multi-parametric data it's possible to obtain the parameterization of stability of landslides and their geotechnical modelling, in order to design potential remediation activities, control during the execution, and verify the effectiveness of the engineering works in different pluviometric conditions.
- The system allows, in an innovative way, a forecasting analysis of landslide movements already in the first evolutionary phases of the micro movements directly along the sliding zone, before reaching the paroxysmal phase, an aim which is not reachable with traditional monitoring systems.
- 2D/3D deformation analysis. D.M.S. 3D system has been specifically studied for 3D measurement in drilling holes, so as to record deformations directly on rocks or soils, and to execute multipiezometric measurements in the same monitoring hole. The system is composed of modules (E.D. 80 millimetre, with packers for direct hole anchorage), linked by special 3D flexible joints with high traction resistance (up to 100 KN) and maximal extension  $> \pm 100$  mm/module.
- Digital RS 485 continuous monitoring H24 (compared to the analog systems) suitable for Early Warning applications including self tests on board and functionality checks that guarantee a reliable monitoring
- High adaptability of the monitoring column to deformations. High space resolution of measurements. The reduced dimensions of the containers units (min = 0.3m) allow a remarkable improvement in the space resolution for the study of located discontinuities, compared with the devices at present on the market (in place inclinometer).
- Robust mechanical construction thanks to stainless steel material AISI 304 or marine AISI 316L and a Joint traction available in the interval 10-100 KN.
- Easy installation in place, and possibility to recover the instrumentation after the monitoring period. At the end of the monitoring period the multi parametric column can

be extracted and installed into different drilling holes with no necessity to disassemble the modules in lab. The system is fully retrievable.

- Modularity and cost reduction. Modularity of container units and joints, joined to the possibility of making the multiparametric monitoring in the same drilling hole, allows a considerable reduction of construction, installation and management cost of the system.
- Early warning full system. For high risk areas it's possible to use an acquisition system in continuous through a control unit which allows data transmission to Technical Services by means of a wireless line. The system allows also an automatic/manual management of 4 incremental alarm thresholds and the automatic/manual activation of acoustic and visual alerting alarms directly at the site monitored. In real time and in remote mode the monitoring staff can verify on receipt of the alarm message, the instability situation by means of the related management software and decide the civil protection measures. The device allows an innovative forecasting analysis of displacement, for civil protection purposes.

### **Limitations**

Main limitations of the DMS systems include:

- The weight of the DMS column does not allow to install manually for length more than 15 m in the 2D version, where a specific machine DMS Reeler or the suspension of a helicopter is necessary.
- The cost of the instrumentation, especially for long systems planned for Early Warning with breaking risk.

### **7.2.5 GB-InSAR: advantages and limitations**

#### Advantages:

Thanks to the new improvements in the technique, especially in the hardware component, GB-InSAR can now be considered a valuable instrument for an early warning system (Casagli et al., 2009), being able to acquire data every 3 minutes, in the best conditions. This represents an important feature in comparison with satellite interferometry, which still has a much worse temporal resolution, measurable in days. The main advantage of this technique is probably that it merges rapid mapping together with near real-time monitoring, which allows one to characterize and follow the evolution of the landslide both in spatial and temporal terms.

Millimetre accuracy on surface motion and deformation can be exploited. The spatial resolution, depending mainly on the distance from the target, usually ranges from few decimetres to few meters.

Another characteristic that enables the use of the GB-InSAR as an early warning tool is its capability of working automatically, continuously and in all weather conditions. Since it performs a remote sensing monitoring, it can be adopted even in cases where a direct access to the unstable slope can be too dangerous or difficult.

Ground-based radar can also be employed in narrow valleys or with steep slopes where satellites can hardly collect information. Furthermore, in a given area, GB-InSAR has a much higher density of measuring points than DInSAR, as it does not require the presence of Permanent Scatterers.

Although the most used band is Ku, many GB-InSAR are able to use several microwave bands (as for satellite interferometry), making them versatile tools.

In the last years more research centres and societies started to produce GB-InSAR apparatuses; this increasing diffusion will favour (and already did) the development of new software, innovative applications and hardware improvements.

#### Limitations:

The GB-InSAR technique suffers from some limitations. One of these is that it is not suitable for monitoring rapid landslides. Only recently it has been possible to monitor movements as fast as 3 m/day.

With respect to satellite interferometry, ground-based interferometry has the same problem of measuring displacements only along the line of sight; moreover the investigated area is much smaller (slope scale) and requires an installation point with certain characteristics: it must be stable, big enough to contain the whole system (which usually requires a 2-3 m long rail), it must be provided with a sufficient power supply, placed in front of the slope and aligned with the direction of movement as much as possible. For the reasons explained above it is not usable for detecting vertical movements or for monitoring horizontal areas (which could be affected by subsidence, for example).

The maximum distance at which the monitoring is proficient is around 4 km, but can vary depending on the atmospheric conditions. In fact, although GB-InSAR is able perform measurements even in bad weather conditions, atmospheric effects can produce noise on data gathered, especially if the distance is high.

Densely vegetated areas represent a problem as they do not maintain coherence.

Another limitation may be represented by the cost, which is currently high.

### **7.2.6 Terrestrial laser scanner: advantages and limitations**

#### **Advantages**

TLS provides high-resolution point clouds over the entire area of interest and can be applied to all types of landslides (slides, topples, falls, flows, lateral spreads, complex mechanisms) (see D4.4) provided that their morphologic expression is visible on the terrain and that the landslide displacements lead to topographic changes.

- Various analyses are possible using TLS data (mapping, structural analysis, surface roughness measurement, volume computation, mechanism, monitoring, spatial failure prediction, modelling, etc.).
- Most TLS instruments are portable, battery-powered and easy to set up, which make TLS applicable to many site settings.
- For most applications no fixed scan position is needed and TLS point clouds can be georeferenced using ground-control points or existing DEMs. Multi-temporal TLS acquisitions can be directly aligned on the reference point cloud, which reduces alignment and georeferencing errors (Oppikofer et al., 2009).
- TLS is a reflectorless and contactless surveying technique (no reflectors or targets needed on the scanned surface), which is very useful in the investigation and monitoring of hazardous or inaccessible landslides and rock walls.
- Data acquisition and treatment can be very quick in emergency situations (e.g. Jaboyedoff et al., 2009a).

### **Limitations**

- TLS needs a direct line-of-sight between the scanner and the landslide, which can lead to occlusions on rugged landslide topographies and irregular coverage and point density. These occlusions impede to obtain a complete landslide displacement field (e.g. Kasperski et al., 2010) and introduce biases in the structural analysis (Sturzenegger et al., 2007; Sturzenegger and Stead, 2009a; Lato et al., 2010).
- Being an optical technique, TLS is influenced by meteorological conditions (air temperature and humidity) and the reflectivity of the scanned surface is greatly reduced when wet. TLS acquisitions should thus only be made under good, stable weather conditions.
- The accuracy of a single point measurement by TLS (relative XYZ coordinates of a point) is around 1 cm and thus significantly higher than comparable optical techniques (e.g. total station). This lower accuracy is however counterbalanced by the high point density.

### **7.2.7 High-resolution terrestrial optical images correlation: advantages and limitations**

#### **Advantages**

A general advantage of correlation of terrestrial optical images for characterizing the surface displacement is the possibility to obtain spatially-distributed information (e.g. velocity maps, displacement maps, deformation maps) without ground based monitoring. It offers also the possibility of retro-analyses of past phenomena if an archive of photographs exists for the area of interest.

The methodology is low-cost as standard CCD cameras (1000-2000€) can be used taking into account that certain pin connections have to be available on the camera for a control by a data logger or a laptop, and it is a very suitable alternative for inaccessible landslides or areas without access to power supply.

The methodology can be very precise: generally, the 2D displacements (in pixel) evaluated by the correlation algorithm have an accuracy of about 0.2 pixel (Casson et al., 2005; Delacourt et al., 2007) in the image plane, corresponding to an accuracy of millimetres to several centimetres for distances of about 100 m in the local coordinate system (Kraus & Waldhäusl, 1994).

The technique can be easily implemented in permanent monitoring systems and it is particularly interesting for monitoring landslides characterized by annual pluri-decimetric displacements. Furthermore, because the proposed methodology does not require ground control points except for determining the external orientation of the camera and for combining displacement pattern observed in image pairs acquired over two years, the methodology can be routinely and automatically applied to new pairs of images. Therefore this technique offers very promising perspectives for operational applications which can be potentially integrated into early warning systems.

Finally, other parameters than the displacement field can be obtained by inversion of the velocity field such as the strain distribution and the macroscopic rheological properties of the landslide material.

#### **Limitations**

The major limitations affecting the displacement calculations and thus potentially limiting the efficiency of this technique for an operational landslide monitoring can be classified in two

---

groups: (i) the parameters affecting the Image Correlation computation and (ii) the external parameters influencing the orthorectification procedure (mainly the position of the camera with respect to the monitoring area).

The orientation of the line of sight (depending on the location and orientation of the camera) to the ground surface has to be considered before installing a permanent monitoring system. Areas of low incidence angles ( $< 5^\circ$ ) are very sensitive to small movements of the camera. Therefore, the angle should be the most perpendicular as possible to the mean displacement vector of the landslide.

The strongest limitations are independent of the acquisition system and are related to the meteorological and illumination conditions and the ground surface changes inducing partial or complete loss of coherence between pairs of images. The presence of snow impedes reliable correlation results and excessive ground deformations between two consecutive years impede valid displacement measurements even if the images are acquired during the same solar time.

The small changes in the camera orientation and the use of a constant DEM are the most important parameters that affect the accuracy of the orthorectification of the displacement field. A regular acquisition of multi-temporal DEMs through airborne or terrestrial laser scanning or stereoscopic photogrammetric views is believed to be a priority to significantly improve the accuracy of the technique. The errors induced by the sub-pixel correlation algorithm are often insignificant compared to the influences of the other parameters cited previously.

### **7.2.8 Seismic monitoring: advantages and limitations**

#### **Advantages**

A general advantage of micro-seismic monitoring on landslides is the possibility to analyse (and understand) from a mechanical viewpoint the failure processes and to search for precursory patterns to material failure. These sub-audible noises can be detected over distances of several tens of meters in hard rocks but are attenuated below detectable level into less than 30m in soft rocks and soils. As a consequence, arrays of conventional seismic geophones on the ground surface near the most active parts of mass movements can provide information about their geometry and dynamic.

According to the rheology of the landslide material, its dynamics and the geometry and characteristics of the monitoring array, seismic monitoring may provide precise information on the spatial and temporal distribution of slide quakes (e.g. forecast) and on the released energy and focal mechanism (e.g. mechanism understanding).

#### **Limitations**

The major limitations affecting the use of seismic monitoring on landslides is the attenuation of seismic waves which may necessitates the installation of a dense array of instruments on the landslides to detect low magnitudes events, and to precisely locate the source. Detailed analyses necessitate the use of relevant 2D or 3D P and S waves models to characterize the sources, especially on ductile materials.

An important limitation is also the maintenance of the equipment in the field which is complex and necessitates a very good coupling between the geophones/seismometers and the material and the location of the array as closest as possible to the most active parts of the landslide. In the absence on a priori knowledge on the slide quake events, very detailed

analyses on the spectral features and the amplitude-versus-time of the signals have to be carried out to characterize the different types of events.

### **7.2.9 Optical fibres: advantages and limitations**

#### **Advantages:**

- Small size and small weight;
- High sensitivity (temperature, strain);
- Immunity to electromagnetic interference;
- Possibility to perform distributed sensing (high number of sensing point, continuous monitoring in a whole area);
- At present this technique is at an experimental stage, in perspective its effectiveness and reliability could be increased.

#### **Limitations:**

- Fragility (optical fibres need to be protected by suitable cabling);
- The installation in soil is not trivial (necessity to transmit strain while preserving fibre integrity);
- Complex interpretation of the results (distributed sensors provide a wealth of data, but interpretation is not always straightforward);
- Temperature-strain cross-sensitivity (if temperature and strain change simultaneously, it is necessary to adopt a method to discriminate the two effects);
- Cost of the interrogation system (but in distributed sensing the costs per measurement point are lower).

### **7.2.10 TDR: advantages and limitations**

#### **Advantages:**

- Fast and reliable measures;
- Small disturbance to the investigated soil;
- Ability to determine moisture profiles with a single measurement using inverse methods for processing data;
- The equipment can be easily adapted to automatically acquire the in situ soil water content.

#### **Limitations:**

- For quantitative measurements a calibration is necessary to determine the relationship between volumetric water content and permittivity;
- High attenuation of the signal for a length of the probe greater than 50cm;
- Long processing time to estimate the moisture profiles with the inverse method.

### **7.2.11 Geoelectrical monitoring: advantages and limitations**

#### **Advantages**

- Continuous and simultaneous monitoring of principal geoelectrical parameters along the landslide mass, i.e.: ground resistivity, self- (or spontaneous-) potential and induced
-

polarisation could indirectly provide important information on internal parameters of the landslide (e.g. geometry of ground water bodies, saturation/porosity/compaction, conductivity of pore fluid and clay content, and their spatial and temporal changes), which could provide information about impending triggering of a landslide even prior to recordable displacements.

- The current state of the art of geoelectric instrumentation allows the necessary high speed of data acquisition and recording of the full receiver signal, which both are necessary to guarantee high quality data and to perform noise analysis.
- Fully remote-controlled data transfer and instrument maintenance via the GPRS and/or the Internet (measurement results, test sequences and log files, containing information about system and GPRS connection status) is available at low cost and reliable quality almost everywhere in Europe; Consequently, immediate availability of information for local stakeholders can be guaranteed.

### **Limitations**

- For a reasonable data interpreting, the geoelectrical monitoring should be complemented with displacement and hydro-meteorological data and needs to be corrected for diurnal and annual temperature effects.
- There is still a significant lack of case studies allowing a sufficient comparison of permanent geoelectrical measurements with displacement data on several types of landslides.
- This method is not appropriate for fast moving landslides (especially if differential movements happen perpendicular to the survey line), since in such a case electrode distances will change with time, making routine processing of the data very difficult (the electrode positions need also to be recorded). However currently some approaches are being investigated (e.g. Wilkinson et al., 2010).
- Until now, there is a critical lack of inversion routines that could handle permanent monitoring data adequately. Some commercial codes (RES2DINV and AGI EearthImager) were tested but did not lead to satisfying results in many cases. Several attempts to solve this problem are currently undertaken by different groups (e.g. within the project “TEMPEL” of the Austrian Academy of Sciences (Geological Survey of Austria and J.H. Kim, duration 2010-2013).

### 7.3 NEEDS FOR RESEARCH AND FUTURE DEVELOPMENTS

The role of scientific research in guiding the technical and technological progress is established once more for ground based monitoring of landslides.

Ground based monitoring systems have been interested by several and relevant improvements during recent years. Many of these new developments have already been consolidated in operative scenarios but enhancements are proposed at a fast rate as scientific research continuously push ground based techniques further, testing them in unattempted and "extreme" conditions and new solutions are found to solve the encountered problems or to reduce the known limitations.

In general ground based methodologies provide an evaluation of the displacement either at the topographic surface or below ground (Table 11). Similarly, a distinction could be made between techniques providing information at a single point or capable to investigate wide areas (Table 11). Gaining a complete understanding of a landslide would require the coupling of these different features (monitoring of its behaviour as at depth as at surface and over the entire landslide body). These features are currently present only in methodologies (seismic monitoring and geoelectrical monitoring (Table 11) that need a relevant work of interpretation of the result.

As a consequence, the coupling of different monitoring techniques will still be necessary in the years to come in order to gain a full insight in the behaviour of large landslides.

**Table 11. Partition of the ground based monitor techniques according to the typology of information provided (superficial/deep and punctual/areal).**

	<b>Superficial investigation</b>	<b>Deep investigation</b>
<b>Punctual information</b>	GPS 3D displacement monitoring gauges Wire extensometers	Automatic inclinometers TDR (few meters max.)
<b>Areal information</b>	GB-InSAR Terrestrial Laser Scanner Optical images correlation	Seismic monitoring Geoelectrical monitoring Optical fibres (few meters max.)

In the following part of the chapter, some limitations common to all the ground based techniques are identified which could be rapidly addressed by researchers and technicians to obtain a consistent increase in the effectiveness of the ground based monitoring systems. The prospected developments could be considered a sort of guideline for the research in this field in the next few years.

#### **Toughness**

Breaking strength and tensile strength are never enough for ground based instrumentation, since it is exposed and should endure every kind of solicitations. The latter include not only thumps and tractions, but also the wearing induced by humidity, water (rainfall, flowing water and backwater), soiling and extreme temperatures. As a consequence the casing of the instrumentation and the various installed components could be improved in terms of employed materials and construction technique to be adaptable to a wider range of ordinary operative conditions and to resist extraordinary circumstances without interrupting the monitoring.

**Freeze-thaw**

At particular latitudes and/or altitudes, freeze-thaw cycles represent a relevant problem. Not only for the already mentioned wearing of the instrumentation, but also because contractions and expansions in the instrumentation (and in case also in the monitored rock mass) can induce errors in the measurements. Several attempts to correct the distortion of the measures on the basis of the temperature already exist, but this is certainly a point which could benefit further improvements either by means of algorithms and softwares or by establishing empirical correlations between temperature and actual displacements. The problem of the contraction/expansion and wearing of the instrumentation could be reduced improving the materials and the construction of the instrumentation.

**Lightening of the equipment and easy installation**

One of the main drawbacks of all the ground-based monitoring techniques is that the landslide (or a location with a clear line of sight) must be physically reached by the instrumentation and by the personnel for the installation and the maintenance works. Therefore, a reduction in the size and weight of the instrumentation, the reduction of cables (progressively substituted by wireless technologies) and every other expedient to ease the installation process would be very helpful and could widen the range of possible applications.

**Remote control**

Ground based applications would benefit from every improvement aimed at reducing the necessity of physically reaching the site of investigation. Therefore, it is expected an improvement in the possibility of remotely setting the instrumentation, acquiring measures and sending the collected data.

**Power supply**

Another relevant issue that should be addressed is the need to supply the necessary amount of energy even to the most complex monitoring systems. Photovoltaic panels' efficiency is constantly increasing and new alternative technologies have been and hopefully will be proposed (e.g. methanol or hydrogen fuel cells).

**Software improvements**

In several emerging ground based techniques a key role is played also by a software component. Hopefully this field will experiment continuous improvements to get in the shortest time the most reliable data possible. New software tools could be created and existing softwares could be optimized to handle systematic errors and it is not excluded that already existing software/algorithms could be adapted to other instrumentations with some adjustments.

**Standardisation**

In the perspective of an increasing use of integrated monitoring/early warning systems in which several different methodologies are managed by a common platform, it could be useful to make the various monitoring techniques able to produce immediately comparable results in terms of units of measure. The use of a common standard (International System) would lighten the automated conversion routines carried out by the integrated monitoring and early warning softwares.

**User-friendly post-processing**

Many emerging ground based instruments provide raw data that need to be post-processed. In some circumstances, especially when very accurate measurements are needed, the data processing could be rather sophisticated. This means a longer time to get the final data and the need of highly trained and expert personnel. The optimisation of the post processing softwares and algorithms, the building of easier to understand systems and easily manageable interfaces are goals that could contribute to get more accurate results from a broader audience.

**Interpretation of the results**

This point is closely linked to the previous one. Some of the emerging ground based techniques do not immediately provide a displacement measure. In turn, their output is another physical factor that needs to be interpreted by expert personnel. This problem is especially relevant for the recently proposed methodologies, which can still be considered on a test phase. In the next few years, research is expected to produce a high number of case studies including different landslide typologies in different physical settings. With time, as the growing number of test cases will help to get a faster, easier and more objective interpretation of the outcomes, research applications will hopefully become well established and could be more broadly used.

**Lower prices**

When using punctual methods (Table 11), permanent monitoring of large areas requires the installation of several devices, therefore at present in such conditions these techniques are still considered expensive and cutting the prices could be an important motivation.

In the framework of all the prospected improvements, the lowering of the prices could be considered unlikely if not impossible. This is true especially for the brand new technologies and the most up-to date technical and scientific answers to the needs of the research. But as a technique experiences some progress, older versions of instrumentations and softwares would hopefully reduce their price.

## **8 EVALUATION OF AIRBORNE AND SPACEBORNE TECHNIQUES**

*UNIFI: Tofani V., Segoni S.*

*with the contribution of all the partners*

This chapter contains the evaluation of the performance of each airborne and spaceborne technique with respect to the various landslide types (as defined by Cruden and Varnes, 1996).

For each landslide type, it is discussed which recent and emerging technology can be used, which advantages and disadvantages it provides, which methodology is more appropriate.

As for ground based techniques (chapter 7), in recent years airborne and spaceborne techniques have been interested by several technical and scientific improvements. That has not led to clearly identify a technology which can be undoubtedly and universally considered better than others. Conversely, the reliability and effectiveness of every airborne and spaceborne technique have been enhanced, providing for each geological problem a wide range of equally good solutions. As a consequence, at present end-users can select the most proper methodology with respect to their specific needs, which can be related to technical issues, economic budget, environmental factors and specific features of the landslide(s) to be monitored. This issue is also addressed by the SafeLand deliverable D4.4 and this chapter is limited to provide a list of the most effective methodologies with respect to the various landslide types (8.1). In addition, the main advantages and limitations of each technique are listed as well (8.2), providing end users with a support for the selection of appropriate airborne and spaceborne techniques for their specific needs.

It should be also stressed that the various proposed methodologies should not be seen one in competition with the other ones; in contrast many of them could conveniently be used in close cooperation to obtain a very effective monitoring system.

## 8.1 LANDSLIDE TYPES

This chapter contains the evaluation of the performance of each airborne and spaceborne technique with respect to the various landslide types (as defined by Cruden and Varnes, 1996). This evaluation can be considered a first crucial step towards the choice of the methodology to adopt for monitoring or detection/mapping purposes, as it allows narrowing down the number of possible solutions to a smallest cluster of techniques which grant high-quality results (Table 12).

**Table 12. Evaluation of the effectiveness and reliability of the emerging airborne and spaceborne techniques for the monitoring and detection/mapping of different landslide types.**

Technique		Effectiveness / reliability				
		slides	topples and falls	flows	lateral spreads	complex mechanisms
Aerial sensors	Detection and mapping	High	Medium (ALS)	High (optical)	Low	Medium
	Monitoring	High	Low	Low	Low	Medium
Satellite, optical	Detection and mapping	High	Low	Medium	Low	Medium
	Monitoring	High	Low	Medium	Low	Medium
Satellite, radar	Detection and mapping	Medium	Not applicable	Medium	Medium	Medium
	Monitoring	High	Not applicable	Medium	Not applicable	Medium
Airborne geophysics	Detection and mapping	Medium	Low	Medium	Low	Medium

### 8.1.1 Slides (rotational and translational)

Generally speaking, almost every airborne and spaceborne technique described in chapter 3 is considered highly effective for the monitoring of slides. All of them can also produce reliable assessments in the detection and mapping phase. As explained in chapter 7.1.1, this judgment is due to the fact that rotational and translational slides are typically associated to a wide range of velocities ranging from medium to very slow and they could be found in very different lithological and geological settings.

Chapter 6.1 shows how some of the emerging airborne and spaceborne techniques have been used to study slides (or complex/composite landslides that encompass a relevant sliding component) in the framework of the SafeLand project (Table 10). In particular, detection and mapping applications can be evaluated in chapters 6.2.2 (satellite optical), 6.2.3 (satellite radar), 6.2.5 (airborne geophysics), 6.2.6 (airborne geophysics); while 6.2.7 reports the monitoring of rockslides using airborne geophysics and 6.2.8 the monitoring by means of satellite radar of a composite landslide with a relevant sliding component.

### **8.1.2 Topples and falls**

This type of movements is mainly characterised by brittle deformations in hard rocks, usually occurring in very steep (or sub-vertical) slopes and usually result in high or very high velocities. All this physical features hamper the application of mobile platforms to the detection\mapping and to the monitoring of this type of landslides. As a consequence, all techniques are generally credited to lead to scarcely reliable assessments or even to not be applicable at all (Table 12). In general, ground based technologies should be preferable for the detection\mapping and for the monitoring of topples and falls, as they grant more reliable performances than mobile platforms.

Despite that, chapter 6.2.1 reports an interesting and successful application of remote sensing to rockfalls, where the used device is an offshore laser scanning.

### **8.1.3 Flows**

The reliability and effectiveness of airborne and spaceborne techniques in the monitoring and detection/mapping of flows is hard to undoubtedly define. The flow typology is very heterogenic and encompasses very slow movements and very rapid flows (such as debris flows) as well. If the latter are excluded (no existing technique is capable of effectively monitor them or to identify them in real time), every airborne and spaceborne technique could be considered capable of obtaining satisfactory results in the monitoring and detection/mapping of flows. Table 12 reports a “medium” reliability score as an average of these two extremes.

Chapter 6 reports several case studies where flows are taken into account. In 6.2.2 and 6.2.3 satellite optical and satellite radar (respectively) are used to detect and map various typologies of landslides, including flows. The case of the mapping survey of a huge debris flow by means of airborne geophysics is contained in chapter 6.2.4; the same technology is also the object of the mapping of various landslides (including flows) in chapter 6.2.5 and 6.2.6.

An example of the monitoring performance of satellite radar in a complex landslide which includes a relevant flow component is included in chapter 6.2.8.

### **8.1.4 Lateral spreads**

The effectiveness of airborne and spaceborne techniques in detecting, mapping and monitoring lateral spreads is generally considered medium or low (Table 12). Unfortunately, no case study concerning lateral spreads is reported in chapter 6.2.

### **8.1.5 Complex mechanisms**

Complex and composite landslides can be generally detected, mapped and monitored with satisfactory results with all the techniques discussed in chapter 3.

Chapter 6.2.8 reports an application concerning the monitoring of a huge complex landslide with satellite radar, while chapters from 6.2.2 to 6.2.6 are centred on various detection and mapping techniques in test cases characterised by the presence of several landslides, including the complex typology.

Anyhow, since in complex and composite mechanisms different types of movement contribute to the landslide, a correct assessment of the best monitoring technique requires to

analyse every single mechanisms separately. Therefore, the previous chapters (8.1.1 to 8.1.4) could be again considered as a reference.

## **8.2 ADVANTAGES AND LIMITATIONS OF AIRBORNE AND SPACEBORNE TECHNIQUES FOR LANDSLIDE DETECTION AND MAPPING**

In the light of the recent developments discussed in chapter 3.1, this chapter synthesises the main advantages of each technique and the open issues and the general drawbacks which still affect them. Each following subchapter is devoted to a specific ground based technique and it was composed by the same authors in charge for the recent trends description reported in chapter 3.1.

### **8.2.1 Aerial Sensors: advantages and limitations for landslide detection and mapping**

The new trend of using UAV (Unmanned aerial vehicles) to get aerial acquisitions has a lot of advantages: UAV can fly under clouds levels, acquiring scenes at a very high resolution (~cm) from classic sensors. Moreover, as sensors can be oriented in many directions, changing the look angle, acquisitions in vertical contexts (i.e. cliffs) are better than traditional airplane photos. There is another useful advantage: as UAV involve less organization, devices and people than airplanes, delays between a catastrophic event, for example, and the scenes acquisitions can be very short; furthermore, campaign are less expensive. Nevertheless, two major limitations have to be underlined: first, UAV are less stable than planes that limit the application for classic photogrammetry, which requires the knowledge of the exact attitude and altitude of the platform; second, this method is only suitable for small areas due to the size of acquired scenes that involves the low altitude during fly.

Regarding InSAR processing from aerial SAR acquisitions, researches have to improve the technology in order to be able to apply it for the monitoring of slow displacements. Indeed, the bad stability of aerial platforms is up to now the major limitation. Nevertheless, this is very promising, allowing acquisitions with very high resolution and with very short temporal and geometrical baselines. As a consequence, processed InSAR scenes can be more reliable with better mean coherence indexes, thanks to these improved acquisitions which drastically decrease noise and decorrelation sources (Bamler and Hartl, 1998; Massonnet and Feigl, 1998).

Finally, all enhancements and optimizations performed within new software and algorithms are looking for the same objectives: being less time consuming with steadily more automatic and robust steps thanks to the enhanced algorithms (Nichol and Wong, 2005; Dymond et al., 2006; Joyce et al., 2008a, 2008b, 2009; Nagai et al., 2009), and giving available tools allowing new types of interpretations of huge dataset thanks to the newest software (Guzzetti et al., 2002; Crosta and Agliardi, 2003; Huggel et al., 2003; Dorren et al., 2006; Jaboyedoff et al., 2007; Lan et al., 2007; Frattini et al., 2008; Horton et al., 2008; Ferrero et al., 2009; Loye et al., 2009; Sturzenegger and Stead, 2009; Gigli and Casagli, 2011; Jaboyedoff and Labiouse, 2011; Michoud et al., submitted). Nevertheless, some of them are still too much processing time consuming (especially for runout assessments) and sometimes, very high resolution dataset, such as ALS-DEM, have to be degraded before processes. Finally, a last precaution has to be mentioned: they will never replace the capability of experts, but they will have to be used as tools, with their own advantages and limitations.

## **8.2.2 Satellite optical: advantages and limitations for landslide detection and mapping**

### **Advantages of new sensor systems**

With the increasingly large fleet of VHR satellites imagery can be acquired timely after major events and with daily temporal resolution at nearly global coverage. The main advantage of VHR imagery is the great density of spatial information, whereas, with more competing satellite operators entering the market, prices constantly decrease. A main advantage of optical datasets are their synergetic values for several other applications such as post-disaster damage assessment and updating of land cover maps and corresponding archives are often available over a given area.

### **Limitations of new sensor systems**

A greater diversity of platforms increases the chance to acquire cloud free imagery of a given area with a specified time frame but atmospheric conditions remain an important factor that, depending on the climate zone and the season, may delay the acquisition of suitable images considerable. For this and other reason satellite tasking for sub-meter images can still be associated with considerable costs.

Higher spatial, spectral (e.g. WorldView-2) and temporal resolutions strongly increase the computational load for the storage and analysis of the datasets. Especially for mappings over wider areas this can slow down the analysis considerably and may make further investments in hardware and software indispensable. This is closely related to the desirable exploitation of spatial context which is typically computational intensive.

Finally it should be noted that the diversity of new space borne platforms exploded in recent years, whereas the number of studies to assess the quality and uncertainties of resulting maps did not hold pace with the technological development. Very few studies compare mapping results among different optical dataset (Joyce et al. 2009) and more careful evaluations of the comparability, uncertainties and the consistency of time series among landslide inventories and deformation maps from different sensors are needed.

### **Advantages and limitations of state-of-the-art analysis methods for optical data**

Pixel-based change detection (typically image differencing) is relatively easy to apply and can be accurate in situations where most surface changes are caused by landslides. In many cases it might also be possible to account for sensor and illumination differences by cross-calibration and image transformation. However, only limited accuracy can be expected from such approaches in situation where other similar surface changes such as deforestation or barren fields are present in the same scene. The selection of an appropriate threshold to distinguish between changed and unchanged areas remains as a general difficulty for the application of such methods. Further problems are usually encountered when pixel-base change detection is applied on VHR imagery because of the higher spectral variance and stronger impacts of small co-registration errors.

Due to a better exploitation of the spatial context within remote sensing images OOA approaches generally yield better results than could be achieved with per pixel analyses (cf. Blaschke 2010). It has been demonstrated that OOA rule sets are not only capable to accurately delineate affected areas but can also be used to distinguish among different landslide types (Barlow et al. 2006; Martha et al. 2010a). One major drawback of expert defined rulesets is still the large amount of manual thresholds defined by an expert. They need

considerable adjustment when the classification system is applied on a different scene. This complicates the transferability of the method to new study areas. In case where multi-temporal images and high-resolution airborne LiDAR DSMs are available the number of individual thresholds can be significantly reduced using image transformations and sample-derived rules (Lu et al. 2011). However, remaining thresholding still renders similar problems as encountered in the context of change detection. For a recent study which addresses such issues using machine learning algorithms we refer again to the SAFELand case study “Object-oriented landslide inventory mapping with VHR imagery using machine learning techniques” presented in 6.2.2.

### **8.2.3 Satellite radar: advantages and limitations for landslide detection and mapping**

With reference to landslide detection/mapping the most advantageous aspects of the multipass DInSAR approach are (Colesanti and Wasowski, 2006):

- The cost-effectiveness for wide-area (hundreds and thousands of km<sup>2</sup>) applications, typical of spaceborne remotely sensed data.
- The high density of benchmarks (up to several hundreds per km<sup>2</sup>).
- The use of “natural” benchmarks not requiring deployment and maintenance.
- The possibility of geo-locating the benchmarks with a precision in the order of 1–5 meters.
- The availability of the extremely valuable ESA ERS archive spanning about 20 years, which enables to carry out retrospective studies. Furthermore, the results of recent studies proved the feasibility of combining new radar data from ENVISAT within ERS data analyses, despite slight differences in critical image acquisition parameters (Duro et al., 2003).
- Regular revisiting time in the order of 20–40 days.

On the whole, the case studies described in the scientific literature highlight that with reference to the detection/mapping of slow-moving landslide phenomena the main benefits regard:

- the definition of the boundaries of already detected mass movements;
- the definition of the states of activity;
- the detection of previously unmapped unstable areas.

However, several limiting factors need to be properly taken into account (Colesanti and Wasowski, 2006):

- Displacement data represent the one dimensional projection in the Line Of Sight (1D LOS projection) of a deformation that can actually occur in all three dimensions (Rocca, 2003; Manzo et al., 2006).
- The ambiguity of phase measurements implies the impossibility to track correctly (i.e., unambiguously) the relative LOS displacement between two scatterers exceeding  $\lambda/4$  (=1.4 cm for ERS) within one revisiting time interval (35 days for ERS), i.e. approximately 14.5 cm/yr. In practice it is extremely difficult to detect LOS displacement rates exceeding 8 – 10 cm/yr in the presence of low density of stable scatterers, such as in the case of landslides where topography and vegetation introduce a limitation in the number of detected scatterers. This limits the use of DInSAR data

only to landslides ranging from extremely to very slow phenomena according to the velocity classification of Cruden and Varnes (1996).

- Limited versatility in terms of (a.) positioning of the measurement points and (b.) revisiting time. Both factors (a.) and (b.) cannot be optimized as degrees of freedom while planning an analysis.
- Finally, it is still difficult to forecast the coherent pixel density in rural areas without carrying out at least several processing steps on a significant number (15–20) of SAR images.

For sake of completeness it is worth stressing that, when dealing with a single landslide analysis, many of the mentioned limitations associated to space-borne DInSAR can be overcome by ground-based differential SAR interferometry GBDInSAR (Canuti et al., 2004; Leva et al., 2003; Tarchi et al., 2003).

Following these suggestions and according to the velocity scale proposed by Cruden and Varnes (1996), Table 13 summarizes the present capability of space-borne and ground-based SAR interferometry to assess different landslide displacement rates (Metternicht et al., 2005).

**Table 13. Capability of spaceborne and ground-based SAR interferometry to assess different displacements rate (after Metternicht et al., 2005).**

Class	Description	Speed	Speed (m/s)	Satellite DInSAR	GB DInSAR
1	Extremely slow	16 mm/year	$5 \cdot 10^{-10}$	Yes	Partly
2	Very slow	1.6 m/year	$5 \cdot 10^{-8}$	Partially	Yes
3	Slow	13 m/month	$5 \cdot 10^{-6}$	No	Yes
4	Moderate	1.8 m/h	$5 \cdot 10^{-4}$	No	Partly
5	Rapid	3 m/min	$5 \cdot 10^{-2}$	No	No
6	Very rapid	5 m/s	5	No	No
7	Extremely rapid			No	No

The case study presented hereafter deals with the abovementioned points following an ongoing research activity that UNISA has been developing jointly with IREA-CNR since 2005.

#### 8.2.4 Airborne geophysics: advantages and limitations for landslide detection and mapping

##### Advantages

Airborne geophysics is a new promising method for landslide investigation. The main advantages of this approach are, i.e.:

- The big advantage of airborne geophysical measurements is that large areas can be surveyed within relatively short survey times. Although the use of helicopters seems to be quite expensive, the method is very effective since several different sensor systems of different kind can be combined, which acquire all data at the same time and at the same location. If a comparable amount of data had to be acquired on the ground, the cost would be even magnitudes higher as with airborne geophysics, if large areas have to be investigated.
- Airborne electromagnetic is the only remote-sensing method which is able not only to survey near surface parameters but to investigate geological structures below the ground surface down to several hundreds of meters.
- Airborne electromagnetics recognizes lithological units with different clay content, porosity and water content at different depths.

- Radiometry, in general, investigates the radioactive content in the soil at the ground surface and it could be applied for reconstructing source areas of mass-movement deposits (U, Th, K), identifying open joints and cracks in hard rock (Th), fault zones in bedrock (U) or degree of chemical weathering (K).
- Ground resistivity and soil moisture could be new parameters for landslide susceptibility assessment and mapping.
- Suitable method for large landslides, earthflows, deep-seated gravitational deformations and for investigating their substrate.

### **Limitations**

- One major limit is terrain roughness: the ground clearance of the sensor needs to be below 90 m, which is very difficult to be kept. Consequently steep and rugged landscape can only be surveyed under the following conditions:
  - Well trained pilots for flying external cargo are needed, which are experienced in flying low altitude surveys;
  - Enough money is available to perform training flights with the system, to wait for optimum weather conditions and to repeat lines with bad data.
  - The engine of the helicopter needs to be strong enough (causing higher costs and a higher background noise level) to allow constant altitude flights in rough terrain.
- Worldwide, the number of available multi-parameter systems is quite limited. Consequently performing an airborne survey will require a significant time of planning in the forefront.
- Legislative regulation for flying with external cargo might differ from country to country; very limiting security regulations are expected for the future.
- This method is not economically feasible for surveying small sites (e.g. below some km<sup>2</sup>). For such small scale slides the application of multi-electrode geoelectric surveys might be cheaper and provides a higher resolution.
- Most inversion routines for AEM require 1D geometry (horizontal layering) of the subsurface. However most resistivity anomalies on landslides exhibit a 3D geometry and the 3D shape of topography (e.g. steep valleys, high cliffs...) cannot be accounted for. Therefore on interpreting airborne results one has to keep these limits in mind.
- AEM is very sensitive to electromagnetic noise caused, e.g., by power lines and electrical cattle fences.
- For gamma measurements, delicate algorithms for correcting the influence of vegetation and topography are needed which still need to be improved.
- For soil humidity measurements algorithms for correcting the influence of vegetation are not available.
- For proper interpretation of airborne (electromagnetic) result, calibration with ground geoelectrical measurements or other ground geophysical methods is highly recommended.
- There is a lack of case studies proving the usefulness of airborne geophysics for landslide investigation. Consequently several test sites are surveyed within SafeLand.

### **8.3 ADVANTAGES AND LIMITATIONS OF AIRBORNE AND SPACEBORNE TECHNIQUES FOR LANDSLIDE MONITORING**

In the light of the recent developments discussed in chapter 3.2, this chapter synthesises the main advantages of each technique and the open issues and the general drawbacks which still affect them. Each following subchapter is devoted to a specific ground based technique and it was composed by the same authors in charge for the recent trends description reported in chapter 3.2.

#### **8.3.1 Aerial sensors: advantages and limitations for landslide monitoring**

To date, aerial sensors are usually not used directly to monitor landslides. The monitoring that can be achieved with aerial sensors is more related to back-analysis of continuous phenomena or single events, comparing non-continuous datasets, such as aerial photos. However, as for the satellite optical monitoring, recent trends in aerial techniques concerning acquisitions and processings (see chapter 3.1.1) have a positive impact on monitoring too.

#### **8.3.2 Satellite optical: advantages and limitations for landslide monitoring**

##### **Advantages and limitations of new sensor systems**

The advantages and limitations of satellite optical for landslide monitoring are the same reported in 8.2.2. In particular it's worth noticing that the main limitations regards on the atmospheric effects, meteorological condition, sun illumination and orbital parameters; moreover the availability of archived VHR acquisitions is very limited and the temporal resolution is not always suitable as it around 20 days and only in specific conditions it can be reduced to few days on demand, moreover the different solar conditions of the two acquisitions and on the variation of surface state due to vegetation growth and anthropic modifications can invalidate the results.

##### **Advantages and limitations of state-of-the-art analysis methods for optical data**

The optical techniques for monitoring (change-detection time series, multi-temporal DEM generation and analysis, digital image correlation) have a potential to supplement and partially replace ground-based measurements. In particular, time series compiled from change detection are potentially useful to incorporate the historical occurrence of landslides, and to progress from simple susceptibility models to a hazard assessments that actually integrates the temporal dimension (e.g. Jaiswal et al. 2011).

Similar enhancements can be expected with methods that enable to extract landslide volumes and displacement rates from spaceborne optical imagery. However, still relatively few studies adopted such methods and further case studies are needed to validate derived volumes and displacement vectors. At present DIC has been applied in only in a few cases and only on satellite images from two time steps. Before the derived displacement vectors might be used as input for kinematic or hazard models further validation studies are necessary. The focus thereby should be the analysis of longer time series of satellite images and a rigorous comparison of derived displacements vectors against ground-based measurements.

### **8.3.3 Satellite radar: advantages and limitations for landslide monitoring**

A general advantage of space-borne images sub-pixel correlation techniques for mapping ground surface deformation comes from the ability to produce maps without ground based instrumentation and offers the possibility of retro-analysis of past phenomena if an archive of data exists for the area of interest.

Respect to space-borne optical imagery, SAR imagery is less sensitive to the weather conditions ensuring that all the acquired images can be used even if an important cloud cover affects the studied area. For our experiment, most of the planned images will be effectively consistent for the processing.

Current RADAR sensors propose interesting repetitiveness (11 days for TerraSAR-X, 8 for COSMO-SKYMED) allowing a good sampling for monitoring evolution of slide displacements consistent with such a sampling (slow landslides).

The precision is limited by the resolution of the data. With sub-metric resolutions, we can expect precision of about 5-10 cm in the best cases. The technique is therefore suitable only for displacement consistent with such value (dm between acquisition dates, if we do not apply stacking techniques to combine different produced deformation maps in order to improve the precision at the cost of a loss in the temporal sampling).

We have to notice that important displacements which consequences could be important changes in the local characteristics of the image could result in a loss of correlation (the technique is based on the identification of local similarities between the two images) and therefore a loss of the reliability of the result. Sudden and important displacements (>decametre) such as rock falls or flows are not the target of the method.

Respect to the optical data, the specific geometry of the SAR acquisition (sampled in azimuth/range) could be a limitation in areas with complex topography (shadowing/lay over effects).

In an operational (without reduced research prices for the data) multi-temporal applications, the price of the data (up to 6k€/images for TerraSAR-X data) could be a limitation. However we think that, in the medium term, the data providers would be able to propose prices more adapted to such applications.

### **8.3.4 Airborne geophysics: advantages and limitations for landslide monitoring**

Airborne geophysical survey is not enough reliable for landslide monitoring due to many technological, processing and financial restrictions. Currently the main applications regard landslide detection and mapping survey. However, it cannot be excluded, that if the technological progress would continue in the future, the method could be applied also for monitoring.

## 8.4 NEEDS FOR RESEARCH AND FUTURE DEVELOPMENTS

Satellite and aerial remote sensing provides a systematic and synoptic view of the Earth playing a fundamental role in acquiring the knowledge of the environmental phenomena in order to understand the history of land surface and predict several hazards. EO data are complementary with ground based networks data and in field observations for landslide analysis.

Currently the application of aerial and satellite remote sensing in landslide analysis is providing good and effective results as described in this deliverable. The contribution of remote sensing imagery, both optical and radar, has proved a powerful instrument for landslides mapping, monitoring and hazard analysis. Landslide mapping and monitoring has profited from the use of both optical and radar images, and especially the coupling of both can provide the best results. In fact, different source data and techniques can be approached depending of the size and velocity of the phenomena investigated.

Anyhow these techniques show some limitations and critical and weak points which have to be addressed by the researchers and technicians to obtain a consistent increase in the effectiveness of the landslide detection, mapping and monitoring.

The main challenge at this regard is the improving of the spatial resolution and the shortening of the revisiting time. The Cosmo-SkyMED (in X band) constellation which has been launched in 2007, has a short revisiting time (12 hours in the better case) such as ALOS mission (in L band) launched in 2006. Nevertheless, several years will be needed before these missions will provide achievements that could be effectively employed in multitemporal processing.

Improvements are expected in optical imagery from the development of Pleiades program by the CNES, scheduled from the beginning of 2010: it is tailored on civil security applications and it consists of two small satellites with a spatial resolution at nadir of 0,7 m with a daily access all over the world and a stereoscopic acquisition capacity.

The full operational use of all the satellite missions and the new ones already on board is outstanding to retrieve data and information tailored on the user's requirements in terms of short revisiting time, high spatial resolution and cost benefit.

In particular for each type of techniques the following specific developments have to be taken into account both for landslide detection/mapping and monitoring:

- **Aerial sensors**

- Despite the many advantages of using the UAV (unmanned aerial vehicles) in landslide detection, mapping and monitoring, some developments has to be addressed especially concerning the applications and the size of acquired scenes.
- Enhancements and optimizations of new software and algorithms in order to be less time consuming with steadily more automatic and robust steps.

- **Satellite optical**

- Decrease in computational time since the higher spatial, spectral and temporal resolutions strongly increase the computational load.
- Need of comparison of mapping results among different optical dataset and more careful evaluations of the comparability, uncertainties and the

consistency of time series among landslide inventories and deformation maps from different sensors.

- Further development of automatic landslide detection and mapping methods reducing as much as possible the manual component of the expert.
- Improvements of optical techniques such as Digital Image Correlation for the measuring displacement rates and landslide volumes.

- **Satellite radar**

- Extend the applicability of A-DInSAR to all type of movements and not only to landslides ranging from extremely to very slow.
- Increase the density of the persistent scatterers in rural areas.

- **Airborne geophysics**

- There is a lack of case studies proving the usefulness of airborne geophysics for landslide investigation; consequently several test sites are surveyed within SafeLand project in order to define the main limitations and the needs for future research.

## 9 CONCLUSION

In this deliverable the most innovative landslide monitoring and remote sensing technologies were reviewed and evaluated, with the aim to address their future scientific and technological developments.

Amongst all the ground based techniques employed in landslide studies, the ones which in recent years showed the most promising improvements were selected and reviewed, emphasizing the recent trends in their development and application and stressing the latest scientific and technological advances.

The same approach was pursued with remote sensing techniques, making a clear distinction between the use for detection and mapping and the use for monitoring purposes.

A relevant part of the deliverable was focused on the application of these innovative techniques within SafeLand case studies, clearly stating which technical and scientific improvements were achieved for each technique thanks to SafeLand project.

Additionally the current use of both ground-based and remote sensing techniques in Europe was evaluated by means of two questionnaires. These questionnaires were used to make a picture of how ground based monitoring and remote sensing technologies are used in landslide study nowadays. They were circulated within and outside Europe to Universities, Research Institutes, Public Institutions and Private Companies.

Based on the literature review, on the aforementioned questionnaires and on the results coming from the Safeland case studies, all the considered ground based, airborne and spaceborne techniques were evaluated listing their main advantages and limitations and highlighting the needs for research and future developments.

It's worth noticing that most of the other deliverables of the Area 4 (D4.3, D4.4, D4.6) are deeply linked to D4.5. In particular in order to avoid a strong content overlapping we make reference for an in-depth examination to the other deliverables:

- D4.1 "Review of monitoring and remote sensing methodologies for landslide detection, fast characterisation, rapid mapping and long-term monitoring", concerning the technical description of the ground-based, airborne and spaceborne techniques examined in this deliverable.
- D4.3 "Creation and updating of landslide inventory maps, landslide deformation maps and hazard maps as input for QRA using remote sensing technology", concerning the methodology for setting up and updating landslide inventories and for feeding and maintaining adaptive hazard maps, providing a common tool for updating these products at regional/catchment scale.
- D4.4 "Guidelines for the selection of appropriate remote sensing technologies for monitoring different types of landslides", concerning the selection of suitable remote sensing techniques by the stakeholders.
- D4.6 "Report on geo-indicator evaluation", concerning a more specific description of the parameters monitored (geoindicators) and an advanced knowledge on the correlation between different indicators, their role as early warning parameters and quantification of thresholds.

---

## 10 REFERENCES

- Aaltonen, J., 2001. Ground Monitoring using Resistivity Measurements in Glaciated terrains. MS. Dissertation, Department of Civil and Environmental Engineering, Royal Institute of Technology, Stockholm, 64 pp.
- Abellán, A., Calvet, J., Vilaplana, J.M., Blanchard, J. (2010). Detection and spatial prediction of rockfalls by means of terrestrial laser scanner monitoring. *Geomorphology* 119(3-4), 162-171. doi:10.1016/j.geomorph.2010.03.016.
- Abellán, A., Jaboyedoff, M., Oppikofer, T., Vilaplana, J.M. (2009). Detection of millimetric deformation using a terrestrial laser scanner: experiment and application to a rockfall event. *Natural Hazards and Earth System Sciences* 9(2), 365-372. doi:10.5194/nhess-9-365-2009.
- Abellán, A., Vilaplana, J.M., Martínez, J. (2006). Application of a long-range terrestrial laser scanner to a detailed rockfall study at Vall de Núria (Eastern Pyrenees, Spain). *Eng.Geol.* 88(3-4), 136-148. doi:10.1016/j.enggeo.2006.09.012.
- Agrawal GP (2008) Applications of nonlinear fiber optics“, Academic Press, 2th Edition.
- Ahl A., Bieber G., 2010. Correction of the attenuation effect of vegetation on airborne gamma-ray spectrometry data using laser altimeter data, *Near Surface Geophysics*, accepted.
- Alba, M., Longoni, L., Papini, M., Roncoroni, F., Scaioni, M. (2005). Feasibility and problems of TLS in modelling rock faces for hazard mapping, in: Vosselman, G., Brenner, C. (Eds.), *Proceedings of the ISPRS Workshop Laser scanning 2005. International Archives of Photogrammetry, Remote Sensing and Spatial Information Sciences*, Enschede, Netherlands, pp. 156-161.
- Allard, M., 2007. On the Origin of the HTEM Species. *Proceedings of Exploration 07: Fifth Decennial International Conference on Mineral Exploration* edited by B. Milkereit, p. 355-374
- Amitrano D., Grasso J.-R., Senfaute G., 2005. Seismic precursory patterns before a cliff collapse and critical-point phenomena. *Geophysical Research Letters*, 32, 8, L08314, doi:10.1029/2004GL022270.
- Amitrano D., Senfaute G., Grasso J.R., Got J.L., Gaffet S., Clement C., 2004. Potential of the seismic monitoring for the understanding of gravitational instability. *AGU Fall Meeting*, paper n°H44A-06, San Francisco.
- Amitrano, D., Gaffet, S., Malet, J.-P., Maquaire, O., 2007. Understanding mudslides through micro seismic monitoring: the Super-Sauze (South-East French Alps) case study. *Bulletin de la Société Géologique de France*. 178 (2), 149-157.
- Angeli, M.G., Gasparetto, P., Pasuto, A. and Silvano, S., 1989. Examples of landslide instrumentation. *Proc. 12th Int. Conf. Soil Mechanics and Foundation Engineering*. Rio de Janeiro. A.A. Balkema. Rotterdam. Vol.3: 1531-1534.
- Angeli, M.G., Gasparetto, P., Silvano, S. and Tonetti, G., 1988. An automatic recording system to detect the critical stability of slopes. *Proc. 5th Int. Symposium on Landslides*, Lausanne. A.A. Balkema. Rotterdam. Vol.1: 375-378.
- Antonello G., Tarchi D., Casagli N., Del Ventisette C., Guerri L., Luzi G., Mugnai F., Leva D., 2008. Microwave interferometric sensors as a tool for space and time analysis of active volcano deformations: The Stromboli case. *Proceedings of the 2008 2nd Workshop on USE of Remote Sensing Techniques for Monitoring Volcanoes and Seismogenic Areas, USEReST 2008*.
- Arattano M., 1999. On the use of seismic detectors as monitoring and warning systems for debris flows. *Natural Hazards*, 20, 197-213.
- Arbeitsgruppe Geologie und Naturgefahren AGN 2004: *GefahrenEinstufung Rutschungen i.w.S.: Permanente Rutschungen, spontane Rutschungen und Hangmuren*. – Bericht, 24. März 2004.
- Archie, G.E., 1942. The electrical resistivity log as an aid in determining some reservoir characteristics. *Trans. AIME*. 146, S. 54-62.
- Atkins, E.R., Smith, G.H., 1961. The significance of particle shape in formation factor-porosity relationships. *J. Petrol. Tech.*, v.13, S. 285-291.
- Auken, E., Pellerin, L., Christensen, N. B., Sørensen, K., 2006. A survey of current trends in near-surface electrical and electromagnetic methods. *Geophysics* 71, G249-G260.
- Avian, M., Kellerer-Pirklbauer, A., Bauer, A. (2009). LiDAR for monitoring mass movements in permafrost environments at the cirque Hinteres Langtal, Austria, between 2000 and 2008. *Natural Hazards and Earth System Sciences* 9(4), 1087-1094.
- Ballais, J.-L., Maquaire, O., Ballais, H. 1984. Esquisse d'une histoire des mouvements de terrain dans le Calvados depuis 2 siècles. In: *Actes du Colloque "Mouvements de terrain"*, Documents du BRGM, N° 83, Ed. BRGM, Orleans, pp. 476-483.

- 
- Bamler, R. and Hartl, P., 1998. Synthetic aperture radar interferometry, *Inverse Problems* 14, 54p.
- Barbieri M., Corsini A., Casagli N., Farina P., Coren F., Sterzai P., Leva D., Tarchi D., 2004. Space-borne and ground-based SAR interferometry for landslide activity analysis and monitoring in the appennines of Emilia Romagna (Italy): Review of methods and preliminary results. European Space Agency, (Special Publication) ESA SP (550), 463-470.
- Barla, G., Antolini, F., Barla, M., Mensi, E., Piovano, G., 2010. Monitoring of the Beauregard landslide (Aosta Valley, Italy) using advanced and conventional techniques. *Engineering Geology*, 116: 3-4, 218-235.
- Barlow, J., Franklin, S., & Martin, Y. (2006). High spatial resolution satellite imagery, DEM derivatives, and image segmentation for the detection of mass wasting processes. *Photogrammetric Engineering and Remote Sensing*, 72, 687-692
- Baron I., Supper R., 2010. A general assessment of landslide investigation and monitoring methods in Europe (preliminary results). – In Supper R. and Baron I. (Eds.): *Monitoring Technologies and Early Warning Systems – Current Research and Perspectives for the Future*. Book of extended abstracts, Open Workshop in frame of the EU FP7 “Safeland” Project, February 24th, 2010, Vienna.
- Baron I., Supper R., Moser G., Gasperl W., 2010. Application of Differential Airborne Laser Scan for effective landslide inventory mapping and activity assessment in forested areas. – *Geophysical Research Abstracts* 12, EGU2010-4649-1, EGU General Assembly 2010
- Baron I., Supper R., Moser G., Gasperl W., 2010. Distinct topographic changes of an earthflow system at Gschliefgraben (Gmunden, Upper Austria) recorded by Differential Airborne Laser Scanning. – In: Krizek et al. (Eds): *Geomorfologicky sbornik* 9: 4, Charles University, Prague. ISBN: 978-80-86561-32-5
- Barton, N. (1982). Modelling rock joint behaviour from in situ block tests: implications for nuclear waste repository design. ONWI-308, Office of Nuclear isolation, Columbus, OH.
- Bell, R., Thiebes, B., Glade, T., Becker, R., Kuhlmann, H., Schauerte, W., Burghaus, S., Krummel, H., Janik, M., Paulsen, H., 2008. The technical concept within the Integrative Landslide Early Warning System (ILEWS). In: *Geotechnologien - Science Report* 14.
- Berardino P., Fornaro G., Lanari R. and Sansosti E. (2002) A New Algorithm for Surface Deformation Monitoring based on Small Baseline Differential SAR Interferograms, *IEEE Trans. Geosci. and Remote Sens.*, 40 (11), 2375-2383.
- Berardino, P., Costantini, G., Franceschetti, G., Iodice, L., Pietranera, L., Rizzo, V. (2003a) Use of differential SAR interferometry in monitoring and modelling large slope instability at Matera (Basilicata, Italy). *Engineering Geology* 68/1–2, 31–51.
- Bernini R, Minardo A, Zeni L (2011) Centimeter-range spatial resolution distributed sensing by BOFDA. 21th International Conference on Optical Fiber Sensors, Ottawa, 15-19 May 2011, Proc. SPIE Vol. 7753, 77532C (2011); doi:10.1117/12.886060.
- Berthier, E, Vadon, H., Baratoux, D., Arnaud, Y., Vincent, C., Feigl, K. L., Rémy, F., & Legrésy B. (2005). Surface motion of mountain
- Bitelli G., Dubbini M., Zanutta A. (2004). Terrestrial laser scanning and digital photogrammetry techniques to monitor landslides bodies, *International Archives of Photogrammetry, Remote Sensing and Spatial Information Sciences* 35, 246–251.
- Bitelli, G., Dubbini, M., Zanutta, A. (2004). Terrestrial laser scanning and digital photogrammetry techniques to monitor landslide bodies, in: Anonymous Proceedings of the XXth ISPRS Congress Geo-Imagery Bridging Continents. International Society for Photogrammetry and Remote Sensing, Istanbul, Turkey, pp. 246-251.
- Blaschke, T. (2010). Object based image analysis for remote sensing. *ISPRS Journal of Photogrammetry and Remote Sensing*, 65, 2-16
- Blikra, L.H., (2008). The Åknes rockslide; monitoring, threshold values and early-warning, in: Chen, Z., Zhang, J., Li, Z., Wu, F., Ho, K. (Eds.), *Landslides and Engineered Slopes. From the Past to the Future - Proceedings of the 10th International Symposium on Landslides and Engineered Slopes*, 30 June - 4 July 2008, Xi'an, China. Taylor & Francis Group, London, pp. 1089-1094.
- Blikra, L.H., Anda, E., Belsby, S., Jogerud, K., Klempe, Ø. (2006a). Åknes/Tafjord prosjektet: Statusrapport for Arbeidsgruppe 1 (Undersøking og overvaking). Åknes/Tafjord project, Stranda, Norway.
- Blikra, L.H., Anda, E., Høst, J., Longva, O. (2006b). Åknes/Tafjord-prosjektet: Sannsynlighet og risiko knyttet til fjellskred og flodbølger fra Åknes og Hegguraksla. Geological Survey of Norway, Trondheim, Norway.
-

- 
- Bonnard, C., Steinmann, G., 1990. Continuous measurement of landslide movements, *Geotechnical Instrumentation in Practice*. Institution of Civil Engineers. Thomas Telford, London, pp. 177–189.
- Bornaz, L., Lingua, A., Rinaudo, F. (2002). Engineering and environmental applications of laser scanner techniques. *International Archives of Photogrammetry and Remote Sensing* 34 Part 3B, 40-43.
- Breiman, L. (2001). Random Forests. *Machine Learning*, 45, 5-32
- Brückl E., Mertl S., 2006. Seismic monitoring of deep-seated mass movements. In: *Disaster Mitigation of Debris Flows. Slope Failures and Landslides*, 571-580.
- Brückl, E., Brunner, F.K., Kraus, K. 2006. Kinematics of a deep-seated landslide derived from photogrammetric, GPS and geophysical data. *Engineering Geology*, 88: 149-159.
- Brunner, F.K., Zobl, F., Gassner, G. 2003. On the capability of GPS for landslide monitoring. *Felsbau*, 21(2):51-54.
- Buckley, S.J., Howell, J.A., Enge, H.D., Leren, B.L.S. and Kurz, T.H., 2008. Integration of Terrestrial Laser Scanning, Digital Photogrammetry and Geostatistical Methods for High-Resolution Modelling of Geological Outcrops, *Proceedings of ISPRS, Beijing, China, 2008*, 6 p.
- Campbell, J.E., 1990. Dielectric properties and influence of conductivity in soils at one to fifty megahertz. *Soil Sci. Soc. Am. J.* 54, 332–341.
- Canuti P., Casagli N., Catani F., Falorni G., Farina P. (2007). Integration of Remote Sensing Techniques in different stages of landslide response. In *Progress in Landslide Sciences* Eds. Kyoji Sassa, Hiroshi Fukuoka, Fawu Wang, Gonghui Wang.
- Canuti P., Casagli N., Ermini L., Fanti R., Farina P. (2004). Landslide activity as a geoinicator in Italy: Significance and new perspectives from remote sensing. *Environmental Geology*, 45(7), 907–919.
- Cardenal, J., Mata, E., Perez-Garcia, J.L., Delgado, J., Andez, M.A., Gonzalez, A., Diaz-de-Teran, J.R. (2008). Close Range Digital Photogrammetry Techniques applied to Landslide Monitoring. *International Archives of the Photogrammetry, Remote sensing and Spatial Information Sciences*. Vol XXXVII. Part B8.
- Casagli N., Tibaldi A., Merri A., Del Ventisette C., Apuani T., Guerri L., Fortuny-Guasch J., Tarchi D., 2009. Deformation of Stromboli Volcano (Italy) during the 2007 crisis by radar interferometry, numerical modeling and field structural data. *Journal of Volcanology and Geothermal Research*, 182: 182-200.
- Casagli N., Tofani V., Adler R. (2009) A look from space. In *Landslides, Disaster Risk Reduction*, Sassa K. and Canuti P. eds.
- Casagli, N., Catani F., Del Ventisette, C., Luzi G., 2010b. Monitoring, prediction, and early warning using ground-based radar interferometry. *Landslides*. 7: 3, 291-301. DOI 10.1007/s10346-010-0215-y.
- Casagli, N., Guerri, L., Righini, G., Ferretti, A., Colombo, D. & Prati, C. (2005). Integrated use of PS and very high resolution optical images for supporting landslide risk management. *URSI, Symposium on Microwave Remote Sensing of the Earth, Oceans, Ice and Atmosphere*, 20-21 April 2005, Ispra, Italy.
- Casagli, N., Tapete, D., Del Conte, S., Luzi, G., Fanti, R., Massagni, S., Leva, D., 2010a. Il monitoraggio satellitare e con radar da terra. In: R. Cecchi (ed.), *Roma Archaeologia. Interventi per la tutela e la fruizione del patrimonio archeologico*. Secondo rapporto. Electa, Roma, 145-157.
- Cascini L., Bonnard Ch., Corominas J., Jibson R., Montero-Olarte J. (2005). Landslide hazard and risk zoning for urban planning and development. State of the Art Report (SOA7). *Proceedings of the International Conference on “Landslide Risk Management”*, Vancouver (Canada). O. Hungr, R. Fell, R. Couture and E. Eberthardt (eds.). Taylor and Francis, London, 199-235.
- Cascini L., Ferlisi S., Peduto D., Pisciotta G., Di Nocera S., Fornaro G. (2008) Multitemporal DInSAR data and damages to facilities as indicators for the activity of slow-moving landslides. In: *Landslides and Engineered Slopes. From the Past to the Future*. Chen Z., Zhang J., Li Z., Wu F., Ho K. (eds.). *Proceeding of the 10th International Symposium on Landslides and Engineered Slopes*, 30 June-4 July 2008, Xi’an (China), Taylor and Francis Group, London. Vol. II, pp. 1103-1109. ISBN 978-0-415-41196-7.
- Cascini L., Fornaro G., Peduto D. (2009). Analysis at medium scale of low-resolution DInSAR data in slow-moving landslide-affected areas. *ISPRS Journal of Photogrammetry and Remote Sensing*, 64(6),598-611. doi:10.1016/j.isprsjprs.2009.05.003
- Cascini L., Fornaro G., Peduto D. (2010). Advanced low- and full-resolution DInSAR map generation for slow-moving landslide analysis at different scales. *Engineering Geology*, 112 (1-4), 29-42, doi:10.1016/j.enggeo.2010.01.003.
- Casson, B., Baratoux, D., Delacourt, D., & Allemand, P. (2003). “La Clapière” landslide motion observed from aerial differential high resolution DEM. *Engineering. Geology*, 68, 123-139.
-

- 
- Casson, B., Delacourt, C., & Allemand, P. (2005). Contribution of multi-temporal remote sensing images to characterize landslide slip surface. Application to the La Clapière landslide (France). *Nat. Hazards Earth Syst. Sci.*, 5, 425-437
- Catani, F., Casagli, N., Ermini, L., Righini, G., Menduci, G. (2005b). Landslide hazard and risk mapping at catchment scale in the Arno River basin. *Landslides* 2: 329-342.
- Catani, F., Farina, P., Moretti, S., Giovanni, N., Strozzi, T. (2005a). On the application of SAR interferometry to geo-morphological studies: estimation of landform attributes and mass movements. *Geomorphology* 66: 119-131.
- Chacón, J., Irigaray, C., Fernández, T., El Hamdouni, R. (2006): Engineering geology maps: Landslides and geographical information systems. *Bulletin of Engineering Geology and the Environment*, 65 (4), 341-411.
- Chambers, J.E., Meldrum, P.I., Gunn, D.A., Wilkinson, P.B., Kuras, O., Weller, A.L., Ogilvy, R.D., 2009. Hydrogeophysical monitoring of landslide processes using automated time-lapse electrical resistivity tomography (ALERT) [extended abstract]. In: *Near Surface 2009*, Dublin, Ireland, 7-9 Sept.
- Chambon G. (2003). Caractérisation expérimentale du frottement effectif des zones de faille. PhD Thesis. Université Paris XI Orsay, ENPC.
- Chen, Y., He, X., Ding, X., Sang, W. 2005. Steep-slope monitoring: GPS multiple-antenna system at Xiaowan Dam. *GPS World*, November 1, 2005, 93-98.
- Chung, C.F., Fabbri, A.G. (2003): Validation of spatial prediction models for landslide hazard mapping, in: *Natural Hazards*, 30, pp. 451-472
- Civil-Protection-Sicily (2010). Landslide and mud food emergency Messina province, Italy, October 1st 2009. In *A.f.a.f.t.E.U.S. Fund* (Ed.) (p. 83): Regione Siciliana - Presidenza, Dipartimento della Protezione Civile
- Clausi, D.A. (2002). An analysis of co-occurrence texture statistics as a function of grey level quantization. *Canadian Journal of Remote Sensing*, 28., 45-62
- Clément, R., Descloitres, M., Günther, T., Oxarango, L., Morra, C., Laurent, J.P., Gourc, J.P., 2010. Improvement of electrical resistivity tomography for leachate injection monitoring. *Waste Management* 30 (2010) 452-464.
- ClimChalp. Slope Monitoring Methods, A State of the Art Report. ClimChalp is an European Regional Development Project, within the framework of the INTERREG IIIB Alpine Space Programme. The Report of the Work Package 6, was released in Munich, 28.2.2008. 179 p. 2008.
- Coe, J.A., Ellis, W.L., Godt, J.W., Savage, W.Z., Savage, J.E., Michael, J.A., Kibler, J.D., Powers, P.S., Lidke, D.J., Debray, S. 2003. Seasonal movement of the Slumgullion landslide determined from Global Positioning System surveys and field instrumentation, July 1998 – March 2002. *Engineering Geology*, 68(1-2): 67-101.
- Colas G, Locat J 1993 Glissement et coulée de La Valette dans les Alpes-de-Haute-Provence. Présentation générale et modélisation de la coulée. *Bulletin de Liaison des Laboratoires des Ponts et Chaussées* 187: 19-28
- Colesanti C., Ferretti A., Prati C., Rocca F. (2003). Monitoring landslides and tectonic motions with the Permanent Scatterers Technique, *Engineering Geology* 68, 3 –14.
- Colesanti C., Wasowski J. (2004). Satellite SAR interferometry for wide-area slope hazard detection and site-specific monitoring of slow landslide. In *Landslides: Evaluation and Stabilization*, Lacerda, Ehrlich, Fontoura, Sayo (eds), Taylor and Francis Group, London, ISBN 0415356652.
- Colesanti C., Wasowski J. (2006). Investigating landslides with space-borne Synthetic Aperture Radar (SAR) interferometry. *Engineering Geology*, 88, 173-199.
- Constable, S. C., Parker, R. L., Constable, C. G., 1987. Occam's inversion: A practical algorithm for generating smooth models from electromagnetic sounding data. *Geophysics*, 52, 289-300.
- Corominas, J., Moya, J., Ledesma, A., Lloret, A., Gili, J.A., 2005. Prediction of ground displacements and velocities from groundwater level changes at the Vallcebre landslide: *Landslides*, 2: 83-96.
- Corominas, J., Moya, J., Lloret, A., Gili, J.A., Angeli, M.G., Pasuto A., Silvano, S., 2000. Measurement of landslide displacements using a wire extensometer. *Engineering Geology*, 55: 149-166.
- Costantini, M., Malvarosa, F., Minati, F., Pietranera, L. (2001). Optimal combination of multiple SAR differential interferometric measurements for monitoring terrain displacements. *Proceedings of the first IEEE/ISPRS Joint Workshop on Remote Sensing and Data Fusion over Urban Areas*, Rome (Italy), 8-9 November 2001, pp. 53-57.
-

- 
- Costantini, M., Malvarosa, F., Minati, F., Pietranera, L., Milillo, G. (2002). A three-dimensional phase unwrapping algorithm for processing of multitemporal SAR interferometric measurements. Proceedings of the IEEE International Geoscience and Remote Sensing Symposium (IGARSS 2002), Toronto (Canada), 24–28 June 2002, vol. 3, pp. 1741–1743.
- Cotecchia, V. (2006). The Second Hans Cloos Lecture. Experience drawn from the great Ancona landslide of 1982. *Bull Eng Geol Env*, 65, 1–41. Springer-Verlag 2006.
- Crosta, G. and Agliardi, F. 2003. A methodology for physically based rockfall hazard assessment. *Nat. Hazards Earth Syst. Sci.*, 3, 407-422.
- Cruden D.M., Varnes D.J. (1996) Landslide types and processes. In: Turner, A.K. and Schuster, R.L. (eds.) *Landslides, Investigation and Mitigation*, Transportation Research Board Special Report 247, Washington D.C., pp. 36-75.
- Dai Z, Liu Y, Zhang L, Ou Z, Zhou C, Liu T (2008) Landslide monitoring based on high-resolution distributed fiber optic stress sensor” *J. Electron. Sci. Technol. China* 6, pp. 416-419.
- Daito, K., Ferretti, A., Kuzuoka, S., Novali, F., Panzeri, P., Rocca, F. (2003). L-band PS analysis: Jers-1 results and TerraSAR-L predictions. Proceedings of the third International Workshop on ERS SAR Interferometry (FRINGE 2003), Frascati (Italy), 2–5 December 2003. ESA SP-550, available also online: <http://earth.esa.int/fringe03/proceedings/>.
- Dalton, F.N., Herkelrath, W.N., Rawlins, D.S., Rhoades, D., 1984. Time domain reflectometry: simultaneous assessment of the soil water content and electrical conductivity with a single probe. *Science* 224, 989–990.
- De Michele, M., Raucoules, D., de Sigoyer, J., Pubellier, M., Chamot-Rooke, N., 2010, Three-dimensional surface displacement of the 2008 May 12 Sichuan earthquake (China) derived from Synthetic Aperture Radar: evidence for rupture on a blind thrust, *Geophysical journal international*, Vol. 183, 1097-1103.
- Debella-Gilo M., & Käab A. Sub-pixel precision image matching for measuring surface displacements on mass movements using normalized cross-correlation. *Remote Sensing of Environment* (2010).
- Debella-Gilo, M., & Käab, A. (2011). Sub-pixel precision image matching for measuring surface displacements on mass movements using normalized cross-correlation. *Remote Sensing of Environment*, 115, 130-142
- Delacourt, C., Allemand P., Casson B., & Vadon H. (2004). Velocity field of the “La Clapiere” landslide measured by the correlation of aerial and Quick-Bird satellite images. *Geophysical. Research Letters*, 31, 1-5.
- Delacourt, C., Allemand, P., Berthier, E., Raucoules, D., Casson, B., Grandjean, P. Pambrun, C. and Varel., E., 2007. Remote-sensing techniques for analyzing landslide kinematics: a review, *Bull. Soc. géol. Fr.*, 178 (2), 89-100.
- Delacourt, C., Raucoules, D. Mouélic, S.L. Carnec, C., Feurer, D., Allemand, P., Cruchet, M. 2009. Observation of a large landslide on la reunion island using differential sar interferometry (JERS and Radarsat) and correlation of optical (Spot5 and aerial) images, *Sensors* , Vol. 9, 616-630
- Déprez, A., Malet, J.-P., Masson, F., Ulrich, P. Continuous monitoring and near-real time processing of GPS observations for landslide analysis: a methodological framework. *Natural Hazards and Earth System Sciences*, 15p. (submitted in Feb. 2011).
- Derron, M., Blikra, L.H., Jaboyedoff, M. (2005). High resolution digital elevation model analysis for landslide hazard assessment (Åkerneset, Norway), in: Senneset, K., Flaate, K., Larsen, J.O. (Eds.), *Landslides and Avalanches: ICFL 2005 Norway*. Taylor & Francis Group, London, pp. 101-106.
- Derron, M.-H., Carrea, D., Fragnol, B., Longchamp, C., Michoud, C., Jaboyedoff, M., Blikra, L.-H., Kristensen, L. and Oppikofer, T., 2011. Off-shore Laser Scanning of coastal cliffs for rockfall hazard assessment by IMU/GNSS coupled Lidar, EGU General Assembly 2011, EGU2011-9706.
- Derron, M.-H., Jaboyedoff, M. (2010). Preface "LIDAR and DEM techniques for landslides monitoring and characterization". *Nat. Hazards Earth Syst. Sci.* 10(9), 1877-1879. doi:10.5194/nhess-10-1877-2010.
- Dewitte, O., Jasselette, J.C., Cornet, Y., Van Den Eeckhaut, M., Collignon, A., Poesen, J., & Demoulin, A. (2008). Tracking landslide displacements by multi-temporal DTMs: A combined aerial stereophotogrammetric and LIDAR approach in western Belgium. *Engineering Geology*, 99, 11-22
- Di, B., Zeng, H., Zhang, M., Ustin, S.L., Tang, Y., Wang, Z., Chen, N., & Zhang, B. (2010). Quantifying the spatial distribution of soil mass wasting processes after the 2008 earthquake in Wenchuan, China: A case study of the Longmenshan area. *Remote Sensing of Environment*, 114, 761-771
- Diaz-Urriarte, R., & Alvarez de Andres, S. (2006). Gene selection and classification of microarray data using random forest. *BMC Bioinformatics*, 7, 3
-

- 
- Dickson, B.L., and Scott, K.M., 1997. Interpretation of aerial gamma ray surveys. *AGSO Journal of Australian Geology and Geophysics*, 17, 187-200.
- Dixon N., Hill R., Kavanagh J., 2003. Acoustic emission monitoring of slope instability: development of an active waveguide system. *Geotech. Eng.*, 156, 83-95.
- Dixon N., Kavanagh J., Hill R., 1996. Monitoring landslide activity and hazard by acoustic emission. *J. Geol. Soc. China*, 39, 437-464.
- Dixon, T.H., 1991. The Global Positioning System. *Review of Geophysics*, 29: 249-276.
- Dorren, L.K.A., Berger, F. and Putters, U.S. 2006. Real-size experiments and 3-D simulation of rockfall on forested and non-forested slopes. *Nat. Hazards Earth Syst. Sci.*, 6, 145-153.
- Dunnicliff J. and La Fonta J.G. (2001) – “In place inclinometers. A significant test program”. *Geotechnical News*, vol. 19, n°1, March, pp. 33-34
- Dunnicliff J. assisted by Green G.E. “Geotechnical instrumentation for monitoring field performance”. (1988-1993) Wiley-Interscience Publication, 577 pp.
- Dunnicliff J. et alii (2005) – “Geotechnical instrumentation for field measurements”. Training course, March 13-15, 2005. The University of Florida.
- Dunning, S.A., Massey, C.I., Rosser, N.J. (2009). Structural and geomorphological features of landslides in the Bhutan Himalaya derived from Terrestrial Laser Scanning. *Geomorphology* 103(1), 17-29. doi:10.1016/j.geomorph.2008.04.013.
- Dupont, M., Taluy, P. 2000. Hydrogéologie du glissement de La Valette (avec carte au 1:50000 des venues d'eau). Internal Report, Université de Savoie, Chambéry, France, 45p [http://eost.u-strasbg.fr/omiv/Publications\\_la\\_valette.html](http://eost.u-strasbg.fr/omiv/Publications_la_valette.html)
- Duranthon, J.-P. 2000. Application de la méthode GPS de localisation par satellite à la surveillance de sites naturels instables. *Bulletin de Liaison des Laboratoires des Ponts et Chaussées*, 228: 47-53.
- Duro, J., Inglada, J., Closa, J., Adam, N., Arnaud, A. (2003). High Resolution Differential Interferometry Using Time Series of ERS and Envisat SAR Data. *Proceedings of the third International Workshop on ERS SAR Interferometry (FRINGE 2003)*, Frascati (Italy), 2–5 December 2003. ESA SP-550, available also online: <http://earth.esa.int/fringe03/proceedings/>.
- Dymond, J.R., Ausseil, A.G., Shepherd, J.D. and Buettner, L., 2006. Validation of a region-wide model of landslide susceptibility in the Manawatu-Wanganui region of New Zealand. *Geomorphology*, 74, 70-79.
- Eberhard, M.O., Baldrige, S., Marshall, J., Mooney, W., & Rix, G.J. (2010). The MW 7.0 Haiti earthquake of January 12, 2010. In, *USGS/EERI Advance Reconnaissance Team report* (p. 58): U.S. Geological Survey Open-File Report.
- Eberhardt E., Spillmann T., Maurer H., Willenberg H., Loew S., Stead D., 2004. The Randa Rockslide Laboratory: Establishing brittle and ductile instability mechanisms using numerical modelling of microseismicity. *Proc. 5th Int. Symp. on Landslides*, Rio de Janeiro, Brazil – Balkema, Rotterdam, 481-487.
- Eidsvig, U., Harbitz, C.B. (2005). Åknes/Tafjord prosjektet. Innledende numeriske analyser av flodbølger som følge av mulige skred fra Åkneset. Norwegian Geotechnical Institute, Oslo, Norway.
- Eisenbeiss, H., 2004. A Mini Unmanned Aerial Vehicle (UAV): System Overview and Image Acquisition, *International Workshop on Processing and visualization using high-resolution imagery*, 18-20 November 2004, Pitsanulok, Thailand, 7 p.
- Eisenbeiss, H., 2007. Applications of photogrammetric processing using an autonomous model helicopter, *IC WG I/V Autonomous Vehicle Navigation*, 6 p.
- Eisenbeiss, H., 2008. The autonomous mini helicopter: a powerful platform for mobile mapping, *The International Archives of the Photogrammetry, Remote Sensing and Spatial Information Sciences*, Vol. XXXVII, Part B1, Beijing 2008, 977-984.
- Evin, M. 1992. Prospection sismique en partie basse de la coulée de La Valette. Internal Report, RTM – Restauration des Terrains en Montagne, Barcelonnette, France [http://eost.u-strasbg.fr/omiv/Publications\\_la\\_valette.html](http://eost.u-strasbg.fr/omiv/Publications_la_valette.html)
- Fallourd, R., Vernier, F., Friedt J.-M., Martin, G., trouvé, E., Moreau, L. & Nicolas, J.-M. (2010). Monitoring temperate glacier with high resolution automated digital cameras – Application to the Argentière Glacier. in: Paparoditis N., Pierrot-Deseilligny M., Mallet C. & Tournaire O. (Eds.), *IAPRS*, Vol. XXXVIII, Part 3B, Saint-Mandé, France., 1-23.
-

- 
- Fardin, N., Feng, Q., Stephansson, O. (2004). Application of a new in situ 3D laser scanner to study the scale effect on the rock joint surface roughness. *Int.J.Rock Mech.Min.Sci.* 41(2), 329-335. doi:10.1016/S1365-1609(03)00111-4.
- Fardin, N., Stephansson, O., Jing, L. (2001). The scale dependence of rock joint surface roughness. *Int.J.Rock Mech.Min.Sci.* 38(5), 659-669. doi:10.1016/S1365-1609(01)00028-4.
- Farina P., Colombo D., Fumagalli A., Marks F., Moretti S. (2006). Permanent Scatterers for landslide investigations: outcomes from the ESA-SLAM project. *Engineering Geology*, 88, 200-217.
- Fecker, E., Rybář J., Stemberk J. (2002): Investigation of a railroad tunnel affected by slow landsliding. – In Rybář, J., Stemberk, J. and Wagner, P. eds „Landslides“, 541-546, Swets & Zeitlinger, Lisse.
- Fell R, Corominas J, Bonnard C, Cascini L, Leroi E, Savage WZ (2008) Guidelines for landslide susceptibility, hazard and risk zoning for land-use planning. *Engineering Geol.* 102:99-111.
- Ferrero, A.M., Forlani, G., Roncella, R. And Voyat, H.I. 2009. Advanced Geostructural Survey Methods Applied to Rock Mass Characterization. *Rock Mech. Rock Eng.*, 42, 631-665.
- Ferretti, A., Perissin, D., Prati, C., Rocca, F. (2005). On the physical nature of SAR Permanent Scatterers. Proceedings of the 2005 URSI Commission F Symposium on Microwave Remote Sensing of the Earth, Oceans, Ice, and Atmosphere, Ispra (Italy), 20–21 April 2005, available online: <http://ursi-f-2005.jrc.it/proceedings.htm>.
- Ferretti, A., Prati, C., Rocca, F. (2000). Nonlinear subsidence rate estimation using Permanent Scatterers in Differential SAR Interferometry. *IEEE Transactions on Geoscience and Remote Sensing* 38 (5), 2202–2212.
- Ferretti, A., Prati, C., Rocca, F., 2001. Permanent scatterers in SAR interferometry. *IEEE Transactions on Geoscience and Remote Sensing* 39 (1), 8–20.
- Fialko, Y., Sandwell, D., Simons, M., and Rosen, P., 2005, Three-dimensional deformation caused by the Bam, Iran, earthquake and the origin of shallow slip deficit, v. 435, 19, doi:10.1038/nature03425.
- Flageollet, J.-C., Helluin, E. 1987. Morphological investigations of the sliding areas along the coast of Pays d'Auge, near Villerville, Normandy, France. In: *Proceedings of the 1<sup>st</sup> International Conference on Geomorphology*, Vol. 1, pp. 477-486.
- Fogolino L., Lovisolo M., Della Giusta A., 2006, Contribution of DMS monitoring systems in the analysis of slide micro-movements for early warning management, risk assesment and evaluation of mitigating actions, *Geophysical Research Abstracts*, Vol. 8, 06122.
- Fornaro, G., Pauciuolo, A., Serafino, F. (2009a). Deformation monitoring over large areas with multipass differential SAR interferometry: a new approach based on the use of spatial differences. *International Journal of Remote Sensing* 30 (6), 1455–1478.
- Fornaro, G., Reale, D., Serafino, F. (2009b). Four-dimensional SAR imaging for height estimation and monitoring of single and double scatterers. *IEEE Transactions on Geoscience and Remote Sensing* 47 (1), 224–237.
- Frattini, P., Crosta, G., Carrara, A. and Agliardi, F. 2008. Assessment of rockfall susceptibility by integrating statistical and physically-based approaches. *Geomorphology*, 94, 419-437.
- Fruneau, B., Achache, J., Delacourt, C. (1996). Observation and Modeling of the Saint-Etienne-de-Tinée Landslide Using SAR Interferometry. *Tectonophysics*, 265, 181–190
- Ganerød, G.V., Grøneng, G., Rønning, J.S., Dalsegg, E., Elvebakk, H., Tønnesen, J.F., Kveldevisvik, V., Eiken, T., Blikra, L.H., Braathen, A. (2008). Geological model of the Åknes rockslide, western Norway. *Eng.Geol.* 102(1-2), 1-18. doi:10.1016/j.enggeo.2008.01.018.
- Genrich, J.F., Bock, Y., 1992. Rapid resolution of crustal motion at short ranges with Global Positioning System. *Journal of Geophysical Research*, 96: 3261-3269.
- Gigli, G. and Casagli, N. 2011. Semi-automatic extraction of rock mass structural data from high resolution LIDAR point clouds. *International Journal of Rock Mechanics & Mining Sciences*, 48, 187–198.
- Gili, J.A., Corominas, J., Rius, J. 2000. Using Global Positioning System techniques in landslide monitoring. *Engineering Geology*, 55: 167-192.
- Gili, J.A., Crosetto, M. & Serral, D. (2009). “Reflectores Radar en el deslizamiento de Vallcebre. Validación y primeros resultados” (in Spanish). Proceed. VII Simposio Nacional sobre Taludes y Laderas Inestables, Barcelona, oct. 2009.
- Giuffredi, F., Zanolini, L., Foglino, L. (2003). Application of a new integrated multi-parametric monitoring system for the analysis of micro-movements in the Civil Protection activities: an example. Proceedings of the Sixth International Symposium on Field Measurements in Geomechanics, Oslo pp. 61-66: Balkema.
-

- 
- Gold MP (1985) Design of a long-range single-mode OTDR. *J. Lightwave Technol.*, vol. 3, pp. 39-46.
- Greco, R., 1999. Measurement of water content profiles by single TDR experiments. In: Feyen, J., Wiyono, K. (Eds.), *Modelling of Transport Processes in Soils*. Wageningen Pers, Wageningen, the Netherlands, pp. 276–283.
- Greco, R., 2006. Soil water content inverse profiling from single 438 TDR waveforms. *J. Hydrol.* 317, 325–339.
- Green, R.O., Eastwood, M.L., Sarture, C.M., Chrien, T.G., Aronsson, M., Chipendale, B.J. et al. 1998. Imaging spectroscopy and the airborne visible/infrared imaging spectrometer (AVIRIS). *Remote Sensing of the Environment*, 65, 227-248.
- Guzzetti, F., Crosta, G., Detti, R. and Agliardi, F., 2002. STONE: a computer program for the three-dimensional simulation of rock-falls. *Computers & Geosciences*, 28, 1079–1093.
- Hanssen, R.F. (2001). *Radar Interferometry: Data Interpretation and Error Analysis*. Kluwer Academic publishers, Dordrecht. 326 pp.
- Haralick, R.M., Shanmugam, K. and Dinstein, I. H. (1973). Textural features for image classification. *IEEE Transactions on Systems, Man and Cybernetics*, 3, 610-621
- Hauck, C., 2001. Geophysical methods for detecting permafrost in high mountains. Ms. Swiss Federal Institute of Technology Zurich, Diss. ETH No. 14163.
- Hayes, G.P., Briggs, R.W., Sladen, A., Fielding, E.J., Prentice, C., Hudnut, K., Mann, P., Taylor, F.W., A. J. Crone, Gold, R., Ito, T., & Simons, M. (2010). Complex rupture during the 12 January 2010 Haiti earthquake. *Nature Geoscience*
- Heikkila, J., & Silven, O. (1997). A four-step camera calibration procedure with implicit image correction. *IEEE Computer Society*, 1106-1112.
- Herring, T.A., King, R.W., McClusky, S.C. 2003a. GLOBK: Global Kalman filter VLBI and GPS analysis program, Version 10.1: Internal Memo- random: Cambridge, Massachusetts Institute of Technology, 87p.
- Herring, T.A., King, R.W., McClusky, S.C. 2003b. GAMIT, GPS analysis at MIT, Release 10.3: Internal Memorandum: Cambridge, Massachusetts Institute of Technology, 182p.
- Hilley G.E., Burgelman R., Ferretti A., Novali F., Rocca F. (2004) Dynamics of slow-moving landslides from Permanent Scatterer Analysis. *Science*, 304, 1952-1955
- Hoek, E., Marinos, P. and Benissi, M., 1998. Applicability of the Geological Strength Index (GSI) classification for very weak and sheared rock masses. The case of the Athens Schist Formation, *Bull. Geol. Env.*, 57 (2), 151-160.
- Honda, K., & M. Nagai (2002), Real-time volcano activity mapping using ground-based digital imagery, *ISPRS Journal of Photogrammetry and Remote Sensing*, 57, 1-2, 159-168.
- Hong, W., Tan, W., Wang, Y., Wu, Y., 2010. Development and experiments of ground-based SAR in IECAS for advanced SAR imaging technique validation, 8th European Conference on Synthetic Aperture Radar, Electronic Proceedings, 7-10 June 2010, Aachen, Germany, 1185 pp.
- Hördt, A., Blaschek, R., Kemna, A., Zisser, N., 2007. Hydraulic conductivity estimation from induced polarisation data at the field scale — the Krauthausen case history. *Journal of Applied Geophysics* 62, Issue 1, 14 May 2007, Pages 33-46.
- Hördt, A., Hanstein, T., Honig, M., Neubauer, F.M., 2006. Efficient spectral IP-modelling in the time domain. *Journal of Applied Geophysics* 59, Issue 2, June 2006, Pages 152-161.
- Horton, P., Jaboyedoff, M. and Bardou, E., 2008. Debris flow susceptibility at a regional scale. 4<sup>th</sup> Canadian Conference on Geohazards, Université Laval, Quebec, Canada, 20-24 May 2008, 8 pp.
- Huang, H., Fraser, D., 1996. The differential parameter method for multifrequency airborne resistivity mapping. *Geophysics*, 61, 100-109.
- Huggel, C., Käab, A., Haeberli, W. and Krummenacher, B. 2003. Regional-scale GIS-models for assessment of hazards from glacier lake outbursts: evaluation and application in the Swiss Alps. *Nat. Hazards Earth Syst. Sci.*, 3, 647-662.
- Itakura M., Kaburaki H. And Arakawa C., 2005. Branching mechanism of intergranular crack propagation in three dimensions. *Physical Review E*, 71, 055102(R) 1-4.
- Iten M, Puzrin AM (2009) BOTDA road-embedded strain sensing system for landslide boundary localization. *Proceedings of the SPIE*, Volume 7293, pp. 729316-729316-12.
- Iten M, Puzrin AM, Hauswirth D (2011) Distributed fiber optic sensor development, testing and evaluation for geotechnical monitoring applications. *Smart Sensor Phenomena, Technology, Networks, and Systems 2011*, San Diego, USA.
-

- Iten M, Puzrin AM, Hauswirth D, Foaleng-Mafang S, Beugnot JC, Thévenaz L (2009) Study of a progressive failure in soil using BEDS. Proc. of SPIE, Vol. 7503, 20th International Conference on Optical Fibre Sensors, Edinburgh, UK, 2009.
- Jaboyedoff, M. and Labiouse, V. 2011. Technical Note: Preliminary estimation of rockfall runout zones. *Nat. Hazards Earth Syst. Sci.*, 11, 819-828.
- Jaboyedoff, M., Baillifard, F., Couture, R., Locat, J., Locat, P. (2004). New insight of geomorphology and landslide prone area detection using Digital Elevation Model(s), in: Lacerda, W.A., Ehrlich, M., Fontoura, A.B., Sayão, A. (Eds.), *Landslides: Evaluation and Stabilization*. Taylor & Francis Group, London, pp. 191-198.
- Jaboyedoff, M., Demers, D., Locat, J., Locat, A., Locat, P., Oppikofer, T., Robitaille, D., Turmel, D. (2009a). Use of terrestrial laser scanning for the characterization of retrogressive landslides in sensitive clay and rotational landslides in river banks. *Canadian Geotechnical Journal* 46, 1379-1390. doi:10.1139/T09-073.
- Jaboyedoff, M., Metzger, R., Oppikofer, T., Couture, R., Derron, M.-H., Locat, J., Turmel, D. (2007). New insight techniques to analyze rock-slope relief using DEM and 3D-imaging cloud points: COLTOP-3D software, in: Eberhardt, E., Stead, D., Morrison, T. (Eds.), *Rock mechanics: Meeting Society's challenges and demands*. Proceedings of the 1st Canada - U.S. Rock Mechanics Symposium, Vancouver, Canada, 27-31 May 2007. Taylor & Francis, London, pp. 61-68.
- Jaboyedoff, M., Oppikofer, T., Abellán, A., Derron, M.-H., Loye, A., Metzger, R., Pedrazzini, A. (2010). Use of LIDAR in landslide investigations: a review. *Nat. Hazards* doi:10.1007/s11069-010-9634-2.
- Jaboyedoff, M., Pedrazzini, A., Loye, A., Oppikofer, T., Güell i Pons, M. (2009b). Earth flow in a complex geological environment: the example of Pont Bourquin, Les Diablerets (Western Switzerland), in: Malet, J.-P., Remaître, A., Bogaard, T.A. (Eds.), *Landslides Processes – From Geomorphologic mapping to dynamic modeling*, Proceedings of the landslide processes conference, pp. 131-137.
- Jackson, P., Taylor-Smith, D., Stanford, P.N., 1978. Resistivity-porosity-particle shape relationships for marine sands, *Geophysics* 43, No. 6, p. 1250-1268.
- Jaiswal, P., van Westen, C., & Jetten, V. (2011). Quantitative assessment of landslide hazard along transportation lines using historical records. *Landslides*, 1-13
- Jiang, R., Jauregui, D.V., & White, K. (2008). Close-range photogrammetry applications in bridge measurement: Literature review. *Measurement*, 41, 823-834.
- Jongmans, D., Garambois, S., 2007. Geophysical investigation of landslides: a review. *Bulletin de la Societe Geologique de France* 178(2), 101-112.
- Joswig, M., 2008. Nanoseismic Monitoring fills the gap between microseismic networks and passive seismic. *First Break*. 26, 121-128.
- Jouniaux, L., Mainault, A., Naudet, V., Pessel, M., Sailhac, P., 2009. Review of self-potential methods in hydrogeophysics. *Comptes Rendus Geosciences*, Volume 341, Issues 10-11, Hydrogeophysique, October-November 2009, Pages 928-936.
- Joyce, K.E., Belliss, S.E., Samsonov, S.V., McNeill, S.J. and Glassey, P.J., 2009. A review of the status of satellite remote sensing and image processing techniques for mapping natural hazards and disasters, *Progress in Physical Geography*, 33 (2), 183-207.
- Joyce, K.E., Dellow, G.D. and Glassey, P.J., 2008a. Assessing image processing techniques for mapping landslides. Proceedings of IEEE International Geoscience and Remote Sensing Symposium, Boston, USA, 1231-1234.
- Joyce, K.E., Dellow, G.D. and Glassey, P.J., 2008b. Methods for mapping landslides in New Zealand using satellite optical remote sensing. 14<sup>th</sup> Australian Remote Sensing and Photogrammetry Conference, Darwin, Australia.
- Joyce, K.E., Samsonov, S., Manville, V., Jongens, R., Graettinger, A., & Cronin, S.J. (2009). Remote sensing data types and techniques for lahar path detection: A case study at Mt Ruapehu, New Zealand. *Remote Sensing of Environment*, 113, 1778-1786
- Kachanoski, R.G., Pringle, E., Ward, A., 1992. Field measurement of solute travel times using time domain reflectometry. *Soil Sci. Soc. Am. J.* 56, 47-52.
- Kamshilin, A., Volkova, E., Leontiev, V., Kuzichkin, O., 2008. On study of the geodynamic processes by geoelectrical Methods. *International Congress on Environmental Modelling and Software*, 8, Russia.
- Kasperski, J., Delacourt, C., Allemand, P., Potherat, P., Jaud, M., Varrel, E. (2010). Application of a Terrestrial Laser Scanner (TLS) to the Study of the Séchillienne Landslide (Isère, France). *Remote Sensing* 2(12), 2785-2802. doi:10.3390/rs122785.
-

- 
- Kemeny, J., Post, R. (2003). Estimating three-dimensional rock discontinuity orientation from digital images of fracture traces. *Computers & Geosciences* 29(1), 65-77.
- Kemeny, J., Turner, K., Norton, B. (2006). LIDAR for rock mass characterization: hardware, software, accuracy and best-practices, in: Tonon, F., Kottenstette, J. (Eds.), *Laser and Photogrammetric Methods for Rock Face Characterization*. ARMA, pp. 49-62.
- Kiessling, D., Schuett, H., Schoebel, B., Krueger, K., Schmidt-Hattenberger, C., Schilling, F., 2009. Geoelectric Monitoring of geological CO<sub>2</sub> storage at Ketzin, Germany (CO<sub>2</sub>SINK project): Downhole and Surface-Downhole measurements. EGU General Assembly 2009, Geophysical Research Abstracts, Vol. 11, EGU2009-11041-1.
- Kneisel, C., 2004. New insights into mountain permafrost occurrence and characteristics in glacier forefields at high altitude through the application of 2D resistivity imaging. *Permafrost and Periglacial Processes* 15 (3), 221-227.
- Kneisel, C., 2006. Mapping and monitoring mountain permafrost using electrical resistivity tomography. *European Geosciences Union 2006, Geophysical Research Abstracts, Vol. 8*, 04181.
- Kochnev, V.A., Goz, I.V., Polyakov, V.S., Murtaev, I.S., Savin, V.G., Zommer, B.K., Bryksin, I.V., 2007. Imaging hydraulic fracture zones from surface passive seismic data. *First Break*. 25, 77-80.
- Kolesnikov Y.I., Nemirovich-Danchenko M.M., Goldin S.V., Seleznev V.S., 2003. Slope stability monitoring from microseismic field using polarization methodology. *Nat. Haz. Earth Sys. Sc.*, 3, 515-521.
- Komac, B., 2001: Geographical Aspects of the Disaster in Log pod Mangartom. *Ujma* 14-15, 2000/2001, Ljubljana. [http://www.urszr.si/slo/tdocs/ujma/2001/p3\\_1.pdf](http://www.urszr.si/slo/tdocs/ujma/2001/p3_1.pdf)
- Konca, A.O., Leprince, S., Avouac, J.-P., & Helmberger, D.V. (2010). Rupture Process of the 1999 Mw 7.1 Duzce Earthquake from Joint Analysis of SPOT, GPS, InSAR, Strong-Motion, and Telesismic Data: A Supershear Rupture with Variable Rupture Velocity. *BULLETIN OF THE SEISMOLOGICAL SOCIETY OF AMERICA*, 100, 267-288
- Košťák B., 2006: Deformation effects in rock massifs and their long-term monitoring. *Quarterly Journal of Engineering Geology and Hydrogeology*, 39, 249 – 258.
- Košťák B., 1977: Terčové měřidlo a jeho použití pro měření velmi pomalých pohybů na poruchách a trhlinách. –*Inženýrské stavby* 5: 213 – 218.
- Košťák B., 1982: Sledování recentního vzniku rozsedlinových jeskyní. –*Sborník referátů ze Symposia o pseudokrasu v ČSSR, Stalagmit*, 23–25. Janovičky u Broumova.
- Košťák B., Avramova-Tacheva E. (1988): A method for contemporary displacement measurement on a tectonic fault. – *Journ. of Geodynamics*, 10, 115-125, Pergamon Press.
- Košťák B., Rybář J., 1978: Measurement of the Activity of Very Slow Slope Movements. –*Grundlagen und Anwendung der Felsmechanik, Felsmechanik Kolloquium Karlsruhe*, 191 – 205. Clausthal.
- Košťák B., Rybář J., 1984: Cykličnost v průběhu porušení svahů. –*Acta Polytechnica – Práce ČVUT v Praze*, 4 (1): 85 – 90. Praha.
- Košťák, B 1991: Combined indicator using Moiré technique. *Proceedings of the 3<sup>rd</sup> International Symposium on Field Measurements in Geomechanics (Oslo) 9-11<sup>th</sup> September 1991*. Brookfield/Balkema, Rotterdam, p. 53-60.
- Košťák, B. (2001): Rock movement analysis of the monument of inanimate nature table hill-Szczeliniec Wielki. – *Szczeliniec*, No 5; 3-39, Kudowa Zdrój.
- Košťák, B., Cruden, D.M., 1990. The Moiré' crack gauges on the crown of the Frank Slide. *Can. Geotech. J.* 27, 835– 840 (Ottawa).
- Košťák, B. (2002): Cycles, trends, impulses in rock movement monitoring. - In Rybář, J., Stemberk, J., Wagner, P. eds „Landslides“, 603-609, Swets & Zeitlinger, Lisse
- Kraus, K. & Waldhäusl, P., (1994). *Photogrammetry, Fundamentals and Standard processes*. vol 1. Hermès (editor), Paris.
- Kulatilake, P., Balasingam, P., Park, J., Morgan, R. (2006). Natural rock joint roughness quantification through fractal techniques. *Geotech.Geol.Eng.* 24(5), 1181-1202. doi:10.1007/s10706-005-1219-6.
- Kurz, T.H., Buckley, S.J., Howell, J.A. and Schneider, D., 2008. Geological Outcrop Modelling and Interpretation using Ground Based Hyperspectral and Laser Scanning Data Fusion. *Proceedings of ISPRS, Beijing, China, 2008*, 6 p.
- La Fonta J.G. and Beth M.B. (2002) – “In place inclinometers, a significant test program”. *SolData-France*
- La Parra, S. and Angel, J., 2005. Low cost navigation system for UAV's, *Aerospace Science and Technology*, 9, 504-516.
-

- 
- Laliberte, A., & Rango, A. (2009). Texture and scale in object-based analysis of subdecimeter resolution unmanned aerial vehicle (UAV) imagery. *IEEE Transactions on Geoscience and Remote Sensing*, 47, 761-770
- Lambiel, C., Baron, L., 2008. Two-dimensional geoelectrical monitoring in an alpine frozen moraine. Proceedings of the 9th International Conference on Permafrost, Fairbanks, Alaska, June 2008, Extended Abstracts volume.
- Lan, H., Martin, C.D. and Lim, C.H. 2007. RockFall analyst: a GIS extension for three-dimensional and spatially distributed hazard modeling. *Computat. Geosci.*, 33, 262-279.
- Lanari, R., Mora, O., Manunta, M., Mallorqui, J.J., Berardino, P., Sansosti, E. (2004). A small baseline approach for investigating deformations on full resolution Differential SAR Interferograms. *IEEE Transactions on Geoscience and Remote Sensing* 42, 1377-1386.
- Lapenna, V., Lorenzo, P., Perrone, A., Piscitelli, S., Rizzo, E., Sdao, F., 2003. High-resolution geoelectrical tomographies in the study of the Giarrossa landslide (Potenza, Basilicata). *Bull. Eng. Geol. Env.* 62, 259-68.
- Lapenna, V., Lorenzo, P., Perrone, A., Piscitelli, S., Rizzo, E., Sdao, F., 2005. 2D electrical resistivity imaging of some complex landslides in Lucanian Apennine chain, southern, Italy. *Geophysics* 70.
- Lato, M., Diederichs, M.S., Hutchinson, D.J., Harrap, R. (2009a). Optimization of LiDAR scanning and processing for automated structural evaluation of discontinuities in rockmasses. *Int.J.Rock Mech.Min.Sci.* 46, 194-199. doi:10.1016/j.ijrmms.2008.04.007.
- Lato, M., Hutchinson, J., Diederichs, M., Ball, D., Harrap, R. (2009b). Engineering monitoring of rockfall hazards along transportation corridors: using mobile terrestrial LiDAR. *Nat. Hazards Earth Syst. Sci.* 9(3), 935-946.
- Lato, M.J., Diederichs, M.S., Hutchinson, D.J. (2010). Bias Correction for View-limited Lidar Scanning of Rock Outcrops for Structural Characterization. *Rock Mech Rock Eng* 43(5), 615-628. doi:10.1007/s00603-010-0086-5.
- Le Mignon, G. 2004. Analyse de scénarios de mouvements de versants de type glissement-coulées. Application à la région de Barcelonnette (Alpes-de-Haute-Provence, France). PhD Thesis, Ecole Nationale des Ponts et Chaussées, Paris, France, 210 p
- Le Mignon, G., Cojean, R. 2002. Rôle de l'eau dans la mobilisation de glissements-coulées (Barcelonnette - France). In: Rybár, J., Stemberk, J., Wagner, P. (Eds.): Proceedings of the 1st European Conference on Landslides, Swets & Zeitlinger, Lisse, pp. 239-245.
- Leprince, S., Barbot, F., Ayoub, J., Avouac, J.-P. 2007. Automatic and precise ortho-rectification, coregistration, and subpixel correlation of satellite images, Application to ground deformation measurements, *IEEE Transactions on Geoscience and Remote Sensing*, 45 (6): 1529-1558.
- Leprince, S., Ayoub, F., Klingler, Y., & Avouac, J.-P. (2007). Co-Registration of Optically Sensed Images and Correlation (COSI-Corr): an Operational Methodology for Ground Deformation Measurements. In, *Geoscience and Remote Sensing Symposium* (pp. 2700-2702). Barcelona, Spain: Institute of Electrical and Electronics Engineers
- LePrince, S., Berthier, E., Ayoub, F., Delacourt, C., & Avouac, J.- P. (2008). Monitoring Earth Surface Dynamics With Optical Imagery. *Eos*, 89, 1-5.
- Les numériques, 2006. Test of the camera Sony DSC-H5, available at: [http://www.lesnumeriques.com/sony-dsc-h5-p951\\_1200\\_16.html](http://www.lesnumeriques.com/sony-dsc-h5-p951_1200_16.html), last access 01.03.2011.
- Les numériques, 2011. Test of the camera Sony Cyber-shot HX7V, available at: [http://www.lesnumeriques.com/sony-cyber-shot-hx7v-p322\\_10463\\_16.html](http://www.lesnumeriques.com/sony-cyber-shot-hx7v-p322_10463_16.html), last access 01.03.2011.
- Leutwiler, A. (2009): [Hrsg. BAFU -Abteilung Gefahrenprävention]: Rutschungen; Dynamik, Gefährdung und Überwachung
- Leva D., Nico G., Tarchi D., Fortuny-Guasch J., Sieber, J. (2003). Temporal analysis of a landslide by means of a ground-based SAR interferometer. *IEEE Transactions on Geoscience and Remote Sensing*, 41(4), 745- 752.
- Li W, Bao X, Li Y, and Chen L (2008) Differential pulse-width pair BOTDA for high spatial resolution sensing," *Opt. Express* 16, 21616-21625.
- Lim, M., Petley, D.N., Rosser, N.J., Allison, R.J., Long, A.J. & Pybus, D. (2005). Combined digital photogrammetry and time-of-flight laser scanning for monitoring cliff evolution. *The Photogrammetric Record*, 20, 109-129.
- Lim, M., Rosser, N.J., Allison, R.J., Petley, D.N. (2010). Erosional processes in the hard rock coastal cliffs at Staithes, North Yorkshire. *Geomorphology* 114(1-2), 12-21. doi:10.1016/j.geomorph.2009.02.011.
-

- 
- Lin, C.-P., 2003. Analysis of nonuniform and dispersive time domain reflectometry measurement system with application to the dielectric spectroscopy of soils. *Water Resour. Res.* 39 (1), 1012.
- Linke, J., & McDermid, G.J. (2010). A Conceptual Model for Multi-Temporal Landscape Monitoring in an Object-Based Environment. *Selected Topics in Applied Earth Observations and Remote Sensing, IEEE Journal of, PP*, 1-7
- Lissak, C., Maquaire, O., Malet, J.-P., Déprez, A., Masson, F., Ulrich, P. & Peters, E. 2010. Multi-technique permanent monitoring of a slow-moving coastal landslide in Normandy. In: Malet, J.-P., Glade, T., Casagli, N. (Eds): *Proceedings of the International conference "Mountain Risks: Bringing Science to Society"*, CERG Editions, Strasbourg, pp. 267-273.
- Liu Y, Dai Z, Zhang X, Peng Z, Li J, Ou Z, Liu Y (2010) Optical fiber sensors for landslide monitoring. *Proceedings of the SPIE, Volume 7844*, pp. 78440D-78440D-6.
- Liu Y, Dai Z, Zhou X, Peng Z, Li J, Ou Z, Liu Y (2011) Optical-fiber stress sensors predict landslides. *SPIE Newsroom*. DOI: 10.1117/2.1201102.003468
- Lovisololo M. and Della Giusta A. (2005) – “Precision of D.M.S. columns from real time in-place measurements and improvement in micro-movements analysis with early warning function”. In: “Computational Methods and Experimental Measurements XII” (Brescia, C.A. and Carlomagno, G.M.). WITpress, Southampton, Boston, pp.177-186
- Loye, A., Jaboyedoff, M. and Pedrazzini, A. 2009. Identification of potential rockfall source areas at a regional scale using a DEM-based geomorphometric analysis. *Nat. Hazards Earth Syst. Sci.*, 9, 1643-1653.
- Lu, P., Stumpf, A., Kerle, N., & Casagli, N. (2011). Object-Oriented Change Detection for Landslide Rapid Mapping. *Geoscience and Remote Sensing Letters, IEEE, PP*, 701-705
- Luzi G., Pieraccini M., Mecatti D., Noferini L., Macaluso G., Galgaro A., Atzeni C., 2006. Advances in ground based microwave interferometry for landslide survey: a case study. *International Journal of Remote Sensing*, Vol. 27, No. 12 / 20 June 2006, 2331 – 2350.
- Luzi, G., (2010). Ground based SAR interferometry: a novel tool for Geoscience. In: *Geoscience and Remote Sensing, New Achievements*, P.Imperatore & D. Riccio (Editors), ISBN: 978-953-7619-97-8. Available at: [http://www.intechopen.com/source/pdfs/10381/InTech-Ground\\_based\\_sar\\_interferometry\\_a\\_novel\\_tool\\_for\\_geoscience.pdf](http://www.intechopen.com/source/pdfs/10381/InTech-Ground_based_sar_interferometry_a_novel_tool_for_geoscience.pdf)
- Luzi, G., Monserrat, O., Crosetto, M., Copons, R., Altimir, J., 2010. Ground-Based SAR Interferometry applied to landslide monitoring in mountainous areas. In: *Mountain risks: bringing science to society: proceedings of the Mountain Risks International Conference, Firenze, Italy, 24-26 November 2010*, ed. by J.-P. Malet, T. Glade and N. Casagli, 307-312. Strasbourg : CERG, 2010. ISBN 2-95183317-1-5. 307-312.
- Maas, H.-G., Schwalbe, E., Dietrich, R., Bäessler, M., & Ewert, H. (2008). Determination of spatio-temporal velocity fields on glaciers in West- Greenland by terrestrial image sequence analysis. *IAPRS, XXXVII*, Part B8 Beijing,China, 1419-1424.
- Majes, B., 2001: Analyses of Landslide and its Rehabilitation. *Ujma* 14-15, 2000/2001, Ljubljana. [http://www.sos112.si/slo/tdocs/ujma/2001/p3\\_3.pdf](http://www.sos112.si/slo/tdocs/ujma/2001/p3_3.pdf)
- Malet, J.P. (2003). Les 'glissements de type écoulement' dans les marnes noires des Alpes du Sud. Morphologie, fonctionnement et modélisation hydro-mécanique. In, *Institut de Physique de Globe* (p. 364). Strasbourg: Université Louis Pasteur
- Malet, J.-P., 2003. Les glissements de type écoulement dans les marnes noires des Alpes du Sud. Morphologie, fonctionnement et modélisation hydro-mécanique. PhD Thesis, Université Louis Pasteur, Strasbourg, France, 364 p.
- Malet, J.-P., Maquaire, O., Calais, E. 2002. The use of GPS for the continuous monitoring of landslides. Application to the Super Sauze earthflow (Alpes-de-Haute-Provence, France). *Geomorphology*, 43: 33-54.
- Manzo, M., Ricciardi, G.P., Casu, F., Ventura, G., Zeni, G., Borgstrom, S., Berardino, P., Del Gaudio, C., Lanari, R., (2006). Surface deformation analysis in the Ischia Island (Italy) based on spaceborne radar interferometry. *Journal of Volcanology and Geothermal Research* 151, 399–416.
- Marescot, L., Loke, M.H., Chapellier, D., Delaloye, R., Lambiel, C., Reynard, E., 2003. Assessing reliability of 2D resistivity imaging in mountain permafrost studies using the depth of investigation index method. *Near Surface Geophysics* 1, 57-67.
- Marescot, L., Monnet, R., Chapellier D., 2008. Resistivity and induced polarization surveys for slope instability studies in the Swiss Alps. *Engineering Geology, Volume 98, Issues 1-2, Pages 18-28*.
- Marschallinger R., Eichkitz C., Gruber H., Heibl K., 2009. The Gschliefgraben Landslide (Austria): A Remediation Approach involving Torrent and Avalanche Control, *Geology, Geophysics, Geotechnics and Geoinformatics*. -*Austrian Journal of Earth Sciences*, 102 (2): 36-51.
-

- 
- Martha, T., Kerle, N., van Westen, C.J., & Kumar, K. (2010a). Characterising spectral, spatial and morphometric properties of landslides for semi-automatic detection using object-oriented methods. *Geomorphology*, 116, 24-36
- Martha, T.R., Kerle, N., Jetten, V., van Westen, C.J., & Vinod Kumar, K. (2010b). Landslide Volumetric Analysis Using Cartosat-1-Derived DEMs. *Geoscience and Remote Sensing Letters, IEEE*, 7, 582 - 586
- Massonnet, D. and Feigl, K.L. 1998. Radar Interferometry and its application to changes in the Earth's surface. *Reviews of Geophysics*, 36, 441-500.
- Mauritsch, H.J., Seiberl, W., Arndt, R., Römer, A., Schneiderbauer, K., Sendlhofer, G.P., 2000. Geophysical investigations of a large landslide in the Carnic Region (case study). *Engineering Geology* 56, 373-388.
- Mazzanti, P., Brunetti, A., 2010. Assessing rockfall susceptibility by Terrestrial SAR Interferometry. In: Mountain risks: bringing science to society: proceedings of the Mountain Risks International Conference, Firenze, Italy, 24-26 November 2010, ed. by J.-P. Malet, T. Glade and N. Casagli, 109-114. Strasbourg : CERG, 2010. ISBN 2-95183317-1-5. 307-312.
- McDermid, G.J., Linke, J., Pape, A., Laskin, D.N., McLane, A.J., & Franklin, S.E. (2008). Object-based approaches to change detection and thematic map update: Challenges and limitations. *Canadian Journal of Remote Sensing*, 34, 462-466
- Meric, O., Garambois, S., Jongmans, D., Wathelet, M., Chatelain, J.-L., Vengeon, J.-M., 2005. Application of geophysical methods for the investigation of the large gravitational mass movement of Séchilienne, France. *Canadian Geotechnical Journal* 42, 1105-1115.
- Méric, O., Garambois, S., Orengo, Y., 2006. Large gravitational movement monitoring using a spontaneous potential network. In: Proc. 19th Annual meeting of SAGEEP, Seattle, USA, EEGS Ed., Denver, USA, 6 p.
- Metternicht G., Hurni L., Gogu R. (2005). Remote sensing of landslides: An analysis of the potential contribution to geo-spatial systems for hazard assessment in mountainous environments. *Remote Sensing of Environment*, 98, 284 – 303
- Michel, R., Avouac J.P., Taboury J., 1999, Measuring ground displacements from SAR amplitude images: Application to the Landers earthquake, *Geophys. Res. Lett.*, v. 26, p. 875-878.
- Michoud, C., Derron, M.-H., Horton, P., Jaboyedoff, M., Queyrel, A., Baillifard, F.-J., Loye, A., Nicolet, P. and Pedrazzini, A. Submitted. Rockfall probabilistic hazard and risk assessment along roads at a regional scale based on slope angle distribution: example in Swiss Alps.
- Michoud, C., Longchamp, C., Derron, M.-H., Jaboyedoff, M., Blikra, L.-H., Kristensen, L. and Oppikofer, T., 2010. Technical report: the terrestrial and offshore laser scanning acquisitions of September 2010 in Sunndalsøra (Møre og Romsdal, Norway) - Techniques, processing and data, Technical report, 10p.
- Mikhail, E., Bethel, J. S., & McGlone, J. C. (2001). *Introduction to Modern Photogrammetry*, Hardcover (edition), New-York.
- Minty B.R.S., Luyendyk A.P.J., Brodie R.C., 1997. Calibration and data processing for airborne gamma-ray spectroscopy, *AGSO Journal of Australian Geology & Geophysics*, 17 (2), p. 51-62.
- Moret, D., Arru'e, J.L., Lo'pez, M.V., Gracia, R., 2006. A new TDR waveform analysis approach for soil moisture profiling using a single probe. *J. Hydrol.* 321, 163-172.
- Motschka, K. (2001): Aerogeophysics in Austria. *Bulletin of the Geological Survey of Japan* 52, 83-88.
- Nagai, M. and Shibasaki, R., 2005. Robust trajectory tracking by combining GPS/IMU and continual CCD images, in Proc. 25<sup>th</sup> Int. Symp. Space Technol. Sci., Kanazawa, Japan, 2006, 1189-1194.
- Nagai, M., Chen, T., Shibasaki, R., Kumagai, H. and Ahmed, A., 2009. UAV-Borne 3-D Mapping System by Multisensor Integration, *IEEE Transactions of Geoscience and Remote Sensing*, Vol. 47 (3), 701-708.
- Nakazato H., Kuroda S., Okuyama T., Sasaki Y., 2006. The aim at a rich rural village utilizing water and soil. Improvement of production basis for improving productivity and exhibiting many-sided functions, and development of management techniques. Improvement of airborne electromagnetic method and three-dimensional resistivity distribution exploration in landslide areas. *Mizu to Tsuchi o Ikashi Yutakana Noson o Mezashite Saishin Nogyo Kogaku Kenkyu Seikashu Heisei 18nen*, pp 216-217.
- Neunhöfer, H., Hemmann, A., 2005. Earthquake swarms in the Vogtland/Western Bohemia region: Spatial distribution and magnitude-frequency distribution as an indication of the genesis of swarms?. *J. Geodyn.* 39, 361-385.
- NGU's geological atlas, available at: <http://www.ngu.no/kart/bg250/>, last access 25.02.2011.
- Nguyen, H.T., Fernandez-Steeger, T.M., Wiatr, T., Rodrigues, D., Azzam, R. (2011). Use of terrestrial laser scanning for engineering geological applications on volcanic rock slopes - an example from Madeira island (Portugal). *Nat. Hazards Earth Syst. Sci.* 11, 807-817. doi:10.5194/nhess-11-807-2011.
-

- 
- Nichol, J., & Wong, M.S. (2005). Satellite remote sensing for detailed landslide inventories using change detection and image fusion. *International Journal of Remote Sensing*, 26, 1913 - 1926
- Niesner, E., Weidinger, J.T., 2008. Results of a continuous geoelectrical monitoring in the forefront of the large landslide event of 2007/2008 in the Gschliefgraben (Gmunden, Upper Austria). EGU General Assembly 2008, Geophysical Research Abstracts, Vol. 10.
- Niesner, E., Weidinger, J.T., 2009. The potential of geoelectrics for landslide forecasting. EGU General Assembly 2009, Geophysical Research Abstracts, Vol. 11.
- Niethammer, U., James, M.R., Rothmund, S., Travelletti, J., Joswig, M., 2011. UAV-based remote sensing of the Super-Sauze landslide: Evaluation and results, *Engineering Geology* (2011), doi: 10.1016/j.enggeo.2011.03.012
- Niethammer, U., Rothmund, S. and Joswig, M., 2009. UAV-based remote sensing of the slow-moving landslide Super-Sauze, in: *Landslide Processes, from geomorphologic mapping to Dynamic Modelling*, Proc. of the Landslide Processes Conference, a tribute to Dr. Theo van Asch, Malet, J.-P., Rémaitre, A. and Bogaard, T. (eds.), Strasbourg, France, 6-7 February 2009, 69-74.
- Nilsson, J.N.U., Sigray, P., Tyler, R.H., 2007. Geoelectric Monitoring of Wind-Driven Barotropic Transports in the Baltic Sea. *Journal of Atmospheric and Oceanic Technology* 24, 1655-1664.
- Nissen, H.H., Moldrup, P., Kachanoski, R.G., 2000. Time domain reflectometry measurements of solute transport across a soil layer boundary. *Soil Sci. Soc. Am. J.* 64, 62-74.
- Noetzli, J., Hilbich, C., Hauck, C., Hoelzle, M., Gruber, S., 2008. Comparison of Simulated 2D Temperature Profiles with Time-Lapse Electrical Resistivity Data at the Schilthorn Crest, Switzerland. 9th International Conference on Permafrost, Book of published papers: 1293-1298.
- Olivares L, Damiano E, Greco R, Zeni L, Picarelli L, Minardo A, Guida A, Bernini R (2009) An Instrumented Flume to Investigate the Mechanics of Rainfall-Induced Landslides in Unsaturated Granular Soils”, *Geotechnical Testing Journal*, vol. 32, no. 2
- Oppikofer, T. (2009). Detection, analysis and monitoring of slope movements by high-resolution digital elevation models. Institute of Geomatics and Analysis of Risk, University of Lausanne, Lausanne, Switzerland.
- Oppikofer, T., Jaboyedoff, M., Blikra, L.H., Derron, M.-H. (2008a). Characterization and monitoring of the Åknes landslide using terrestrial laser scanning, in: Locat, J., Perret, D., Turmel, D., Demers, D., Leroueil, S. (Eds.), 4th Canadian Conference on Geohazards: From Causes to Management. Presse de l'Université Laval, Université Laval, Québec, Qc, Canada, pp. 211-218.
- Oppikofer, T., Jaboyedoff, M., Blikra, L.H., Derron, M.-H. (2009). Characterization and monitoring of the Åknes rockslide using terrestrial laser scanning. *Nat. Hazards Earth Syst. Sci.* 9(3), 1003-1019. doi:10.5194/nhess-9-1003-2009.
- Oppikofer, T., Jaboyedoff, M., Keusen, H.-R. (2008b). Collapse at the eastern Eiger flank in the Swiss Alps. *Nat. Geosci.* 1(8), 531-535. doi:10.1038/ngeo258.
- Oppikofer, T., Jaboyedoff, M., Pedrazzini, A., Derron, M.-H., Blikra, L.H. (in press). Detailed DEM analysis of a rockslide scar to improve the basal failure surface model of active rockslides. *Journal of Geophysical Research* doi:10.1029/2010JF001807.
- Optech Inc., 2011. LiDAR manufacturers, available at: <http://www.optech.ca/>, last access 01.03.2011.
- Oswald, B., Benedickter, H.R., Bächtold, W., Flußler, H., 2003. Spatially resolved water content profiles from inverted time domain reflectometry signals. *Water Resour. Res.* 39 (12), 1357.
- PDNA (2010). Haiti Earthquake PDNA: Assessment of damage, losses, general and sectoral needs. In G.o.t.R.o. Haiti (Ed.), *Annex to the Action Plan for National Recovery and Development of Haiti* (p. 115). Port au Prince, Haiti: Government of the Republic of Haiti
- Pedrazzini, A., Oppikofer, T., Jaboyedoff, M., Guelli Pons, M., Chantry, R., Stampfli, E. (2010). Assessment of rockslide and rockfall problems in an active quarry: case study of the Arvel quarry (Western Switzerland), in: Zhao, J., Labiouse, V., Dudt, J.-P., Mathier, J.-F. (Eds.), *Rock Mechanics in Civil and Environmental Engineering*. CPC/Balkema, pp. 593-596.
- Peduto D. (2008). Analysis of ground deformations related to subsidence and landslide phenomena via DInSAR techniques. Ph.D.Thesis (In English). University of Salerno, Italy, May 2008. Tutor: Cascini L.; co-tutor: Fornaro G.
- Perissin, D., Prati, C., Ferretti, A. (2005). Spaceborne SAR anatomy of a city. Proceedings of FRINGE 2005, Frascati (Italy), 28 November– 2 December 2005. ESA SP-610, available also online: <http://earth.esa.int/workshops/fringe2005/proceedings/>.
-

- 
- Perrone, A., 2001. Electrical and Self-Potential tomographic techniques for landslide monitoring: first results on Southern Apennine Chain (Italy). II international Workshop on Geo-Electro-Magnetism / Abstract, Memorie dell'Accademia Lunigianese di Scienze "G. Capellini" Vol. LXXI (2001), Scienze Matematiche, Fisiche e Naturali, La Spezia.
- Pesci A., Baldi B., Bedin A., Casula G., Cenni N., Fabris M., Loddo F., Mora P., & Bacchetti M. (2004). Digital elevation models for landslide evolution monitoring: application on two areas located in the Reno River Valley (Italy). *Annals of Geophysics*, 47, 1339-1353.
- Pesci, A., Teza, G., Casula, G., Loddo, F., De Martino, P., Dolce, M., Obrizzo, F., Pingue, F. (2011). Multitemporal laser scanner-based observation of the Mt. Vesuvius crater: Characterization of overall geometry and recognition of landslide events. *ISPRS J. Photogramm.* 66(3), 327-336. doi:10.1016/j.isprsjprs.2010.12.002.
- Petkovšek, B., 2001: Geological Characteristic of the Stože Landslide. Ujma 14-15, 2000/2001, Ljubljana. [http://www.urszr.si/slo/tdocs/ujma/2001/p3\\_5.pdf](http://www.urszr.si/slo/tdocs/ujma/2001/p3_5.pdf)
- Petro L, Vlčko J, Ondrášik O, Polascanova E 2004: Recent tectonics and slope failures in the Western Carpathians. *Engineering Geology* 74, 103 – 112.
- Pfaffhuber A., Grimstad E., Domaas U., Auken E., Halkjær M., 2010. The hunt for sliding planes in a phyllitic rock slide in Western Norway using airborne electromagnetic mapping, EGU General Assembly 2010, Geophysical Research Abstracts, 12, EGU2010-4492.
- Picarelli L, Urciuoli G, Russo C (2004) Effect of groundwater regime on the behaviour of clayey slopes. *Canadian Geotechnical Journal*, vol. 41, no 3, 1 pp. 467-484.
- Pieraccini M., Mecatti D., Noferini L., Macaluso G., Luzi G., Atzeni C., 2007. Radar interferometric per il monitoraggio di frane, ghiacciai e valanghe. Atti 11° conferenza ASITA, Torino 6-9 Novembre 2007.
- Pieraccini M., Tarchi D., Rudolf H., Leva D., Luzi G., Atzeni C., 2000a. Interferometric radar for remote monitoring of building deformations., *Electronics Letters*, 36, 6, 569-570.
- Pieraccini M., Tarchi D., Rudolf H., Leva D., Luzi G., Bartoli G., Atzeni C., 2000b. Structural static testing by interferometric synthetic radar. *NDT&E International*, 33, 8, 565-570.
- Pieraccini, M., Casagli, N., Luzi, G., Tarchi, D., Mecatti, D., Noferini, L. & Atzeni, C., 2003 Landslide monitoring by ground-based radar interferometry: a field test in Valdarno (Italy). *International Journal of Remote Sensing*, 24(6), 1385-1391.
- Plaza, A., Benediktsson, J.A., Boardman, J.W., Brazile, J., Bruzzone, L., Camps-Valls, G., Chanussot, J., Fauvel, M., Gamba, P., Gualtieri, A., Marconcini, M., Tilton, J.C. and Trianni, G. 2009. Recent advances in techniques for hyperspectral image processing, *Remote Sensing of Environment*, 113, S110–S122.
- Prokop, A., Panholzer, H. (2009). Assessing the capability of terrestrial laser scanning for monitoring slow moving landslides. *Natural Hazards and Earth System Sciences* 9(6), 1921-1928. doi:10.5194/nhess-9-1921-2009.
- R. Greco, A. Guida: "Field measurements of topsoil moisture profiles by vertical TDR probes". *Journal of Hydrology*, 2008, Vol 348, pp. 442-451.
- Rabatel, A., Deline, P., Jaillet, S., Ravel, L. (2008). Rock falls in high-alpine rock walls quantified by terrestrial lidar measurements: A case study in the Mont Blanc area. *Geophys.Res.Lett.* 35(10), 10502. doi:10.1029/2008GL033424.
- Rau, J.-Y., Chen, L.-C., Liu, J.-K., & Wu, T.-H. (2007). Dynamics monitoring and disaster assessment for watershed management using time-series satellite images. *Geoscience and Remote Sensing, IEEE Transactions on*, 45, 1641-1649
- Regalado, C.M., Munoz Carena, R., Socorro, A.R. & Hernandez Moreno, J.M. Time domain reflectometry models as a tool to understand the dielectric response of volcanic soils, *Geoderma*, 2003, 117, 313-330.
- Reid, M.E., Baum, R.L., LaHusen, R.G., Ellis, W.L. 2008. Capturing landslide dynamics and hydrologic triggers using near-real-time monitoring. In: Chen, Z.-Y., Zhang, J.-M., Ho, K., Wu, F.-Q., Li, Z.-K. (Eds): *Landslides and Engineered Slopes, from the Past to the Future*. Proceedings of the Tenth International Symposium on Landslides and Engineered Slopes, Taylor & Francis Group, London, 179-191.
- Rocca, F. (2003). 3D Motion recovery with multi-angle and/or left right Interferometry. Proceedings of the third International Workshop on ERS SAR Interferometry (FRINGE 2003), Frascati (Italy), 2–5 December 2003. ESA SP-550, available also online: <http://earth.esa.int/fringe03/proceedings/>.
-

- 
- Roering, J.J., Stimely, L.L., Mackey, B.H. and Schmidt, D., 2009. Using DInSAR, airborne LiDAR, and archival airphotos to quantify landsliding and sediment transport, *Geophysical Research Letters*, 36, 5 p.
- Rosser, N.J., Petley, D.N., Dunning, S.A., Lim, M., Ball, S. (2007). The surface expression of strain accumulation in failing rock masses, in: Eberhardt, E., Stead, D., Morrison, E. (Eds.), *Rock mechanics: Meeting Society's challenges and demands. Proceedings of the 1st Canada - U.S. Rock Mechanics Symposium, Vancouver, Canada, May 27-31, 2007*. Taylor & Francis Group, London, pp. 113-120.
- Rosser, N.J., Petley, D.N., Lim, M., Dunning, S.A., Allison, R.J. (2005). Terrestrial laser scanning for monitoring the process of hard rock coastal cliff erosion. *Quarterly Journal of Engineering Geology and Hydrogeology* 38(4), 363-375. doi:10.1144/1470-9236/05-008.
- Roth, K., Schulin, R., Fluhler, H., Attinger, W., 1990. Calibration of time domain reflectometry for water content measurement using a composite dielectric approach. *Water Resour. Res.* 26, 2267–2273.
- Roth, M., Dietrich, M., Blikra, L.H., Lecomte, I., 2005. Seismic monitoring of the unstable rock slope at Åknes, Norway. *NORSAR, Report for the International Centre for Geohazards*.
- Rowlands, K.A., Jones, L.D., Whitworth, M. (2003). Landslide Laser Scanning: a new look at an old problem. *Quarterly Journal of Engineering Geology and Hydrogeology* 36(2), 155-157.
- Rudolf H., Leva D., Tarchi D., Sieber A.J., 1999. A mobile and versatile SAR system. *Proc. IGARSS 99*, 592-594.
- Sasaki Y., Nakazato H., 2004. Inversion of airborne EM data accounting for terrain and inaccurate flight height, *SEG Expanded Abstracts* 23, 648.
- Sass, O., Viles, H.A., 2010. Wetting and drying of masonry walls: 2D-resistivity monitoring of driving rain experiments on historic stonework in Oxford, UK. *Journal of Applied Geophysics* 70, 72–83.
- Schlumberger, 1987. *Log Interpretation Charts*, Houston, Schlumberger Educational Services.
- Scholz, C.H., 1968. The frequency-magnitude relation of microfracturing in rock and its relation to earthquakes. *BSSA*. 58 (1), 399-415.
- Schorlemmer, D., Wiemer, S., 2004. Earthquake statistics at Parkfield: 1. Stationarity of b values, *J. Geophys. Res.*, 109. B12308, doi: 10.1029/2004JB003235.
- Seiberl, W., A. Ahl, and E. Winkler, 1998. Interpretation of airborne electromagnetic data with neural networks: *Exploration Geophysics*, 29, 152-156.
- Seijmonsbergen, A.C., Van Westen, C.J., Rupke, J. and Krieg, W. (1988): *Geomorphologische, geotechnische und Naturgefahren-Karten des Hinteren Bregenzerwaldes (Vlb., Austria).- Karten mit Erläuterungen – Projektbericht*.
- Siehl A. (1996): *Umweltradioaktivität*, Ernst & Sohn, Berlin.
- Singhroy, V., Mattar, K.E., Gray, A.L. (1998). Landslide characteristics in Canada using interferometric SAR and combined SAR and TM images. *Advances in Space Research*, 3, 465–476.
- Sjödahl, P., 2006. Resistivity investigation and monitoring for detection of internal erosion and anomalous seepage in embankment dams. MS. Doctoral Thesis, Lund University, 96 pp.
- Slater, L., Ntarlagiannis, D., Wishart, D., 2006. On the relationship between induced polarization and surface area in metal-sand and clay-sand mixtures. *Geophysics* 71, A1-A5.
- Slob, S., Hack, H., Turner, A.K. (2002). An approach to automate discontinuity measurements of rock faces using laser scanning techniques, in: Dinid da Gama, C., Riberia e Sousa, L. (Eds.), *Proceedings of ISRM EUROCK 2002, 25-28 November 2002, Funchal, Portugal*. Sociedade Portuguesa de Geotecnia, pp. 87-94.
- Soto MA, Bolognini G, Di Pasquale F (2011) Long-range simplex-coded BOTDA sensor over 120km distance employing optical preamplification. *Opt. Lett.* 36, 232-234.
- Spillmann T., Maurer H., Green G. A., Heincke B., Willenberg H., Husen S., 2007. Microseismic investigation of an unstable mountain slope in the Swiss Alps. *J. Geophys. Res.*, 112.
- Spillmann, T., Maurer, H., Green, A.G., Heincke, B., Willenberg, H., Husen, S., 2007. Microseismic investigations of an unstable mountain slope in the Swiss Alps. *J. Geophys. Res.* 112, B07301.
- Squarzoni, C., Delacourt, C., Allemand, P. 2003. Nine years of spatial and temporal evolution of the La Valette landslide observed by SAR interferometry. *Engineering Geology*, 68(1-2): 53-66.
- Squarzoni, C., Delacourt, C., Allemand, P. 2005. Differential single-frequency GPS monitoring of the La Valette landslide (French Alps). *Engineering Geology*, 79(3-4): 215-229.
- Stemberk J. (2002): Slope and tectonic movement trial in Moravskoslezské Beskydy Mts. – In Rybář J., Holzer R., Kopecký M. eds „1st ECL Field Trip Guide, Post-Conference Field Trip, 24-27, Prague
-

- 
- Stemberk J., Jánoš V. (2003): Svahové deformace na Radhošťském hřebenu v Moravskoslezských Beskydech, mapové listy 25-23-09 a 25-23-10 v měřítku 1 : 10 000. – Zprávy o geologických průzkumech 2002, ČGS, Praha
- Strozzi, T., Farina, P., Corsini, A., Ambrosi, C., Thüning, M., Zilger, J., Wiesmann, A., Wegmüller, U., Werner, C. (2005). Survey and monitoring of landslide displacements by means of L-band satellite SAR interferometry. *Landslides*, 2 (3), 193–201.
- Stumpf, A., & Kerle, N. (forthcoming). Object-oriented mapping of landslides using Random Forests. *Remote Sensing of Environment*
- Sturzenegger, M., Stead, D. (2009a). Close-range terrestrial digital photogrammetry and terrestrial laser scanning for discontinuity characterization on rock cuts. *Eng.Geol.* 106(3-4), 163-182. doi:10.1016/j.enggeo.2009.03.004.
- Sturzenegger, M., Stead, D. (2009b). Quantifying discontinuity orientation and persistence on high mountain rock slopes and large landslides using terrestrial remote sensing techniques. *Nat. Hazards Earth Syst. Sci.* 9(2), 267-287. doi:10.5194/nhess-9-267-2009.
- Sturzenegger, M., Yan, M., Stead, D., Elmo, D. (2007). Application and limitations of ground-based laser scanning in rock slope characterization, in: Eberhardt, E., Stead, D., Morrison, T. (Eds.), *Rock mechanics: Meeting Society's challenges and demands. Proceedings of the 1st Canada - U.S. Rock Mechanics Symposium, Vancouver, Canada, May 27-31, 2007.* Taylor & Francis, London, pp. 29-36.
- Supper R., Ahl A., Römer A., Jochum B., Bieber G., 2007. A complex geo-scientific strategy for landslide hazard mitigation – from airborne mapping to ground monitoring, *Advances in Geosciences*, 14, 1-6.
- Supper R., Baron I., Ita A., Winkler E., Jochum B., Motschka K. (2010b): Airborne Geophysical Survey and Innovative Landslide Monitoring at Gschlifgraben, Austria. – Near Surface 2010, 16th European Meeting of Environmental and Engineering Geophysics, Zurich, Switzerland, 6 - 8 September 2010, 5 pp. CD.
- Supper R., Baron I., Jochum B., Ita A., Motschka K., Winkler E. (2010a): Airborne geophysics and geoelectric and inclinometric monitoring at the Gschlifgraben landslide. – In.: Supper R. & Baron I. (Eds.): *Landslide Monitoring Technologies & Early Warning Systems, Current Research and Perspectives for the Future, Book of extended abstracts. Open Workshop within the frame of the EU FP7 “SafeLand” Project, February 24th, 2010, Vienna.* Berichte der Geologischen Bundesanstalt 82: 50-56. ISSN 017 - 8880
- Supper, R., Ahl, A., Römer, A., Jochum, B., Bieber, G., 2008. A complex geo-scientific strategy for landslide hazard mitigation – from airborne mapping to ground monitoring. *Advances in Geosciences* 14, 1-6.
- Supper, R., Baron, I., Jochum, B., Ita, A., Winkler, E., Motschka, K., Moser, G., 2010. From structural investigation towards multi-parameter early warning systems: geophysical contributions to hazard mitigation at the landslide of Gschlifgraben (Gmunden, Upper Austria), *Terra Abstracts, European Geosciences Union 2010*, accepted.
- Supper, R., Hübl, G., Jaritz, W., 2002. Geophysical Surveys for the investigation and monitoring of landslide areas. *Proceedings of the Environmental and Engineering Geophysical Society, 8th Meeting Aveiro, Portugal.*
- Supper, R., Jochum, B., Seiberl, W., Arndt, R., 2000. Geoelectrical multielectrode measurements for surveying and monitoring of landslide areas. *Proceedings of the “Workshop on Advanced Techniques for the Assessment of Natural Hazards in Mountain Areas”, p.99, Igls, Austria.*
- Supper, R., Römer, A., 2003. New Achievements in Developing a High Speed Geoelectrical Monitoring System for Landslide Monitoring. *Proceedings of the Environmental and Engineering Geophysical Society, 9th Meeting Prag, Prag.*
- Supper, R., Römer, A., Avian, M., Kellerer-Pirklbauer, A., 2007. Geoelectrical measurements for permafrost monitoring at the Hoher Sonnblick, Salzburg, Austria. *EGU General Assembly 2007, Geophysical Research Abstracts, Vol. 9.*
- Supper, R., Römer, A., Jochum, B., 2009. Geoelectrical measurements for natural hazard monitoring. *SEGJ 9th International Symposium, Extended Abstracts, Sapporo.*
- Supper, R., Seiberl, W., Hübl, G., 2001. Combined Airborne Electromagnetics and Ground Geoelectrics for Landslide Investigations. *II international Workshop on Geo-Electro-Magnetism / Abstract, Memorie dell'Accademia Lunigianese di Scienze “G. Capellini” Vol. LXXI (2001), Scienze Matematiche, Fische e Naturali, La Spezia.*
-

- 
- Supper, R.; Stotter, Ch.; Schattauer, I.; Motschka K. (2004): The Problem of High resolution positioning and the importance of innovative DEM generation for environmental airborne geophysics. – 32nd International Geological Congress, Florence, Scientific Sessions: abstracts (part 1) – 175: CD
- Suriñach, E., Vilajosana, I., Khazaradze, G., Biescas, B., Furdada, G., Vilaplana, J.M., 2005. Seismic detection and characterization of landslides and other mass movements. *Nat. Hazards Earth Syst. Sci.* 5, 791-798.
- Swisstopo, 2011. False-colour infrared (FCIR) orthophoto mosaic of Switzerland, available at: [http://www.swisstopo.admin.ch/internet/swisstopo/en/home/products/images/ortho/swissimage/SWISS\\_IMAGE\\_FCIR.html](http://www.swisstopo.admin.ch/internet/swisstopo/en/home/products/images/ortho/swissimage/SWISS_IMAGE_FCIR.html), last access 23.03.2011.
- Tang, H., Jia, H., Hu, X., Li, D., & Xiong, C. (2010). Characteristics of landslides induced by the great Wenchuan earthquake. *Journal of Earth Science*, 21, 104-113
- Tapete, D., Casagli, N., Fanti, R., Del Ventisette, C., Cecchi, R., Petrangeli, P., 2011. Satellite and ground-based radar interferometry for detection and monitoring of structural instability in archaeological sites. *Geophysical Research Abstracts* Vol. 13, EGU2011-8387, European Geosciences Union (EGU) General Assembly, April 3-8, 2011, Vienna (Austria). Available at: <http://meetingorganizer.copernicus.org/EGU2011/EGU2011-8387.pdf>
- Tarchi D., Leva D., Sieber A.J., 2000a. SAR Interferometric Techniques from Ground Based System for the Monitoring of Landslides. *Proc. IGARSS 2000*.
- Tarchi D., Nesti G., Prati C., Rocca F., 1998. *Proc. PIERS Workshop on Advances in Radar Methods*, 230-233.
- Tarchi D., Rudolf H., Luzi G., Chiarantini L., Coppo P., Sieber A.J., 1999. SAR Interferometry for structural changes detection: a demonstration test on a dam. *Proc. IGARSS 99*, 1522–1524
- Tarchi D., Rudolf H., Pieraccini M., Atzeni C., 2000b. Remote monitoring of buildings using a ground-based SAR: application to cultural heritage survey. *International Journal of Remote Sensing*, 21, 18.
- Tarchi, D., Basso, M., Farina, P., Leva, D., Casagli, N., Del Piccolo, A., Moretti, S., Luzi, G., Pieraccini, M., Mannucci, G. & Tavelli, S., 2002. Applicazione dell'interferometria radar da terra per il controllo dei movimenti franosi: la frana del Ruinon in Valfurva (SO). In: P. Canuti & A.J. Sieber (Editors), *Pubblicazione CNR-GNDCI n.2543*. Tipografia Grifo, Perugia, 79 pp. (CNR GNDCI Pub.No.2543).
- Tarchi, D., Casagli, N., Fanti, R., Leva, D., Luzi, G., Pasuto, A., Pieraccini, M. & Silvano, S., 2003a. Landslide monitoring by using ground-based SAR interferometry: an example of application to the Tessina landslide in Italy. *Engineering Geology*. 68(1-2), 15-30. (CNR GNDCI Pub.No.2484).
- Tarchi, D., Casagli, N., Leva, D., Luzi, G., Moretti, S., Pieraccini, M. & Sieber, A.J., 2003b. Monitoring landslide displacements by using ground-based SAR interferometry: application to the Ruinon landslide in the Italian Alps. *Journal Geophysical Research*, 108(6). (CNR GNDCI Pub.No.2510).
- Tarchi, D., Ohlmer, E., Sieber, A.J., 1997. Monitoring of Structural Changes by Radar Interferometry. *Research in Nondestructive Evaluation*, 9, 213-225.
- Teza, G., Galgaro, A., Zaltron, N., Genevois, R. (2007). Terrestrial laser scanner to detect landslide displacement fields: a new approach. *Int.J.Remote Sens.* 28(16), 3425-3446.
- Teza, G., Pesci, A., Genevois, R., Galgaro, A. (2008). Characterization of landslide ground surface kinematics from terrestrial laser scanning and strain field computation. *Geomorphology* 97(3-4), 424-437.
- Tilch, N. and Schwarz, L. (2010): Erstellung von Dispositionskarten für Massenbewegungen – Herausforderungen, Methoden, Chancen, Limitierungen.- Vortrag Innsbrucker Hofgespräche 26.05.2010, Innsbruck. [[http://bfw.ac.at/050/pdf/IHG260510\\_Tilch\\_Schwarz.pdf](http://bfw.ac.at/050/pdf/IHG260510_Tilch_Schwarz.pdf)]
- Tilch, N., Kociu, A., Ribitsch, R., Schmid, F., Proske, H., Andrecs, P., Hagen, K., Lang, E., Hermann, S. & Loizenbauer, J. (2009): Abschätzung der Risikodisposition für Rutschungen und Hangbewegungen am Beispiel Gasen/Haslau (Stmk).- *FloodRisk II - Vertiefung und Vernetzung zukunftsweisender Umsetzungsstrategien zum integrierten Hochwassermanagement*. Ergebnispräsentations-veranstaltung 29./30.06.2009, Wien; [[http://www.geologie.ac.at/pdf/Poster/poster\\_2009\\_floodrisk\\_II.pdf](http://www.geologie.ac.at/pdf/Poster/poster_2009_floodrisk_II.pdf)]
- Topp, G.C., Davis, J.L., Annan, A.P., 1980. Electromagnetic determination of soil water content: measurement in coaxial transmission lines. *Water Resour. Res.* 16, 574–582.
- Travelletti, J., Delacourt, C., Allemand, P., Malet, J.-P., Schmittbuhl, J., Toussaint, R., Bastard, M. A multi-temporal image correlation method to characterize landslide displacements with a terrestrial camera. *International Journal of Photogrammetry & Remote-Sensing*, 15p. (submitted in December 2010).
- Travelletti, J., Malet, J.-P. (accepté, in press). Characterization of the 3D geometry of flow-like landslides: a methodology based on the integration of multi-source data. *Engineering Geology*, 21p. (accepté, in press).
- Travelletti, J., Malet, J.-P., Samyn, K., Grandjean, G., Jaboyedoff, M. Control of landslide retrogression by discontinuities: evidences by the integration of airborne- and ground-based geophysical information. *Landslides, Journal of the International Consortium on Landslides*, 21p. (submitted in Déc. 2010).
-

- 
- Travelletti, J., Oppikofer, T., Delacourt, C., Malet, J.-P., Jaboyedoff, M. (2008). Monitoring landslide displacements during a controlled rain experiment using a long-range terrestrial laser scanning (TLS). *International Archives of Photogrammetry and Remote Sensing* 37 Part B5, 485-490.
- Tsutsui, K., Rokugawa, S., Nakagawa, H., Miyazaki, S., Chin-Tung Cheng Shiraishi, T., & Yang, S.-D. (2007). Detection and Volume Estimation of Large-Scale Landslides Based on Elevation-Change Analysis Using DEMs Extracted From High-Resolution Satellite Stereo Imagery *IEEE Transactions on Geoscience and Remote Sensing Letters*, 45, 1681 - 1696
- Utsu, T., 1965. A method for determining the value of b in the formula  $\log N = a - bM$  showing the magnitude-frequency relation for earthquakes. *Geophys. Bull. Hokkaido Univ.* 13, 99-103.
- van der Werff, H.M.A., & van der Meer, F.D. (2008). Shape-based classification of spectrally identical objects. *ISPRS Journal of Photogrammetry & Remote Sensing*, 63, 251–258
- Vannini E., Vannucci S., Zanicchi M., Mastorci G., con la consulenza di Puccinelli A., 2004. Progetto preliminare finalizzato al consolidamento del versante di Castagnola in comune di Framura - Relazione geologica preliminare con allegati. Committente: Comunità Montana Riviera Spezzina. EPTA Consult p.s.c.r.l., 47 pp.
- Vidrih, R., Ribičič, M., 1999: Slope Failure Effects in Rocks at Earthquake – Posočje, April 12.1998 and European Macroseismic Scale (EMS-98). *Geologija*, 41, 365-419 (1998), Ljubljana. <http://www.geologija-revija.si/dokument.aspx?id=774>
- Vidrih, R., Ribičič, M., 2004: The earthquake on July 12, 2004, in Upper Soča Valley (NW Slovenia) – preliminary geological and seismological characteristic. *Geologija*, 47/2, 199-220, Ljubljana. <http://www.geologija-revija.si/dokument.aspx?id=451>
- Vlcko J, Jezny M, Pagacova Z (2005) Influence of thermal expansion on slope displacements (C101-2). In: Sassa K, Fukuoka H, Wang F, Wang G (eds.) *Landslides – Risk Analysis and Sustainable Disaster Management*, Springer, pp 71-74.
- Walter, M., Arnhardt, C., Joswig, M. 2011 (accepted, in press). Seismic monitoring of rockfalls, subsurface fracture processes, and superficial fissure development at the Super-Sauze, French Alps, mudslide. *Engineering Geology*, 12p. (to be published in May 2011).
- Walter, M., Joswig, M., 2008. Seismic monitoring of fracture processes generated by a creeping landslide in the Vorarlberg Alps. *First Break*. 26, 131-135.
- Walter, M., Joswig, M., 2009. Seismic characterization of slope dynamics caused by softrock landslides: The Super-Sauze case study, in: Malet, J.-P., Rémaitre, A., Boogard, T. (Eds), *Proceedings of the International Conference 611 on Landslide Processes: from geomorphologic mapping to dynamic modelling*, Strasbourg, CERG Editions, pp. 215-220.
- Walter, M., Niethammer, U., Rothmund, S. and Joswig, M., 2009. Joint analysis of the Super-Sauze (French Alps) mudslide by nanoseismic monitoring and UAV-based remote sensing, *Near Surface Geoscience*, 27, 53-60.
- Walter, M., Niethammer, U., Rothmund, S., Joswig, M., 2009. Joint analysis of the Super-Sauze (French Alps) mudslide by nanoseismic monitoring and UAV-based remote sensing. *First Break*. 27(8), 75-82.
- Wang B, Li K, Shi B, Wie G (2009) Test on application of distributed fiber optic sensing technique into soil slope monitoring. *Landslides*, vol. 6, no. 1, pp. 61-68, DOI: 10.1007/s10346-008-0139-y
- Wasowski J., Gostelow P. (1999). Engineering geology landslide investigations and SAR Interferometry. *Proceedings of FRINGE'99*, Liege, Belgium. <http://www.esa.int/fringe99>.
- Weber, D., Herrmann, A., 2000. Reconstitution de l'évolution géomorphologique de versants ins Tables par photogrammétrie numérique: l'exemple du glissement de terrain de Super-Sauze (Alpes-de-Haute-Provence, France). *Bulletin de la Société Géologique de France*. 171, 637-648.
- Weerts, A.H., Huisman, J.A., Bouten, W., 2001. Information content of time domain Reflectometry waveforms. *Water Resour. Res.* 37 (5), 1291–1299.
- Whalley, W.R., 1993. Considerations on the use of time domain reflectometry (TDR) for measuring soil water content. *J. Soil Sci.* 44, 1–9.
- White, D. J., Take, W. A. & Bolton, M. D., (2003). Soil deformation measurement using particle image velocimetry (PIV) and photogrammetry. *Géotechnique*, 53, 619-631.
- Wiesmann, A., Werner, C., Strozzi, T., Wegmüller, U., 2008. Measuring deformation and topography with a portable radar interferometer. 13th FIG Symposium on Deformation Measurement and Analysis, 4<sup>th</sup> IAG Symposium on Geodesy for Geotechnical and Structural Engineering, LNEC, Lisbon, May 12-15.
- Wilkinson P.B., Chambers J.E., Meldrum P.I., Gunn D.A., Ogilvy R.D., and Kuras O., 2010: Predicting the movements of permanently installed electrodes on an active landslide using time-lapse geoelectrical resistivity data only, *Geophysical Journal International* 183, 543-556.
-

- Willenberg H., Evans K.F., Eberhardt E., Loew S., Spillmann T., Maurer H., 2004. Geological, geophysical and geotechnical investigations into the internal structure and kinematics of an unstable sliding mass in crystalline rock. 9th Internat. Symp. on Landslides, Rio de Janeiro, 489-494.
- Winsauer, W.O., Shearin, H.M., Jr., Masson, P.H., Williams, M., 1952. Resistivity of brine saturated sands in relation to pore geometry. AAPG Bull., v. 36, p. 253-277.
- Wust-Bloch, H., Joswig, M., 2006. Pre-collapse identification of sinkholes in unconsolidated media at Dead Sea area by “nanoseismic monitoring” (graphical jackknife location of weak sources by few, low-SNR records). Geophys. J. Int. 167, 1220-1232.
- Yang, X., & Chen, L. (2010). Using multi-temporal remote sensor imagery to detect earthquake-triggered landslides. *International Journal of Applied Earth Observation and Geoinformation*, 12, 487-495
- Yaramanci, U., 2000. Geoelectric exploration and monitoring in rock salt for the safety assessment of underground waste disposal sites. *Journal of Applied Geophysics* 44, 181-196.
- Zebker, H.A., Rosen, P.A., Hensley, S., 1997. Atmospheric effects in Interferometric Synthetic Aperture Radar Surface Deformation and topographic maps. *Journal of Geophysical Research* 102 (B4), 7547–7563.
- Zhang, L., & Gruen, A. (2006). Multi-image matching for DSM generation from IKONOS imagery. *ISPRS Journal of Photogrammetry and Remote Sensing*, 60, 195-211.
- Zlotnicki, J., Nishida, Y., 2003. Review on Morphological Insights of Self-Potential Anomalies on Volcanoes. *Surveys in Geophysics* 24, 291-338.
- Zongjian, L., 2008. UAV for mapping – low altitude photogrammetric survey, *Remote Sensing and Spatial Information Sciences*, Vol. XXXVII, Part B1, Beijing 2008, 1183-1186.